EXPERIMENTAL AND NUMERICAL INVESTIGATIONS ON THE CAVITATION PHENOMENON IN A CENTRIFUGAL PUMP

A THESIS SUBMITTED IN PARTIAL FULFILMENT OF THE REQUIREMENTS FOR THE DEGREE OF DOCTOR OF PHILOSOPHY AT THE UNIVERSITY OF HUDDERSFIELD

By

Ahmed Ramadhan Mohsin Al-Obaidi

B.Sc. University of Technology, Baghdad, Iraq, 1998

M.Sc. University of Technology, Baghdad, Iraq, 2001

Director of Research: Professor Rakesh Mishra

Leader of Energy, Emissions and the Environment Research Group

School of Computing and Engineering

University of Huddersfield

UK

January 2018

بسم الله الرحمن الرحيم

صدق الله العظيم

ABSTRACT

Centrifugal pumps play an important role in engineering applications since they are commonly used in industrial and residential systems, covering wide range of flow rates. Improving the performance of turbomachines such as the centrifugal pumps can be difficult to achieve, since the flow is turbulent with unsteady behaviour and cavitation. Cavitation is a complex phenomenon that is commonly considered as one of the main causes of deterioration in pump performance. Diagnosing cavitation and detecting its level of severity are essential for maintaining the pump's reliability. Continuous condition monitoring of the pump is important to increase its operational life, decrease maintenance costs and hence, enhance the reliability of the pump. Early detection of cavitation can also improve the pump's life expectancy by adopting various preventative actions. In this research, the first technique used for detecting cavitation is Computational Fluid Dynamics because it can provide suitable visualisation and reasonably accurate information, regarding the behaviour of fluid flow in the pump. In this work, both qualitative and quantitative analyses were carried out through a wide range of operating conditions and different geometrical configurations of a centrifugal pump under single-phase and cavitation conditions. Both, global and local flow field characteristics were investigated for better understanding. For qualitatively analysis, contours of static pressure and velocity magnitude under single-phase conditions and vapour volume fractions contour under cavitation conditions were adopted. On the other hand, the head and pressure variation in both time and frequency domains were analysed for qualitative analysis. The results showed that, as the pump rotational speed, number of impeller blades, and the outlet impeller diameter increase the head of the pump increases as well as the occurrence of cavitation. Based on the extensive numerical investigations for variety of operational and geometrical parameters, novel semi-empirical correlations under single-phase and cavitation conditions for the pump head and power coefficients were developed. Developments of aforementioned relations were carried out using multiple regression analysis technique. The second and third research areas consist of an extensive experimental analysis on the effects of operating conditions on the pump performance to predict cavitation using vibration and acoustic signature analyses. Detailed experimental investigations were carried out for the detection and diagnosis of cavitation, with the aid of sophisticated equipment and sensors. The condition monitoring was experimentally carried out in both, time and frequency domains analyses. Time domain method was applied to analyse the vibration and acoustic signals in time waveform analysis (TWFA). These

signatures were analysed using different statistical parameters such as peak, root mean square (RMS), peak-to-peak and variance. In addition, transforming and analysing these signals in frequency domain was made by using Fast Fourier Transform technique. Analyses of these signals in frequency domain were also carried out using different statistical parameters such as mean and RMS features under wide various frequency ranges. The results revealed that using cavitation detection index (CDI) was a powerful technique, which can be used in both time and frequency domains for detecting cavitation and comparing the sensitivity of the vibration and acoustic techniques in estimating earlier stage of cavitation. Moreover, vibration technique was more sensitive to detect different levels of cavitation, especially inception of cavitation as compared to acoustic technique. This research has also found that the range of frequency between 0Hz to 15kHz was more sensitive to detect cavitation in the pump at the early stages. However, further investigation indicated that a frequency range of 1Hz to 2kHz was also effective on predicting the cavitation. Based on these findings, it can be suggested to use low range of frequency sensors (accelerometer and microphone) to capture the cavitation phenomenon instead of higher range of frequency, which are more expensive.

In addition, it was found that all three techniques adopted in this investigation such as; CFD, vibration and acoustic techniques are well capable to analyse cavitation behaviours under different operating conditions. Moreover, it was observed that the numerical results and vibration technique can detect the inception of cavitation within a pump earlier than the acoustic technique. The results also revealed that, the combined use of these techniques (numerical and experimental) could increase the reliability. The combined method can be a considered to be a robust method, which can provide detailed information about the performance of the pump and detection/diagnosis of cavitation within a centrifugal pump. Hence, this will assist in prolonging the life of the pump and protect the system from emergency shutdown.

DECLARATION

- The author of this thesis (including any appendices and/or schedules to this thesis) owns any copyright in it (the ―Copyright) and he has given The University of Huddersfield the right to use such Copyright for any administrative, promotional, educational and/or teaching purposes.

- Copies of this thesis, either in full or in extracts, may be made only in accordance with the regulations of the University Library. Details of these regulations may be obtained from the Librarian. This page must form part of any such copies made.

- The ownership of any patents, designs, trademarks and any and all other intellectual property rights except for the Copyright (the ―Intellectual Property Rights) and any reproductions of copyright works, for example graphs and tables (―Reproductions), which may be described in this thesis, may not be owned by the author and may be owned by third parties. Such Intellectual Property Rights and Reproductions cannot and must not be made available for use without the prior written permission of the owner(s) of the relevant Intellectual Property Rights and/or Reproductions.

ACKNOWLEDGEMENTS

In the beginning, I would like to pay my undivided gratitude to almighty Allah for providing me the opportunity to be on this planet and take a part in the advancement of the human race with my best capability. To the mentor of humanity and its guide from the darkness of ignorance to the light of knowledge, the Prophet Mohammed and his household (peace be upon them all). I am highly indebted to my parents for their constant encouragement and support in all stages of my life. My words fall short to thank them.

I would like to express my deep thanks and sincere indebtedness to Prof. Rakesh Mishra at the University of Huddersfield, for supervising this research and for his efforts to put the research work on the right path. I would like also to acknowledge the considerable amount of help and support provided by my co-supervisor Dr. Taimoor Asim to complete this thesis. Sincere gratitude should have got to the Republic of Iraq/Ministry of Higher Education and Scientific Research/Al-Mustansiriya University/Faculty of Engineering/Department of Mechanical Engineering who funded my scholarship; without whose support I could not achieve this. Warm thanks should also go to the Iraqi Cultural Attaché in the London/UK who took care of my paper work during my study and offered me help whenever needed. In addition, I would like to thank all my colleagues at the Energy, Emissions and Environment Research group at the University of Huddersfield. Last but not the least, I would like to acknowledge the researchers around the globe whose work was reproduced in this thesis without permission, in the form of figures (mostly in Chapters 1 and 2). I presume that they wouldn't have disagreed to reproduce their work if I would have contacted them, which I wouldn't able to do due to shortage of time and in some cases due to insufficient contact information.

At last but not least, I wish to thank my family; my wife and my children (Mustafa, Zahraa, Abdullah, and Abbas), my brothers, and sisters for their devoted care, quiet sacrifices, and indispensable role.

CONTENTS

No. word count for all chapters: 88680 words

LIST OF FIGURES

LIST OF TABLES

NOMENCLATURE

A	Cross-sectional area	m^2
BPF	Blade passing frequency	Hz
CFD	Computational Fluid Dynamics	
CDI	Cavitation Detection Index	
CMT	Condition Monitoring Techniques	
d_1	Suction pipe diameter	m
d_2	Discharge pipe diameter	m
D1	Inlet impeller diameter	m
D2	Outlet impeller diameter	m
FDA	Frequency Domain Analysis	
f	Darcy friction factor	
g	Gravitational acceleration	m/s^2
H	Head of the pump	m
Hf	Friction losses in pipes	m
Hi	Safety factor including all suction side losses (friction losses in valves, pipes, fittings and pump inlet)	m
Hs	Static suction head	m
H_t	Total head	m
H_{tin}	Total suction head	m
H_{tout}	Total discharge head	m
L	Length of pipe	m

N	Pump rotational speed	rpm
N1	Number of vapour bubbles per unit volume of fluid	
n	Total numbers of signals	
NPSH	Net Positive Suction Head	m
NPSHA	Net Positive Suction Head Available	m
NPSHR	Net Positive Suction Head Required	m
P	Power	W
P_1	Suction pressure	Pa
P_2	Discharge pressure	Pa
P_{atm}	Atmospheric pressure	Pa
p_l	Liquid pressure	Pa
P_v	Vapor pressure	Pa
Ps	Suction pressure	Pa
Q	Flow rate	l/min
R_B	Bubbles radius	mm
R_c	Mass transfer source terms connected to the growth and collapse of the vapour bubblesHz	
Rf	Rotational frequency	Hz
RMS	root mean square value	
$S_{\bar{x}}$	Mean uncertainty value	
TDA	Time Domain Analysis	
TWFA	Time Wave Form Analysis	
t_w	Wall shear stress	Pa

u^*	Friction velocity	
V	V Mean velocity of the fluid flowing in the pipe	m/s
V_1	Velocity at suction side of the pump	m/s
V_2	Velocity at discharge side of the pump	m/s
x_i	Total of elements	
$\bar{x}$	The set of elements	
x_k	Set of signals	
y+	Dimensionless wall distance	
Z	Number of impeller blades	
Z_1	Elevation in suction side of the pump	m
Z_2	Elevation in discharge side of the pump	m

SYMBOLS

ρ	Water density	(Kg/m^3)
μ	Dynamic Viscosity	(Pa-sec)
v	Kinematic viscosity of the liquid	(m^2/s)
ϒ	Specific Weight	(N/m^3)
ρ_v	Vapour density	(kg/m^3)
ρ_l	liquid density	(kg/m^3)
$\propto v$	Vapour volume fraction	
ρ_m	Mean density	(kg/m^3)

τ	Shear stress	Pa
σ_x	Standard deviation	
л	Pi	

SUBSCRIPTS

a	Available
atm	Atmospheric
B	Bubbles
f	Friction
i	Inlet
k	Sample of signal
l	Liquid
o	Outlet
r	Required
t	Total
v	Vapour
w	Wall

CHAPTER 1

INTRODUCTION

Centrifugal pumps are broadly used in manufacturing and for domestic purposes. The principle function of the centrifugal pump is to transfer fluid through the flow system and to increase the energy of the fluid. This chapter includes a brief history of pumps and introduces pumps by referring to their applications and types. For a better knowledge of the working principle of the centrifugal pump, the parts of the pump are explained along with the performance curve of the pump. Besides, this chapter presents the issues encountered (cavitation) during the operation of a centrifugal pump. In addition, it provides the influence of cavitation on the pump. Moreover, it introduces various monitoring techniques that can be applied for detecting and predicting cavitation with a particular emphasis on condition monitoring. Furthermore, it describes the motivation, aims of the research as well as the thesis structure.

1.1. Brief Introduction to Pumps History

The requirement to transfer liquid from one position to another, affects almost all walks of life. In the past, different numbers of tools have been used in order to move liquid. The Egyptians invented the shadoof device to transfer water in 2000 BC. The simple design of the shadoof included a long suspended rod with a bucket at one end and a weight at the other end [1] as shown in Figure 1-1 (a) [2].

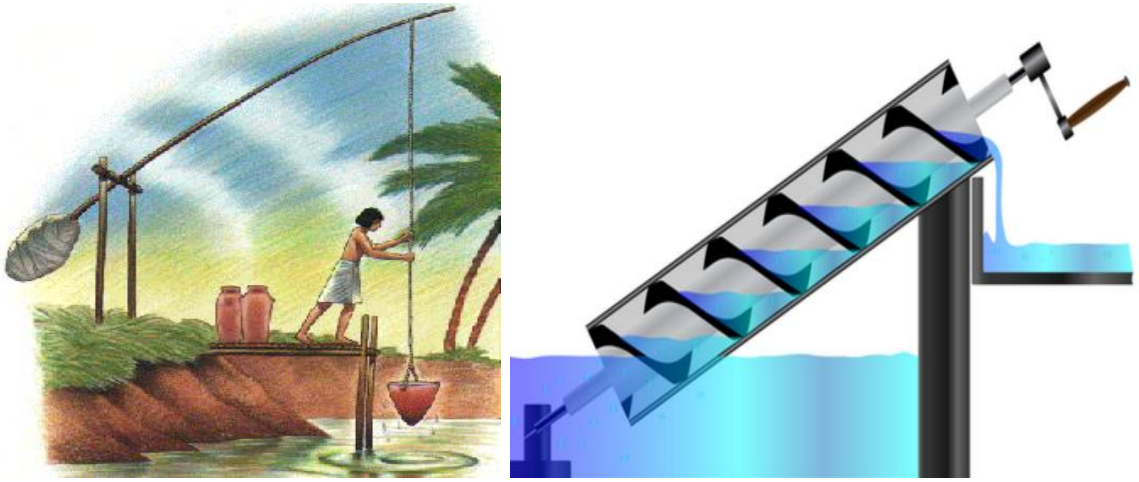

(a) (b)

Figure 1-1: (a) The Egyptian shadoof [3], and (b) Archimedean screw pump [4]

The Greek mathematician Archimedes invented the "screw pump" in 200BC, which is still used in the third world to irrigate agricultural fields since it can be operated without consuming electrical power [1] as depicted in Figure 1-1 (b). Later Agostino Ramelli, an Italian engineer, invented the first sliding vane water pump in the year 1588. Another invention of the pump was by a German engineer Pappenheim in the year 1636 when he designed a double deep-toothed gear pump. Otto van Guericke invented a new type of pump (piston vacuum pump) in the year 1650. He used leather washers in order to prevent leakage between the piston and cylinder. Sir Samuel Moreland invented the plunger pump in the year 1675, which was capable of raising high quantities of water. Denis Papin a French-born scientist developed the first centrifugal pump in the year 1687. It was designed to have straight vanes and it used for local drainage. In addition, Revillion invented the modern screw pump in the year 1830. Henry R. Worthington invented the first engine for direct acting steam pumping in 1845. Furthermore, the first all-metal pump was casted and assembled by Goulds in 1849. John Appold (British inventor) introduced the first curved blade centrifugal pump in 1851 [1,5,7]. The next section illustrates the applications and types of pumps.

1.2. The Applications of Pumps

Generally, most of the industrial processes require the transfer of fluids from one place to another. Therefore, the pump is an indispensable and essential component for industry as it is extensively used for the above purpose. Pumps are used in many applications such as agriculture, nuclear power plants, chemical plants, pharmaceutical and petroleum plants [8]. Figure 1-2 depicts the use of pumps for various industrial applications.

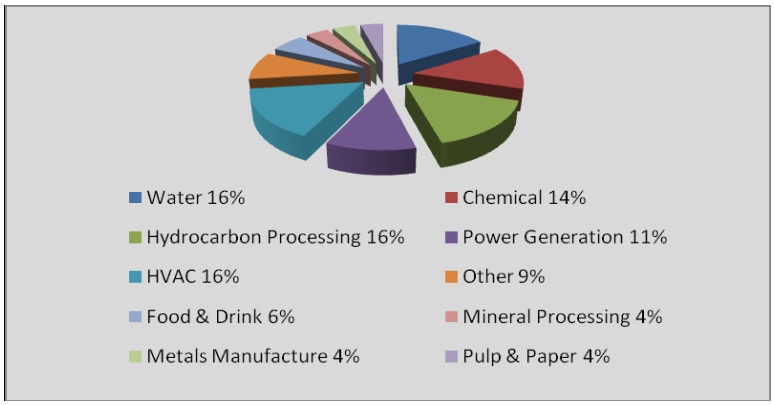

Figure 1-2: The applications of pumps in industry [9]

1.3. Types of Pumps

The size of pumps varies depending on the applications and their types. The classification of pumps depends on their operating principles. Figure 1-3 illustrates the categories of pumps. According to this Figure, most of pumps can be classified into two main categories, namely positive displacement and dynamic pumps. Displacement pumps can be further sub-categorised as rotary and reciprocating pumps, while dynamic pumps can be sub-categorised as axial pumps and centrifugal pumps [10].

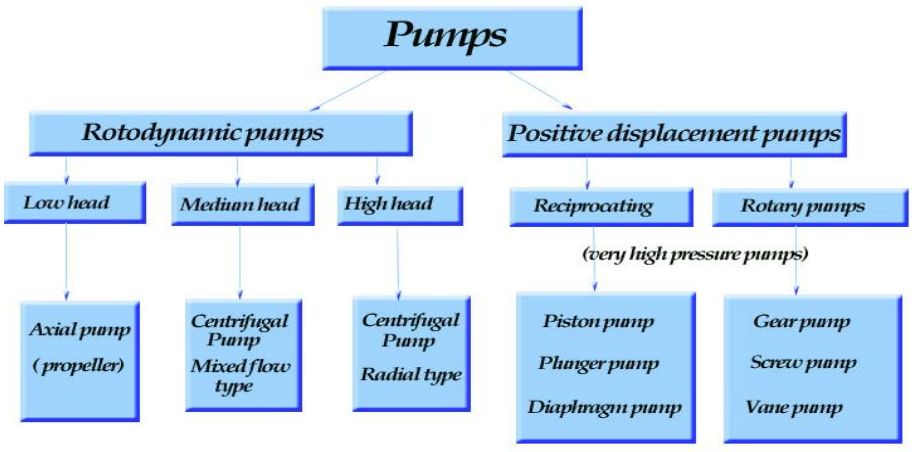

Figure 1-3: Types of pumps [11]

To make the research more effective, in this work, focus is paid to centrifugal pumps. The following sections explain some significant mechanical construction aspects and characteristics of the cavitation phenomenon in centrifugal pumps.

1.4. Centrifugal Pumps

Generally, the centrifugal pump is a mechanical device that utilizes a rotating impeller to transfer electrical energy into hydraulic energy. Figure 1-4 depicts the volute, impeller and other common parts in pumps are broadly used in industrial applications. Liquid enters through the inlet pipe and moves towards the low-pressure region at the impeller eye. The rotation of the impeller pushes the liquid between vanes outward into the volute or diffuser. This phenomenon creates a vacuum at the eye of the impeller that increasingly draws liquid into the pump and generates a low-pressure region at the impeller eye region. The volute/casing is a stationary part that converts the kinetic energy of the liquid into liquid pressure [12].

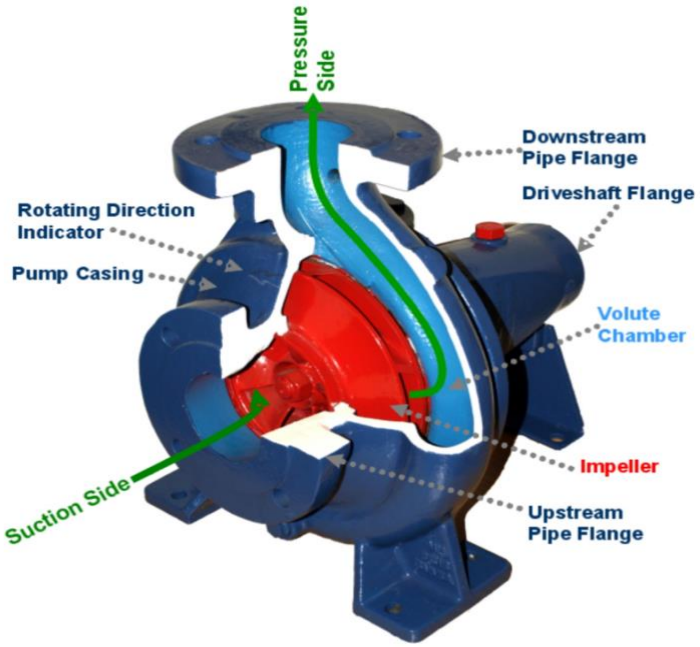

Figure 1-4: Centrifugal pump components [13]

Centrifugal pumps are widely used in industry and the reasons behind that are their high efficiency, a wide range of applications, ease of maintenance and operation. Figure 1-5 depicts the principal of operation and construction of centrifugal pumps [12].

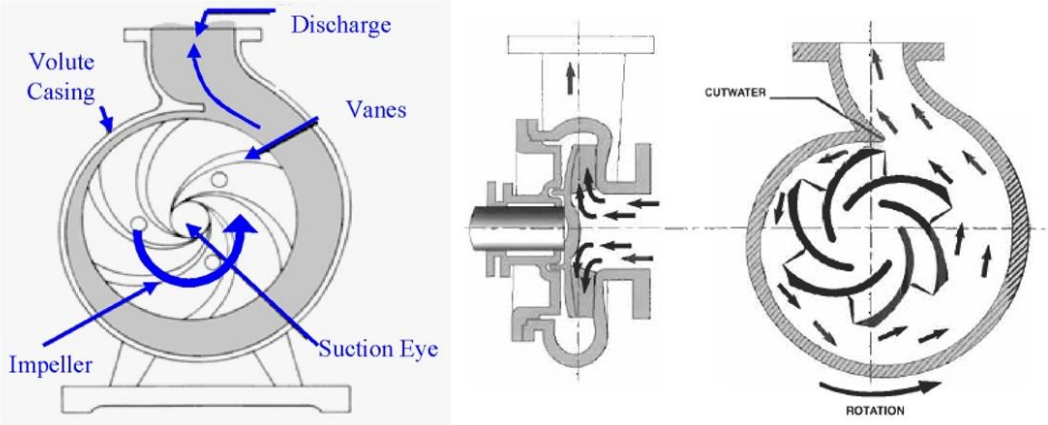

Figure 1-5: Construction and principal of working in centrifugal pumps [14]

1.4.1. Centrifugal Pump Components

Generally, there are numerous designs of centrifugal pumps available for every given application. This section will provide a general description of the mechanical components of centrifugal pumps [7].

1.4.2. Impeller

The impeller is the first major part of a centrifugal pump. The fluid enters into the impeller at the eye of the impeller, and then flows through the impeller channels formed by the blades between the hub and shroud, as shown in Figure 1-6. Figure 1-7 depicts the locations of suction side, pressure side, leading edge, trailing edge of blade, inlet, and outlet diameters of the impeller. Any fault in the impeller may lead to poor performance and reduces the pump's efficiency [9]. In general, there are three types of impellers i.e. open impellers, semi-open impellers and closed impellers [12].

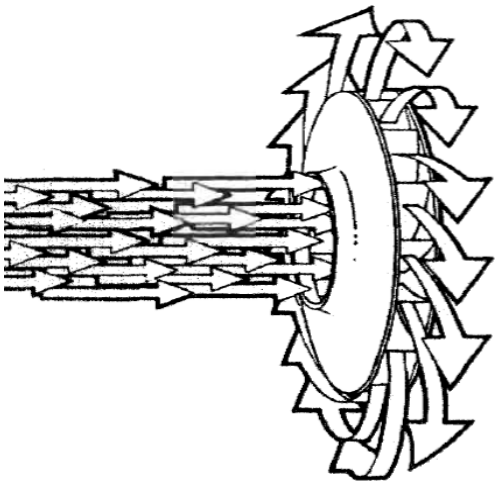

Figure 1-6: Flow directions in impeller [15]

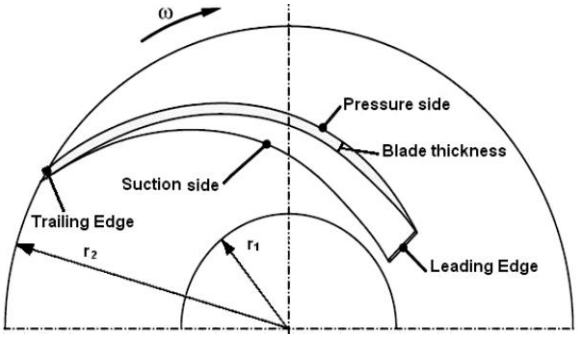

Figure 1-7: Pressure and suction sides, leading and trailing edges in the impeller blade [16]

1.4.3. Construction of Impellers

As mentioned in the previous section, there are three types of impellers, which were categorised based on having a cover on the top of the impeller known as a shroud. These three types of impellers are described below:

Open Type

Figure 1-8 (a) depicts an open impeller, which merely comprises blades attached to the shaft, having no cover or shroud. This type of impeller has shorter and weaker blade structure as compared to other types. Usually, the primary purpose of open type of impeller is for clog resisting applications [12]. Commonly, open type impellers have low efficiency as compared to other types of impellers [12].

Semi-Open Type

From Figure 1-8 (b) it is evident that these impellers are composed of a circular plate (shroud) only attached to one side of blades. The advantage of semi-open impeller is that the circular plate over one side of blades stiffens the blades and provides structural strength to the system as compared to open impeller. The semi-open impeller is commonly used for liquids containing small amounts of suspended solids in medium diameter pumps [12].

Closed Type

This kind of impeller has a circular plate attached to both sides of blades to maximise the strength as shown in Figure 1-8 (c). They are frequently used in different types of pumps, and can be applied with fluids that do not contain suspended solids. This type of impellers are broadly used for liquids free of impurities in centrifugal pumps [12].

(a) Open type (b) Semi-open type (c) Close type

Figure 1-8: Types of impellers [17]

1.4.4. Volute

The component that contains the impeller is usually denoted as the volute, which is also referred to as casing as well. The volute is composed of a curved passage that increases in area where it approaches the discharge port. The volute of centrifugal pumps is a casing that receives the liquid being pumped through the impeller. A volute converts kinetic energy of the liquid into pressure by decreasing flow velocity [18]. Commonly, centrifugal pumps have four kinds of volutes that are widely utilised, such as single, double, diffuser and circular volutes, as shown in Figure 1-9 [12].

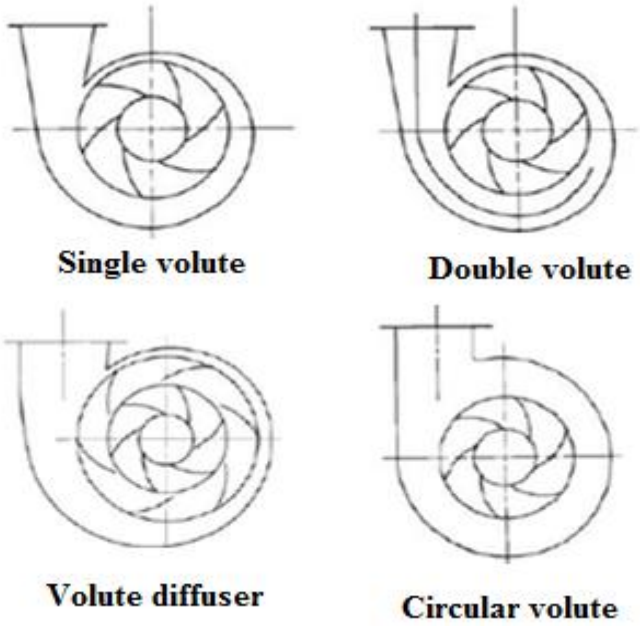

Figure 1-9: Types of volute for centrifugal pumps [12]

1.5. Performance Curves of Centrifugal Pumps

The performance of the pump is measured via different standard quantities such as head, flow rate and pump rotational speed [19]. Usually, the performance curve of the pump is presented by plotting head and power against the flow rate.

1.5.1. Flow Rate

The flow rate parameter is one of the most significant parameters in centrifugal pumps. Generally, the flow rate is defined as the volume of liquid that passes through a particular cross-section area per unit time. Several factors influence the flow rate such as pump size, liquid properties, rotational speed, pump geometry, pump suction, impeller size, and the pressure conditions [9]. The flow rate can be calculated via the below equation:

$$Q = V\,A \tag{1-1}$$

Where, A denotes a cross-sectional area (m^2), and V represents the mean velocity of the liquid flowing in the pipe (m/s).

1.5.2. Head

The head of the pump is a major factor in centrifugal pumps, and it can be measured in length scale, having an SI unit of metre (m) [18]. Figure 1-10 illustrates the relationship between static and dynamic head at suction and discharge sides of the pump. The total head of a pump can be calculated as below equation [13].

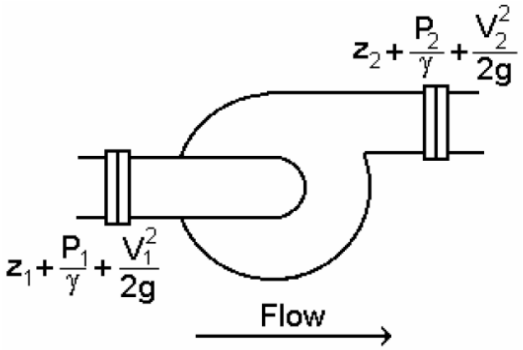

Figure 1-10: Inlet and outlet centrifugal pump parameters

$$H = \left(\frac{P_2}{\rho g} + Z_2 + \frac{V_2^2}{2g}\right) - \left(\frac{P_2}{\rho g} + Z_2 + \frac{V_2^2}{2g}\right) - Hf \tag{1-2}$$

1.6. Pump Characteristic Curves

For each pump, manufacturers provide the characteristic curve of the pump. There are four characteristic curves:

- H versus Q: Differential head of the pump versus flow rate.
- Efficiency versus Q: Efficiency versus flow rate of the pump.
- Power versus Q: Input power versus flow rate.
- NPSHR versus Q: Net Positive Suction Head Required versus flow rate.

Typically, the centrifugal pump's performance curves are developed by plotting efficiency, power and head against the flow rate of the pump as depicted in Figure 1-11. Therefore, the best efficiency point (BEP) will indicate the point on the performance curve of the pump that results in the maximum efficiency of the pump. Working beyond the BEP causes significant decrease in the performance and operational life of the pump [12]. The net positive suction head (NPSH) represents the difference between the liquid's absolute pressure in the system and the vapour pressure of the liquid at a given temperature. Therefore, the value of NPSH is a significant parameter in designing a centrifugal pump because when the liquid pressure drops below the vapour pressure, that leads to increase the potential for cavitation occurrence [12].

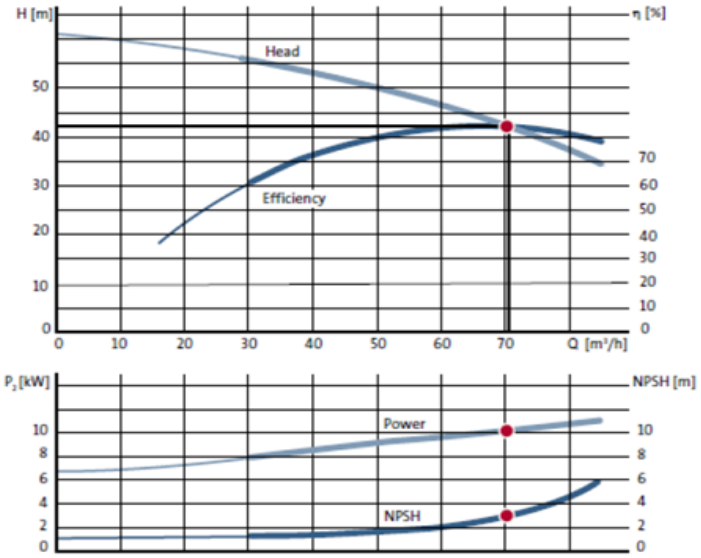

Figure 1-11: Centrifugal pump performance curves [12]

Usually, pump manufacturers supply NPSHR curve for the inlet pressure of the pump where severe cavitation may happen. However, this value differs with the physical properties of the liquid and surface roughness of pipes [20].

1.6.1. The Affinity Laws

Affinity laws are derived from the basis that flow rate, head and power. Fluid flow rate defined by the following [18]:

$$Q = \mathrm{UA} = \begin{cases} \mathrm{A}\ \alpha\ \mathrm{r}^2 \alpha\ \mathrm{D}^2 \\ \mathrm{U}\ \alpha\ \mathrm{N}.\mathrm{r}\ \alpha\ \mathrm{N}.\mathrm{D} \end{cases} \quad (1\text{-}3)$$

$$\mathrm{Q}\ \alpha\ \mathrm{N}.\mathrm{D} \quad (1\text{-}4)$$

Head is a function of two variables velocity and diameter as indicated in below equation [18]:

$$\mathrm{H}\ \alpha\ (\mathrm{N}.\mathrm{D})^2 \quad (1\text{-}5)$$

Power, P, defines as a function of flow and head is then denoted by referring to equations [18]:

$$\mathrm{P} = \mathrm{Q}.\mathrm{H} \quad (1\text{-}6)$$

$$\mathrm{P}\ \alpha\ (\mathrm{N}.\mathrm{D})^3 \quad (1\text{-}7)$$

All above equations represent the general affinity laws applicable for pumps. These laws can be defined as mathematical equations between different variables including capacity of the pump (Q), head (H), pump rotational speed (N), power (P) and impeller diameter (D). The capacity of pump (Q), according to the affinity laws is directly proportional to the pump rotational speed ratio as well as the ratio of the impeller diameters as given in below equations [18]:

$$\mathrm{Q}_2 = \mathrm{Q}_1 * \frac{\mathrm{N}_2}{\mathrm{N}_1} \quad (1\text{-}8)$$

$$\mathrm{Q}_2 = \mathrm{Q}_1 * \frac{\mathrm{D}_2}{\mathrm{D}_1} \quad (1\text{-}9)$$

Also, the pump head is proportional to the square of the pump rotational speed and the impeller diameter as shown in equations (1-10) and (1-11) [18].

$$\mathrm{H}_2 = \mathrm{H}_1 * \left[\frac{\mathrm{N}_2}{\mathrm{N}_1}\right]^2 \quad (1\text{-}10)$$

$$\mathrm{H}_2 = \mathrm{H}_1 * \left[\frac{\mathrm{D}_2}{\mathrm{D}_1}\right]^2 \quad (1\text{-}11)$$

The power is proportional to the cube of the pump rotational speed and the impeller diameter as shown in below equations [18].

$$\mathrm{P}_2 = \mathrm{P}_1 * \left[\frac{\mathrm{N}_2}{\mathrm{N}_1}\right]^3 \quad (1\text{-}12)$$

$$P_2 = P_1 * \left[\frac{D_2}{D_1}\right]^3 \quad (1\text{-}13)$$

1.7. Failure in Centrifugal Pumps

Centrifugal pumps can fail during their long operational services as a consequence of issues that emerge inside the liquid (e.g. cavitation) and mechanical faults (e.g. impeller and bearing faults). The following section provides a brief overview of the most common failure in centrifugal pumps.

1.7.1. Cavitation

The term cavitation is originated from the word 'cavus', which means hollow or cavity. The Webster dictionary defines “cavitation” as rapid formation and collapse of flowing fluid in low-pressure area [21]. It is known that cavitation is regarded as one of the most common issues that occurs at the inlet side of the pump [12]. The fast collapsing of vapour bubbles causes high local pressure that results in pitting and severely damages the impeller blades as well as generating vibration and noise. Consequently, the collapsing bubbles decrease the performance of the pump [22].

1.7.2. The Effects of Cavitation on Performance of the Pump

Cavitation is an unwanted phenomenon in a centrifugal pump as it causes reduction in efficiency, and increase in vibration, noise, and erosion. The measured NPSHA and NPSHR are very important parameters for comprehending the occurrence of cavitation within a pump [21]. When a pump operates under cavitation conditions for a long period of time, the following can occur:

- Early bearing failure
- Pitting marks on the internal volute casing wall and the impeller blades
- Early mechanical seal failure
- Failure or fatigue in the shaft or other part of the pump

1.7.3. Mechanisms of Damages Caused Through Cavitation

When cavity implosions are sufficiently strong, cavitation erosion occurs and may affect nearby solid material. Cavitation erosion can be recognised through the specific rough marks

on the surface of the pump components when it runs under cavitation conditions for a lengthy period of time [23].

Collapse of Bubbles

This mechanism is related to the phenomenon where the collapsing bubbles become unstable resulting in their collapse on a nearby solid surface. Observations reveal that the development of spherical asymmetry takes the shapes of a rapidly accelerating jet liquid, allowing the bubble to enter from the furthest side of the wall as shown in Figure 1-12 [24].

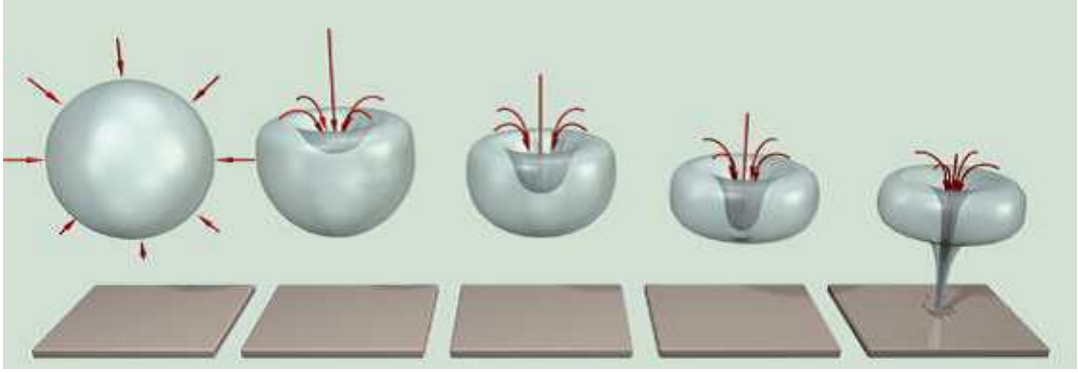

Figure 1-12: Collapse of bubbles due to cavitation [25]

This cavitation mechanism inside the centrifugal pump through the bursting bubbles causes several unfavourable impacts such as deterioration of the pump performance (reduce the head and efficiency), erosion and pitting the material of the pump [26]. Therefore, evaluating the level of cavitation and detecting this issue at an early stage is very important in the pump [27].

1.8. Cavitation in Centrifugal Pumps

Generally, inception of cavitation describes the starting stage of cavitation within a pump. However, at this stage it is necessary to differentiate between appearance and disappearance of cavitation conditions. In centrifugal pumps, the term cavity demonstrates the dynamic formation of internal bubbles in the fluid, which grow and then collapse as the fluid flows through a pump [21]. Figure 1-13 depicts two conditions inside the centrifugal pump without and with cavitation. The following section provides a brief overview of the cavitation symptoms within a centrifugal pump.

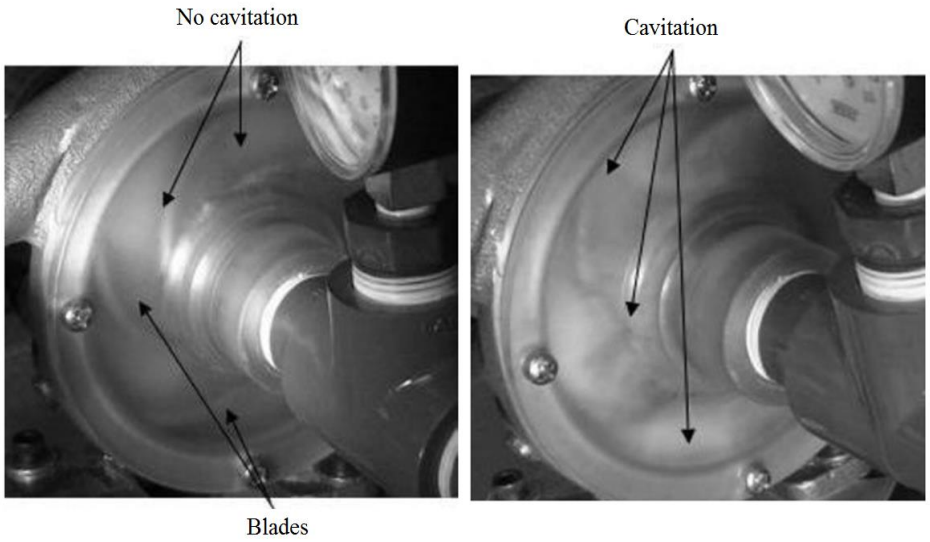

Figure 1-13: Centrifugal pump without and with cavitation [12]

1.8.1. Cavitation Symptoms

There are several symptoms that indicate the occurrence of cavitation within the pump. The occurrence of cavitation has significant impact on the performance of the pump and in severe cases; it might damage essential components of the pump. Therefore, it is essential to identify the symptoms of cavitation occurrence, which are described in the following section.

- **Decrease the Head of the Pump**

A sudden decrease in the head of the centrifugal pump is one of the important indicators of cavitation occurrence, when the flow rate increases the pressure at the eye of impeller decreases. After a certain flow rate, an increase in flow rate will reduce the pressure at the eye of impeller this will cause cavitation in the pump.

- **Pump Pitting and Corrosion**

When the centrifugal pump operates under cavitation conditions for a long time, the cavitation damages important pump parts such as blades, impeller and volute. There are several important factors that can affect pitting in the centrifugal pump, such as high flow rate, level of cavitation (inception, development, or full development) and the pump rotational speed.

- **Noise and Vibration**

Noise and vibration are two commonly used indicators that are used in identifying the presence of cavitation in the centrifugal pump. The noise and vibration in the system during cavitation

are the result of bubbles implosion close to the solid surface. The vapour bubbles collapse when they reach high-pressure points in the pump, which causes flow pulsation and pressure fluctuations. These pulsations affect the casing of the pump thus causing noise and vibration. The level of the noise and the vibration intensity depends on the size and number of bubbles. During the cavitation, the amplitude of the vibration and noise change dramatically. The vibration and noise signals can be used as the input to the data acquisition system for detailed analysis of cavitation process. The use of these parameters allows cavitation to be detected at early stage.

According to the above, it can be clearly seen that cavitation causes deterioration in performance of the pump and increases the level of vibration as well as noise resulting in damage to the pump components. So, an intensive pump monitoring is needed where cavitation is suspected. In Chapters 5, 6 and 7 in the current study, further detailed information is presented regarding to the flow field analysis and detection of cavitation using CFD technique, and how to collect and analyse vibration and noise signals and how to use these techniques to detect cavitation in a centrifugal pump.

1.8.2. Damage Caused by Cavitation

As mentioned in the previous section, cavitation in the pump is caused by the formation, subsequent collapse and implosion of vapour bubbles. The occurrence of collapse with adequate friction energy causes erosion inside the casing wall [21]. Figure 1-14 below shows the damage on impeller of the centrifugal pump caused by cavitation. The vapour bubbles collapse might generate extreme shock waves and intense local pressure that could cause significant damage to the surface of the metal. This damage removes the thin surface causing corrosion. Commonly, erosion is considered as one of the symptoms of the cavitation process within pumps [29]. The operation of the pump under cavitation conditions for a long period of time can lead to serious damage in the system, particularly to the impeller. Thus, it can cause pitting at the suction vane edges, discharge vane edges, the shroud of the impeller blades as well as the casing of the pump. In severe cases, cavitation can make holes in the impeller of the pump and damage the vanes to a level that may lead the impeller to become entirely ineffective [30].

Figure 1-14: Cavitation damage in centrifugal pump impellers [31, 32]

The following section provides a brief overview of the techniques for prediction of cavitation that were used in the current study for detecting and diagnosing cavitation within a pump at early stage as a basic platform for condition monitoring.

1.9. Techniques for Detecting Cavitation

A brief introduction to techniques that were used in this study for detecting cavitation will be given in the next section.

1.9.1. Numerical Simulation using CFD Technique

Currently, CFD analysis technique is being widely used in the turbomachines industry for analysis and design of artefacts such as turbines, compressors and various kinds of pumps. In addition, using CFD code to analyse the flow field within a centrifugal pump enables designers to have quantitative and qualitative information about likely operational behaviour of such systems. The results from numerical simulation can provide reasonably accurate information regarding to the behaviour of fluid flow in the pump. It can also be used to determine pump performance as well as to predict cavitation at the early stage. The application of CFD is relatively cheap as compared to the experiments and it offers more information regarding the flow field within a pump. However, both numerical and experimental techniques provide detailed and effective results. The CFD technique will be discussed in more detail in Chapter five.

Brief Description of the Numerical Simulation Methodology for the Centrifugal Pump using CFD

The flow field within the centrifugal pump, particularly in the blade passages and volute, has an important effect on the performance of the pump. However, carrying out experiments to measure this flow field can prove to be difficult. Therefore, CFD code can be used for this purpose because it is a useful and powerful tool to study and analyse the behaviour of the flow inside the pump. In the present study, numerical simulation methodology was used for the centrifugal pump under single-phase and cavitation conditions. This brief methodology includes four main stages as illustrated in Figure 1-15. The first stage consists of preparation of the geometry of pump parts. The second stage includes creating the meshing for each part. The third important stage in this methodology is solver setup. This stage includes providing the types of domain properties, selecting the turbulence model, boundary conditions, mesh interfaces between different parts, convergence controls and numerical schemes. The final stage is to select effective parameters to monitor in the pump and then run the simulation to calculate the results, as well as collect the stored data during the post processor stage for analyse. The results can be validated with the experimental data.

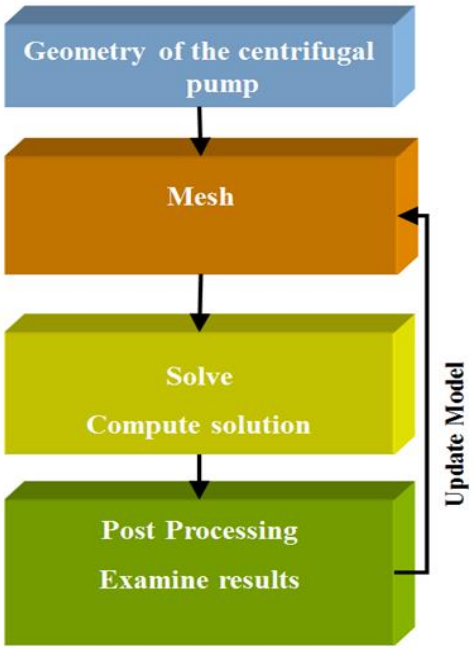

Figure 1-15: Numerical methodology for the centrifugal pump using CFD code

1.9.2. Experimental Techniques for Detection of Cavitation

The detection and diagnostics of cavitation within centrifugal pumps using vibration and acoustic techniques were experimentally investigated in this study using condition monitoring system, and a brief explanation of these techniques is presented in this section.

Brief Description of Condition Monitoring System using Vibration Technique

Recently, different types of condition monitoring approaches were used and developed, for example airborne acoustics, vibration, lubricant, acoustic emission, motor current, voltage and temperature analyses. The vibration technique is widely used in different types of machines for fault detection. The reasons includes how ease of use and also take the measurements, as well as its sensitivity to diagnosing machine faults using wide range of frequencies and temperatures. Hence using vibration technique for condition monitoring systems for different applications was shown to be effective [33]. The condition monitoring system consists of six main parts as shown in Figure 1-16. These parts are the machine under investigation such as turbines, compressors, and pumps. The vibration sensor (accelerometer), data acquisition system for collecting data, the PC for saving data, the interface software programme between the data acquisition and the user in order to display the vibration signal. The final part of the analysis encompasses the use of a software (MATLAB code) in analysing the data [34]. Further detailed information regarding this technique will be provided in Chapter six.

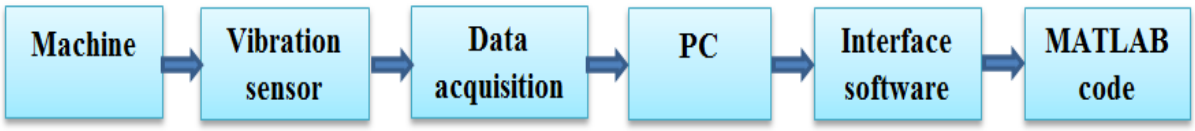

Figure 1-16: Experimental methodology for the vibration signal processing

1.9.3. Experimental Acoustic Analysis Technique

Brief Description of Condition Monitoring System using Acoustic Technique

Acoustic technique has become widely used in different fields such as psychology, engineering, physics, music, speech, and neuroscience. In general, the sound in flow systems is produced due to several reasons, for example, vibration changes in airflow, supersonic flow and friction between parts [35]. The acoustic technique has several advantages such as, it can be used to collect data from the machine under different temperatures and different operation conditions and it can be used to detect different types of faults in the machines directly during

operation conditions. Using acoustic technique is relatively easy and the cost of acoustic sensor is the same as that of the vibration sensor. The vibration and acoustic signals have a very similar condition monitoring system procedure. Figure 1-17 illustrates the various steps in using acoustic technique for condition monitoring purposes. Chapter seven in this thesis will discuss this technique in a more detailed manner and the following section provides a brief overview of the condition monitoring system.

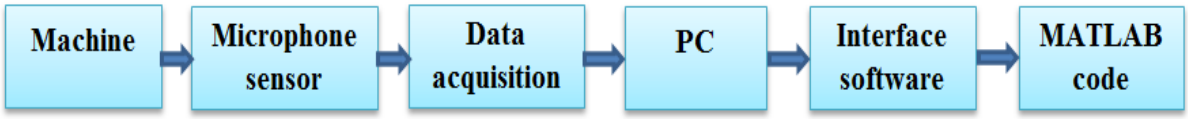

Figure 1-17: Experimental methodology for the acoustic signal processing

1.10. Condition Monitoring

Condition monitoring has made more acceptable and helpful for many process industries. These monitoring systems can give useful information regarding different problems or faults that can occur in the damaged components of the pump. In addition, it helps to improve the performance of the pump or it can be recognised when the pump needs to be refurbished or replaced.

1.10.1. Condition Monitoring System Process

In recent years, most industries have broadened their interest on condition monitoring systems. In order to decease the maintenance cost and increase the reliability of machines. According to the standard ISO 17359:2011, the condition monitoring process can be divided into five important sections as shown in Figure 1-18 [36].

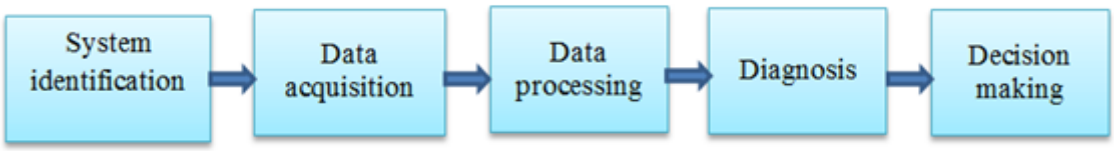

Figure 1-18: Condition monitoring system process [36]

- **System Identification**

The condition monitoring system process includes analysis of the function of the system, such as; identifying the types of a failure in the system and selecting the components that have to be

considered for condition monitoring. Furthermore, it consists of all information regarding to the research techniques and the existing historical data for the study.

- **Data Acquisition System**

This includes collecting and saving useful data that was collected using suitable sensors. It is a very important section in condition monitoring system because it consists of several steps such as measuring and recording data, type of sensor, number and position of the sensor and type of signals that were collected.

- **Data Processing**

This is the third significant section in the condition monitoring process; the first stage in this section is to remove any unwanted noises in the collected data from the environment. This can be achieved by using filter function to filter out most of the unwanted noise. This data can then be processed using the suitable technique to extract suitable features, which can be used to define the performance of the system. For instance, Fast Fourier Transform technique was widely used to convert data from time domain to the frequency domain.

- **Diagnosis**

The purpose of diagnosis is to determine the location, severity of the damage and fault in the system. Different faults in the machine can be diagnosed by collecting data when the machine is working under different operating conditions. The general trend is to collect data when the machine is working under healthy and faulty conditions. This data (healthy and faulty) will be analysed to identify the variance. The level of the variance indicates the current condition of the system, which will help to make decision for the next step.

- **Decision Making**

The diagnosis is to provide useful information regarding what happens in the system. The condition of the system and the required level of maintenance are defined based on the analysis of the features used for diagnostic purposes [36].

1.10.2. Advantages of Condition Monitoring

Current improvements in the field of sensors, computer hardware, and software, have resulted in an increase of interest in condition monitoring. Various studies and analyses were conducted

on the cost and benefits of condition monitoring process. The following section will present some of these findings on the advantages of condition monitoring [37]:

- Increase the revenue approximately by 30%
- Drop in maintenance cost by 50 - 80%
- Decrease spare parts inventory by 30%
- A 20 to 60% performance improvement
- Other advantages that can be obtained by plants through the use of condition monitoring systems include the following points:

- A decline in forced and unexpected shutdowns
- An enhancement in equipment availability and reliability
- Extended machine operating life
- Enhanced safety margins
- An overall increase in the output quality and performance of the machine

According to the Figure 1-19, it can be observed clearly that the total maintenance cost for pumps is 70% whereas other machines have this cost to be nearly below 20%. Therefore, to save on maintenance cost and enhance productivity, it is very important to improve the schedule of pumps' maintenance [9].

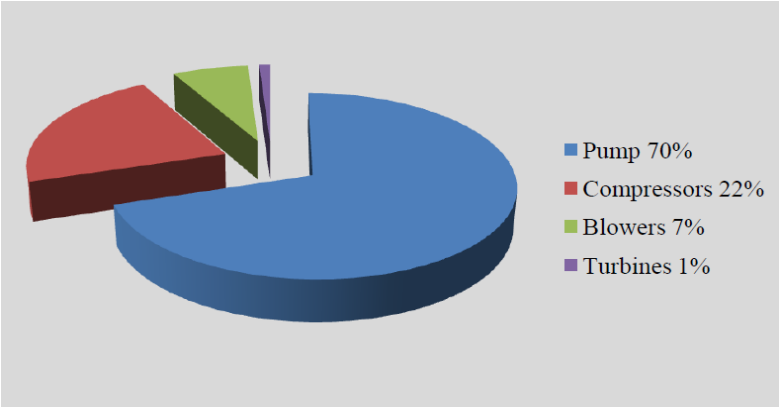

Figure 1-19: Cost of maintenance for different rotating machines [9]

1.11. Research Motivation

Centrifugal pumps are widely used in numerous applications such as agriculture, wastewater treatment plants, oil and gas industry, food industry, and power plants. An average useful life of the industrial centrifugal pump is stated to be about thirty years. However, the actual satisfactory life span of pumps relies on the characteristics of the liquid, the working

environment and the regularity and quality of maintenance. Investigation of the cavitation in the centrifugal pump is necessary to figure out a plan of preventative maintenance which in-turn, can increase the life of operation of pumps [38]. The detection of cavitation level in a centrifugal pump and analysing this phenomenon is an essential part to improve maintenance and enhance the reliability of the pump. Early detection of cavitation can enhance the pump's life expectancy by adopting various preventative actions. Due to the occurrence of cavitation, in extreme cases, the life of the pump can decrease from about 10-15 years to 2 years [39]. For these reasons, the cavitation in a centrifugal pump was taken into consideration in this study. Therefore, it needs continuous condition monitoring in order to increase life of the pump and decrease the cost of maintenance. Any faults or damage in pumps will cause many problems within the system such as; leakage, high level of noise and vibration, damage to the pump parts which will lead to a breakdown of the whole system, resulting in a significant amount of loss in time and money. This research study develops an effective diagnosis method of cavitation in the centrifugal pump using different techniques to increase the reliability of cavitation detection. This will be carried out with the help of various tools such as numerical analysis using CFD technique. Currently, the numerical simulation technique was used to design and analyse different types of machines such as water turbines and pumps as this technique is capable of providing the internal flow field within a machine. It also offers useful information regarding the internal flow dynamics and hence this information can be used for design conditions. In this study, CFD technique is proposed to be used to simulate and mimic the flow within a centrifugal pump at various operational conditions under the transient condition for single-phase and cavitation conditions. In order to comprehend the flow structure within a pump for both single-phase and cavitation conditions, an extensive study will be carried out on the effects of various geometric parameters on the performance of a centrifugal pump. It is also proposed to use experimental techniques such as, vibration and acoustic analyses. The aim of this study is to find a reliable system to identify accurate and effective cavitation detection and diagnosis of the centrifugal pump with most appropriate technique/s. The technique should be able to predict the inception of cavitation at an earlier stage, which will help in prolonging the life of the pump and protect the system from emergency shutdown. This research involves evaluation of these techniques and this study will be aimed at finding the most effective method for monitoring cavitation in the centrifugal pump.

1.12. Research Aims

The specific research aims formulated for this research study are described in this section whereas the objectives of this study will be discussed after carrying out an extensive literature review in the next chapter. Based on the motivation of this study, the research aims were broken down into the following:

1. CFD based investigation of flow and geometrical parameters on single-phase and cavitation behaviour in the centrifugal pump.
2. Experimental investigations on condition monitoring of the centrifugal pump using vibration analysis technique for detecting and diagnosing cavitation phenomenon in a centrifugal pump using time domain analysis (TDA) and frequency domain analysis (FDA).
3. Experimental investigations on condition monitoring of the centrifugal pump using acoustic analysis technique for detecting and diagnosing cavitation in a centrifugal pump using time domain analysis (TDA) and frequency domain analysis (FDA).

1.13. Thesis Structure

This thesis consists of eight chapters, the contents of which are briefly described as follow:

Chapter one: The main aim of Chapter one is to present an introductory review of the centrifugal pump and its significance in our daily lives. It provides an overview of different applications where centrifugal pumps are used along with the common operational issues. Therefore, the current chapter describes the centrifugal pump parts and explains the cavitation phenomenon. Moreover, it provides an account of different monitoring techniques that can be applied for detecting cavitation with a particular focus on condition monitoring.

Chapter two: This chapter provides an elaborate review of the literature on centrifugal pumps. It contains already published researches that concern the effect of operational conditions, different geometrical parameters and cavitation detection based on analysis with CFD and experiments using condition monitoring investigations for centrifugal pumps. To bridge the knowledge gaps in the literature regarding this field of study.

Chapter three: This chapter concentrates on CFD technique that was used to mimic the flow field within the centrifugal pump computationally. Also, this chapter presents the usage of CFD, along with a methodology for the prediction of performance and detection of cavitation in the centrifugal pump.

Chapter four: This chapter describes the construction and design of the centrifugal pump's experimental setup and detailed configurations of the system such as, the piping system and description of all the applied sensors, data acquisition systems and equipment. As well as the procedure for measurement system in order to monitor and detect cavitation in the pump, that was used in the experimental setup.

Chapter five: This chapter consists of a detailed analysis of all the results obtained using CFD code regarding the prediction of pump performance and detection of cavitation. Both quantitative and qualitative analyses were carried out to comprehend the flow structure within a pump under both single-phase and cavitation conditions. The investigation under different impeller geometrical parameters related to pressure fluctuations in time and frequency domains in the pump were analysed. Moreover, semi-empirical correlations for the head and power coefficients of the pump based on single-phase and cavitation were developed.

Chapter six: This chapter includes all the measurements and analyses of the experimental vibration signals obtained from the centrifugal pump. It provides the analysis of a number of statistical parameters to detect the cavitation in the pump in the time domain analysis. The vibration signal is then converted into to the frequency domain using FFT technique in order to obtain more information regarding the occurrence of cavitation within a pump.

Chapter seven: This chapter describes the acoustic technique that was adopted for detecting and diagnosing cavitation in the centrifugal pump. This chapter also provides the measurement and analysis of the experimental acoustic signals acquired from the pump using similar technique adopted in Chapter six. Also, it includes comparison between vibration and acoustic techniques in order to find the more effective technique for detecting cavitation under different operating conditions. Furthermore, it provides the evaluation of the methods utilised in this thesis in order to detect cavitation.

Chapter eight: This chapter includes the conclusion of this thesis and it summarises the contribution of this research. Finally, it provides the recommendations for future work.

A detailed literature review is presented in the next chapter, which focuses on the aforementioned research aims in order to find knowledge gaps in the existing literature.

CHAPTER 2

LITERATURE REVIEW

After obtaining information regarding to the centrifugal pump and the effects of cavitation occurrence on its performance in the previous chapter, a detailed review of the literature in centrifugal pumps is presented in this chapter. The central areas presented in the current chapter are associated with the pump and it contains detailed review of the published studies concerning the three main aims of investigation, as mentioned in Chapter one, with a view to identifying the knowledge gaps. Finally, the scope of research was determined and research objectives were formulated based on the knowledge gaps identified in the literature.

2.1. Introduction

Many researcher have attempted to comprehend the hydrodynamics of centrifugal pumps. Most of these studies investigated the effect of different operational conditions and geometrical parameters on the performance of centrifugal pumps via at least different well-known analyses techniques such as CFD, vibration and acoustic. According to the current study aims, which focuses on the employment of all above-mentioned techniques, and based on the acquired results a comparison can be made between the reliability of the three techniques for detecting and diagnosing of cavitation. As one of aims of the present investigation is establishing the effect of geometric and operation parameters on the pump performance and cavitation behaviour, the first part of review is focussed around this aspect. The following section will illustrate some of these findings.

2.2. CFD Based Investigation of Flow and Geometrical Parameters on Single-Phase and Cavitation Behaviour in Centrifugal Pumps

In order to understand the characteristics of the centrifugal pump and when the cavitation phenomenon take place, operating the pump under single-phase and cavitation conditions give a agood picture regarding to the characteristics of the this phenomenon. Therefore, the next section will review and discuss the research works that were investigated the effects of the operational conditions and geometrical parameters on the flow field behaviour and thereby on the pump performance in both cases, single-phase and cavitation.

2.2.1. Investigation of Flow and Geometrical Parameters on the Centrifugal Pump under Single-Phase Operational Conditions

The flow field within a centrifugal pump was investigated by many researchers using CFD, for example, the work done by Kim et al. [40], where authors studied the effect of outlet angle of blades on performance of the pump. The investigation was carried out under using 60m head and 600rpm rotating speed as the operating condition. The results indicated that the head increases by 2.5m as the outlet angle of a blade increases whereas, the efficiency decreases approximately by 0.3% as shown in Figure 2-1. The focal point of this study was the effect of the outlet angle of blades. No information was obtained in their study regarding to the effect of different geometrical parameters.

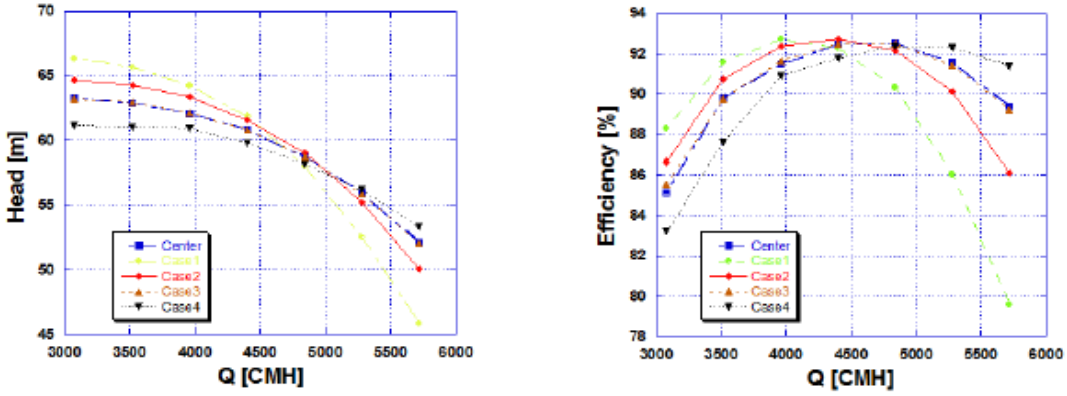

Figure 2-1: Head and efficiency curves of the pump [40]

Sidhesware and Hebbal [41] investigated a hydraulic design of a metallic centrifugal pump. The authors carried out the flow simulation of a pump under different flow rates. They found that the pump's head decreases as the flow rate increases. In addition, the pressure distributions over the suction and pressure side of blades were found to be non-uniform. There was no information regarding prediction of cavitation in a pump. Moreover, their study focussed on a limited range of flow rates.

Rajendran and Purushothaman [42] conducted a numerical investigation to analyse the flow structure in the impeller of a pump with water at 25^{o}C as the working fluid. The pump has six blades, inlet and outlet impeller diameters of 150mm, 280mm and outlet blade angle of 20^{o}. The pump was operated at a rotational speed of 925rpm having a 10m head and 0.0125m^{3}/s flow rate. Findings show that the pressure at the pressure side of blade was higher than suction side and it increases from the leading edge to trailing edge. The minimum pressure inside the impeller was located at the leading edge of blades. However, their study does not reveal any information regarding occurrence of cavitation and focuses on the pressure field under the same geometrical parameters.

Patel and Doshi [43] investigated the effect of outlet angle of impeller blades on the pump under different specific speeds of 28.91, 38.47 and 53.48, respectively. Their study showed that the outlet blade angle plays a significant role on the pump performance. The head and efficiency increased with the outlet blade angle increased as shown in Figure 2-2. However, no analysis of the pressure field within the pump was presented.

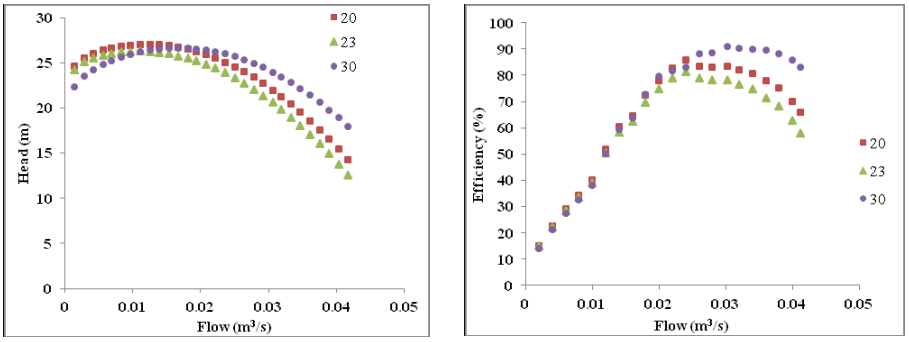

Figure 2-2: Head and efficiency under different outlet blade angles [43]

Shah et al. [44] analysed the flow field within a pump, the numerical simulation was carried out under steady state for six different flow rates. In addition, they used two turbulence models: shear stress transport (SST) k-ω and (RNG) models. Findings show that k-ω SST turbulence model provides better results as compared to RNG model. The numerical result proved that the head and the efficiency were higher than experimental results by 5% to 7%. However, this investigation was limited to single-phase and under steady state conditions, there was no any expression for the head or power coefficients.

Kagami et al. [45] investigated an automotive centrifugal pump using CFD. They used a multiple rotating frame (MRF) approach. The numerical results were in a good agreement with the experimental results under different rotational speeds. The pressure distribution was similar for all the impeller channels. Also, the results showed that a slight decrease in pressure in the circumferential direction of the volute. This work was carried out under steady state conditions and like other previous aforementioned studies, the effects of other geometrical parameters were not revealed in their work.

Houlin et al. [46] studied the effect of different CFD algorithms to simulate the inner flow field in the pump. These algorithms were SIMPLE (Semi-Implicit Method for Pressure-Linked Equations) and SIMPLED (Semi-Implicit Method for Pressure-Linked Equations Development). The results of their study showed that the SIMPLED was slightly higher accuracy than the SIMPLE by 2% and it was closer to the experimental results at the design operating condition. However, there was no information regarding the flow field analysis inside the pump for example, pressure and velocity distributions.

Yang et al. [47] investigated the effect of pump volute shape on the performance characteristics by using CFD. They used a single-stage centrifugal pump and design parameters used were Q=210m^3/h, H=100m, N=3000rpm, inlet and outlet impeller diameters of 100mm and 280mm.

The number of blades used was seven. Four different volute cross-section shapes namely, round, horseshoe shaped, trapezoid and rectangular were analysed to evaluate the performance. They found that the round cross-section provided the highest head, whereas the trapezoid and rectangular volute had nearly the same efficiency as shown in Figure 2-3. Furthermore, the study was focused on the effect of different volute cross section areas. Moreover, the effect of head coefficient of the pump under different geometrical parameters was not investigated.

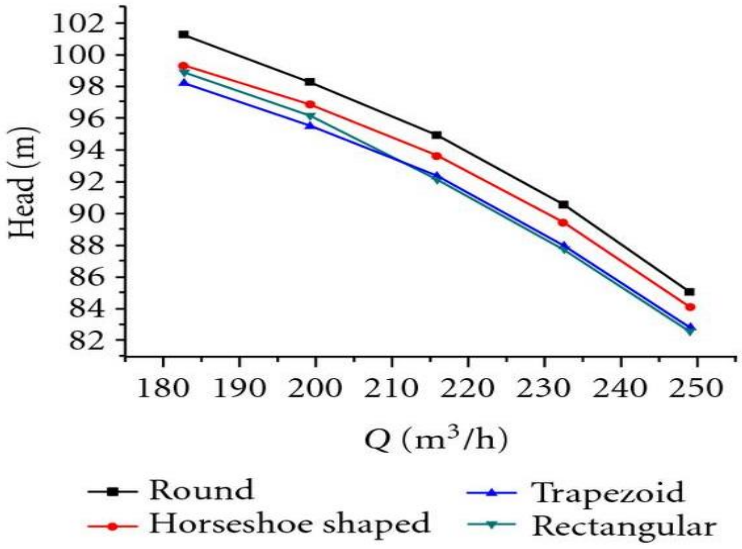

Figure 2-3: Head curves for different volute shapes [47]

Chakraborty et al. [48] correlated the performance of the pump with different number of blades. They studied a 2-D centrifugal pump under steady state for different blade numbers of 5, 6 and 7. The geometry of the pump includes an arc shaped blade with inlet and outlet blade angles of 25º and 33º, inlet and outlet impeller diameters of 80mm and 168mm. Volute inlet and outlet diameters of 80mm and 52mm. The results showed that the increase in efficiency was from 72.60 to 73.71%. Their work demonstrated that the optimum number of blades for efficiency was found to be seven. In addition, the total and static pressures were increased as the number of blades increased.

Gupta et al. [49] investigated the pressure and velocity distribution inside the pump. They noticed that the separation in flow takes place at the leading edge. In addition, the pressure at the suction side of impeller appeared to be the lowest pressure, and the highest pressure occurred at the outlet of the impeller as shown in Figure 2-4. However, their study includes a limited details and no information was provided regarding to the effect of different operational conditions on pressure fluctuations in the pump under single-phase and cavitation conditions.

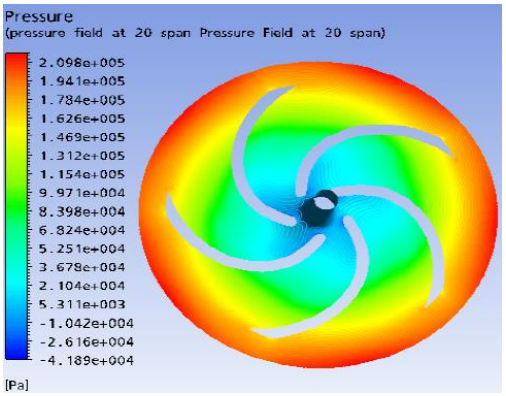

Figure 2-4: Static pressure distributions in the impeller [49]

Chakraborty and Pandey [50] studied the influence of the number of blades on a pump performance. They selected the different number of blades and the design parameters for the pump were inlet and outlet blade angles of 25º and, 33º. Impeller inlet and outlet diameters of 80mm and 168mm. Results indicated that the static pressure increases gradually with the increased number of blades and 10 blades were found to be optimum in terms of efficiency as shown in Figure 2-5. However, their study was limited to an investigation and focused only on the effect of number of blades.

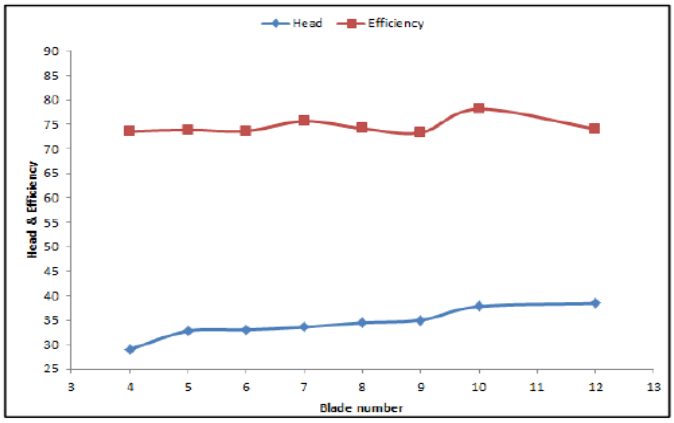

Figure 2-5:Performance of the pump under different number of blades [50]

Shi et al. [51] predicted the performance of the pump under different outlet widths of the impeller. They conducted their investigation for a single stage pump with H=13m, Q=20 m^3/h, N=2850rpm, blade inlet and outlet angles of 26º and 22º. Varied the blade outlet width in the range of 9, 10, 11, 12mm. They used multiple reference frame (MRF). The results indicated that the head and power increase with the increase of the outlet width of the impeller as shown in Figure 2-6. However, the effect of occurrence of cavitation under different operation

conditions such as wide range of flow rates and pump rotational speeds were not taken into consideration.

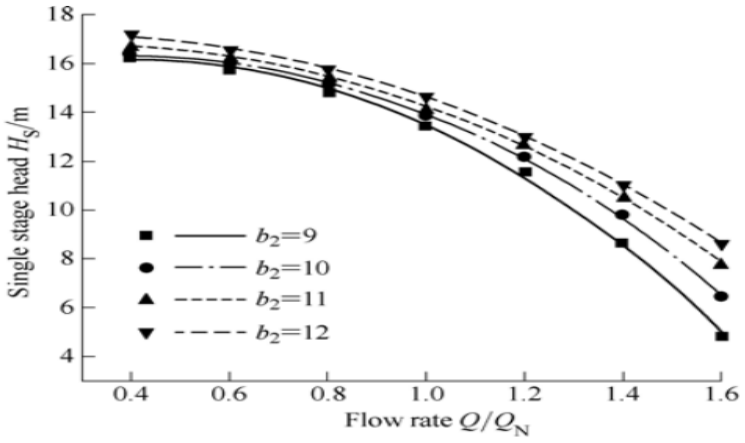

Figure 2-6: Pump head under different outlet widths [51]

Liu et al. [52] investigated the flow field inside the pump at shut-off conditions. They validated numerical results via particle image velocimetry (PIV) measurements. The analysis of flow field on the pump showed that the velocity in the volute diffusion area was low and there were two eddies in each of the impeller flow passages as shown in Figure 2-7 (a). The curve of the head fluctuations during shut-off condition displayed some periodic fluctuations as shown in Figure 2-7 (b). However, no information regarding pressure fluctuations and detection of cavitation in the pump.

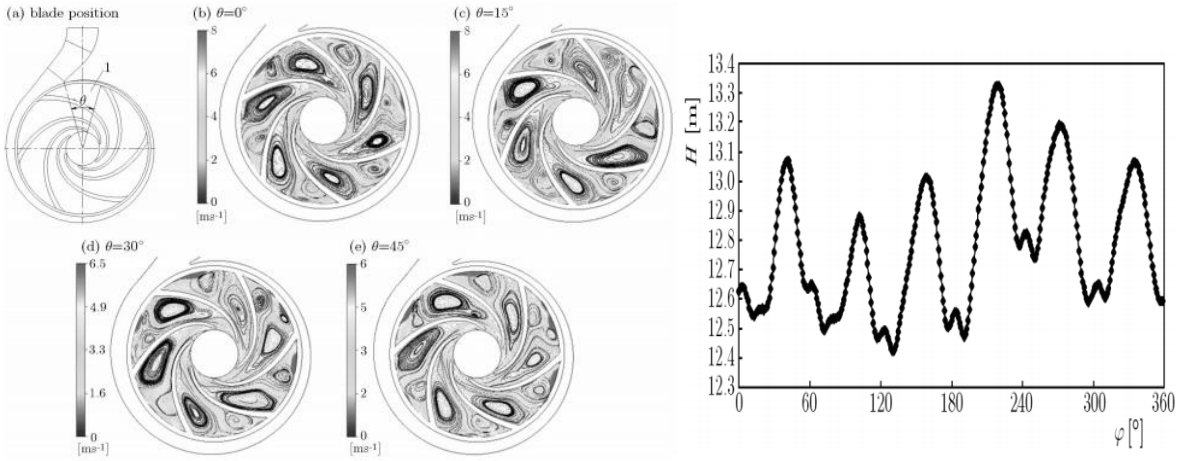

(a) (b)

Figure 2-7: (a) Velocity distributions and (b) Head fluctuation in the pump [52]

Yulin et al. [53] simulated the flow field within the centrifugal pump. The design parameters included Q=46.65(l/min), N=1000rpm, H=1.36m, inlet and outlet impeller diameters of 55.14mm, and 100mm, and the impeller was composed of seven blades. The results showed

that the comparison between the numerical results for the velocity at steady and unsteady within a pump under design flow rate using PIV measurement, indicating that the numerical unsteady flow was found to be closer to experimental data. Moreover, the authors focused only on the flow field for the velocity distribution in the pump and thus, no information was presented regarding to the pressure distribution.

Barrio et al. [54] investigated the flow field near the volute tongue area of the pump for various flow rates. The design parameters used were N=1620rpm, outlet impeller diameter of 0.210m and an impeller that is composed of seven blades. They found that the lowest flow rate displayed a larger counter-rotating vortex for the relative flow at the outlet of the impeller channels near the tongue area. However, this study has just focused on the effect of unsteady flow near the tongue region and no information was revealed regarding to the pressure fluctuations under different geometrical parameters.

Meakhail et al. [55] studied unsteady flow within the centrifugal pump for two different types of impellers. The design parameters used were Q=0.7813kg/s, inlet and outlet diameters for the first impeller were 140mm, and 70mm. For the second impeller's inlet and outlet diameters were chosen to be 270mm and 105mm. Both impellers were designed with seven blades, and N=2800rpm. Their results showed that the increase of pressure in the impeller was uniform for both pumps, which then gradually increased from suction to the outlet of the pump. The pressure distribution for the smaller impeller pump was uniform in the volute zone than the larger. For low flow rates, separation was seen to appear and for high flow rate, no separation was seen in the pump. However, no information regarding occurrence of cavitation was presented.

Zhang et al. [56] investigated unsteady flow within the pump by changing the operating process. The design parameters used were flow rate in the range of 34m^3/h to 110m^3/h, head of 35m, inlet and outlet impeller diameters of 140mm, and 230mm, an impeller with three blades, and N=4500rpm. They observed that at the beginning of different operating conditions, large-scale vortices existed in the flow passages at different times. In addition, the pressure gradually started to increase from inlet to outlet of the impeller as shown in Figure 2-8.

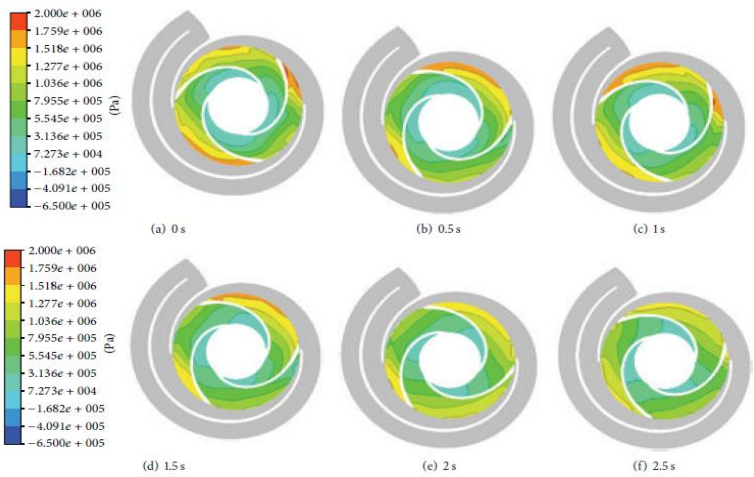

Figure 2-8: Static pressure variations at unsteady flow [56]

Cui et al. [57] studied transient flow at low specific speed for the pump under various operating conditions. The design parameters used were Q=1.5m^3/h, H=15m, inlet and outlet impeller diameters of 40mm, 105mm, and N=2900rpm. They found that the interaction between volute and impeller has a strong effect on the pressure distribution causing uneven pressure fluctuations in the volute circumference. Additionally, the highest-pressure fluctuations were noticed close to the volute tongue zone. However, no information regarding to the effects of the various operation conditions such as air injection and pump rotational speed on the occurrence of cavitation were made available.

C. Dai et al. [58] used a 3-D pump model with unsteady conditions and two turbulence models SST k-ω and RNG k-ε. The design parameters used were Q=2m^3/h, H=2.8m, N=940rpm, inlet and outlet impeller diameters of 30mm and 53mm. The impeller had eight blades. They observed that the SST k-ω model was more accurate than RNG k-ε model. Furthermore, at the tongue zone the pressure coefficient was observed to change under different flow rates as shown in Figure 2-9. However, no information regarding to the pressure distribution and cavitation in the pump were presented.

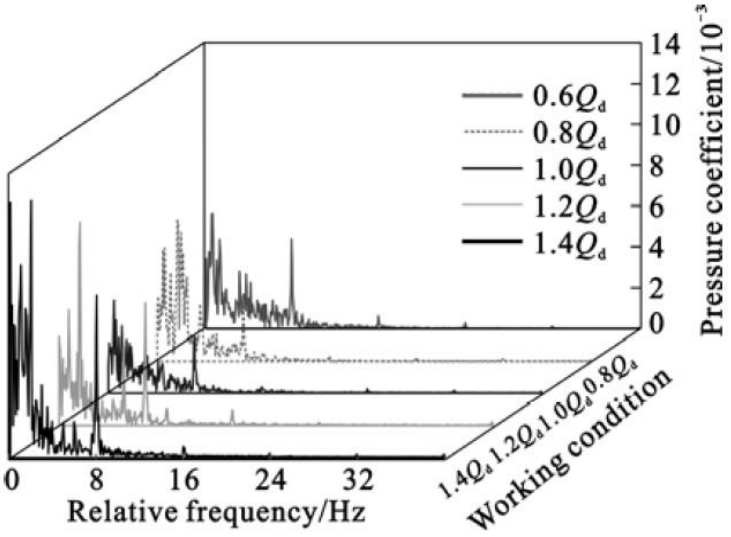

Figure 2-9: Frequency spectra at tongue region due to pressure fluctuations [58]

2.2.2. Investigation the Effect of Flow and Geometrical Parameters on Cavitation Behaviour in Centrifugal Pumps

In the literature, many researchers have attempted to investigate cavitation in centrifugal pumps using various approaches such as numerical and experimental. One of these studies was carried out by Koné et al. [59] where authors attempted to detect the pump cavitation using visual observation through the use of a high-speed camera. The design parameters used were flow rate in the range of 0.3 to 1.1(l/s), N=3000rpm, water temperature between 20 to 90^{o}C, inlet and outlet impeller diameters 54mm, and 175mm. The impeller had six blades. They found that the inception of cavitation appears before the performance of the pump starts to decrease. Also, when flow rates and temperatures increased the cavitation increased as well. The cavities colour was changed with the change of water temperature as shown in Figure 2-10. However, the authors just focussed on studying the effect of cavitation under different water temperatures. No information about pressure fluctuations or pressure and velocity distributions within the pump were reported in their work.

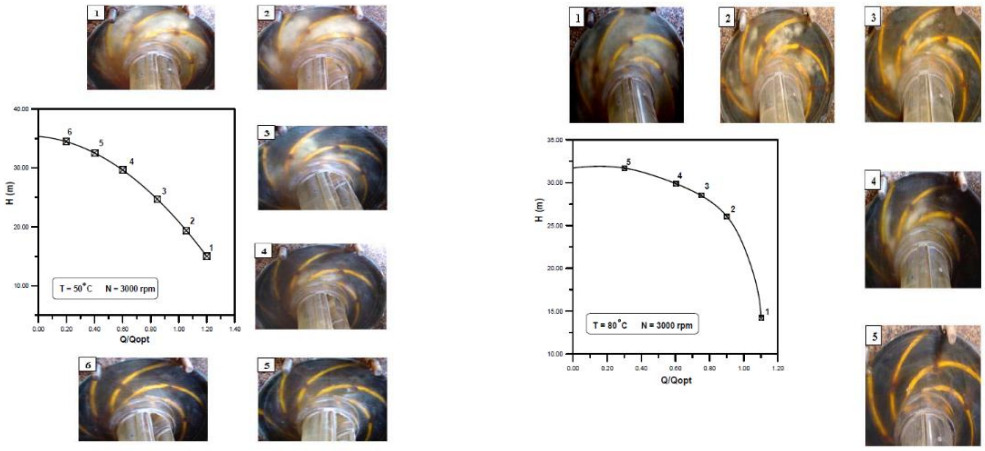

(a) (b)

Figure 2-10: Observation of cavitation within the centrifugal pump [59]

Abbas [60] investigated cavitation within the centrifugal pump numerically. The design parameters used were Q=16kg/s, N=3000rpm, inlet and outlet impeller diameters of 36mm and 80mm and an impeller was designed with six blades. The results showed that the formation of bubbles occurs in a lower pressure area. In addition, the cavitation happens on the surface of blades at the leading edge. Then, the cavitation zones move from leading to trailing edge at lower NPSH values. When the cavity length reaches the maximum chord length of the blade, the head-NPSH curve begins to drop, Figure 2-11 depicts the curve of NPSH and Head. However, the author did not study the effects of other geometrical parameters. Also, his study was under a limited range of boundary conditions.

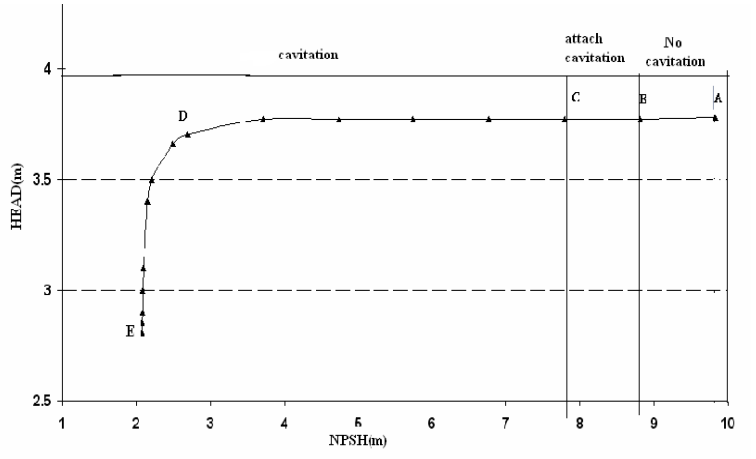

Figure 2-11: NPSH-Head curve at flow rate of 16 kg/s and N= 3000rpm [60]

Later, Kim et al. [61] conducted numerical analysis on a centrifugal pump and compared it with experimental results. The design parameters used were the flow coefficient of 0.09, head coefficient of 0.42, outlet impeller diameter 128mm, N=2400rpm, and the impeller was made

of five blades. From numerical and experimental outcomes, they found that accuracy could be changed due to the loss that happens in the pump between the shaft and the bearing as well the casing and the impeller that was not considered in the numerical analysis. However, no information regarding to the flow distribution and analysis of the pressure fluctuations within the pump was provided in their work. Moreover, the head or power coefficients of the pump were not considered.

Li et al. [62] studied the effect of different outlet blade widths which are 11, 13 and 16mm on the pump performance under cavitation conditions. The investigation was carried out under various operating condition and impeller design parameters were Q=340(l/min), H=15m, N=3700rpm, 19^{o} and 30^{o} inlet and outlet blade angles. Also, they used seven blades, 60mm and 98mm inlet and outlet diameter of impeller. Their results showed that as the outlet blade width increased, the pump head gradually increased and the low static pressure region at the impeller eye decreased as well as cavitation also increased as shown in Figure 2-12. However, this study was based only on a limit of the geometrical parameters. Also, no information regarding the velocity distribution.

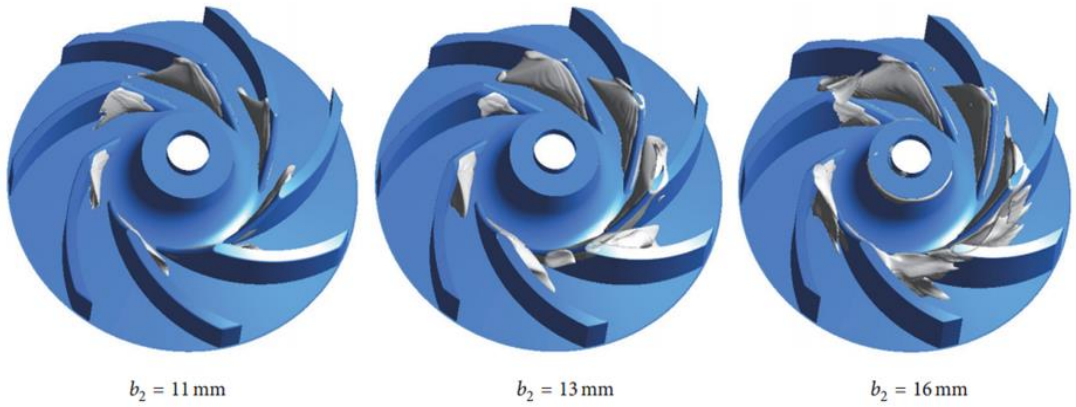

Figure 2-12: Volume vapour fraction distribution under different outlet blade widths [62]

Niazi et al. [63] numerically and experimentally investigated the cavitation within the centrifugal pump. Their studies were carried out under different flow rates and impeller parameters, which include six number of blades, 75 and 165mm inlet and outlet impeller diameters as shown in Figure 2-13. Their results showed that cavitation occurs at the suction side of blades and it also increases with low pressure at this particular region as illustrated in Figure 2-13. However, their study focuses only on occurrence of cavitation under limited boundary conditions (only flow rate). Their study does not reveal any information on the pressure fluctuations inside the pump.

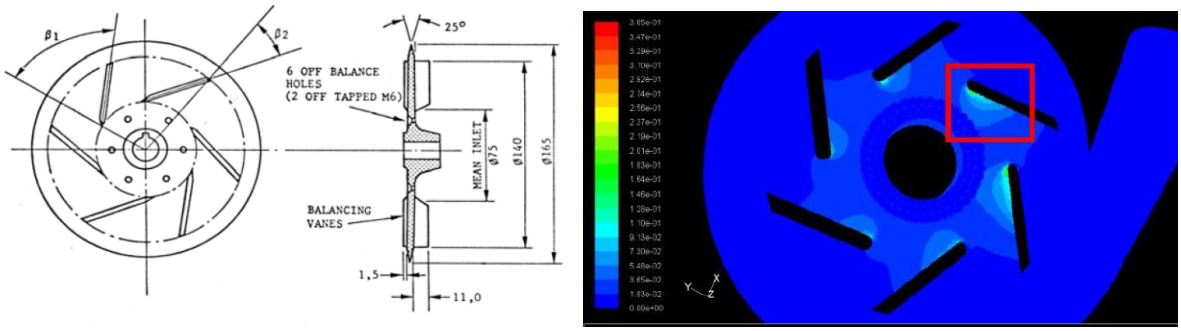

Figure 2-13: Geometrical parameters and volume fraction distribution for the pump [63]

XiaoJun et al. [64] investigated the effect of impeller leading edge on cavitation in the centrifugal pump. They used a 3-D pump with six impeller blades which they investigated under operating condition with a specific operating speed of ns=88.6, H=34m head, Q=50m^3/h and N=2900rpm. The results showed that the occurrence of the head drop in the pump was due to the generation of the vortex flow in the rear area of the cavity. Their results demonstrated that the appropriateness of using the numerical solution for the cavitation flow in the pump. The accuracy of the prediction for the flow regimes was estimated to be within 5% as shown in Figure 2-14. However, the authors only focused on studying the effects of cavitation at the impeller leading edge on the pump with limited information regarding the flow field analysis.

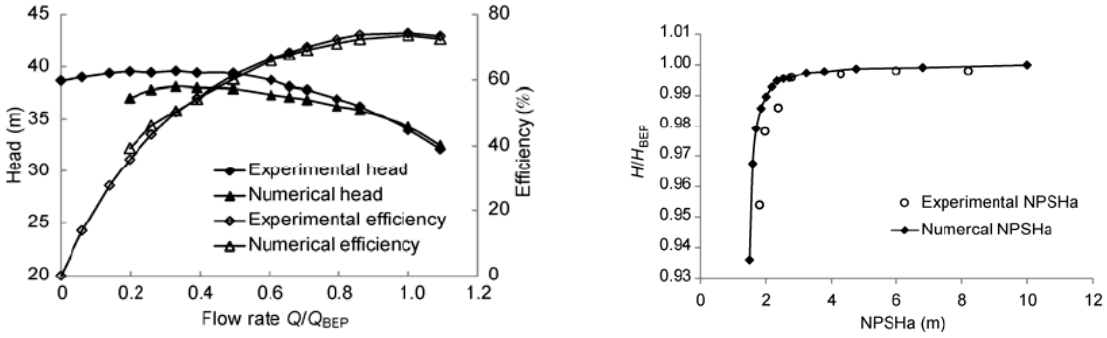

Figure 2-14: Pump Performance in non-cavitation and cavitation conditions [64]

Misiewicz and Skrzypacz [65] investigated the effects of the inlet blade angles of the impeller on the performance of the pump under cavitation conditions. The design parameters of the pump used were flow rate coefficient of 0.087, head coefficient between 0.759 and 0.787, N=2850rpm, inlet and outlet impeller diameters of 32mm and 90mm using a six blade impeller. They also studied various inlet blade angles of 16°, 38°, 56° and 72° respectively. From their results, they found at a constant flow rate, the NPSHR decreased when the inlet angle increased. The numerical technique provided possibilities for predicting cavitation in the impeller. Their

observation was under limited boundary conditions also pressure fluctuations within the pump were not considered.

Hassan and Kamal [66] studied the impact of cavitation in the centrifugal pump. They used a two-dimensional model for the pump and the geometrical parameters carried out in their investigation were a three-blade impeller having inlet and outlet diameters of 46mm and 120mm respectively. The results showed that head and efficiency of the pump decreased with a decreased in NPSHA. Furthermore, they observed an inversely proportional relationship between the temperature and NPSHA and they noticed that a reduction of NPSHA increased the pump's noise level. However, the investigation was carried out under steady state conditions, the head and power coefficients of the pump under cavitation conditions were not considered.

Kesba et al. [67] studied the influence of cavitation on different types of materials for the impeller. The design parameters for the pump used in their research were Q=18m^3/h, H=23.5m and N=2900rpm. They experimentally studied the influence of cavitation on the performance of the pump with three types of materials such as cast iron, aluminium and bronze. The results showed that the efficiency of the pump were 8.15%, 15.18%, and 5.31% for cast iron, aluminium and bronze respectively. However, a comparison and evaluation investigation between different techniques to detect cavitation were not carried out.

Lie et al. [68] investigated cavitation in the centrifugal pump at off-design conditions. The design parameters for their pump used were Q=340m^3/h, H=30m, outlet impeller diameter of 329mm, and N=1450rpm with six blades impeller. They found that cavitation at the blade leading edges of the impeller has maximum pressure fluctuations, which was about 2.54 times higher than that for non-cavitating flow in the pump. This was due to the violent disturbances that has occurred because of cavitation near the blade leading edges.

Fukaya et al. [69] studied the effects of impeller speed on cavitation intensity within the pump. The flow rate at the best efficiency point was 7.6m^3/min and an impeller diameter of 302mm with the impeller comprising of six blades. The results showed that the cavitation intensity was increased when impeller speed increased, Figure 2-15 showed the cavitation intensity distributions at various rotational speeds. However, no information regarding the pressure and velocity distributions were presented.

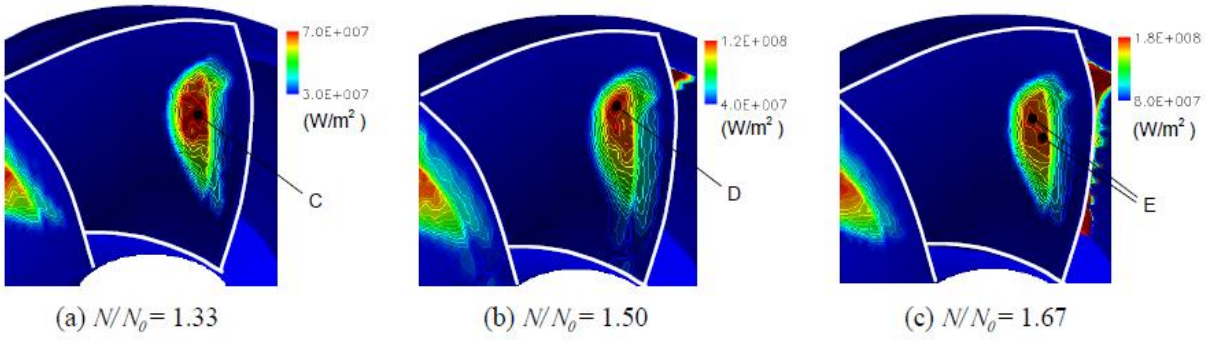

Figure 2-15:Cavitation intensity distributions at various rotational speeds [69]

Al-Hashmi [70] carried out statistical analysis of acoustic signal in detection of cavitation in centrifugal pump. The design parameters used for the pump were H=38m, N=2800rpm, inlet suction and outlet discharge diameters of 0.0508m, and 0.01375m, and the impeller made up of five blades. Their results showed that at flow rates larger than 340(l/min), the cavitation starts when NPSHA was lower than NPSHR. At higher flow rates, more cavitation, turbulence, friction and velocity influences are generated. However, the effect of different operation conditions such as air injection, suction valve opening, and pump rotational speed on the detection of cavitation were not investigated.

Steinmann et al. [71] investigated unsteady cavitation flow within pump. From their numerical result, the pump power and head were approximately 6% higher than their experimental results. Changing the vapour volume fraction from 0 to 10%, cavitation occurred at the leading edges at the impeller as shown in Figure 2-16. Also, the CFD results showed no cavitation appearance at Best Efficiency Point (BEP). However, this study was only based on the limited flow rates and no information regarding to the analysis of pressure fluctuations in time and frequency domains were presented.

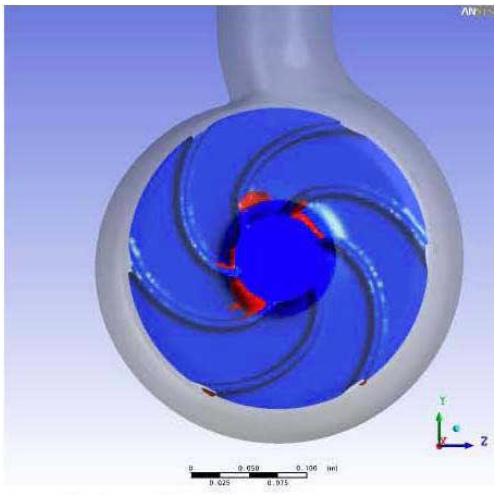

Figure 2-16: Detection of cavitation in the pump [71]

Shukla and Kshirsagar [72] predicted cavitation in the centrifugal pump for different inlet impeller diameters of 225mm, 330mm and 425mm. The design parameters of the pump used in their research were Q=0.508m^3/s, H=60m, N=1450rpm, inlet impeller diameter of 330mm and impeller with five blades. Their results showed that the head drop for (225mm diameter) was at a high NPSHR, though the head drop for (445mm diameter) was approximately the same as that of (330mm diameter) as showed in Figure 2-17. Also, when the NPSH decreased, the cavitation increased between the blades as illustrated in Figure 2-18. However, this study includes a limited investigation on the effects of the inlet impeller diameter on cavitation in the pump and no information regarding the pressure and velocity distribution were reported.

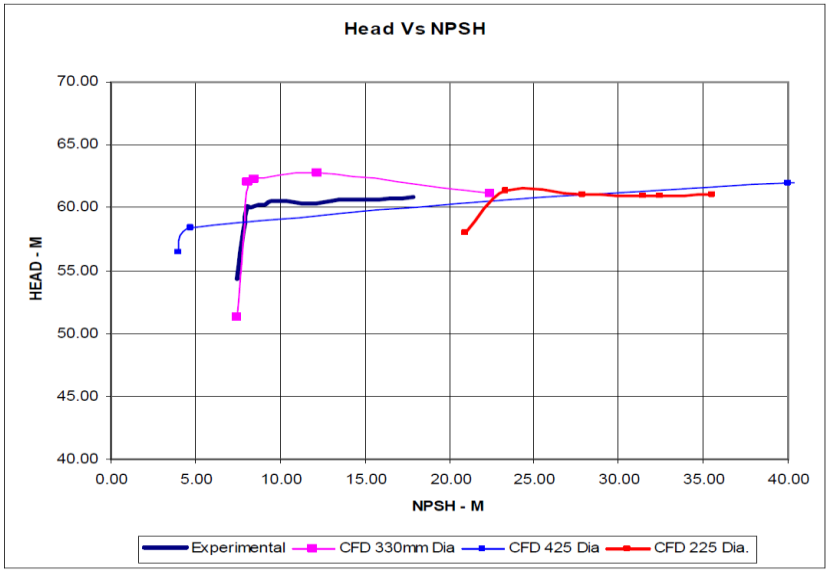

Figure 2-17: Head-NPSH curves under different inlet impeller diameters [72]

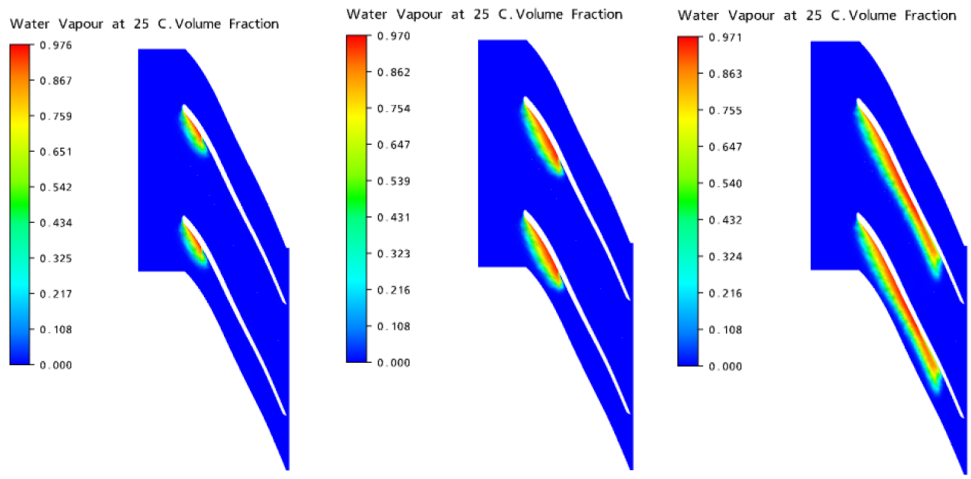

(a) 10m NPSH (b) 7.5m NPSH (c) 7m NPSH

Figure 2-18: Cavitation in the impeller passages under different NPSH values [72]

Zhu et al. [73] investigated the cavitation in transient flow during the collapse of a nuclear power pump. They used boundary conditions were H=32m, Q=35m^3/h, N=2900rpm and an impeller with six blades. They observed that when the pump began operating, the volume fraction was zero in the flow passages of the impeller and after that, the cavitation increased quickly due to the decrease in pressure in the suction line. Additionally, the occurrence of cavitation was near the impeller inlet diameter at low pressure. However, a comparison between different approaches to find effective technique for predicting cavitation was not conducted.

Liu et al. [74] studied the effects of the empirical coefficient pump head and cavitation number with different bubble diameters under cavitation flow in the pump. The parameters used for the test pump include Q=0.014m^3/s, outlet impeller diameter of 168mm, N=2900rpm and an impeller with five blades. They considered three different bubble diameters which were 2×10^{-4}m, 2×10^{-6}m and 2×10^{-8}m respectively. Their results, when compared with the experimental results, showed that the accuracy of the prediction of the pump's cavitation performance improved as the bubble diameters reduced.

Homa and Wróblewski [75] investigated the modelling of flow for cavitation in the pump. In their flow modelling, they used in their pump Q=23.08kg/s, N=985rpm, water temperature was 25°C. They observed that the minimum pressure in a rotor occurs close to the leading edges of blades. In that zone, the vapour bubbles might appear even with NPSHA higher than NPSHR. The cavitation cloud was seen to cover the entire zone beyond the blades of the rotor when

there was decreased in the inlet pressure as shown Figure 2-19. However, no information regarding to the pressure fluctuations were presented.

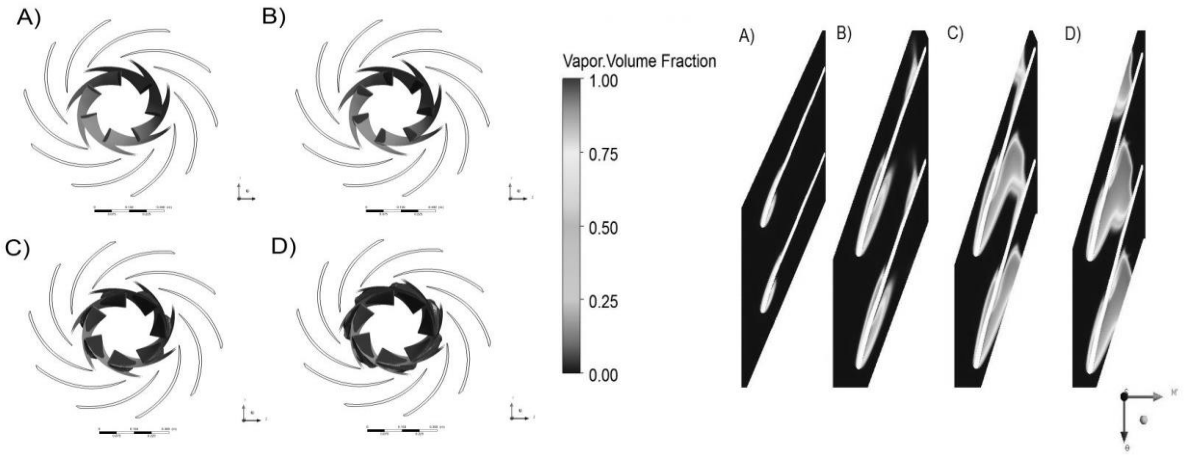

Figure 2-19: Vapour volume fraction distributions at different pressures A) 110kPa B) 55kPa C) 40kPa and D) 39kPa [75]

2.2.3. Summary of Literature Review Concerning the Effects of Flow and Geometrical Parameters on the Single-Phase and Cavitation Behaviour in Centrifugal Pumps

Different researchers have investigated the effect of various parameters and operation conditions on the centrifugal pump performance, after critical review of the literature presented above, the following can be noted:

1. There is a lack of information in most of the above investigations, which were conducted at constant geometrical parameters of pumps and under limited operation conditions.
2. These studies are severely limited and lacked of the local flow field transient analysis under different combinations of geometrical parameters of the pump for different operating conditions (with and without cavitation conditions). For instance, the local and global interrelations among pressure, velocity, vapour volume fraction distributions, pressure fluctuations in time and frequency domains as well as the pump head were not studied in an integrated manner.
3. There was a necessity for better comprehension of the flow structure within the centrifugal pump as well as the effect of geometric and operational conditions on detection and diagnosis of cavitation within the pump. Thus, cavitation is still not well analysed whether numerically or experimentally.

4. There were no reports on development of semi-empirical correlations for calculating the head and power coefficients of the pump in the literature as a function of different geometrical parameters under single-phase and cavitation operating conditions.
5. There may be extra information and description as well as the sensitivity of the method used regarding detection of cavitation, which means that most of the authors used two detection techniques or less from those available techniques such as CFD, vibration and acoustic techniques.
6. There is a lack of information in most of the above studies regarding a comparison and evaluation investigation among different techniques, such as CFD, vibration, and acoustic to detect and diagnose cavitation within the centrifugal pump.

In the view of the research aims, the use of CFD technique in the detection of cavitation in centrifugal pumps was surveyed and discussed. However, in order to achieve the rest of the research aims, the next section will consist of literatures, using the experimental investigations on condition monitoring of the centrifugal pump, using vibration and acoustic techniques for the purpose of cavitation detection in the centrifugal pump. Furthermore, the works that considered both the time and frequency domains will be reviewed.

2.3. Experimental Investigations on Condition Monitoring using Vibration and Acoustic Techniques for Detecting Cavitation in Centrifugal Pumps

In the literature, many researchers have attempted experimentally to investigate and discuss the pump performance with and without cavitation using various conditioning monitoring methods, one of these studies was carried out by Zhang et al. [76] where authors attempted to study the vibration features in the centrifugal pump that has a special slope in the volute. They collected vibration signals at various flow rates and compared the performance obtained between the slope volute and conventional spiral volute as shown in Figure 2-20 (a). The results showed that the vibration level of the slope volute pump was lower than the vibration level of the conventional pump as illustrated in Figure 2-20 (b). They therefore found that using slope volute pump could effectively decrease the vibration level in the pump. However, no information regarding the influence of cavitation on the pump performance. Also, the pressure and velocity distribution were not reported.

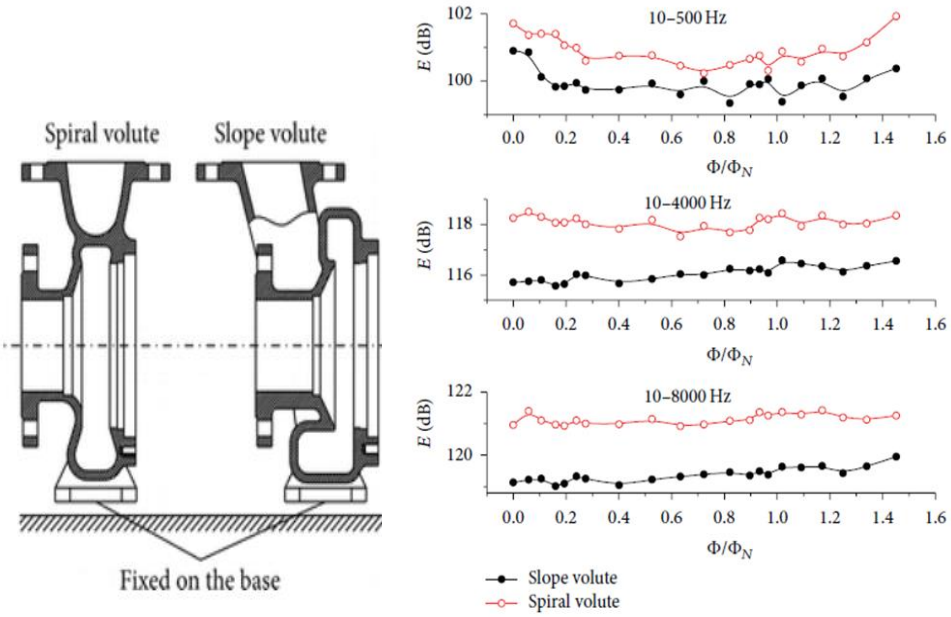

(a) (b)

Figure 2-20: (a) Spiral and slope volutes (b) Level of vibration in the centrifugal pump [76]

Stopa et al. [77] detected incipient of cavitation in centrifugal pump using a tool known as Load Torque Signature Analysis (LTSA) as shown in Figure 2-21. It uses electrical signals from the motor to compute the torque that the pump develops via its frequency spectrum information and determines the occurrence and intensity of the cavitation. Their results revealed that the LTSA tool presents a response pattern close to those normally shown by pressure sensor when used in such an application. The LTSA tool can detect the cavitation using a single component impeller passing frequency as shown in Figure 2-22.

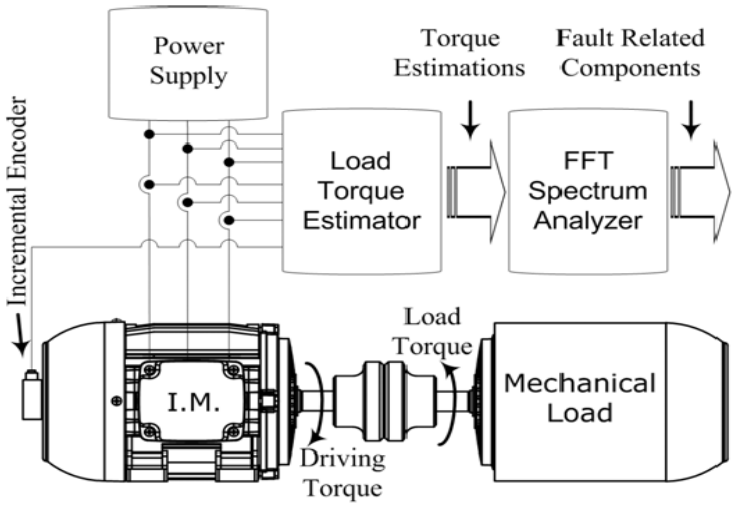

Figure 2-21: Block diagram of the LTSA [77]

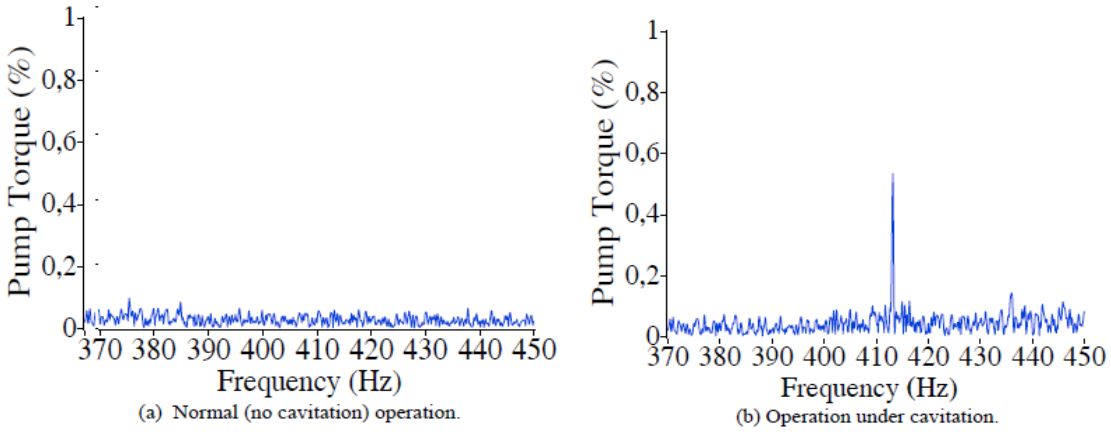

Figure 2-22: Frequency spectrum of LTSA under normal and cavitation conditions [77]

Chudina [78] used noise as an indicator in investigating cavitation within the pump. The author carried out analysis of the noise signal in frequency domain under different operating conditions. The results showed that the cavitation increased at high flow rate particularly at the high range of frequency as shown in Figure 2-23. However, the author studied cavitation in the pump only by using the noise technique and no information regarding to the pressure and velocity distributions. There is also no information regarding analysis of the noise signal in time domain.

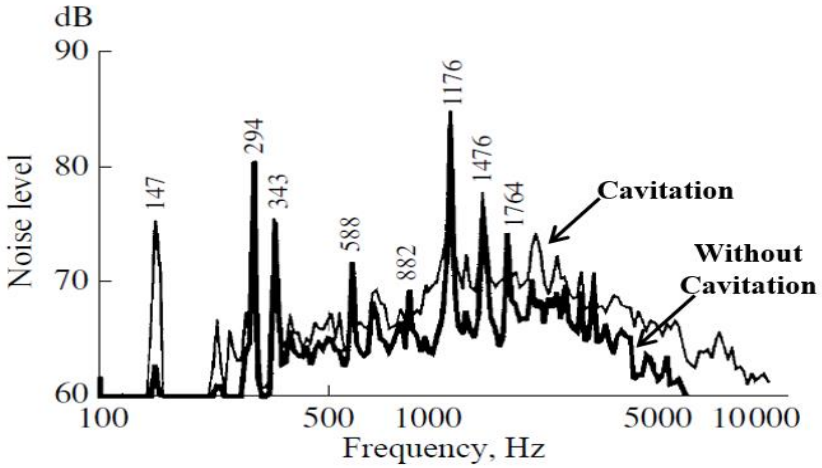

Figure 2-23: Acoustic signal in frequency domain under cavitation condition [78]

Cernetic et al. [79] detected and monitored of cavitation in the pump by using vibration and acoustic signals. They used two types of centrifugal pumps, the first one was closed impeller with six blades and made of metal alloy, the second one was semi-open impeller with six blades and made of plastic material. The results showed that each pump has different vibration spectra and noise levels with various discrete frequencies. In addition, they found that the difference between vibration and noise under cavitation and non-cavitation conditions was between 30 to

40dB. However, they did not present any information regarding to the pressure and velocity distributions or any sensitive technique and sensitive frequency range in detecting cavitation.

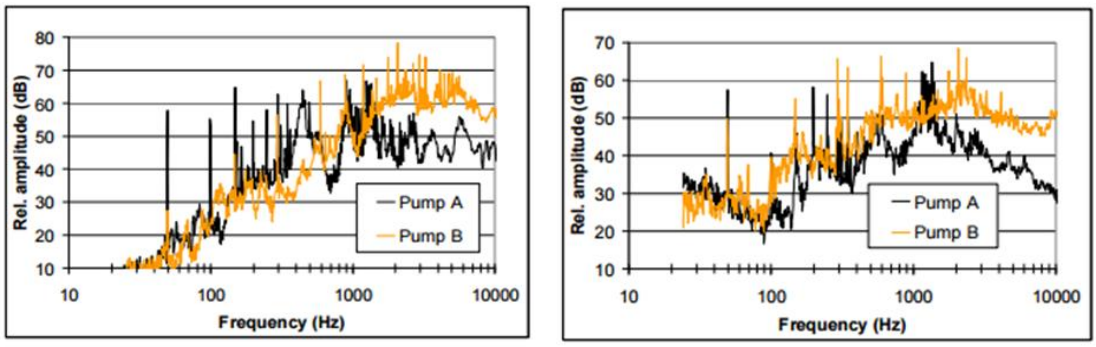

(a) Vibration (b) Acoustic

Figure 2-24: Vibration and acoustic spectra for two pumps under cavitation and non-cavitation conditions [79]

Albarik et al. [80] investigated and diagnosed centrifugal pump faults through the use of vibration signal. They used a closed impeller pump with some parameters of the pump considered in their design such as Q=30m^3/h, H=55m N=2900rpm. They predicted the relationship between the NPSHA and NPSHR by decreasing the discharge valve progressively with the suction valve fully opened. NPSHR for the system increased when flow rate increased. The results showed that when the flow rate increases the level of vibration increases as well. However, the authors just used vibration signal technique to investigate faults in the pump. Hence, no information regarding the influence of cavitation and pressure fluctuations in time and frequency domains were reported.

Suhane [81] studied the effect of radial clearance on pressure pulsations by using vibration and acoustic signals under different radial clearances between impeller and diffuser of 1.5mm, 3.7mm, and 6.8mm. The horizontal type pump was used in this study together with diffuser. The impeller was designed using eight blades while that of the diffuser composing of seven vanes. Results indicated that at high flow rate, both vibration and acoustic levels were high. The vibration and acoustic levels were minimum at the maximum radial clearance between impeller and diffuser. In addition, when the value of radial clearance increases, the lower pressure fluctuations occur.

Farokhzad et al. [82] experimentally investigated the relationship between vibration signal and the type of fault within the centrifugal pump under different operating conditions. They tested two different configurations; the first one was broken impeller and the second one was with

faulty seal conditions. The results showed that an important change in the trend of vibration signal was occurred as a function of fault at various operating conditions. The value of RMS for healthy pump conditions was moderate and stable, but this increased in value due to the broken impeller and faulty seal as shown in Figure 2-25.

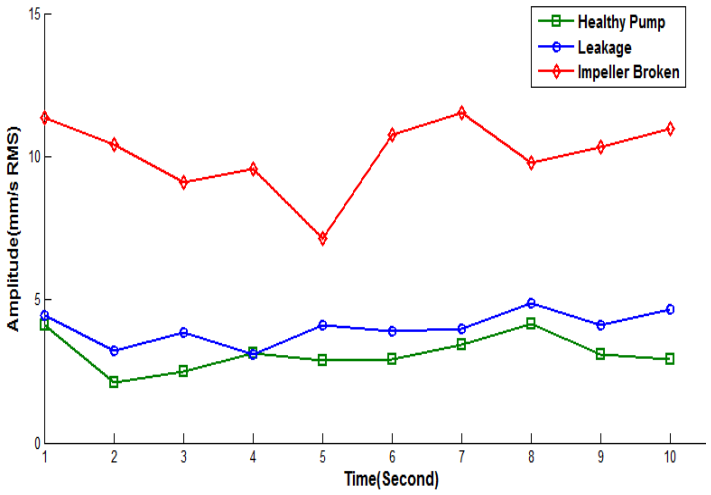

Figure 2-25: Vibrations trend under healthy, impeller broken and seal faulty [82]

Luo et al. [83] researched on statistical features of vibration signals in the centrifugal pump. The parameters used for the test pump were Q=50m^3/h, H=32m and N=2900rpm. The number of blades used for their impeller was six, impeller inlet and outlet diameters of 75mm and 174mm. The results showed that when the pump works under flow instability conditions, the dynamic characteristics of the pump changes. Therefore, the statistical analysis of vibration signal (probability density factor PDF, standard deviation and Kurtosis) could be used to predict unstable flow in the pump. The statistical features of vibration signal in time domain and frequency domains were good indicator for predicting intensity changes and the onset of cavitation in the pump. However, the study of cavitation under different operation conditions were not conducted.

Cdino M. al. [84] detected cavitation in the pump using the sound signal. The specifications of the pump were Q=0.150m^3/s, H=80m and N=2535rpm. Their results showed that when cavitation becomes fully developed, the sound level increase to a higher level compared to that without cavitation as shown in Figure 2-26. The noise occurrence on the pump depends on the flow rate, speed of the pump and the instability of the pump. Moreover, instability can occur due to cavitation causing vibration, noise, deterioration of the performance of the pump, material erosion and pitting. However, no information was provided to compare different techniques under different frequency ranges for detecting cavitation.

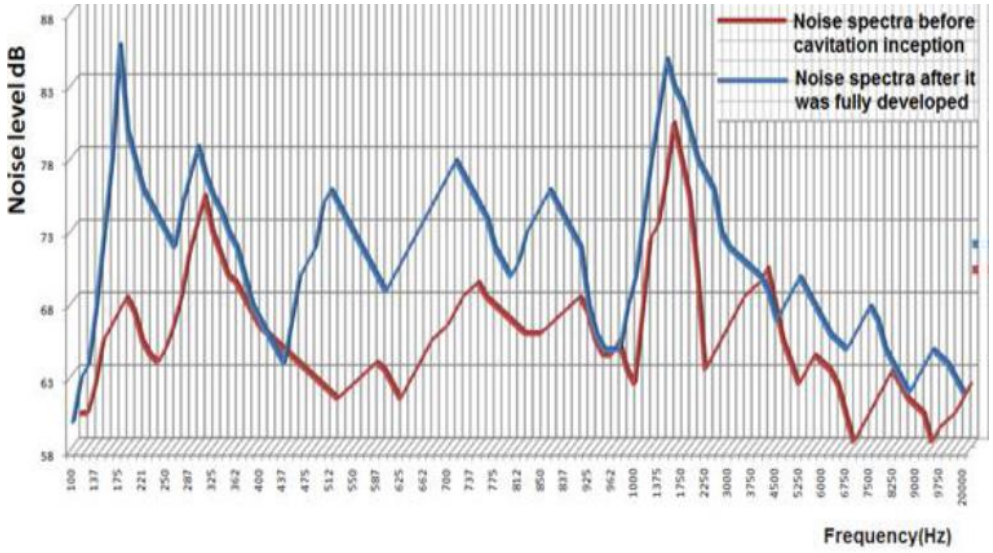

Figure 2-26: Acoustic frequency under no cavitation and cavitation conditions [84]

Sakthivel et al. [85] conducted an investigation about the usage of a set of statistical features for diagnosing faults in the centrifugal pump such as kurtosis, standard deviation, skewness, variance, range, maximum value and minimum value. Such statistical features allowed them to extract both normal and faulty conditions from the vibration signals. Their study for faulty conditions comprises of impeller faults as well as bearing faults making their outcome a promising method for diagnosing practical fault application in the pump. However, there is no information regarding the influence of cavitation and effect of different geometrical parameters or the pressure and velocity distributions.

Tan and Leong [86] detected cavitation in the pump using vibration signals. They tested the pump under different flow rates. The design parameters of their pump were a six vane diffuser and the motor was coupled to three phase with N=2500rpm. Their results showed that the vibration amplitude increased significantly under cavitation when compared to normal operating conditions. The possible reason for this increase was due to the formation and collapse of bubbles particularly at the eye of the impeller. However, information regarding pressure or velocity distributions of the flow field in the pump or sensitive frequency range for detection of cavitation were not presented.

Mc Cormick and Nandi [87] examined the usage of artificial neural networks (ANN) to monitor the rotating machinery condition from the time series of vibration. Such approach assumes the use of automatic categorisation of the machine condition through extraction of features from many approaches such as neural network. The assumption of extracting methods is based on

the zero lag higher-order statistics applicable to both horizontal and vertical vibration time series. The feedback of adaptive learning and momentum technique is utilised for training the ANN. The feedback approach is examined in a test rig that was designed to create unbalanced shaft and rub faults. The outcomes from such a method showed that the combination of moments of the complex time series with its acquired derivative moments can help in the achievement of detecting faults successfully by more than 90%.

Al Thobiani et al. [88] studied the cavitation in the centrifugal pump through the use of acoustic and vibration signals. Assessments with different statistical parameters such as kurtosis, variance and peak factor. The outcome revealed that kurtosis and peak factors are not sufficient for indicating cavitation in the pump. However, their finding recommends that spectral entropy is more accurate for detecting cavitation. Their study was under a limited range of boundary conditions at different flow rates only. Moreover, study of the occurrence of cavitation under different operation conditions such as air injection, different suction valve openings and rotational speeds was not carried out.

C̆udina and Prezelj [89] detected cavitation in pump using acoustic method. The results of their study showed that the spectrum of the acoustic was related with inception and development of cavitation within a pump. In addition, the level of the spectra frequency peak increased with the inception of cavitation, which further increased, with the development of the cavitation and it reached a maximum value when the cavitation process was fully developed. However, their study just used the acoustic technique under limited boundary conditions using frequency domain analysis.

Nasiri et al. [90] analysed the vibration signal for detecting cavitation in pump by using neural networks. They used two statistical features such as crest factor and kurtosis as an input to build a neural networks technique to detect cavitation. They introduced three monitoring conditions such as normal, developed and fully developed of cavitation as shown in Figure 2-27. In order to test such network, they used the feed forward back propagation. Their findings revealed the reliability of the method to detect cavitation in the pump. However, the author just used crest factor and kurtosis features to investigate cavitation under a limited range of boundary conditions and a comparison between different techniques such as CFD, vibration and acoustic to find sensitive frequency range and effective method for detecting cavitation was not carried out.

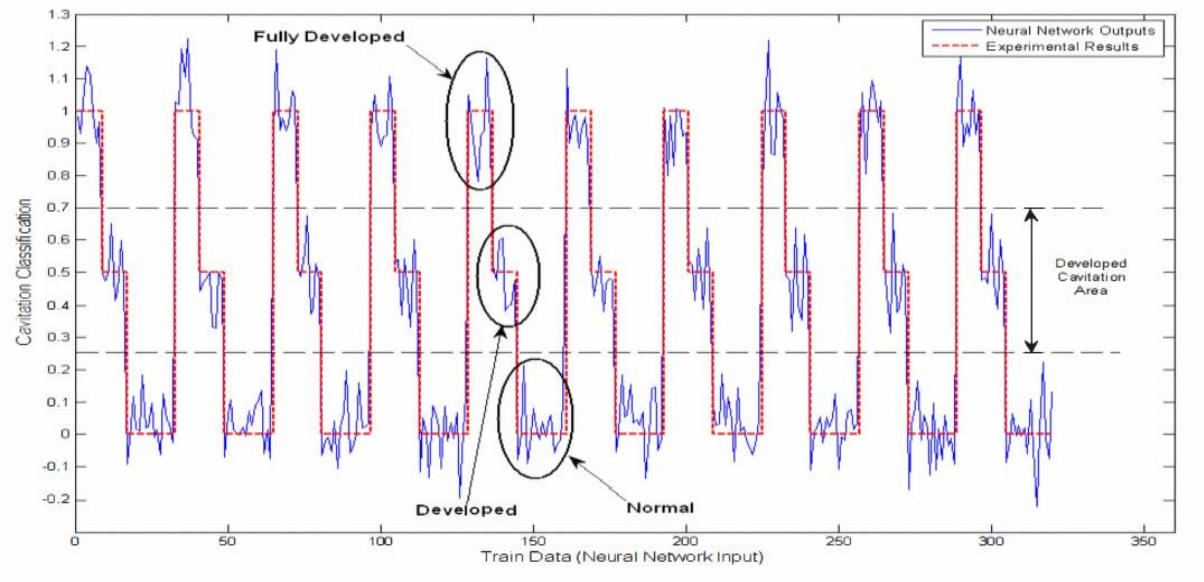

Figure 2-27: Compare between the experimental and network results with and without cavitations [90]

Zargar [91] detected cavitation within the centrifugal pump related to the oil industry for cooling circulation water systems. The author detected cavitation by analysing the vibration signal in time waveform and frequency domain using FFT method. The author found that the vibration amplitude in time and frequency analyses suddenly increased under cavitation conditions as compared to without cavitation. This phenomenon leads to a decrease in the performance of the pump. However, the author just used vibration technique to detect cavitation. Moreover, no information regarding study of sensitive frequency range for detection of cavitation under different operation conditions.

2.3.1. Summary of Literature Review Concerning Experimental Investigations on Condition Monitoring using Vibration and Acoustic Techniques for Detecting Cavitation in Centrifugal Pumps

The literature review that is presented above, for predicting cavitation in centrifugal pumps and the effect of this phenomenon on the performance of the pump, has highlighted gaps in the knowledge base and the following can be noted:

1. There is a lack of information related to the use of different frequency ranges in frequency domain analysis that might be more sensitive to detect cavitation within the centrifugal pump.

2. The cavitation is still not well analysed/discovered, particularly when the pump operates under a wide range of operational conditions such as various flow rates, pump rotational speeds, decrease in the suction valve openings and effects of air injection.
3. There is a shortage of information regarding the comparison of different techniques such as CFD code, vibration and acoustic to find the effective techniques in order to detect different levels of cavitation (no cavitation, inception, development, and full development of cavitation).
4. Inter-dependence of the local flow field analysis with indicators of the global performance with a variety of operating conditions and different combinations of geometrical parameters using CFD technique were not conducted in more detail.

This research study attempts to fill these gaps by using different techniques numerically using CFD and experimentally using vibration and acoustic condition monitoring techniques for detecting cavitation within a centrifugal pump.

2.4. The Scope of Research

Through the research and studies that were reviewed in this chapter it can be concluded that the performance of the centrifugal pump is influenced by a combination of many functional factors such as pressure, velocity, head, power and cavitation. Interestingly, cavitation has major effects on pump performance where the greatest drop in the performance might be due to the cavitation. The cavitation causes many problems in the pump such as deterioration in performance of the pump, increase in the levels of vibration and noise as well as it causing erosion of pump material (impeller and volute). For the above-mentioned reasons, the cavitation in a centrifugal pump was taken into consideration in this study. The detection of cavitation level in a pump and analysing this phenomenon is an important aspect to improve maintenance and enhance the reliability of the pump. This study will investigate and discuss the pump performance and detection/diagnosis of cavitation in the pump under different wide ranges of operation conditions. This will be carried out numerically and experimentally using different analyses techniques in order to increase the reliability of cavitation detection within a pump. Based on the above studies reviewed in this current chapter, the research scope regarding a centrifugal pump was designed.

The first research area includes extensive analysis of the flow field, the pump performance and detection of cavitation. CFD tools will be considered to conduct the analysis in the first research area. Using CFD technique more information regarding the internal flow field can be provided.

Furthermore, the analysis will be carried out under the transient conditions using sliding mesh technique (SMT) for single-phase and cavitation conditions. In order to understand the flow structure within a pump, an extensive local and global analyses is going to be carried out for the effects of different operating conditions on the performance of a pump. Moreover, quantitative and qualitative analyses were also conducted to predict and diagnose different levels of cavitation in the pump under a wide range of operating conditions and different geometrical parameters. Based on the above analysis and the acquired results, novel semi-empirical correlations of the head and power coefficients for the centrifugal pump will be developed.

To better comprehend of the pump performance and detection of cavitation the second and third research areas consist of an extensive experimental analysis on the effects of different operating conditions on the pump performance under cavitation conditions using different techniques such as, vibration and acoustic techniques. There will be a focused on the condition monitoring of the pump system which is experimentally carried out using both time and frequency domains. Analyse the above vibration and acoustic signals by using different statistical parameters such as peak, root mean square (RMS), peak-to-peak and variance features in order to provide a good indication regarding detection of cavitation. Also, for further investigations and to better understand the prediction of the inception and development of cavitation levels in the pump, more specific features are required. These features can be found through transforming and investigating vibration and acoustic signals in the frequency domain by using FFT technique. Also, for further investigations in obtaining a more detailed information regarding the cavitation inception, analysing these signals in frequency domain were carried out using different statistical parameters such as mean and RMS features under various frequency ranges. Moreover, the comparison between vibration and acoustic analyses techniques under a wide range of operational conditions in both time and frequency domains was carried out. The aim of this study is to compare and find an adequate and reliable technique to detect and diagnose of cavitation in centrifugal pumps. Therefore, in this research an evaluation was carried out of these techniques and this study will be aimed at finding the most effective technique for monitoring and detecting cavitation. Furthermore, these techniques should be able to detect the inception of cavitation at an earlier stage.

2.5. Research Objectives

Based on the research aims presented in the previous chapter and after conducting a detailed literature review, the following objectives were formulated which will assist in achieving the research aims presented in Chapter one and enable bridging the knowledge gap noticed in the literature:

1. To analyse the flow field within the centrifugal pump based on single-phase at different operating conditions using sliding mesh technique under transient approach.

2. To predict the cavitation phenomenon within the centrifugal pump by using cavitation model in CFD at various operating conditions using sliding mesh technique under transient approach.

3. To investigate the effect of the different impeller geometrical parameters including (number of impeller blades, inlet and outlet impeller diameters) on the performance of the centrifugal pump under single-phase and cavitation conditions.

4. To develop semi-empirical relations for the head and power coefficients in the centrifugal pump under single-phase and cavitation conditions.

5. To detect the cavitation in the centrifugal pump based on vibration technique. The objective comprises developing MATLAB code to analyse and process the acquired data from vibration signal in both time and frequency domains under different flow rates.

6. To investigate the cavitation within the centrifugal pump based on vibration technique under various pump rotational speeds.

7. To detect the cavitation within the pump based on vibration technique under different suction valve openings.

8. To study the effect of air injection on the performance of the centrifugal pump and detect the cavitation occurrence within a pump based on vibration technique.

9. To detect the cavitation in the centrifugal pump based on acoustic technique under different flow rates.

10. To investigate the cavitation in the pump based on acoustic technique under various pump rotational speeds.

11. To detect the cavitation within the pump based on acoustic technique under various suction valve openings.

12. To analyse the cavitation in the centrifugal pump based on acoustic technique using air injection.

13. To compare between vibration and acoustic techniques to find the sensitive frequency range and to conclude on the better effective technique for detecting and diagnosing cavitation in the centrifugal pump.

In order for this study to reach a satisfactory conclusion of the above-mentioned research objectives, it uses CFD code and experimental study using condition monitoring based methods for detecting and diagnosing cavitation in the centrifugal pump. The next chapter explain the numerical modelling techniques incorporated in this current work.

CHAPTER 3

NUMERICAL MODELLING OF THE CENTRIFUGAL PUMP USING CFD CODE

To investigate the objectives of this research, CFD based technique was used to numerically simulate the transient flow of water within the centrifugal pump. Sliding Mesh Technique (SMT) was employed to mimic the rotation of the impeller. This chapter details the methodology used for the detection of cavitation as well as to evaluate the pump's performance. A detailed explanation on the solver settings and boundary conditions is presented in this chapter for both single-phase flow and cavitation conditions in the centrifugal pump.

3.1. Introduction

CFD code is widely used in designing, modelling and solving different industrial applications that are quite complex as it provides a good accuracy. CFD is often used for analysing the distribution and management of flow variables in various industrial processes such as compressors, pumps, turbines, furnace and boilers, hot rolling industries and other applications where thermal management and mixing are very important. The optimisation can assist in providing a very large energy saving. It is however now very important to have a tool such as a real-time CFD in analysing, controlling and optimising on-line various processes for industrial applications [92].

CFD is a tool used for the simulation of the behaviour of fluid flow by the use of high-speed computers. There are well known mathematical equations that define the behaviour of fluid, gases and air in terms of the conservation of energy, mass and momentum equations. As the power of the computer increased in the early 1970's, the aerospace industry began to pioneer the development of software in approximating solutions to all of these equations for complicated flows around air and that of space craft. For the last few decades, the CFD being developed has reached an advanced level to where solutions that are very accurate can be achieved for more complex flows including chemical reaction, particle tracking and heat transfer [93].

Using CFD code can help build the 3-D domain using the computer. A computational mesh can then be introduced into this domain. This mesh then divides the flow domain region into several cells or control volumes. It is also for these models to contain several millions of these control volumes or cells. The CFD code is then used in solving the fluid motion equations such as conservation of energy, mass and momentum for every single cell. The results that would be obtained can then be plotted as different colour contours in order to show the variation of different parameters of flow in the domain, at any location. Therefore, analysis of the different flow pressure, velocities, species concentrations, temperatures and other parameters can then be obtained from the results. Animations, which are computer-generated, can be also created, offering visualisation of flow in observing the "real-time" flow motion. Quantitative and qualitative analyses in CFD code were used in analysing the results obtained [93].

3.1.1. Advantages of CFD Code

In this section the main advantages of CFD analysis is described briefly:

1. It relatively reduces cost and saves time in order to build different new designs.
2. It is now possible to analyse various flow problems that if done experimentally, it could be expensive and quite difficult.
3. The use of CFD code can provide the capacity and capability in investigating the different types of systems under a wide range of operating conditions that are over their limits.
4. The detailed design and analysis, the level of which CFD code can be applied is unlimited.
5. To facilitating calculus, it is a requirement in simplifying the phenomenon mathematically. If this simplification was done properly, the result obtained from CFD can then be more accurate.
6. CFD code provides different types of model that are best at describing multi-phase flows, turbulence phenomenon and other problems that are quite difficult to analyse.
7. Any location in the flow domain of interest is allowed in CFD for the designer to examine and also interpret its performance through some flow and thermal parameters.
8. In experiments, only at a limited number of locations permit the extraction of data in the system in places where gauges and sensors are placed [94].

3.2. Running of the CFD Code

Computational fluid dynamics is designed for the analysis of fluid flow issues. Therefore, they provide simple access and powerful solutions to the entire commercial CFD, which contains complicated interfaces which is then left for users to input parameters of problems and study their outcomes. The entire code involves three main components which are:

1. Pre–Processor
2. Solver
3. Post–Processor

Pre–processing stage is further divided into two i.e. geometrical modelling and meshing of the flow domain. Geometrical modelling comprises of construction of the geometry of the flow domain (passages through which fluid flows), via operator–interface, in order to follow the transformations of such inputs into an appropriate shape that can be used by the solver. The flow domain is then spatially discretised into very small sections (called elements) on which the governing equations of fluid flow are solved iteratively using finite volume approach. This is known as the meshing process. Selection of the physical/turbulence models, applying appropriate boundary conditions and setting-up the convergence criteria are all part of the solver stage. This stage also involves providing initial conditions and running of the

simulations. The post-processing stage comprises of gathering the data for the various fluid and flow related parameters. Figure 3-1 depicts the numerical model steps using CFD code.

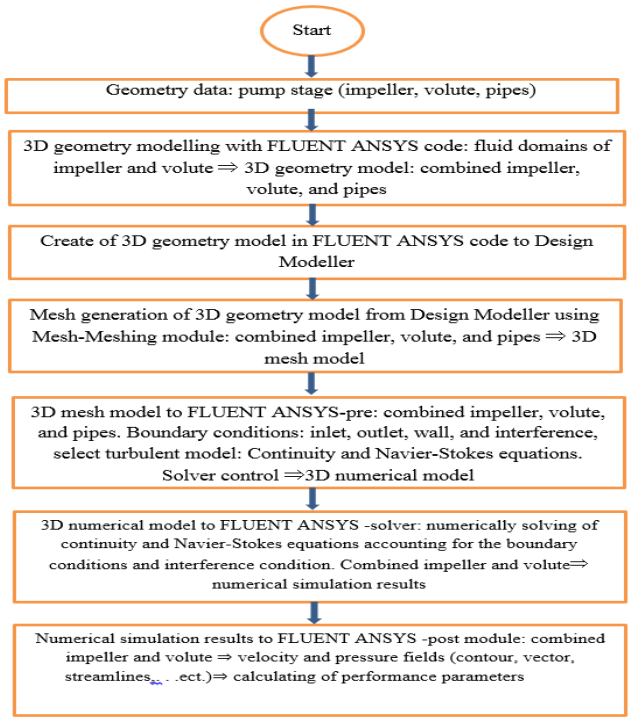

Figure 3-1: CFD code steps [95]

3.3. Governing Equations of Fluid Flow

As discussed in the previous section, governing equations of fluid flow are being iteratively solved on each mesh element within the flow domain. The governing equations that were used in the present work are:

1. Mass Conservation
2. Momentum Conservation

It should be noted that CFD codes are based on control volume approach, where the fluid is regarded as continuum.

3.3.1. Mass Conservation

The first stage of derivative of a mass conservation equation is to record the equation of mass balance for the liquid component:

Increase of mass rate in liquid element	=	Net rate of flow of mass into liquid element	(3-1)

For each liquid, there is constant density, the mass conservation equation is:

$$Div\, u = 0 \tag{3-2}$$

The net flow of mass out of the element across its boundaries is described. The previous equation can be written as:

$$\frac{\partial u}{\partial x} + \frac{\partial v}{\partial y} + \frac{\partial w}{\partial z} = 0 \tag{3-3}$$

This equation (3-3) represents the three-dimension mass conservation or continuity at a given point in an incompressible fluid.

3.3.2. Momentum Conservation

The second law of Newton illustrated the rate of momentum change of a liquid particle which is equal to the sum of the forces acting on the particle:

The rate of momentum change of a liquid particle = Sum of the forces acting on the particle (3-4)

Liquid particles have two types of forces. These forces are the body forces and surface forces. Body forces contain centrifugal and electromagnetic forces while, surface forces contain viscous, pressure and gravity force. It is a common practice to focus on the contributions of the latter (surface forces) as the discrete term in the momentum equations. In addition, the influence of body forces is also included as a source term. To find the x–element of the momentum equation of the rate change a liquid particle is setting equal to the total force in the x–direction on the component because of surface stresses, added to it the rate of increase of x– momentum because of sources, the equation is as next:

$$\rho \frac{Du}{Dt} = \frac{\partial(-p+\tau_{xx})}{\partial x} + \frac{\partial \tau_{yx}}{\partial y} + \frac{\partial \tau_{zx}}{\partial z} + S_{Mx} \tag{3-5}$$

The y and z–components of momentum equation are given by:

$$\rho \frac{Dv}{Dt} = \frac{\partial \tau_{xy}}{\partial x} + \frac{\partial(-p+\tau_{yy})}{\partial y} + \frac{\partial \tau_{zy}}{\partial z} + S_{My} \tag{3-6}$$

$$\rho \frac{Dw}{Dt} = \frac{\partial \tau_{xz}}{\partial x} + \frac{\partial \tau_{yz}}{\partial y} + \frac{\partial(-p+\tau_{zz})}{\partial z} + S_{Mz} \quad (3\text{-}7)$$

3.3.3. Navier–Stokes Equations

In a Newtonian liquid, the viscous stresses are related to the ratios of deformation. Generally, Newtonian fluid is incompressible therefore, the viscous stresses are only double, to the linear deformation, times the dynamic viscosity local rate. The Navier–Stokes equations are as following:

$$\rho \frac{Du}{Dt} = -\frac{\partial p}{\partial x} + \frac{\partial}{\partial x}\left[2\mu \frac{\partial u}{\partial x} + \lambda\, div\, u\right] + \frac{\partial}{\partial y}\left[\mu\left(\frac{\partial u}{\partial y} + \frac{\partial v}{\partial x}\right)\right] + \frac{\partial}{\partial z}\left[\mu\left(\frac{\partial u}{\partial z} + \frac{\partial w}{\partial x}\right)\right] + S_{Mx} \quad (3\text{-}8)$$

$$\rho \frac{Dv}{Dt} = -\frac{\partial p}{\partial y} + \frac{\partial}{\partial x}\left[\mu\left(\frac{\partial u}{\partial y} + \frac{\partial v}{\partial x}\right)\right] + \frac{\partial}{\partial y}\left[2\mu \frac{\partial v}{\partial y} + \lambda\, div\, u\right] + \frac{\partial}{\partial z}\left[\mu\left(\frac{\partial v}{\partial z} + \frac{\partial w}{\partial y}\right)\right] + S_{My} \quad (3\text{-}9)$$

$$\rho \frac{Dw}{Dt} = -\frac{\partial p}{\partial z} + \frac{\partial}{\partial x}\left[\mu\left(\frac{\partial u}{\partial z} + \frac{\partial w}{\partial x}\right)\right] + \frac{\partial}{\partial y}\left[\mu\left(\frac{\partial v}{\partial z} + \frac{\partial w}{\partial y}\right)\right] + \frac{\partial}{\partial z}\left[2\mu \frac{\partial w}{\partial z} + \lambda\, div\, u\right] + S_{Mz} \quad (3\text{-}10)$$

Recently, CFD is being used to predict the performance of pumps [96]. In the present study, two types of numerical simulation were carried out in order to investigate the characteristics of the pump performance and visualise the flow field within a centrifugal pump. The first category was a numerical simulation under single-phase operating conditions. The second was to simulate cavitation under different operating conditions. In the former the flow was water and in the latter (cavitation model) the flow includes a two-phase mixture of water and vapour as the working fluid under transient analysis approach. In the next sections explanation will be given for the numerical research works that were carried out in this study to investigate the flow field behaviour and pump performance in both cases single-phase and cavitation conditions.

3.3.4. Geometry

CFD tool is commercially available and was utilised to investigate the three-dimensional turbulent fluid flow within a centrifugal pump under various operational conditions. Therefore, such code was extensively utilised by acknowledging satisfactory agreements between experimental and numerical results [6]. A numerical model of a pump in the present study was simulated with five impeller blades, the impeller was designed as a rotating part while the other parts of the geometry such as volute, inlet and outlet pipes were stationary as shown in Figure

3-2. All specifications of the centrifugal pump used in this investigation are summarised in Table 3-1. In order to simulate and mimic the 3-D centrifugal pump model in a real world scenario, the numerical model in this study was used the same specifications, dimensions, and geometrical parameters corresponding to the experimental model (F32/200AH from Pedrollo Company) in order to conduct, compare, and validate the numerical results with experimental results.

Table 3-1 Specifications of the centrifugal pump

Parameter	Value
Inlet diameter of the impeller	30mm
Outlet diameter of the impeller	215mm
Pump rotational speed	2755 rpm
Number of blades	5
Thickness of blade	4mm
Impeller type	Backward type
Length of the inlet pipe	1m
Length of the outlet pipe	1m
Inlet blade angle	17.09^{o}
Outlet blade angle	17.28^{o}

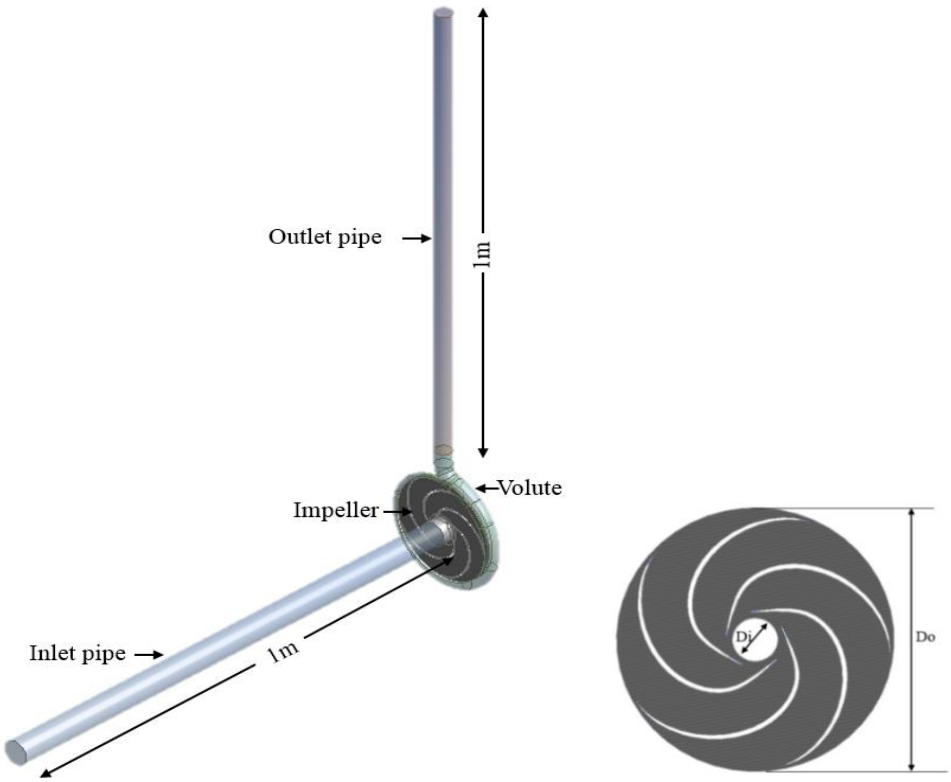

Figure 3-2: Geometry of the centrifugal pump model

3.3.5. Meshing of the Flow Domain

The flow domain needs to be spatially discretised into a number of small parts, each one called a mesh element, so that the fluid flow governing equations can be solved on them. This study uses an unstructured tetrahedral meshing within the flow domain because of excessive mixing and irregular geometric profile of the impeller and volute geometry. Moreover, in order to accurately capture the near-wall effects on the fluid flow, a dense mesh is generated in the near-wall regions of the flow domain. A mesh size of 1.6mm was specified for the impeller and the volute regions, while a mesh size of 3.5mm was used for the inlet and outlet sections. Mesh independence tests were carried out in order to find the optimal mesh sizing for accurate prediction of fluid flow within the domain, the details of which are presented in Chapter 5. The mesh elements within the impeller and the volute are shown in Figure 3-3.

3.3.6. Calculate the Dimensionless Wall Distance (y+)

In order to calculate y+ which is dimensionless value can use the following equations:

- **Friction Velocity**

It can be calculated using Eq. (3-11).

$$u^* = \sqrt{\frac{t_w}{\rho}} \tag{3-11}$$

Where t_w and ρ are represented the wall shear stress, and the fluid density.

- **Dimensionless Wall Distance y+**

The y+ value is calculated by using Eq. (3-12).

$$y^+ = \frac{u^* y}{v} \tag{3-12}$$

Where, v represents the kinematic viscosity of the liquid, y and u* are defined as the distance and the friction velocity to the nearest wall. It is generally acceptable in numerical simulation using CFD code that the turbulent flow is to be valid in the area where y+ equal 30 [97-99]. Therefore, the average value of y+ in this current study was around 30 for all centrifugal pump parts. Table 3-2 summarises the calculation of y+ for impeller under different flow rates. For more details, APPENDIX A represents all y+ calculation results for volute, inlet and outlet pipes.

Table 3-2 Calculation of y+ for impeller

No.	Flow rate	Density	Kinematic viscosity	Shear stress	u*	Y	y+
	(l/min)	(kg/m^3)	($m^2/s * 10^{-6}$)	(Pa)		(m)	
1	100	998.2	1.004	109.76	0.3315	0.000092	30.38
2	150	998.2	1.004	149.52	0.3870	0.000080	30.83
3	200	998.2	1.004	192.26	0.4388	0.000070	30.59
4	250	998.2	1.004	242.14	0.4925	0.000062	30.41
5	300	998.2	1.004	305.35	0.5530	0.000055	30.29
6	320	998.2	1.004	328.04	0.5732	0.000052	29.69

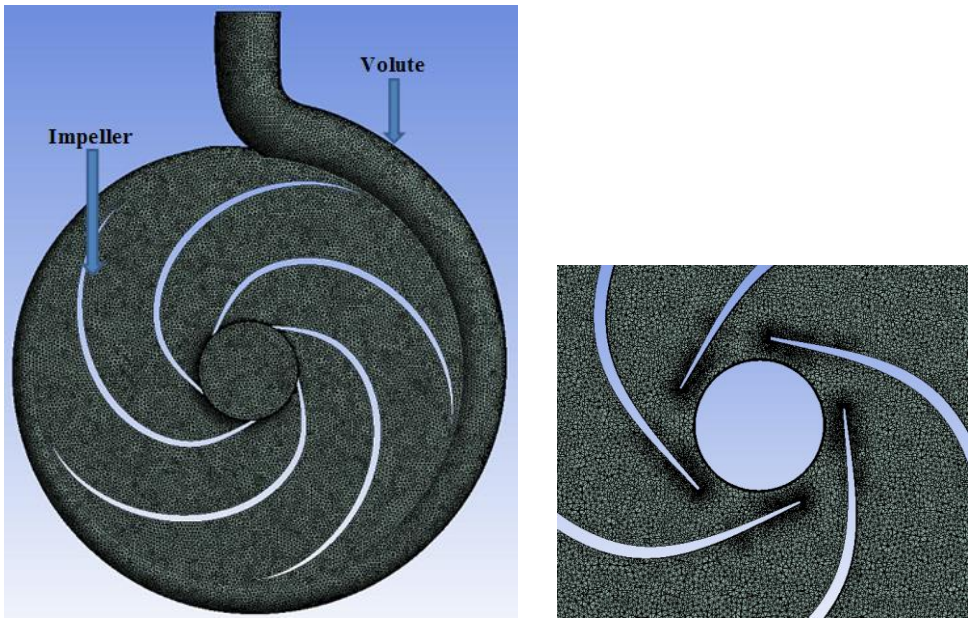

(a) (b)

Figure 3-3: (a) Mesh of the centrifugal pump (b) Mesh in the impeller

3.4. Solving Settings in CFD Code for the Centrifugal Pump

The following sections provide the solver settings details that were used in this study.

3.4.1. The Physical Models Selection

In this study, for the flow diagnostics, a pressure-based solver was selected due to the fact that the density of working fluid is water, remains constant. In addition, to obtain more accurate results from the numerical simulation a transient solver was chosen for the flow diagnostics of the pump. In order to provide accurate simulation results, it is essential to choose the turbulence model suitable for the simulation calculation as the turbulence model describes the Reynolds stresses distributions in the flow domains. This model is quite essential, as the flow fields within a centrifugal pump under different operation conditions are highly turbulent and

unsteady. Due to the complex separation and recirculation during the transient flow process, a reliable turbulence model selection is significant to simulate the performances more accurately. Therefore, in this study, the SST k-ω model was used in order to provide accurate results inside the centrifugal pump. The important reason behind selecting the k-ω model is due to this model being capable of capturing the extreme pressure gradients and the wake regions. In addition, this model can detect the variations in the flow parameters within a pump with reasonable accuracy.

3.4.2. Boundary Conditions under Single-Phase Conditions

In this study, sliding mesh was used to simulate the pump under single-phase conditions. The boundary conditions for the single-phase flow simulation are set at the inlet with different flows rates. The inlet velocity ranges from 0.85m/s to 3.1m/s, and outlet boundary condition is set as the outflow [100-102]. The experimental data for the centrifugal pump was obtained in the lab as detailed in Chapter 4, which was analysed in order to develop a performance prediction model for the pump. The centrifugal pump design condition parameters and water physical properties are summarised in Table 3-3.

Table 3-3 Design condition parameters and are material properties of the centrifugal pump

Design flow rate	Head	Rotational speed	Atmospheric Pressure	Fluid	Density	Kinematic viscosity
(l/min)	(m)	(rpm)	(Pa)	(-)	(kg/m^3)	($m^2/s *10^{-6}$)
300	38	2755	101325	Water	998.2	1.004

3.4.3. Sliding Mesh Technique

The sliding mesh must be used for an unsteady flow when a time accurate solution for a rotator and stator interaction is needed. The sliding mesh model is an accurate approach in simulating flows as compared to Moving Reference Frame (RMF). In the technique of sliding mesh, two or more zones of cells are manipulated. Each of these cell zones are bounded by at least one cell zone of interface meeting the opposing cell zone as shown in Figure 3-4. The interface regions of the nearest cell zones are linked with one another in order to create a mesh interface. The two cell regions move relatively to one another along the mesh interface. While, calculating the cell regions slide in relation to each other along the mesh interface in separate steps. As the flow is inherently unstable, a time-bounded solution procedure is required. The sliding mesh model permits adjacent meshes to slide in relation to each other [103].

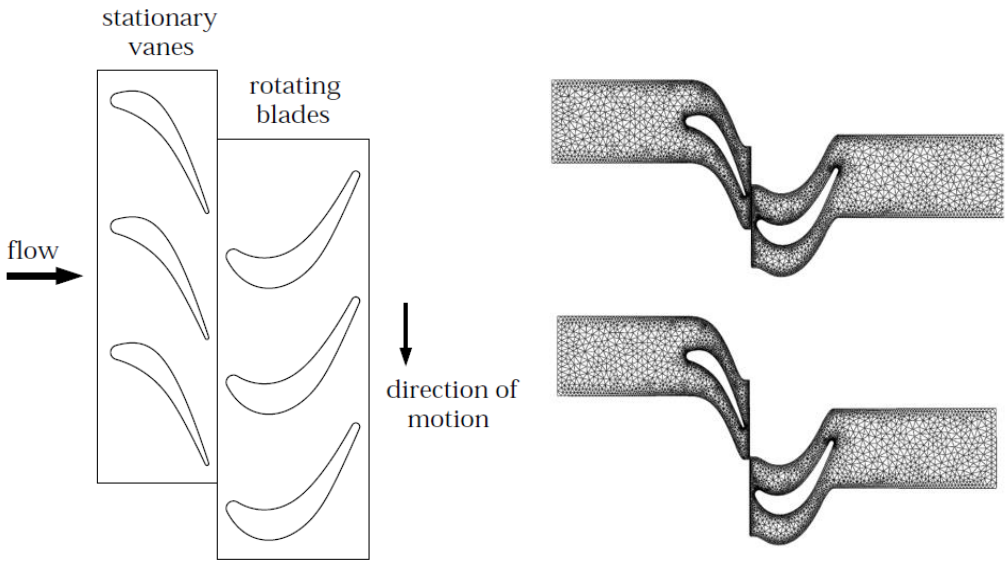

(a) (b)

Figure 3-4: (a) Interaction between rotor-stator, and (b) Slides of rotor mesh with respect to the stator [108]

Figure 3-5 depicts example of two-dimensional grid interface, it can be seen that the interface regions are composed of different faces include A-B, B-C, D-E and E-F. Hence, the intersection of these regions makes the faces a-d, d-b, and b-e. These faces produced in the area where the two cell regions overlap d-b, b-e, and e-c were grouped to form an interior region. Whereas, the remaining faces include a-d and c-f are paired up to form a periodic region [108].

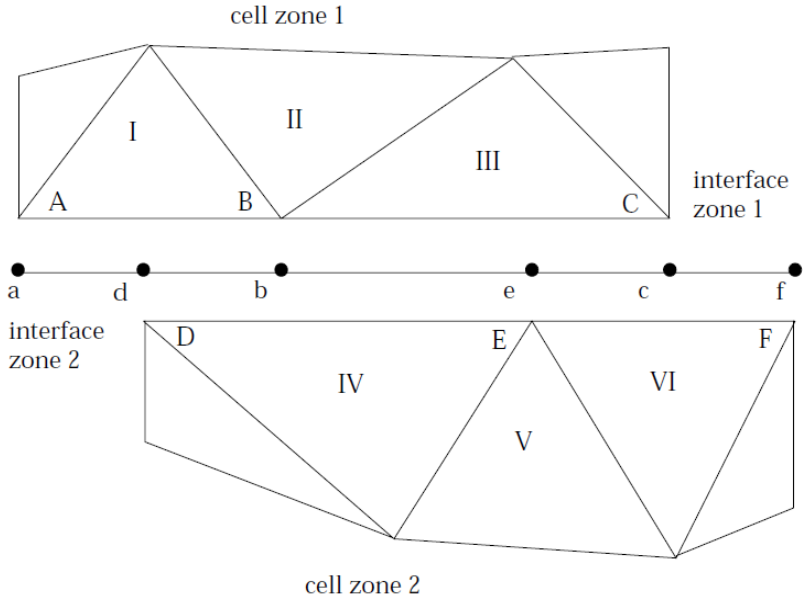

Figure 3-5: 2-D grid interface [108]

3.5. Solver Setting for the Single-Phase Conditions

The solver settings are necessary to precisely predict the behaviour of liquid flow in the flow domain. In the current study, for the single-phase flow the SIMPLE (Semi-Implicit Method for Pressure-Linked Equations) algorithm for pressure–velocity coupling was used. Due to the use of such algorithm provides faster converges as well as it more accurate for flows within and around different geometries [104]. SIMPLE algorithm implements the velocity and pressure corrections to attain the pressure field and the mass conservation. The momentum equations are recorded based on the pressure gradient collected from the previous iteration or an initial guess of pressure distribution profile to achieve velocity profile. If the initial pressure distribution does not satisfy the continuity equation, pressure and velocities are corrected until they satisfy the continuity equation [104]. A Green–Gauss Node based approach was adopted to compute the gradients. This approach solves a constrained minimisation problem to restructure the exact values of a linear function at a node from surrounding cell–centred values on arbitrary unstructured meshes while preserving a second-order spatial accuracy. In most of the CFD solvers, discrete values of the scalars are stored at the cell centres. However, for the convection term, face values are required. The face values are the result of the interpolation of cell centred values. An upwind spatial discretisation scheme is adopted for this interpolation because in this scheme, the face value is calculated from quantities in the cell upstream, or upwind relative to the direction of the normal velocity. To obtain better accuracy in pressure, momentum, turbulent kinetic energy and turbulent dissipation rate, 2^{nd} order upwind scheme were adopted [104]. In this thesis, Double Precision unsteady solver was used because it offers more precise results. For pressure, density, body force, momentum and energy, the under relaxation factor was set at 0.3, 1, 1, 0.7 and 1 respectively in order to obtain better converge from the numerical solution.

3.6. Interaction between the Impeller and Volute

The flow field within a centrifugal pump is highly complicated the relative rotation between volute and impeller causes unstable flow and hence leads to the generation of more pressure fluctuations and increased level of noise and vibration. As a result, that leads to a decrease in a pump life due to fatigue which in-turn affects the pump performance [105]. However, the knowledge regarding analysis of transient pressure fluctuations in both time and frequency domains due to interactions between the impeller and volute under different operating conditions and various geometrical parameters are still not conclusive and need more

investigation. Therefore, to achieve this knowledge in this study, numerical technique by CFD code was used in order to study the effect of interactions. Further detailed information regarding this interaction between the impeller and volute will be provided in Chapter five.

In order to investigate the occurrence of cavitation within the centrifugal pump, it is necessary to calculate the performance under single-phase first and then taking these results as the basis for the initial conditions of cavitation calculation. Therefore, a detailed discussion of suitable solver settings and boundary conditions is presented in this next section under cavitation conditions.

3.7. Cavitation Model in the Centrifugal Pump

Information regarding cavitation model is provided in this section as it was used in CFD code. Such cavitation model is useful to simulate and mimic cavitation influences in two-phase flows when a mixture model is employed [106].

3.7.1. The Overview Regarding the Cavitation in CFD

The fluid at constant temperature is subjected to a decline in pressure, which might fall under the saturated vapour pressure. Such reduction in pressure initiates the process of vaporisation of liquid at constant temperature, which is named as cavitation. Additionally, the fluid contains dissolved or ingested micro bubbles of non-condensable gases, which might grow and lead to form cavities under reducing pressure. In this study, the implementation of cavitation is based on what is called cavitation model, which represents the second-order effects (e.g. bubble dynamics phase change, non-condensable gases, turbulent and pressure fluctuations). What distinguishes such a model is its ability to represent multiphase N-phase flows, multiphase type transport flows, the impact of slip velocities between the fluid and vapour phases, as well as thermal impacts and compressibility of fluid and vapour phases [106].

3.7.2. Cavitation Model

The characteristics of the two-phase cavitation model are:

- The cavitation model under investigation includes merely two phases and these phases are liquid-water and water-vapour.
- The model takes into consideration bubble formation (evaporation) and the collapse of bubbles (condensation).

Such cavitation model provides the following abilities:

- The cavitation model represents the mass transfer between the liquid-water and water-vapour.
- It is well-matched with most available turbulence models in FLUENT.
- It is applicable to be solved with the mixture energy equation.
- It can be used with both sliding mesh and non-conformal interfaces.
- It can be used with both incompressible and compressible fluid or vapour phases under the assumption that the non-condensable gases are always compressible.
- The usage of mass transfer model parameters for cavitation (e.g. liquid surface tension coefficient, vaporisation pressure) could be either constant or a function of temperature [106].

3.7.3. Schnerr and Sauer Model

The Schnerr-Sauer model is used to predict cavitation flow in many applications such as propellers, hydrofoils, and pumps, and it can be used in the centrifugal pump in order to detect cavitation where the Schnerr-Sauer model is defined as [107]:

$$R_c = 3\frac{\rho_v \rho_l \propto_v}{\rho}\frac{(1-\propto_v)}{R_B}\sqrt{\frac{2\,p_v - p}{3p_l}} \qquad P < P_v \tag{3-13}$$

$$R_c = 3\frac{\rho_v \rho_l \propto_v}{\rho}\frac{(1-\propto_v)}{R_B}\sqrt{\frac{2\,p_v - p}{3p_l}} \qquad P > P_v \tag{3-14}$$

Where, R_c is the mass transfer rate, ρ, ρ_v, ρ_l are denoted the fluid density, vapour and liquid fluid density respectively. $\propto v$ represents the vapour volume fraction. R_B represents bubbles radius which can be calculated by using the equation:

$$R_B = \left[\frac{3\propto_v}{4\pi N1(1-\propto_v)}\right]^{1/3} \tag{3-15}$$

Where, p_v, p_l are represented vapour and liquid pressures, and N1 is the number of vapour bubbles per unit volume of fluid.

3.7.4. Solver Settings for the Cavitation Model

In this study, the simulation was conducted using the Coupled algorithm for the pressure-velocity coupling. Furthermore, the following schemes are utilised:

The coupled solver is chosen in order to solve the momentum equations that could lead to faster convergence and a more robust calculation [108, 109]. The coupled solver is used to simulate the cavitation flows especially in rotating machineries such as pumps, turbines impellers and inducers [108]. In order to correct the pressure between iterations, the PRESTO scheme is utilised [110]. The PRESTO can be used when the flows have highly swirling, including steep pressure gradients and the flow domains have curved boundaries such as pumps, fans, and turbines [111]. For momentum, density, turbulent dissipation rate and turbulent kinetic energy, second order upwind schemes were used as the second order upwind provides a more accurate calculation compared to the first order upwind.

3.7.5. Relaxation Factors

Generally, small relaxation factors are recommended to be used for momentum equations ranging from 0.05 to 0.4. In addition, the pressure-correction equation should have a relaxation factor ranging from 0.2 to 0.7. Furthermore, the vaporisation mass and density (e.g. source term in the vapour equation) can be relaxed in order to enhance convergence. Usually, the density relaxation factor ranges from 0.3 to 1.0 value, while that of the vaporisation mass may be appropriately set between 0.1 and 1.0 [106].

3.8. Prediction of Cavitation in the Centrifugal Pump Using CFD

A 3-D computational model of the centrifugal pump was used in CFD code. Because of the high geometric complexity of the pump, the unstructured grid cells are generated to define the geometry as mentioned earlier. A sliding mesh is applied to consider the interaction of an impeller and volute. The SST k-ω model, coupled algorithm and multiphase mixture were selected in FLUENT, in this study the convergence precision of residuals is set to be 10^{-6}. The head and NPSH of a centrifugal pump can be found in the next equations [112]:

$$H = \frac{Po - Pi}{\rho g} \tag{3-16}$$

$$NPSH = \frac{P - Pv}{\rho g} \tag{3-17}$$

Where Pi, Po are the total inlet and outlet pressure, ρ is the fluid density, g is the gravitational acceleration, and Pv is the vapour pressure.

3.8.1. The Performance of Cavitation in Centrifugal Pumps

In order to investigate cavitation in pumps, it is necessary to calculate the performance under single-phase first, and then taking the results as the basis for the initial conditions of cavitation calculation [116-118].

3.8.2. Boundary Conditions for the Cavitation Model

1. The boundary condition at the inlet is velocity.
2. The outlet is the static pressure to obtain the pressure distribution and the volume fraction of gas liquid phase [119].

3.9. Convergence Criteria

It is critical to take into consideration the convergence criterion factor. The convergence criterion for the continuity in three dimensions was taken as 10^{-6} in order to obtain more accurate results.

After describing the numerical simulation model based on both single-phase and cavitating model conditions for the centrifugal pump in the above sections, the next chapter will describe the design and construction of the centrifugal pump experimental setup including all parts, sensors, and equipment.

CHAPTER 4

EXPERIMENTAL SETUP

This chapter explains design and construction of the centrifugal pump test rig and associated experimental setup. In addition, it provides detailed information about the entire experimental equipment such as piping system and descriptions of all the sensors that were used in this study such as pressure transducers, accelerometer, microphone, flow metres, and data acquisition system. It also describes the procedure for the measurement system in order to monitor and detect cavitation in the pump. This chapter also provides a brief explanation regarding to the techniques that were used in order to detect cavitation such as vibration and acoustic techniques in both time and frequency domains. Furthermore, it includes the uncertainty analysis and calibration procedure for different sensors.

4.1. The Experimental Setup for the Centrifugal Pump

The main aims of the present study are to determine the pump performance and detect cavitation in the centrifugal pump numerically and experimentally. CFD code, which was already explained in Chapter 3, will be used to analyse the pump performance and the detection of cavitation as will be detailed later in Chapter 5. The detection of cavitation experimentally was carried out by using different sensors such as accelerometer, microphone and pressure transducers at suction and discharge of the pump. To achieve these aims experimentally, it was essential to construct and design an appropriate experimental setup for the centrifugal pump. The designing of this experimental setup will be discussed in more details in the next section.

Figure 4-1 and Figure 4-2 depict the different parts and dimensions for the flow loop system of the centrifugal pump, and Table 4-1 provides the flow loop components and equipment. The centrifugal pump can supply water to the tank with a maximum pressure of about 10bar. The selected flow loop system was re-circulatory and included a plastic water tank, PVC clear pipes and PVC connections components. The inlet pipe diameter of the pump was 2 inches. Also, the outlet pipe diameter of the pump used was 1.25 inches. Thus, a reducing coupling of 1.25 to 1.5 inches was used to connect the outlet pipe to the water flow meter line. The tank was made of plastic with dimensions of 95×90×110cm. All pipes were transparent pipes as shown in Figure 4-3, the reason behind that is to permit observation when the cavitation occurs. The connections of the flow loop of the centrifugal pump and the water tank are made through use of various sizes of PVC pipes. APPENDIX B provides more details of piping system components.

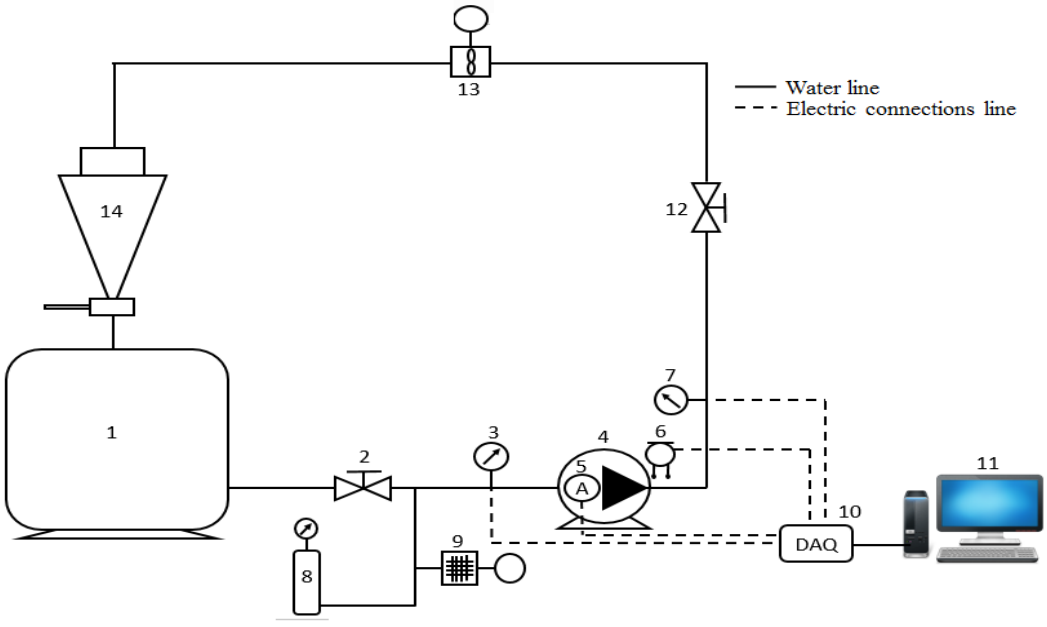

1- Water tank
2- Suction valve
3- Suction pressure transducer
4- Centrifugal pump
5- Accelerometer sensor
6- Microphone sensor
7- Discharge pressure transducer
8- Air supply
9- Air flow meter
10- Data acquisition system
11- PC
12- Discharge valve
13- Water flow meter
14- Hopper

Figure 4-1: Components of Experimental setup for flow loop system

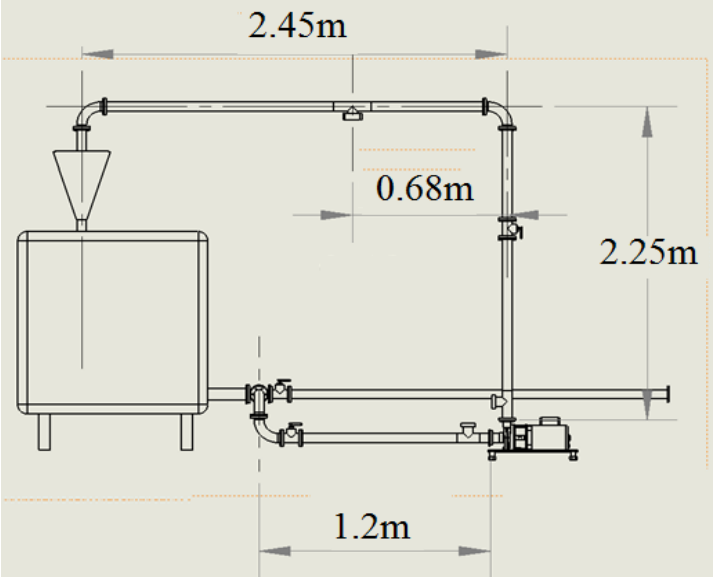

Figure 4-2: Dimensions of the flow loop system

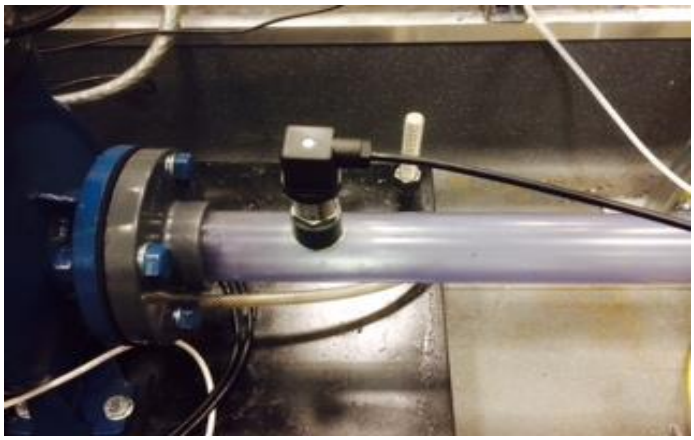

Figure 4-3: The transparent pipe

Table 4-1 Experimental setup components

No.	Components	Quantity	Notice
1	Centrifugal pump	1	

2	Water flow meter	1	Discharge pipe of the pump
3	Low pressure transducer	1	Suction pipe 0-5 bar
4	High pressure transducer	1	Discharge pipe of Pump 10 bar
5	Accelerometer	1	Attached with outlet volute of the pump
6	Acoustic microphone	1	Near the outlet volute of the pump
7	Speed controller	1	To control the pump rotational speed
8	Power supply	1	20 volt for two pressure transducers at suction and discharge sides of the pump
9	Air flow meter	1	Suction pipe
10	Thermometer	1	To measure water temperature
11	Hopper	1	To calibrate the water flow meter
12	Data Acquisition	1	To collect different data from different sensors
13	PC	1	To collect, save, and analysis data from different sensors

4.1.1. Procedure on how Measurement are Taking within the Experimental Setup

It would be essential to measure the following system parameters in the experimental setup of the centrifugal pump:

- Measurement of the inlet water temperature using thermometer.
- Measurement of the water flow rate using a TM150 from GPI 1½ inch flow meter.
- Measure water pressure signals at inlet and outlet using IMP-Industrial Pressure Transmitter types IMP-G5000-6A4-BCV-03-000 for 5bar and IMP-G1002-7A4-BCV-03-000 for 10bar.
- Measurement of the air flow using an air flow meter type mass flow meter FMA 1700/1800 series from OMEGA Engineering INC.
- Measure vibration signal in the pump using the accelerometers type IEPE (small size, high sensitivity) model CA-YD-1182 position at the outlet volute near tongue region.
- Measure the acoustic signal using a free-field accurate microphone model CHZ-223 and ICP microphone preamplifier model YG-201 position at approximately 50mm from the outlet of the centrifugal pump. APPENDIX B provides more details of the procedure for operating the flow loop system.

4.1.2. Construction of the Experimental Setup

The experimental setup in this research study was particularly designed and built in order to study the detection of cavitation within a centrifugal pump. It was built at the fluid laboratory inside the Technology Building at the University of Huddersfield and this process took ten months to be completed. Typically, an experimental setup should be capable of operating and

monitoring the cavitation phenomenon in the centrifugal pump through the use of different monitoring techniques. So, various kind of sensors are incorporated for measuring various parameters; for example, water temperature, water flow rate, air flow rate, vibration signal, acoustic signal, and pressure at inlet and outlet pipes. All of these parameters are useful to detect and diagnose cavitation in the pump. The experimental setup in this study was appropriately conducted using different test measurements under various ranges of operating conditions. This specific pump setup was chosen amongst other setups that were widely used for industrial applications in the detection of cavitation. Selecting the proper size and correct type of the pump can considered as a fundamental procedure in determining the experimental setup. This is because the pressure and capacity of the pump determines the specified requirement for all other components in the setup such as pipes, tank, flow meter, and pressure transducers. Another significant factor in selecting the pump is the size of the design space in constructing the experimental setup. In this work, the design and construction of the experimental setup was classified into four important steps. The first step includes the design of the flow loop of the pumping system. The second step identifies all requirements such as the installation of the entire piping system and parts needed for the experimental setup. The third step is identifying what is needed in the loop such as installation of all sensors including the water flow meter, airflow rate, pressure transducers, accelerometer, microphone and other equipment. The fourth step is to connect all sensors with data acquisition system and PC. Figure 4-1 above depicts the schematic diagram of the experimental setup used in present investigation.

4.1.3. Centrifugal Pump

Figure 4-4 depicts the centrifugal pump that was applied in this experimental work. The made of the applied pump is the F32/200AH series standardised centrifugal pump from Pedrollo Company. This type of pump consists of a single stage and closed type impeller. It is powered by a 4kW, 5.5HP, 3-phase driven motor. The current is 8.9A and voltage ranges between 380 to 400V. The design parameters for this pump are flow rate of up to 380(l/min), head of about 46m at the designed flow rate, five impeller blades and design rotational speed of 2900rpm. APPENDIX B summarises the overall dimensions such as positions and sizes of the suction and discharge parts and other dimensional characteristics that comply with such standards. It is recommended from manufacturer’s data sheet to use clean water for the pump in order to avoid any chemical damage to the pump parts. Therefore, the design of such pump allows

simpler dismantling without disconnecting the pump body from the pipeline, which has made it very suitable for experimental work in case any change to the motor, impeller, or bearings is required. Table 4-2 summarises the technical specifications of Pedrollo F32/200AH pump and motor.

Figure 4-4: Centrifugal pump type F32/200AH

Table 4-2 Technical specifications of Pedrollo F32/200AH centrifugal pump [120]

Pump Manufacturer	Pedrollo
Type of the Centrifugal pump	F32/200AH
Head	44 –55m
Capacity	6–30m^3/h
Rotational speed	2900rpm
Number of blades	5 blades
Maximum pressure	10bar
Type of impeller	Closed, brass
Number of impeller stages	Single
Power supply	4kW
Frequency	50Hz
Maximum current	8.9A
Maximum voltage	400V

4.2. Types of Sensors for Monitoring Systems

Generally, sensors are regarded as important parts of a measurement system. The core functions of the sensors are to obtain a physical parameter as well as transform it into a signal that can be collected using the acquisition system. Usually, different types of sensors can be used for measuring and detecting the physical parameters in order to monitor machine condition, for

example, temperature, noise, vibration, current and speed signals [121]. In the next sections all sensors will be described.

4.2.1. Vibration Sensor

Commonly, vibration is the widely utilised parameter in the condition monitoring of rotating systems such as pumps, turbines and compressors.

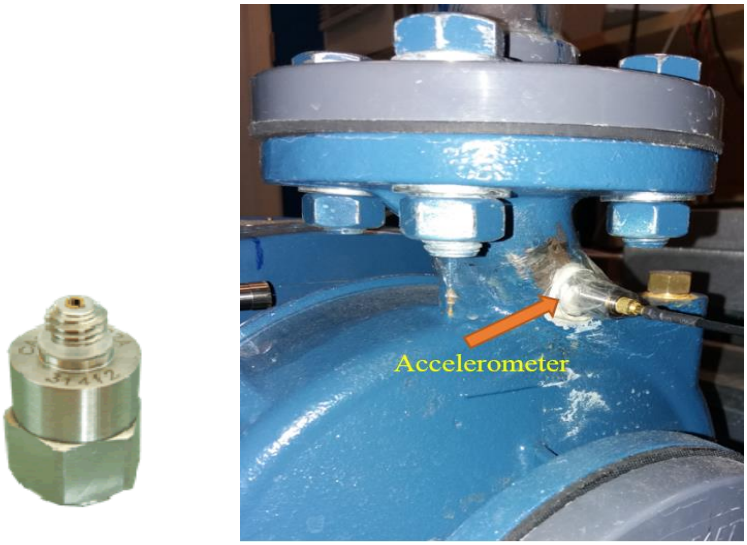

Figure 4-5: Accelerometer and its location on the centrifugal pump

As mentioned in Chapter one, the cavitation process in the pump includes the start of formation and collapse of huge bubbles. As a result of the bubbles collapsing this generates vibration in the pump. Therefore, the vibration within the pump provides a good indication of the occurrence of cavitation. Consequently, cavitation could be predicted and diagnosed by monitoring vibration signals through the use of an appropriate sensor such as accelerometers. In this current study the accelerometer type IEPE model CA-YD-1182 was used at the outlet volute near tongue region as depicted in Figure 4-5. The accelerometer range of frequency is between 0Hz to 15kHz and the operation temperatures range between -40 and +120°C. Table 4-3 summarises all the accelerometer specifications.

Table 4-3 Specifications of the accelerometer sensor [122]

Vibration accelerometer sensor	
Axial sensor sensitivity (20±5°C)	100mV/g
Measurement sensor range (peak)	50g
Transverse of the sensor sensitivity	≤5 %
Frequency response range (0.5dB)	0.5 to 15,000 Hz
Mounting frequency resonance	40,000 Hz
Polarity	Positive

Range of the operating temp.	-40 to +120 °C
Shock of the sensor limit (±peak)	3,000g
Operating accelerometer current	+2 to +10 mA (typical 4mA)
Output accelerometer signal	≤6V
Noise (1 to 20kHz)	＜0.5 mg
Base strain accelerometer sensitivity	0.2mg/με
Magnetic sensitivity	1.5g/T
Thermal transient of the sensor sensitivity	10mg/°C
Output accelerometer impedance	＜100 Ω
Weight	9g

4.2.2. Microphone (Acoustic Sensor)

In Chapter one of this thesis, it was explained that as cavitation occurs in pumps, the noise level increases. Therefore, in this study a microphone was used in order to monitor and obtain more information regarding the cavitation. A free-field accurate microphone model CHZ-223 is employed for gaining the acoustic signal. It is obvious that the location of the microphone is very important to record the best acoustic signals. Therefore, in this study, several tests were carried out to ascertain the optimum microphone position. Hence, it was found that the best position needs to be about 50mm in distance from the outlet of the pump to the mounted microphone as depicted in Figure 4-8, the diameter of the microphone is 12.7mm (0.50inch), sensitivity 250Hz 31.6mV/Pa, the operating temperature between -10ºC and +50ºC. Table 4-4 summarises the technical specification of the microphone that was utilised on the experimental setup of the centrifugal pump.

Table 4-4 Specifications of the microphone sensor [123]

Acoustic microphone sensor	
Microphone diameter	12.7mm (0.50”) without grid ;13.2mm (0.52”) with grid
Height	16.0mm (0.63”) without grid ; 17.2mm (0.68”) with grid;
Weight of microphone	9g
Case	material MONEL
Mounting to amplifier	11.7 mm – 60UNS
Sensing element	Electret condenser
Sensitivity	(250Hz） 31.6mV/Pa (at 250Hz,open-circuit,–30dB±2dB ref.1 V/Pa)
Range of frequency	20Hz to 20kHz
Dynamic range	>140dB SPL within 3% distortion
Thermal noise	<20.0dB
Temperature coefficient-0.01dB within the range	-10ºC and +50ºC

Figure 4-6: Microphone

4.2.3. Microphone Pre-amplifier YG-201

The second most important part of the microphone is the preamplifier (type YG-201 ICP). Microphone preamplifier helps to condition the output signal. This simple pre-amplifier can be seen in Figure 4-7. The operating temperature range of this pre-amplifier is between -40°C and +85°C, the power requirements is between 2 to 20mA with nominal power of 4mA, connector type is the BNC connector and has a dimension of 12.7mm (1/2")×70mm (including the connector). Table 4-5 summarises the specifications of the YG-201 ICP Microphone Preamplifier.

Figure 4-7: Microphone Preamplifier

Table 4-5 Specifications of the YG-201 ICP microphone preamplifier [124]

Microphone preamplifier	
Frequency Response of the preamplifier (ref. 250Hz)	16Hz to 100 kHz, ±0.5dB
Nominal attenuation	-0.3dB
Input impedance	2GΩ, <0.4pF
Output impedance	100Ω
Maximum output voltage	5.0Vrms(Corresponding to 134dB SPL (Sound Pressure Level) for microphone sensitivity of 50mV/Pa)
Noise	<5.0μV A-weighting <15.0μV Lin., 22.4Hz - 22.4 kHz
Power supply requirements	ICP supply, 2 to 20mA. Nominal 4mA
Type of connector	Connector type BNC
Dimensions	12.7mm (1/2") × 70mm (including connector)

Preamplifier mounting Thread	11.7mm -60UNS (for standard 1/2 inch microphones)
Range of operating temperature	-40°C to +85°C
Humidity range	0 to 98%RH

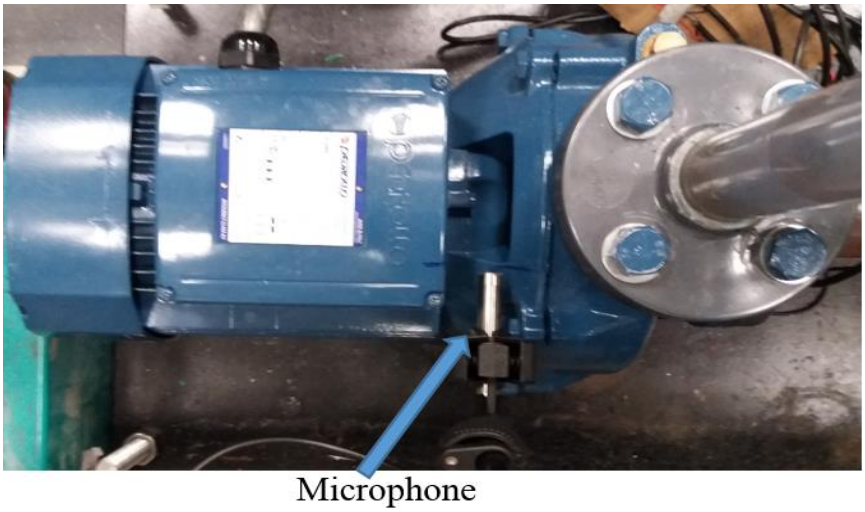

Figure 4-8: Microphone and its location on the centrifugal pump

4.2.4. Pressure Transducers

As already described in Chapter one, the impeller of the pump applies a force on the liquid being pumped. At the pump inlet, the level of pressure has an important influence on the performance of the pump. Cavitation occurs in the pump when the pressure at the inlet of the pump, which is named as the net positive suction head available NPSHA, is equivalent to or below the vapour pressure of a fluid. Therefore, monitoring of pressure at the pump inlet and outlet is regarded as another significant method of detecting and monitoring cavitation. Thus, pressure sensors are installed at the inlet and the outlet pipes of the pump to measure pressure signals. In this study, measuring the maximum pressure at the discharge pipe was carried out by the pressure transducer made by Impress Control (model number IMP-G5000-6A4-BCV-03-000). The pressure range on this transducer is between 0 to 10bar. To measure the low-pressure at the suction pipe, another pressure transducer was used, also from Impress Control (model number IMP-G1002-7A4-BCV-03-000), having different pressure range from 0 to 5bar. The operating temperature for both transducers is between -20 to +80°C with accuracy of less than ±0.25%, with supply voltage of between 9-32V DC. The pressure transducers are chosen according to the estimate of the predicted pressure in the experimental setup. According to the manufacturer's guidelines, the pressure of water in a pumping system ranges from 0 to 5bar also the pump's maximum operating pressure is 10bar. Figure 4-9 shows the pressure transducers used in this study. Table 4-6 and Table 4-7 summarise the technical specifications

for both pressure transducers. In order to calculate the head across the pump in this experimental work, two pressure transducers were used. Both pressure transducers were positioned two diameters (2D) downstream of the inlet pipe and inlet flange of the pump, and two diameters (2D) upstream of the outlet pipe from outlet flange of the pump [2].

Table 4-6 Specifications of the suction pipe pressure transducer [125]

Manufacture	IMP - Industrial Pressure Transmitter
Type	IMP-G5000-6A4-BCV-03-000
datum of pressure	Gauge
Range of pressure	0 - 5 Bar
Output signal	0 - 5V / 4-wire
Accuracy of the transducer (Combined NL&H)	<±0.25% / FS (Full Scale)
Accuracy of the transducer (Thermal Zero Shift)	<±0.04% / FS / °C
Type of connection	Large Plug & Socket (GDM3009, DIN43650)
Process connection	1/4" NPT (National Pipe Thread Taper) male
O Ring material	Viton
Length of cable	3metre (industrial PVC)
Specials Code	No special requirements
Diaphragm material	Aluminium oxide 96% (Ceramic Al2O3)
Process connection material	Process connection material
Range of temperature	-20 to +135°C
Operating temperature	-20 to +80°C
Voltage supply	9 - 32V dc

(A) (B)

Figure 4-9: Pressure transducers at (A) Pump inlet (0-10bar), and (B) Outlet (0-5bar)

Table 4-7 Specifications of the discharge pipe pressure transducer [125]

Manufacture	IMP - Industrial Pressure Transmitter
Type	IMP-G1002-7A4-BCV-03-000
Datum of pressure	Gauge
Range of pressure	0 - 10 Bar
Output	0 - 5V / 4-wire
Accuracy of the transducer	<±0.25% / FS

(Combined NL&H)	
Accuracy of the transducer (Thermal Zero Shift)	<±0.04% / FS / °C
Type of connection	Large Plug & Socket (GDM3009, DIN43650)
Process connection	1/4" NPT (National Pipe Thread Taper) male
O Ring material	Viton
Length of Cable	3metre (industrial PVC)
Specials code	No Special Requirements
Diaphragm material	Aluminium oxide 96% (Ceramic Al2O3)
Process connection material	Process connection material
Range of temperature	-20 to +135°C
Operating temperature	-20 to +80°C
Voltage supply	9 - 32V dc

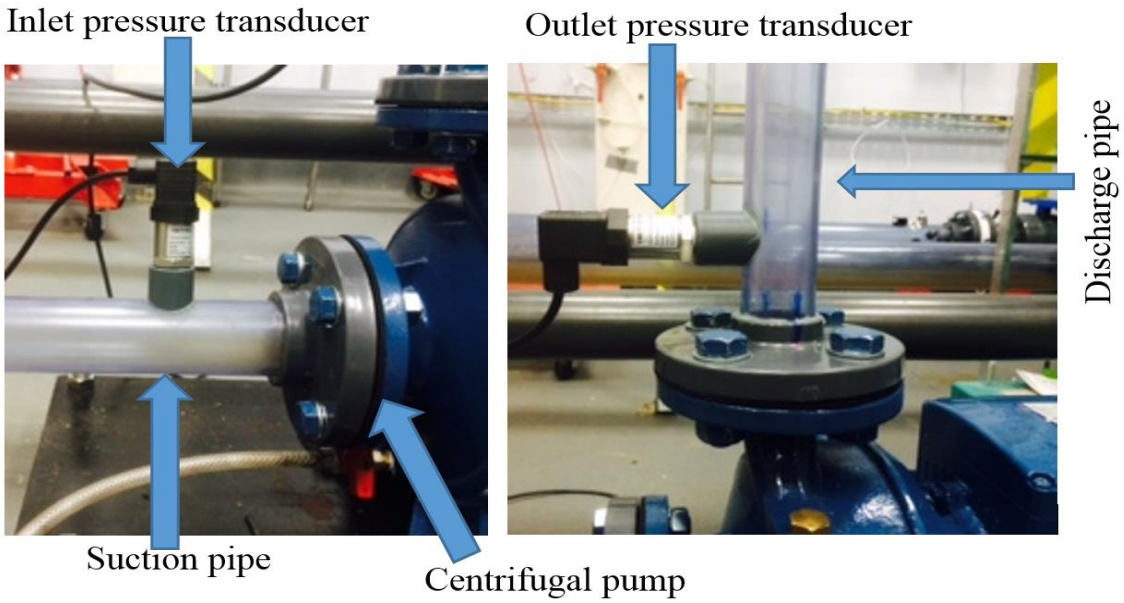

Figure 4-10: Pressure transducers and their location at the pump inlet and outlet

4.2.5. Water Flow Meter

The flow rate at which fluid is moved or pushed by the pump to the desired point is defined as the pump capacity. According to some previous studies [84, 88] the flow rate is influenced by cavitation. Therefore, it is essential to monitor flow rate on the centrifugal pump experimental setup. However, in this study, the water flow meter model chosen is the TM150 from GPI. The 1 ½ inch TM series water flow meter as shown in Figure 4-11. Moreover, Table 4-8 summarises the technical specification details of this flow meter. According to the manufacturer's guidelines, the flow meter was installed 5D downstream of the inlet flow pipe diameter and 10D upstream of the outlet flow pipe diameter, in order to make sure that the flow inside the pipe was fully developed [126].

Figure 4-11: Water flow meter

Table 4-8 Specifications of the water flow meter [127]

Flow meter manufacturer	GPI
Type of Flow meter	TM150, 1 ½ in
Type of Fitting	Schedule 80 Spigot (pipe) end 1 ½ in.
Accuracy of the flow meter	±3.0 % of reading
Range of flow rate	10 to 100 GPM 38 to 380 LPM
Operating temperature	+32 to +140 ºF 0 to +60 ºC
Powered supply	5 Year Lithium battery
Display reading	LCD 6 digits
Reads	Gallons litres
Electronic choice	Computer (Local) Rate of Flow, Field Calibration, Batch, and Cumulative Total options
Rating of pressure	225 PSIG 15.3 bar at 73º F / 23º C

4.2.6. Air Flow Meter

This experimental work also makes use of an air flow meter, which is a mass flow meter type FMA 1700/1800 series from OMEGA Engineering INC as shown in Figure 4-12. This mass flow meter measures the amount of air injection through the suction side of the centrifugal pump. It works under an ambient temperature of between 0 and 50°C, and the transducer power of about 12 VDC. All specifications of this flow meter are summarised in Table 4-9.

Figure 4-12: Air flow meter

Table 4-9 Specifications of the FMA air flow meter [128]

Air flow meter	
Accuracy	±1.5% of full scale
Pressure coefficient	0.01% of full scale per psi (0.07 bar)
Response time	800 msec time constant; 2 seconds (typical) to within ±2% of set flow rate over 25 to 100% of full scale
Power supply requirements	12 to 26 Vdc power @200 mA maximum
Maximum pressure gas	1000 psig (70 kg/cm² gauge)
Ambient and gas Temperature	0 to 50°C
Materials in fluid contact	Aluminium models: Anodized aluminium, 316 SS, brass and FKM O-rings Stainless Steel models: 316 SS and FKM O-rings
Output air flow meter signal	Linear 0 to 5 Vdc: 1000 Ω minimum load 4 to 20 mA: 50 to 250 Ω loop resistance
Power of the transducer	12 Vdc @ 200 mA maximum
Weight of air flow meter	1.1 kg

4.2.7. Power Supply

This experimental test was used power supply type (Rapid 10A 0-30V Triple Output Digital DC Regulated) from PROTO-PIC as shown in Figure 4-13 in order to power the two pressure transducers. The input voltage for the power supply is 230V AC 50Hz and the output voltage varying from 0-30V DC with a rated output current 10A. Table 4-10 summarises the specifications of this power supply.

Figure 4-13: Power supply

Table 4-10 Specifications of the power supply [129]

Manufacture	PROTO-PIC Company
Input supply voltage	230V AC 50Hz
Output voltage supply variable	0-30V DC
Output current rated	10A
Output voltage 1	5V DC 500mA (max. 1A)
Output voltage 2	12V DC 500mA (max. 1A)
Noise and ripple	5mV
Load regulation	30mV
Line regulation	10mV
Cooling systems	Thermostatically
Power supply dimensions	205 x 125 x 280mm
Weight of the power supply	6.5kg

4.2.8. Thermometer

A dual channel temperature type K thermocouple with backlight LCD thermometer was used in this experimental work as shown in Figure 4-14 in order to measure the water temperature and hence to calculate the water vapour pressure via this water temperature from tables of water properties. This thermometer consists of two main parts, the first being the temperature sensor (thermocouple) type (K) and the second part is LCD screen.

Figure 4-14: Thermometer

4.2.9. Data Acquisition System

The main aim in using the data acquisition system was to record and collect the signals from all of sensors that are used, including an analogue device and signal conditioning units. This DAQ system displays all of the different types of signals from the sensors/transducers on the PC screen or an oscilloscope in the form of values and curve plots. Figure 4-16 depicts the schematic diagram to connect all sensors with data acquisition system used for this current study. The type of data acquisition used in this study is Voltage/IEPE (Integrated Electronics Piezo Electric) data acquisition system (USB 2.0) YE6232-16 channels, from Global Sensor Technology (GST), which was made by Sinocera as shown in Figure 4-15. It was used to capture the voltage signals from different sensors and then transfer these signals to digital signals.

Each sensor, such as pressure transducers at inlet and outlet pipes, is connected to a power supply between 0 and 30 volts. They are then connected to the data acquisition system by coaxial BNC cables which then connects to PC through a USB port. The accelerometer and microphone with preamplifier are connected directly to the same data acquisition system by coaxial BNC cables and connect to a PC through a USB port. Figure 4-15 shows the data acquisition system. The output data collected from the different sensor such as an accelerometer, microphone and pressure transducers are then fed into this data acquisition system. The sampled frequency of this particular data acquisition was set at 96kHz which collected data being fed and saved it on the PC for analysis in time and frequency domain. The technical specifications for the voltage/IEPE data acquisition system include IEPE power supply of 4mA/+24VDC. DC signal frequency range of 30kHz (-3dB±1dB). DAQ accuracy of

±0.5%, sample rate of 96kHz, operating temperature is between 0 and 50°C. Humidity of between 20 and 80% RH, and power supply AC of 220V/50Hz as shown in Table 4-11.

Figure 4-15: Voltage/IEPE data acquisition system

Table 4-11 Technical specifications for voltage / IEPE data acquisition system

Manufacture	Global Sensor Technology (GST) which was made by Sinocera Company
Channels	16/32(Selectable)
A/D bits	24bit (Σ-Δ)
Input DAQ Mode	V/IEPE (Integrated Electronics Piezo Electric)/TEDS (Transducer Electronic Data Sheet)
Power Supply	4mA/+24VDC
Range of the signal input	≤±10VP
Range of the signal frequency	DC-30kHz (-3dB±1dB)
Filter	Independent Anti-filtering
Accuracy of the DAQ	±0.5%
Maximum sample rate	96kHz/CH, Parallel
Type of interface	USB2.0
Modes of trigger	Signal trigger; external trigger
Operating temperature	0 to 50°C;
Range of Humidity	20 to 80% RH
Dimensions of the DAQ (mm)	426W×88H×300D
Weight of the DAQ	4Kg
Power supply	AC220V50Hz/110V60Hz
Type of software	YE7600 Software used for general test and analysis
Cable	interface cable, Input cable, and power cable

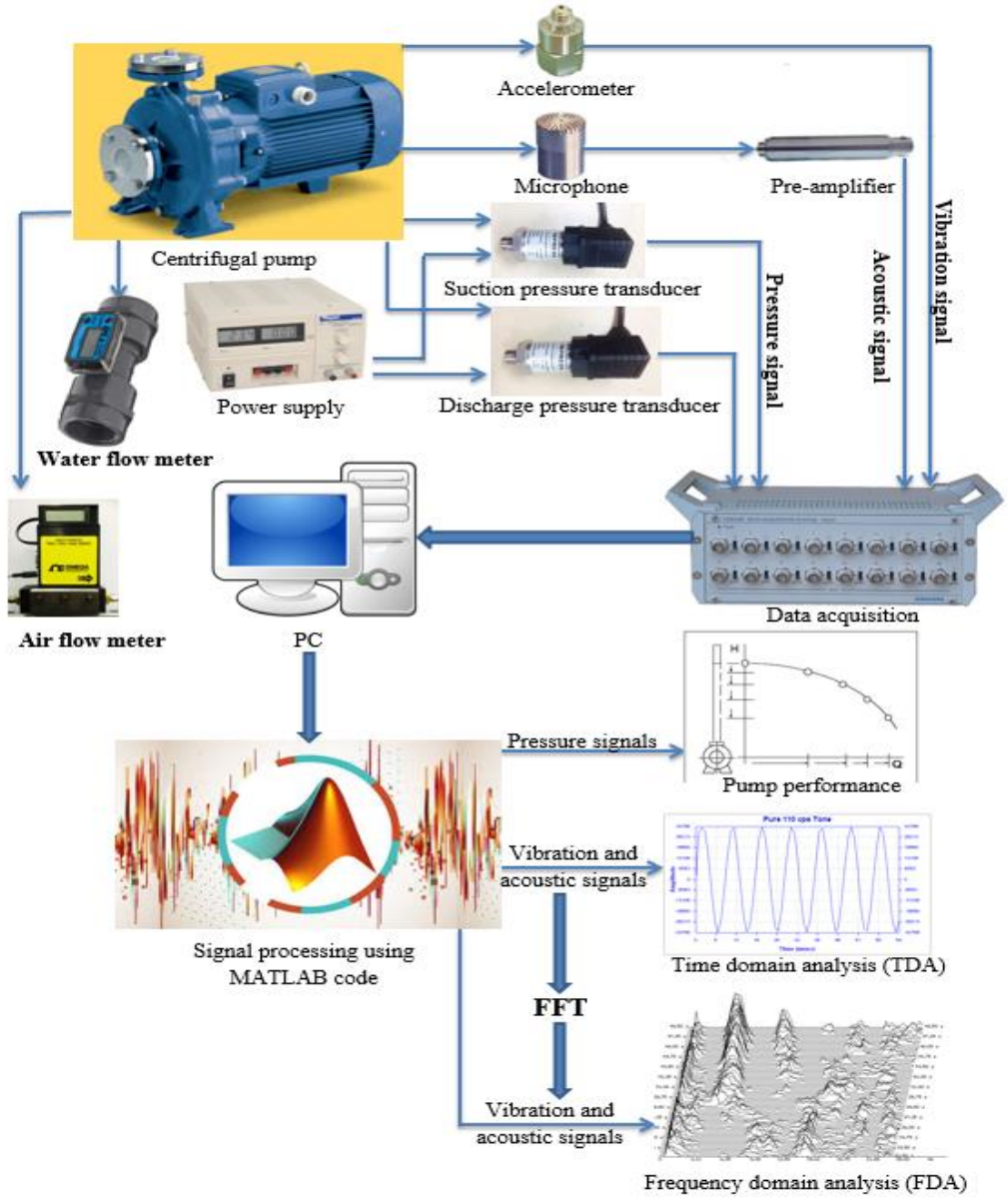

Figure 4-16: Schematic diagram for connection different sensors with the data acquisition system and signal processing system

4.2.10. Interface Software Panel

Interface software panel provides an interface between the user and the data acquisition system for monitoring, collecting, saving and getting visual data from the experimental setup, by using different monitoring sensors in order to process and analyse the data through the use of programming languages (e.g. MATLAB code). Thus, another aim of this study is to develop MATLAB code to analyse and process the acquired data from different sensors such as pressure, vibration and acoustic signals in time and frequency domains. The interface panel software can be changed through various operations parameters (e.g. sampling of data time,

and sampling of frequency). Figure 4-17 shows the interface software panel that was used in this study.

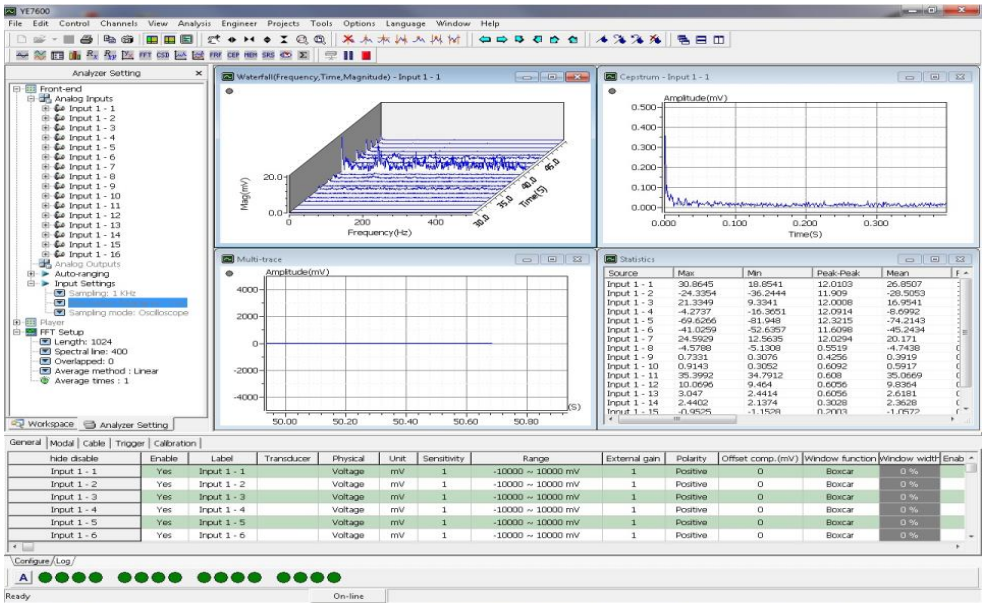

Figure 4-17: Interface software panel type (YE6232)

The next section will briefly explain the various techniques that were used in this experimental study in order to detect cavitation in the centrifugal pump.

4.3. Signal Processing and Data Analysis in Time and Frequency Domains for Condition Monitoring of Cavitation in the Centrifugal Pump

This study has proposed to use different techniques in order to achieve and analyse different form of results, as well as to increase the reliability of detection of cavitation in a centrifugal pump.

4.3.1. Time Domain Analysis

The correct and useful condition monitoring for any machine as well the detection and diagnosis of any faults usually depends on the usage of suitable signal analysis approaches. These approaches are always divided into two categories in condition monitoring: The first approached is the time domain analysis. It is an important technique to analyse different types of signals such as vibration, acoustic and pressure in order to detect and diagnose any problems or fault in machines. This technique is used due to its simple and low-cost method of fault detection. Generally, the time domain is used to analyse the energy level in the signal and therefore, dominated by those components in the signal by using time wave form analysis

(TWFA). Conventional statistical parameters such as peak, RMS, peak-to-peak and variance features of the signal are used in the time domain offering vital information about the presence of any problem in the machine such as faults and cavitation. Commonly, the time domain needs relatively inexpensive and unsophisticated tools. The second approached is the frequency domain. Varieties of sensors were used which depended on the various parameters and frequency ranges of interest [9]. In this experimental study, different techniques are used to detect inception and development of cavitation in the centrifugal pump as explained below:

1- Detection of Cavitation by using Vibration Analysis Technique

This first approach is to evaluate the use of vibration signals for monitoring cavitation in a pump through the use of accelerometer. The mounted accelerometer in the machine should be positioned near or close to the high source of vibration. The background noise may contaminate and corrupt the measured signal since cavitation can increase the broadband frequency. In addition, the vibration signal can be analysed in time and frequency domains in order to establish a relationship between the amplitude of the signal and occurrence of cavitation within a pump. Further detailed information regarding this technique will be provided in Chapter six.

2- Detection of Cavitation by using Acoustic Analysis Technique

The noise as a result of cavitation, normally called cavitation noise, generates bubbles nucleation which randomly collapse. This current study will use acoustic technique under a wide range of pump operation conditions in order to find the relationship between the acoustic signals to detect cavitation. Also, it provides the analysis of acoustic signals in time domain through the use various features in order to predict and diagnose the cavitation under various operation conditions. For further analysis, the acoustic signals were converted from time domain to frequency domain analysis via of FFT. This technique can be suitable to predict cavitation in the pump. In addition, this study concentrates on analysing the acoustic signals in the frequency domain based on different range of frequencies. Further detailed information regarding acoustic technique will be provided in Chapter seven.

3- Detection of Cavitation by using Pressure Signal

For condition monitoring, this study was used different pressure transducers at both the inlet and outlet of the pump to measure the pressure signals in order to determine the pump head as well as to detect and diagnose the cavitation in the pump through calculation of NPSH. Furthermore, the outcomes achieved by such technique are presented for detecting cavitation

on the experimental setup of the pump. Furthermore, using pressure signal is valuable for the condition monitoring of rotating systems such as different types of pumps.

4.3.2. Conventional Statistical Measures from the Time Domain Analysis

The study will use conventional statistical measures to analyse signal that were obtained from time domain by using the statistical features below:

Analysis of Data using the Peak Value of the Signal

It is an important statistical parameter and is used to calculate the peak value of the signal [9]

Analysis of Data using Root Mean Square (RMS) Value

The RMS value of the signal is employed widely in condition monitoring for machines in order to indicate the energy level of the signal. Further, this statistical feature is used to evaluate the effect of signal fluctuations in any machine and it can be defined by using the equation given below [12]:

$$RMS = \sqrt{\frac{1}{N}\sum_{i=1}^{N} {x_i}^2} \tag{4-1}$$

Where, x_i and N are represented the element signal and the total number of elements respectively.

Analysis of Data using the Peak-to-Peak Value of the Signal

This is an important statistical parameter and represents the distance from the minimum peak to maximum peak of the signal.

Analysis of Data using Variance Value

The fourth statistical parameter that was used in this study is to measure and analyse signals that are obtained from time domain variance value and it can be given as below [12]:

$$Variance = \frac{\sum(xi-\bar{x})^2}{N-1} \tag{4-2}$$

Where, xi, N, and $\bar{x}$ are represented the set of elements, the total of elements, and the mean value of elements respectively.

4.3.3. Frequency Domain Analysis

The Fast Fourier transform technique is extensively used to transform the signal from time domain into the frequency domain on the assumption that the frequency elements of the signal are always directly related to the mechanical condition of the machine components. The Fourier transform produces a frequency spectrum, which is the average of the signal over the sampling period [9]. The outcome of the Fast Fourier transforms offers the amplitude of the signal with frequency. The Fourier transforms and its inverse for continuous signals mathematically can be defined as below [12]:

$$F(\omega) = \int_{-\infty}^{\infty} X(t) e^{j2\pi * f t} dt \tag{4-3}$$

And inverse of FFT can be written as:

$$X(t) = \int_{-\infty}^{\infty} F(\omega) e^{j2\pi * f t} d\omega \tag{4-4}$$

Where, X(t) and F(ω) are the time and frequency signals, and $j = \sqrt{-1}$

$$\omega = 2\pi f \tag{4-5}$$

Where, ω represents angular frequency, and f=1/T, T represents time in second.

$$e^{j2\pi ft} = \cos 2\pi ft + \sin 2\pi ft \tag{4-5}$$

Conventional Statistical Measures from the Frequency Domain Analysis

For further analysis, this work was used different conventional statistical information to analyse signals that were obtained from frequency domain by using below statistical values:

Analysis of Data using the Mean Value of the Signal

The mean value of a signal is denoted by the Greek symbol μ, it represents the average value and can be calculated by using Eq. (4-7) [130].

$$\mu = \frac{1}{N} \sum_{i=0}^{N-1} x_i \tag{4-7}$$

Analysis of Data using Root Mean Square (RMS) Value

The RMS can be calculated from frequency domain (spectrum), representing the value from zero to 70.7% of the maximum (peak) amplitude for the spectrum [131].

4.4. Calculate Total Head of the Centrifugal Pump

In this experimental study, the total head of the centrifugal pump can be calculated under different operational conditions as following:

Velocity at the Suction Side of the Pump

This velocity at the suction side of the pump can be calculated by using below equation:

$$V_1 = \frac{4Q}{\pi {d_1}^2} \tag{4-8}$$

Where, Q, V_1, and d_1 are represented the flow rate (l/min), water velocity in suction pipe (m/s), and suction pipe diameter (m) respectively.

Velocity at the Discharge Side of the Pump

This type of velocity can be calculated using Eq. (4-9):

$$V_2 = \frac{4Q}{\pi {d_2}^2} \tag{4-9}$$

Where, V_2, and d_2 are denoted the water velocity in discharge pipe (m/s) and discharge pipe diameter (m).

Friction Head (Hf)

This type of friction head can be calculated using the below equation:

$$Hf = f\left(\frac{L}{d}\right)\left(\frac{V^2}{2g}\right) \tag{4-10}$$

Where, f, L, and D are defined the Darcy friction factor, pipe length (m), and pipe diameter (m).

Static Suction Head (Hs)

This head represents the vertical distance from the centre line of the pump to the free water level in the tank.

Head at the Suction Side

To calculate the total head at the suction side the following equation can be used:

$$H_{tin} = Z_1 + \frac{P_1}{\rho g} + \frac{{V_1}^2}{2g} \quad (4\text{-}11)$$

Head at the Discharge Side

The total head at the discharge side can be calculated by Eq. (4-12):

$$H_{tout} = Z_2 + \frac{P_2}{\rho g} + \frac{{V_2}^2}{2g} \quad (4\text{-}12)$$

Total Head in the Centrifugal Pump

Total head in the pump can be calculated as follow:

$$H_t = H_{tin} - H_{tout} - Hf - Hs \quad (4\text{-}13)$$

Where, H_{tout} and H_{tin} are represented the total head at the inlet and outlet of the pump.
In order to calculate the NPSH in this study the experimental data for Net Positive Suction Head required (H-NPSHR) curve of the centrifugal pump that was provided by its manufacturer (Pedrollo company pump model F32/200H) and the NPSHA can be calculated under several operational conditions as follows:

$$NPSHa = \frac{P_{atm}+P_s}{\rho g} + \frac{V^2}{2g} - \frac{P_v}{\rho g} - H_i \quad (4\text{-}14)$$

4.5. The Uncertainty Analysis Measurement Procedure

There is no doubt that measurements are quite significant in many applications such as communicating technical details, monitoring systems processes and establishing scientific facts. Therefore, all industries spend a lot of money in order to obtain and maintain measurement from different test equipment. These measurements should be as accurate as possible and should be closely analysed during any test measurement procedure. The first stage

in analysing the uncertainty measurement in any process is to identify the physical quantity to be measured. Such quantity can be directly measured through the use different types of sensors. Furthermore, at this step of the analysis measurement, it is significant to describe the experimental setup, technical specifications for sensors and any other equipment to be used. Moreover, the process of obtaining the measurement from test setup needs to be clearly explained; all information can then be utilised in order to identify the processes of the error measurement before finally calculating the uncertainty [132]. This study was calculated the uncertainty measurement using standard deviation σ_x of the sampled data by using below equation.

$$\sigma_x = \sqrt{\sum_{k=1}^{n} \frac{(x_k - \bar{x})^2}{n}} \quad (4\text{-}15)$$

Where, x_k denotes a set of signals, n represents the total number of signals, and $\bar{x}$ is the mean value of signals.

The uncertainty in the mean value can be calculated by using below equation;

$$S_{\bar{x}} = \frac{\sigma_x}{\sqrt{n}} \quad (4\text{-}16)$$

Where, σ_x represents the standard deviation, n denotes the sample size of single.

Based on the different data that was collected and acquired from different sensors in the experimental setup of the centrifugal pump, then using the above equations Eq. (4-15) and (4-16) it can be calculated the uncertainty value for different sensors as follows:

Calculate the mean value of the signal:

$$\bar{X} = \frac{1}{n} \sum_{i=1}^{n} xi \quad (4\text{-}17)$$

$$\bar{X} = \frac{1}{2880000} \sum_{i=1}^{2880000} 695520 \ = 0.2415 \text{m/s}^2$$

Calculate the standard deviation of the signal:

In order to calculate the standard deviation of the signal can be used Eq. (4-15).

$$\sigma_x = \sqrt{\sum_{i=1}^{2880000} \frac{(x_k - 0.2415)^2}{2880000}} = 73.8279 \text{m/s}^2$$

Calculate the estimated standard uncertainty of the signal used Eq. (4-16).

$$S_{\bar{x}} = \frac{73.8279}{\sqrt{2880000}} = 0.0435\text{m/s}^2$$

Calculate the mean estimated standard uncertainty used below equation:

$$Eu = \frac{\sum_{t=1}^{t} S_{\bar{x}}}{n_t} = \frac{0.0435+0.0417+0.0421}{3} = 0.0424\text{m/s}^2$$

Where, n_t representsthe number of tests.

Based on the above procedure, the mean uncertainty values of other sensors can be calculated as shown in Table 4-12 which summarises the mean values of uncertainty for different sensors that were used in this experimental study.

Table 4-12 Mean value of the uncertainty calculations for different sensors

	Vibration sensor	Acoustic sensor	Suction pressure transducer	Discharge pressure transducer
Mean uncertainty value	(m/s^2)	(Pa)	(Pa)	(Pa)
	0.0424	0.0012	18.80	2.232

4.6. Pressure Transducer Calibration Procedure

In order to ensure and increase the confidence in the sensitivity of the pressure transducers used in this current experimental setup, they are first calibrated before they can be used in the experimental setup. For this purpose, the next section explains this calibration measurement procedure for the pressure transducer. Also, the schematic of the pressure transducer calibration procedure is shown in Figure 4-19. To carry out the calibration, the following equipment was used:

- Air supply with pressure regulator.
- Calibration pipe as shown in Figure 4-18 (a).

(a) (b)

Figure 4-18: (a) Calibration pipe, and (b) Clamp to prevent a possible failure in the pipe

Figure 4-18 (b) depicts the clamp which was used to prevent a possible failure in the pipe due to high level of pressure inside the calibration pipe.

- Power supply for pressure transducer.
- Digital multi-meter in order to read the pressure transducer output.

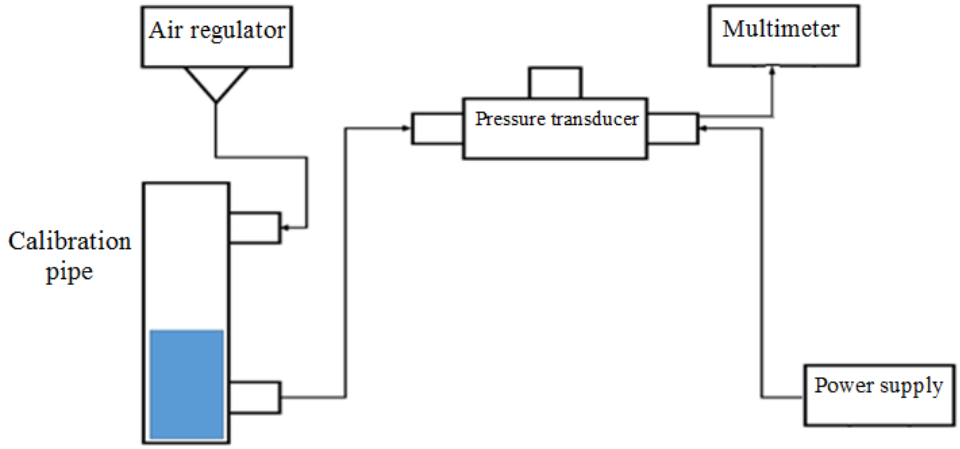

Figure 4-19: Scheme of pressure transducer calibration procedure

In this study, in order to calibrate the pressure transducer the following steps were carried out:

- Fill half of the volume of calibration pipes with water.
- Fix calibration pipes in a vertical position, with the water in the bottom part.
- Connect an air regulator in the top stud of the calibration pipe.
- Connect pressure transducer to the bottom studs of the calibration pipe.
- Connected the pressure transducer wires to the voltage power supply (0 to 32 VDC).
- Connected the output wires pressure transducer to the digital multi-meter.
- Set air regulators to 1 bar.
- Read voltage in the digital multi-meter, this voltage will be the offset for further readings.
- Set the air regulator to 2, 3, 4, 5, and 6 bar then read voltages.
- Calculate the corresponding pressure and create the curve data.
- Repeat the above steps to calibrate another pressure transducer.

After the calibration measurements and calculation of the voltages and pressures for both pressures transducers, the output voltage (V) and the pressure (bar) are plotted in Figure 4-20 (a) and (b). From these figures, two equations can be found by the regression line as shown in figures below, these equations can be used for further analysis in the centrifugal pump to calculate pressures at the inlet and outlet of the pump.

$$P_s = 0.9873V + 0.0220 \quad (4\text{-}18)$$

$$P_d = 0.9903V + 0.0164 \quad (4\text{-}19)$$

Where, P_s represents pressure at suction line, P_d denotes pressure at discharge line, and V is corresponding voltage.

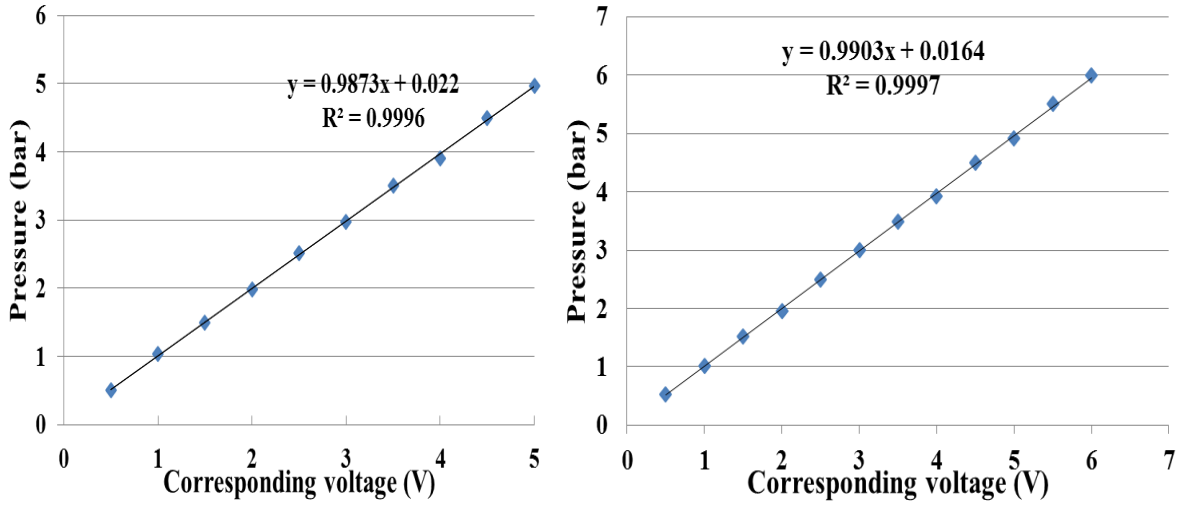

(a) (b)

Figure 4-20: (a) Calibration results for pressure traducers 5bar, and (b) For pressure traducers 10bar

4.7. Water Flow Meter Calibration Procedure

This section provides details of calibration of water flow meter using the hopper available in the University of Huddersfield, Technology Building, Fluids Lab. Such hopper is used for the calibration purposes of the water flow meter. Also, the schematic of the water flow meter calibration procedure is shown in Figure 4-21. To carry out the calibration, the following equipment was used:

➢ **The setup parts include:**

- Hopper
- Off the shelf PLC (Programmable logic controller) (DAD141.1)
- S-shaped Load Cell
- Knife valve
- Solenoid valve

The hopper is the first part of the four running flow loops in the fluid's lab. It is situated right above the main water reservoir/tank. At the bottom of the hopper a pneumatically, as well as

electronically, controlled knife valve is connected. This valve is used to fill and drain the hopper upon reaching a set point.

- **Measurement**

The hopper is connected to a s-shaped load cell to measure the gross weight of the hopper and the collected water.

- **Actuation**

Once the hopper reaches a set point (programmable), the knife valve is actuated electronically. The setup required for the actuation involves pressurising the knife valve at about 4 bar, using the pressure regulator available in the fluids lab. A solenoid valve is connected to the knife valve for electronic triggering. Once the set point is reached and registered by the PLC (Programmable logic controller), it will set the output 0 low to control the solenoid valve in order to drain the hopper.

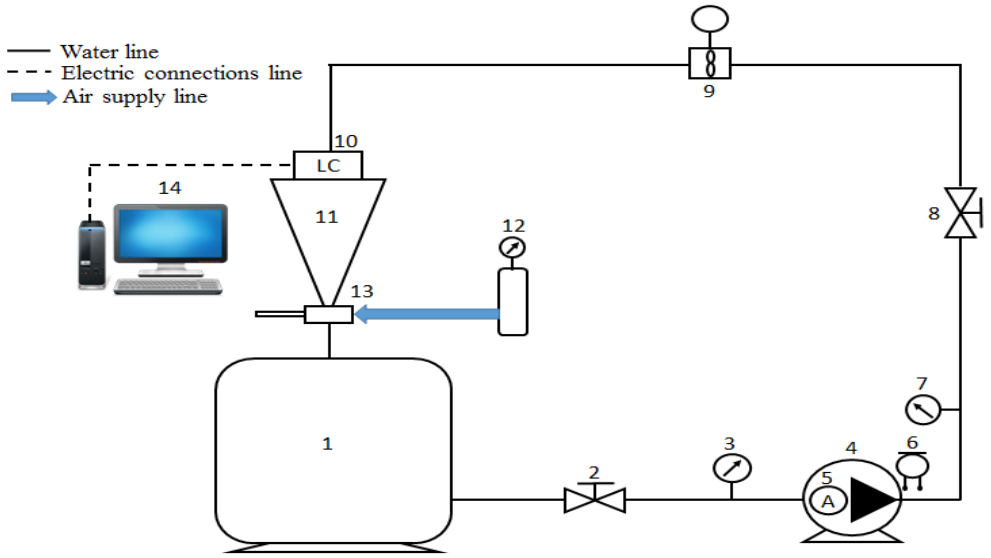

1- Water tank
2- Suction valve
3- Suction pressure transducer
4- Centrifugal pump
5- Accelerometer sensor
6- Microphone sensor
7- Discharge pressure transducer
8- Discharge valve
9- Water flow meter
10- Load cell
11- Hopper
12- Air supply
13- Knife valve
14- PC

Figure 4-21: Scheme of water flow meter calibration procedure

- **Setup Procedure**

In this study, in order to calibrate the water flow meter, the following steps were used:

1. Provide 4 bar pressure to the knife valve to close the valve using the pressure regulator as shown in Figure 4-22 (a). Make sure the valve is at close position (Normal closed) (NC).

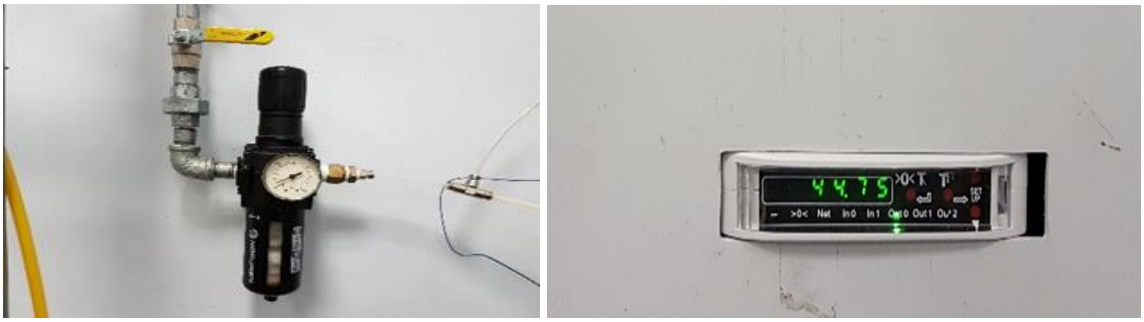

Figure 4-22: (a) Pressure regulator, and (b) Power the PLC unit

2. Power the PLC unit through the power socket and wait for the PLC display to initialise as shown in Figure 4-22 (b). Once the initialisation is completed the static weight of the hopper will appear on the display. At this stage, the PLC is ready.
3. This PLC unit is connected to the university network.
4. Using the PC available in the fluids lab access the DOP4 software.
5. Once the software is executed and if the PLC unit is powered ON and connected to the network, it should appear in the Selected Devices dialogue box with the correct static IP.
6. The data transmission from the PLC can be tested by clicking the Start Test Stream button. It will provide with a real time weight signal. If a reading is present, as shown below figure the unit is connected and ready.

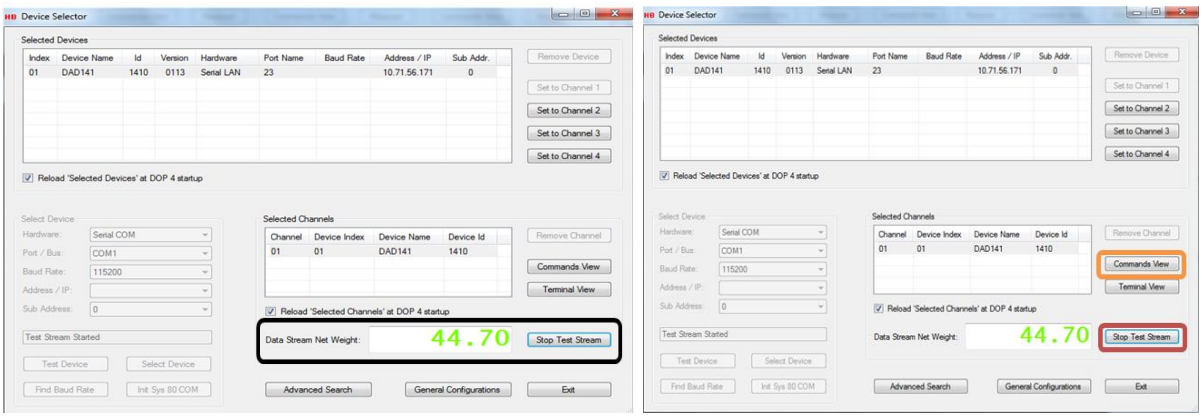

(a) (b)

Figure 4-23: (a) Data transmission from the PLC to program, (b) Device selector

7. After testing the test stream, click on stop test stream button and then click on commands view button.
8. In Commands view mode click on Sequencer.

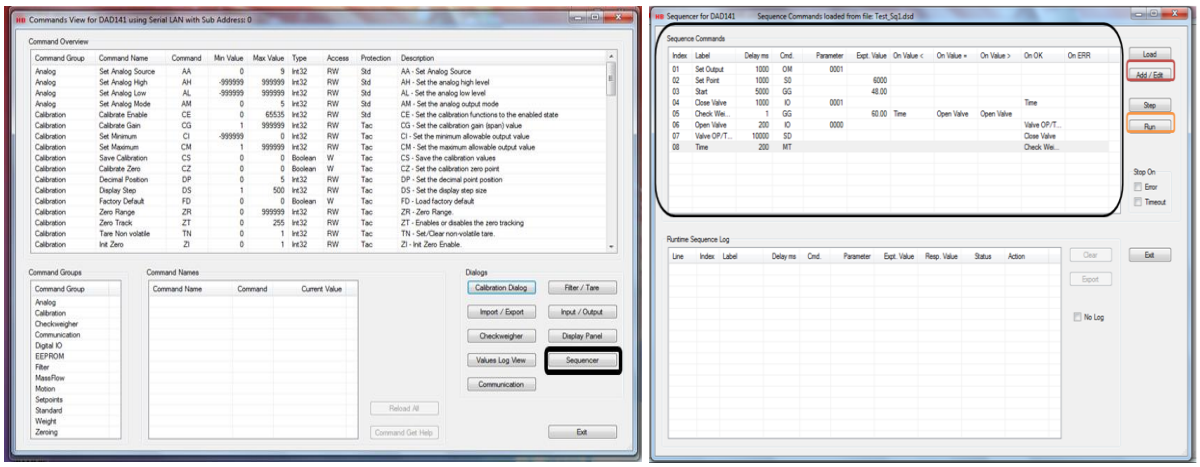

(a) (b)

Figure 4-24: (a) Commands view, and (b) Sequence commands window

9. In the Sequencer window click on the Load button to load the sequence program file. The (Test_Sq1.dsd) file is available on the desktop under (LoadCellSequencer) folder.
10. After loading the file, the pre-programmed sequence can be seen in the Sequence Commands window. To start the sequence, click on Run button and the commands will be running in sequence. To edit any command, select the command and press Add/Edit button.
11. Once the sequence is started a Runtime Log can be seen in the window below, Runtime Sequence Log. This log is used to create (a .csv) file using the Export button.

a. N.B. The measuring time interval for each sample can be set by editing the time command. This is the time PLC takes between measuring each reading from the Load Cell; currently set at 200ms.

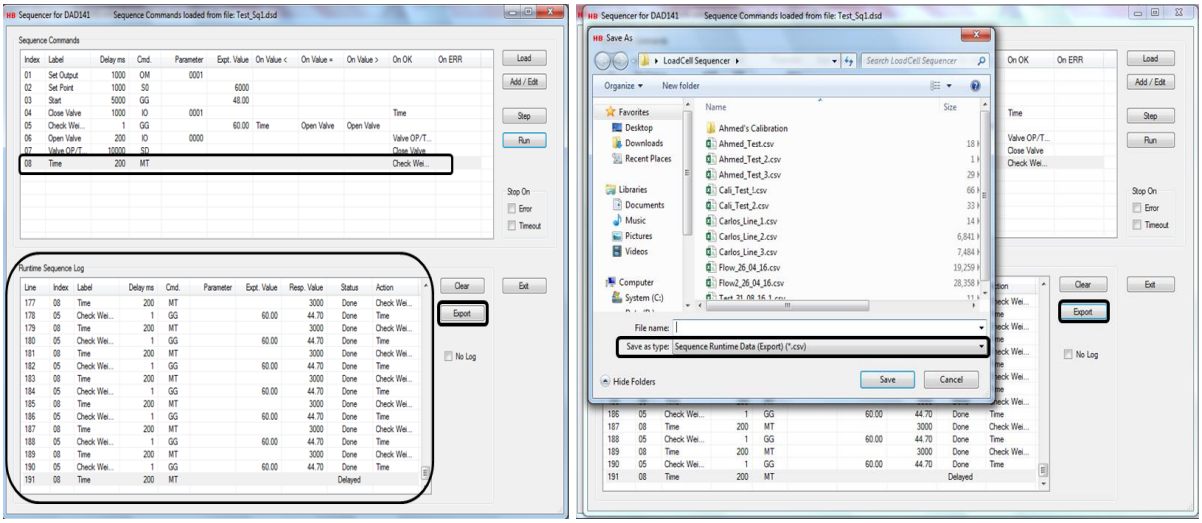

(a) (b)

Figure 4-25: (a) Runtime Sequence Log, and (b) Save data

12. After pressing the Export button, the following window will appear as shown in Figure 4-25. Choose the Save as type to be (.csv) and save your data in the appropriate drive or network location for post-analysis. Furthermore, Once the file was saved Clear button can be pressed to re-do the test.

➢ **Post Processing of the Collected Data**

1. Open the appropriate (.csv**)** file and the following columns should appear in the spread sheet.

	A	B	C	D	E	F	G	H	I	J	K
1	Line	Index	Label	Delay ms	Cmd.	Parameter	Expt. Value	Resp. Value	Status	Action	
2	1	7	Valve OP/Time	10000	SD			0	Done	Close Valve	
3	2	4	Close Valve	1000	IO	1		OK	Done	Time	
4	3	8	Time	200	MT				1000	Done	Check Weight
5	4	5	Check Weight	1	GG		60		47.85	Done	Time
6	5	8	Time	200	MT				1000	Done	Check Weight
7	6	5	Check Weight	1	GG		60		48.1	Done	Time

Index	Label	Delay ms	Cmd.	Parameter	Expt. Value	Resp. Value	Status	Action	Time
8	Time	200	MT			1000	Done	Check Weight	0.1
5	Check Weight	1	GG		60	47.45	Done	Time	0.2
8	Time	200	MT			1000	Done	Check Weight	0.3
5	Check Weight	1	GG		60	47.55	Done	Time	0.4
8	Time	200	MT			1000	Done	Check Weight	0.5
5	Check Weight	1	GG		60	47.75	Done	Time	0.6
8	Time	200	MT			1000	Done	Check Weight	0.7
5	Check Weight	1	GG		60	48.7	Done	Time	0.8
8	Time	200	MT			1000	Done	Check Weight	0.9
5	Check Weight	1	GG		60	49.4	Done	Time	1
8	Time	200	MT			1000	Done	Check Weight	1.1
5	Check Weight	1	GG		60	49.95	Done	Time	1.2
8	Time	200	MT			1000	Done	Check Weight	1.3
5	Check Weight	1	GG		60	50.35	Done	Time	1.4
8	Time	200	MT			1000	Done	Check Weight	1.5

Figure 4-26: (a) Data in excel sheet, (b) Data in excel sheet

2. Create a timing column for time intervals.

a. Each command interval is of 100ms i.e. 0.1sec.

b. Start the time from 0.1+previous row and populate the time column.

3. Filter out all the command rows as follows:

a. Select the Label column.
b. Click the Sort & Filter button from the home tab and click Filter.
c. The Label column should now have a drop down arrow.
d. Click on the drop down menu to deselect the time row.

4. After deselecting the time row the new timing interval will be of 200ms i.e. 0.2sec as set in the sequencer program earlier. The Resp. Value column will indicate the rise in weight over time for the hopper.
5. Further columns needed for flow calculations for various flow rates are as follows:

Absolute Time (Sec)	Absolute weight (kg)	(kg/sec)	Load Cell (l/min)	Reading Flow meter (l/min)	Difference (%)
4.8	13.2	2.75	165	172	4.069767

a. Absolute time and weight can be calculated by summing the rise time and weight from the point when the valve was closed (Close Valve) till the valve was next opened (Open Valve).
b. To calculate absolute time $5.1 - 0.3 = 4.8$ sec.
c. To calculate absolute weight $60 - 46.8 = 13.2$Kg.
d. From these two calculations mass flow (Kg/s) $\frac{13.2\text{Kg}}{4.8\text{sec}} = 2.75\text{Kg/sec}$
e. To calculate mass flow (l/min) $2.75 * 60 = 165\ (\text{l/min})$.
f. To calculate the difference between the calculation and reading from flow meter.

$\left(\frac{172-165}{172}\right) * 100\% = 4.2\%$

Check We	1	GG		60	46.8	Done	Time	0.3
Check We	1	GG		60	46.95	Done	Time	0.5
Check We	1	GG		60	47.1	Done	Time	0.7
Check We	1	GG		60	48.1	Done	Time	0.9
Check We	1	GG		60	48.3	Done	Time	1.1
Check We	1	GG		60	48.8	Done	Time	1.3
Check We	1	GG		60	49.4	Done	Time	1.5
Check We	1	GG		60	49.95	Done	Time	1.7
Check We	1	GG		60	50.6	Done	Time	1.9
Check We	1	GG		60	51.2	Done	Time	2.1
Check We	1	GG		60	51.7	Done	Time	2.3
Check We	1	GG		60	52.3	Done	Time	2.5
Check We	1	GG		60	53	Done	Time	2.7
Check We	1	GG		60	53.55	Done	Time	2.9
Check We	1	GG		60	54	Done	Time	3.1
Check We	1	GG		60	54.55	Done	Time	3.3
Check We	1	GG		60	55.55	Done	Time	3.5
Check We	1	GG		60	55.95	Done	Time	3.7
Check We	1	GG		60	56.3	Done	Time	3.9
Check We	1	GG		60	57.15	Done	Time	4.1
Check We	1	GG		60	58	Done	Time	4.3
Check We	1	GG		60	58.4	Done	Time	4.5
Check We	1	GG		60	58.8	Done	Time	4.7
Check We	1	GG		60	59.4	Done	Time	4.9
Check We	1	GG		60	60	Done	Open Valve	5.1

Figure 4-27: Final data (time and weight) in excel sheet

After the calibration measurements were carried out and calculation of the time and water weight for the water flow meter obtained, the output reading of the water flow meter (l/min) and the calculated water flow rate (l/min) are plotted in Figure 4-28. From this figure, it can be found that the calculation flow rate value using the above process is close to the water flow meter reading (both results having a close match) and this agreement signifies that the calibration results are reasonable. Furthermore, the result analysis also displayed that the average deviation of the calculated results for calibration compared to that of the flow meter reading results is approximately around 4%.

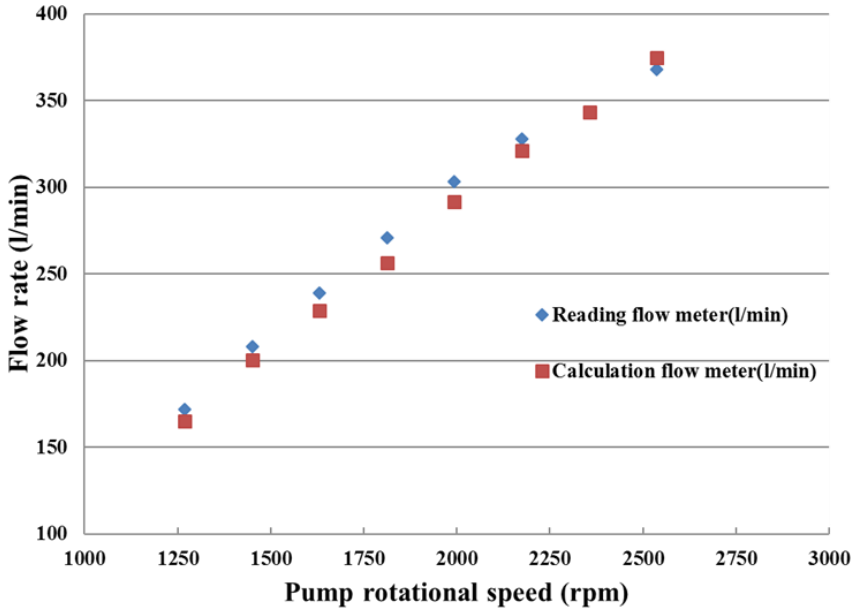

Figure 4-28: Calibration water flow meter results

After explaining the numerical simulation of the flow inside the centrifugal pump in Chapter three, different outcomes were gathered from CFD in the next chapter. Detailed investigations of these outcomes are provided in Chapter 5. The next chapter presents the analysis and discusses the flow field behaviour within the centrifugal pump based on single-phase and cavitating model under different operating conditions and various impeller geometrical parameters using the CFD code.

CHAPTER 5

PREDICTION OF PERFORMANCE AND DETECTION OF CAVITATION WITHIN A CENTRIFUGAL PUMP USING CFD TECHNIQUE

All the results obtained by numerical simulations that carried out via CFD code regarding to the prediction of the pump performance and detection of cavitation within the centrifugal pump are presented in this chapter. Both qualitative and quantitative analyses were conducted on all of these results to better understand the flow structure within a centrifugal pump, under both single-phase and cavitation conditions. Also, the investigation using different geometrical parameters of the pump in both time and frequency domains are analysed. Moreover, semi-empirical correlations for head and power coefficients of the pump based on single-phase and cavitation were developed.

5.1. Introduction

The usage of CFD plays a significant role in fluid mechanics. Improvements that were made on the capabilities of the computer over the years have allowed for numerical approaches through the CFD to be used to improve in predicting the performance of centrifugal pumps. In this current chapter, the transient numerical calculations using CFD code are carried out under different operating conditions and for various geometrical parameters for the flow field within a pump under single-phase and cavitation conditions. This chapter is divided into four sections. The first section includes the mesh independence, time independence and y+ sensitivity analyses. Also, this section comprises of the validation of the obtained results from the CFD with experimental results. The second section in this chapter corresponds to the unsteady investigation of the pump. For this aim, the pump was run at different flow rates under single-phase and cavitation conditions for five revolutions. Also, in the same second section, the pump head at last revolution was analysed based on single-phase and cavitation phase under various operation conditions using transient simulation approach. The third section, analyses the unsteady behaviour of the pump with different impeller geometrical parameters such as a number of blades, the inlet and outlet impeller diameters. Detailed qualitative and quantitative analyses was performed on local flow parameters (e.g. static pressure, flow velocity, vapour volume fraction, pump head and pressure fluctuations in both time and frequency domains). Quantitative and qualitative analyses were also conducted in the prediction of cavitation in the centrifugal pump. Finally, based on the extensive numerical investigations of these parameters various semi-empirical correlations at different impeller geometrical parameters under single-phase and cavitation conditions for the pump head and power coefficients were developed using multiple regression analysis technique.

5.2. Analysis of the Flow Field and Performance of the Centrifugal Pump using Transient Numerical Approach

In order to investigate the flow field within a centrifugal pump through the use of numerical simulation for predicting the performance of pump and detecting cavitation under different operation conditions were carried out. To analyse the effect of interaction between impeller and volute, numerical simulations were conducted that take into account various locations of the impeller blades relative to the volute tongue region using sliding mesh technique. Details regarding to all numerical results for the centrifugal pump, model reliability including mesh

independence test, time independence test, y+ sensitivity test and validation will be represented in the next sub sections.

5.2.1. Mesh Independence Test

Testing the mesh independence is important because meshing can lead to less or more accurate outcomes. Despite to the proposed number of mesh elements whether is high or low mesh independent test is basically aiming to grantee the stability of results when the number of elements is changed. In this study three meshes consisting of 1.25 million, 2.5 million, and 5 million mesh elements were selected, as displayed in Table 5-1. The outcomes of these three cases showed that the changes in the heads predicted within the centrifugal pump are less than 0.2% amongst the three meshes under consideration. Thus, from the table below, it can be concluded that the mesh with 2.5 million elements is capable of accurately predicting the flow features and therefore it was selected for further analysis of the centrifugal pump. According to the differences in head, it can be seen that the change in the percentage is low.

Table 5-1 Results of mesh independence of the centrifugal pump

No.	No. of elements	Head	Difference in head
		(m)	(%)
1	1.25 million	38.83	
2	2.5 million	38.75	0.211
3	5 million	38.84	0.231

5.2.2. Time Steps Independence Test

Time step independence can lead to less or more accurate outcomes of the Computational Fluid Dynamics. This study includes the usage of three different time steps. The outcomes of time steps are summarised in the Table 5-2 shows that the variance in the head within the centrifugal pump is less than 1.11% between the three-time steps under consideration. Therefore, the time step with $3.0248*10^{-4}$sec was selected for further analysis.

Table 5-2 Results of time steps independence of the centrifugal pump

No.	Time step	Head	Difference in head
	(s)	(m)	(%)
1	$6.04960*10^{-5}$	38.01	
2	$1.81488*10^{-4}$	38.44	1.11
3	$3.02480*10^{-4}$	38.75	0.79

5.2.3. y+Sensitivity Test

To obtain more accurate results from the numerical simulation using CFD code, it is important to calculate the y+ sensitivity of the all centrifugal pump parts in the computation domain. For this reason also, this study compared three different y+ values at the same design flow rate for the pump in order to study the effect of y+ value on the head of the pump. Table 5-3 summarises the pump head under the different y+ values. It can be clearly seen that the head difference for all cases under investigation was less than 1.8% or less. This confirms that for numerical simulations, the influence of the y+ value has little impact on the results.

Table 5-3 Calculation y+ sensitivity test

No.	y+	Head	Difference in head
		(m)	(%)
1	20	39.48	
2	30	38.75	1.8
3	40	38.28	1.2

5.2.4. Validation

The validation of the outcomes is considered as one of the most significant steps when conducting numerical studies. In other words, it means that the results gained from the numerical simulations are compared with experimental findings to verify accurately that the numerical model symbolises the physical model of the actual system. Thus, the entire geometric, flow and solver-related parameters and variables become vital in validation studies. In the present study, the experimental data for the centrifugal pump was provided by experimental investigations to validate the model used in the CFD. The head at both the suction and discharge sides of the pump was calculated using both Eqs. (4-11) and (4-12). Also, the total head across a pump was calculated using Eq. (4-13). Figure 5-1 depicts the variation in the head for both numerical and experimental results. It can be seen that there is a good agreement between CFD and the experimental results. The analysis of the above figure showed that the average deviation between the CFD results when compared with experimental results for the head is about 6%. From previous analysis it can be seen that both results match closely with each other and this agreement confirms that the CFD results are reasonable. It can be concluded from the above findings that the numerical analysis is reasonably well validated.

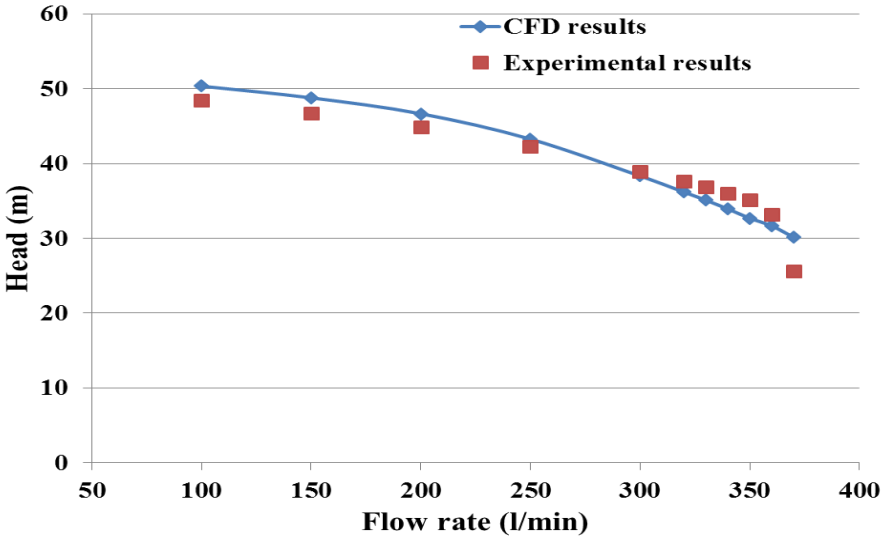

Figure 5-1: Validation of the numerical and experimental results

5.2.5. Computational Results Based on Transient Analysis Approach

In this study, two types of numerical simulation were carried out to investigate the pump performance and visualise the flow field within a centrifugal pump. The first was a numerical simulation under single-phase operating conditions [58]. The second was simulation under cavitation operating conditions. The complex internal flow field within the pump in transient conditions was investigated under different operating conditions. In order to capture unsteady flow interaction between the rotor-stator interface, the relative position of the impeller blades needs to be changed for every time step [133]. For the simulation of the transient situation, the time step is selected as $3.0248*10^{-4}$sec corresponding to pump rotational speed of 2755rpm as mentioned in section 5.2.2., the residual is set at 10^{-6} [134].

5.2.6. Flow Field Analysis at Design Flow Rate

Before analysing the influence of the impeller geometrical parameters on the performance output of the centrifugal pump under single-phase and cavitation conditions. It is essential first to investigate and analyse the structure of the flow field in the pump so that related to local and global flow. In the next section, the pressure and velocity distributions within a centrifugal pump were investigated.

5.2.7. Static Pressure and Velocity Magnitude Distributions under Design Flow Rate

The flow within a centrifugal pump is highly affected by the shape of the impeller and volute [23]. In order to predict the performance of the pump, it is vital to be aware as to how transformation of energy takes places in various parts of the pump. Such phenomenon can be comprehended by studying the behaviour of the flow field within the pump [44].

Figure 5-2 (a) depicts the variations of static pressure in the centrifugal pump having five impeller blades. The inlet and outlet impeller diameters used are 30mm and 215mm, and pump rotational speed chosen is 2755rpm under design flow rate of 300(l/min). When the water flows into the pump through the inlet of an impeller, the fluid starts to rotate with the impeller blades. Also, the pressure and velocity begin to change. Additionally, it is observed from the case under investigation, that the static pressure distributions are similar for all impeller passages. The pressure field in the pump shows that the pressure on impeller blades increases from inlet at the leading impeller edges to trailing edges along the radial direction within the impeller blade-to-blade passages. Maximum pressure was noticed at the outlet of the volute. Furthermore, it is notable that the pressure near the suction side of blades at the inlet eye of impeller near or close to the leading edge is particularly low. It can be observed that this particular area in the impeller has lower pressure value as compared to another area in the pump.

Furthermore, Figure 5-2 (b) depicts velocity variations for further investigation of the flow structure in the pump. Study of the velocity magnitude contour in the centrifugal pump provides good information about velocity change in the pump. The variation of velocity magnitude in the central plane of the pump under design flow rate is depicted in this figure. It can be seen that the velocity within a pump increases from the inlet to outlet. Also, high velocity occurs at the pressure side of the impeller blades as shown in this figure. It can be observed that the flow velocities at the suction side of blades are quite low with the minimum value reaching 0.27m/s during the rotation of the impeller. In addition, the flow velocities near the pressure side of blades are higher than suction sides of blades and maximum velocity is 24.34m/s. In addition, when the kinetic energy within a pump is converted into pressure energy in the volute, the velocity is always reduced. The reason behind this is due to the design of the volute, which has significantly different cross-section areas, and these cross-sectional area are continuously increasing to reach the higher cross-section area at the outlet volute region.

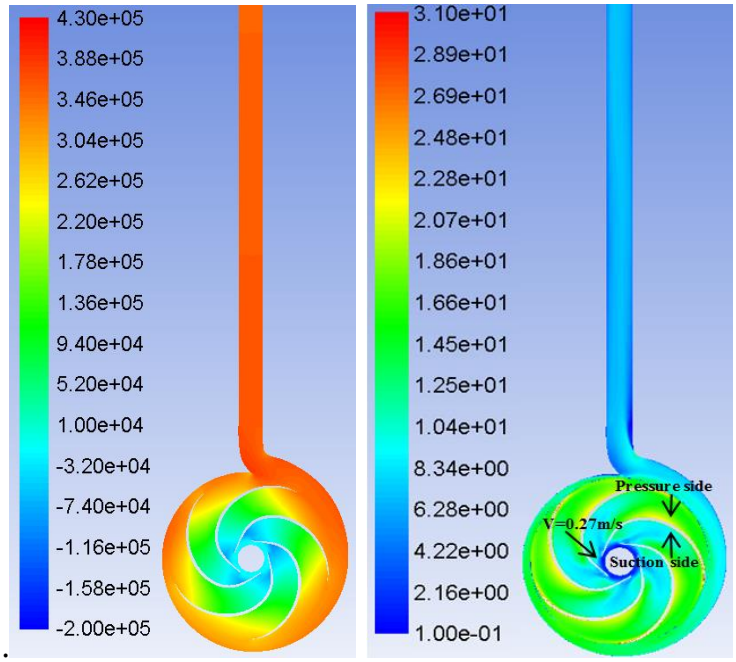

(a) (b)

Figure 5-2: Variations in (a) Static pressure and (b) Velocity magnitude of the pump having Q=300(l/min), Z=5, do=215mm, di=30mm, and N=2755rpm

5.2.8. Performance of the Centrifugal Pump under Transient Conditions

For this present study, in order to investigate the turbulent flow within the pump under single phase, 3-D unsteady Reynolds-Averaged Navier–Stokes (RANS) equations were solved using CFD code. For transient simulation, the rotor–stator method interfaces were used. Because of the transient technique the rotor (impeller) – stator (volute) was changed dependent on the change in the angular position of the impeller.

5.2.9. Instantaneous Pump Head under Design Flow Rate

In the transient investigation, the centrifugal pump was run at 2755rpm for five revolutions at the design flow rate of 300(l/min). To quantify the performance of the pump considered here, the instantaneous head for one revolution of the pump was depicted in Figure 5-3. It can be seen that the instantaneous head's waveform is almost uniform at a particular rotational speed and the peak-to-peak head remains nearly constant at an appropriate pump speed. It is obvious that the variation in the head of the centrifugal pump is cyclic with the number of peaks and valleys are equal to the same number of impeller blades. Also, the inner flow within the pump is very complex. The maximum peak head value is around 40.28m while the minimum valley value is around 36.47m.

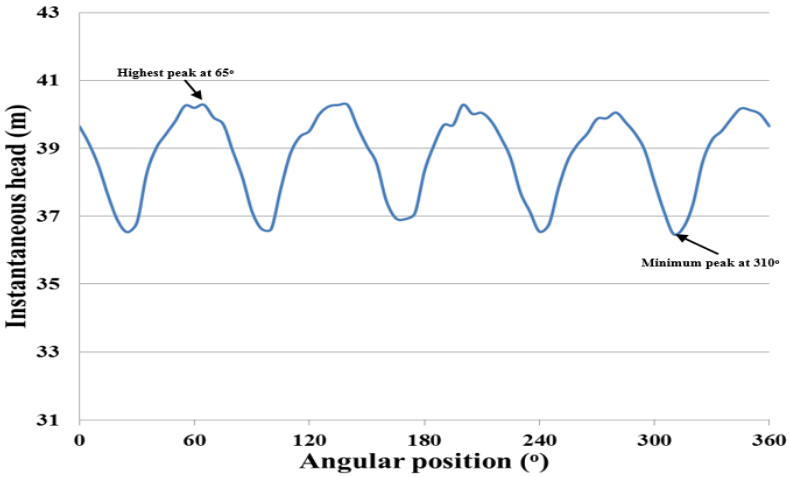

Figure 5-3: Instantaneous head variations of the pump having Q=300(l/min), Z=5, do=215mm, di=30mm, and N=2755rpm

5.2.10. Pressure and Velocity Variations at Peak and Valley Instantaneous Head of the Centrifugal Pump

Generally, the centrifugal pump is a mechanical device that utilises a rotating impeller to transfer electrical energy into hydraulic energy. Water enters through the inlet pipe and moves towards the impeller eye. The rotation of the impeller pushes the water between impeller blades outwards into the volute. This phenomenon creates a vacuum at the eye of the impeller and it generates a low-pressure region at this area. When the volute cross-section area increases, this leads to velocity of the water in the volute to decrease and hence the water pressure increases. To comprehend the dynamics of flow within a pump and the trend of the instantaneous head, it is important to analyse the flow structures that correspond to the peaks and valleys as viewed in Figure 5-4. Therefore, Figure 5-5 display the pressure and velocity variations in the centrifugal pump at such angular locations that corresponds to the peak and valley in the instantaneous head of the centrifugal pump.

It can be observed that the pressure between blades also increases and this increase starts from the leading edge of the impeller blade to the trailing edge. The pressure at the suction side of impeller blades was lower than at the pressure side of impeller blades. In one revolution, the numbers of peaks are equal to five, simultaneously the numbers of valleys are equal to 5. Thus, this form of wave is created through the transient motion of the impeller blades. To investigate this particular phenomenon, the highest peak and valley points were selected. The highest peak happened at 65^{o} angular position of the impeller while the minimum valley happened at 310^{o} angular orientation of the impeller.

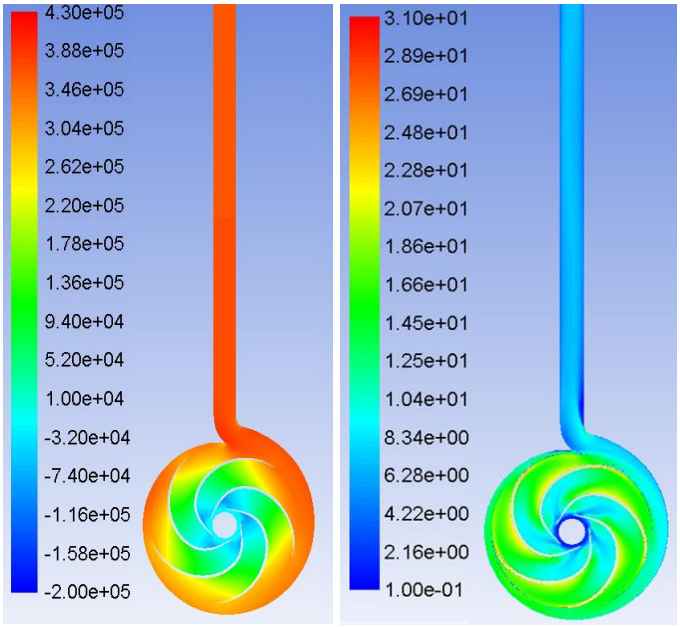

(a) (b)

Figure 5-4: Variations in (a) Static pressure and (b) Velocity magnitude at peak fluctuation pressure of the pump having Q=300(l/min), Z=5, do=215mm, di=30mm, and N=2755rpm

It can be noticed that in Figure 5-3, the peaks and valleys in pump instantaneous head occur due to two important reasons. Firstly, when the tongue area is in between two impeller blades. The second reason is when one of the impeller blades has passed the tongue region and the other blade is approaching it. Based on the above results, it can be concluded that the analysis of transient numerical simulation results can provide useful information regarding flow fields within a centrifugal pump such as velocity and pressure distributions. The relative position of the rotor part (impeller) and stationary part (volute) cause unstable flow and generate more pressure fluctuations. Hence, increase the level of vibration and noise in the pump especially at the volute tongue region. This particular region causes more energy losses due to the high interaction between the impeller and volute.

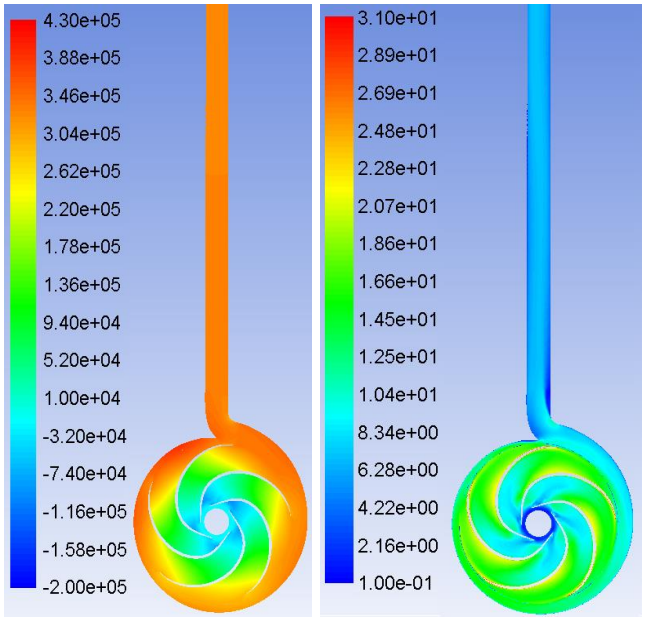

(a) (b)

Figure 5-5: Variations in (a) Static pressure and (b) Velocity magnitude at lowest fluctuation pressure of the pump having Q=300(l/min), Z=5, do=215mm, di=30mm, and N=2755rpm

5.2.11. Analysis the Effect of Volute Tongue Region on Variations of Static Pressure

In order to better comprehend the internal flow field during transient conditions within a pump, the variation of static pressure for the impeller and volute was analysed under different impeller positions. As discussed above, the variations of static pressure close to the volute tongue region were higher than other regions in the pump. Figure 5-6 depicts the rotation of the impeller and variations in the static pressure around the volute tongue region at different blade angular positions in respect to the volute tongue region. The angular position (θ) was changed from 0° to 6°. The centrifugal pump has a design flow rate of 300(l/min), Z=5, do=215mm, di=30mm, N=2755rpm. In this figure, the five blades were displayed in the impeller flow channels. Two blades are named blade 1 and blade 2 as highlighted. It can be observed in this figure that the highest static pressure happens especially close the tongue area inside the pump and the pressure is increased from near the volute tongue to the outlet region of volute along the direction of flow. However, the pressure close to the tongue region was higher than those other regions within the pump. This is mostly due to the high interactions between the impeller and volute, particularly near or close to the volute tongue region. From the above investigation of the dynamic interaction between the volute tongue region and impeller. It can be concluded that the interaction between impeller and volute tongue region is due to the relative position of the impeller blades with respect to tongue region. Furthermore, based on the above findings

regarding the variations of pressure in the pump, the results showed that there are high interactions between the impeller and volute close to the volute tongue region and this particular area of the volute has a high impact on the pressure variations.

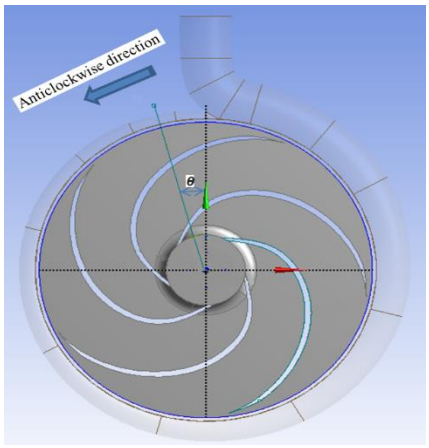

Impeller rotating direction

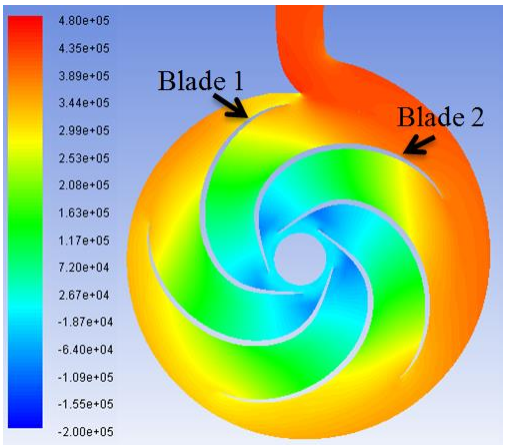

(a) θ =0º

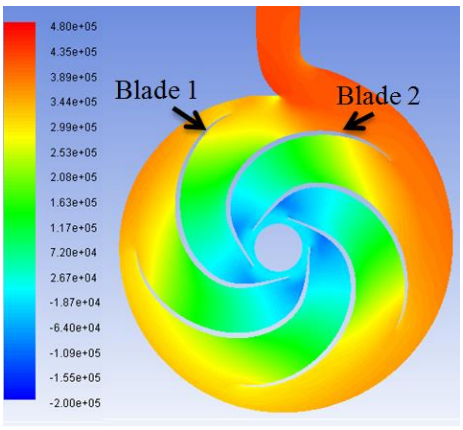

(b) θ =3º

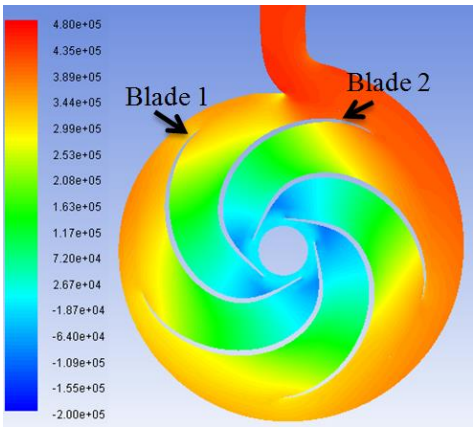

(c) θ =6º

Figure 5-6: Direction of the impeller and variations of static pressure close to the volute tongue region at various angular positions

5.3. Effect of Different Flow Rates in the Centrifugal Pump

For further analysis, this section includes studying the effect of different flow rates on the static pressure variations, velocity magnitude variations within a centrifugal pump and the performance of the pump.

5.3.1. Pressure Variations in the Centrifugal Pump under Various Flow Rates

Further investigations regarding flow field within a pump the numerical simulations using CFD were carried out under different flow rates in order to investigate the velocity and pressure

variations inside the pump. Figure 5-7 depicts the static pressure variation under various flow rates namely 100, 150, 200, 250, 300, and 320(l/min) respectively. The corresponding operating conditions can be designated as condition A (number of impeller blades is five, inlet and outlet impeller diameters are di=30mm, do=215mm, and N=2755rpm). For accurate comparison purposes, all the static pressure contours under various flow rates displayed in this figure were drawn on a similar scale. From these figures, it can be seen that the changes of the flow structure in the pump takes place as flow rate increases from lower to a higher value. It is interesting to note the change of pressure variations in the impeller and volute at inlet and outlet of the pump. It is obvious that the distributions of static pressure under different flow rates have the same trend for all cases under investigation. The pressure gradually increases from the inlet area of the impeller to the outlet area along the radial direction of the impeller. The maximum pressure was found to occur at the outlet of the volute and close to the tongue region. It can also be seen that the pressure on the suction surface of blades of the impeller, especially at the eye of impeller, is smaller than that on the pressure surface. Also, the result showed that when the pump operates at higher flow rate, the low pressure area at the inlet of the impeller increases, causing cavitation to occur and then develops further as the flow rate keeps increasing. The reason behind the occurrence of cavitation is due to the decrease in pressure in this region which goes lower than the water vapour pressure. From this figure, it can be seen that with increase in flow rate, the static pressure at the pump decreases particularly at high flow rate. Furthermore, based on the above analysis, it can be concluded that the static pressure in the impeller, and volute were highly affect under the different flow rates.

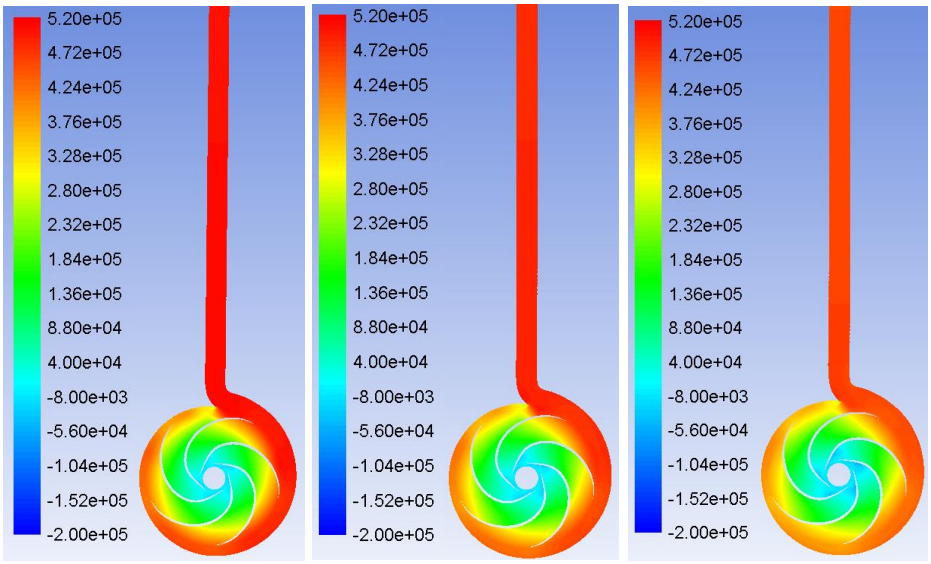

Q=100(l/min) Q=150(l/min) Q=200(l/min)

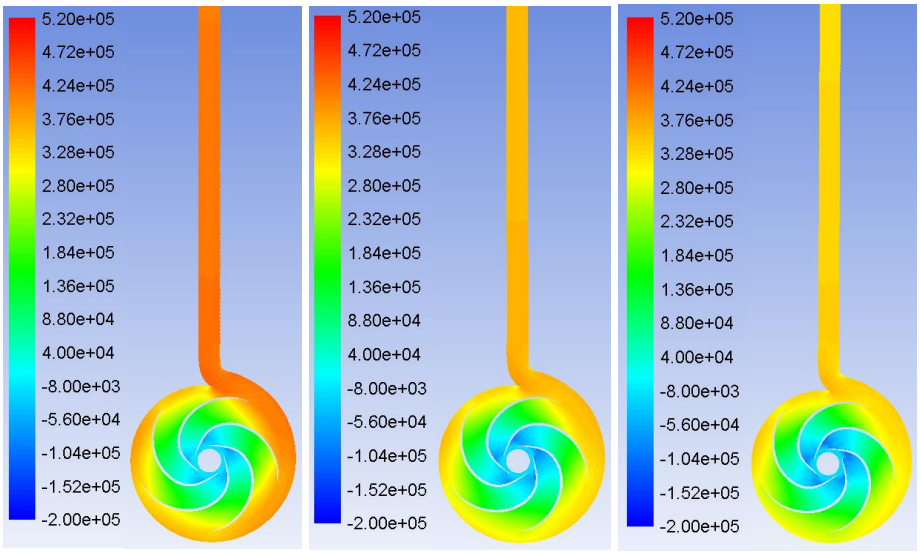

Q=250(l/min) Q=300(l/min) Q=320(l/min)

Figure 5-7: Static pressure variations in the centrifugal pump under various flow rates at 2755rpm

5.3.2. Velocity Variations in the Centrifugal Pump under Various Flow Rates

Figure 5-8 depicts the velocity magnitude variations of the pump under various flow rates which were 100, 150, 200, 250, 300, and 320(l/min) respectively. The simulation corresponds to condition A. For accurate comparison purposes, all the velocity magnitude contours at various flow rates displayed in this figure were drawn on the similar scale. It can be seen that the velocity within a pump is gradually increased from the inlet of the impeller to outlet for all of the cases under investigation. The higher velocity occurs near the volute tongue region, an interesting point to note is that there are different flow velocities across the impeller blades, at

the suction and pressure sides, as shown that in Figure 5-8. Furthermore, it can be observed that the regions of low velocity for the suction sides of blades are moving along the blades starting from the leading edge to trailing edge of blades. Also, it can be clearly observed that the magnitude of velocity in the impeller is higher than in the volute. This is because the volute has an asymmetrical cross section area and this cross section is increased up to the volute outlet. This means that when the cross section area is increased, the velocity of water within the volute is decreased. This then leads to the velocity of water being decreased and the pressure of water being increased.

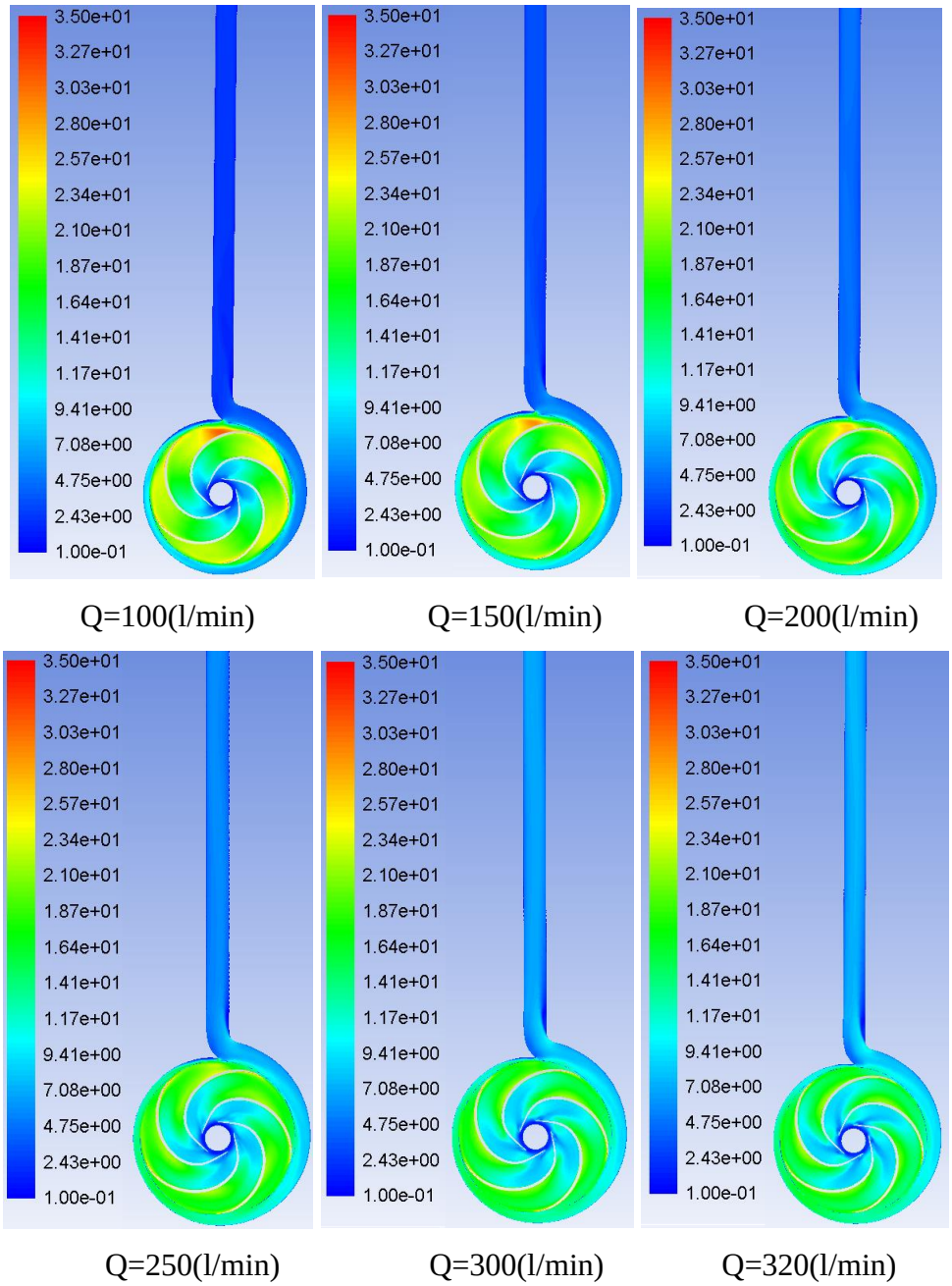

Figure 5-8: Velocity variations in the centrifugal pump under various flow rates at 2755rpm

To analyse the influences of different operational conditions on the instantaneous head of the pump, six flow rates namely100, 150, 200, 250, 300, and 320(l/min) were selected and compared. Figure 5-9 (a) depicts the instantaneous head and (b) average head of the centrifugal pump at various flow rates. It is worth observing that the instantaneous head decreases when the flow rate is increased, supported by the fact that there are five peaks and valleys depending on the number of blades and the results revealed that the higher value of the instantaneous head was at flow rate of 100(l/min). The average head at different flow rates are 50.25, 48.87, 46.89, 43.60, 38.75, and 37.65m respectively, as shown in Figure 5-9 (b). Based on above analysis, it can be concluded that the flow rate has an important influence on the head of the pump.

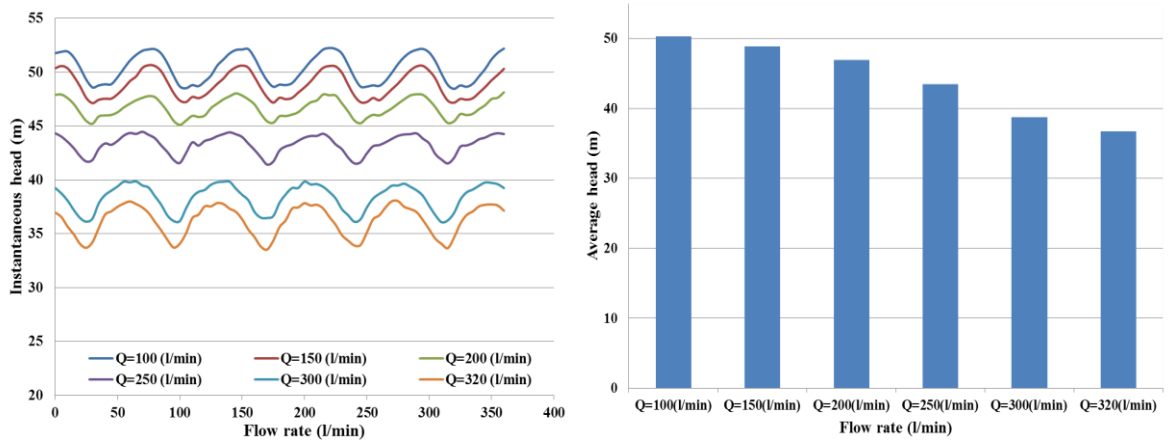

(a) (b)

Figure 5-9: Variations in (a) Instantaneous head and (b) Average head of the pump under various flow rates at N=2755rpm

5.3.3. Comparison between Numerical and Experimental Head Fluctuations

To obtain more information regarding the head fluctuations within a pump, the numerical calculation of the head was compared with experimental results under various flow rates. Figure 5-10 depicts head variations under numerical and experimental results at N= 2755rpm. It is observed that the numerical simulation results showed similar patterns as compared to the experimental results. Also, the results show that the amplitudes of peak-to-peak head for the numerical calculations are smaller than the experimental results. Furthermore, the changes in trend of the head fluctuations in a pump can be analysed using statistical results such as average, minimum, maximum, and RMS features. Table 5-4 provides the comparison between numerical and experimental results under different flow rates. It can be observed that the values of these features are decreased as the flow rate of the pump is increased.

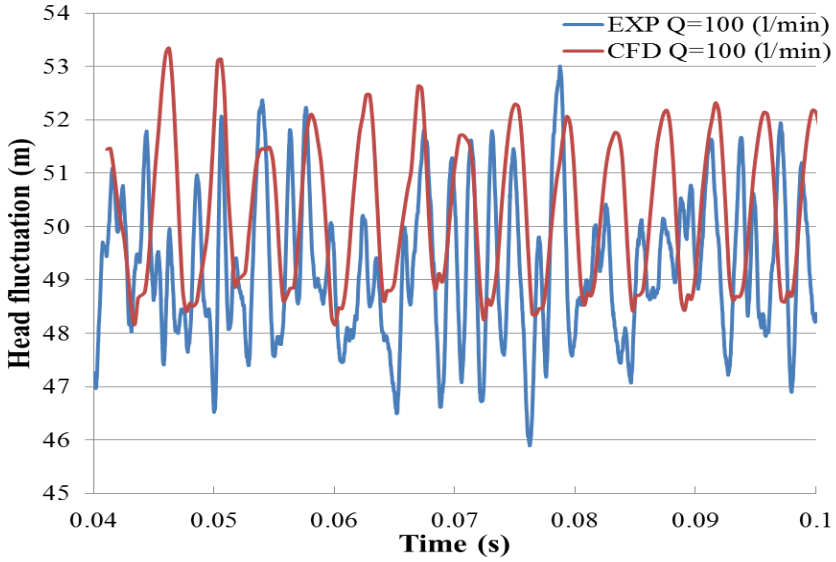

Figure 5-10: Comparison of the head fluctuations from the experimental and numerical results

Numerical results are in agreement with experimental results and maximum differences between them are approximately around 3% for the average value, 9% for the minimum value, 8% for the maximum value and 2% for RMS value respectively, as listed in this table. The difference between numerical and experimental results can be due to several reasons. Firstly, the mechanical losses occurring in the pump which is caused by the contact between the shaft and bearings and between the shaft and seal. The second reason is due to the gap between the volute and impeller. Thirdly, due to hydraulic losses caused by friction losses, vortexes, and separation due to change in flow direction that happens at the passages of the impeller. In addition, the geometry and flow field within the pump are very complex and fully turbulent, with complex impeller blade curvature, which has considerable effect on the flow field developed either within the blade passages or inside the volute.

Table 5-4 Comparison between experimental and numerical results for head fluctuations

No.	Flow rate	Head	EXP. Head	CFD Head	Difference in head
(-)	(l/min)	(m)	(m)	(m)	(%)
1	100	Avg.	49.24	50.27	2.04
		Min.	45.89	48.15	4.69
		Max.	53.01	53.33	0.60
		RMS	7.017	7.114	1.36
2	150	Avg.	47.41	48.79	2.82
		Min.	43.28	46.98	7.87
		Max.	52.79	50.81	-3.89
		RMS	6.886	7.004	1.68
3	200	Avg.	45.46	46.88	3.02
		Min.	40.89	44.98	9.09
		Max.	50.37	48.28	-4.32
		RMS	6.743	6.846	1.50

4	250	Avg.	42.22	43.45	2.83
		Min.	37.73	41.50	9.08
		Max.	47.32	44.87	-5.46
		RMS	6.498	6.592	1.43
5	300	Avg.	38.27	38.78	1.31
		Min.	32.93	36.22	9.08
		Max.	43.30	40.48	-6.96
		RMS	6.186	6.207	0.32
6	320	Avg.	37.06	36.75	-0.84
		Min.	32.76	34.09	3.90
		Max.	41.73	38.61	-8.08
		RMS	6.088	6.033	-0.91

To further understand the head fluctuations was investigated through the use of different statistical features such as average, minimum, maximum, RMS features of head fluctuations. Figure 5-11 depicts the comparison between the trends of the numerical and experimental results using the above mentioned features under various flow rates and at N=2755rpm. It is obvious that the above features have the same trends and gradually decrease when the flow rate is increased. Also, the results found that small difference between the numerical and the experimental average head. However, it can be further observed that the maximum numerical head results are lower than experimental head results and the reason behind that is due to the unstable flow in a pump can cause more mechanical and hydraulic losses which will cause more pressure fluctuations. Also, the flow field within a pump is known to be very complex, fully turbulent, and unsteady and the rotating impeller with highly complex blade curvature has a considerable effect on the complex flow field developed either within blade passage or inside the volute. Additionally, the numerical and experimental results for above mentioned features showed a similar trend.

Based on the above analysis, it can be seen that the general behaviour trend of the average head pump numerically and experimentally was in agreement with the one shown in previous studies for various types of pumps [135-138]. However, comparative investigations between numerical results under transient flow conditions and experimental results using different features such as minimum, maximum and RMS of the head were not commonly carried out in most of these studies.

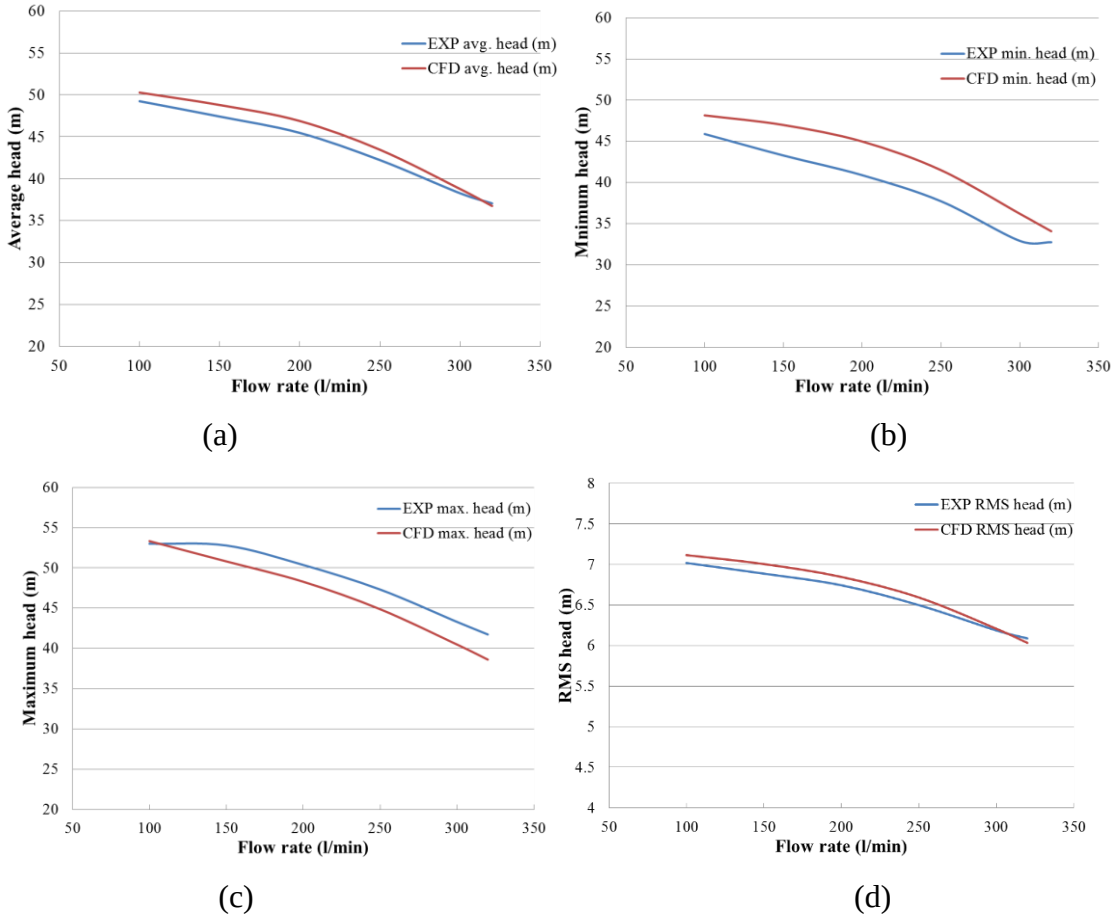

Figure 5-11: Trends of the numerical and experimental results using different statistical features of head fluctuations

5.4. Effect of Pump Rotational Speed on the Performance of the Centrifugal Pump

As mentioned and clearly observed in the previous sections, the flow field behaviour and pump performance directly change depending on the different operating conditions. Therefore, the flow pattern behaviour such as pressure and velocity fields, as well as the flow field instabilities within a pump, depends on various operational conditions. Hence, all of these parameters can affect the flow field and performance of the pump under various pump rotational speeds. Further investigation was carried out in this section, including studying the effect of pump rotational speed on the pressure variations, velocity variations within a pump and performance of the pump.

5.4.1. Effect of the Pump Rotational Speed on the Pressure Variations

The effects of rotational impeller speeds of the pump were investigated under transient approach. The flow field analyses of the static pressure and velocity variations in the pump were presented in this section.

Figure 5-12 depict the static pressure variations corresponding to operating conditions B (number of impeller blades is five, inlet and outlet impeller diameters are di=30mm, do=215mm, and under various rotational speeds of 2320, 2610, and 2755rpm) and at three angular positions 0°, 30° and 60°. For precise comparison, the pressure variation contours under the different pump rotational speeds depicted in Figure 5-12 were presented on a similar scale. It can be seen that from this figure that the pressure is gradually increased from inlet of impeller to outlet and reaches the maximum value at the outlet of impeller blades with lower pressure region being at the eye of the impeller. This flow behaviour within a pump was noticed for all analysed relative impeller positions and for all above cases under investigation. In addition, it is obvious that the pressure values are increased as rotational impeller speed is increased and the higher pressure was obtained at N=2755rpm. Moreover, the result showed that the pressure increases close to the tongue region, this occurs due to the high interaction between impeller and volute in this particular region. The flow field analysis in the impeller shows that there are different pressures on both sides of the impeller blades. In addition, it is observing that from this figure there is a considerable influence on the flow field in the volute zone of the pump when the pump operates at different rotational speeds. Furthermore, based on the above results, it can be seen that the pump rotational speed has a high effect on the pressure variations

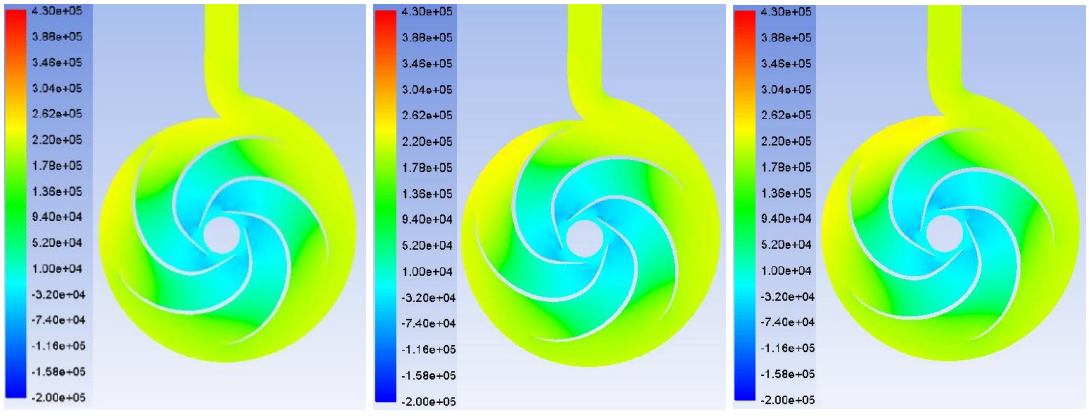

(a) θ =0º (b) θ =30º (c) θ =60º

N=2320rpm

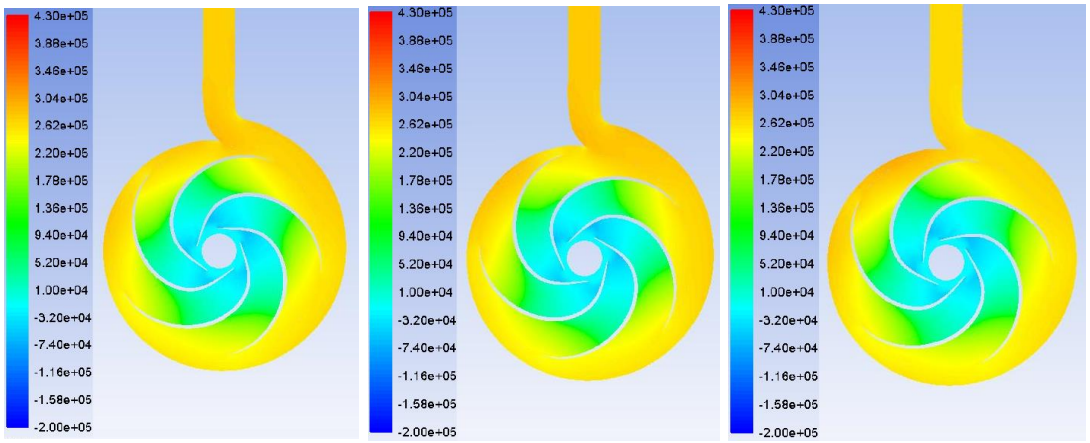

(a) θ =0º (b) θ =30º (c) θ =60º

N=2610rpm

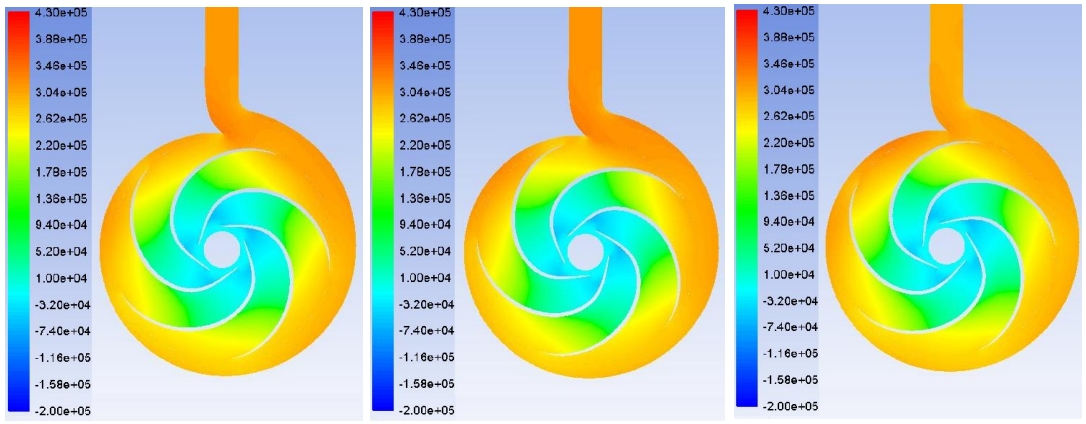

(a) θ =0º (b) θ =30º (c) θ =60º

N=2755rpm

Figure 5-12: Effect of various rotational speeds on the static pressure variations in the pump at Q=300(l/min) under different angular positions

5.4.2. Effect of Pump Rotational Speed on the Velocity Variations

Figure 5-13 depicts the velocity magnitude distribution under different pump rotational speeds of 2320, 2610, and N=2755rpm respectively, and at three angular positions 0°, 30° and 60°. The flow rate considered is design flow rate 300(l/min) with the number of blades similar to the earlier investigation being five. Also, do=215mm and, di=30mm, with results reported at the middle section of the centrifugal pump under transient conditions. It can be observed that for different pump rotational speeds the velocity magnitude inside a pump is gradually increased from the inlet of the impeller to outlet. The velocity at the blades pressure side is higher than the blades suction side for all cases under investigations and it increases as pump rotational speed increases. In addition, the velocity becomes lower when the water goes into

the volute, In addition, the velocity magnitude in the impeller was higher than in the volute. Due to the volute having an asymmetrical cross section area. This means that when the cross section area increases, the velocity of water within the volute decreases leading to an increase in the water pressure as the velocity of water decreases. Furthermore, it is obvious that the velocity magnitude is increased when pump rotational speed is increased and higher velocity was observed at N=2755rpm. The information presented in this figure, regarding the velocity, can be seen to show that the pump rotational speed has a high effect on the velocity in the centrifugal pump.

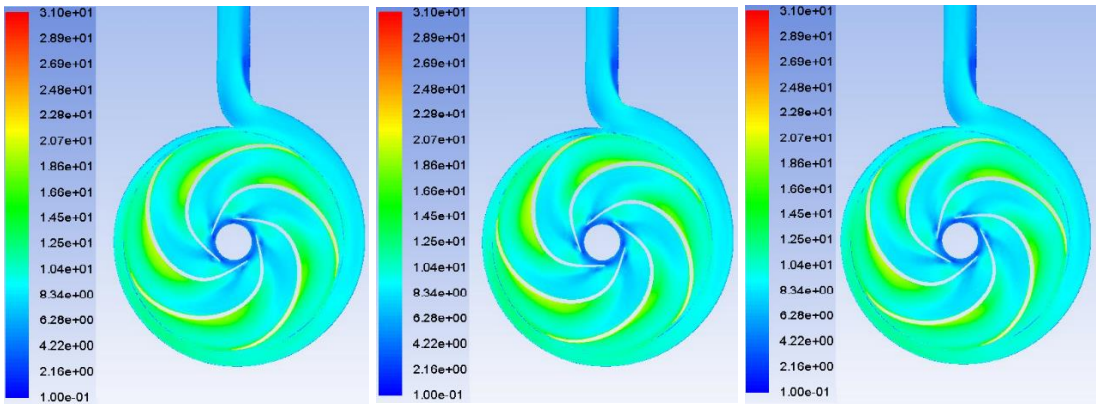

(a) θ =0º (b) θ =30º (c) θ =60º

N=2320rpm

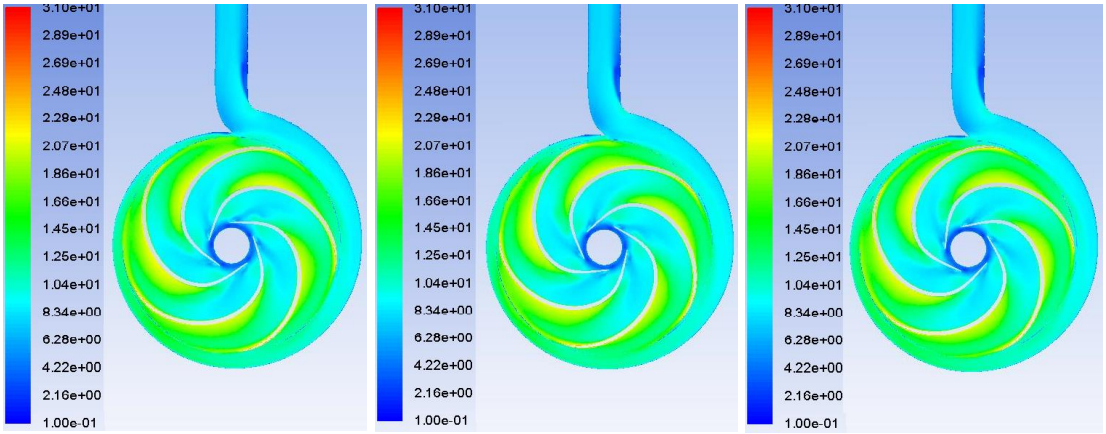

(a) θ =0º (b) θ =30º (c) θ =60º

N=2610rpm

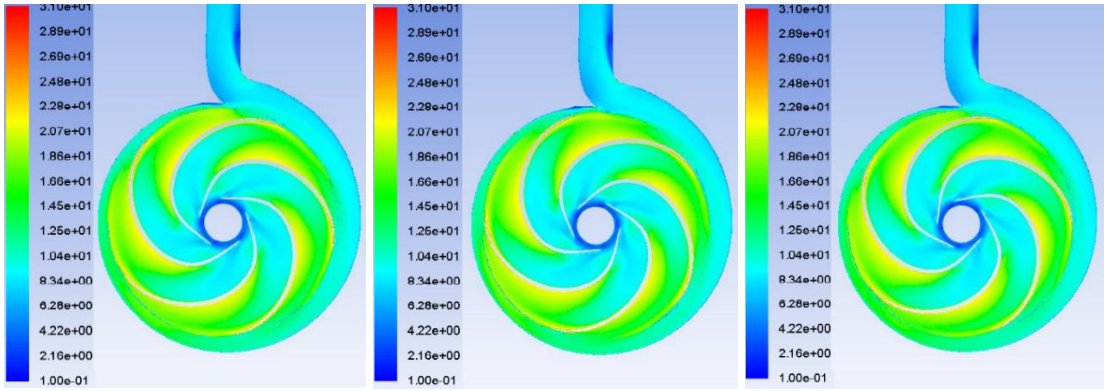

(a) θ =0^o (b) θ =30^o (c) θ =60^o

N=2755rpm

Figure 5-13: Effect of various rotational speeds on the velocity magnitude variations in the pump at Q=300(l/min) under different angular positions

5.4.3. Effect of change in Rotational Speed on the Instantaneous Head

For further investigation based on transient conditions, the centrifugal pump performance is simulated to correspond with condition B. Figure 5-14 depicts the relationship between instantaneous head and various rotational speeds for the one revolution. It can be clearly observed that the instantaneous head of the pump is smaller for N=2320rpm then increases when the impeller rotational speed is increased and higher value of instantaneous head obtained was for N=2755rpm. Also, the waveform trend of instantaneous head at different speeds remains approximately constant. It can be seen that there are the same number of peaks and valleys in one revolution, which are equal to the same number of blades of the impeller, namely five, for all cases under investigation. The unsteady motion of the impeller blades causes these peaks and valleys across the volute tongue region. For further details Table 5-5 provides statistical analysis results such as average, minimum, maximum and (max.-min.) values of the instantaneous head under various pump rotational speeds. By studying this table, it is obvious that all of the above statistical features for the instantaneous head have the same trends; they increase as pump rotational speed increases. Based on the results above, it can be concluded that the pump rotational speed has an important effect on the head of the pump, and that the pump head increases as rotational speed increases.

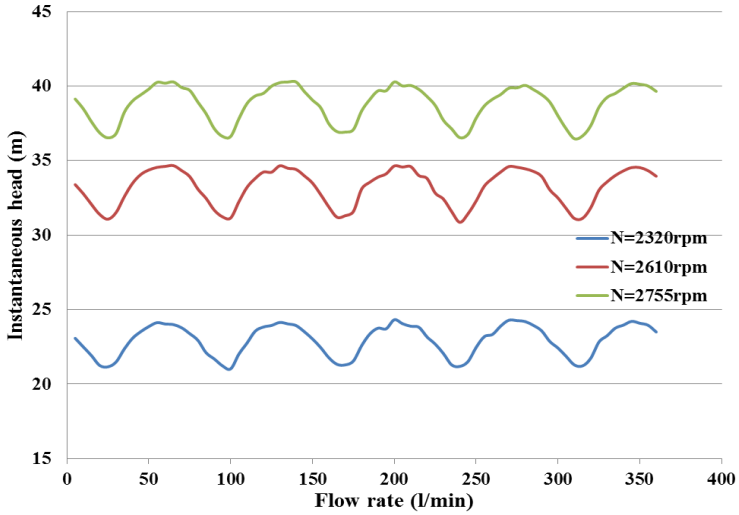

Figure 5-14: Instantaneous head variations of the pump under various rotational speeds

Table 5-5: Statistical analysis results of the instantaneous head for pump under different rotational speed

Pump rotational speed	Head (m)			
(rpm)	Average	Minimum	Maximum	Max - Min
2320	22.90	20.95	24.24	3.28
2610	33.19	30.86	34.66	3.80
2755	38.75	36.47	40.28	3.81

Based on the above understandings, the prediction of the pump head was carried out using CFD under different pump rotational speeds, shows a good agreement with experimental results as shown in Figure 5-15.

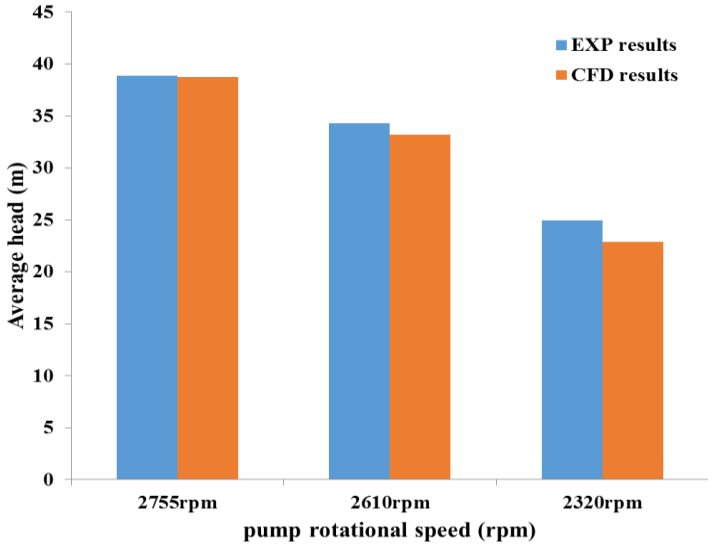

Figure 5-15: Comparison between numerical and experimental average head of the pump under various rotational speeds at Q=300(l/min)

5.5. Analysis of the Pressure Fluctuations in the Centrifugal Pump

The internal flow field in pumps are complex and there are several reasons behind their complexity. Firstly, it is due to the high interaction between fluid and impeller blades as well as the interaction between the rotor part (impeller) and stationary part (volute) especially at volute tongue region as analysed and discussed in the previous sections. Secondly, it is due to the effect of turbulence and the complex unsteady effects within the pump. Thirdly, the most important reason is the occurrence of cavitation. For Further investigations for pressure fluctuations analyses in the impeller and volute at different monitoring points will be discussed in the next section.

5.5.1. Monitoring Points on the Impeller and Volute for the Centrifugal Pump

Many monitoring points are set in the impeller and volute of the pump to investigate and develop comprehensive understanding of the pressure fluctuations within the centrifugal pump under various geometrical parameters and different operational conditions of the pump. For this purpose, there are 15 points that were marked in the volute, including 6 points inside the volute which are set at every 60^{o}, 3 points are set close to the tongue region and in addition 6 points are set at the outlet of the volute, a further 8 points are set in the impeller. The monitoring points for volute are referred to as VP1 to VP15 and for impeller are called IP1 to IP8. Figure 5-16 depicts the distribution of the monitoring points within a centrifugal pump.

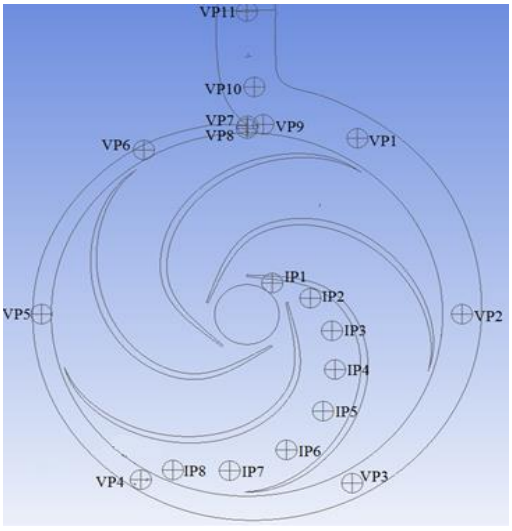

Figure 5-16: Distribution of monitoring point's positions in the centrifugal pump

5.5.2. Analysis of the Pressure Fluctuations of the Pump in Time Domain

Based on the above findings from the previous sections, it can be seen that the numerical calculations using CFD code were reasonable. Therefore, this numerical technique is used to analyse the characteristics of pressure fluctuations in both time and frequency domains analyses within a centrifugal pump, with various operation conditions as illustrated in the next sections. Pressure fluctuations within a pump are unavoidable; hence, they have a high effect on the characteristic for the transient flow field analysis inside the pump. Therefore, studying pressure fluctuation characteristics provides reliable information regarding the pump. Such detail includes the effect of the interaction between the impeller and volute when the pump operates under different operation conditions and various geometrical parameters.

5.5.2.1. Pressure Fluctuations at the Angular Position around the Volute under Design Flow Rate

Figure 5-17 depicts the pressure fluctuations for the volute at 12 monitoring points of the pump the corresponding operating conditions can be designated as condition A (five impeller blades, inlet and outlet impeller diameters of 30mm and 215mm respectively, under design flow rate of 300(l/min) and N= 2755rpm). It can be seen that all the curves for the different monitoring points have five peaks and five valleys with the same number of impeller blades. Table 5-6 provides further quantitatively results of pressure fluctuations on 12 monitoring points at the volute using different statistical features such as average, minimum, maximum and the difference between minimum and maximum. The results found that pressure fluctuations in the volute are increased or decreased for all monitoring points dependent on locations of these points, with respect to volute tongue and outlet volute regions. Furthermore, the maximum pressure values are at points VP6, and VP8 (391.66kPa, 386.58kPa) which are higher than that at other points. The reason behind this is due to locations of these points being nearer the volute tongue and outlet volute regions; as well the interactions between the rotator (impeller) and stator (volute) having high influences on the inner flow field. Based on the information represented in this section, the results of pressure fluctuations around the volute showed that the cross-section area of the volute have a high effect particularly close or near the tongue region.

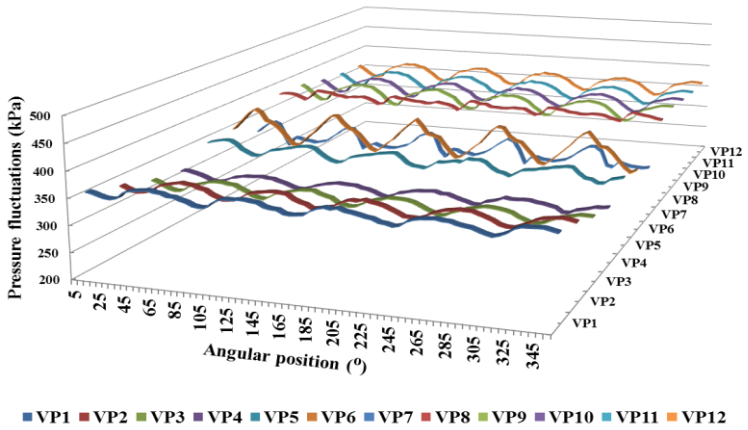

Figure 5-17: Pressure fluctuations around the volute at Q=300(l/min), Z=5, do=215mm, di=30mm, and N=2755rpm

Table 5-6: Statistical analysis results of the static pressure fluctuations in the volute at Q=300(l/min), Z=5, do=215mm, di=30mm, and N=2755rpm

Statistical features	VP1 (kPa)	VP2 (kPa)	VP3 (kPa)	VP4 (kPa)	VP5 (kPa)	VP6 (kPa)	VP7 (kPa)	VP8 (kPa)	VP9 (kPa)	VP10 (kPa)	VP11 (kPa)	VP12 (kPa)
Avg.	352.4	335.59	311.08	300.12	334.35	353.10	309.60	377.10	365.68	359.45	354.68	354.47
Min.	339.1	321.52	296.06	288.27	317.80	315.23	286.86	364.77	340.85	337.28	332.58	332.31
Max.	363.3	348.02	322.16	308.09	347.16	391.66	337.35	386.58	382.55	374.72	369.80	369.61
Min.-Max.	24.25	26.50	26.09	19.82	29.36	76.43	50.49	21.81	41.69	37.44	37.22	37.30

5.5.2.2. Pressure Fluctuations along the Angular Position within the Impeller

In order to investigate the pressure fluctuations in the impeller passages quantitatively, different monitoring points were used as shown in Figure 5-16 in section 5.5.1. Figure 5-18 depicts the pressure fluctuations at the impeller of the pump which the corresponding operating conditions can be designated as condition A, for eight monitoring points. It can clearly be seen that the pressure fluctuation amplitudes at the impeller outlet are higher than the pressure fluctuation amplitudes at impeller inlet. In addition, the pressure fluctuations are increased as the distance from the impeller eye is increased and the maximum value is at the outlet of the impeller diameter as mentioned earlier. The pressure fluctuations are increased near the volute tongue and the high-pressure are noticed at points IP7 and IP8. According to this figure, the pressure fluctuations curves for points IP1 and IP2 are relatively flat. The results of the pressure fluctuations as depicted in this figure showed that the larger pressure fluctuations can be seen at monitoring point IP8, where the maximum value for pressure fluctuation is 354.85kPa as shown in Table 5-7. Furthermore, the minimum pressure fluctuations were at monitoring point IP1 due to the location of this point being close to the eye of the impeller and this particular region has a low-pressure area. Based on the above analysis regarding the pressure fluctuations

at the impeller, the results showed that the radius of the impeller and the volute tongue region have a high effect on the pressure fluctuations.

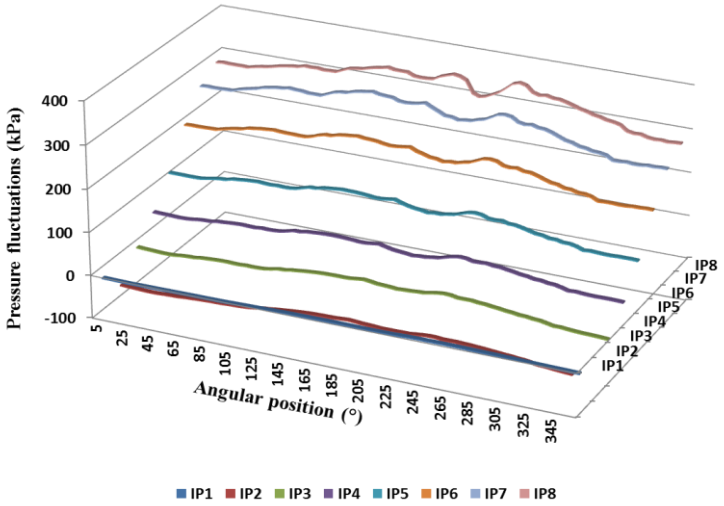

Figure 5-18: Pressure fluctuations in the impeller and the pump having Q=300(l/min), Z=5, do=215mm, di=30mm, and N=2755rpm

Table 5-7: Statistical analysis results in the impeller at Q=300(l/min), Z=5, do=215mm, di=30mm, and N=2755rpm

Statistical features	IP1 (kPa)	IP2 (kPa)	IP3 (kPa)	IP4 (kPa)	IP5 (kPa)	IP6 (kPa)	IP7 (kPa)	IP8 (kPa)
Avg.	-16.48	-55.32	3.44	55.63	123.04	211.81	279.78	312.71
Min.	-19.78	-71.26	-13.52	39.68	104.06	185.72	248.68	277.86
Max.	-13.57	-43.27	21.09	73.79	143.79	236.94	309.88	354.85
Min.-Max.	-6.21	-27.98	7.57	15.95	18.98	26.10	31.10	34.85

For further analysis regarding the change in pressure within a centrifugal pump, Figure 5-19 depicts the average pressure at 8 monitoring points within the impeller for the pump under different flow rates namely 100, 150, 200, 250, 300, 320(l/min) at constant N=2755rpm. It can be seen that the negative pressure is exhibited at the inlet of the impeller particularly at monitoring points IP1 to IP2, as well as at point 3 for flow rate of 320(l/min). It can be seen that the low-pressure region in the eye of the impeller decreases as flow increases. This is because this particular area of the impeller has lower pressure and hence, may cause cavitation due to the decrease in the water pressure in this region below the water vapour pressure. The results also showed that the average pressure at the impeller increases with distance from the eye and can be seen from monitoring points IP1 to IP8 under the different flow rates. Also, the highest value for the average pressure was at point IP8 for the different flow rates. Furthermore, it can be clearly observed that the average pressure decreases as flow rate increases for various cases under investigation. Table 5-8 and Table 5-9 summarise the maximum and minimum

pressure fluctuations of the 8 monitoring points at the impeller under different flow rates. Based on above results it can be concluded that the pressure in the impeller increases when the distance from the eye along the radius of the impeller increases. The low pressure at the eye of the impeller decreases as flow rate increases.

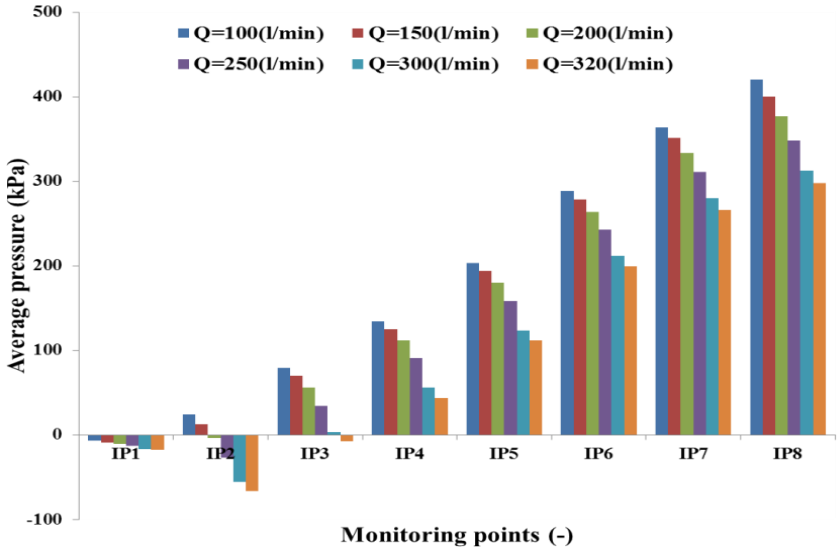

Figure 5-19: Average pressures in the impeller under different flow rates

Table 5-8: Maximum static pressure fluctuations at the impeller under different flow rates

Flow rate (l/min)	IP1 (kPa)	IP2 (kPa)	IP3 (kPa)	IP4 (kPa)	IP5 (kPa)	IP6 (kPa)	IP7 (kPa)	IP8 (kPa)
100	-4.47	40.23	99.45	159.46	233.67	326.66	409.66	470.67
150	-5.93	29.24	91.09	151.25	226.02	318.75	400.81	457.71
200	-6.03	14.93	76.03	135.82	210.44	301.81	381.60	428.62
250	-9.51	-9.84	52.22	110.55	183.08	274.59	350.48	388.64
300	-13.57	-43.27	21.09	73.79	143.79	236.94	309.88	354.85
320	-14.26	-49.70	13.80	68.80	140.91	235.56	308.84	355.82

Table 5-9: Minimum static pressure fluctuations at the impeller under different flow rates

Flow rate (l/min)	IP1 (kPa)	IP2 (kPa)	IP3 (kPa)	IP4 (kPa)	IP5 (kPa)	IP6 (kPa)	IP7 (kPa)	IP8 (kPa)
100	-8.86	12.43	57.67	102.66	159.34	232.52	294.25	314.41
150	-10.76	2.95	51.16	96.32	152.81	224.27	285.00	309.30
200	-13.19	-15.38	42.03	93.50	151.08	225.01	286.12	311.56
250	-16.17	-40.58	21.12	74.80	138.67	216.97	278.07	310.70
300	-19.78	-71.26	-13.52	39.68	104.06	185.72	248.68	277.86
320	-20.17	-81.59	-25.98	24.44	89.53	173.06	234.22	261.64

Figure 5-20 depicts the average pressure at 12 monitoring points around the volute for the centrifugal pump under different flow rates namely 100, 150, 200, 250, 300, 320(l/min) at N=2755rpm. It can be seen that the average pressure has the same trend for different cases under investigation. Also, the results showed that for different monitoring points around the volute, the pressure decreases as flow rate increases, except for monitoring points VP6 and VP7, where the average pressure is slightly increased when the pump operates near or higher

than the design flow rate. This is due to the fact that the locations of these points are near to the tongue region. Additionally, it can be observed that the maximum value of pressure was at volute outlet. Table 5-10 and Table 5-11 summarise the maximum and minimum pressure fluctuations of the 12 monitoring points within the volute under different flow rates. Furthermore, based on the above analysis, with regard to the variations of pressure in the volute, the results showed that the volute cross-section area especially at tongue region and flow rate have a high effect on the pressure variations.

Table 5-10: Maximum static pressure fluctuations at the volute under different flow rates

Flow rate (l/min)	VP1 (kPa)	VP2 (kPa)	VP3 (kPa)	VP4 (kPa)	VP5 (kPa)	VP6 (kPa)	VP7 (kPa)	VP8 (kPa)	VP9 (kPa)	VP10 (kPa)	VP11 (kPa)	VP12 (kPa)
100	497.13	493.66	483.02	457.91	435.36	420.39	364.83	452.74	512.24	511.06	510.27	509.24
150	476.98	469.38	452.97	426.62	410.03	388.77	344.96	448.74	494.26	492.97	491.71	490.73
200	448.43	438.82	417.40	393.26	394.74	378.30	331.23	438.64	466.73	463.84	462.55	461.27
250	411.84	399.28	374.24	353.83	371.77	384.39	326.44	420.21	429.36	424.72	422.47	421.32
300	363.39	348.02	322.16	308.09	347.16	391.66	337.35	386.58	382.55	374.72	369.80	369.61
320	344.02	328.08	301.67	290.92	340.78	393.86	337.34	366.76	362.53	354.97	348.69	348.81

Table 5-11: Minimum static pressure fluctuations at the volute under different flow rates

Flow rate (l/min)	VP1 (kPa)	VP2 (kPa)	VP3 (kPa)	VP4 (kPa)	VP5 (kPa)	VP6 (kPa)	VP7 (kPa)	VP8 (kPa)	VP9 (kPa)	VP10 (kPa)	VP11 (kPa)	VP12 (kPa)
100	478.89	469.42	449.35	426.96	423.09	364.88	285.12	0.00	471.20	473.71	472.95	471.89
150	462.82	448.28	423.03	396.66	400.09	358.27	264.13	427.60	457.05	458.41	457.16	456.12
200	437.26	420.11	390.38	362.63	375.32	356.39	273.43	412.31	435.10	435.28	433.89	432.62
250	395.90	378.15	347.84	328.39	350.49	342.53	286.09	396.56	396.77	394.84	392.59	391.46
300	339.14	321.52	296.06	288.27	317.80	315.23	286.86	364.77	340.85	337.28	332.58	332.31
320	314.38	298.29	274.12	273.20	304.26	303.37	288.67	342.99	314.24	310.60	304.59	304.75

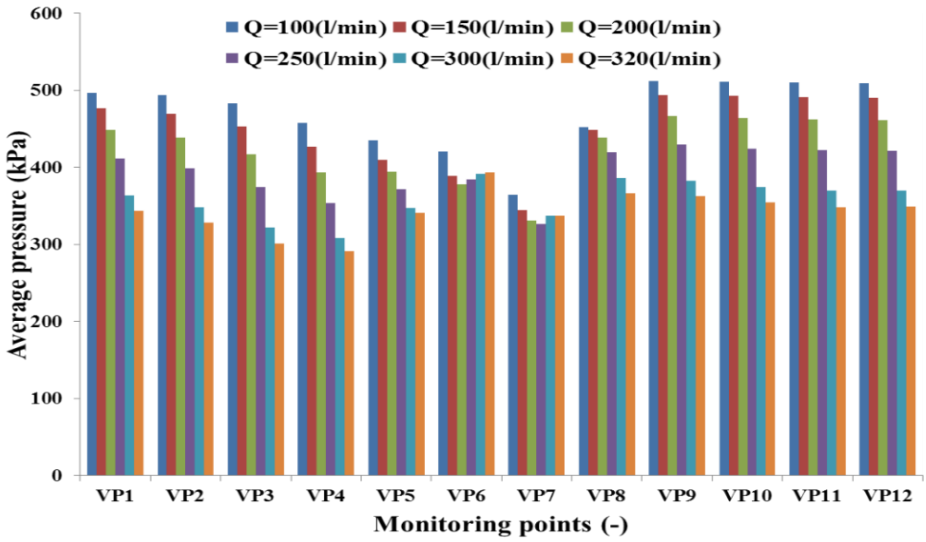

Figure 5-20: Average pressures around the volute under different flow rates

For further investigation the pressure fluctuations within a pump were analysed in frequency domain using FFT as can be seen in the next section.

5.5.3. Analysis of the Pressure Fluctuations of the Pump in Frequency Domain

The Fast Fourier Transform converts the time domain data into frequency domain and generates a complex spectrum of the sampled signals under study, it is commonly utilised in different engineering fields such as electrical, mechanical and computer engineering [12]. The outcome of the FFT in the present study offers the amplitude of pressure fluctuations with frequency [12]. There are two dominant frequencies in the centrifugal pump, the first being the rotational frequency (Rf) and its related harmonics, and can be calculated through the use of the below equation:

$$Rf = (N/60) \text{ or } (\text{impeller rotational speed}/60) \quad (5\text{-}1)$$

The second one is Blade Passing Frequency (BPF) and its related harmonic which can be calculated by using Eq. (5-2):

$$BPF = (\text{impeller rotational speed}/60) * \text{number of blades, or } BPF = (N/60) * Z \quad (5\text{-}2)$$

These types of frequencies are generated due to the movement of impeller blades.

Figure 5-21 depicts the 3-D figure of volute pump frequency and its harmonics against pressure amplitude for all the monitoring points, the corresponding operating conditions A. This figure depicts the pressure fluctuation amplitudes with their frequencies for the different monitoring points on the volute. At the volute, the maximum pressure fluctuation amplitude for all the monitoring points are at BPF 236.14Hz. This type of frequency is generated because of the interaction between the impeller blades and the volute, close to the volute tongue region, where the BPF value was quite higher than that of the other region. In addition, the frequency for all monitoring points is significant at first harmonic. Further analysis of the frequency results exhibit that the deviation of calculation outcomes for transient conditions compared with calculation by equation (5-2) for the BPF is about 2.78%, where the BPF from above equation is equal to 229.58Hz. Furthermore, the numerical results showed that all curves of monitoring points have a similar trend but at different maximum amplitude values based on the location of these monitoring points close, near or far, relative to the volute tongue region as shown in Table 5-12. Based on the information represented in this section, with regard to the pressure fluctuation amplitudes around the volute, the results revealed that unsteady flow and asymmetric cross-section area of the volute have a high effect on increased or decreased values of the pressure fluctuations amplitude, particularly near the tongue region.

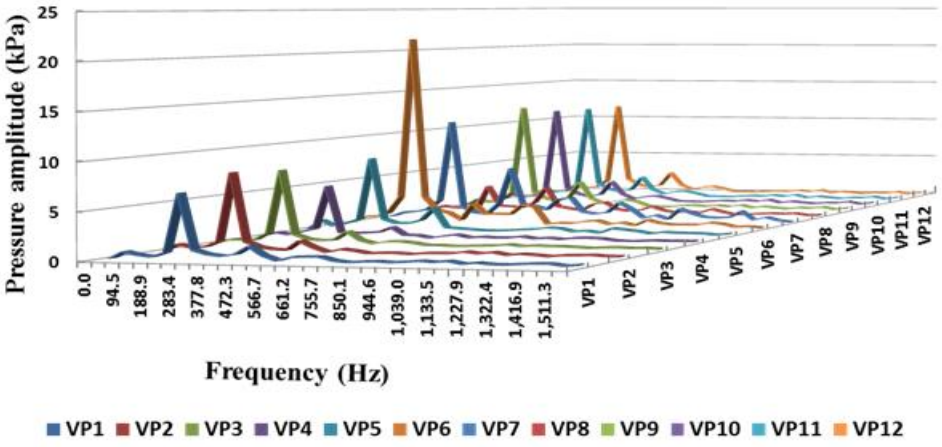

Figure 5-21: Frequency spectra around the volute and the pump having Q=300(l/min), Z=5, do=215mm, di=30mm, and N=2755rpm

Table 5-12: Maximum amplitude of pressure fluctuations at the volute and the pump with Q=300(l/min), Z=5, do=215mm, di=30mm, and N=2755rpm

Frequency	Maximum amplitude of pressure fluctuations for 12 monitoring points at the impeller (kPa)											
Hz	VP1	VP2	VP3	VP4	VP5	VP6	VP7	VP8	VP9	VP10	VP11	VP12
236.14	6.73	8.23	7.91	5.58	8.11	21.55	11.42	3.09	12.41	11.66	11.54	11.55

Figure 5-22 depicts the three dimensional figure of impeller pump frequency (shaft frequency) and its harmonics against pressure amplitude for all monitoring points. This figure shows the variations in the amplitude of the pressure fluctuation against frequencies for all the monitoring points and the amplitude of the frequency was quite significant at the first harmonic. Also, the pressure fluctuation increases with radius of the impeller increases and the maximum value of the pressure fluctuation is at the outlet of the impeller diameter. In addition, in the impeller, the maximum pressure fluctuation for entire monitoring points is at frequency equal 47.23Hz. The pressure fluctuation gradually decreases with increasing frequency for all points and the amplitude of pressure fluctuations at monitoring point IP8 was larger than other points as displayed in Table 5-13. The analysis showed a 2.77% deviation from the calculated results for transient conditions when compared with equation (5-1) for the impeller rotational frequency. Based on the above investigation regarding the amplitude of the pressure fluctuations at the impeller, the results revealed that unsteady flow and impeller diameter has a high effect on the pump pressure amplitudes.

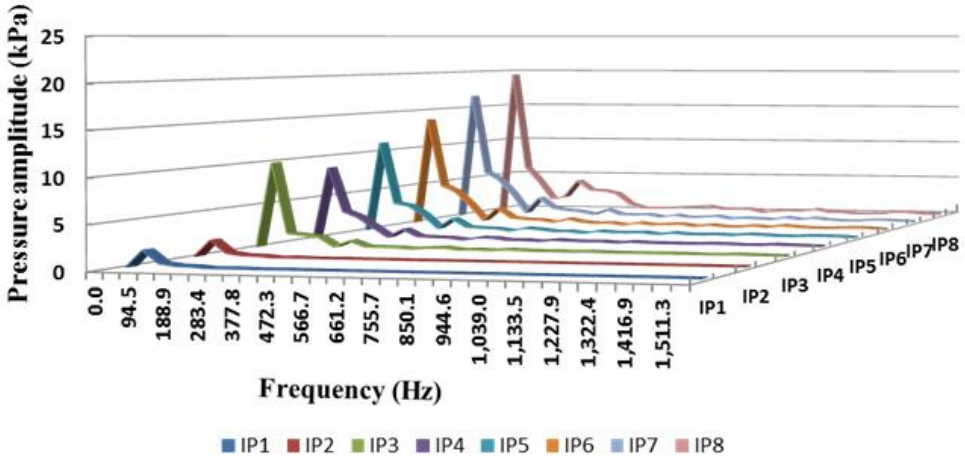

Figure 5-22: Frequency spectra in the impeller and the pump having Q=300(l/min), Z=5, do=215mm, di=30mm, and N=2755rpm

Table 5-13: Maximum amplitude of static pressure fluctuations at the impeller and the pump with Q=300(l/min), Z=5, do=215mm, di=30mm, and N=2755rpm

Frequency	Maximum amplitude of pressure fluctuations for 8 monitoring points at the impeller (kPa)							
Hz	IP1	IP2	IP3	IP4	IP5	IP6	IP7	IP8
47.23	1.89	1.89	10.00	8.73	11.24	13.82	16.66	19.45

5.6. Cavitation Detection in the Centrifugal Pump

Undoubtedly, cavitation has undesirable effect in any turbomachinery system such as turbines and pumps. Due to cavitation effects, various types of problems occur such as performance deterioration, damage to the turbomachinery components and increase in the level of noise and vibration. In this current study, an attempt was made to investigate the effect of cavitation within a centrifugal pump using numerical analysis. The performance analysis of the pump and detection of cavitation was carried out under various operating conditions. The results were presented in the form of vapour volume fraction contour and in the form of the pump head for qualitative and quantitative analyses respectively. Vapour volume fraction is a significant parameter in detecting cavitating flow conditions within a centrifugal pump, varying from between 0 and 1. When the value of vapour volume fraction is equal 1, this means 100% of vapour bubbles have occurred.

5.6.1. Detection of Cavitation in the Impeller of the Centrifugal Pump

This section will discuss and analyse the detection of cavitation using numerical simulation inside the pump. This tool is being used to reveal the significant characteristic mechanism of cavitation in the pump. In order to achieve this, CFD code was used to simulate the two-phase

flow (water-liquid and water-vapour). This study will be carried out under various flow rates in order to study the effect of these wide ranges of flow rates. The flow rates include 150, 200, 250, 300, 320, 330, 340, 350, 360, and 370(l/min) respectively, under cavitation conditions. In order to investigate the inception and development of cavitation within the inner flow fields of centrifugal pump under various flow rates, the vapour volume fraction distribution of cavitation is analysed in this section.

Figure 5-23 shows the distribution of vapour volume fraction near the inlet of an impeller under various flow rates. Generally, cavitation occurs in the vicinity of low-pressure region. The results showed that the cavitation inception and development on the impeller could be classified into four levels as per the increase in the vapour volume fraction. The following points emerged from the present investigation:

- Level 1: No cavitation occurrence in this stage is noticed

When the range of flow rate is between 150 and 250(l/min), the cavitation does not occur as depicted in Figure 5-23 (a) to (c).

- Level 2: The stage of small inception of cavitation

When the range of flow rate is between 300 and 320(l/min), the cavitation mostly occurred on the suction surface of the impeller blades passages. Thus, it can be observed that the cavitation zone is small, and then it slowly increases. However, the cavitation increase at this stage is slow, showing inception of cavitation as depicted in Figure 5-23 (d) and (f).

- Level 3: The stage growth of cavitation

When the range of flow rate is between 320 and 350(l/min), a rapid cavitation growth occurs on the impeller and the location of cavitation extends to inlet sides of passages. The cavitation zone develops, and then from this range cavitation rapidly grows in the impeller of the pump. Furthermore, it is obvious that from this figure the maximum vapour volume fractions are mostly distributed in a specific area nearby the entrance of the impeller, particularly in the eye of impeller.

- Level 4: The stage of development of cavitation

In this final stage when the flow rate is higher than 350(l/min), the cavitation mostly develops in all the passages of the impeller. Also, it can be clearly seen that the centrifugal pump under this flow rate has the highest vapour volume fraction at near and around the inlet of impeller compared with other flow rates. Under this flow rate, the smaller bubbles increase rapidly, thereafter causing blockages to the flow of water and consequently causing a reduction in the performance of the pump. The maximum vapour volume fractions were mostly distributed in

a special area near the inlet surface of blades of an impeller, subsequently progressively increasing along each passage of an impeller. Also, it can be seen that the vapour volume fraction increases along the radial direction, and then starts to block the inlet passages of the impeller under high flow rates. This indicates that the performance of the centrifugal pump significantly decreases under high flow rate.

As a result, from above findings, it can be concluded that the numerical analysis using CFD code provides a good indication regarding the behaviour of cavitation within a centrifugal pump under a wide range of operational conditions.

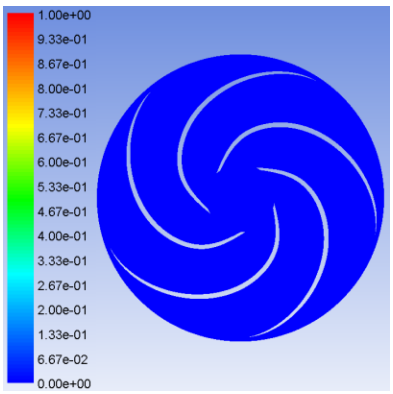

(a)150(l/min)

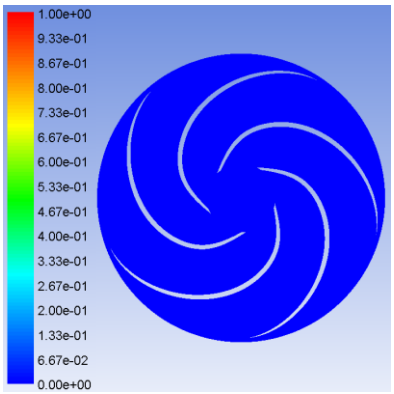

(b) 200(l/min)

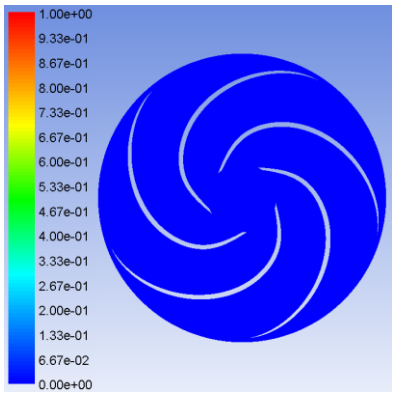

(c) 250(l/min)

No cavitation

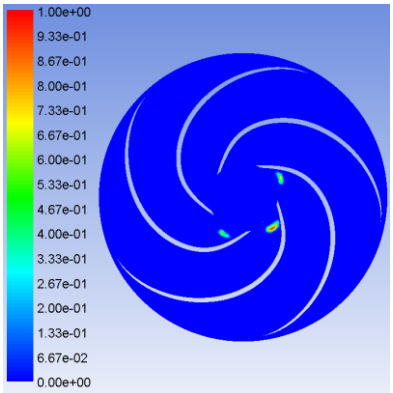

(d) 300(l/min)

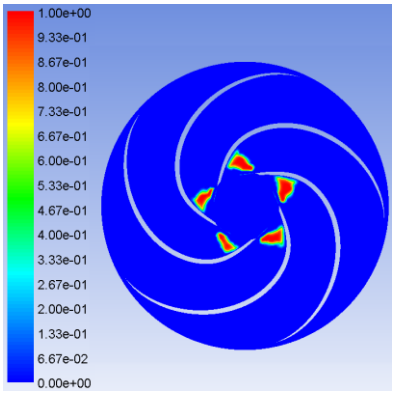

(e) 320(l/min)

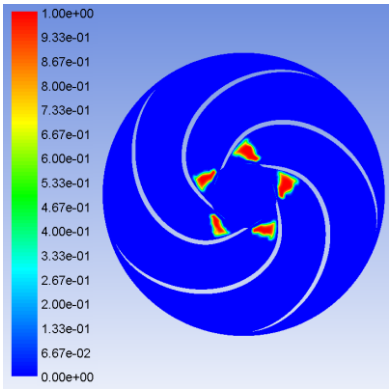

(f) 330(l/min)

Inception of cavitation

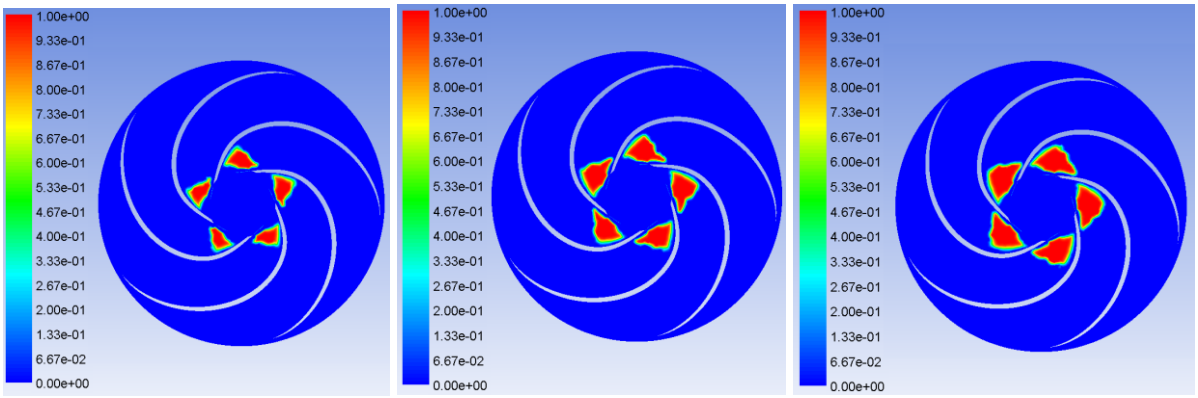

(g) 340(l/min) (h) 350(l/min) (i) 360(l/min)

Development of cavitation

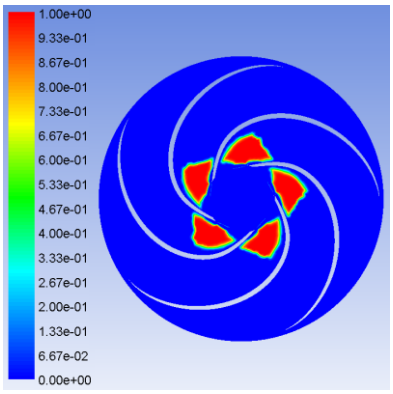

(j) 370(l/min)

Fully development of cavitation

Figure 5-23: Vapour volume fraction distributions under different flow rates at 2755rpm

Based on the above numerical results the following conclusions can be noted:

- The results showed that cavitation in turbomachines, like the centrifugal pump, is a significant phenomenon that affects the performance of the pump. Also, analysing the level of cavitation, as well as investigating their impact on the flow field pattern within a pump, needs to be further studied. In addition, the ability to compute and analyse cavitation using CFD code is important due to it can help in linking local flow features with global performance characteristics of the pump.
- The position, level and characteristics of the cavitation within a centrifugal pump were investigated. Also, the numerical simulation for flow in the pump under various operating conditions was carried out. Additionally, the results revealed that the cavitation mainly occurred at the inlet eye of impeller flow region with no cavitation occurring at the volute flow region.

- The numerical investigation results found that it can capture the different levels of cavitation in the pump. Also, these numerical results revealed that the cavitation cannot be observed at low range flow rates. While at high range flow rates, bubble formation occurs and the cavitation were observed to occur, meaning that the occurrence of cavitation increases as the flow rate increases.
- Based on the above analysis, the results showed that the flow rate has a high effect on cavitation, particularly at the eye of the impeller region.
- Numerical simulation using CFD technique accurately predicts the behaviour of the flow field and cavitation within a centrifugal pump.
- The results showed that the use of CFD was good tool for detecting the different levels or stages of cavitation such as no cavitation, inception, development and full development within a centrifugal pump under various operation conditions.

5.6.2. Instantaneous Pump Head at Different Flow Rates with Two-phase Modelling Approach

The effects of different operating conditions on the instantaneous head of the centrifugal pump with two-phase modelling approach at various flow rates were investigated. The flow rates of 150, 200, 250, 300,320, 330, 350, 360, 370(l/min) were selected for this study. The instantaneous head at various flow rates are compared, and the results are depicted in Figure 5-24. It can be clearly seen that the different operational conditions have a significant and clear influence on the instantaneous head at the pump. Moreover, the same trend can be seen as for single-phase modelling approach that is instantaneous head decreases when the flow rate is increased. That supported by the fact that there are five peaks and valleys depending on the number of blades, the average heads are 47.48, 45.56, 42.59, 38.11, 36.04, 34.55, 32.78, 30.58,28.52, and 25.70m respectively. Based on the information represented in this section, the results of the effect of cavitation on the head under different flow rates showed that the flow rate has a high effect on the pump head.

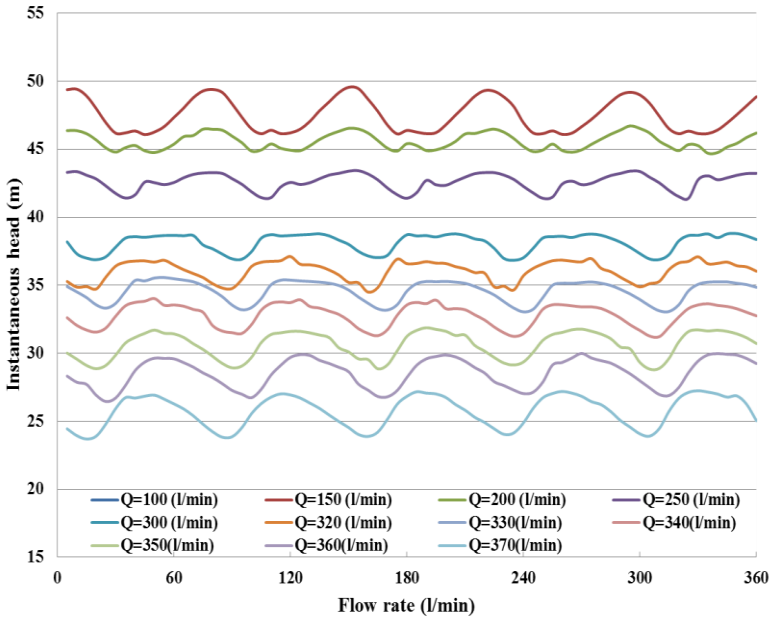

Figure 5-24: Instantaneous head of the centrifugal pump under cavitation conditions and various flow rates at 2755rpm

5.6.3. The Transient Cavitation Behaviour under Design Flow Rate in One Revolution Cycle

Figure 5-25 depicts the inception of cavitation in the passages of the impeller at operational conditions were flow rate of 300(l/min), Z=5, do=215mm, di=30mm, and N=2755rpm, in one revolution cycle at six different angular positions. Location of small areas of cavitation at the inlet of the impeller, close to the leading edges of blades on the flow passage can be seen due to the lower pressure zone within this domain. Also, the cavitation area is approximately the same during the impeller rotating in on the cycle. Furthermore, cavitation under the design flow rate of Q=300(l/min) was inception of cavitation. According to the specification of America hydraulic standard association, cavitation development occurs when the head is decreased by 3% [114, 139].

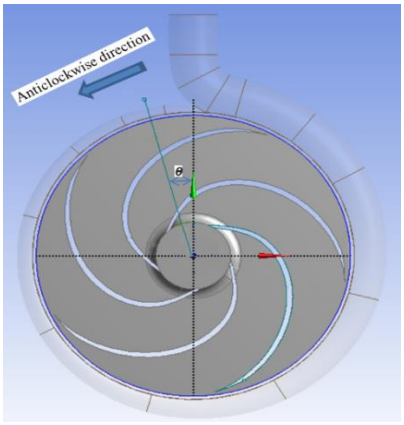

Anticlockwise impeller direction

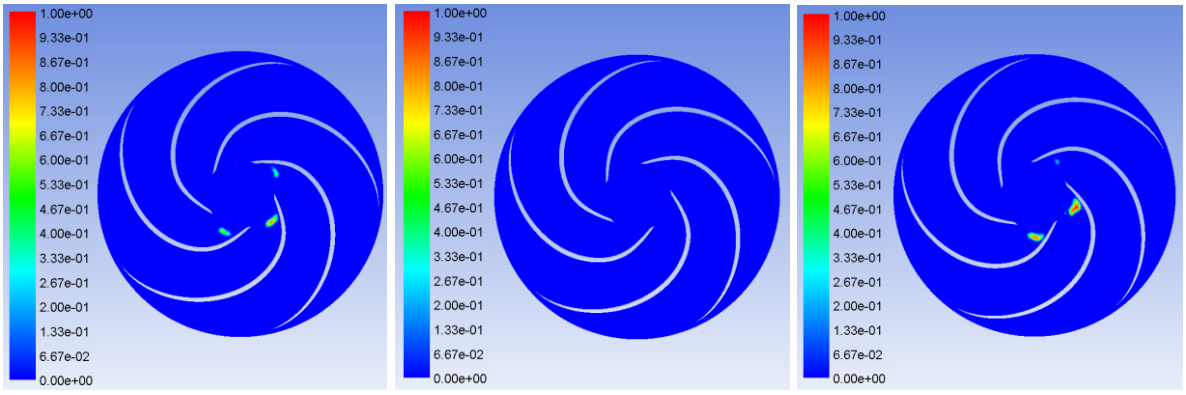

θ=60º θ=120º θ=180º

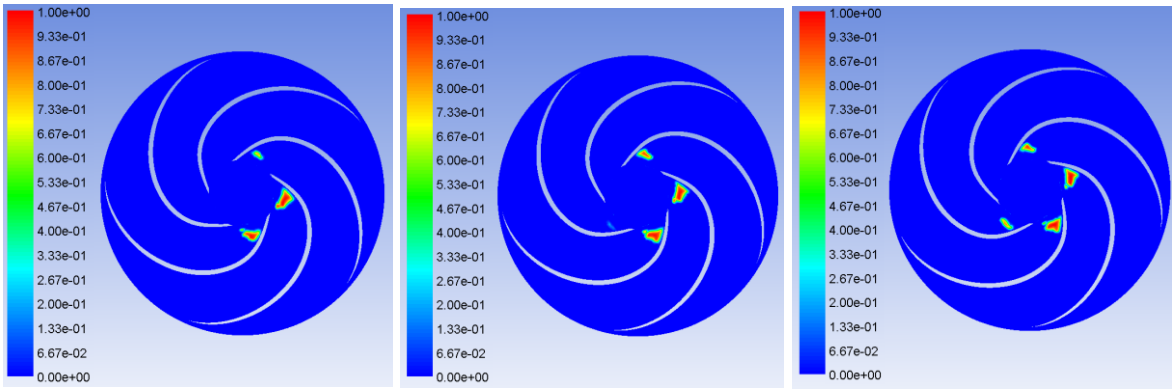

θ=240º θ=300º θ=360º

Figure 5-25: Impeller direction and behaviour of the vapour volume fraction distributions in the passages of impeller at different angular positions

5.6.4. Pressure Variations under Cavitation Condition at Different Flow

Figure 5-26 depicts the vapour volume fraction and pressure variations contours under the condition of inception and development of cavitation at different flow rates (300, 350 and 370l/min). For accurate comparison purposes, all the pressure variations and vapour volume fraction distribution contours displayed in this figure were plotted on a similar scale. It can be

seen that the cavitation appears at the inlet eye of impeller near the blade's leading edges at a flow rate of 300(l/min). It (cavitation) then extends and develops in the passages of the impeller at flow rates of 350 and 370(l/min). This occurs because of the decrease of the low-pressure region at the inlet eye of the impeller. When the pressure decreases at the eye of impeller, cavitation increases particularly at this region. However, cavitation on every passage remained approximately the same at 350 and 370(l/min) flow rates. It can be seen from the above findings that the cavitation inception and development in the centrifugal pump is highly dependent on the low-pressure region at the inlet eye of impeller. Again, based on the above analysis illustrated in this section, regarding the cavitation, the results showed that the flow rate has a high effect on the cavitation within a pump.

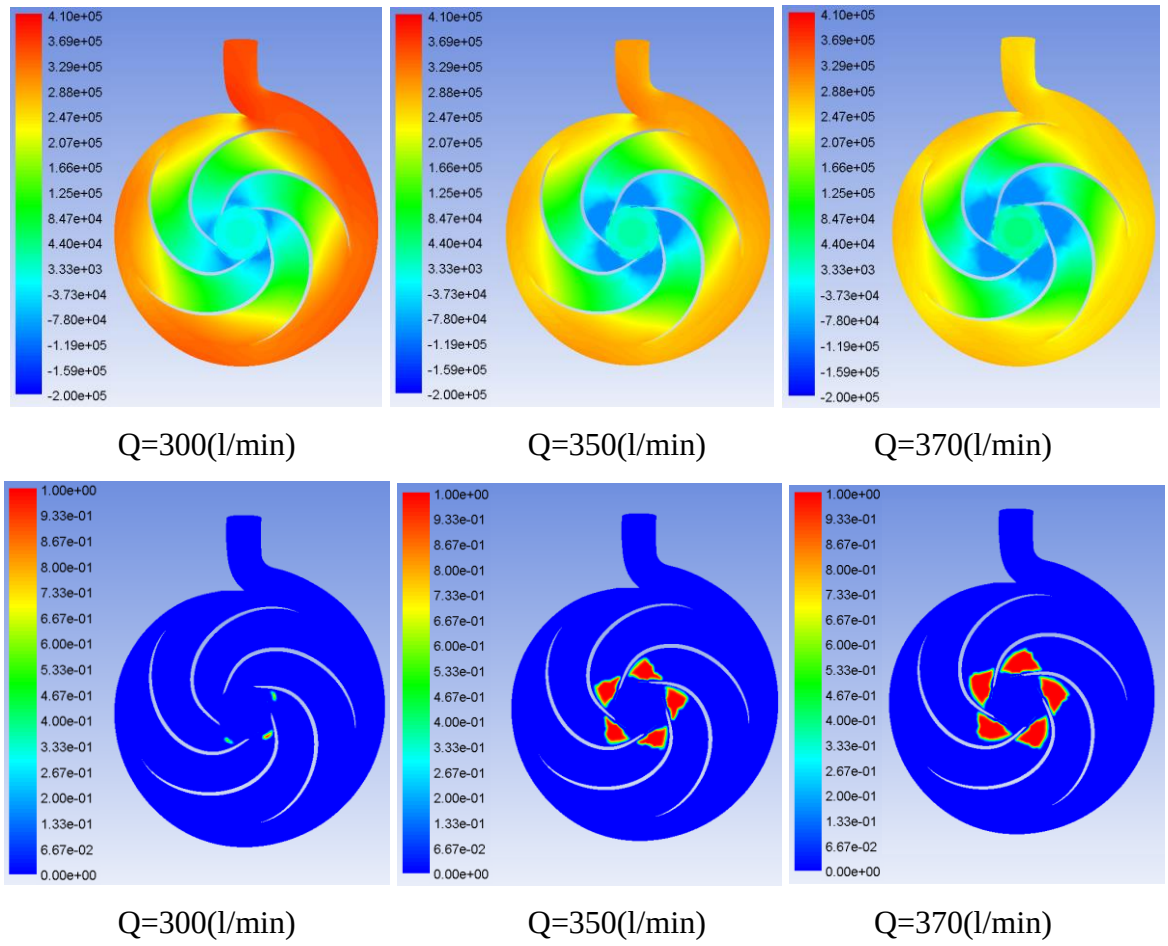

Figure 5-26: Static pressure and volume fraction variations contours in the centrifugal pump under 300, 350 and 370(l/min)

5.6.5. Detection of Cavitation within the Centrifugal Pump under Different Flow Rates

The head of the centrifugal pump was calculated under both single-phase and cavitation conditions as depicted in Figure 5-27. These curves displaying numerical results from CFD

predictions corresponding to N=2755rpm. It can be observed that the head of the pump decreases as the flow rate increases, with the curve of the head under cavitation conditions lower than the curve for single-phase. Furthermore, the result showed that from flow rate of 150 to 250(l/min), both curves corresponding to single-phase and cavitation conditions are quite close. This is due to the fact that no cavitation occurred under this flow rate range, which then led to no significant change occurring at the head of the pump. Also, cavitation zone can be seen to form at the inlet of the impeller. It can be seen that the low pressure in the eye of the impeller decreases as the flow rate increases as shown in the previous section. The inception of cavitation occurred when the flow rate is around 300(l/min) because of the head decreased, when compared with that of the single-phase condition under the same flow rate, which is about a 0.577% difference. According to the specification of American hydraulic standard association, the cavitation development occurred with a 3% decrease in the head [140]. The numerical results indicated that cavitation starts to develop after a flow rate of 340(l/min) within the impeller of the pump. Also, fully developed of cavitation occurred on the suction surface, close to the inlet of the impeller, after a flow rate of about 370(l/min) in the pump. This is due to the existence of a lower pressure zone within this area which further causes a decrease in head when compared with single-phase condition. Based on the above analysis, it is clear that the inception of cavitation starts from 320 to 340(l/min) because of the fact that the head drop at flow rate 340(l/min) was about 3.39%. However, the development of cavitation occurred at flow rate of 350(l/min) because the head drop at this flow rate was around 6.4%. The highest head drop comparison between single-phase and cavitation conditions occurred at flow rate of 370(l/min) which was around 14.6%.

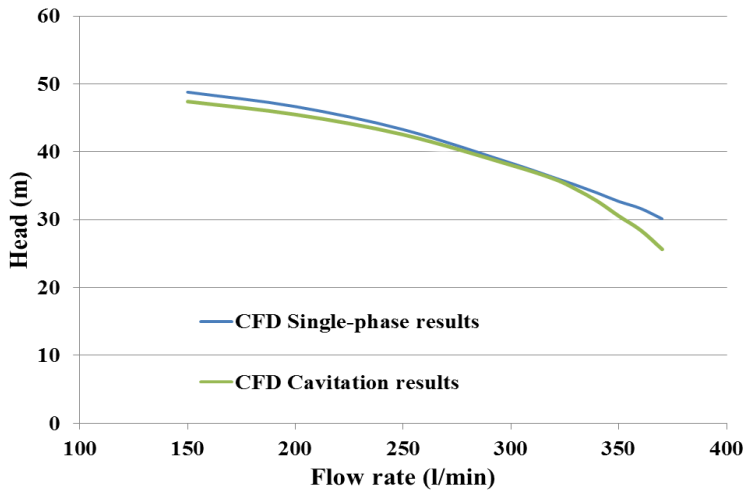

Figure 5-27: Characteristic curves of the centrifugal pump under single-phase and cavitation conditions

5.6.6. Detection of Cavitation Behaviour in the Centrifugal Pump under Different NPSH

This section further analyses the flow structure within the centrifugal pump under cavitation model by decreasing the value of the outlet pressure, the value of NPSHA is reduced and the cavitation curves are obtained as discussed in the following section [141]. The NPSH was calculated by using Eq. (4-14). The value of NPSHR is determined when the head of the pump is decreased under 3% [114], according to the American Hydraulic Standards Institute [139].

Figure 5-28 depicts the results of simulation within the centrifugal pump by varying the volume fraction with various NPSH values and the pump operated under design operating conditions with flow rate of 300(l/min), Z=5, do=215mm, di=30mm, and N=2755rpm. The NPSH are 9.93, 8.93, 7.91, 6.89, 5.86, and 4.85m, corresponding to letters A, B, C, D, E and F respectively in Figure 5-28, within the centrifugal pump. As seen in the previous section, in order to make the cavitation regions within an impeller more apparent, it can be visualised through the use of vapour volume fraction contours. The appearance of a cavity first occurs on the suction side nearby the blade leading edges within the impeller flow passages in the low pressure region. Thereafter, the cavitation zone becomes greater at the inlet impeller, as depicted in Figure 5-28 (F). The numerical results found that when the value of the NPSHA was decreased, the cavity extends in the impeller channels and may cause a flow blockage. Furthermore, cavitation will fill the spaces within the inter blade passage alongside the blades of an impeller. The head of the pump begins to drop as revealed in Figure 5-28. This figure shows that as a result of a sudden drop in the pump head, the cavitation bubbles become larger. In this situation, the pump performance becomes abnormal and high-pressure fluctuations begin to occur due to the collapse of the bubbles, causing damage to the blades of the impeller. The numerical results showed that cavitation increases as the NPSH decreases and severe cavitation occurs within the pump when the NPSH continues to decrease, which occurs at the inlet of the impeller at the suction side of blades. This is due to the fact that this region has low pressure when compared to other regions in the pump. As a result, the formation of cavitation occurs faster at low values of NPSH.

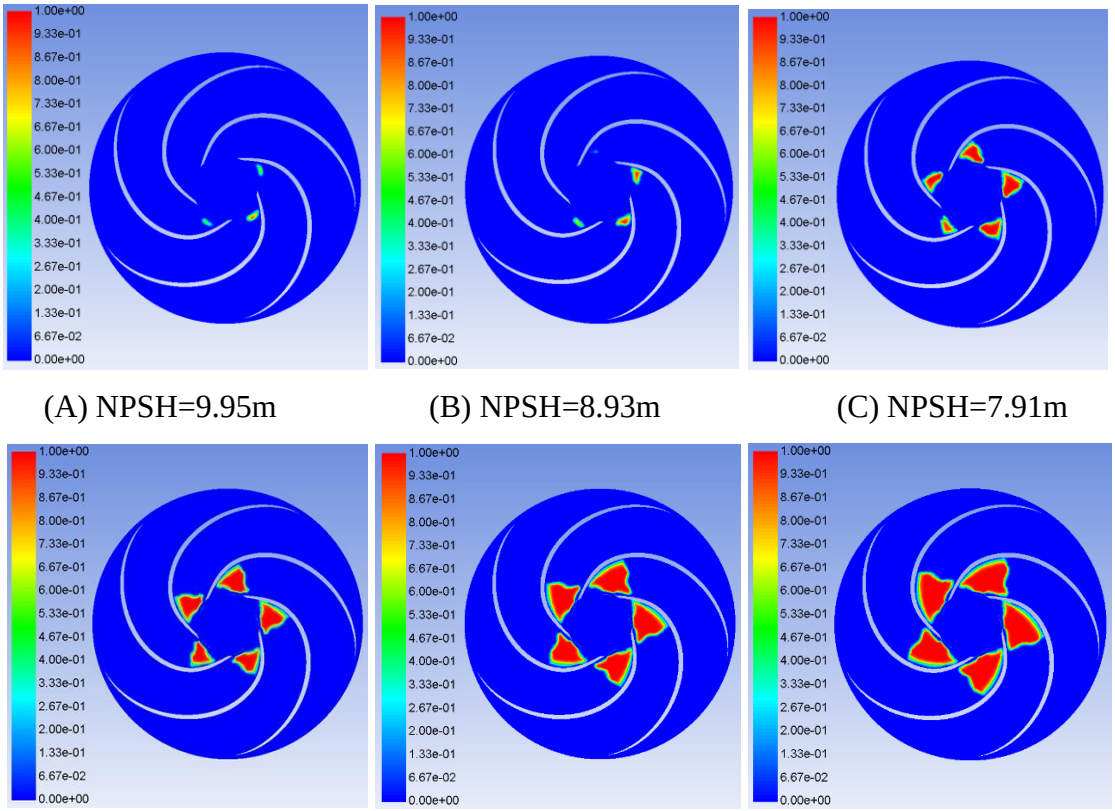

(A) NPSH=9.95m (B) NPSH=8.93m (C) NPSH=7.91m

(D) NPSH=6.89m (E) NPSH=5.87m (F) NPSH=4.85m

Figure 5-28: Variation of vapour volume fraction distributions with various NPSH at Q= 300(l/min), Z=5, do=215mm, di=30mm, and N=2755rpm

5.6.7. Pressure Variations under Cavitation Condition at Different NPSH

For further investigation regarding cavitation conditions within the pump under different NPSH, Figure 5-29 depicts the pressure variation contours at the flow rate of 300(l/min) and N=2755rpm under various NPSH. Pressure increase can be seen from the inlet to the outlet of the impeller. Also, the pressure at blades' suction side of the impeller channel is lower than the pressure side for all cases under investigation. These numerical findings for pressure variations have a similar trend as compared to the numerical result by the single-phase method. In addition, it can be seen that the low-pressure region at the inlet eye of the impeller increases as NPSH decreases. The reason for this is due to the small cavitation area, which appears at the inlet eye of the impeller near the blades leading edges; cavitation then extends and develops in the passages of impeller at low value of NPSH. This is due to the decrease in the low-pressure region at the inlet eye of the impeller as shown in the pressure variations contour. When the pressure decreases and reaches its minimum value, cavitation increases, particularly at this region. In addition, when the pump continuously operates under lower values of NPSH, erosion

occurs more rapidly on the blades of the impeller due to cavitation, at lower values of NPSH. It can be concluded that from the findings above the cavitation inception and development in the pump is highly dependent on the low-pressure region in the inlet eye of the impeller and NPSH.

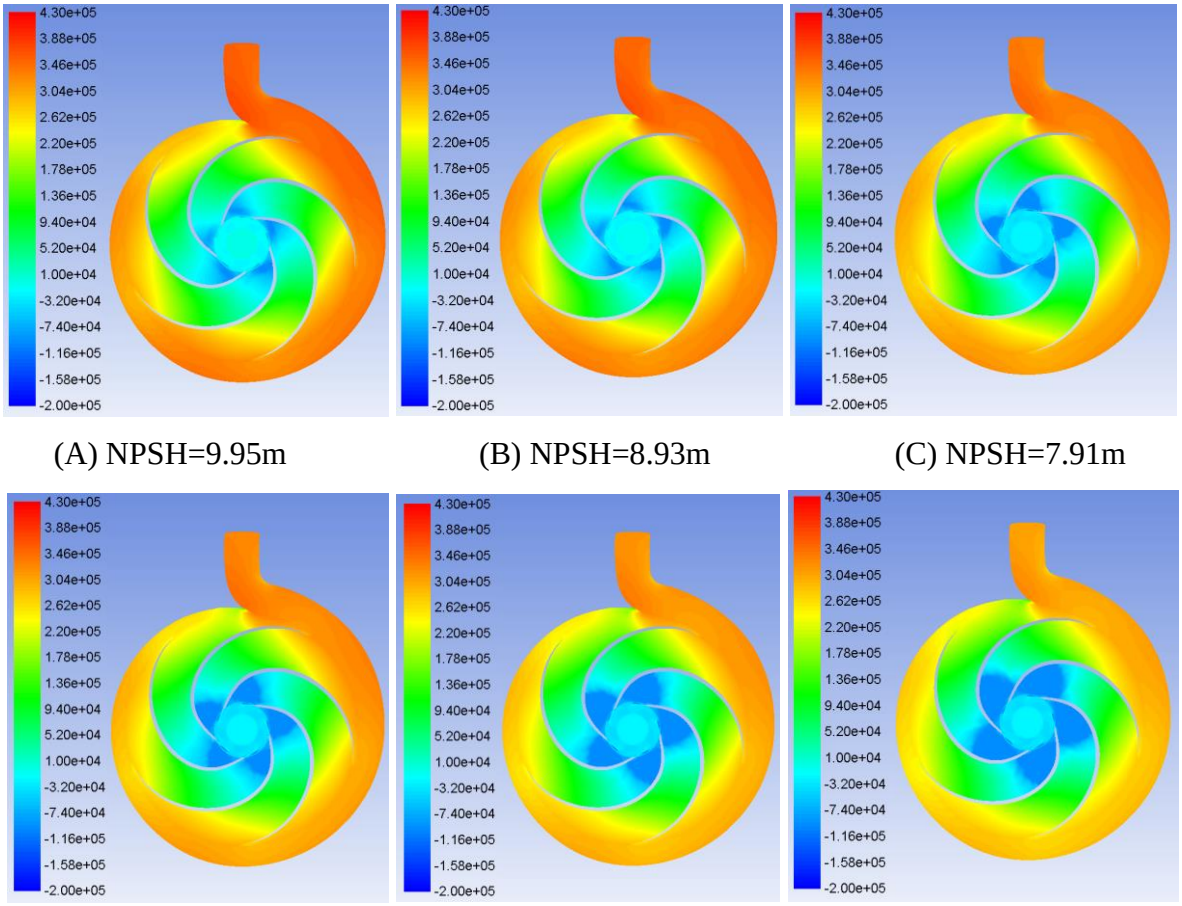

(A) NPSH=9.95m (B) NPSH=8.93m (C) NPSH=7.91m

(D) NPSH=6.89m (E) NPSH=5.87m (F) NPSH=4.85m

Figure 5-29: Variation in static pressure distributions with various NPSH at Q=300(l/min), Z=5, do=215mm, di=30mm, and N=2755rpm

Figure 5-30 depicts the average pressure in the impeller at 8 monitoring points at the design condition of Q=300(l/min) and N=2755rpm under different NPSH. It can be observed that the pressure at the inlet of an impeller decreases when the NPSH deceases in all the cases being investigated. Also, it can be seen that amplitudes of pressure fluctuations increase as the distance along the radius of the impeller is increased. In addition, both the negative pressure and positive pressures can be seen. The negative pressure occurs at the inlet of the impeller, which causes cavitation, noise and vibration on the impeller.

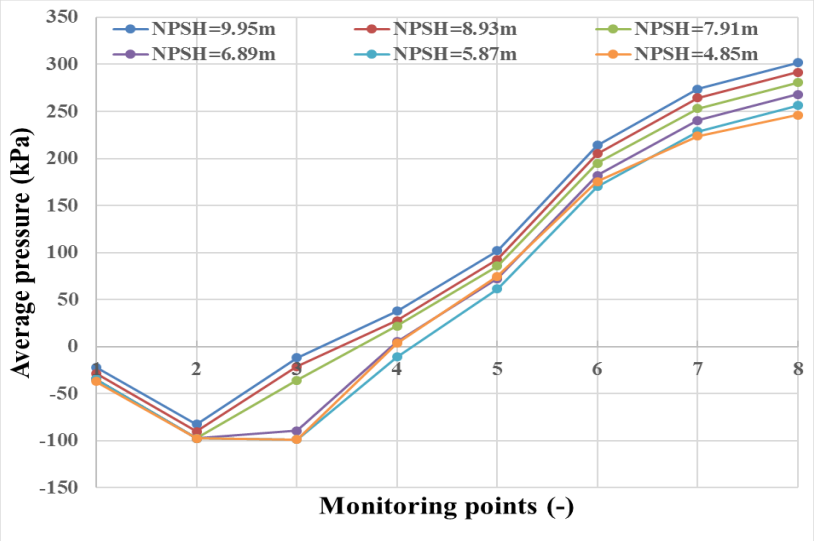

Figure 5-30: Static pressure at the impeller with various NPSH at Q=300(l/min), Z=5, do=215mm, di=30mm, and N=2755rpm

5.6.8. Instantaneous Head under Cavitation Condition at Different NPSH

Figure 5-31 depicts the instantaneous head under different NPSH of the pump at the design flow rate of 300(l/min). It can be clearly seen that there are five peaks and valleys of the instantaneous head. In addition, when the NPSH decreases, the instantaneous head also decreases and when the NPSH is reduced, cavitation starts to develop in the pump as shown in Figure 5-28. For further qualitative analysis of the centrifugal pump performance under different NPSH, Table 5-14 provides the statistical analysis parameters such as minimum, maximum and average instantaneous head. It can be seen from this table that the above statistical parameters decrease as NPSH is reduced and as a result, cavitation occurs because of the reduced NPSH as already explained in the previous section.

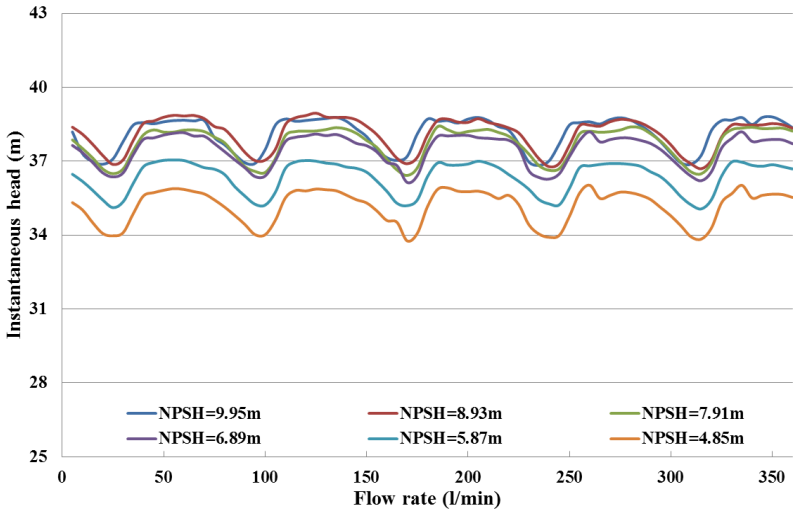

Figure 5-31: Instantaneous head variations of the pump under different NPSH

Table 5-14: Statistical analysis results of the pump head under different NPSH

Head	NPSH=9.9	NPSH=8.9	NPSH=7.9	NPSH=6.8	NPSH=5.8	NPSH=4.8	NPSH=3.8
(m)	(m)	(m)	(m)	(m)	(m)	(m)	(m)
Average	38.11	38.10	37.71	37.45	36.34	35.16	33.97
Minimum	36.83	36.69	36.42	36.13	35.06	33.76	32.68
Maximum	38.79	38.95	38.40	38.19	37.05	36.02	34.80

Figure 5-32 depicts the relationship between the head of the pump and NPSH. It shows the head drop of the pump under flow rate of 300(l/min) corresponding to points A, B, C, D, E, F and G. In this figure, the curve of head-NPSH can be divided into three parts. The first part shows when the NPSH is equal to between 6.89m and 9m, an inception of cavitation occurs in this region. The second part displays the occurrence of the development of cavitation when the NPSH is equal to 5.87m corresponding to head drop of about 4.36%. The third and final part illustrates the full development of cavitation when the NPSH is equal to 3.83 m with a head drop of 10.84%. Furthermore, when the NPSH decreases, the cavitation on the suction side of the pump begins to develop as illustrated in Figure 5-28. Table 5-15 summarises the relationship between the head of the pump and NPSH based on various NPSH values. It can be found from this table that the NPSHR of centrifugal pump at Q=300(l/min) is 5.87m at point (E) due to the head drop in this case being under 4.36% as mentioned earlier. Based on the above analysis, it can be observed that the general behaviour trend of the NPSH against head of the pump was in agreement with the one proven in previous studies of different types of pumps [60, 72, 142, 143]. However, the flow field analysis of static pressure distributions under different NPSH, and using different statistical analysis of the pump head under different NPSH using different features such as average, minimum, maximum and (min-max), were not commonly carried out in most of these studies.

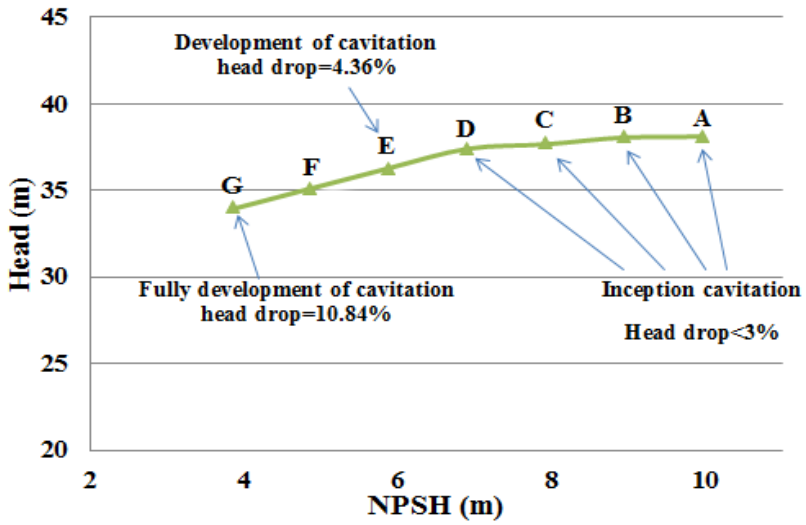

Figure 5-32: Cavitation characteristics prediction curve for the pump having flow rate 300(l/min), Z=5, do=215mm, di=30mm, and N=2755rpm

Table 5-15: Relationship between the head of the pump and NPSH at Q=300(l/min), Z=5, do=215mm, di=30mm, and N=2755rpm

Case	Head	NPSH	Difference in Head
(-)	(m)	(m)	(%)
A	38.11	9.95	
B	38.10	8.93	0.02
C	37.71	7.91	1.03
D	37.45	6.89	1.72
E	36.34	5.87	4.63
F	35.16	4.85	7.73
G	33.97	3.83	10.84

5.7. Numerical Analysis of Cavitation within a Centrifugal Pump under Different Pump Rotational Speeds

As seen in previous sections, the numerical results revealed that the cavitation has an important effect on the performance of the pump. For further analysis, the purpose of current section is to investigate the effect of various pump rotational speeds on cavitation flows within a centrifugal pump.

5.7.1. Detection of Cavitation under Variable Speeds

As already mentioned and observed in previous sections, the inception and development of cavitation within a pump directly depends on the different operating conditions. Therefore, the flow pattern behaviour distribution such as the vapour volume fraction in the pump can be predicted at various operational conditions. Figure 5-33 depicts the distribution of vapour

volume fraction contours within an impeller at various rotational speeds of 2320, 2610, and 2755rpm, at different flow rates of 300, 330 and 350(l/min). It can be observed that at 300(l/min) flow rate, there was no occurrence of cavitation at rotational speeds of 2320 and 2610rpm, but small cavitation occurs when the speed goes up to 2755rpm. The numerical results showed that occurrence of cavitation changes with various pump rotational speeds and flow rates. Also, cavitation increases as the pump rotational speed and flow rate increase starting from the inlet of the impeller close to the leading edge under different rotational speeds and flow rates. The length of the cavity is increased with a decrease in low pressure at the inlet impeller (eye). The possible reason might be due to the increase in the pump rotational speed leading to the increase in the flow velocity within an impeller, hence, the pressure at the eye of the impeller continually decreases, and as a result, the cavitation intensity will increase within a pump. In addition, at 2755 rpm, cavitation was affected highly at the suction of the impeller compared to the rotational speed at 2610 and 2320rpm. Furthermore, based on the above analysis, the numerical results found that the pump speed and flow rate have a high effect on the development of cavitation within a pump.

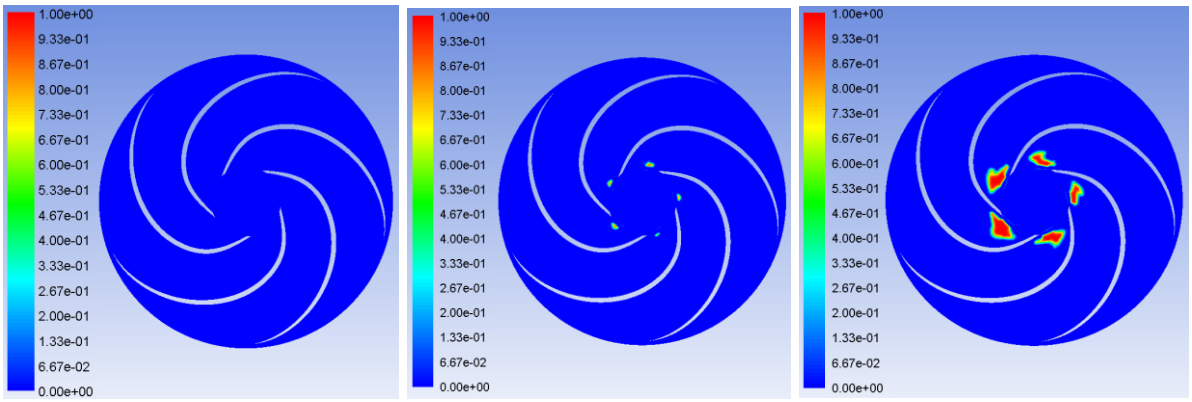

300 (l/min) 330(l/min) 350(l/min)

N=2320rpm

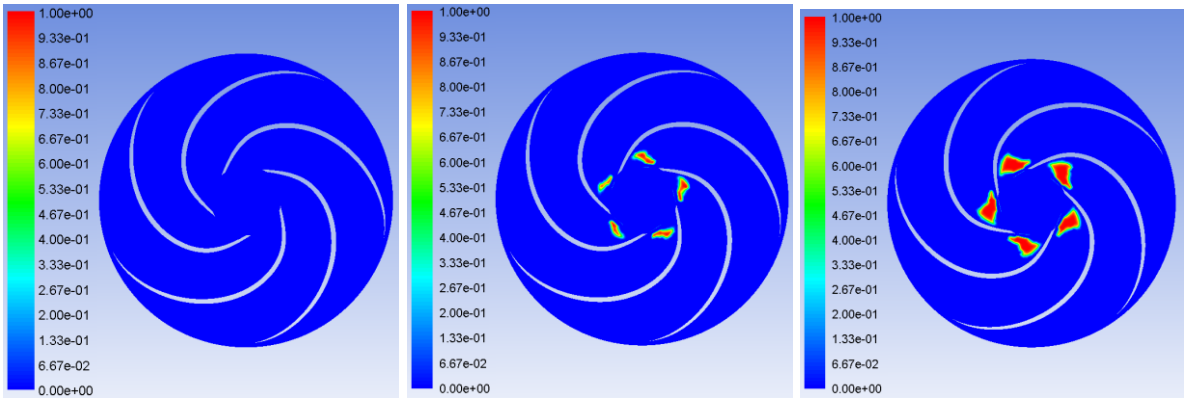

300(l/min) 330(l/min) 350(l/min)

N=2610rpm

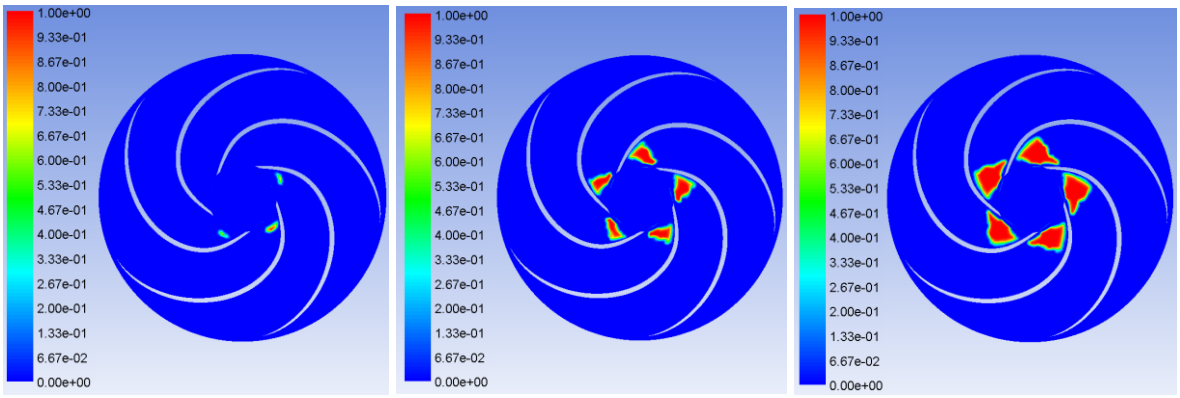

300(l/min) 330(l/min) 350(l/min)

N=2755rpm

Figure 5-33: Variation of volume fraction distributions under various rotational speeds and flow rates

Due to the high complexity of geometry and flow inside the pump, there are still various issues relating to the behaviour of the flow pattern in pumps, which necessitate their study under different geometrical parameters. Carrying out investigations using experimental tests on the pump with various geometrical parameters can be costly and time-consuming due to its numerous requirements and setups. Therefore, for these reasons, it would difficult to carry out comprehensive analysis of the flow field behaviour for different geometrical parameters and various operating conditions within the centrifugal pump. Hence, the numerical analysis using CFD code has currently become quite an effective and suitable technique to investigate and discuss the flow field within the pump. Therefore, in the next section, analysis and discussion regarding the effects of different geometrical parameters on the flow field behaviour and pump performance in cases with and without cavitation will be presented. Moreover, different semi-empirical equations were developed to estimate the head and power coefficients for the pump under single-phase and cavitation conditions is novel contribution in this work.

5.8. Effect of Impeller Geometrical Parameters under Single-Phase and Cavitation Conditions

As clearly seen in the previous sections, the different operating conditions have a significant effect on the flow field behaviour and the pump performance. For further analysis, the 3-D centrifugal pump model considered in the current investigation was analysed with various geometrical parameters as the geometrical parameters play an important role in the

performance of the pump. The main goal for this study is to carry out extensive numerical calculations using CFD code, in order to determine and study the influences of the number of impeller blades, inlet and outlet impeller diameters on the characteristic of the pump performance under single-phase and cavitation conditions as shown in the following parts.

5.8.1. Effect of Number of Impeller Blades (Z) on Performance of the Centrifugal Pump under Single-Phase and Cavitation Conditions

There was limited information regarding the effect of geometrical variations on the pressure, velocity distributions, pressure fluctuations and the occurrence of cavitation within the centrifugal pump. Therefore, this work provides detailed results regarding the investigation of static pressure, velocity magnitude, vapour volume fraction variations and pressure fluctuations based on both time and frequency domains analyses and pump head fluctuations. In addition, the effect of different geometrical parameters on the cavitation condition within a pump was established.

This chapter focuses on the numerical analysis of the transient behaviour of the centrifugal pump for three important parameters. These parameters include the number of blades (Z), the outlet impeller diameter (do), and the inlet impeller diameter (di). Further analysis of the above geometrical parameters is required to investigate the effect of these parameters on the performance and cavitation detection in the pump.

To some degree, the pump performance characteristics, such as pressure, velocity, pressure fluctuations and head are highly impacted by the number of blades, which for most pumps is a significant design parameter. If the number of blades is high, the crowding out effect phenomenon at the impeller is severe and the velocity of flow increases. In addition, increases in the interface between fluid stream and the blade will also cause an increment in the hydraulic loss. Hence, using the suitable number of impeller blades for the pump can provide better pump performance [144]. In order to analyse the effect of the number of impeller blades on the performance of the pump under single-phase and cavitation conditions, three different number of impeller blades 3, 4, and 5 were selected for the analysis purpose. Keeping flow rate at the design operating conditions of 300(l/min), inlet and outlet impeller diameters di=35mm and 220mm, and N=2755rpm constant. The complete set of results can be seen in APPENDIX C. The next section represents the results obtained from the calculation of the different number of impeller blades.

Figure 5-34 depicts the static pressure variations within the centrifugal pump corresponding to operating conditions were flow rate of 300(l/min), inlet and outlet impeller diameters of 35mm and 220mm and N=2755rpm and Z=1,2, and 3 blades. It can be noticed that the pressure is increased gradually from the inlet to the outlet of the impeller. Under these operating conditions, the static pressure of the blade's pressure surface is higher than the suction surface. The lower pressure inside the impeller is positioned at the suction surface of the blade. The high-pressure regions for Z=4 are higher than for Z=3 by 6.7%, and for Z=5 is higher than Z=4 by about 3.57%. Based on the above analysis, it can be seen that when the the number of impeller blades increase the static pressure also increases.

On further analysing for the flow structure within the centrifugal pump, Figure 5-35 depicts the velocity magnitude variations at the middle section of the pump. It can be seen that the velocity increases from inlet to exit of the impeller at the design flow rate through the passages between the blades. In addition, it can be seen that the high-velocity region for Z=4 is higher than for Z=3 by 4.65%. Furthermore, velocity for Z=5 is slightly higher for Z=4 by 2.27%.

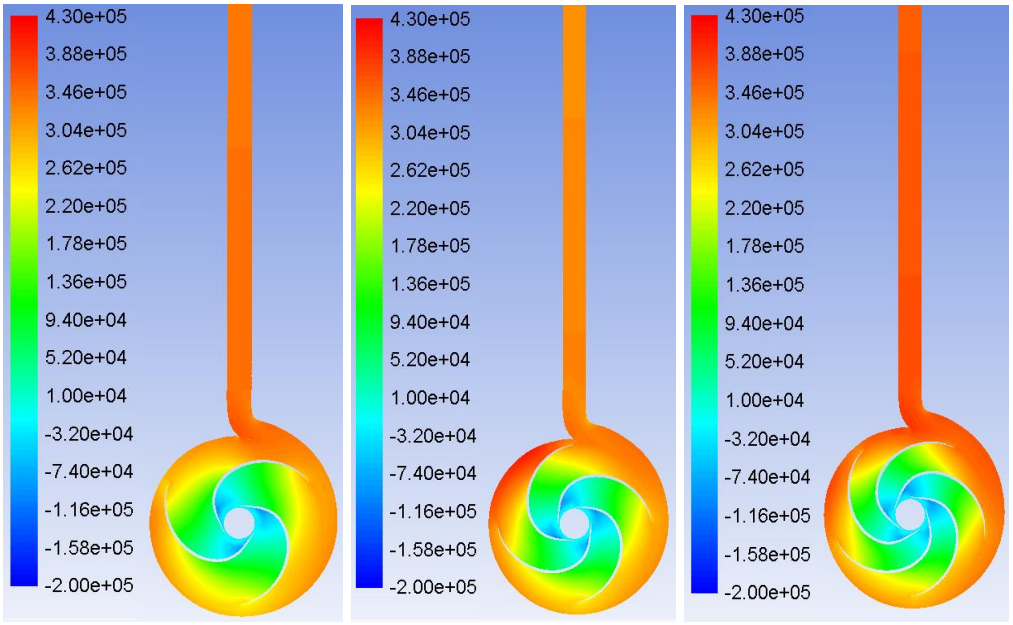

Figure 5-34: Static pressure variations of the pump under different number of blades

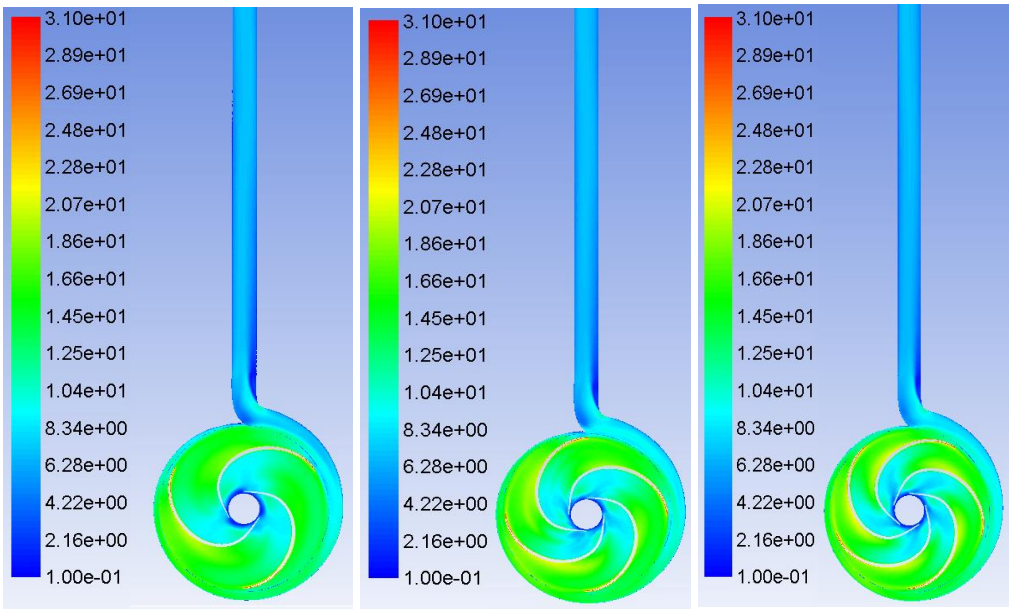

Figure 5-35: Velocity magnitude variations of the pump under different number of blades

Many monitoring points are set in the volute and impeller in order to analyse the pressure fluctuation in the pump under different impeller geometrical parameters as shown in the following section.

Figure 5-36 (a) depicts the pressure fluctuations for 12 monitoring points on the volute with a flow rate of 300(l/min), do=220mm, di=35mm, N=2755rpm and Z=1, 2, and 3 blades. It is obvious that the pressure fluctuations at the monitoring points are increased near or close to the tongue region then decreased when they are located far from the tongue area. In addition, the highest-pressure fluctuations are at the area near the tongue and in the outlet pipe of the volute regions. The higher-pressure fluctuation in the volute at for Z=4 is higher than that for Z=3 by about 6.34%. Furthermore, the pressure fluctuation in the volute at for Z=5 is slightly higher than for Z=4 by 2.67% as presented in Table 5-16.

Table 5-16: Statistical analysis results of the static pressure fluctuations at the volute under different number of blades

Z=3												
Statistical features	VP1 (kPa)	VP2 (kPa)	VP3 (kPa)	VP4 (kPa)	VP5 (kPa)	VP6 (kPa)	VP7 (kPa)	VP8 (kPa)	VP9 (kPa)	VP10 (kPa)	VP11 (kPa)	VP12 (kPa)
Avg.	316.72	299.49	278.94	280.60	326.12	347.12	328.15	331.16	326.89	323.41	314.41	316.07
Min.	284.13	286.44	257.67	264.37	283.70	284.30	294.24	296.67	277.04	278.51	270.12	271.40
Max.	341.39	314.49	297.88	291.58	348.12	436.84	346.48	349.46	359.04	354.60	345.24	347.20
Min.-Max.	32.59	13.04	21.28	16.23	42.42	62.82	33.91	34.49	49.85	44.90	44.30	44.67
Z=4												
Avg.	345.38	327.20	301.17	296.59	344.02	369.06	353.41	359.02	357.40	353.95	347.04	347.29
Min.	322.90	300.65	288.55	280.43	325.81	315.79	326.58	332.91	318.00	320.28	313.58	313.85
Max.	362.67	346.52	311.15	305.02	352.66	433.73	369.49	375.26	383.35	377.14	370.21	370.37

Min.-Max.	39.76	45.87	22.60	24.59	26.84	117.94	42.92	42.35	65.35	56.86	56.64	56.52
Z=5												
Avg.	355.61	336.05	308.13	298.79	349.07	379.17	363.69	368.87	367.43	364.05	357.36	357.79
Min.	343.46	322.62	293.80	289.98	328.01	334.46	343.15	350.66	340.58	342.65	336.13	336.52
Max.	366.36	347.99	317.86	304.31	364.90	425.20	376.31	380.57	385.82	380.14	373.40	373.89
Min.-Max.	22.90	25.36	24.06	14.33	36.89	90.74	33.16	29.91	45.25	37.49	37.27	37.37

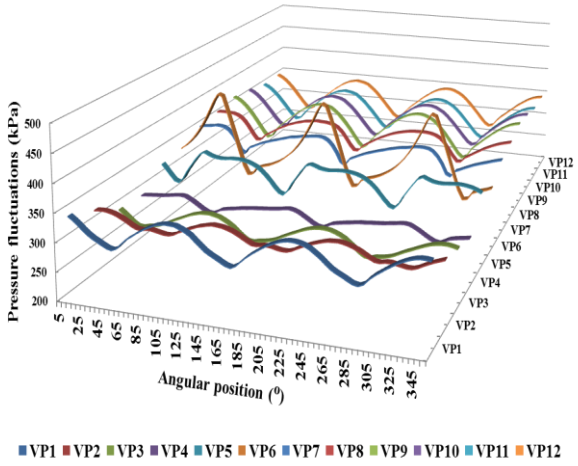

(a)

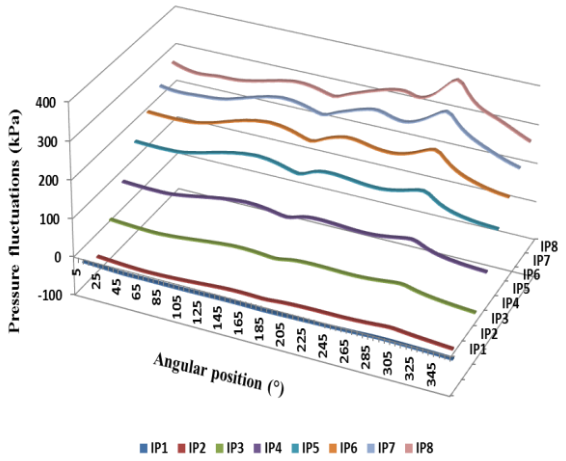

(b)

Z=3

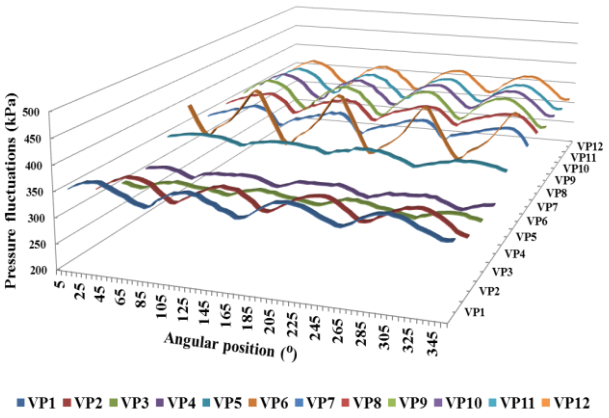

(a)

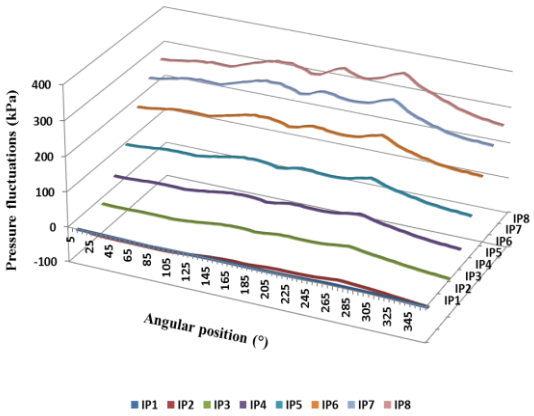

(b)

Z=4

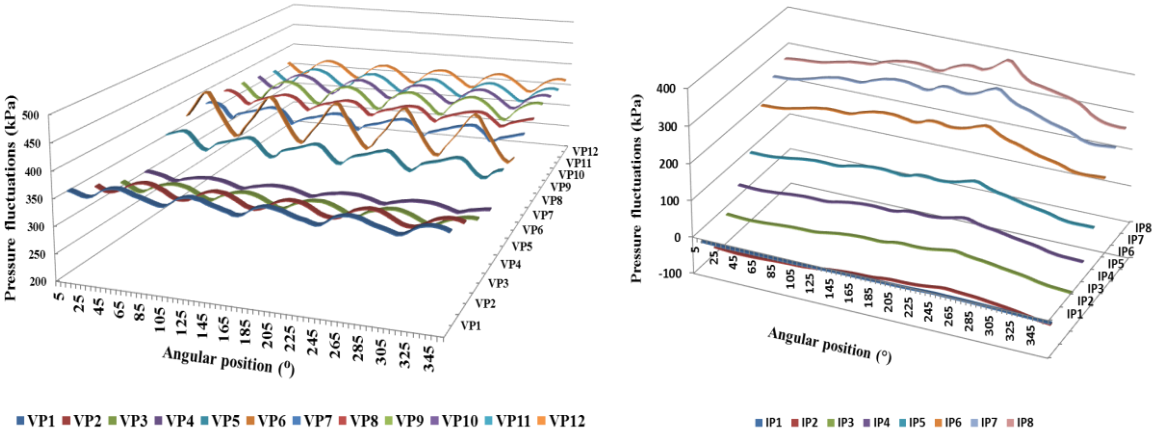

(a) Z=5 (b)

Figure 5-36: (a) Pressure fluctuations around the volute and (b) at the impeller of the pump under different number of blades

Figure 5-36 (b) depicts the pressure fluctuations along the angular location within the impeller under different number of blades. It can be seen that the pressure fluctuations at the inlet of an impeller are low and the pressure fluctuations are increased when the distance along the radius of the impeller is increased, with the maximum value found at the outlet of the impeller diameter. The maximum pressure fluctuations are at points IP7 and IP8 as summarised in Table 5-17. This is due to increased interaction between the impeller and volute, which have high effects on the impeller flow close to this particular area. This figure also displays that the static pressure has maximum values within the tongue region. In addition, pressure fluctuation in the impeller at IP8 for Z=4 is slightly higher than that for Z=3 by about 2.01%. Pressure fluctuation in the impeller at IP8 for Z=5 is slightly higher than for Z=4 by 4.71%.

Table 5-17: Statistical analysis results of the static pressure fluctuations at the impeller under different number of bladess

Z=3								
Statistical features	IP1 (kPa)	IP2 (kPa)	IP3 (kPa)	IP4 (kPa)	IP5 (kPa)	IP6 (kPa)	IP7 (kPa)	IP8 (kPa)
Avg.	-28.59	-47.08	21.43	94.28	174.79	229.04	270.87	296.28
Min.	-32.26	-57.81	6.44	75.24	149.56	195.40	229.34	251.77
Max.	-23.18	-35.66	37.82	114.95	203.52	274.58	339.57	388.72
Min.-Max.	-9.08	-22.15	31.38	39.72	53.96	79.18	110.23	136.95
Z=4								
Avg.	-20.16	-56.28	1.16	55.40	121.52	206.68	269.91	302.35
Min.	-23.63	-67.94	-12.25	38.88	100.52	180.25	235.80	262.54
Max.	-16.23	-41.59	20.11	78.95	149.15	239.26	309.92	355.73
Min.-Max.	-7.40	-26.34	7.87	40.07	48.63	59.02	74.11	93.19
Z=5								
Avg.	-23.41	-60.30	2.20	54.30	118.57	229.06	287.87	317.32
Min.	-26.82	-77.55	-17.21	34.26	95.56	194.49	244.35	269.16
Max.	-19.20	-40.03	27.10	83.03	151.20	270.44	341.34	389.09
Min.-Max.	-7.61	-37.52	9.89	48.76	55.65	75.95	96.99	119.93

Figure 5-37 (a) depicts the amplitudes of pressure fluctuations against frequencies for the 12 monitoring points around the volute for these cases under consideration. It can be seen that in the volute the maximum pressure fluctuation amplitude for all monitoring points is at a BPF. However, the maximum pressure fluctuation amplitudes were at VP6 and VP9 as indicated in Table 5-18. The reason behind that is due to the location of these points being near the tongue region. In addition, at point PV4, the pressure fluctuation amplitude reaches the lowest point due to its location, far away from the volute tongue area. It can be observed that the maximum pressure fluctuation amplitude in the volute at points VP6 for Z=4 was lower than for Z=3 by 45.25%, and for Z=5 is lower than for Z=4 by 15.58%. This happened due to the distance between blade to blade for Z=3 was higher than Z=4, hence that leads to the value of peak-to-peak for Z=3 being higher than Z=4 by 22.86%, and for Z=4 being higher than Z=5 by 23.15%.

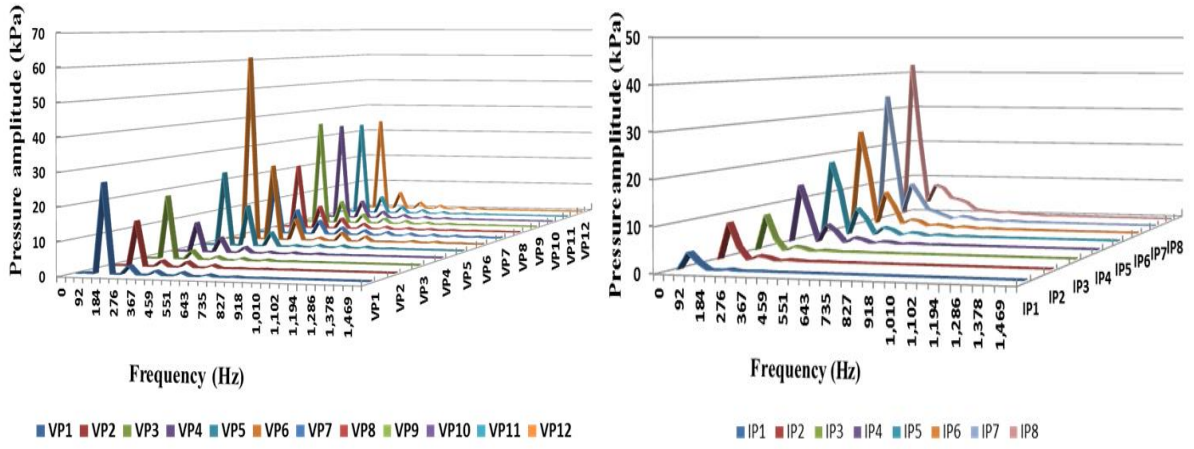

(a) Z=3 (b)

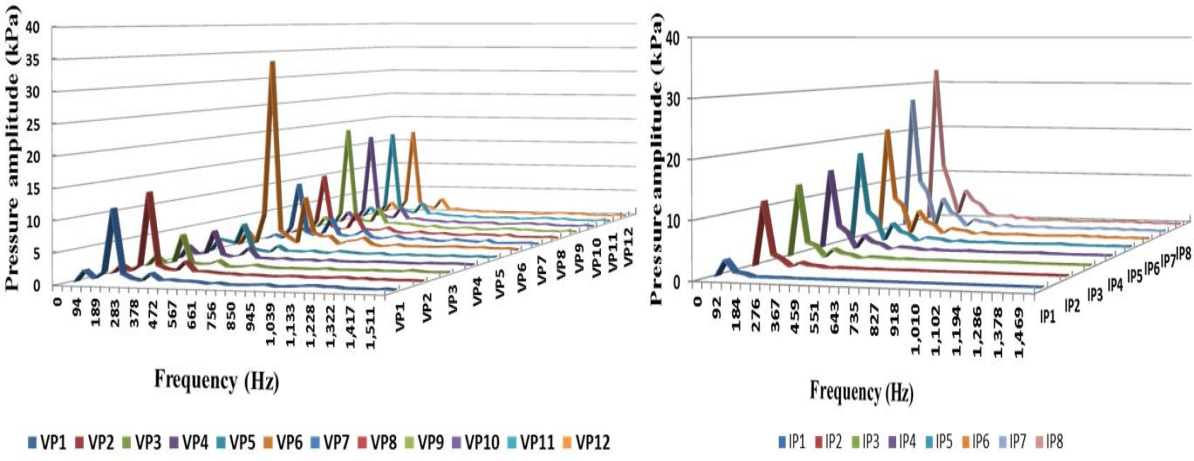

(a) Z=4 (b)

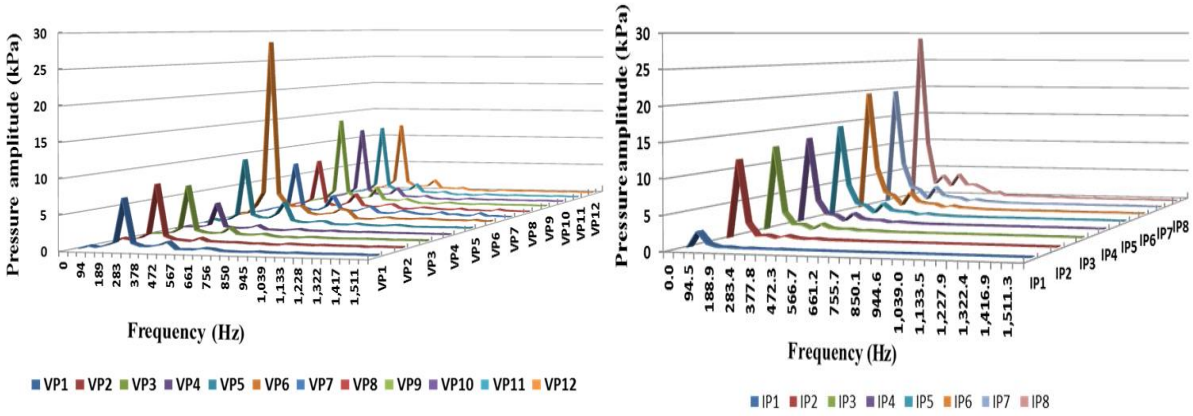

(a) Z=5 (b)

Figure 5-37: (a) Frequency spectra around the volute and (b) in the impeller under different number of blades

Table 5-18: Maximum amplitude of static pressure fluctuations at the volute under different number of blades

Z=3												
Frequency	Maximum amplitude of pressure fluctuations for 12 monitoring points at the impeller (kPa)											
Hz	VP1	VP2	VP3	VP4	VP5	VP6	VP7	VP8	VP9	VP10	VP11	VP12
137.75	26.72	13.64	19.44	9.33	23.80	61.19	18.40	21.88	35.87	34.09	33.54	33.95
Z=4												
Hz	VP1	VP2	VP3	VP4	VP5	VP6	VP7	VP8	VP9	VP10	VP11	VP12
188.91	11.69	13.32	5.29	4.82	4.92	33.50	10.28	10.95	19.15	17.18	17.12	17.01
Z=5												
Hz	VP1	VP2	VP3	VP4	VP5	VP6	VP7	VP8	VP9	VP10	VP11	VP12
236.14	7.18	8.38	7.40	4.01	10.02	28.28	8.09	7.91	14.32	12.17	12.08	12.10

Figure 5-37 (b) depicts obvious variations in the amplitudes of pressure fluctuations with frequencies for 8 monitoring points at the impeller under different number of blades. The first maximum amplitude of pressure fluctuations for entire points is at rotational frequency. Table 5-19 summaries the amplitudes of pressure fluctuation at (Rf) in the impeller. It can be clearly seen that the amplitudes of pressure fluctuations increase as the distance along the radius of the impeller is increased. The pressure fluctuation amplitudes in the impeller are lower than in the volute. Additionally, it can be observed that the maximum amplitude pressure fluctuation on the impeller at point IP8 for Z=4 is lower than that for Z=3 by around 22.20%, and the maximum pressure fluctuation amplitude at the impeller for Z=4 is higher than for Z=5 by 11.798%. This is because of the (max. pressure – min. pressure) value for the peak-to-peak for Z=3 is also higher than that for Z=4 and Z=5.

Table 5-19: Maximum amplitude of static pressure fluctuations under different number of blades

Z=3	
Frequency	Maximum amplitude of pressure fluctuations for 8 monitoring points at the impeller (kPa)

Hz	IP1	IP2	IP3	IP4	IP5	IP6	IP7	IP8
45.92	3.80	8.33	8.33	13.84	18.19	25.00	33.81	42.19
Z=4								
Hz	IP1	IP2	IP3	IP4	IP5	IP6	IP7	IP8
45.92	2.87	11.42	13.10	14.71	17.07	21.05	26.70	32.83
Z=5								
Hz	IP1	IP2	IP3	IP4	IP5	IP6	IP7	IP8
47.23	2.28	11.53	12.67	13.28	14.55	19.60	19.60	28.96

Figure 5-38 depicts the transient simulation of cavitation in the centrifugal pump having a flow rate of 300(l/min), do=220mm, di=35mm, N=2755rpm, and Z=1, 2, and 3 blades. It can be seen that there is no cavitation in case Z=3, and the vapour volume fractions zone within the impeller of the pump for Z=4, and 5 models are slightly higher than that of Z=3, due to these cases operate under flow rate of 300(l/min).

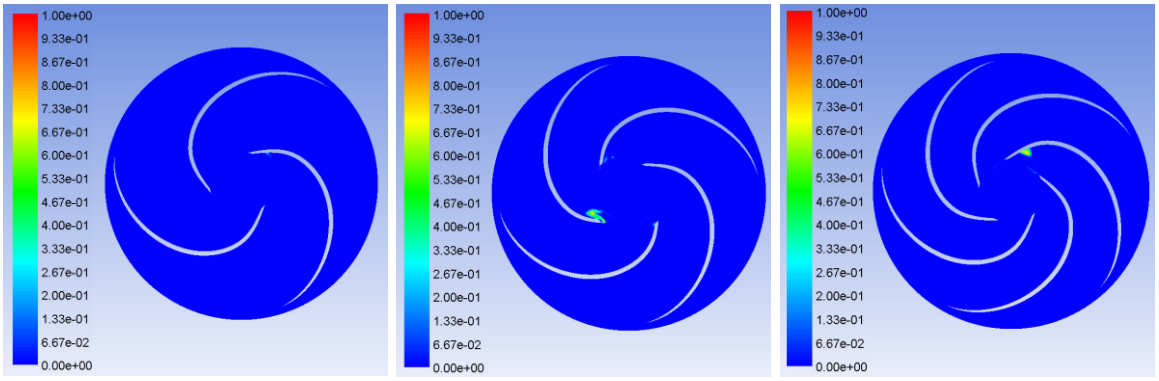

Z=3 Z=4 Z=5

Figure 5-38: Volume fraction distributions for the pump under different number of blades

For comparison purposes between the above models, Figure 5-39 (a) and (b) depict the instantaneous head of the aforementioned cases under single-phase and cavitation conditions. It can be clearly seen that for the model that has Z=5, the average head under single-phase and cavitation conditions are considerably higher than for the other two models Z=4 and Z=3 by 11.09% and 2.64%, and under cavitation condition by 11.04% and 3.16% respectively. In comparison, between the models when Z=4 and Z=5, the maximum instantaneous head for Z=5 is seen to be higher than that of Z=4. The results showed that as the number of impeller blades increases, the head of the centrifugal pump increases.

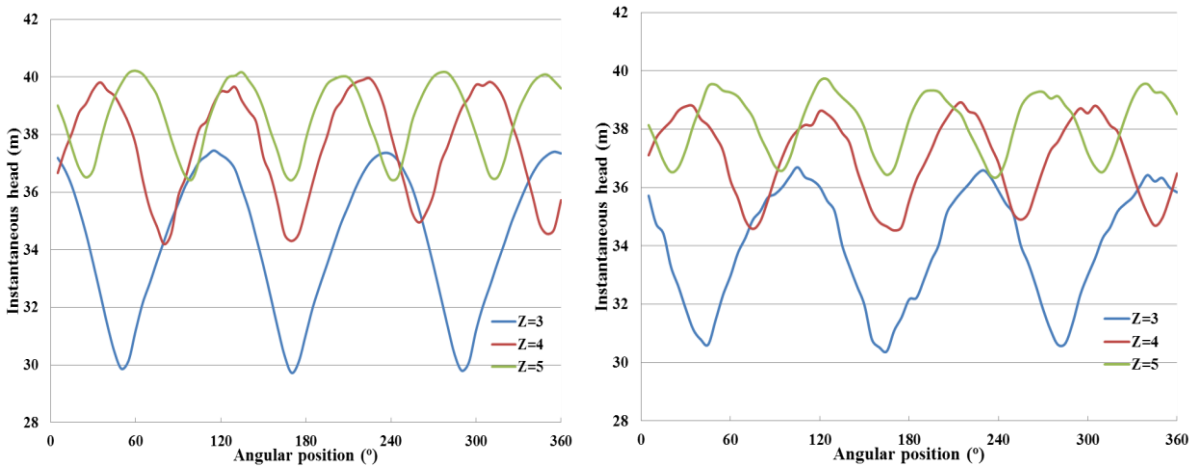

Figure 5-39: Instantaneous head variations of centrifugal pump models having different number of blades (Z) under single-phase and cavitation conditions

APPENDIX C presents the complete CFD results for single-phase and cavitation conditions. Figure 5-40 depicts some of these results. It can be seen that when the flow rate, pump rotational speed, inlet and outlet impeller diameters and are kept constant and number of impeller blades (Z) is increased, the average head of the pump increases under both single-phase and cavitation conditions. Also, there is a slight difference between the head for both single-phase and cavitation under different number of impeller blades. The head for the single-phase is slightly higher than the head for the cavitation condition by 1.02, 1.54, and 1.01% for when Z=3, 4, and 5 respectively. All of these cases under investigation were conducted under design flow rate of 300(l/min) and the level and severity of cavitation was found to be relatively small under this flow rate. In addition, the results showed that as the number of blades increases, the head of the pump increases. The maximum performance of the centrifugal pump corresponds with the optimum value of the number of blades (Z), which in the current study is five blades.

Based on the findings in this thesis, it can be observed that the general behaviour of pressure fluctuations in time and frequency domains, as well as the head using CFD was in agreement with previous studies for different types of pumps [101, 145-147]. However, in the current study, comprehensive investigations on the global and local flow fields analysis and comparative investigations to estimate the effects of different geometrical parameters were carried out. Moreover, developing different semi empirical correlations for the head and power coefficients of the centrifugal pump under single-phase and cavitation at transient flow conditions were not carried out in most of these studies.

Further quantifying the performance of the pump, Table 5-20 provides the statistical analysis results of the instantaneous head such as the maximum, minimum, average, and (max–min) amplitude under single-phase and cavitation condition at different number of blades.

Table 5-20: The statistical analysis results of the instantaneous head under single-phase and cavitation conditions at different number of blades

Single-phase			
Head (m)	Z=3	Z=4	Z=5
Average	34.31	37.57	38.59
Minimum	29.72	34.19	36.41
Maximum	37.44	39.94	40.21
Max - Min	7.72	5.75	3.79
Cavitation condition			
Head (m)	Z=3	Z=4	Z=5
Average	33.96	36.99	38.20
Minimum	30.38	34.52	36.39
Maximum	36.69	38.91	39.71
Max - Min	6.309	4.392	3.315

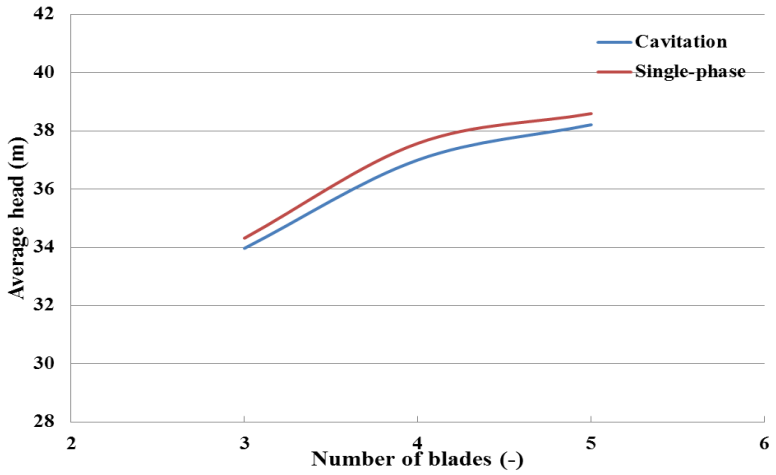

Figure 5-40: Effect of number of impeller blades on performance of the centrifugal pump under single-phase and cavitation conditions

The numerical results showed that as the number of impeller blade increases, static pressure also increases, hence, the pump head increases. Also, under different number of impeller blades, the low pressure region occurs at the inlet eye of the impeller, particularly at the suction side of blades near the leading edges. Also, when the blade number increases, it leads to the region of low-pressure area increasing, causing cavitation to increase due to the decrease in the low-pressure region at this particular area. Therefore, the number of impeller blade has a high influence on the pump characteristics and cavitation within the centrifugal pump.

5.8.1.1. Detection of Cavitation under Different Number of Impeller Blades at Different Flow Rates

Figure 5-41 depicts the vapour volume fraction variations under various flow rates namely 300, 330, and 350(l/min). The number of impeller blades that have been used are 3, 4, and 5, inlet and outlet impeller diameters used are di=35mm, do=220mm, and N=2775rpm was the speed of operation. The numerical results found that the occurrence of cavitation changes with the number of impeller blades and flow rates. It can be seen that at 300(l/min) flow rate, there was no occurrence of cavitation at Z=3, but small cavitation occurs when the number of impeller blades goes up to Z=5. Also, cavitation initiates from the leading edge of the impeller and the magnitude of the cavitation increases as the number of impeller blades and flow rate increase. In addition, the length of the cavity is increased when low pressure at the inlet impeller (eye) decreases. The possible reason behind that is due to an increase in the number of impeller blades and flow rate, leading to pressure at the eye of impeller continually decreases. In addition, at Z=5 blades, cavitation was affected highly at the suction of the impeller compared to the number of blades at 4 and 3, especially at high flow rate. Furthermore, based on the above analysis, the numerical results showed that the number of blades and flow rates have a high effect on cavitation within a pump, particularly at the eye of impeller region.

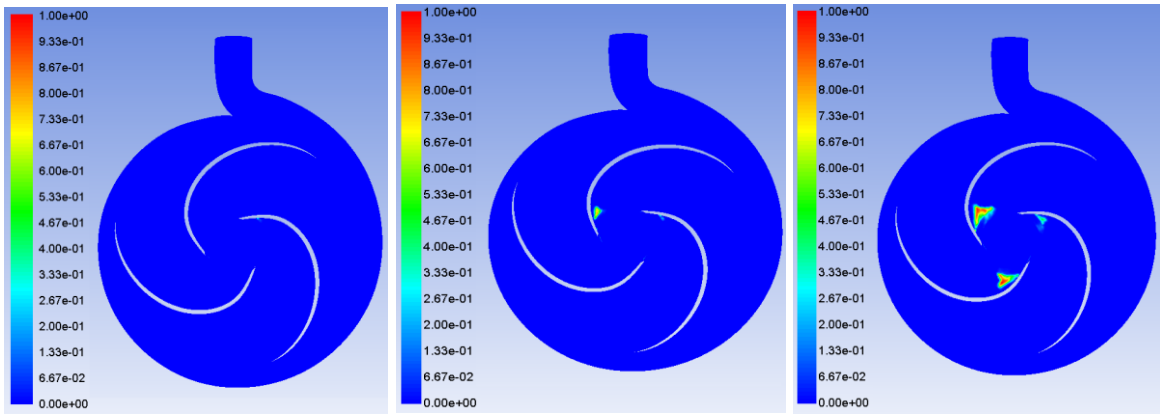

Q=300(l/min) Q=330(l/min) Q=350(l/min)

Z=3

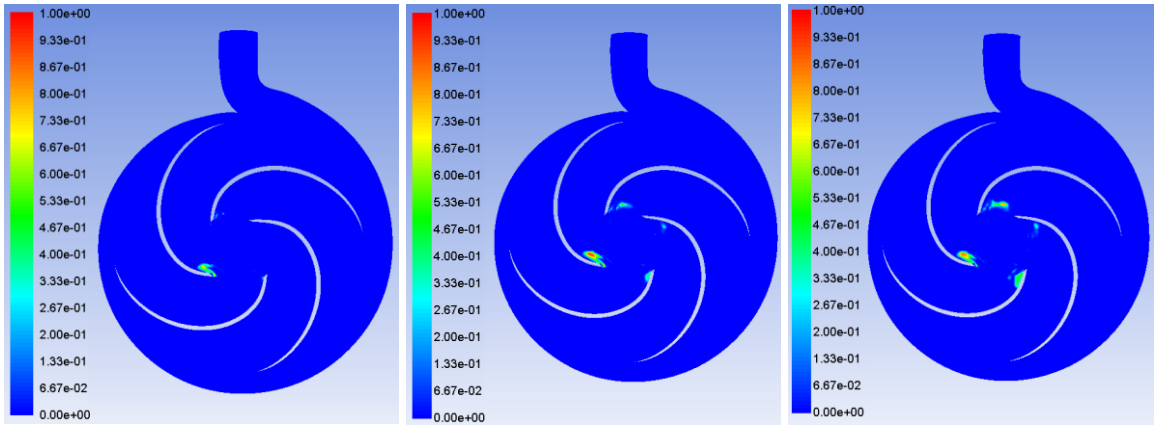

Q=300(l/min) Q=330(l/min) Q=350(l/min)

Z=4

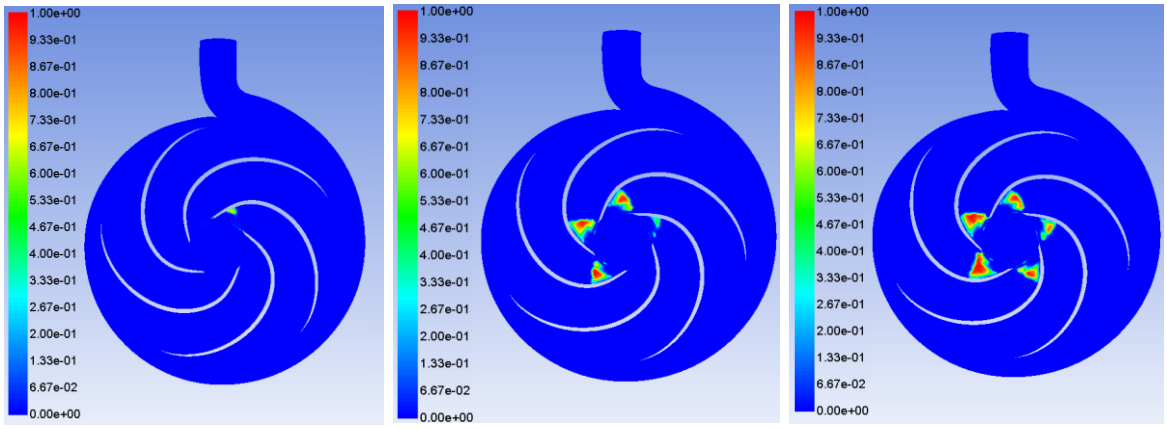

Q=300(l/min) Q=330(l/min) Q=350(l/min)

Z=5

Figure 5-41: Volume fraction distributions for the centrifugal pump under different number of impeller blades and flow rates

5.8.2. Effect of Outlet Impeller Diameter on the Performance of Centrifugal Pump under Single-Phase and Cavitation Conditions

As seen in previous sections, the pump geometrical parameters have a high impact on flow field behaviour and performance of the pump under both single-phase and cavitation conditions. Therefore, in order to investigate the wide range of geometrical parameters in this section, the detailed analysis on the effect of outlet impeller diameter was carried out. In industry it is important to provide different impeller diameters. There are different reasons behind that, firstly in order to increase the capacity of the pump through impeller replacement. Secondly, for the pump to be reused for different applications. Thirdly, to increase the performance of the pump [144]. In order to analyse the effect of outlet impeller diameter (do) on the performance of the centrifugal pump three outlet impeller diameters (do), values of

200mm, 210mm and 220mm were selected, keeping flow rate at design flow rate 300(l/min), Z=5, di=35mm and N=2755rpm. APPENDIX C presents the results for different Computational Fluid Dynamics simulations based on investigations being carried out on the flow of the pump under various impeller outlet diameters.

Figure 5-42 depicts the pressure variations within the centrifugal pump having a flow rate of 300(l/min), Z=5, di=25mm, N=2755rpm, and do=200. 210, and 220mm. It can be observed that the pressure gradually increases from the inlet area to outlet, along the radius direction of the pump. For example, lower pressure occurred at the inlet of the impeller, whereas the maximum value of the static pressure occurred at the outlet of pump near tongue region. It is established from this figure that the value of static pressure of impeller blades on pressure surface is clearly greater than that on the suction surface. In addition, the lowest static pressure exists at the leading edge of blades at the inlet side of impeller. This pressure for do=210mm is considerably higher when compared to do=200mm by 16.84%. Furthermore, the maximum pressure for do=220mm is slightly higher than for do=210mm by around 0.02%.

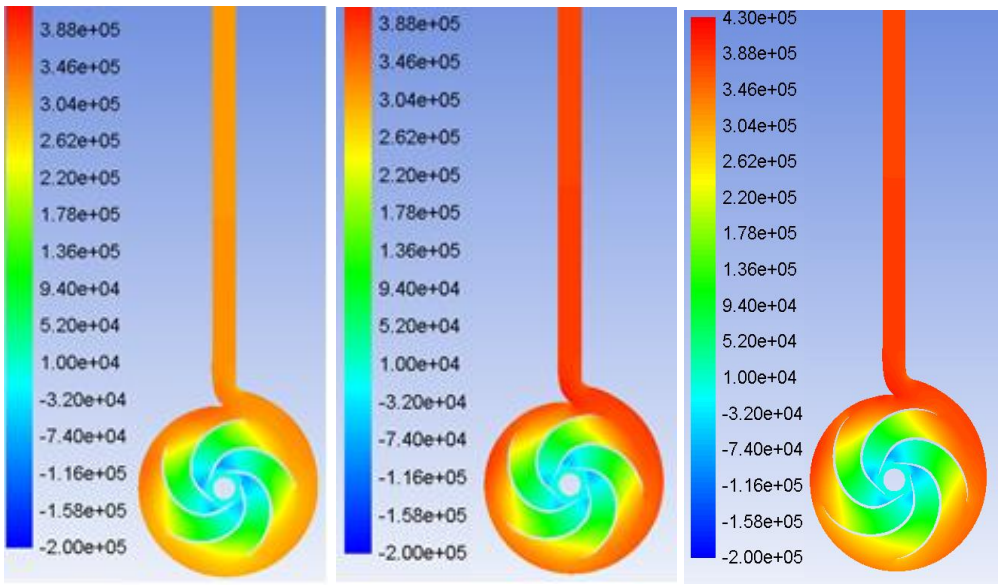

do=200mm do=210mm do=220mm

Figure 5-42: Static pressure variations of the pump under different outlet impeller diameters

Figure 5-43 depicts that the flow velocity variations are increased at the pressure surface of the impeller's blades, it then decreases within the volute. Velocity for do=210mm is seen to be slightly lower when compared with do=200mm by around 0.2%. Also, the maximum velocity for do=220mm is around 23.71m/sec.

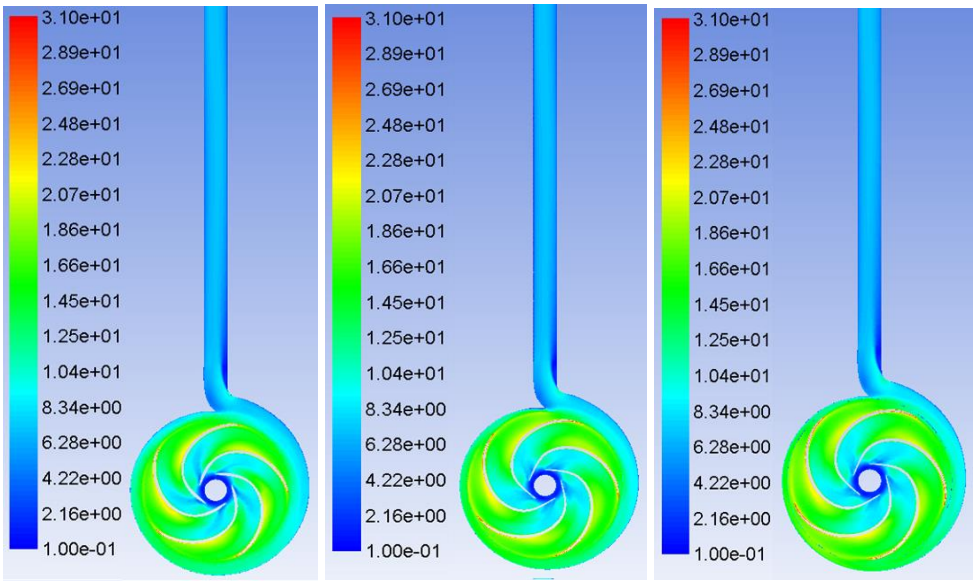

do=200mm do=210mm do=220mm

Figure 5-43: Velocity magnitude variations of the pump under different outlet impeller diameters

Figure 5-44 (a) depicts the pressure fluctuations for 12 monitoring points for the centrifugal pump having flow rate of 300(l/min), Z=5, di=25mm, N=2755rpm, and do=200, 210, and 220mm. It can be observed that there are five peaks and valleys with the same number of blades on the impeller. In addition, the pressure fluctuation at monitoring point VP6 is higher than other points and the minimum pressure fluctuation was noticed at VP3 as shown in Table 5-21. The pressure fluctuations curves for the outlet volute monitoring points VP10, VP11 and VP12 have similar trends due to the flow in the volute outlet pipe having approximately the same velocity. It can be observed that the average pressure fluctuation in the volute at VP6 for do=210mm is higher than for do=200mm by 6.74%. Furthermore, the maximum pressure fluctuation in the volute at VP6 for do=220mm is higher than for do=210mm by 7.4%.

Table 5-21: Statistical analysis results of the static pressure fluctuations at the volute under different outlet impeller diameters

do=200mm												
Statistical features	VP1 (kPa)	VP2 (kPa)	VP3 (kPa)	VP4 (kPa)	VP5 (kPa)	VP6 (kPa)	VP7 (kPa)	VP8 (kPa)	VP9 (kPa)	VP10 (kPa)	VP11 (kPa)	VP12 (kPa)
Avg.	320.49	309.17	294.69	295.74	329.49	349.13	329.50	343.86	330.43	324.05	318.29	318.21
Min.	311.57	300.31	286.52	289.19	317.86	319.84	316.60	333.51	314.29	309.44	303.85	303.72
Max.	328.33	317.74	302.33	302.91	344.49	379.94	347.41	353.77	344.01	336.56	330.69	330.62
Min.-Max.	16.76	17.43	15.81	13.72	26.63	60.10	30.81	20.26	29.71	27.13	26.85	26.89
do=210mm												
Avg.	374.00	358.48	336.51	329.29	363.56	382.85	344.02	388.13	386.16	379.97	374.57	374.69
Min.	366.48	350.09	328.07	323.36	355.37	356.89	330.10	382.22	370.90	366.14	360.80	360.91
Max.	381.33	367.00	344.15	335.39	372.22	407.41	358.80	393.10	399.24	392.16	386.59	386.75
Min.-Max.	14.86	16.91	16.08	12.03	16.85	50.52	28.71	10.88	28.35	26.02	25.78	25.84
do=220mm												
Avg.	369.70	350.33	322.53	313.93	364.85	394.42	378.02	383.24	381.27	378.05	371.49	371.76

Min.	357.29	335.36	307.42	303.65	342.15	348.26	356.29	363.89	354.11	356.54	350.08	350.31
Max.	380.84	363.10	333.20	320.93	381.29	439.99	391.17	396.30	399.68	394.62	387.93	388.26
Min.-Max.	23.55	27.74	25.78	17.28	39.14	91.73	34.88	32.41	45.57	38.07	37.85	37.94

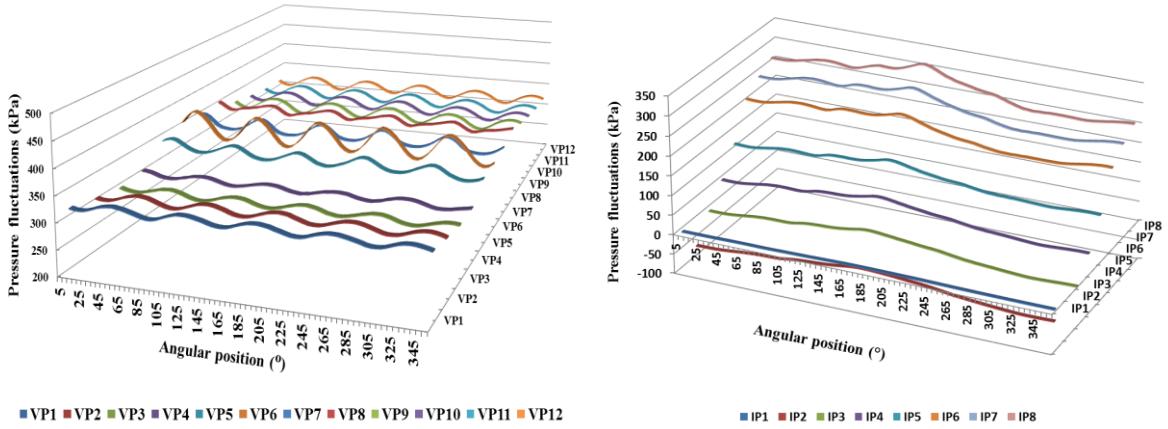

(a) do=200mm (b)

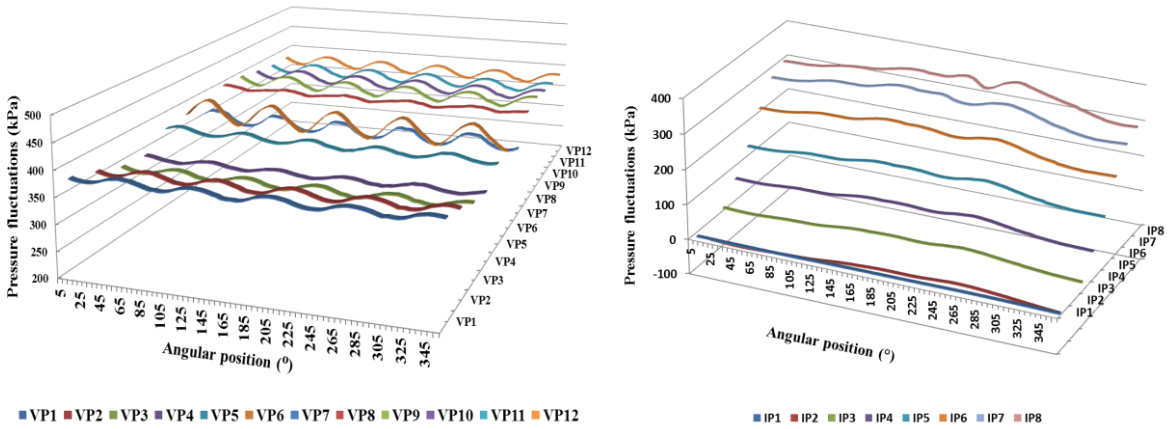

(a) do=210mm (b)

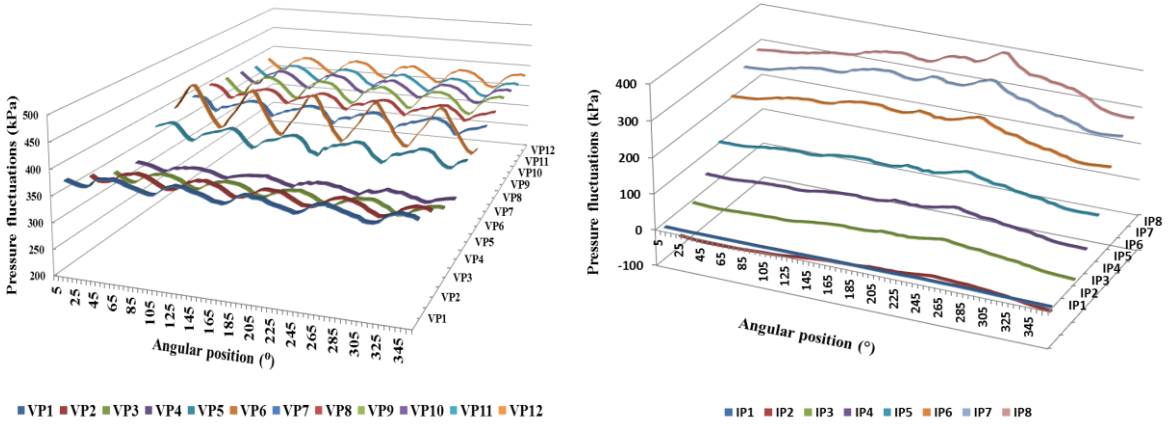

(a) do=220mm (b)

Figure 5-44: (a) Static pressure fluctuations around the volute and (b) at the impeller under different outlet impeller diameters

Figure 5-44 (b) depicts the pressure fluctuations along the angular location within the impeller. It can be seen that the pressure fluctuations in time domain are increased with distance along the radius of the impeller is increased, and the maximum pressure fluctuations at outlet impeller at points IP7, and IP8 are higher than that at other points as summarised in Table 5-22. The maximum pressure fluctuation in the impeller at IP8 for do=210mm is higher than for do=200mm by 12.48%. Furthermore, the pressure fluctuation in the volute at IP8 for do=220mm is higher than for do=210mm by 10.8%.

Table 5-22: Summary of the statistical analysis results of the static pressure fluctuations at the impeller under different outlet impeller diameters

do=200mm								
Statistical features	IP1 (kPa)	IP2 (kPa)	IP3 (kPa)	IP4 (kPa)	IP5 (kPa)	IP6 (kPa)	IP7 (kPa)	IP8 (kPa)
Avg.	-2.09	-57.36	3.92	57.39	121.93	207.68	243.31	269.75
Min.	-3.98	-71.42	-10.81	41.75	108.03	187.67	219.87	244.18
Max.	0.52	-39.50	25.16	81.96	147.71	237.76	278.84	313.96
Min.-Max.	-3.46	-31.91	14.35	40.21	39.68	50.09	58.97	69.78
do=210mm								
Avg.	-3.73	-36.51	25.98	82.49	150.04	235.06	300.29	324.25
Min.	-5.44	-49.78	12.55	68.16	133.84	213.35	272.33	292.48
Max.	-1.90	-23.60	40.83	99.51	169.14	255.72	325.08	358.74
Min.-Max.	-1.71	-13.27	13.43	14.33	16.20	21.71	27.96	31.77
do=220mm								
Avg.	-4.13	-49.25	13.82	66.17	130.30	241.18	301.88	330.82
Min.	-6.02	-66.93	-4.27	48.09	109.42	206.02	258.40	282.68
Max.	-1.94	-29.33	37.26	93.78	160.48	279.64	352.21	398.98
Min.-Max.	-4.08	-37.60	32.99	45.69	51.06	73.63	93.81	116.29

Figure 5-45 (a) depicts the pressure fluctuations amplitudes for all monitoring points in frequency domain. This figure shows the frequency spectrum at 12 monitoring points under design flow on the volute surface, under different outlet impeller diameters. The pressure fluctuations amplitudes at monitoring points near the tongue region are obviously higher than that at other positions in the volute. Also, the maximum pressure fluctuation amplitude for all monitoring points is at BPF 229.58Hz due to the number of impeller blades (Z) being five. The maximum pressure fluctuations are at VP6 and VP9 as shown in Table 5-23. The maximum pressure fluctuation for do=200mm is lower than for do=210mm by 41.58%. Furthermore, the maximum pressure fluctuation at the impeller for do=220mm is higher than two models, the reason behind this being there is a small clearance between impeller and volute for this model that leads to the pressure fluctuation amplitudes being higher than the other above models.

Table 5-23: Maximum amplitude of static pressure fluctuations at the volute under different outlet impeller diameters

do=200mm												
Frequency	Maximum amplitude of pressure fluctuations for 12 monitoring points at the impeller (kPa)											
Hz	VP1	VP2	VP3	VP4	VP5	VP6	VP7	VP8	VP9	VP10	VP11	VP12
229.58	7.05	7.75	6.84	5.60	11.21	27.97	14.27	7.39	13.49	12.13	12.03	12.05
do=210mm												
Hz	VP1	VP2	VP3	VP4	VP5	VP6	VP7	VP8	VP9	VP10	VP11	VP12
229.58	4.58	6.63	4.86	3.25	4.65	16.34	9.85	2.55	8.98	8.22	8.14	8.15
do=220mm												
Hz	VP1	VP2	VP3	VP4	VP5	VP6	VP7	VP8	VP9	VP10	VP11	VP12
229.58	9.92	11.83	10.73	5.95	14.30	40.52	12.13	12.13	20.25	17.09	16.93	16.95

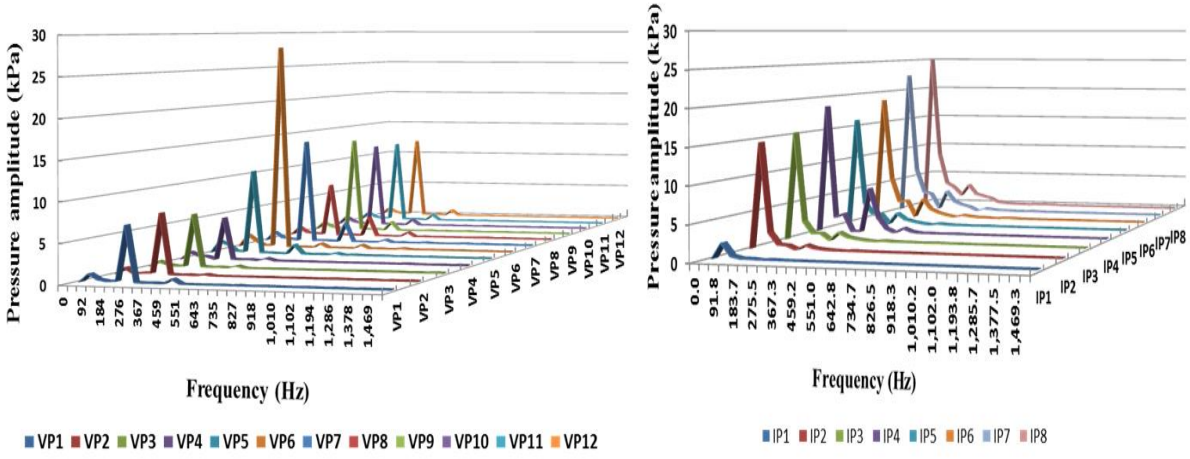

(a) do=200mm (b)

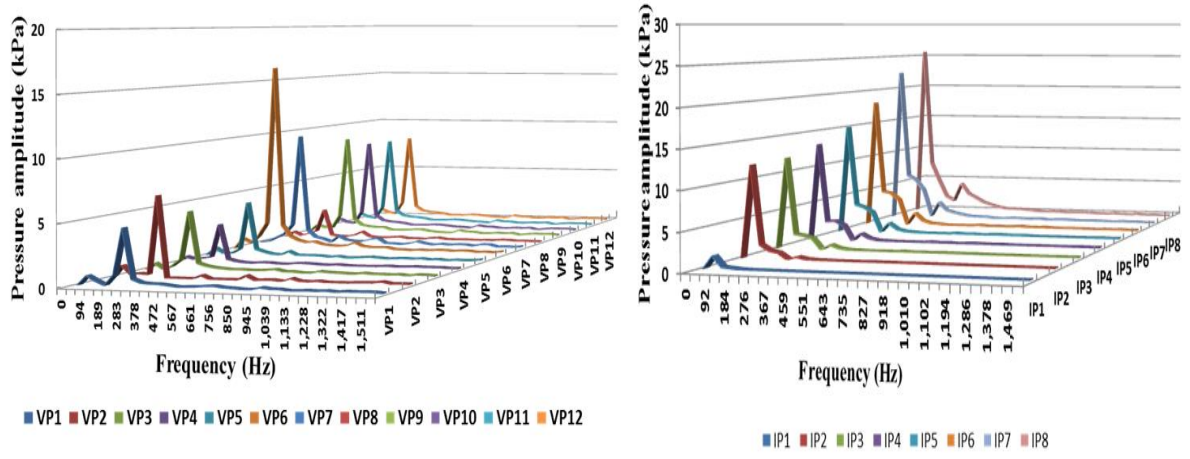

(a) do=210mm (b)

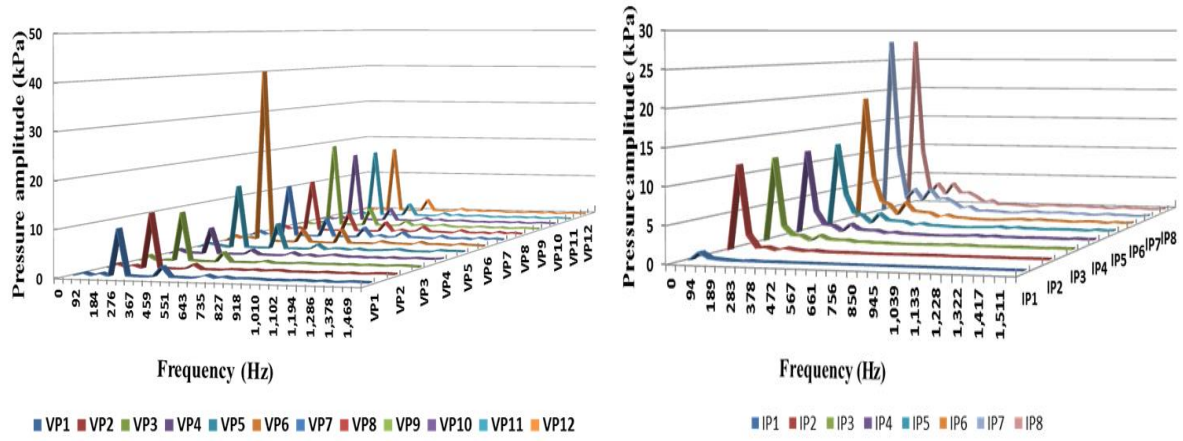

(a) do=220mm (b)

Figure 5-45: (a) Frequency spectra along the volute and (b) at the impeller under different outlet impeller diameters

Figure 5-45 (b) depicts frequency characteristics of pressure fluctuations for the impeller under different outlet impeller diameters. The first maximum amplitude of pressure fluctuations for all monitoring points is at rotational frequency 45.92Hz. It can be clearly seen from Table 5-24 the amplitudes of pressure fluctuations were increased with radius of impeller increased. Furthermore, the pressure fluctuation amplitude of the first harmonic is clearly higher than that of other harmonics in the impeller. The maximum pressure fluctuation amplitude at the impeller for do=210mm is slightly higher than for do=200mm by around 1.9%. Furthermore, the maximum pressure amplitude fluctuation at the impeller for do=220mm is higher than do=210mm.

Table 5-24: Maximum amplitude of static pressure fluctuations at the impeller under different outlet impeller diameters

do=200mm								
Frequency	Maximum amplitude of pressure fluctuations for 8 monitoring points at the impeller (kPa)							
Hz	IP1	IP2	IP3	IP4	IP5	IP6	IP7	IP8
45.92	2.11	14.68	15.39	18.69	16.07	18.75	22.49	25.07
do=210mm								
Hz	IP1	IP2	IP3	IP4	IP5	IP6	IP7	IP8
45.92	1.62	12.01	12.12	13.27	15.08	18.20	22.41	25.56
do=220mm								
Hz	IP1	IP2	IP3	IP4	IP5	IP6	IP7	IP8
45.92	1.10	11.72	11.88	12.08	12.41	19.04	28.12	28.12

Figure 5-46 depicts the vapour volume fraction on the pump's impeller and it can clearly be seen that the vapour volume fraction for do=200mm was very slightly small at the impeller blades channels and no cavitation occurred for two cases do=210 and 220mm, due to these cases operated under flow rate of 300(l/min).

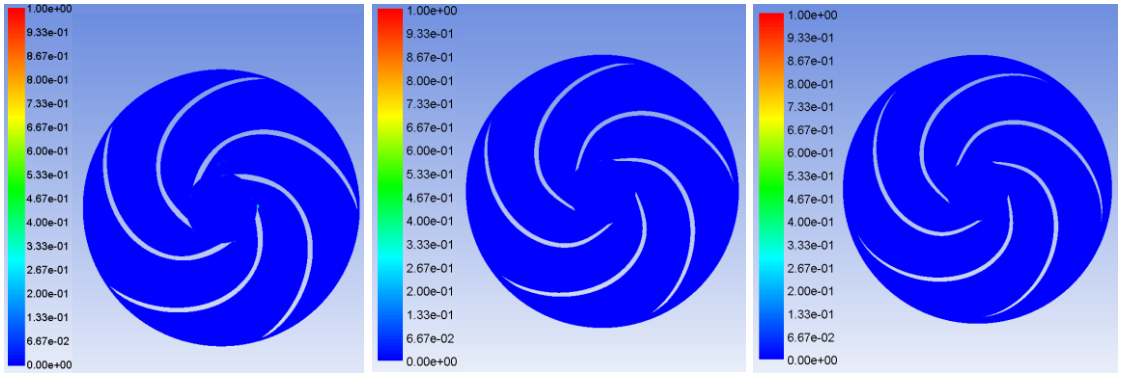

do=200mm do=210mm do=220mm

Figure 5-46: Volume fraction distributions of the pump under different outlet impeller diameters

For comparison purposes between the above models under single-phase and cavitation conditions, Figure 5-47 (a) and (b) depict the instantaneous head for the cases mentioned above under single-phase and cavitation conditions on a single scale. It can be seen that the head is considerably higher for do=220mm than for when do=200mm for both single-phase and cavitation conditions.

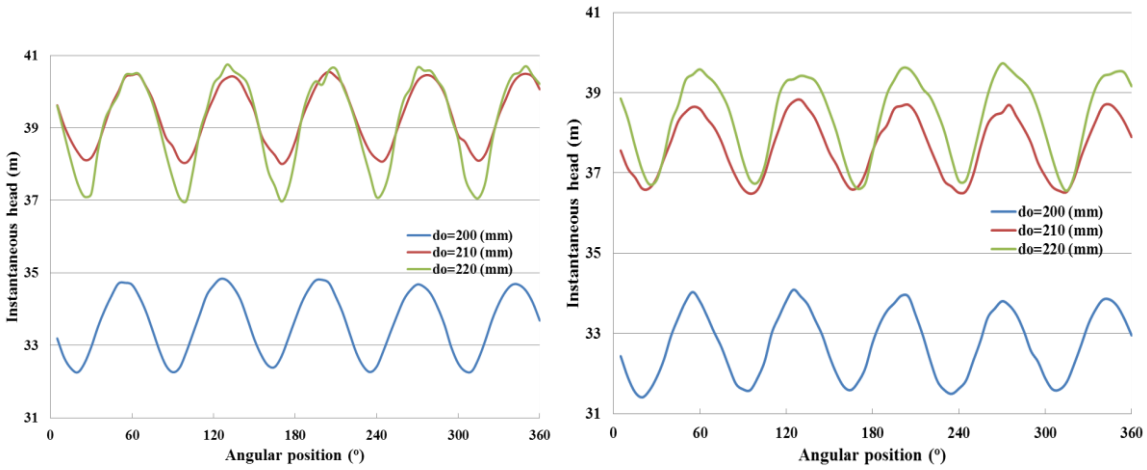

(a) (b)

Figure 5-47: Instantaneous head variations of centrifugal pump having different impeller outlet diameter under single-phase and cavitation conditions

Figure 5-49 below depicts the effect of do, and APPENDIX C presents complete CFD results. As mentioned earlier in previous sections, when Z and di values are constant while the value of do increases, it can be seen that variances between peaks to valleys for this model (do=220mm) are considerably higher than the other two models. The common reason behind this is due to the fact that there is a small clearance between the impeller and the volute for the

model for when do=220mm, making the pressure fluctuations significantly higher when compared to the other two models. It can be observed that the two curves have the same trend as shown in Figure 5-48. The average head curve under cavitation condition is lower than for single-phase curve. In addition, there is no significant change on the head between when do=220mm and do=210mm for both single-phase and cavitation. However, the head for when do=220mm is higher than for when do=200mm under both single-phase and cavitation conditions by around 14.13% and 14.69%, as shown in this figure. It can also be seen that there is a slight difference between the head for both single-phase and cavitation under the different outlet impeller diameters (do). The head for the single-phase condition is slightly higher than for the cavitation condition. Due to the fact that all these cases under investigation were operating under flow rate of 300(l/min), very small cavitation has then occurred in the pump.

Further quantifying the performance of the aforementioned centrifugal pump under single-phase and cavitation conditions at different outlet impeller diameters. Table 5-25 shows the maximum, minimum, average, maximum, and (max – min) amplitude in the instantaneous head.

Table 5-25: Statistical analysis of the centrifugal pump instantaneous head under single-phase and cavitation conditions under different outlet impeller diameters

Single-phase			
Head (m)	do=200mm	do=210mm	do=220mm
Average	33.60	39.34	39.13
Minimum	32.25	38.01	36.97
Maximum	34.83	40.54	40.74
Max - Min	2.57	2.54	3.77
Cavitation condition			
Head (m)	do=200mm	do=210mm	do=220mm
Average	32.73	37.65	38.37
Minimum	31.40	36.48	36.55
Maximum	34.08	38.82	39.73
Max - Min	2.680	2.338	3.174

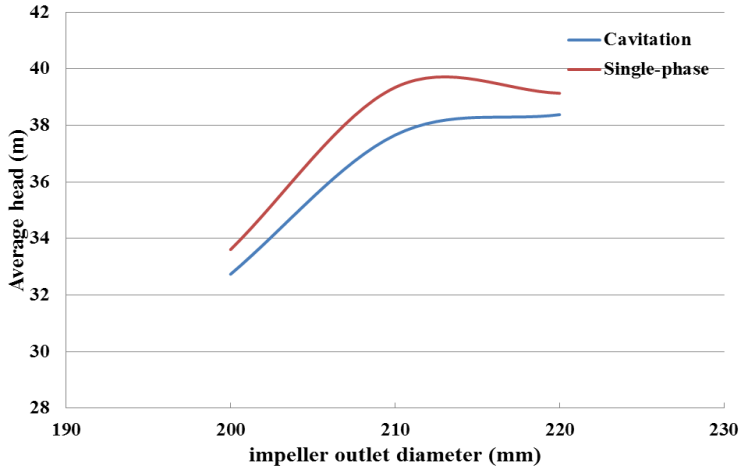

Figure 5-49: Effect of impeller outlet diameter on the performance of centrifugal pump under single-phase and cavitation condition

5.8.2.1. Detection of Cavitation under Different Outlet Impeller Diameters and Flow Rates

Figure 5-50 depicts the vapour volume fraction variations under various flow rates namely 300, 330, and 350(l/min). The outlet impeller diameters are 200mm, 210mm, and 220mm, inlet impeller diameters of di=25mm, and Z=5, and N=2775rpm for all cases under investigation. The numerical results showed that the occurrence of cavitation changes with outlet impeller diameters and flow rates. It can be seen that at 300 and 330(l/min) flow rates; there was very small occurrence of cavitation at different outlet impeller diameters. In addition, cavitation increases as the outlet impeller diameter and flow rate increase, starting from the inlet of the impeller close to the leading edge, under a different outlet impeller diameters and flow rates. The length of the cavity is increased with low pressure and at the inlet impeller decreased. The reason for this due to an increase in the outlet impeller diameters and flow rates, leading to pressure at the eye of impeller continually decreasing and as a result, the cavitation intensity will increase within a pump. In addition, at do=220mm blades, cavitation was affected at the suction of impeller compared to the different outlet impeller diameters at 210mm and 200mm, especially at high flow rate. It can be seen that as the low pressure decreases, the visual observation of the cavitation gradually increases with increase in the outlet impeller diameter. Based on the above analysis, the numerical results showed that the outlet impeller diameter and flow rate have a high effect on the development of cavitation within a pump, particularly at the eye of impeller region.

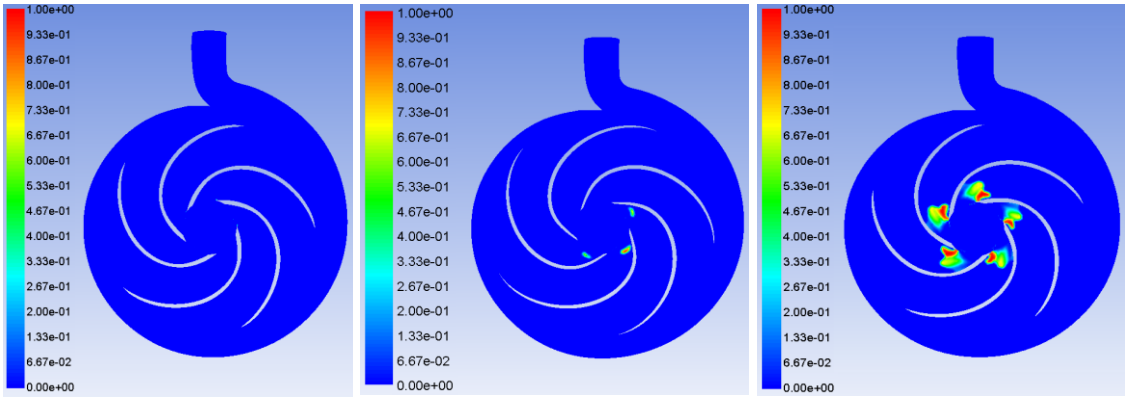

Q=300(l/min) Q=330(l/min) Q=350(l/min)

do200Z5di25

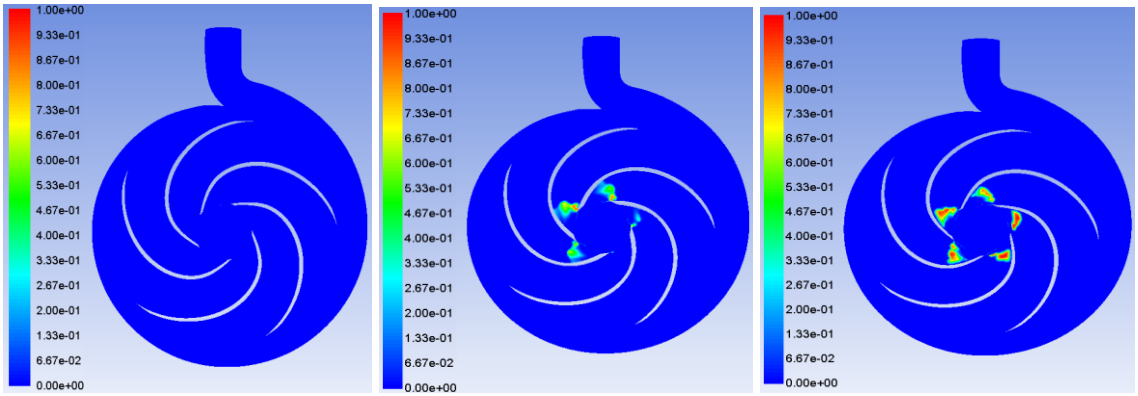

Q=300(l/min) Q=330(l/min) Q=350(l/min)

do210Z5di25

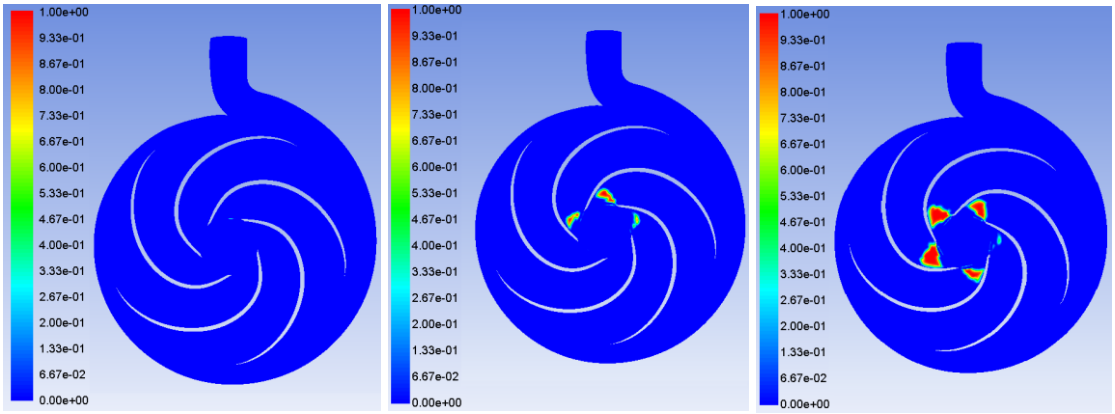

Q=300(l/min) Q=330(l/min) Q=350(l/min)

do220Z5di25

Figure 5-50: Volume fraction distributions for the pump under different outlet impeller diameters and flow rates

5.8.3. Effect of Inlet Impeller Diameter on the Performance of the Centrifugal Pump under Single-Phase and Cavitation Conditions

In order to analyse the effect of the inlet impeller diameter (di) on the performance of the centrifugal pump under single-phase and cavitation conditions, three (di) values of 25mm, 30mm, and 35mm were selected for this analysis purpose. The centrifugal pump flow rate is kept at 300(l/min), Z=3, do=210mm and N=2755rpm. APPENDIX C summarises the complete set of results.

Figure 5-51 depicts the pressure variations within the centrifugal pump having a flow rate of 300(l/min), Z=3, do=210mm, N=2755rpm, and di=25, 30, and 35mm. It can be observed that a high-pressure region exists between the impeller outlet and tongue volute area, as the pressure becomes lower at the inlet of the impeller. Furthermore, the pressure becomes comparatively low at the eye of the impeller when compared to the higher pressure at the impeller outlet section. Moreover, it can be noticed that the high-pressure for di=30mm is comparatively lower than when di=25mm by around 3.52%. Furthermore, the high-pressure for di=35mm is slightly lower than in the case for when di=30mm by 1.01%. This suggests that the average head output for this case will be slightly lower than for when di=35mm.

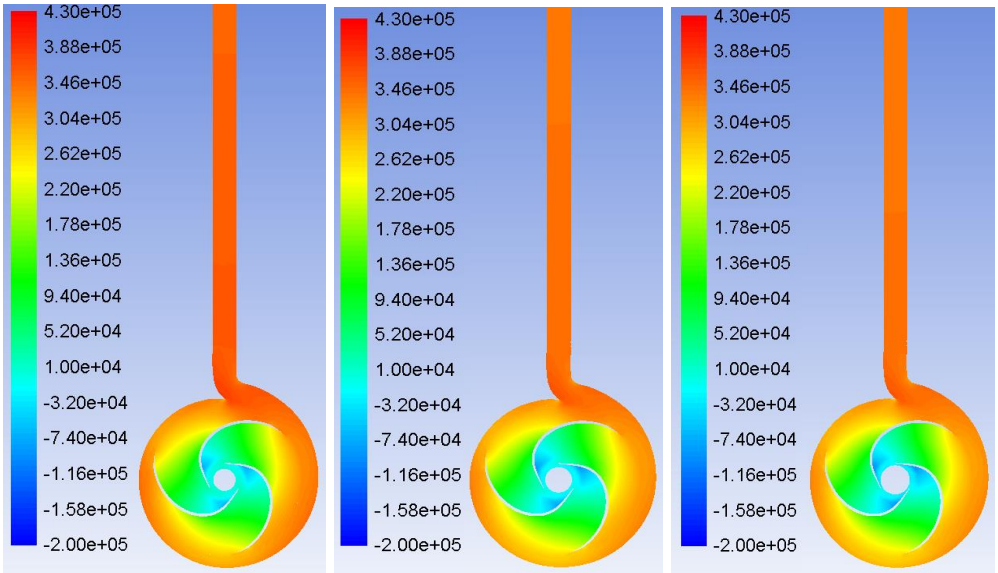

Figure 5-51: Static pressure variations of the pump under different inlet impeller diameters

Figure 5-52 depicts the velocity variations within the pump. It can be seen that the flow velocity is considerably high at the pressure side of blades due to the orientation of blades. The velocity

goes up to as high as 21.39m/sec for case (di=25mm). It can be seen that the flow velocity has no significant change in the velocity variations when compared with these cases.

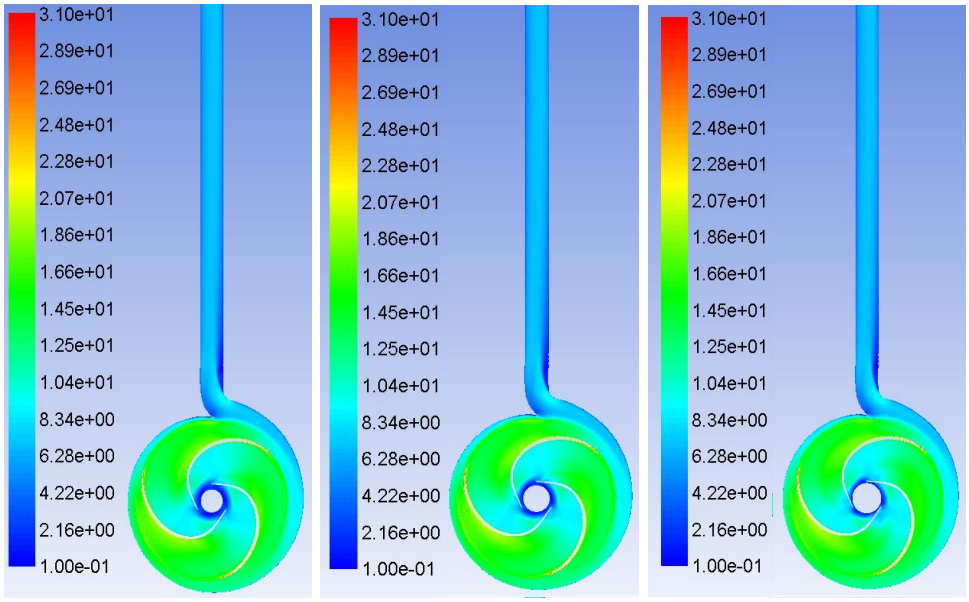

di=25mm di=30mm di=35mm

Figure 5-52: Velocity magnitude variations of the pump under different inlet impeller diameters

Figure 5-53 (a) depicts the pressure fluctuations for 12 monitoring points at volute of the pump under different inlet impeller diameters. The trend for pressure fluctuations at all various monitoring points are almost the same. The pressure fluctuations show a cyclical variation pattern and appear in the form of a sine wave. It can be observed that there are three peaks and valleys, which is equal to the same number of blades on the impeller. In addition, the pressure fluctuation at monitoring points VP6 is higher than that at the rest of the points. The minimum pressure fluctuation was found at VP3 with a pressure as shown in Table 5-26 this point is not close to the tongue region. In comparison with the case of when di=25mm, the amplitude of maximum pressure fluctuations at the volute for when di=30 and 35mm were slightly lower than when di=25mm.

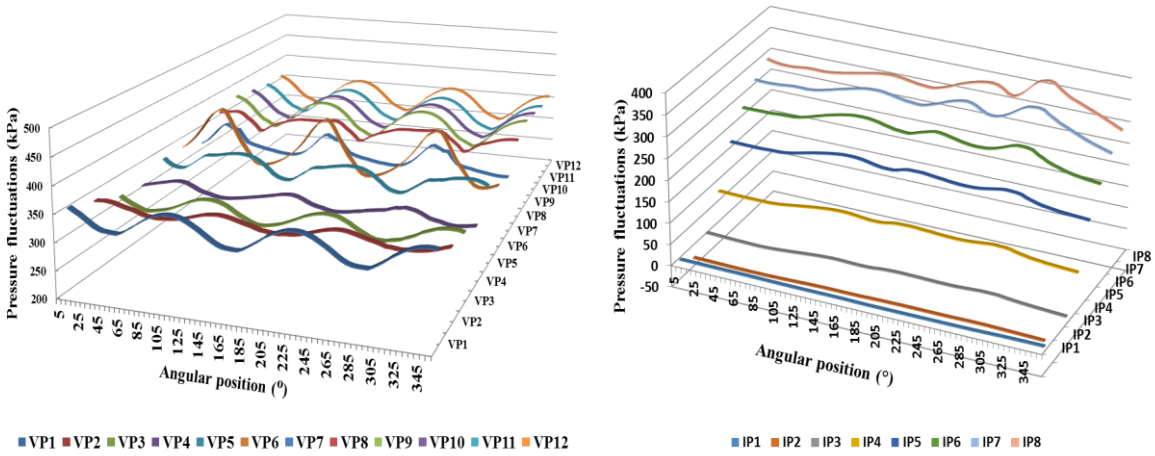

(a) di=25mm (b)

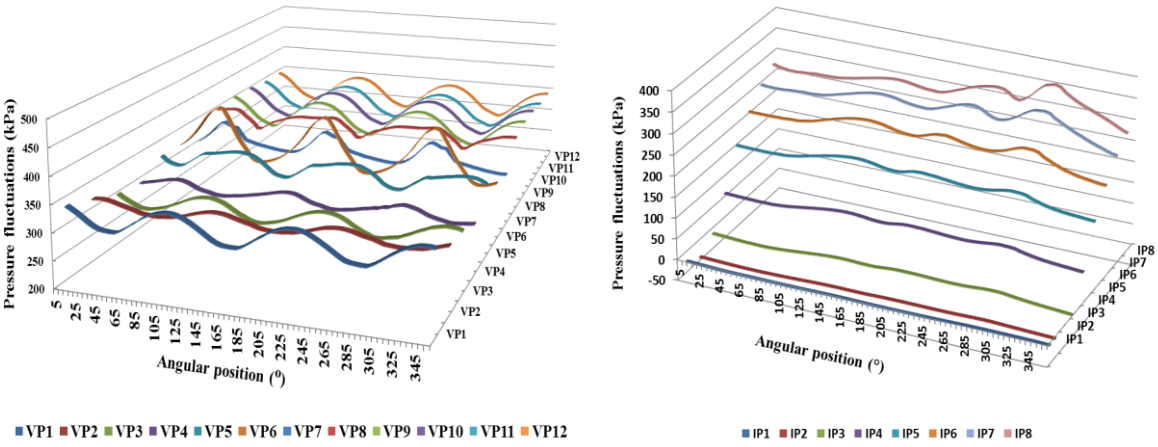

(a) di=30mm (b)

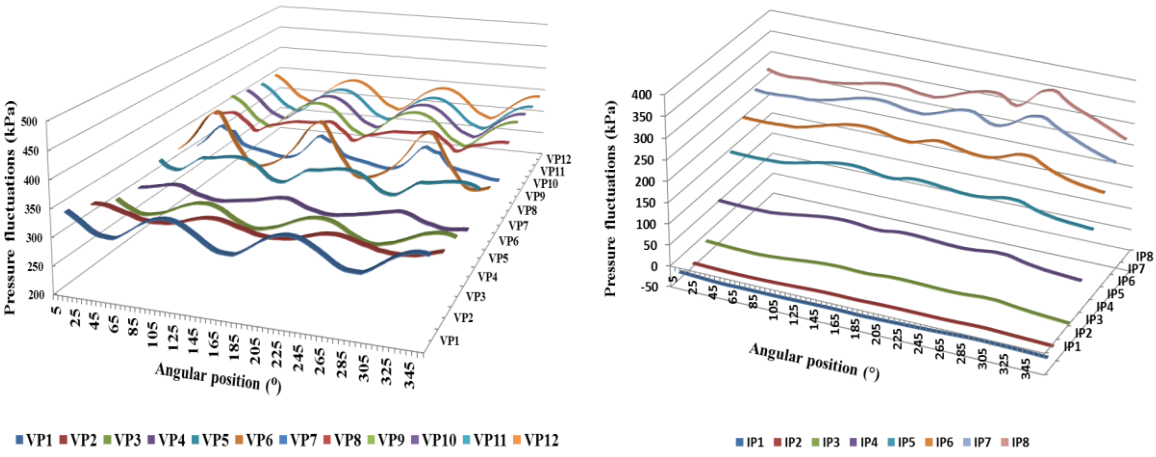

(a) di=35mm (b)

Figure 5-53: (a) Static pressure fluctuations in the volute and (b) At the impeller under different inlet impeller diameters

Table 5-26: Summarises statistical analysis results of the static pressure fluctuations at the volute under different inlet impeller diameters

di=25mm												
Statistical features	VP1 (kPa)	VP2 (kPa)	VP3 (kPa)	VP4 (kPa)	VP5 (kPa)	VP6 (kPa)	VP7 (kPa)	VP8 (kPa)	VP9 (kPa)	VP10 (kPa)	VP11 (kPa)	VP12 (kPa)
Avg.	335.45	322.38	306.96	307.95	340.65	355.35	326.77	349.98	346.49	339.68	333.12	333.63
Min.	310.45	312.20	288.55	296.58	315.17	310.85	308.39	323.80	309.40	304.64	298.28	298.64
Max.	358.10	334.21	325.03	321.19	357.70	416.98	360.30	363.39	374.27	367.76	360.91	361.67
Min.-Max.	47.65	22.00	36.49	24.60	42.53	106.12	51.91	39.60	64.87	63.12	62.63	63.02
di=30mm												
Avg.	321.77	308.69	293.19	294.09	326.82	341.71	313.09	336.33	326.02	326.02	319.49	319.99
Min.	297.63	299.16	274.98	283.40	302.44	297.69	294.58	311.20	291.98	291.98	285.67	286.05
Max.	344.70	320.37	311.31	307.51	342.99	402.12	345.38	349.51	354.03	354.03	347.38	348.02
Min.-Max.	47.06	21.21	36.33	24.10	40.55	104.43	50.80	38.31	62.05	62.05	61.71	61.98
di=35mm												
Avg.	319.20	306.15	290.32	291.26	323.53	338.58	309.31	332.89	330.39	323.54	317.08	317.56
Min.	295.46	296.54	272.41	281.34	299.67	295.25	289.40	310.93	295.00	290.16	283.90	284.22
Max.	341.53	317.42	307.91	303.32	339.30	398.13	342.23	346.39	357.67	350.99	344.43	345.06
Min.-Max.	46.07	20.88	35.50	21.98	39.63	102.88	52.82	35.45	62.67	60.83	60.53	60.83

Figure 5-53 (b) depicts the pressure fluctuations along the angular location at the impeller. The maximum pressure fluctuations were at the impeller outlet for points IP7 and IP8, which were higher than the rest of points as summarised in Table 5-27. When di=25mm, the amplitude of the average pressure fluctuation at the impeller at IP8 for when di=30mm is lower than for when di=25mm by about 3.3%. In comparison with the previous model, the maximum pressure fluctuations at the impeller for when di=35mm has no significant change from that of the previous model.

Table 5-27: Summarises statistical analysis results of the static pressure fluctuations at the impeller under different inlet impeller diameters

di=25mm								
Statistical features	IP1 (kPa)	IP2 (kPa)	IP3 (kPa)	IP4 (kPa)	IP5 (kPa)	IP6 (kPa)	IP7 (kPa)	IP8 (kPa)
Avg.	0.61	-21.87	12.82	88.56	183.44	246.11	292.06	313.30
Min.	-0.58	-25.23	3.77	76.90	167.79	223.13	262.20	281.16
Max.	2.06	-19.18	20.03	98.49	196.75	271.22	335.52	371.53
Min.-Max.	1.48	-6.05	16.26	21.59	28.95	48.09	73.32	90.37
di=30mm								
Avg.	-17.29	-33.61	-0.69	74.38	169.69	232.63	278.34	299.91
Min.	-19.29	-38.15	-11.24	60.97	152.12	208.87	247.02	266.71
Max.	-14.74	-29.71	7.61	85.24	184.03	258.45	322.78	359.24
Min.-Max.	-4.56	-8.44	-3.63	24.27	31.91	49.58	75.76	92.52
di=35mm								
Avg.	-28.59	-33.73	-3.94	70.14	165.08	228.68	275.29	296.48
Min.	-32.26	-38.56	-15.16	56.65	147.24	204.88	244.17	262.87
Max.	-23.18	-29.57	4.79	81.25	179.39	254.77	319.93	355.71
Min.-Max.	-9.08	-8.99	-10.37	24.60	32.15	49.88	75.76	92.84

Figure 5-54 (a) depicts that the amplitudes of pressure fluctuations with their frequencies for 12 monitoring points around the volute under different inlet impeller diameters. It can be noticed that the dominant frequency for the entire monitoring points is at the BPF, which is equal to 144.9Hz, due to the number of impeller blades used (three blades). However, the maximum pressure fluctuations amplitude at VP6 and VP9 as shown in Table 5-28. This is due

to locations of where these points are which near the tongue. In addition, at point VP2, the pressure fluctuation amplitude reaches its lowest, due to the location being far away from the volute tongue area. Additionally, the maximum pressure fluctuation amplitude at the volute for when di=30mm is lower than when di=25mm. In comparison with the case for when di=30mm, the maximum pressure fluctuation amplitude at the volute for when di=35mm is lower than the previous model by about 1.8%.

Table 5-28: Maximum amplitude of static pressure fluctuations at the volute under different inlet impeller diameters

di=25mm												
Frequency	Maximum amplitude of pressure fluctuations for 12 monitoring points at the impeller (kPa)											
Hz	VP1	VP2	VP3	VP4	VP5	VP6	VP7	VP8	VP9	VP10	VP11	VP12
141.69	16.70	7.08	12.62	7.47	13.13	35.01	15.75	10.18	21.23	20.89	20.70	20.81
di=30mm												
Hz	VP1	VP2	VP3	VP4	VP5	VP6	VP7	VP8	VP9	VP10	VP11	VP12
141.69	16.71	7.07	12.54	12.54	7.31	12.82	34.95	15.74	10.11	21.20	20.68	20.78
di=35mm												
Hz	VP1	VP2	VP3	VP4	VP5	VP6	VP7	VP8	VP9	VP10	VP11	VP12
141.69	16.43	7.07	12.28	6.96	12.52	34.30	15.92	8.86	20.86	20.53	20.36	20.46

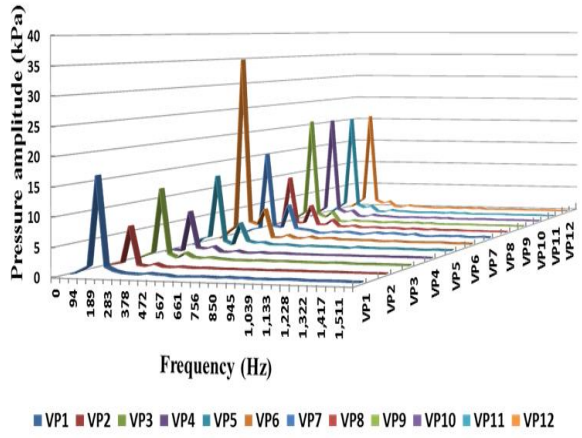

(a)

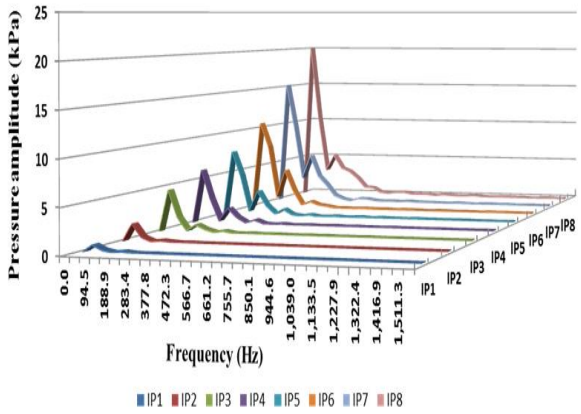

(b)

di=25mm

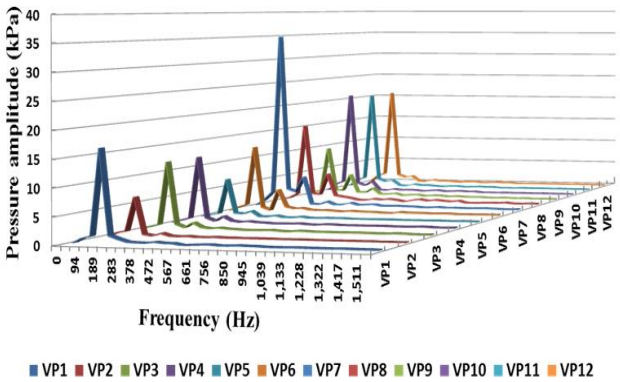

(a)

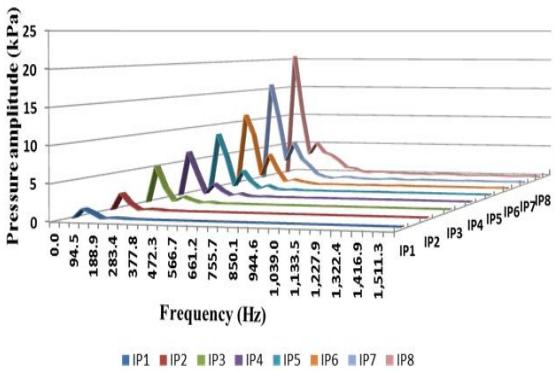

(b)

di=30mm

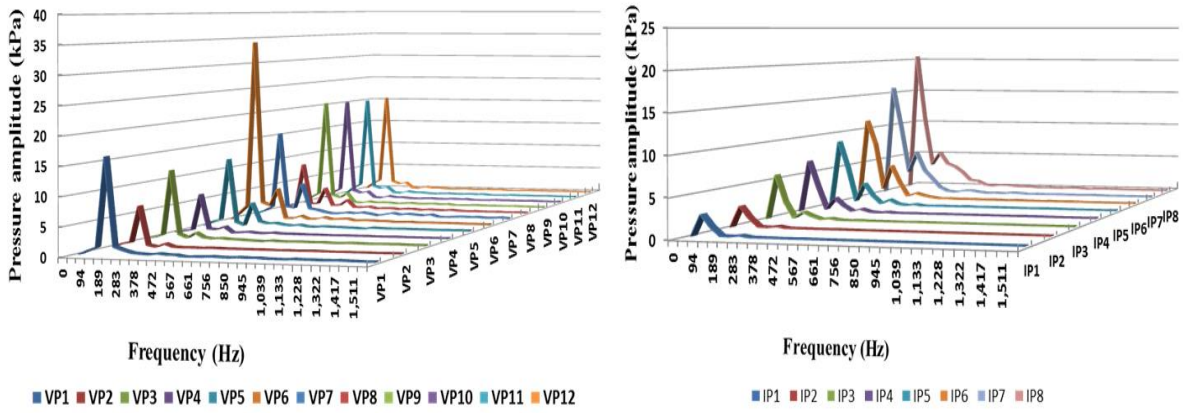

(a) di=35mm (b)

Figure 5-54: (a) Frequency spectra around the volute and (b) At the impeller under different inlet impeller diameters

Figure 5-54 (b) shows the variances in the amplitudes of pressure fluctuation with frequencies for eight monitoring points at the impeller. The maximum pressure fluctuation amplitudes gradually increase from the inlet of the impeller to the outlet at the impeller flow passages. The first maximum amplitude of the pressure fluctuations for all points is at frequency 47.23Hz due to the rotation frequency (Rf) of impeller and is equal to (N/60). Table 5-29 summarises the amplitudes of pressure fluctuations at (Rf) in the impeller. In addition, it can be observed that the maximum pressure fluctuation amplitude at the impeller for when di=30mm is slightly lower than for when di=25mm by about 2.47%. In comparison, the results for maximum pressure fluctuation amplitude for di=30mm shows no significant change when compared to the previous case (di=30mm).

Table 5-29: Maximum amplitude of static pressure fluctuations at the impeller under different inlet impeller diameters

di=25mm								
Frequency	Maximum amplitude of pressure fluctuations for 8 monitoring points at the impeller (kPa)							
Hz	IP1	IP2	IP3	IP4	IP5	IP6	IP7	IP8
47.23	0.75	1.90	4.72	6.22	7.71	10.69	15.28	20.06
di=30mm								
Hz	IP1	IP2	IP3	IP4	IP5	IP6	IP7	IP8
47.23	1.31	2.36	5.32	6.65	8.70	11.20	15.86	20.57
di=35mm								
Hz	IP1	IP2	IP3	IP4	IP5	IP6	IP7	IP8
47.23	2.67	2.67	5.78	6.85	8.86	11.30	15.83	20.52

Figure 5-55 depicts the centrifugal pump under cavitation conditions. The pump used for this study has a flow rate of 300(l/min), Z=3, do=210mm N=2755rpm, and di=25, 30, and 35mm. It can be observed that there is very minimal cavitation zone occurrence at the inlet of the

impeller of the pump for di=25mm. The lowest pressure for this impeller happens close to the inlet. In this region, the vapour bubbles occur during the operation of the pump. Firstly, the vapour bubbles occur close to this area and then increase as the inlet pressure was reduced. However, in comparison cases di=30 and 35mm with di=25mm it can be seen that there was no cavitation occurred in these cases.

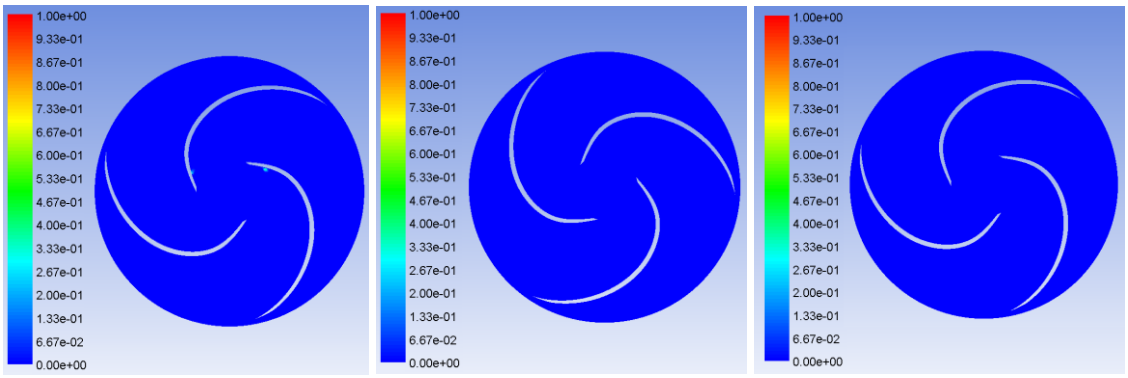

di=25mm di=30mm di=35mm

Figure 5-55: Volume fraction distributions for the pump under different inlet impeller diameters

Figure 5-56 (a) and (b) depicts the instantaneous head of the aforementioned cases under single-phase and cavitation conditions on a single scale for comparison purposes. It can be seen that for when di=25mm, the head is slightly higher than for the other two models under single-phase and cavitation conditions. Therefore, it can be observed that as (di) increases, the head of the pump slightly decreases.

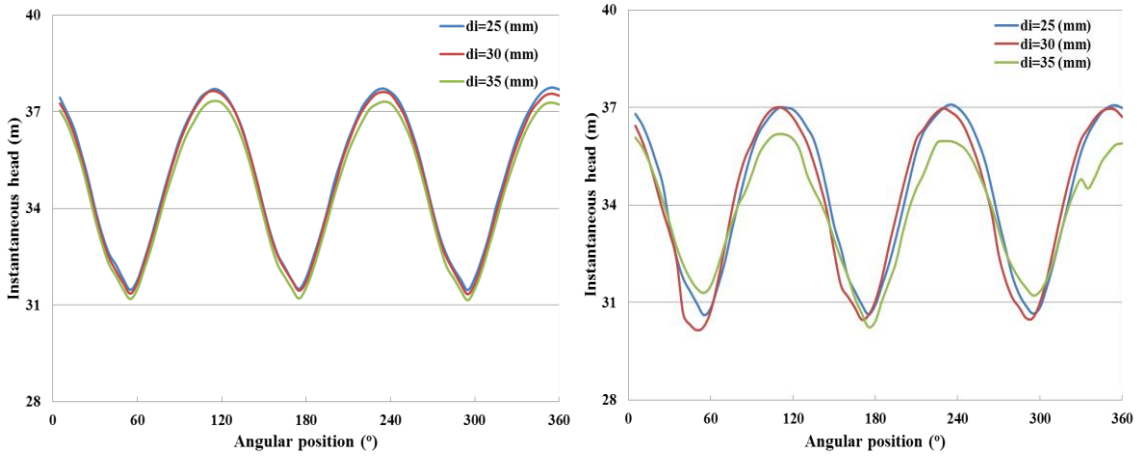

Figure 5-56: Instantaneous head variations of centrifugal pump having different impeller outlet diameter under single-phase and cavitation conditions

The complete CFD outcomes were displayed in APPENDIX C. Figure 5-57 depicts the effect of impeller inlet diameter (di) on the performance pump under single-phase and cavitation conditions. It can be found that for a given Z and do, as di increases, the average head of the pump very slightly decreases under both single-phase and cavitation conditions. Also, there is a slight difference between the head for both single-phase and cavitation under different inlet impeller diameters and the head for single-phase is slightly higher than cavitation condition by 1.97, 1.37, and 2.34% for di=25, 30, and 35mm respectively. The reason behind this is due to all the cases under investigation being operational under flow rate of 300(l/min) and under this flow rate cavitation in the pump was very small.

For further quantification on the performance output of the aforementioned centrifugal pump, under different inlet impeller blades Table 5-30 shows the statistical analysis of the instantaneous head.

Table 5-30: Statistical analysis of the instantaneous head of the pump under cavitation conditions at different inlet impeller diameters

Single-phase			
Head (m)	di=25mm	di=30mm	di=35mm
Average	34.94	34.82	34.57
Minimum	31.46	31.33	31.14
Maximum	37.75	37.64	37.33
Max - Min	6.28	6.30	6.18
Cavitation condition			
Head (m)	di=25mm	di=30mm	di=35mm
Average	34.25	34.10	33.76
Minimum	30.60	30.13	30.23
Maximum	37.08	37.01	36.18
Max - Min	6.480	6.863	5.94

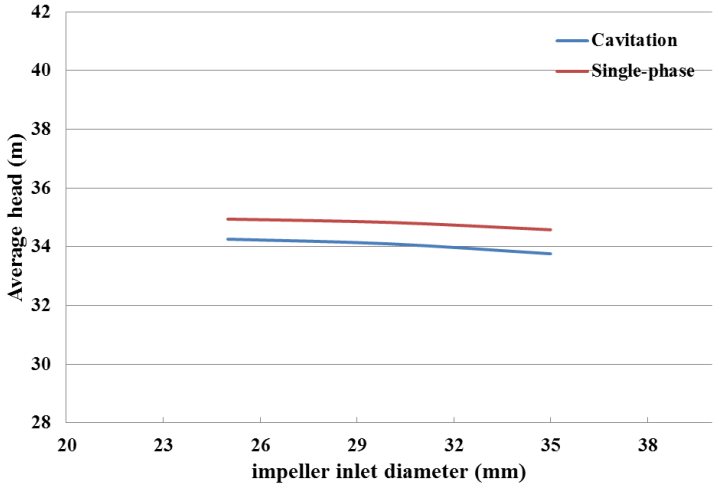

Figure 5-57: Effect of impeller inlet diameter on performance of the centrifugal pump under single-phase and cavitation conditions

5.8.3.1. Detection of Cavitation under Different Inlet Impeller Diameters and Flow Rates

Figure 5-58 the vapour volume fraction variations distributions under various flow rates, namely 300, 330, and 350(l/min). The inlet impeller diameters are 25mm, 30mm, and 35mm, the number of impeller blades is three. The pump rotational speed was kept constant at 2775rpm for all cases under investigation. The numerical results showed that the occurrence of cavitation changes with different inlet impeller diameters and flow rates. It can be seen that at 300(l/min) flow rate, there was very small occurrence of cavitation at inlet impeller diameter di=25mm. In addition, cavitation slightly increases as the inlet impeller diameters and flow rate increase, starting from the inlet of impeller close to the leading edge, under different inlet impeller diameters and flow rates. Moreover, the length of the cavity is slightly increased with low pressure at the inlet impeller (eye) decreased. The possible reason is due to increase the inlet impeller diameters and flow rate, leading to the pressure at the eye of impeller continually decreasing and as a result, the cavitation will slightly increase within a pump. In addition, at do=35mm blades, cavitation was slightly affected at the suction of impeller compared to the different inlet impeller diameters at 25mm and 30mm. It can be seen that as the low pressure decreases, the small visual observation of the cavitation gradually increases with increase in the inlet impeller diameter.

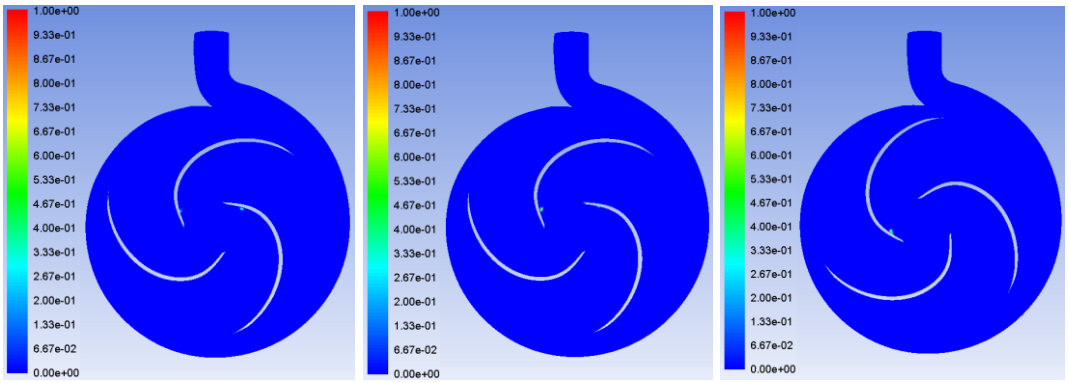

Q=300(l/min) Q=330(l/min) Q=350(l/min)

di25Z3do210

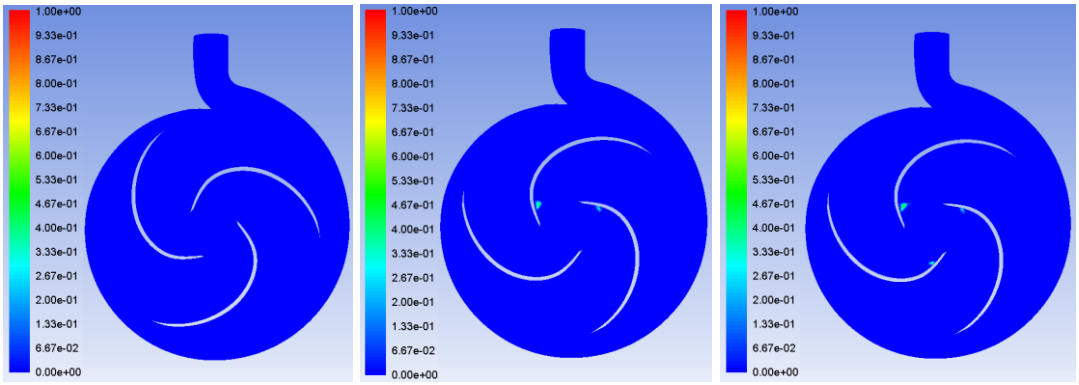

Q=300(l/min) Q=330(l/min) Q=350(l/min)

di30Z3do210

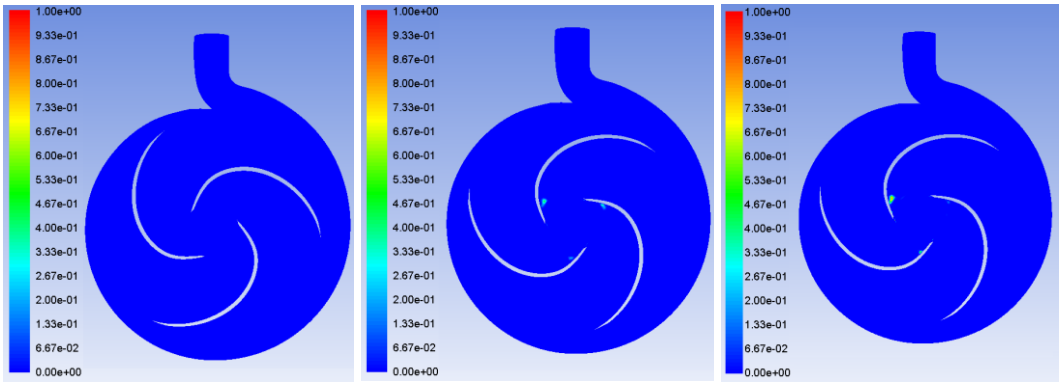

Q=300(l/min) Q=330(l/min) Q=350(l/min)

di35Z3do210

Figure 5-58: Volume fraction distributions for the pump under different inlet impeller diameters and flow rates

5.9. Expression for Head and Power Coefficients (CH) and (CP) Based on Impeller Geometrical Parameters

Detailed analysis into the influence of the impeller geometrical parameters on the performance of a centrifugal pump were carried out in the previous sections, where for practical purposes, the range for the impeller geometrical parameters was limited. The trends showed that increase in the number of impeller blades (Z) enhances the performance of a centrifugal pump whilst decrease in the inlet impeller diameter (di) slightly increases the head of the pump.

In order to quantify these outcomes in the centrifugal pump, multiple regression investigations were carried out and the results gained from CFD simulations. The three geometrical variables involved in this study are the number of impeller blades (Z), inlet and outlet impeller diameters (di and do), while the output target parameter was selected as the head and power coefficients

of the pump. The head and power coefficients can be represented with regards to the impeller geometrical parameter of the pump as following:

$$\mathrm{CH} = \mathrm{f}\,(\mathrm{Z}, \mathrm{do}, \mathrm{di}) \tag{5-3}$$

$$\mathrm{CP} = \mathrm{f}\,(\mathrm{Z}, \mathrm{do}, \mathrm{di}) \tag{5-4}$$

The author is not aware of any published papers in previous literature review in which such an expression was developed in centrifugal pump under single-phase and cavitation conditions. From CFD simulations results under single-phase conditions summarised in APPENDIX C, multiple regression analysis was performed and the following equations for the head and power coefficients of the pump were developed:

$$CH = \frac{115.21\ g\ (\frac{do}{di})^{-0.940}\ \mathrm{Z}^{0.1971}}{\omega^2\ di} \tag{5-5}$$

$$CP = \frac{686.8\ (\frac{do\ Z}{di})^{-0.876}\ (\frac{di\ Z}{do})^{-0.0658}\ Pavg\ Z}{\rho\ \omega^3\ do^4\ di} \tag{5-6}$$

Furthermore, under cavitation conditions the head and power coefficients of the pump were also developed:

$$\mathrm{CH} = \frac{112.65\ g\ (\frac{do}{di})^{-0.9205}\ \mathrm{Z}^{0.165}}{\omega^2 di} \tag{5-7}$$

$$CP = \frac{618.2\ (\frac{do\ Z}{di})^{-0.849}\ (\frac{di\ Z}{do})^{-0.0575}\ Pavg\ Z}{\rho\ \omega^3\ do^4\ di} \tag{5-8}$$

The above equations can be formulated to calculate the head and power coefficients for different configurations of the centrifugal pump. In order to validate these equations, they were compared with the results summarised in APPENDIX C. The accuracy of the head and power coefficients were more than 90% and 83%. The error was within ±10% and ±17%. The proper reasons for these errors could be attributed due to the numerical diffusion within the solver (numerical errors–iterative convergence errors), or due to the mechanical losses occurring in the pump which is caused by the contact between the shaft and bearings and between the shaft and seal. Also, the losses that occurs in the pump, which is due to the gap between the volute and impeller. In addition, hydraulic losses, which is an important loss, caused by friction losses, vortexes, and separation due to change in flow direction that happens at the passages of the

impeller. Moreover, the geometry and flow field within the pump are very complex and fully turbulent, with complex impeller blade curvature, which has considerable effect on the flow field developed either within the blade passages or inside the volute. Furthermore, due to statistical reasons like scattered data that might be a result to numerical calculations.

5.10. Summary of the Analysis of a Centrifugal Pump under Single-phase, Cavitation Conditions and Different Impeller Geometrical Parameters

Detailed flow diagnostics within the centrifugal under single-phase and cavitation conditions and effect of different impeller geometrical parameters showed the following results:

1- The pressure gradually increases from inlet to outlet impeller of the pump. Pressure at the impeller outlet is higher than the pressure at other parts of the impeller when the impeller rotates close to the tongue region of the volute.
2- The velocity gradually increases from the inlet to outlet impeller of the pump also. The high velocity occurs at the outlet of the impeller close to the tongue region.
3- The instantaneous head's waveform is almost uniform at a particular rotational speed.
4- The highest peaks in the pump's instantaneous head occur due to two important reasons, when the tongue area is approximately in-between the two impeller blades, and when one impeller blade has passed the tongue region and the other blade is approaching it.
5- The interaction between impeller and volute tongue region is actually according to the relative position of the impeller blades with respect to tongue region.
6- The pressure variations within a centrifugal pump increase as the rotational impeller speed is increased.
7- There are two dominant frequencies, the rotational frequency (Rf), and Blade Passing Frequency (BPF) and their related harmonics.
8- The cavitation phenomenon within a centrifugal pump occurs at the low-pressure region at the eye of impeller near the blade leading edges.
9- The numerical results showed that the distribution of volume fraction within a pump first occurs at the inlet eye of the impeller close to the leading blade.
10- This study concludes that the cavitation on the impeller can be classified into four levels (no cavitation, inception, development, and fully development of cavitation).
11- The results show that the cavitation in the pump increases as pump rotational speed increases.

12- The results show that as the number of impeller blades increases, the head of the centrifugal pump increases as well as the occurrence of cavitation also increases.
13- The head is considerably higher for when do=220mm than for when do=200mm for both single-phase and cavitation conditions. Moreover, when the outlet impeller diameter increases the occurrence of cavitation also increases.
14- When the inlet impeller (di) increases, the head of the centrifugal pump slightly decreases as well as the occurrence of cavitation also slightly increases.
15- CFD can be a useful tool to predict and analyse the outcome characteristics and performance of the centrifugal pump with reasonable accuracy under single-phase and cavitation conditions.
16- The detailed investigations of cavitation characteristics were presented in this study in order to provide useful information and guidance regarding the inception and development of cavitation within the centrifugal pump.

Based on previous analysis, the numerical results using CFD technique has provided detailed information with regards to analysing the flow field behaviour and predict pump performance, as well as cavitation detection under a different range of operating conditions. However, in order to increase in the reliability of cavitation detection in the pump. The use of different techniques using CFD, vibration and acoustic investigation techniques can provide a more robust detection of cavitation within a pump. Hence, study and detection of cavitation experimentally has become a significant aspect in pumps to give better understanding and provide confident and reliable results. Moreover, the experimental results allow us to understand the relationships between the occurrences and development of cavitation with vibration and acoustic signals. In order to study the cavitation in the pump in a real world scenario, data experimental techniques, using vibration and acoustic investigations in the next chapters can be further compared with the CFD technique as a basis for developing a comparison system between the different techniques for detecting and diagnosing different levels of cavitation within a centrifugal pump. Attempts would be made to find the most effectiveof these techniques in order to increase the accuracy and reliability of detection of cavitation within a centrifugal pump under wide a range of operating conditions.

CHAPTER 6

PREDICTION OF CAVITATION WITHIN A CENTRIFUGAL PUMP USING VIBRATION ANALYSIS TECHNIQUE

Cavitation is a problem that occurs in any pump and contributes highly towards the deterioration in the performance of the pump. In industrial applications, it is vital to detect and decrease the effect of cavitation in pumps. After obtaining detailed information regarding the pump performance and the effect of cavitation occurrence within a centrifugal pump using CFD technique as in the previous chapter, achieving some of the other research aims would lead to increase the reliability of cavitation detection in the pump. The use of various techniques, such as vibration and acoustic analyses, can provide a more robust detection of cavitation in the pump. In this chapter therefore, focus is on detecting and diagnosing the cavitation using vibration technique. The results obtained for vibration signal in time and frequency domains were analysed in order to achieve a better understanding regarding detection of cavitation. The effects of different operating conditions related to the cavitation were investigated in this chapter using different statistical features in time domain. Moreover, FFT technique for frequency domain was also applied.

6.1. Diagnosis of Cavitation within the Centrifugal Pump using Vibration Analysis Technique

In the current study, various experimental measurement techniques such as vibration, acoustic (sound) and pressure, based on different pump operation conditions, were used in order to simultaneously find the relationship between vibration and acoustic signals. This is for the purpose of detecting cavitation within the centrifugal pump. In this chapter, the sources of pump vibration during different operational conditions were evaluated. Further to this, explanations of how the inception and development of cavitation influences the pump vibration level were provided. The chapter includes the analysis of vibration signals in the time domain format using time wave form analysis (TWFA), followed by various statistical features to predict and diagnose cavitation under various operating conditions. For further analysis on the characteristic of cavitation inside the pump, the vibration signal in time domain is converted to frequency domain by employing the Fast Fourier Transform technique. This is for the purpose of predicting cavitation. This chapter further focuses on analysing the vibration signal in frequency domain based on different range of frequencies. Furthermore, analyses on the vibration amplitude in frequency domain by using different features, such as mean and RMS on the vibration amplitude values were also carried out. This analysis is essential in order to obtain a better understanding and gain more information regarding the detection of the occurrence of cavitation for various frequency ranges and hence, finding the sensitive frequency range for predicting cavitation.

6.2. Vibration Sources in the Centrifugal Pump

The vibration in centrifugal pumps might occur from various types of sources, comprising of hydraulic and mechanical excitation forces. These results in an increase in vibration levels that may decrease the performance of the pump and lead to damage in the pump parts, such as the impeller and volute. This also leads to a decrease in pumps bearing life and seal failures [15, 18]. Measurements of vibration in centrifugal pump can be utilised for several applications, including quality control and condition monitoring investigations and also for research development. Vibration in pumps have two central sources, the first one is hydraulic and the second is mechanical. The next section will explain these types of vibration sources [18].

6.2.1. The Vibration Occurrence from Hydraulic Sources in the Centrifugal Pump

Vibration in centrifugal pumps occurs as a result of several operational issues including flow distribution at high velocity, interaction between the rotating part such as the impeller, and the stationary part (e.g. volute). Furthermore, hydraulic sources of vibration in a pump includes blades passing forces, hydraulic imbalance, recirculation flow, cavitation, system instabilities, water hammer and so on [15].

6.2.2. The Vibration Occurrence from Mechanical Sources in the Centrifugal Pump

As described in the experimental setup in Chapter four, the pumping system comprises of several parts. This pumping system includes the centrifugal pump, an electrical motor and its related flow loop piping system, such as pipes, elbows, fittings and valves. There are various kinds of physical processes that create vibration within a pump, such as hydraulic interaction with the piping system, improper installation or maintenance, application for the pump, manufacturing designs and different types of faults [148]. Typically, the mechanical vibration sources in the pump generates from several sources such as pressure fluctuations created in the fluid, imbalance, misalignment between shafts connections and damaged bearings [149]. Other mechanical sources include; mechanical forces, improper usage of the pump as provided in the installation manual and the conditions emerging from the pump incorrect assembly, and also from wear [15].

6.2.3. Cavitation as another Important Source of Vibration in the Centrifugal Pump

As mentioned in Chapter one, when cavitation occurs in the different types of machines (e.g. propellers, turbines and various kinds of pumps), it leads to drop in pressure, particularly at the eye of impeller. As a result, it leads to an increase in the level of noise and vibration, which causes an increase in pressure fluctuations within a pump [15]. When cavitation starts to occur within the pump, the formation of bubbles takes place. As cavitation continues, the bubbles collapse close to the surface of the impeller, which eventually erodes the impeller and causes pitting on the surface of the impeller and volute. Since the formation and collapse of bubbles happens randomly, the inception and development of cavitation can cause high noise and vibration [15].

Over the last decade, there was an increasing interest in using condition monitoring methods for detecting cavitation. There are several reasons behind choosing this method as it decreases the costs of machines maintenance resulting in increased productivity and safety in industry.

In this chapter, the vibration signal will be analysed as it is an important technique in condition monitoring for the centrifugal pump in order to predict the inception and development of cavitation occurrence. For this experimental work, in order to study the wide range of operational conditions and also to detect the different levels of cavitation, the centrifugal pump was subjected to various flow rates, pump rotational speeds, decrease in the suction valve openings and also air injection at the suction side of the pump. The flow rate was changed by throttling the ball valve at the discharge pump side and then being adjusted step by step. Furthermore, the analysis of vibration signals under the different operation conditions, aforementioned, using both time and frequency domains are performed using MATLAB code in the next sections.

6.3. Effect of Various Flow Rates to Predict the Performance and Cavitation within a Centrifugal Pump

For analysis purposes, the effects of various flow rates on the pump performance and to predict cavitation were investigated in this section. The pump was operated experimentally at different flow rates as summarised in Table 6-1. Keeping pump rotational speed N=2755rpm constant corresponding to 0.95Nd where Nd represented the design pump rotational speed and it is equal 2900rpm. The reason behind choosing this particular pump speed for analysis purposes is because of the maximum pump rotation speed for this experimental setup was 0.95 of Nd. Also in this section, the same operating conditions as used in the previous chapter, were chosen for comparison purposes between the results from CFD and the experimental results, in order to validate both results as shown in section 5.2.4. The complete set of results can be seen in this chapter.

Table 6-1 Range of flow rate for the pump under N=2755rpm

Flow rate (l/min)																
378	370	365	362	352	342	331	320	310	302	276	252	227	200	177	152	103

6.3.1. Performance Output of the Centrifugal Pump

One key aim in this experimental study is to calculate the pump head. Therefore, several experimental measurements were conducted to find the pump performance under various operation conditions. The suction and discharge pressure signals of the pump can be obtained through the use of two pressure transducers at suction and discharge sides of the pump. The data includes pressure signals and calculated heads are processed through use of MATLAB code as shown in next section.

6.3.2. Analysis on the Instantaneous Outlet Pressure of the Centrifugal Pump under Various Flow Rates

Figure 6-1 depicts the raw data of the instantaneous outlet pressure from the centrifugal pump in time domain, under different flow rates starting from 103(l/min) to 378(l/min) with N= 2755rpm. It can be seen also that the instantaneous outlet pressure signals changes as the flow rate changes. The magnitude of the pressure decreases with increases in flow rate. The possible reasons are due to the hydraulic and mechanical losses as well as the effect of the occurrence of cavitation leading to causing more unstable flow within the pump. However, it can be observed that these changes in the instantaneous outlet pressure do not provide a clear picture regarding the detection of cavitation in the pump. Therefore, further investigations are required to detect cavitation using different statistical features in order to analyse the instantaneous outlet pressure signals in time domain in the next section.

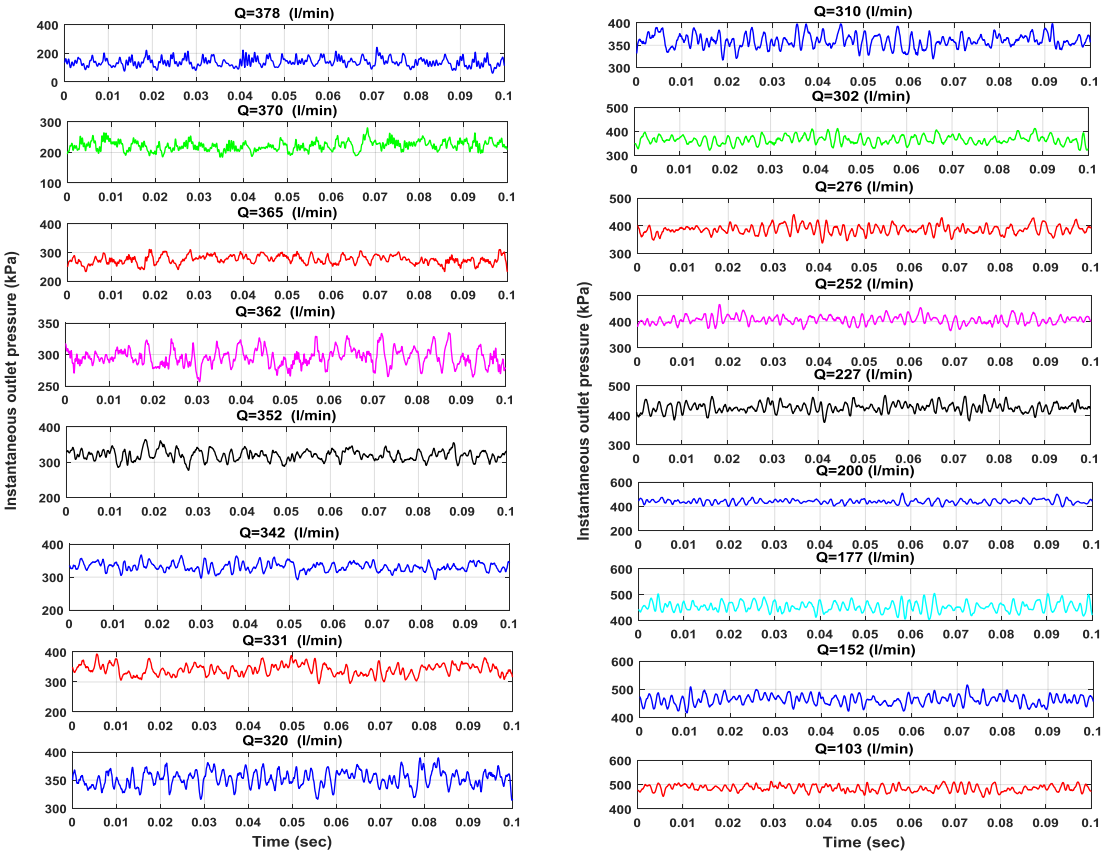

Figure 6-1: Instantaneous outlet pressure of the pump under different flow rates and N= 2755rpm

As mentioned earlier in the previous figure, time domain was used to analyse the raw data of the instantaneous outlet pressure signals under various flow rates using different statistical features. Figure 6-2 depicts the trend of peak, mean, minimum and RMS features for the outlet

pressure signals under different flow rates from 103(l/min) to 378(l/min) with N=2755rpm. It is evident that trends of all above mentioned features are decreased with increased flow rate due to the same reasons as given above. Also, the trend of these features rapidly decreases when the pump operates at a flow rate higher than 350(l/min). The reasons for this are due to the high interaction between impeller and volute and due to the occurrence and development of cavitation within a pump.

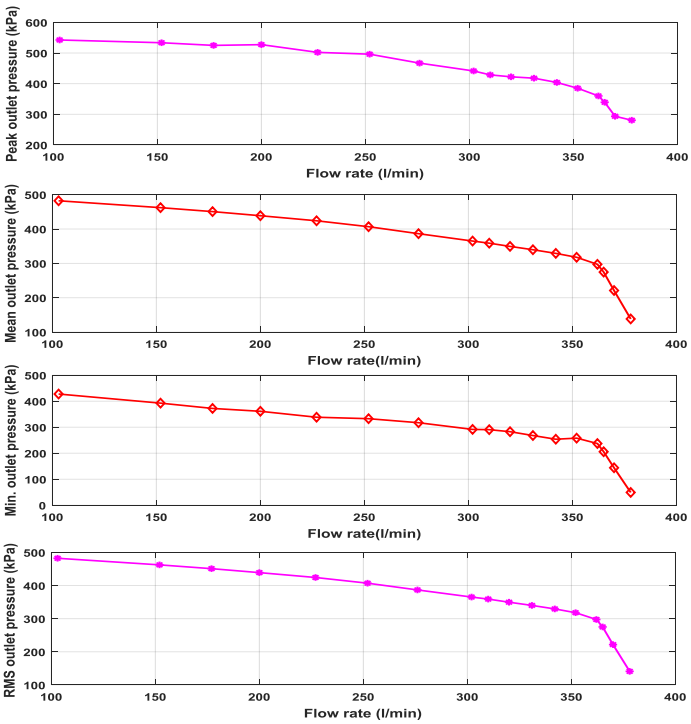

Figure 6-2: Trend of the peak, mean, minimum, and RMS features of the outlet pressure signals under different flow rates

6.3.3. Calculation of the Head and NPSH of the Centrifugal Pump under Various Flow Rates

Figure 6-3 depicts the measurements of the pump head under various flow rates which was also summarised in Table 6-1 for N= 2755rpm. It can be observed that the head gradually decreases when flow rate increases. The head changes in a periodic manner as the pressure changes in the pump. There are three main possible reasons for this, the first being the high interaction between the impeller and tongue volute region which is generated by the impeller rotational speed. The second reason is related to the non-uniform distribution of pressure in the volute due to the asymmetrical cross-section area of the volute, and finally, the important reason, is the occurrence of inception and development of cavitation. It can also be seen from this figure

that when the pump operates under high flow rate, it leads to a decrease in the head within the pump and then also leads to reduction in pressure at the inlet eye of the impeller below the water vapour pressure. This results in cavitation which will develop in the pump when the flow rate is increased. Further investigation also shows that the head rapidly decreases when the pump operates at flow rate higher than 350(l/min). The reason being the occurrence of cavitation. However, this phenomenon will be analysed and then discussed in details in this chapter using the vibration technique.

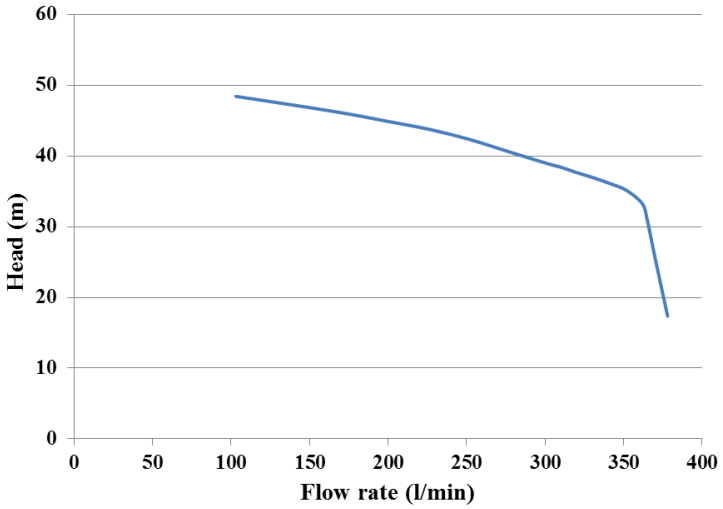

Figure 6-3: Head of the centrifugal pump at N= 2755rpm

The effect of cavitation on the performance of the centrifugal pump under different operation conditions will be discussed. Such conditions include various flow rates, different pump rotational speeds, various suction valve openings and air injection. It is important to first calculate the NPSH of the pump under different flow rates. The cavitation characteristics of the centrifugal pump that are an important part of this study are plotted in Figure 6-4. This figure depicts the NPSHA and NPSHR against different flow rates [150]. For this purpose, the pump flow rate can be changed through progressively throttling the discharge valve and then keeping the suction valve open at 100% and keeping N= 2755rpm. The experimental data for the H-NPSHR curve for the centrifugal pump was provided by the manufacturer (Pedrollo company pump model F32/200H).

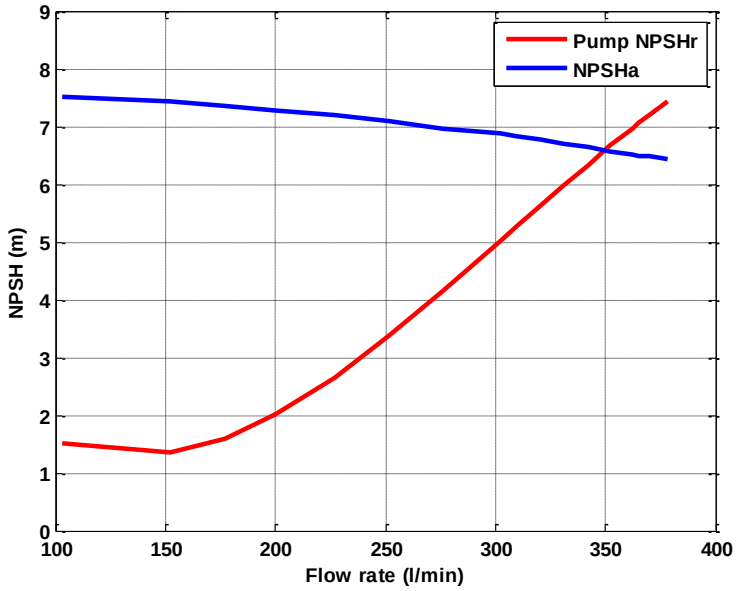

Figure 6-4: The cavitation characteristics of the centrifugal pump under different flow rates

From this figure, the different regions of cavitation are quite apparent. The first one being when the pump works under low flow rate, resulting in no cavitation to occur in this region. At this point, the NPSHA is higher than the NPSHR. For the second region, the flow rate is higher than 350(l/min) and in this region, cavitation begins to occur in the pump where the inter-section between the two curves for NPSHA and NPSHR already occurred. This means the development of cavitation starts at this point. The third important region is when cavitation within the pump starts to increase as the flow rate increases more than 350(l/min) due to decrease in the pressure at the eye of the impeller, hence, at this point, the NPSHA becomes smaller than the NPSHR. Also, it can be seen from this figure that cavitation has occurred at flow rate between higher design flow rate range of 300(l/min) and 350(l/min). It is also worth noting that these experimental results are in agreement with that of the CFD result in Chapter five for detecting cavitation in the pump. Furthermore, based on the above results regarding the relationship between the NPSHA and NPSHR. It can be seen that the values of NPSHA and NPSHR have a high effect on the performance of the pump.

In this study, investigations and discussions regarding the performance of the centrifugal pump under cavitation conditions were carried out using vibration technique. The details of the influences of various experimental operating conditions are discussed and analysed in details in the following sub section.

6.3.4. Predicting Cavitation within a Centrifugal Pump using Vibration technique under Various Flow Rates

In this research, an attempt was made to investigate the pump behaviour under the effect of normal operating and cavitation conditions, through the application of vibration technique. This technique necessitates particular sensors such as an accelerometer and accurate signal evaluation processing technique in order to analyse the vibration signal related to the cavitation condition within a pump under different operating conditions. Results corresponding to the vibration signal under various flow rates, through calculations and analysis of the signal amplitude in time and frequency domains within the pump, were presented to predict cavitation. Simultaneous evaluation of the different experimental measurements based on normal operation (without cavitation) and cavitation conditions were performed using MATLAB code. These signals are sampled, collected and saved through the use of dynamic data acquisition and analysis system model YE7600 from Global Sensor Technology.

During each experimental test, for the vibration signal sampling process, the pump rotation speed was kept constant at the different flow rates. In these experimental measurements, each experimental test was repeated at least 3 times. In order to obtain and provide more reliable consistent data sets, collecting and repeating each operation test helps to comprehend the characteristics of the vibration signals. Hence, acquire more dependable diagnostic features for predicting cavitation within the pump. This study collects and then analyses the vibration signals under various flow rates as summarised in Table 6-1. At the input, the voltage signal obtained from the accelerometer was collected then sampled at 96kHz in the data acquisition system. Furthermore, the numbers of data points in each of these experimental measurements were equal to 2880000 points. In order to measure vibration in the system, an accelerometer was used as the most appropriate vibration sensor [151]. There are several reasons behind using this type of sensor. Firstly, it can be used for wider ranges of frequency. Secondly, it is easy to install on the machine. Thirdly, it is reliable for vibration measurement and finally, it can be used effectively to predict various conditions such as healthy or faulty equipment [20].

Currently, there are many applications associated with pumps in industry. Therefore, condition monitoring in pumps has become a significant application as it can allow the extension of the life of the pump as well also decrease the cost of maintenance. In this research, a methodology was proposed for detecting the inception and development of cavitation. Figure 6-5 depicts the flow chart of this methodology used for the analysis of the vibration data for detecting

cavitation under a wide range of operation conditions. The methodology used in this research consists of different stages and the brief details of these experimental stages are as follows:

- The first stage includes collecting the experimental raw vibration signals from the centrifugal pump under the different ranges of operating conditions.
- Analysing the vibration signal based on time domain. Firstly, to compare the various raw vibration signals under the different operation conditions using the graph of the time wave form analysis (TWFA). Secondly, is to analyse the vibration signal using different statistical features such as peak, RMS, peak-to-peak and variance values.
- Detect various levels of cavitation (no cavitation, inception, development and full development of cavitation) within a pump by using the above features.
- Compare between the above mentioned features to find the sensitive feature in order to detect different levels of cavitation.
- Analyse the vibration signals based on frequency domain using FFT technique. Firstly, analyse the raw vibration signal based on various frequency ranges (low and high frequency ranges).
- Find the sensitive frequency range for detecting different levels of cavitation in the pump using waterfall figures to compare between vibration signals under different conditions.
- Analysing the amplitude of the vibration signals under different frequency ranges and wide range of operating conditions based on frequency domain analysis using different statistical features such as mean and RMS vibration amplitudes.
- Detect different levels of cavitation within a pump by using the above features.
- Compare between the above features in order to find the sensitive frequency range in frequency domain and detect different levels of cavitation within a pump.

The details of analysing the vibration data in time and frequency domains under different range of operation conditions and frequency ranges using above methodology, are presented in the next sections.

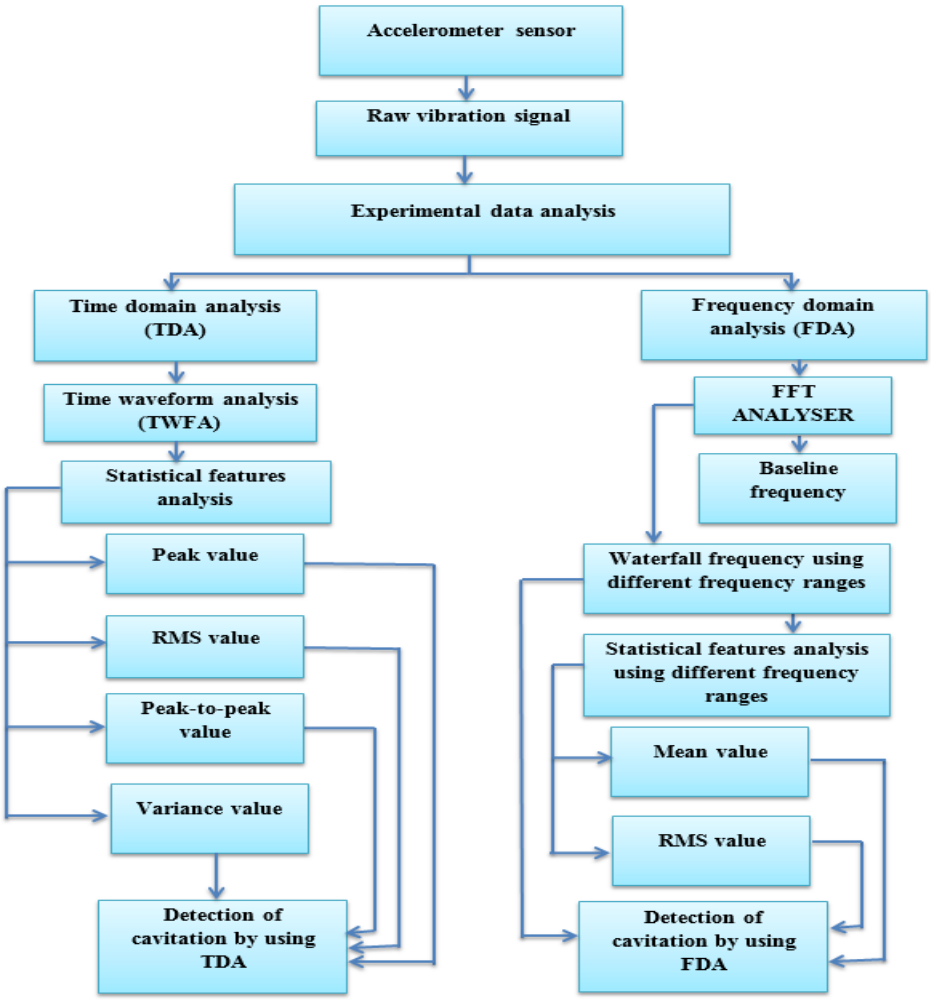

Figure 6-5: Flow chart analysis of vibration data processing

6.3.5. The Vibration Signal Analysis Based on Time Domain (Wave Form) under Various Flow Rates

The time wave form analysis (TWFA) of vibration acceleration signal was compared under normal and cavitation operating conditions. The experimental results were depicted and grouped based on different flow rates. Figure 6-6 depicts the relationship between the amplitude and time for the vibration wave form signals under various flow rates are listed in Table 6-1 at N=2755rpm. It can be seen that there are different levels of vibration amplitudes as the flow rate changes. For example, when the pump operates under the low range of flow rate such as between 152 and 302(l/min) the levels of vibration amplitudes are almost the same. It is also noticing that at a low range of flow rate the levels of vibration amplitudes are lower than that when the pump operates under high flow rate. However, at the high range of flow rate for example, from 331 to 352(l/min), the vibration levels began to increase. Obviously, at the

range of flow rate from 362 to 378(l/min), the values of vibration amplitudes rapidly increase. The results depict that the vibration amplitude increases when the flow rate increases. Two possible reasons can be considered for this phenomenon, one being due to the interaction between the impeller and volute tongue region. The second main reason is mostly due to the inception of cavitation-taking place at the high flow rate, which will develop when the flow rate is increased. In this case, the trend of the vibration amplitude was more random with high peaks when compared with normal operating conditions. The reason behind that is due to generate very small bubbles and these small bubbles collapse leading to change in the shape and amplitude of the vibration signals. It can be seen that the occurrence of cavitation is one key reason that causes instability in the flow in a pump. By comparing figures from (a) to (p), it can be concluded that vibration signals are sensitive to predicting cavitation.

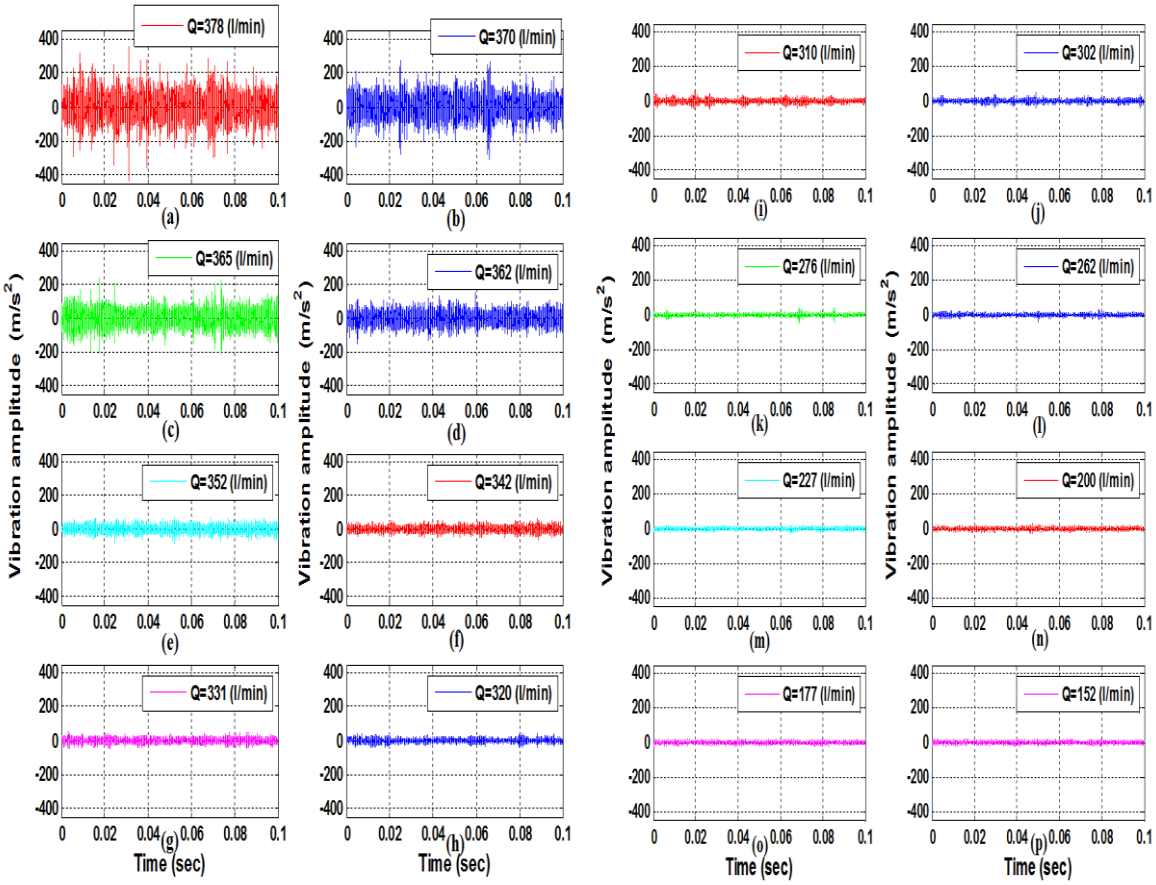

Figure 6-6: Analysis of the vibration signal in TWFA under various flow rates at N=2755rpm

To extract useful features, statistical analysis is used in condition monitoring method, which depends strongly on the kind of signal under investigation. In order to obtain further information with regards to analyse the vibration signals. This section includes analysis of the vibration signal in time domain, through the use of various types of statistical features to obtain

a clear idea regarding how the vibration amplitude is changed under different flow rates, and to predict and diagnose the cavitation within a pump.

6.3.6. Analysing of the Vibration Signal using Peak and RMS Features in Time Domain

As mentioned earlier, to analyse the sample of vibration signals under various operation conditions, different statistical features of vibration signals were used in time domain including peak and RMS features. These features are a useful tool and widely used in condition monitoring by referring to the signal energy content. Figure 6-7 depicts the analysis of vibration signal for a centrifugal pump using the above statistical values. In order to detect the inception and development of cavitation conditions. Various types of operational conditions of flow rates, such as at low flow rate from 100 to 250(l/min), design flow rate at 300(l/min) and high flow rate from 320 to 378(l/min) have to be conducted whilst the pump rotational speed is kept constant at 2755rpm. It can be seen that from these figures there is a small indication of the variance in vibration level at flow rates below 350(l/min). However, at a flow rate above 350(l/min), the vibration level witnesses a significant increase. The results showed that the same trend occurs for all the statistical features corresponding to the vibration signals under the different flow rates. The trend of all these statistical parameters rapidly increase when the centrifugal pump operates over flow rate of 350(l/min). One of the main reasons for this is because of the occurrence of cavitation at this particular flow rate. Also, pressure fluctuations reaching to the highest peak inside the pump this occur close to tongue region. It can be noticed that for a flow rate between 100 to 300 (l/min), the RMS value is lower than that of the peak values. This is due to the flow instabilities within the pump under high flow rates. It can also be noticed that the rapidly increase was earlier for the peak feature as compared to the RMS feature. The results depict that using peak and RMS features in time domain have the capability to predict cavitation in the pump. On this basis and from the above findings, it can be concluded that cavitation was the central problem behind the increase in the level of vibration. Hence, the vibration signal analysis in the time domain can be considered as an indication to first determine the pump's condition, in addition to when cavitation was occurred in the pump. Furthermore, the peak feature value was more sensitive as compared to RMS feature for detecting occurrence of cavitation.

Different statistical parameters to monitor the trend of vibration amplitude, such as peak-to-peak and variance values, can be used to predict cavitation as can be seen in the next section.

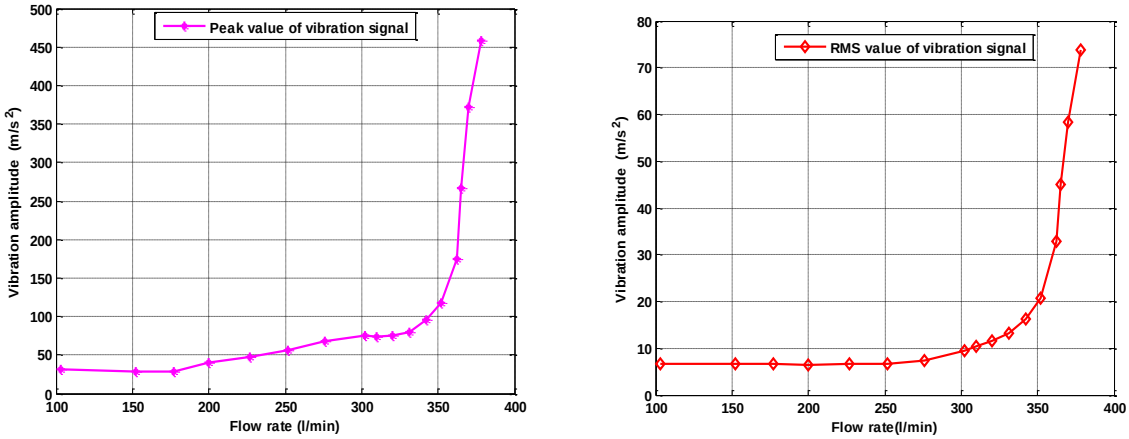

(a) Peak (b) RMS

Figure 6-7: Trend of (a) Peak and (b) RMS values of the vibration signal within the centrifugal pump at N=2755rpm

6.3.7. Analysis of the Peak-to-Peak and Variance Values Based on Time Domain

The relationship between the vibration level and various flow rates within a centrifugal pump can provide more information regarding the cavitation through the use of other different types of statistical features. For further analysis, the vibration signals in time domain in Figure 6-8 depicts the peak-to-peak and variance features, under various flow rates, as summarised in Table 6-1, at N=2755rpm. It can clearly be seen that the values of peak-to-peak and variance have approximately the same trend as compared to trends of peak and RMS values as shown in Figure 6-7 above. It can be observed that there is no significant change in peak-to-peak and variance values when the centrifugal pump operates under low flow rate from 100 to 300(l/min). Also, as seen at a flow rate beyond 350(l/min), the vibration amplitudes witnessed a rapid increase as shown in these figures. For comparison between different flow rates, the level of vibration amplitude was rapidly changed with the increase of the flow rate value, particularly in the flow rate from 350 to 378(l/min). When the pump operates at low flow rate, no cavitation occurred. Whereas, at high flow rate, inception of cavitation then begins to occur at the pump and as the flow rate increases continuously, cavitation also increases, leading to the pump working under a fully developed of cavitation. In other words, it can be seen that when the NPSHA is smaller than the NPSHR, that leads to cavitation occurrence as shown in Figure 6-4. It can also be observed that the peak-to-peak value increases rapidly when compared to the variance value. From the above findings, it can be concluded that the peak-to-peak value was more sensitive as compared with variance value. Also, the result shows that the

use of statistical features such as peak-to-peak and variance values in order to analyse the vibration data in time domain acquired from experimental measurements, can be a suitable technique to identify the inception and development of cavitation in the pump under different operational conditions.

Furthermore, the analysis of variation in the levels of vibration amplitude, within a centrifugal pump under different experimental measurements of flow rate in time domain agreed with characteristics of cavitation that was presented using the NPSH curve.

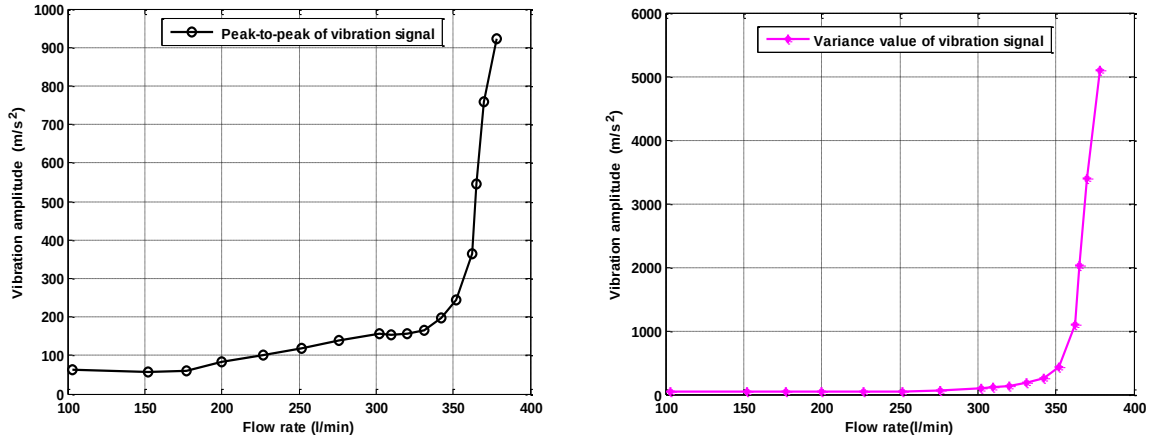

(a) Peak-to-peak (b) Variance

Figure 6-8: Trend of (a) Peak-to-peak and (b) Variance values of the vibration signal in the pump at N=2755rpm

More investigations and understandings to predict and diagnose the inception and development of cavitation in the centrifugal pump are required. These features can be found through transforming and analysing vibration signals in the frequency domain by using FFT technique. The details of analysis of vibration data in frequency domain, under different range of flow rates and frequency ranges are presented and discussed in the next section.

6.3.8. The Analysis of Vibration Signals Based on Frequency Domain under Various Flow Rates

The cavitation in the pump can be identified by finding the variation in vibration signal amplitudes in frequency domain as discussed in detail in the next section.

6.3.9. The Analysis of Baseline Frequency in the Centrifugal Pump

Figure 6-9 depicts the frequency of the vibration signals for the centrifugal pump under design flow rate of 300(l/min) and based on the range of frequency from 0Hz to 1kHz and N=2755rpm. It can be seen that the frequency range between 0Hz to 1kHz and the characteristics of the frequencies that occurred in the pump are due mostly to the periodicity in the flow within the pump. Due to the interaction between impeller blades and flow being pumped and high interaction between the impeller blades with stationary parts (e.g. the volute tongue region) as mentioned earlier. It can be observed that two main dominated frequencies were generated. Both ranges of dominated frequency are associated with the shaft rotating frequency (Rf), the blade passing frequency (BPF) and their harmonics. Also, the first rotational frequency under design flow rate has occurred at 45.91Hz and its second, third and fourth harmonics have occurred at 91.8, 137.7, and 183.6Hz respectively. In addition, the first blades passing frequency is taking place at 229.58Hz, and its second harmonic has occurred at 459.16Hz. It can be noticed that there are some additional frequencies and these frequencies are generated due different sources, such as the driving motor and the cooling fan that was used in order to cool the pump motor.

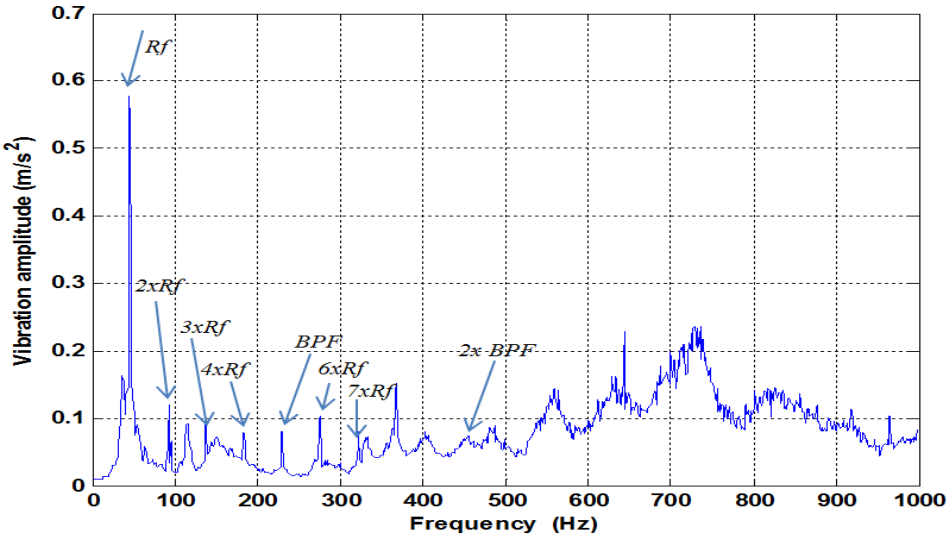

Figure 6-9: Baseline frequency of vibration signal range from 0Hz to 1kHz at design flow rate at N=2755rpm

Many researchers into pump applications have used high vibration frequency at a range higher than 20kHz to predict and diagnose any faults and failures [78, 79, 86, 90]. In this current study, an attempt was carried out to use and analyse low frequency range, less than 20kHz, for detecting cavitation. The important reason behind using the latter technique is to decrease the

cost of the accelerometer. The details of using this method in frequency domain under different flow rates, are presented in the next section.

6.3.10. The Analysis of Vibration Signals Based on Frequency Domain under Various Flow Rates and Frequency Ranges

To further investigation, frequency domain analysis was carried out in studying the effect of the different of the flow rates on the vibration amplitude. For this purpose, in the next section a three-dimensional figure was used. This figure allows comparison of more than one vibration amplitude signal in frequency domain allowing it to be illustrated how the vibration amplitude changes within the centrifugal pump under various operational conditions. For this purpose, in order to study the effect and sensitivity of using different frequency ranges and also to analyse and detect the inception and development of cavitation by using vibration signal in frequency domain. The frequency range is divided into four main parts to obtain an apparent conception concerning the dominant frequencies in the pump: The first part deals with a low range of frequency starting from 0Hz to 1kHz. The second part deals with the range of frequency starting from 1kHz to 2kHz, the third part starting from 2kHz to 10kHz and final part from 10kHz to 15kHz as illustrated in the next section.

6.3.11. Prediction of Cavitation within a Pump at Frequency Range from 0Hz to 2kHz

Figure 6-10 depicts the three-dimensional figure of vibration signals in the frequency domain based on the different range of frequencies. The first one is at low range frequency (a) from 0Hz to 1kHz and the second one (b) is at range of frequency between 1kHz and 2kHz under various flow rates and N= 2755rpm. It can be seen from both figures, there are small variances in the level of vibration amplitude in the pump when it is operating less than 300(l/min). However, it can be observed that there is a significant increased in the level of vibration amplitude when the pump is operated under flow rate higher than 350(l/min) for both range of frequencies from (0Hz-1kHz) to (1kHz-2kHz). One important reason is due to the occurrence of cavitation. Also it is observing that under flow rate higher than 350(l/min), the development of cavitation has already occurred. The dominated frequencies for both frequency ranges are associated with the shaft rotating frequency, BPF and their harmonics.

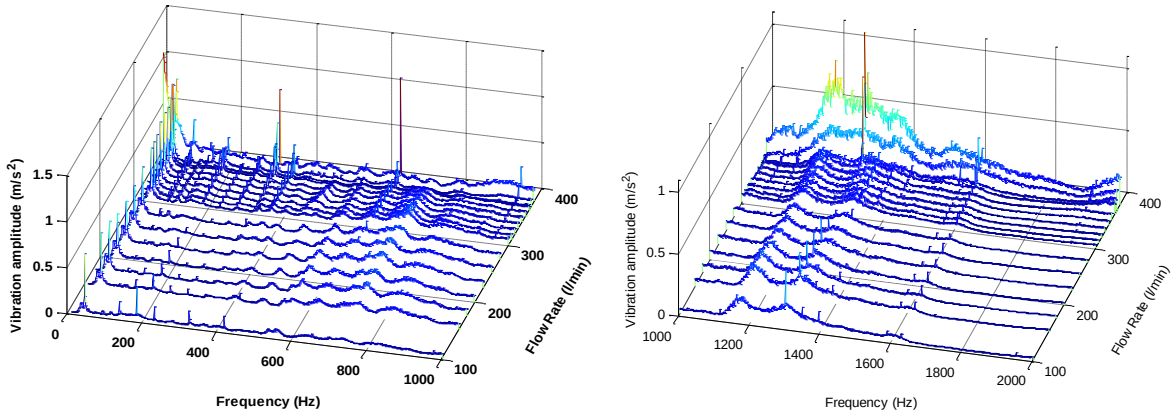

(a) (b)

Figure 6-10: Vibration signal in frequency domain under various flow rates and the frequency range from (a) 0Hz-1kHz to (b) 1kHz-2kHz at 2755rpm

6.3.12. Prediction of Cavitation within a Pump at Frequency Range from 2Hz to 15kHz

Figure 6-11 depicts the three-dimension vibration signal in frequency domain and the frequency ranges are from (a) 2Hz to10kHz and (b) 10kHz to 15kHz, under various flow rates and the N=2755rpm. It can be seen that these range of frequencies have the same trends as compared to previous figures for level of vibration amplitude. However, the vibration amplitude increases when the flow rate increases. It is also observing that the vibration amplitudes under high flow rates have much higher intensities as compared to the low flow rate due to the inception of cavitation at the flow rate lower than 350(l/min). After the inception of cavitation has occurred, variations in the level of vibration amplitude increase as flow rate increases. When the cavitation increases continuously, it means the pump is operating under conditions that the cavitation was developed fully, leading to the level of increased amplitudes in the vibration signal, particularly under higher flow rates. It can be observed that high-frequency range was more sensitive for detecting cavitation, particularly at high flow rate, as compared to low-frequency range.

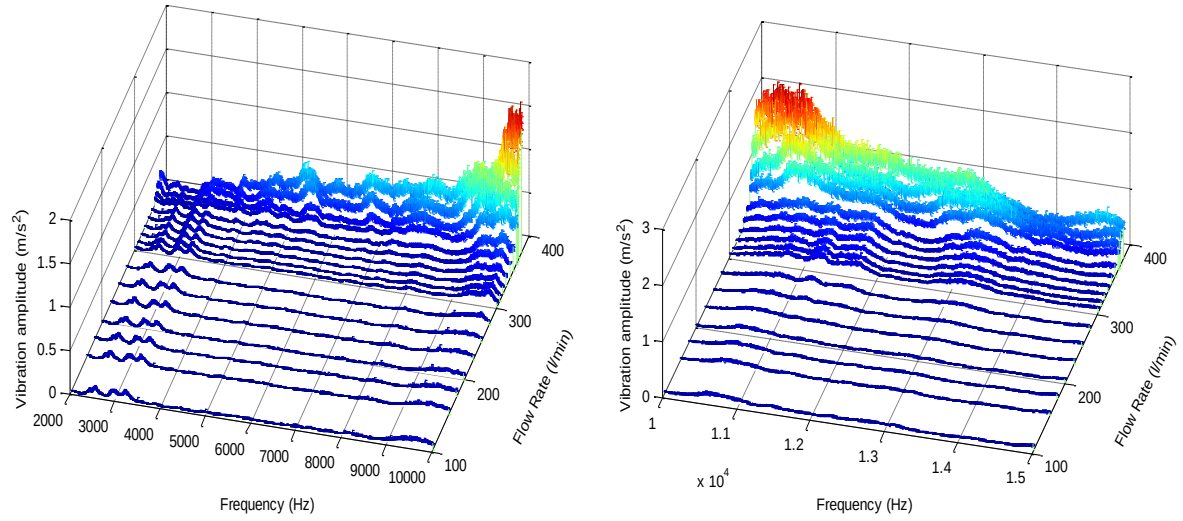

(a) (b)

Figure 6-11: Vibration signal in frequency domain under various flow rates and the frequency range from (a) 2Hz-10kHz to (b) 10kHz-15kHz at 2755rpm

From the above findings, it can be concluded that when the flow rate increases, the vibration amplitude also increases. This has led to the provision of a good indication as to when cavitation occurs within the pump.

It can be seen that from above figures, the range of frequency 10kHz-15Hz was more sensitive to detect cavitation within a pump as compared to the other range of frequencies. However, it can be observed that the range of frequency 1kHz-2Hz was also sensitive to detect cavitation. The results showed that the vibration, within a centrifugal pump, are due to the occurrence of cavitation that characteristically causes increase in the level of vibration amplitude, which can be noticed under the different range of frequencies between 0 to 15kHz.

6.3.13. Analysis of the Vibration Amplitude in Frequency Domain using Different Statistical Features

As shown in the previous section, 3-D figures are used in order to analyse the level of vibration amplitude based on different range of frequencies. It can provide more knowledge regarding the inception and development of cavitation in the pump. However, during this experimental work, analysis of the vibration signal based on the frequency domain also helps to detect cavitation within a pump. Moreover, comparing the vibration amplitude under various operation conditions helps to match the variations in the level of vibration amplitude with the different characteristics of cavitation of the pump. This section includes analyses of the vibration amplitude signal in frequency domain, by using different statistical features such as

mean and RMS vibration amplitude. For comparison purposes in this study, the vibration under different range of frequencies will be analysed during the investigation in order to find the sensitive range of frequency to detect cavitation.

6.3.14. Analysis of the Vibration Amplitude in Frequency Domain using Mean Vibration Amplitude Feature

Figure 6-12 depicts the analysis of vibration signal using mean vibration amplitude value for various range of frequencies namely (0Hz–1kHz), (1kHz–2kHz), (2kHz–10kHz), and (10kHz–15kHz) respectively, under operational conditions, including flow rate as summarised in Table 6-1, and N= 2755rpm. The same trend can be seen in the vibration amplitude under both low and high range of frequencies. The minimum vibration amplitude occurs at low flow rate less than the design flow rate 300(l/min). No significant change in the level of vibration amplitude at this operation occurs. However, the results showed that a rapid increase in the level of vibration amplitude for the high flow rate which is higher than design flow rate that is in excess of 350(l/min). This increase occurred due to the fact that NPSHR was higher when compared to the NPSHA. These results show a good agreement with the results obtained from the previous section. It can therefore be concluded that the level of vibration amplitude provides a good indication to predict and diagnose cavitation in the pump.

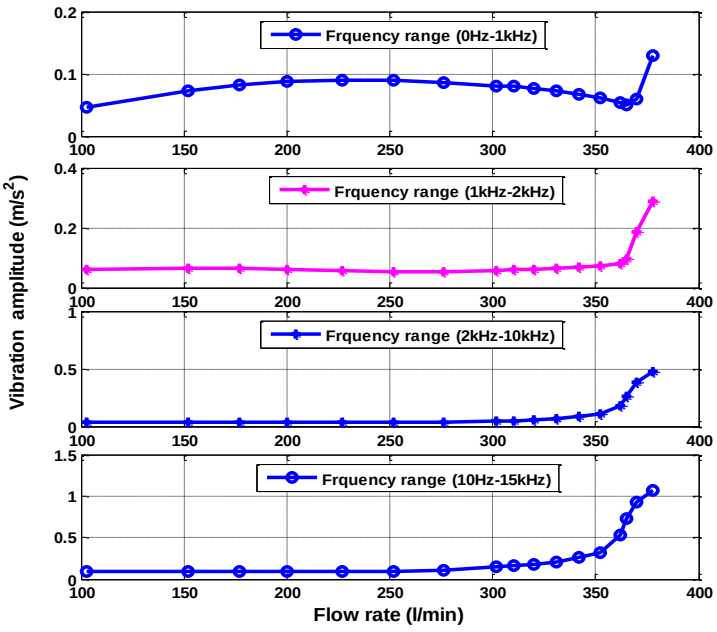

Figure 6-12: Mean vibration amplitude value of the frequency range from 0Hz to 15kHz at 2755rpm

6.3.15. Analysis of the Vibration amplitude in Frequency using RMS Vibration Amplitude Features

For further analysis of the vibration signal in frequency domain, Figure 6-13 depicts the analysis of vibration signal using RMS vibration amplitude feature for different range of frequencies, namely (0Hz–1kHz), (1kHz–2kHz), (2kHz–10kHz), and (10kHz–15kHz), under operational conditions, including different flow rates and N=2755rpm. It can be clearly seen that the RMS value has the same trend as the mean vibration amplitude feature, but different values of the vibration amplitudes. It can be seen that there is no significant change in the vibration amplitude between 100 and 300(l/min) but the vibration amplitudes are rapidly increased at the high flow rate higher than 350(l/min). This means at this point, the pump operated under cavitation conditions due to NPSHR is higher than NPSHA.

The analysis of variation in levels of vibration amplitude within a centrifugal pump in frequency domain, under different flow rate and of frequency ranges using mean and RMS features, were in agreement with characteristics of cavitation that was presented using NPSH curve.

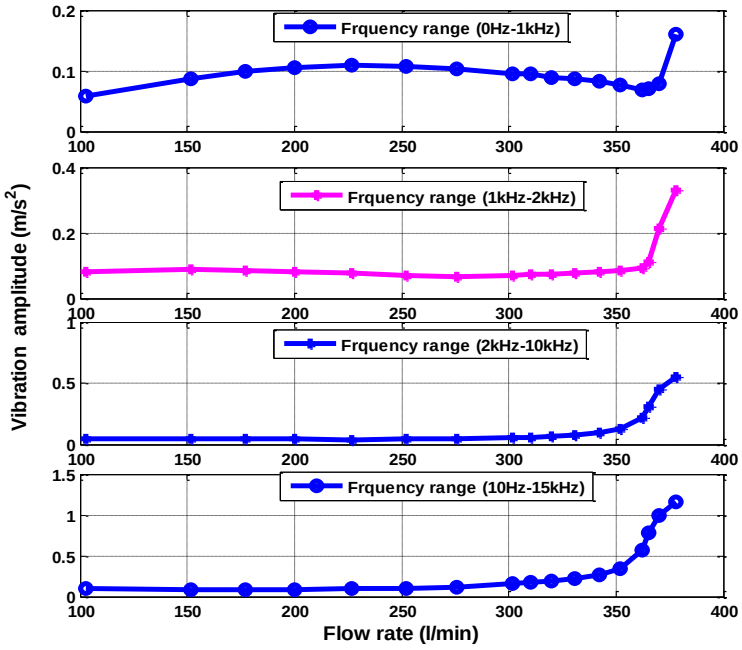

Figure 6-13: RMS vibration amplitude value of the frequency range from 0Hz to15kHz at 2755rpm

During the experimental investigation in this study, it was observed that the low range of frequency between 1Hz to 2kHz is sensitive to predict cavitation. From above result it can be concluded that the analysis of vibration signals based on different ranges of frequencies from

0Hz to 15kHz are effective in order to predict cavitation, particularly within the range of broadband frequency between 1 and 2kHz. As a result, an accelerometer with low range of frequency can provide a good indication to predict and diagnose cavitation in the pump, which leads to a decrease in the cost of sensor, as compared to using an accelerometer with high range of frequency.

After the investigation and discussion, the performance and prediction of cavitation within a centrifugal pump under various flow rates. The details of the influences of different pump rotational speeds on the performance and prediction of cavitation, through the use of vibration technique in time and frequency domains are analysed in the following sections.

6.4. Effect of Various Pump Rotational Speeds to Predict Cavitation in a Pump using Vibration Technique

As mentioned and clearly observed in the previous chapter, the pump performance depended directly on the different operating conditions. Therefore, the flow pattern behaviour such as pressure, velocity, occurrence of cavitation and instabilities in the flow field within a centrifugal pump, can be changed at various operational conditions.

Further analysis on the vibration signal for this research would be presented in order to predict cavitation. The effect of various pump rotational speeds 2610, 2320, and 2030rpm, corresponding to 0.9Nd, 0.8Nd, and 0.7Nd where Nd denotes the design rotational speed and is equal to 2900rpm were selected for analysis purposes. The pump rotational speed was precisely controlled by using the electronic inverter in the control panel. The range of pump capacity (flow rate) was changed depending on the rotational speed. The following sections represent the results obtained from the experimental calculation of the pump under different pump rotational speeds.

6.4.1. Centrifugal Pump Head at Different Rotational Speeds

Figure 6-14 depicts the head of the pump under different pump rotational speeds. It can be observed that the head in the pump follows a continuous downward trend with increasing flow rate at various rotational speeds under investigations. Also, it can be seen that the head under N=2755rpm is considerably higher than for the other three cases N=2610rpm, N=2320rpm, and N=2030rpm. The results showed that the pump starts to operate under cavitation conditions at a flow rate higher than the design flow rate and then increases at a flow rate higher than

350(l/min). This means that when a pump operates at the high flow rate, it leads to a decrease in the inlet suction pressure faster than at low flow rate. Hence, cavitation will occur quicker. From the above findings, it can be concluded that the head of the pump increases as the pump rotational speed also increases. The pump rotational speeds are proportional to cavitation occurrence within the pump. This means when rotational speeds increase, occurrence of cavitation also increases due to the decreased pressure at the inlet eye of impeller which goes lower than the vapour pressure.

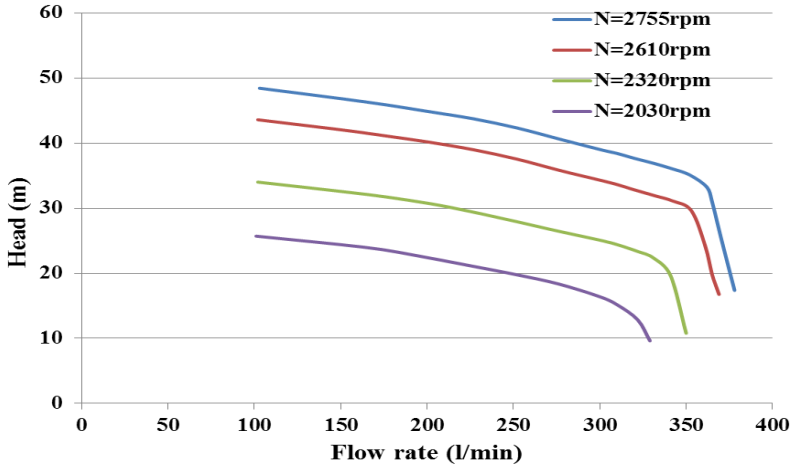

Figure 6-14: Comparison between head of the pump under different rotational speeds

6.4.2. Analysis of the Vibration Signal in Time Domain at Different Rotational Speeds

In this section, the vibration signals were analysed in time domain using the different statistical features as in the previous case (N=2755rpm). In order to obtain more information regarding change in the vibration amplitude under the different flow rates and different pump rotational speed to predict the cavitation within a pump.

6.4.3. Analysis of the Vibration Signal using Various Statistical Features

Based on time domain analysis, Figure 6-15 depicts the statistical features such as peak, RMS, peak-to-peak and variance values under different pump rotational speeds. It can be seen that the maximum peak feature for N=2755rpm is considerably higher than for the other three cases. For instance, for N=2610 rpm, it is higher by 13.38%, for N=2320rpm by 15.48%, and N=2030rpm by 36.60%. The maximum RMS value for N=2755rpm is higher than the remaining three cases already listed by 11.72%, 29.98%, and 52.53%. The highest peak-to-peak for N=2755 rpm is higher than for the other cases by 13.025%, 13.45%, and 33.24% and also the maximum variance value by 16.66%, 42.19%, and 75.93% respectively as given in

Table 6-2. From the above findings, it can be concluded that the pump rotational speeds are proportional to the increase in the vibration amplitude. This means that when the pump rotational speed increases, the vibration amplitude also increases due to the cavitation occurrence within a pump. When vapour bubbles form due to cavitation for a long period of time, these bubbles collapse that causes drop in performance of the pump and also damages some parts of the pump due to erosion on the surfaces of the pump.

Table 6-2 Summary of the maximum statistical features of the vibration amplitude in time domain under different rotational speeds

Rotational speed (rpm)	Peak (m/s^2)	RMS (m/s^2)	peak-to-peak (m/s^2)	variance (m/s^2)
2755	457.66	73.82	921.14	5099.6
2610	396.38	65.17	801.16	4249.5
2320	386.80	54.28	797.22	2947.6
2030	294.71	35.04	614.86	1227.0

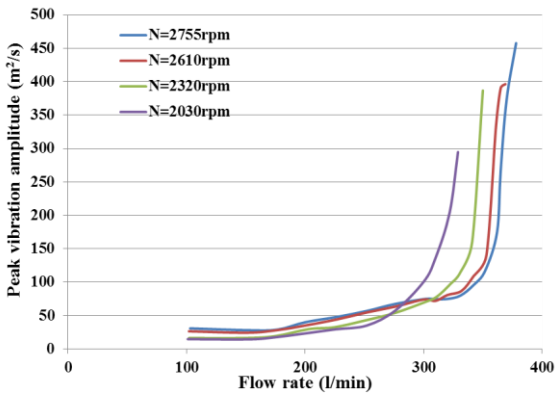

(a) Peak

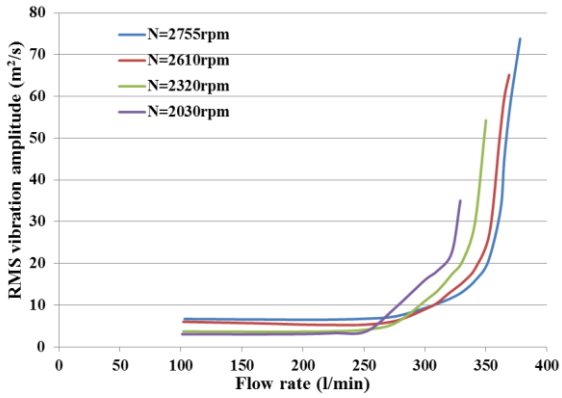

(b) RMS

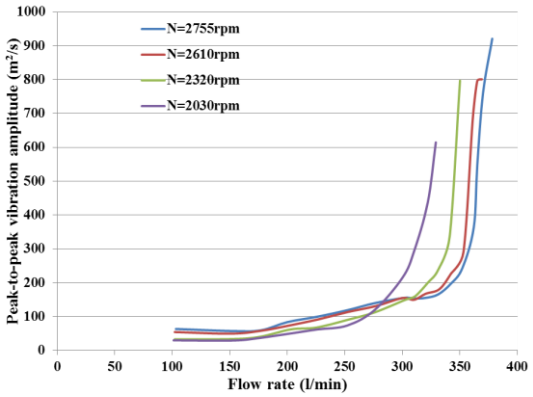

(c) Peak-to-peak

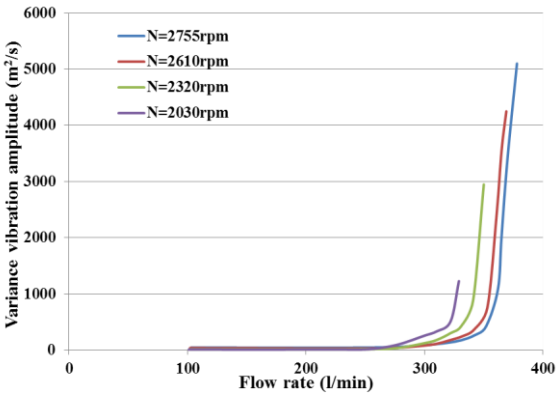

(d) Variance

Figure 6-15: Comparison between different statistical features of the vibration asignal in time domain under different rotational speeds

6.4.4. Analysis of the Vibration Signal in Frequency Domain at Different Pump Rotational Speeds

Figure 6-16 depicts the vibration signal in frequency domain, the frequency ranges are from (a) 0Hz to 1kHz and (b) 1kHz to 2kHz under different rotational speeds of 2610, 2320, and 2030rpm. It can be clearly observed that the vibration peak amplitude occurred, as expected, at two dominated distinctive frequencies for both frequency ranges. The first one is the rotational frequency and the second one is the blade passing frequency, and their harmonics. These harmonics increase with an increase in flow rates. Furthermore, these frequencies show clearer variances between them at various flow rates, with the same continuous pattern for frequency range between 0Hz and 1kHz. Therefore, in this study, focus is on using the low range of frequencies for detecting the occurrence of cavitation within a pump. It is also worth mentioning that the amplitude of vibration signal in frequency domain shows an apparent change in the level of vibration amplitudes when the pump operates at high rotational speed.

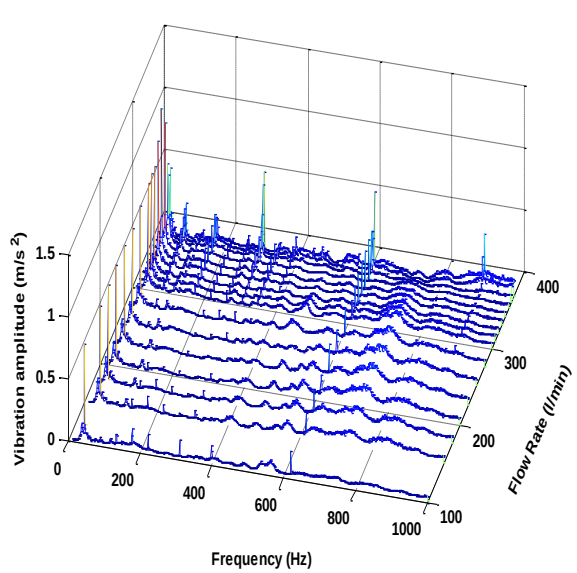

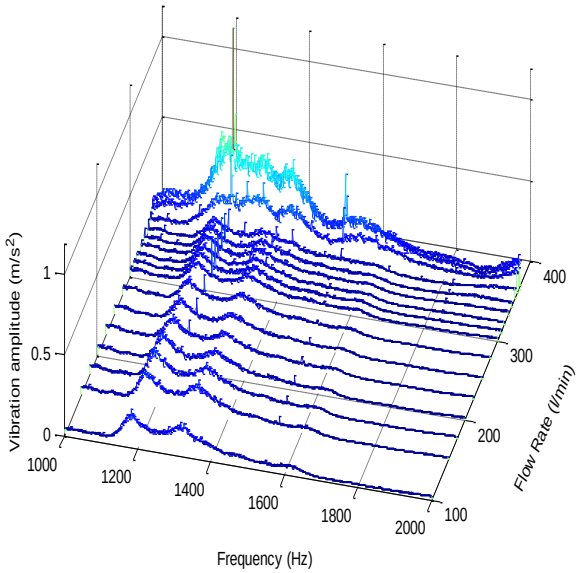

(a) N=2610rpm (b)

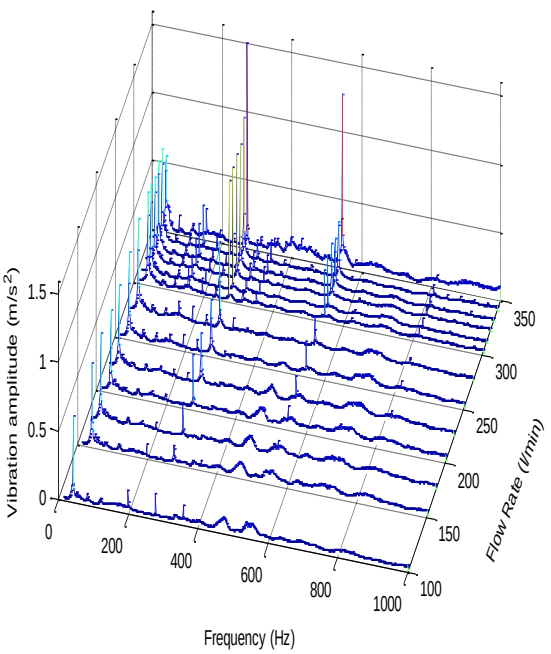

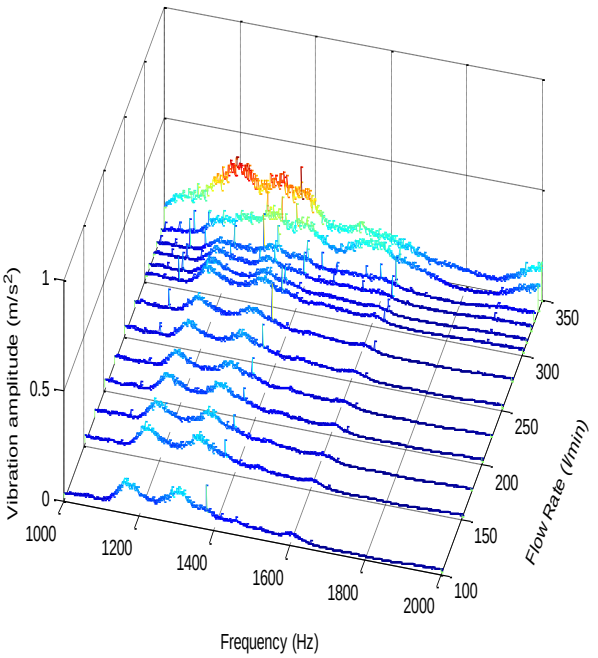

(a) N=2320rpm (b)

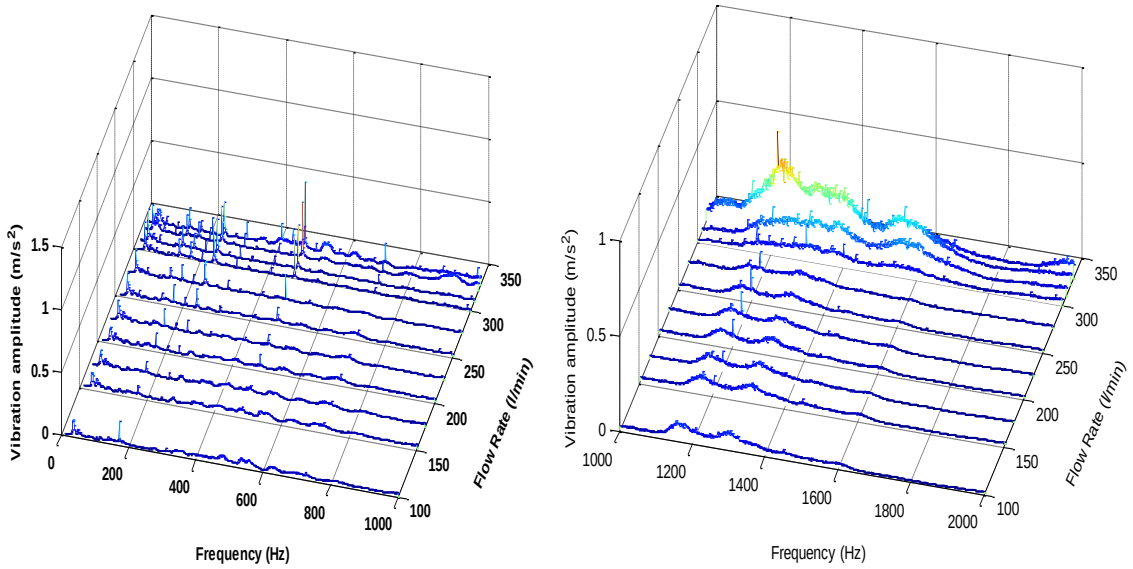

(a) N=2030rpm (b)

Figure 6-16: Vibration signal in frequency domain under different rotational speeds and the frequency range from (a) 0Hz-1kHz to (b) 1kHz-2kHz

For comparison purposes between the above cases, based on frequency domain, Figure 6-17 depicts the mean vibration amplitude values of the aforementioned cases under different pump rotational speeds and for the different range of frequencies which include 0Hz-1kHz, 1kHz-2kHz, 2kHz-10kHz, and 10kHz-15kHz. It can be clearly seen that the maximum mean feature under N=2755rpm is considerably higher than for the other three cases. Furthermore, the results from the frequency domain analysis demonstrated that the mean vibration amplitude value for various ranges of frequencies can be used to predict different levels of cavitation within a pump, especially at low range frequencies from 1Hz to 2kHz. However, it can be clearly seen that high ranges of frequency are sensitive to predict cavitation as compared to the low range of frequency as shown in these figures.

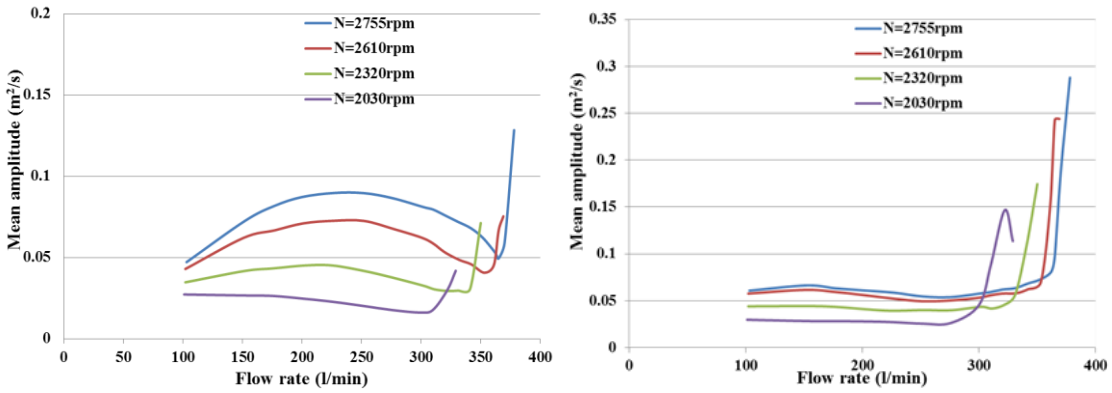

(a) 0Hz-1kHz (b) 1kHz-2kHz

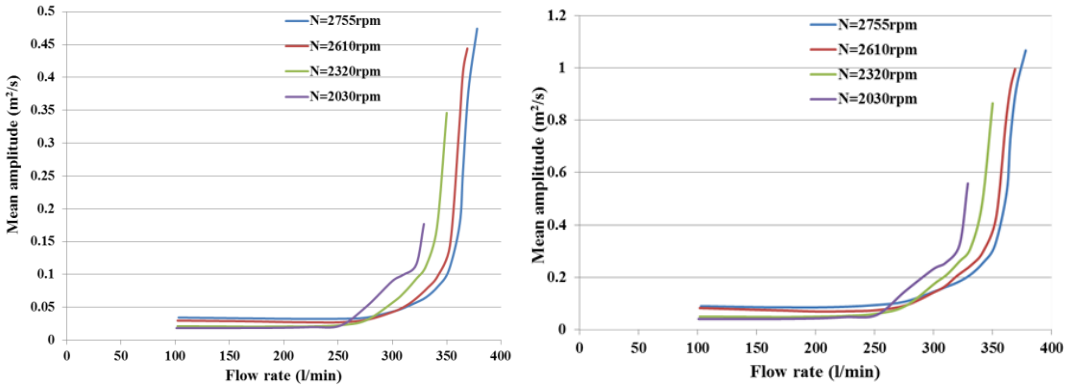

(c) 2kHz-10kHz (d) 10kHz-15kHz

Figure 6-17: Comparison between mean vibration amplitude in frequency domain for different rotational speeds and frequency ranges

In regard to the changes in vibration amplitude of the mean value for the centrifugal pump under different pump rotational speeds and various range of frequencies, including 0Hz-1kHz, 1kHz-2kHz, 2kHz-10kHz, and 10kHz-15kHz. Table 6-3 provides more detailed comparison between all of the above cases under investigation. The values for the mean feature for N=2755rpm, for different range of frequencies, are considerably higher than for all three cases (N=2610, N=2320, and N=2030rpm) as summarised in this table. It can be seen that the analysis of the vibration signals in frequency domain, using mean amplitude features, under different pump rotational speed shows that when the rotational speed increases, vibration amplitude also increases due to increases in the occurrence of cavitation within a pump under the different frequency ranges.

Table 6-3 Comparison between mean vibration amplitude values in frequency domain, under different rotational speeds at 0kHz-15kHz

Rotational speed	Mean value 0Hz-1kHz	Mean value 1kHz-2kHz	Mean value 2kHz-10kHz	Mean value 10kHz-15kHz
(rpm)	(m/s^2)	(m/s^2)	(m/s^2)	(m/s^2)
2755	0.128	0.288	0.474	1.066
2610	0.075	0.243	0.444	0.995
2320	0.071	0.174	0.345	0.864
2030	0.041	0.113	0.176	0.558

For comparison purposes between the above cases based on frequency domain analysis, Figure 6-18 depicts the RMS feature for the aforementioned cases under different rotational speeds and for the different range of frequencies which include 0Hz-1kHz, 1kHz-2kHz, 2kHz-10kHz, and 10kHz-15kHz. It can be clearly seen that the maximum RMS feature for N=2755rpm is considerably higher than for the other three cases. Also, the results from frequency domain

analysis have demonstrated that RMS vibration amplitude values for various range of frequencies can be used to predict cavitation within a centrifugal pump, especially at the low range frequency between 1kHz and 2kHz.

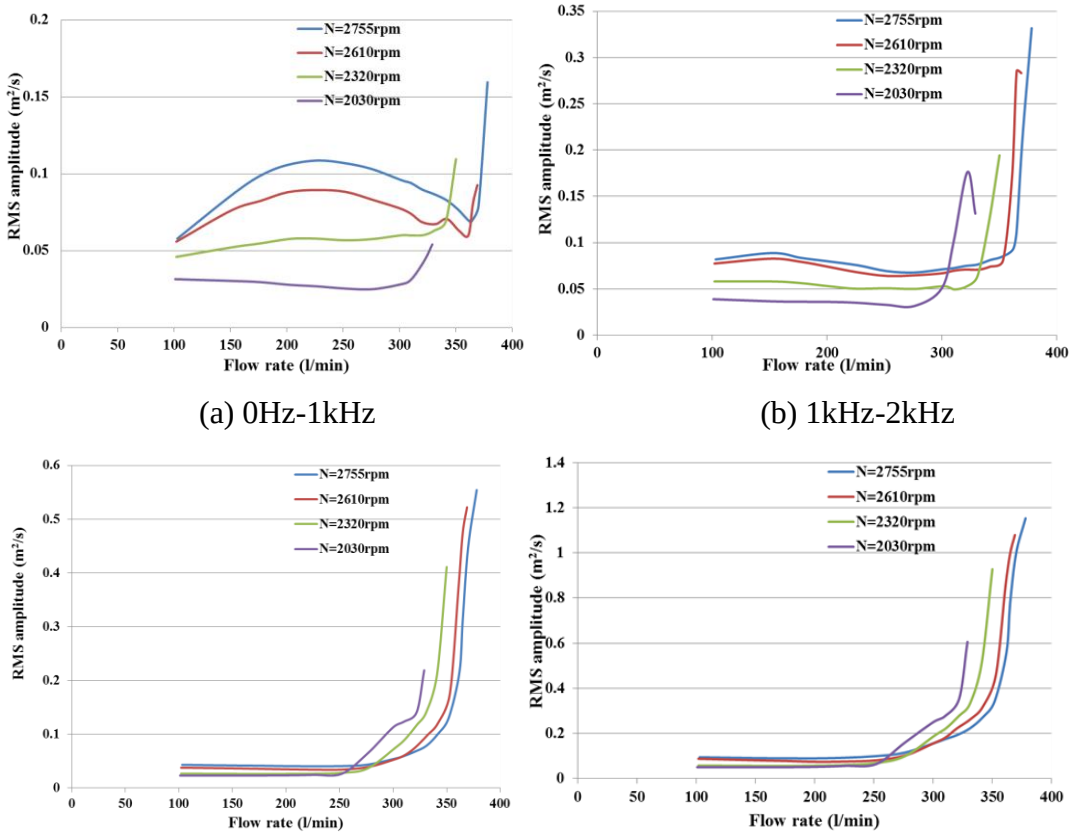

(a) 0Hz-1kHz (b) 1kHz-2kHz

(c) 2kHz-10kHz (d) 10kHz-15kHz

Figure 6-18: Comparison between RMS vibration amplitude values in frequency domain for different rotational speeds aqnd frequency ranges

In regard to the changes in vibration amplitude and trends of the RMS value for the centrifugal pump under different rotational speeds and for various range of frequencies, Table 6-4 provides the comparison between all the above cases under investigation. The values of RMS features for N=2755rpm for different range of frequencies are considerably higher than for all three case (N=2610, N=2320, and N=2030rpm) as summarised in this table.

Table 6-4 Comparison between RMS vibration amplitude values in frequency domain under different rotational speeds at 0kHz-15kHz

Rotational speed	RMS value 0Hz-1kHz	RMS value 1kHz-2kHz	RMS value 2kHz-10kHz	RMS value 10kHz-15kHz
(rpm)	(m/s^2)	(m/s^2)	(m/s^2)	(m/s^2)
2755	0.1595	0.3318	0.5543	1.153
2610	0.1095	0.2855	0.5221	1.0789
2320	0.0926	0.1944	0.4111	0.9276

2030	0.0540	0.1762	0.2189	0.6055

In summary, the different level of vibration amplitudes due to various operation conditions in the pump were analysed. Hence, the frequency at which cavitation occurs was obtained through analysis of the experimentation process. The results showed that there is a significant difference in the trend of vibration amplitude, as a function of various operational conditions, such as flow rate and pump rotational speed, as shown in both tables and figures in the previous section. These frequencies can provide good information regarding diagnosing the occurrence of cavitation within a pump. Also in this research study, the results showed that the use of vibration technique in both time and frequency domains were given a good understanding in predicting the different levels of cavitation (no cavitation, inception, development, and fully developed of cavitation) in a pump under different operational conditions.

6.5. Summary of the Analysis of Different Flow Rates and Pump Rotational Speeds using Vibration Technique

Based on above results in this section, several conclusions were drawn regarding the effect of different flow rates and pump rotational speeds on the vibration signal and performance of the centrifugal pump.

1. The head of the centrifugal pump gradually decreases when flow rate is increased due to the hydraulic and mechanical losses as well as different levels of cavitation occurrence within a pump.
2. When the pump operates under low flow rates, no cavitation occurs but at a flow rate greater than 350(l/min) cavitation occurs.
3. The level of cavitation in a pump was directly linked with the pump flow rate.
4. The vibration signal analysis in time domain using different statistical features can be considered as a first indication to determine when cavitation was occurred in the pump.
5. The peak and peak-to-peak features were the most sensitive to detect cavitation when compared to RMS and variance features.
6. The level of vibration stability of a pump is associated directly with the pump rotational speed.
7. The frequency domain analysis was a satisfactory technique to predict the inception and development of cavitation in a pump.
8. The pump has generated two main dominant frequencies the shaft rotating frequency and the BPF.

9. Usin mean and RMS vibration amplitude values to analyse the vibration signal in frequency domain, provides more information regarding the prediction of cavitation.
10. The head for N=2755rpm is considerably higher than that of the other cases.
11. The analysis of the variation in the level of vibration amplitude under different flow rate in time domain by using different statistical features and also in frequency domain under different ranges of frequencies, were in agreement with the characteristics of cavitation that was presented using the NPSH curve.
12. Based on time domain analysis the maximum statistical features values for N=2755rpm are considerably greater than for the other cases.
13. Based on frequency domain analysis, using mean and RMS feature values for different ranges of frequencies namely the maximum values for the above features for N=2755rpm is considerably higher than for the other cases.
14. It was found that from the analysis, the vibration signal using mean and RMS amplitudes features, for the different range of frequencies revealed that using low-frequency range between 1kHz and 2kHz was sensitive to predict cavitation in the pump. Therefore, it is possible to use an accelerometer that has a low range of frequency which would decrease the cost of the sensor when compared to a high range of frequency sensor.
15. Based on the above findings, the severity of cavitation can be gauged by increasing the level of vibration amplitude value. It provides a good indication regarding the occurrence of the severity of cavitation within a centrifugal pump.
16. The analysis of variation in the level of vibration amplitude in a pump, under different experimental flow rate measurements, agreed with the characteristics of cavitation that was predicted using CFD code in Chapter five.

6.6. Effect of the Suction Valve Opening on the Level of Vibration to Predict Cavitation within a Centrifugal Pump

As clearly observed in the previous sections, the pump performance and occurrence of cavitation directly depends on the different operating conditions. In order to cover a wide range of operation conditions for detecting cavitation in this section, investigations on the effect of various suction valve openings on cavitation in the pump were carried out.

In order to analyse the various levels of cavitation at different operation conditions, the effect of the decrease in the inlet suction pressure of the centrifugal pump, by controlling the inlet suction valve opening, was investigated using this experimental setup. Hence, the vibration,

and pressure signals under different inlet valve openings and different flow rates namely 103, 200, 302(l/min were collected for this purpose. The inlet suction valve is first fully open (100%) at the beginning. Then changed through throttling the suction valve progressively, step by step for every 10% by using a protractor instrument that measures angles as shown in Figure 6-19, until cavitation occurs due to decreasing the inlet pressure at the inlet pipe by keeping the pump rotational speed constant at 2755rpm. This process is based on the collection of experimental measurements at different suction valve openings and various flow rates. The collection of the experimental data allows evaluation of different indicators connected to cavitation condition within a pump. Such indicators include the performance of the pump, the head-suction valve-opening curve and vibration generated by cavitation, which are analysed in both time and frequency domains. All of these indicators provide useful information regarding predicting cavitation in the pump with high certainty. The next section presents the results obtained from the experimental calculation under different inlet suction valve openings. Each experimental test in this study was repeated at least three times.

Figure 6-19: Protractor instrument for measuring angles at suction valve of the pump

6.6.1. Performance of the Centrifugal Pump under Different Suction Valve Openings at Flow Rate of 103(l/min)

To analyse the effect of inlet suction valve openings on the performance of the centrifugal pump under various flow rates through the use of vibration technique, it is important first to investigate and calculate the NPSH against head of the pump in relation to the different inlet valve openings, presented in the next section.

Figure 6-20 depicts the NPSH-Head curve for the pump based on some operating conditions such as flow rate of 103(l/min) and N=2755rpm. It can be seen that when the NPSH decreases from 7.5m to 6.5m, no significant change in the pump head is evident and no cavitation was occurred in this region. When the NPSH goes lower than 5.5m, the head is decreased by 3%

and inception of cavitation occurs. Furthermore, it can be seen that when the NPSH value also decreases, the pump head rapidly decreases and the development of cavitation then increases. The reason is due to the pressure at the suction line of the pump which gradually decreases when the suction valve opening decreases leading to a decrease in NPSH.

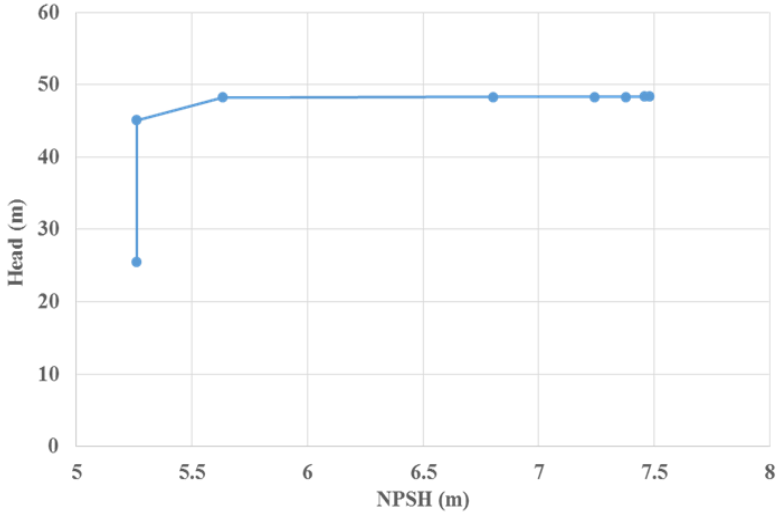

Figure 6-20: The cavitation characteristics NPSH-Head curve of the pump

The pump performance is also analysed in relation to the different inlet suction valve openings. Figure 6-21 depicts the pump head via the inlet suction valve openings curve for the pump based on operational conditions such as flow rate of 103(l/min) and N=2755rpm. The head drop curve for the pump can be seen correspond to inlet suction valve openings of 100, 90, 80, 70, 60, 50, 40, and 35%. In this figure, the head drop curve can be seen to be divided into three parts because of the decrease in the inlet suction pressure. The first part shows inlet suction valve openings between 100% and 50%. It can be further observed that there is no significant change in the head of the pump and no cavitation occurs in this region. The second part displays the development of cavitation occurring when inlet suction valve opening was at 40% due to the head drop of 7.85%. The final part illustrates full development of cavitation when the inlet suction valve opening was at 35% as the head drop was 37.66%. It can be concluded that when decreasing the inlet suction valve openings, this leads to the lowering of the inlet suction pressure and cavitation on the suction side of the pump starts occurring and developing.

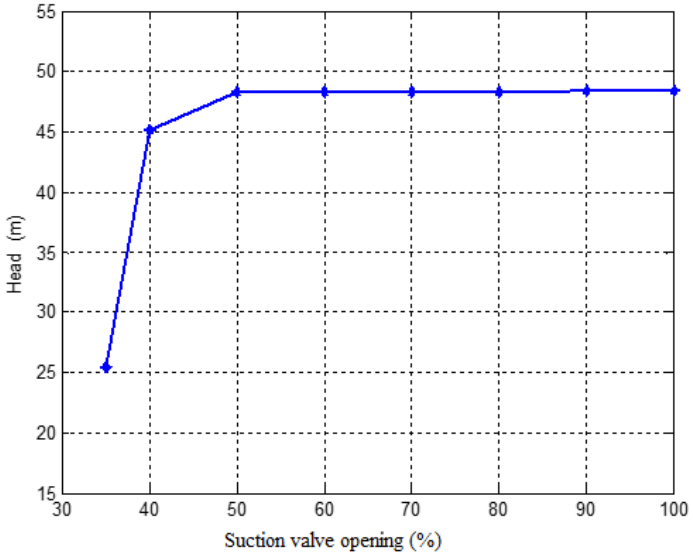

Figure 6-21: The relation between head and different suction valve openings at 103(l/min)

6.6.2. Analysis of the Level of Vibration in Time Domain under Different Suction Valve Openings at Flow Rate of 103(l/min)

The primary goal of this section is to investigate the relationship between the suction valve openings and occurrence of cavitation in the pump. For this purpose, the vibration signal was analysed in time domain using the same various statistical features as used in the previous sections. In order to obtain more detailed information regarding the change in the vibration amplitude under different inlet suction valve openings.

Figure 6-22 depicts the analysis on the vibration signal for the pump using peak, RMS, peak-to-peak and variance values at a flow rate of 103(l/min), N=2755rpm and under different inlet suction valve openings. It can be seen that all these features include three parts, the first shows no significant change in the level of vibration amplitude when the pump operates between suction valve openings 100% and 40%. The second indicates that the trends of the peak, RMS peak-to-peak and variance values rapidly increase when the pump operates between suction valve openings of 40% to 35%. The reason for this is due to the decrease in the suction pressure below the water vapour pressure, leading to cavitation starting to develop. The third part includes the maximum vibration due to when the inlet suction pressure continuously decreases under these conditions and cavitation fully develops causing deterioration in the performance of the pump.

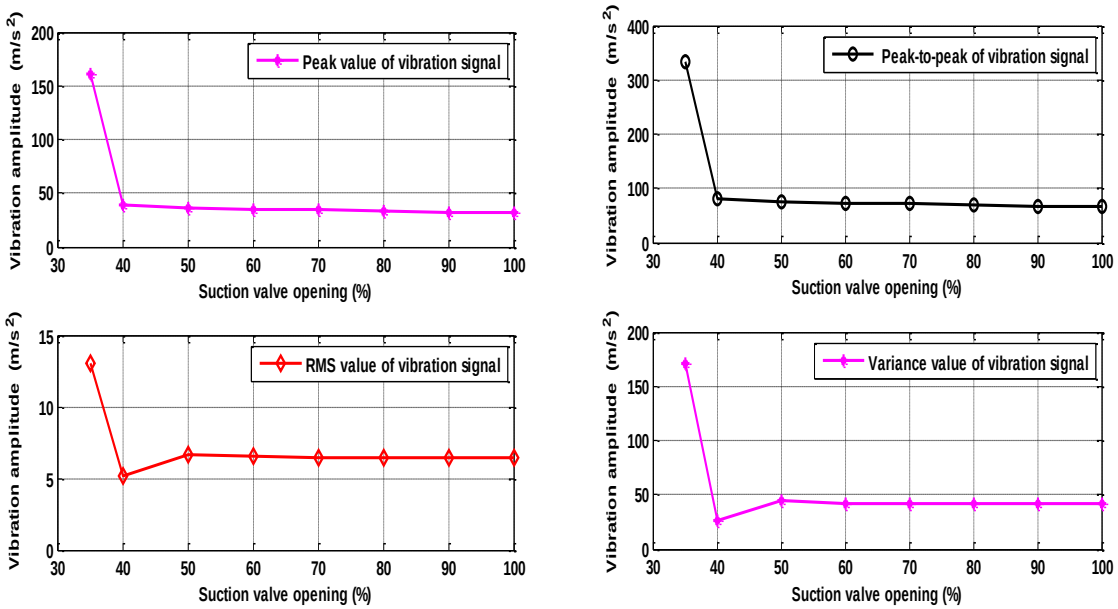

(a) Peak and RMS (b) Peak-to-peak and variance

Figure 6-22: Trends of various statistical features of the vibration signal nuder different suction valve openings at 103(l/min)

6.6.3. Analysis of the Level of Vibration in Frequency Domain under Different Suction Valve Openings at Flow Rate of 103(l/min)

Figure 6-23 depicts the vibration signal in frequency domain under various test measurements of inlet suction valve openings and the operation conditions at flow rate of 103(l/min), N=2755rpm and range of frequency of 0Hz-1kHz and 1kHz-2kHz. It can be clearly observed that the vibration peak amplitude was occurred at two dominated distinctive frequencies as expected. The first one is rotational frequency 45.9Hz and the second is BPF 229.5Hz, and their harmonics. From this figure, it can be seen there is no significant change in the level of vibration amplitude when the pump operates between suction valve openings of 100% and 50%. However, at this range of frequency, a change in the vibration amplitude can be seen when the pump operates between suction valve openings of 40% to 35%.

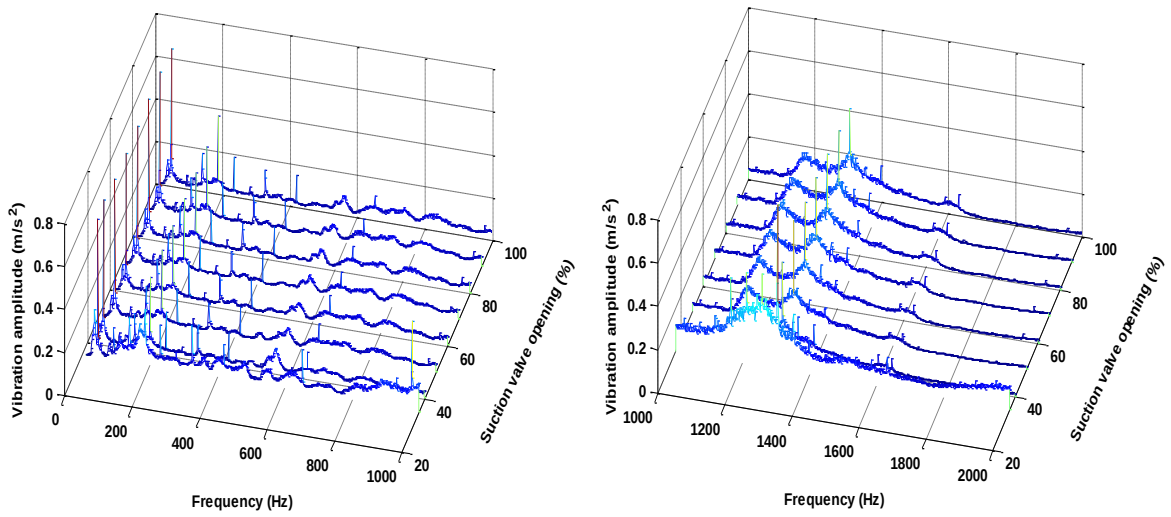

(a) 0Hz-1kHz (b) 1kHz-2kHz

Figure 6-23: Vibration signal in frequency domain under various suction valve openings and frequency ranges at 103(l/min)

From the above analysis, it can be concluded that the high peak amplitude in frequency domain for the vibration signal is clearly evident within a pump operating under cavitation conditions at suction valve openings from 40% to 35%. This is due to the random formation and collapse of the bubbles in the pump, causing unstable flow and more pressure fluctuations that lead to producing high levels of vibration in the pump. It can also be noted that analysing the level of vibration amplitude at frequency range between 0Hz and 2kHz, provides a suitable indication to predict cavitation within a pump.

For more analysis regarding vibration signal in frequency domain, Figure 6-24 and Figure 6-25 depict the mean and RMS vibration amplitude values that were calculated from the frequency domain under different inlet suction valve openings for a range of frequencies, namely 0Hz-1kHz, 1kHz-2kHz, 2kHz-10kHz, and 10kHz-15kHz respectively, with a flow rate of 103(l/min) and N=2755rpm. It can be seen that the mean and RMS vibration amplitude values for the various range of frequencies have approximately the same trend under different inlet suction valve openings. It is also worth noting here that no significant change occurs at the inlet suction valve openings between 100% and 50%. However, changes occur when the inlet suction valve opening is between 40% and 35%. This is due to the occurrence of cavitation within a pump. It can be concluded that the low frequency range from 0Hz to 2kHz can be sensitive in detecting cavitation in the pump.

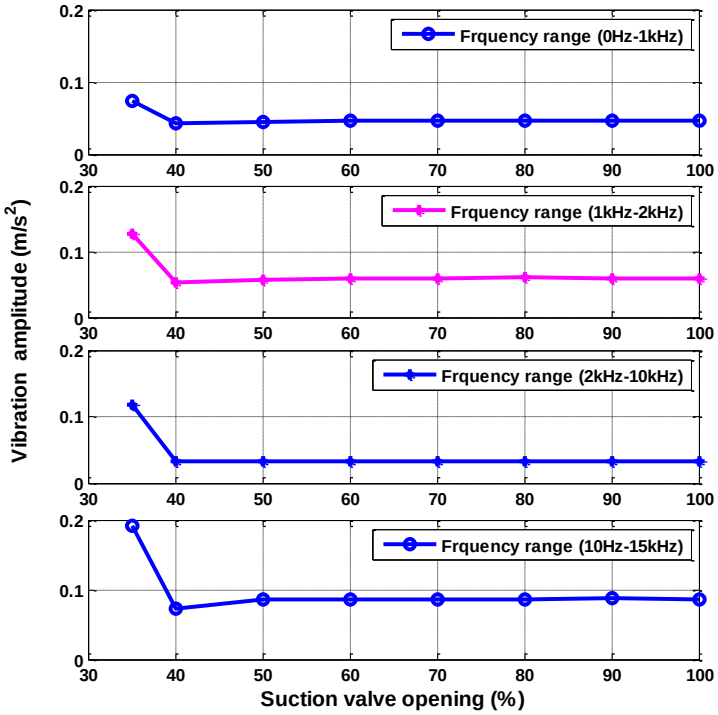

Figure 6-24: Mean vibration amplitude value of the vibration frequency range from 0Hz to 15kHz at 103(l/min)

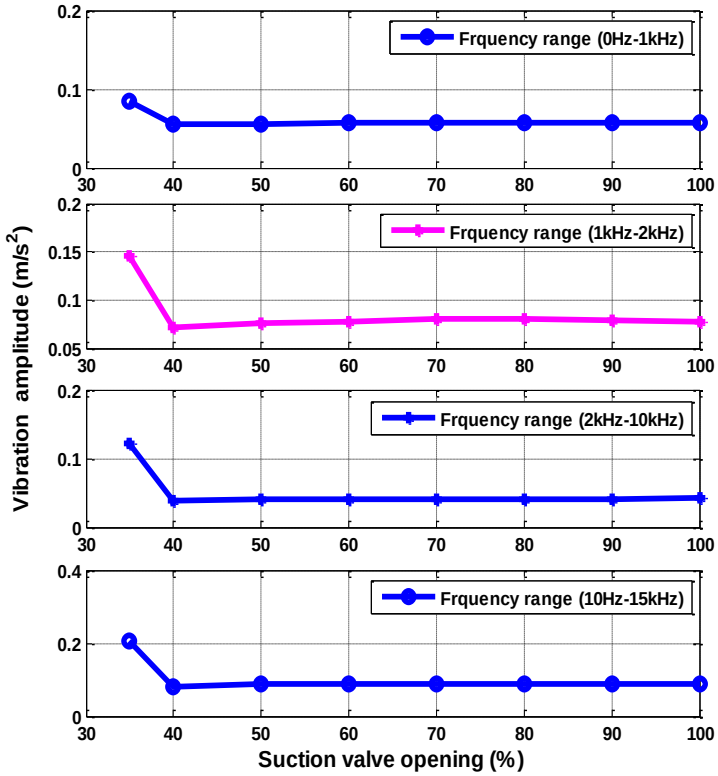

Figure 6-25: RMS vibration amplitude value of the vibration frequency range from 0Hz to 15kHz at 103(l/min)

6.6.4. Performance of the Centrifugal Pump under Different Suction Valve Openings at Different Flow Rates

For comparison purposes between the different cases (Q=100(l/min), Q=200(l/min) and Q=302(l/min)), investigating the effects of decrease in the suction valve on the performance of the centrifugal pump. Figure 6-26 depicts the head of the different cases under different inlet valve openings at the suction side of the pump. It can be clearly seen that the head for Q=100(l/min) is considerably higher than for the other two flow rates 200(l/min) and 302(l/min). The results showed that at flow rate of 100(l/min), the pump start operates under cavitation conditions when inlet suction valve opening was 40%. However, at flow rate of 200(l/min) started at 50%, and at the flow rate of 302(l/min) was at 60% respectively. That means when a pump operates at the high flow rate it leads to a decrease in the inlet suction pressure faster than at low flow rate and hence this leads to the fact that cavitation will occur quicker. From the above findings, it can be concluded that the inlet suction valve openings are inversely proportional with cavitation occurrence within the pump, meaning that when the inlet suction valve opening is decreased this leads to cavitation being increased.

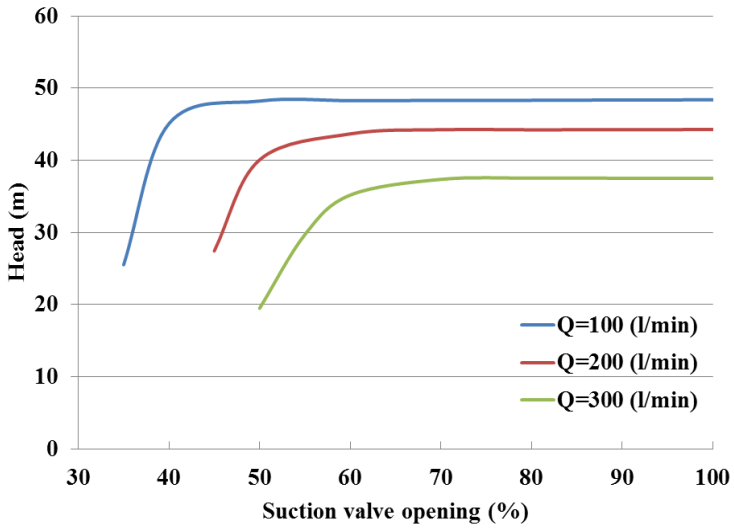

Figure 6-26: Effect of different suction valve openings on the performance of a pump

6.6.5. Analysis of the Level of Vibration in Time Domain under Different Suction Valve Openings and Flow Rates

Further comparison between the different cases (Q=100(l/min), Q=200(l/min) and Q=302(l/min)) under investigation was analysed in time domain in order to obtain more information regarding the occurrence of cavitation. Figure 6-27 depicts the statistical features such as peak, RMS, peak-to-peak and variance values of the aforementioned cases under

different flow rates and various suction valve openings. It is clearly seen that the maximum peak feature under the different suction valve openings at Q=302(l/min) is considerably higher than for the other cases Q=200(l/min) and Q=103(l/min) by 42.21%, and 43.33%. Also, the maximum RMS value by 51.83% and 59.45% is considerably higher than for the other cases. In addition, the maximum peak-to-peak value is higher than for the other cases by 40.97%, and 41.86%. Moreover, the maximum variance value is also higher than for the previous cases by 76.80%, and 83.73% respectively. The reason for this is due to the decrease in the suction valve openings, causing the occurrence of cavitation within a pump and hence this leads to an increase in the level of vibration. From above findings, it can be concluded that the suction valve openings are inversely proportional to the increase of the vibration amplitude as shown in Table 6-5 meaning when the suction valve opening is decreased this leads to increase cavitation within a centrifugal pump resulting in an increase in the vibration amplitude.

Table 6-5 Summarises the maximum statistical features of the vibration amplitude in time domain under different flow rates

Flow rate (l/min)	Peak (m/s^2)	RMS (m/s^2)	peak-to-peak (m/s^2)	variance (m/s^2)
103	173.11	13.32	365.23	177.54
200	176.53	15.90	370.83	253.22
302	305.52	33.01	628.29	1091.6

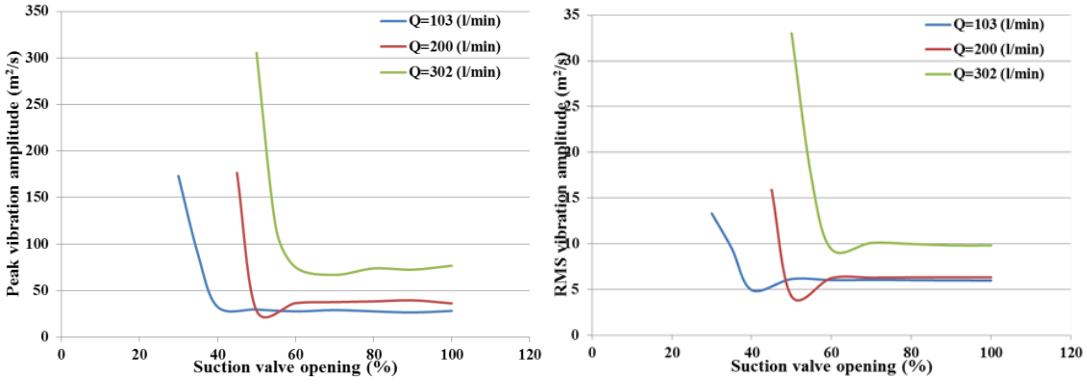

(a) Peak (b) RMS

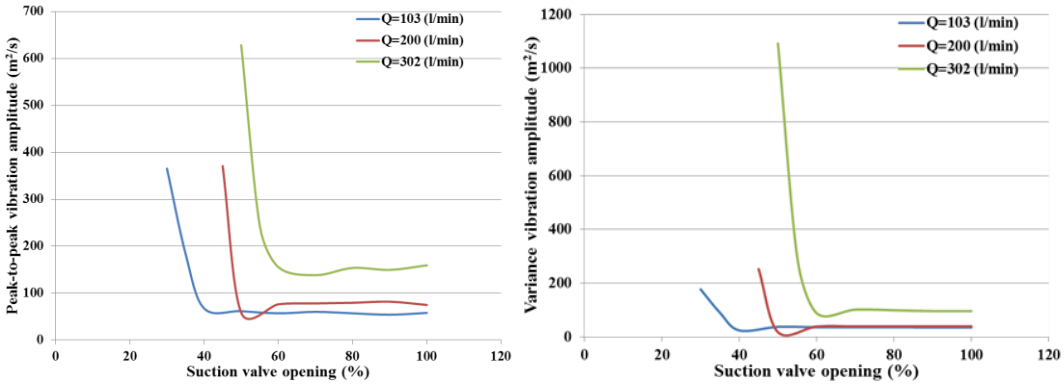

(c) Peak-to-peak (d) Variance

Figure 6-27: Comparison between different statistical features of the vibration signal in time domain under different suction valve openings and flow rates

6.6.6. Analysis of the Level of Vibration in Frequency Domain under Different Suction Valve Openings and Flow Rates

Figure 6-28 depicts the analysis on the vibration signal under different suction valve openings and flow rates (Q=200(l/min) and Q=302(l/min)), N=2755rpm, and frequency range of between (a) 0Hz-1kHz to (b) 1kHz-2kHz operational conditions. It can be seen that the first peak vibration amplitude was at frequency 45.9Hz and represents the rotation frequency. The second, third and fourth harmonics were 91.8, 137.7, and 183.6Hz respectively. The second dominate peak vibration amplitude was at frequency 229.5Hz, and is denoted as the BPF and its harmonics. It can be seen that the peak vibration amplitude is increased where cavitation exists within the pump. In addition, it can be seen for case (Q=200(l/min)) there is no change in the level of vibration amplitude under inlet suction valve openings between 100 and 60%. However, the change in vibration amplitude was relatively higher at inlet suction valve openings from 50 to 45% as compared to inlet suction valve openings between 100 and 50% due to the cavitation conditions. Furthermore, for case (Q=302(l/min)) the change in vibration amplitude was relatively higher at inlet suction valve openings between 60 and 50% when compared to the inlet suction valve openings between 100 and 60%.

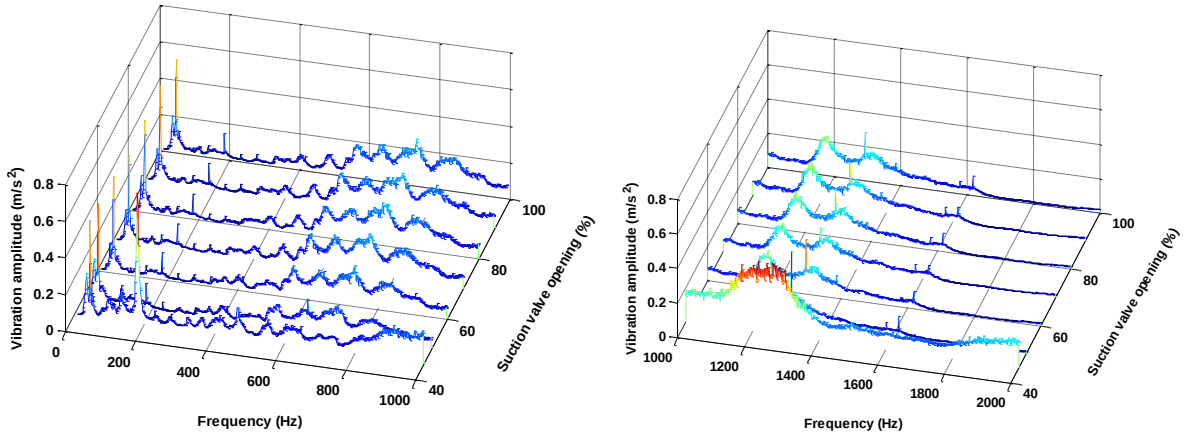

(a) Q=200(l/min) (b)

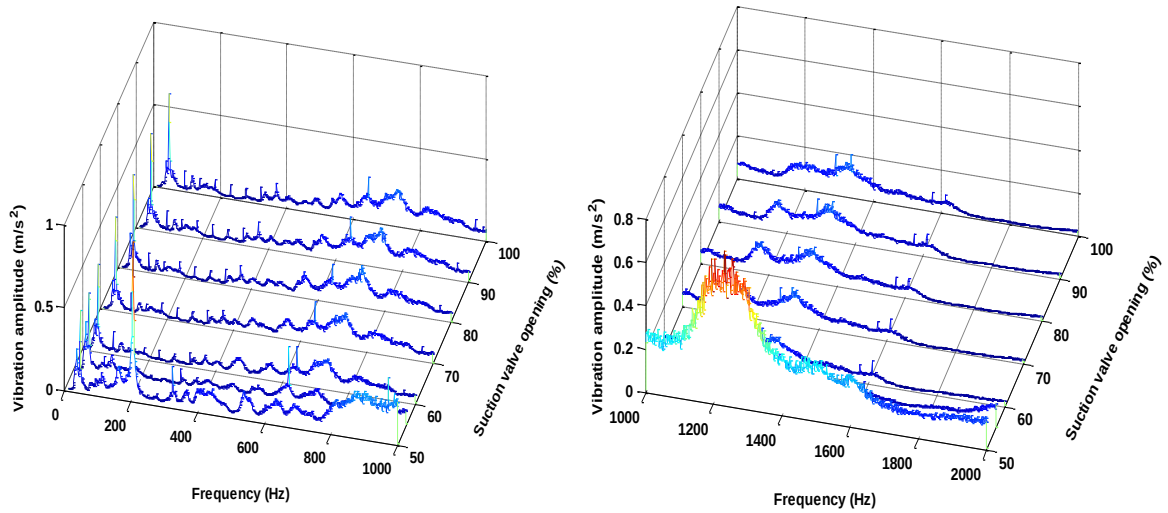

(a) Q=302(l/min) (b)

Figure 6-28: Vibration signal in frequency domain under various suction valve openings and the frequency range of (a) 0Hz-1kHz to (b) 1kHz-2kHz at different flow rates

For more comparison purposes based on frequency domain, Figure 6-29 depicts the statistical feature such as mean vibration amplitude value of the aforementioned cases under different flow rates and various suction valve openings and for various range of frequencies namely (0Hz-1kHz), (1kHz-2kHz), (2kHz-10kHz), and (10kHz-15kHz). It can be clearly seen that the mean feature under the different suction valve openings at Q=302(l/min) is considerably higher than for the other cases Q=200(l/min) and Q=103(l/min), due to cavitation process in the pump. From the above findings, it can be concluded that the analysis on the vibration signal in frequency domain, using mean value, provides a good indication regarding the occurrence of cavitation within a centrifugal pump due to the decrease in the suction valve opening.

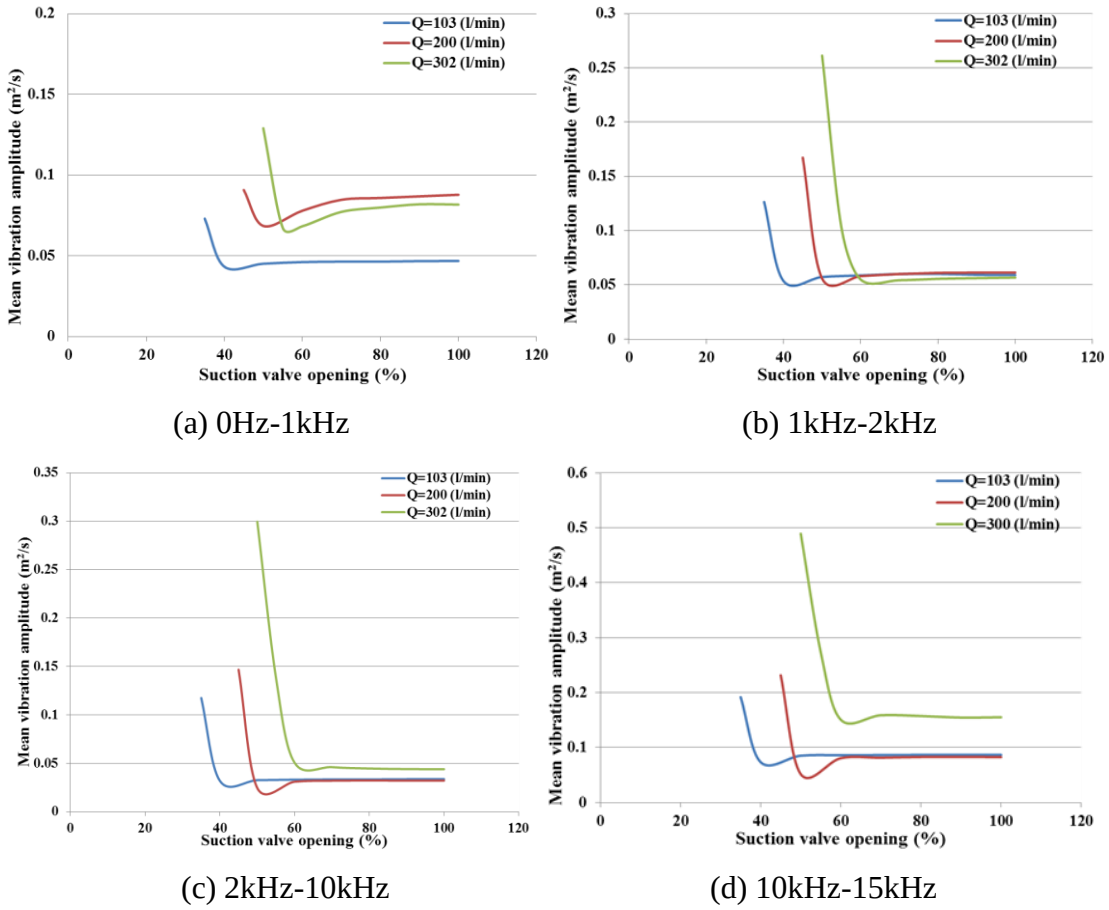

(a) 0Hz-1kHz (b) 1kHz-2kHz

(c) 2kHz-10kHz (d) 10kHz-15kHz

Figure 6-29: Comparison between mean vibration amplitude values in frequency domain for different frequency ranges under different suction valve openings

For more analysis on the vibration signal based on the frequency domain, Figure 6-30 depicts the RMS vibration amplitude value of the aforementioned cases under different flow rates and various suction valve openings and for various range of frequencies, which include (0Hz-1kHz), (1kHz-2kHz), (2kHz-10kHz) and (10kHz-15kHz). It can be clearly seen that the RMS feature has the same trend for the mean vibration amplitude value but with different values. It can be seen that the RMS value for Q=302(l/min) was considerably higher than for the other cases Q=200(l/min) and Q=103(l/min) as shown in Table 6-6 and Table 6-7. It can be concluded that the analysis of vibration signal in frequency domain, using RMS value, provides another indication regarding the occurrence of cavitation within a pump due to decrease at the suction valve opening.

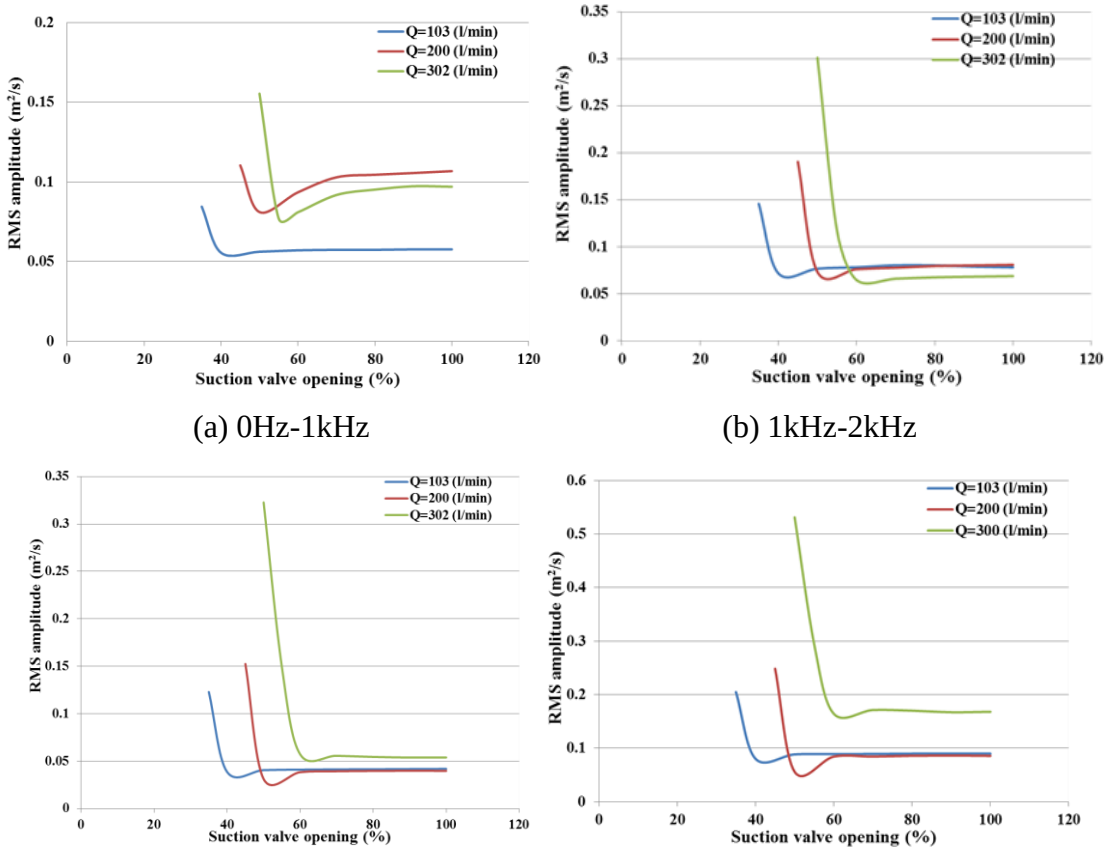

(a) 0Hz-1kHz (b) 1kHz-2kHz

(c) 2kHz-10kHz (d) 10kHz-15kHz

Figure 6-30: Comparison between RMS vibration amplitude values in frequency domain for different frequency ranges under different suction valve openings

Table 6-6 Result summary of the maximum mean vibration amplitude for different flow rates and frequency range of 0Hz-15kHz

Flow rate	Mean value 0Hz-1kHz	Mean value 1kHz-2kHz	Mean value 2kHz-10kHz	Mean value 10kHz-15kHz
(l/min)	(m/s^2)	(m/s^2)	(m/s^2)	(m/s^2)
103	0.0730	0.1264	0.1175	0.1918
200	0.0908	0.1673	0.1467	0.2315
302	0.1290	0.2613	0.2996	0.4892

Table 6-7 Result summary of the maximum RMS vibration amplitude for different flow rates and frequency range of 0Hz-15kHz

Flow rate	Mean value 0Hz-1kHz	Mean value 1kHz-2kHz	Mean value 2kHz-10kHz	Mean value 10kHz-15kHz
(l/min)	(m/s^2)	(m/s^2)	(m/s^2)	(m/s^2)
103	0.0844	0.1457	0.1228	0.2049
200	0.1103	0.1903	0.1524	0.2484
302	0.1553	0.3011	0.3227	0.5311

6.7. Summary of the Analysis of Different Suction Valve Openings

Based on above results, the effect of different suction valve openings on the vibration signal and performance of the centrifugal pump are obtained.

1. The head of the pump decreases as the inlet suction valve opening decreases.
2. As the inlet suction valve opening decreases, it leads to the lowering of the inlet suction pressure and cavitation on the suction side of the pump starts to occur.
3. The vibration signal analysis in time domain, using different statistical features can provide a good indication to determining when cavitation in the pump under different suction valve openings.
4. The results of the various statistical features in time domain increases with decrease in the suction valve openings.
5. Analysis on the vibration signal in frequency domain showed that the vibration peak amplitude occurred at two dominant distinctive frequencies as expected, the rotational frequency and the BPF.
6. The mean and RMS vibration amplitudes features from frequency domain under different inlet suction valve openings and various frequency ranges were observed different regions. The first region shows that there is no significant change in vibration amplitudes. In the second region, vibration amplitudes increase due to the cavitation occurrence within a pump.
7. The mean and RMS features increase with decrease in the suction valve openings and the above mentioned statistical features value also increase as flow rate increases.
8. The vibration signal in time domain can provide a primary indication regarding the detection of the inception and severity of the different levels of cavitation within a pump. Also, secondary indication can be quantified in the frequency domain analysis under different frequency ranges, making the experimental results in detecting cavitation more reliable.

6.8. Effect of Different Amounts of Air Injection using Vibration Technique

Investigating the various degrees of cavitation within the centrifugal pump in this section was carried out by studying the effect of air injection into the suction side of the pump. To simulate various cavitation flows based on different operation condition, air injection was used. It can be controlled either by air injection through the pressure supply by the air valve at the suction side of the centrifugal pump where the quantity of air injection can be measured by using air flow meter FMA 1700/1800 series from OMEGA Engineering INC was chosen for this study.

All the vibration signals of a pump were collected through the use of accelerometer as mentioned in previous sections. The digital form of the vibration signal was transferred and saved on a PC by a USB port. Following this, all these signals were processed by extracting the various features in both time and frequency domains.

In this experimental measurement, different amounts of air are injected into the suction side of the pump. Also, the pump was tested under various flow rates starting from to 100(l/min) to 370(l/min) corresponding to different operation conditions (low flow rate) and cavitation conditions (high flow rate). For this experimental work, higher amounts of air cannot be injected within the suction pipe. There are two possible reasons behind this, the first being due to the high injection of air this cause's unstable flow within the suction pipe and the pump, this leads to a rapid decrease in the performance of the pump and the second reason is the high air injection causes clogging at the inlet of the pump.

6.8.1. Performance Output of the Centrifugal Pump under Air Injection

The one important aim of this experimental study is to calculate the pump head. Therefore, several experimental measurements were conducted to find the pump performance under various air injections.

6.8.2. Calculated Head of the Centrifugal Pump at 0.4(l/min) Air Injection

Figure 6-31 depicts the pump head under different experimental flow rates with and without air injection. The amount of air injection in this case was 0.4(l/min) and N=2755rmp. It is evident that the head under both cases (with and without air injection) in the pump has a continuous downward trend with increasing flow rate. In addition, the results showed that there is no significant change between both cases when the pump works under operating conditions between 150 and 300(l/min). However, it can be seen that there is a slight difference between both cases after 300(l/min) and drop in the pump head for air injection was noticed as compared to without air injection condition. There are two possible reasons behind this decrease in the trend of the head. The first is due to hydraulic losses and additional losses due to air injection bubbles and the second reason is due to more pressure fluctuations within a pump which causes the formation and collapse of the bubbles from both the occurrence of cavitation and from air injection.

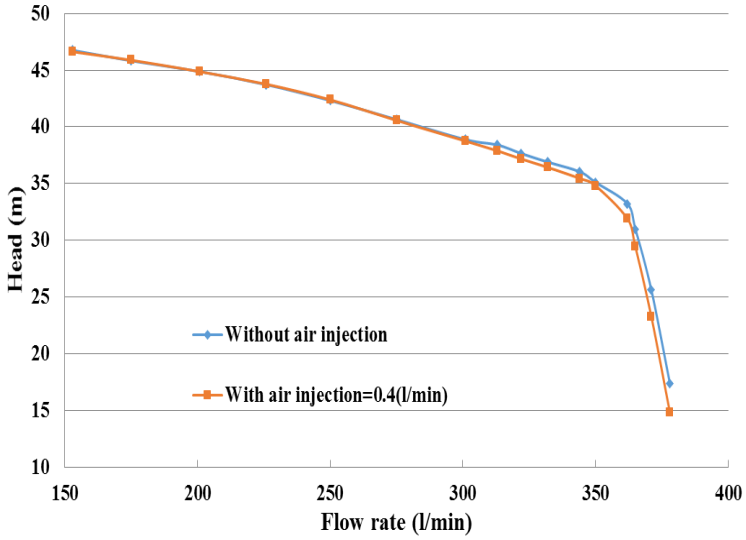

Figure 6-31: Head of the centrifugal pump with and without air injection at 2755rpm, and air injection 0.4(l/min)

Earlier detection of cavitation in the centrifugal pump, under different air injections is through the use of vibration technique. It is essential to first investigate and calculate NPSH of the centrifugal pump and then relate it with the different flow rates and air injection. The cavitation characteristics of the pump that were monitored as an important part of this study was plotted in Figure 6-32. This figure depicts the NPSHA and NPSHR against different flow rates regarding the inception and development of cavitation in the pump with air injection of 0.4(l/min). To achieve this purpose, the pump flow rate can be changed through progressively throttling the discharge valve and keeping the suction valve fully open (100%) whilst keeping the pump rotational speed constant at 2755rpm. From this figure, it can be clearly observed that when the pump operates under low flow rate, no cavitation occurs. This is due to the NPSHA being higher than the NPSHR. However at flow rate greater than 350(l/min), cavitation occurs in the pump and intersection between both curves (NPSHA and NPSHR) occurs. That means the development of cavitation starts at this point and it will increase when flow rate is increased more than 350(l/min) therefore, at this stage the NPSHA is smaller than the NPSHR.

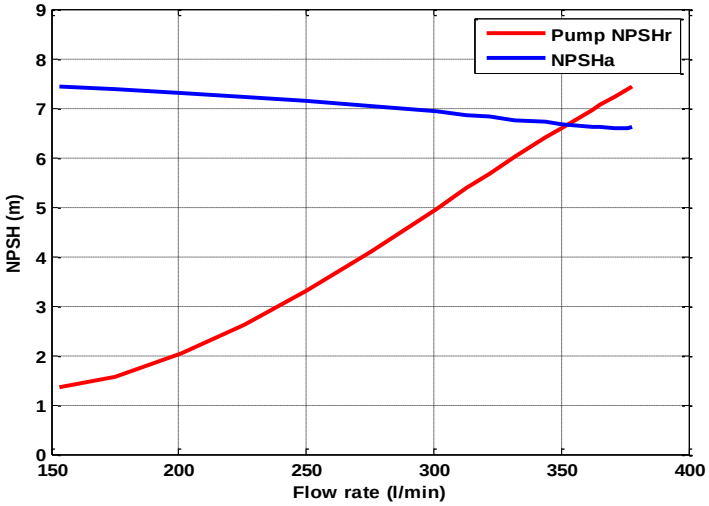

Figure 6-32: The cavitation characteristics of the pump under different flow rates and air injection 0.4(l/min)

6.8.3. The Vibration Signal Analysis Based on Time Domain under Amount of Air Injection of 0.4(l/min)

Figure 6-33 depicts the vibration signal wave form for the pump in time domain obtained at 0.4(l/min) air injection rate. These signals are collected at N=2755rpm and under various flow rate conditions (under normal and cavitation conditions) studied in this experimental test. As seen from this figure, the different levels of the vibration amplitudes depend on the various flow rates. It can be seen that when the pump works under low flow rate, for instance between 150 and 300(l/min), the levels of vibration amplitudes are lower than when the pump is operating under high flow rate resulting in the vibration amplitude signal being increased as flow rate is increased due to three possible reasons. The first is due to air injection within a pump. The second is due to the high interaction between the impeller and volute tongue region and the final reason, which is the most important, is due to the occurrence of cavitation at the high flow rate. It can be clearly seen that there are different levels of vibration amplitudes when the pump operates at normal conditions (without cavitation) and under cavitation conditions with air injection. In this case, the trend for the vibration amplitude was more random with high peaks when compared with normal operating conditions. By comparing these figures, it can be concluded that the vibration signals are sensitive to predict cavitation with air injection within a pump.

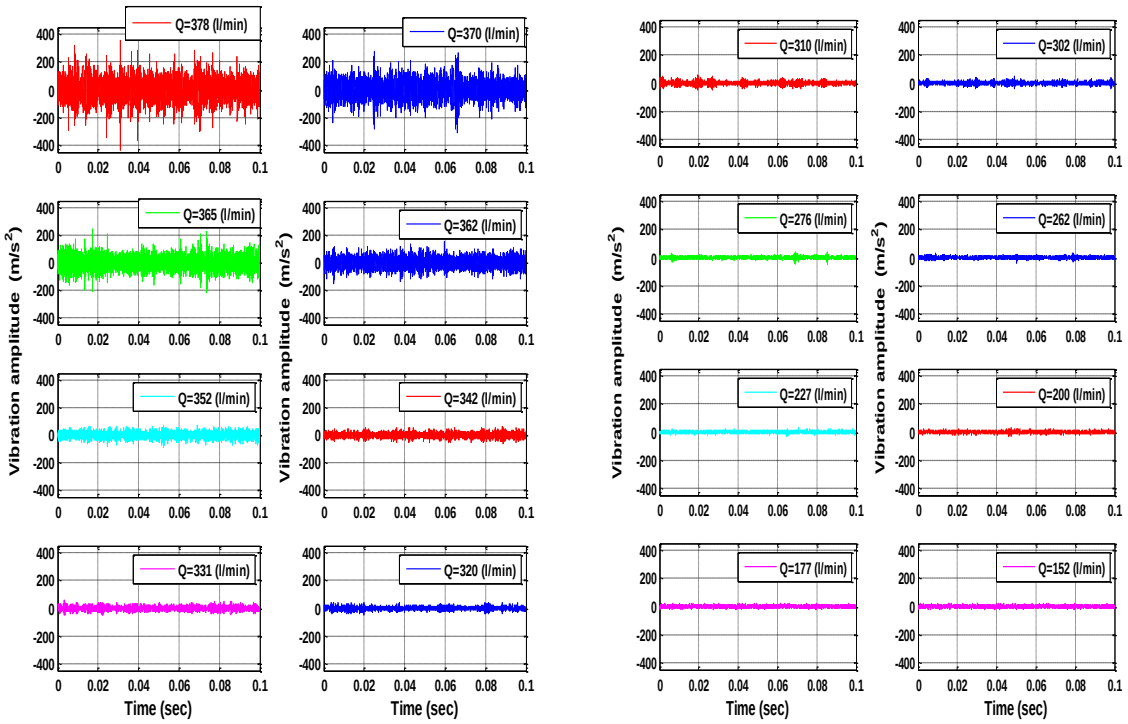

Figure 6-33: Analysis of the vibration signal in TWFA at N=2755rpm and air injection of 0.4(l/min)

6.8.4. Analysis of the Vibration Signal Based on Time Domain at 0.4(l/min) Rate of Air Injection

Further analysis on the vibration signal in time domain, with and without air injection was conducted in this section using the same different statistical features which were used in previous sections which include peak, RMS, peak-to-peak and variance features. Figure 6-34 depicts the analysis on the vibration signals for the centrifugal pump, using the above mentioned features at different flow rates, air injection at 0.4(l/min) and N=2755rpm operational conditions. It can be seen from this figure (with and without air injection) that there is a small indication of variance in the vibration level at flow rates below 350(l/min). However, the results from experimental measurements revealed that these statistical features of vibration signals have the same trend under the different flow rates. The vibration level witnesses a significant rapid increase when the pump operates at flow rate higher than 350(l/min). It can be observed that the trends for the vibration signals using peak and peak-to-peak features with air injection, starts to ascend before the trends for the vibration signals without air injection at flow rate higher than 340(l/min). The reason for this is due to the effect of the air injection in a pump and the occurrence of cavitation at high flow rate which causes more unstable flow

within a pump. It is noticed that the use of peak and peak-to-peak features were more sensitive to investigate the effect of air injection when compared to RMS and variance features. The experimental results showed that the analysis of variation in the level of vibration amplitudes in a pump, under different experimental flow rate measurements, with and without air injection in time domain, agreed with the characteristics of cavitation that was depicted in Figure 6-32.

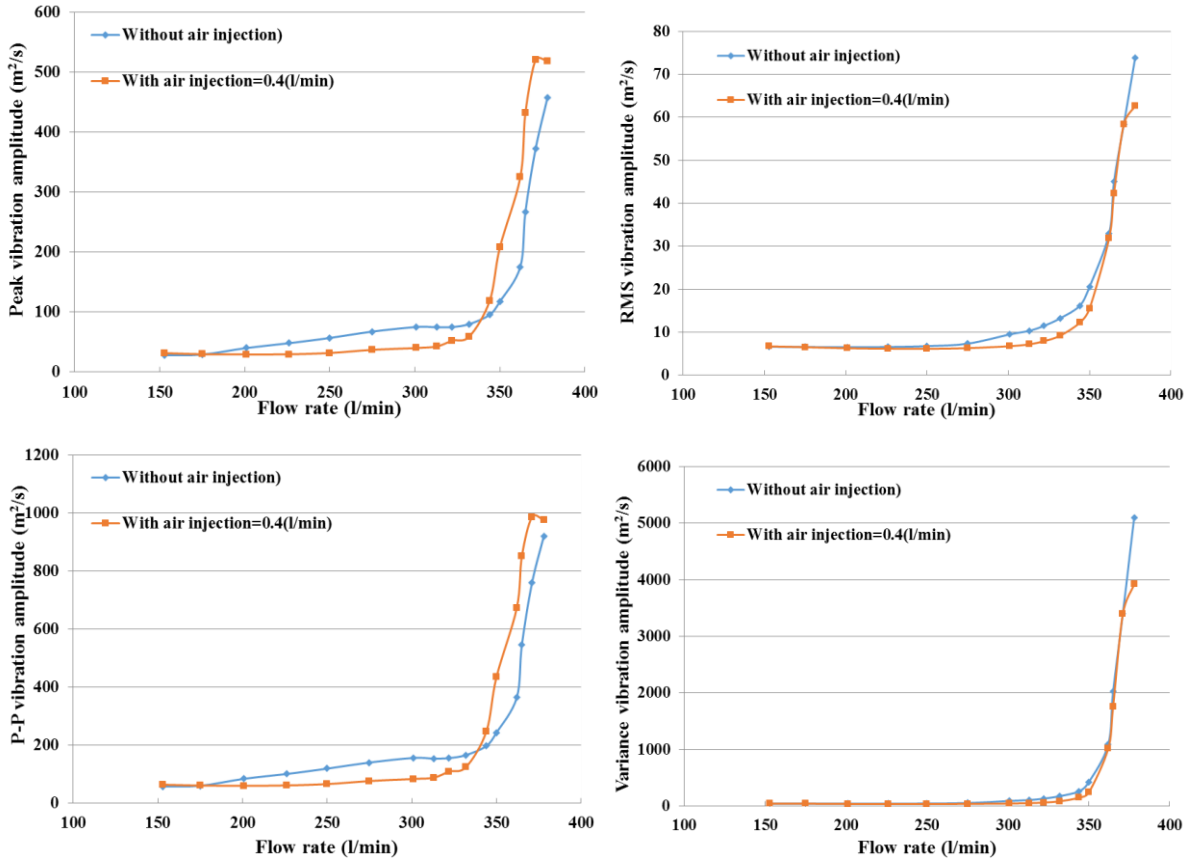

Figure 6-34: Trends of peak, RMS, peak-to-peak, and variance values of the vibration signal at 2755rpm with and without air injection

6.8.5. Analysis of the Vibration Signal Based on Frequency Domain at 0.4(l/min) Rate of Air Injection

Frequency domain analysis was carried out under different air injection rates in order to investigate the changes in the level of vibration amplitude. Figure 6-35 depict the analysis on the vibration signal under the different ranges of frequencies (a) 0Hz-1kHz and (b) 1kHz-2kHz) at various flow rates, N=2755rpm and air injection of 0.4(l/min). Different types of frequencies were observed to have appeared. The first was the rotational frequency of 45.91Hz, whilst the second was the BPF 229.5Hz and their harmonics. It can be seen that the vibration amplitude

increases as flow rate increases due to the occurrence of the inception and development of cavitation in the pump and also due to the effect of air injection within a pump.

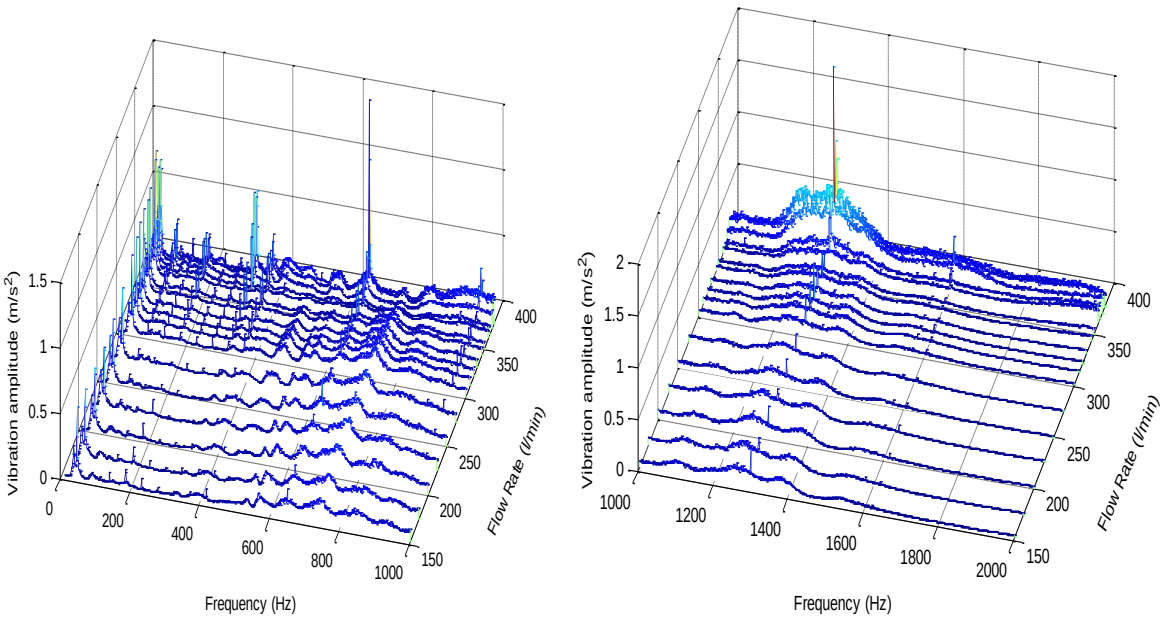

(a) (b)

Figure 6-35: Vibration signal in frequency domain at various flow rates with the frequency range from (a) 0Hz-1kHz to (b) 1kHz-2kHz at 2755rpm and air injection of 0.4(l/min)

Figure 6-36 and Figure 6-37 depict using mean and RMS vibration amplitude features, with and without air injection to analyse the vibration signal in frequency domain. These features were investigated under different range of frequencies which include a) 0Hz-1kHz, b) 1kHz-2kHz, c) 2kHz-10kHz, and d) 10kHz-15kHz, at different flow rates, air injection of 0.4(l/min), and N=2755rpm operational conditions. It can be observed that the plots for the above-mentioned features displayed the same trend when compared to the results obtained in the previous sections under different operational conditions. This case under investigation has different vibration amplitude due to the effect of air injection in the flow pattern within a pump as well as the cavitation occurrence. It can be seen that trends for the mean and RMS vibration amplitudes values have small changes at flow rate between 100 and 350(l/min) for both cases (with and without air injection). However, the trends for the above mentioned features for both cases are rapidly increased after flow rate of 350(l/min). There are two possible reasons for this observation. The first is mostly due to the interaction between impeller/volute as well as cavitation occurrence within a pump. The second one is due to the amount of air injection which causes more instability in the flow pattern inside the pump and hence, leads to increasing

pressure fluctuations in the pump due to more interactions between the air injection bubbles and the collapsed bubbles as a result of the cavitation process.

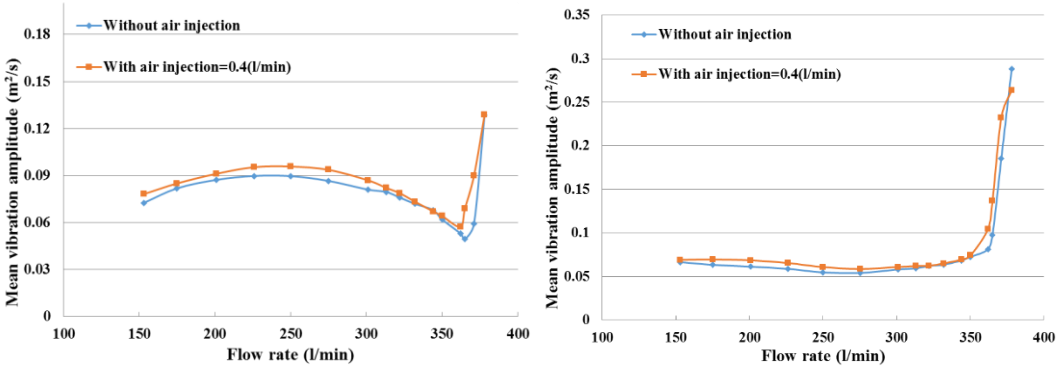

(a) 0Hz-1kHz (b) 1kHz-2kHz

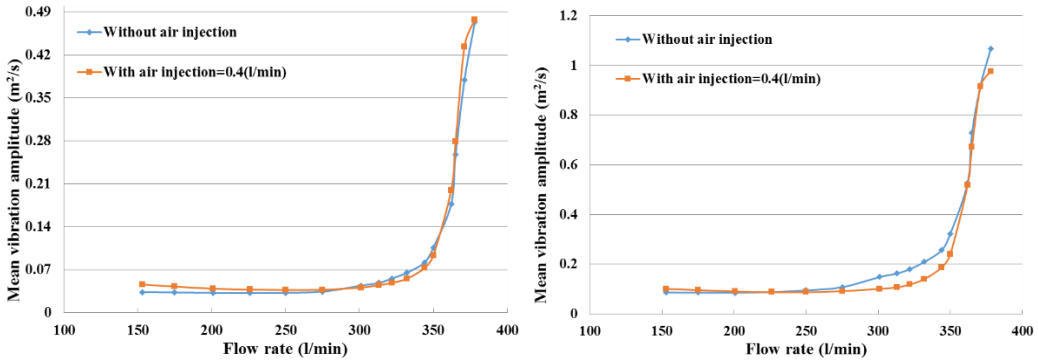

(c) 2kHz-10kHz (d) 10kHz-15kHz

Figure 6-36: Mean vibration amplitude value of the frequency range from 0Hz to 15kHz at 2755rpm with and without air injection

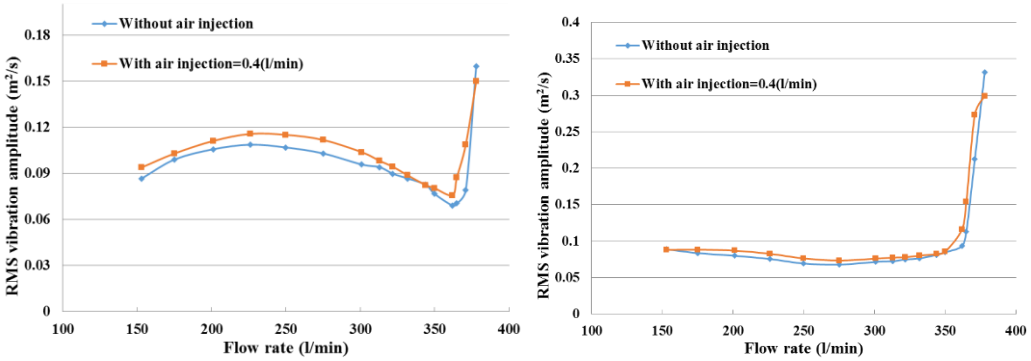

(a) 0Hz-1kHz (b) 1kHz-2kHz

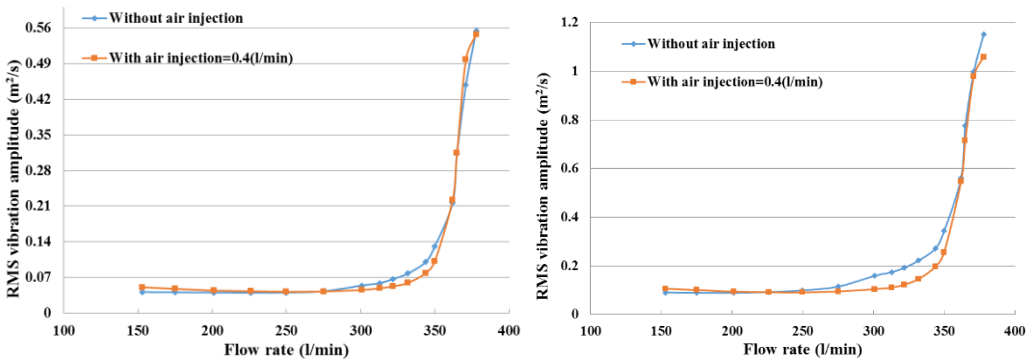

(c) 2kHz-10kHz (d) 10kHz-15kHz

Figure 6-37: RMS vibration amplitude value of the frequency range from 0Hz to 15kHz at 2755rpm with and without air injection

For this study, the effect of the different amounts of air in the suction side of the pump on the performance and detection of cavitation through the use of vibration signals was investigated experimentally. The results showed that when the amount of air injection increases, it leads to decrease in the performance of the pump. Furthermore, the behaviour of the water and air (two-phase) mixtures within a centrifugal pump can be highly complex, having a striking impact on the performance of the pump. The results analysis on the vibration signal obtained in both time and frequency domains are discussed, and the results obtained experimentally with air injection are investigated in the next section. In practice, analysis on vibration signal with air injection in the centrifugal pump faces several difficulties due to inadequate information in this field.

The entrance air inside the pump could increase the level of vibration and noise. In this current study, different amounts of air injections were conducted in order to study the effect of these air injections on pump performance. How these amounts of air injection relate to changes in the vibration signals are also investigated and also obtain more information regarding the prediction of cavitation within a pump. Furthermore, cavitation within a pump was directly monitored by measuring the vibration signal near the volute tongue region, through the use of an accelerometer.

6.8.6. Calculation of the Head of the Centrifugal Pump at Different Air Injection Rates

Figure 6-38 depicts the pump head under different flow rates and air injections. The amounts of air injection were 0.4, 1, and 1.8(l/min) and N=2755rmp. It can be seen that the head under both cases (with and without air injection) in the pump has a continuous downward trend with increasing flow rate. In addition, the results showed that the pump head was decreased with air

injection increased when the pump operates under a flow rates. Due to hydraulic losses and additional losses caused by air injection bubbles and the second reason is due to more pressure fluctuations within a pump, which causes the formation and collapse of the bubbles from both the occurrence of cavitation and air injection.

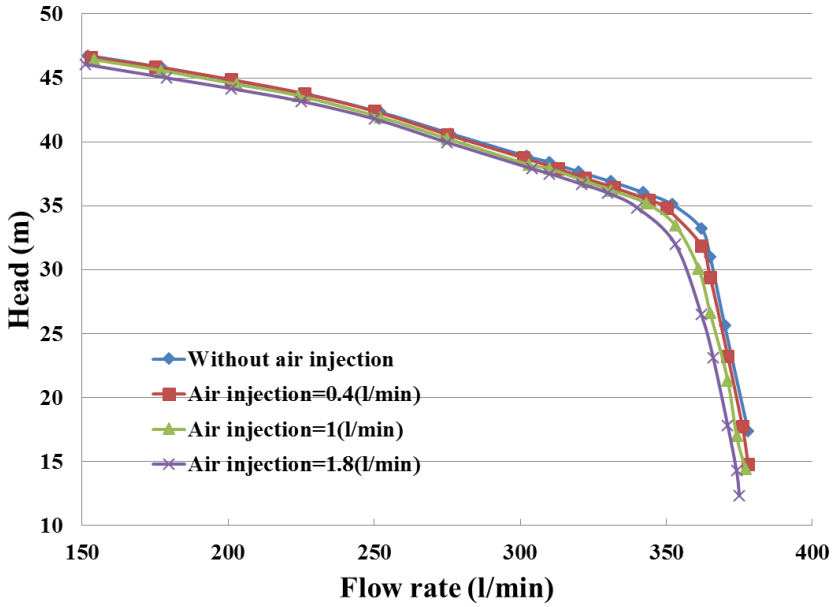

Figure 6-38: Head of the pump with and without air injection under different air injections

6.8.7. Time domain Analysis on the Vibration Signal for at Different Air Injection Rates

For comparison purposes between the different cases the amounts of air injection were 0.4, 1, and 1.8(l/min), in time domain analysis, all of the results that were obtained from the experimental setup for the centrifugal pump showed to follow the same trend for the peak, RMS, peak-to-peak and variance features as illustrated in Figure 6-39. These results indicated that no significant change occurs in the vibration amplitude at flow rate lower than 350(l/min). However, the rapid increase in the vibration amplitude was at flow rate higher than 350(l/min). This increase in the vibration amplitude can be explained due to the increase in the formation of bubbles that causes cavitation. The additional air bubbles leads to decrease in pressure at the eye of impeller, below the water vapour pressure. Hence, for this case, the NPSHA becomes lower than NPSHR value and at this point cavitation increases and then develops fully within the pump. Furthermore, high amount of air injection within the suction side of the pump can be collected back which forms a pocket around the impeller, particularly at the eye of the impeller which causes more losses in the pump and then possibly leading to air binding. As a result of air binding, problems such as the impeller spinning in the air occurs that may lead to

increase in the pressure fluctuations and also increase in the heating of the pump. This can then lead to damage to the bearing, impeller and the volute of the pump.

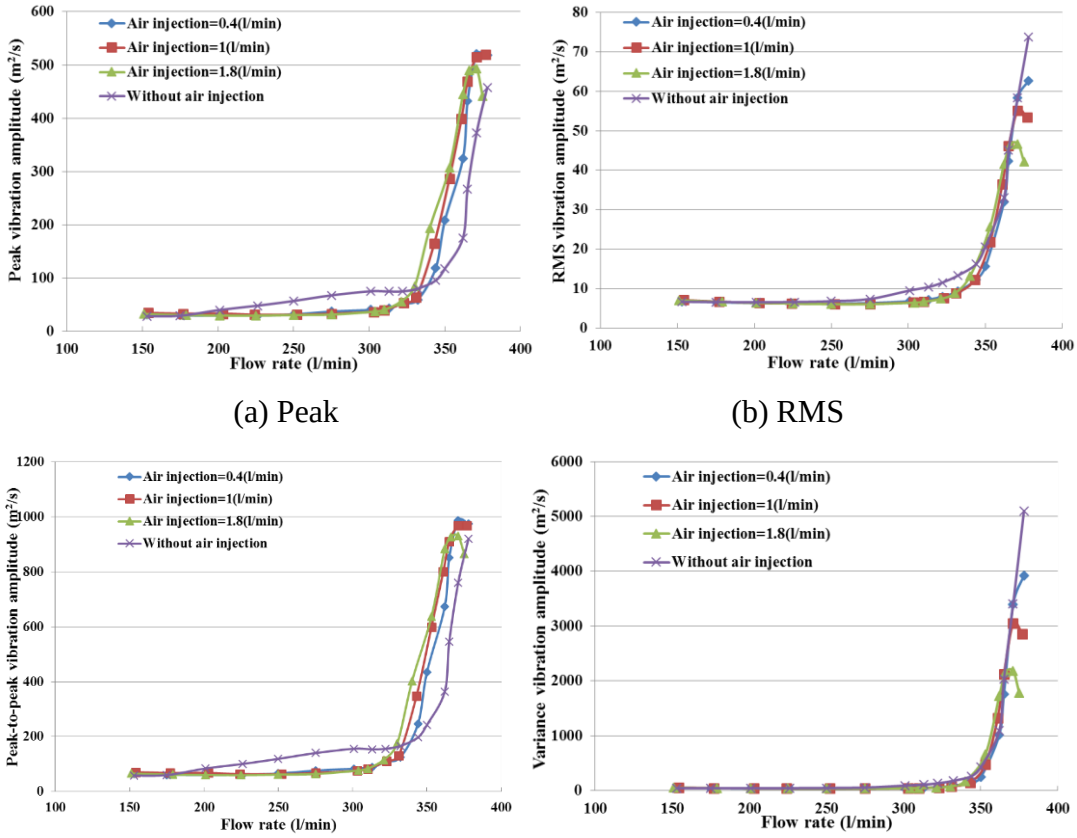

(a) Peak (b) RMS

(c) Peak-to-peak (d) Variance

Figure 6-39: Comparison between different statistical features of the vibration signals in time domain different air injections

For more results on the maximum peak, RMS, peak-to-peak and variance features of the pump, Table 6-8 and Table 6-9 provide the comparison between above cases. The maximum and minimum values of peak and peak-to-peak for air injection 0.4(l/min) were higher than another cases. The reasons for this is because the pressure fluctuations for air injection at 1(l/min) are higher than air injection at 1, and 1.8(l/min). Pressure fluctuations within the centrifugal pump are generated due to several reasons, which include interactions between the impeller (rotor) and volute (stator), especially at the volute tongue region. In addition, another reason is due to secondary flow together with the inner pump flow. Finally, the primary reason for this pressure fluctuation generation is the occurrence of cavitation and also due to the air injection within a pump.

Table 6-8 Summary of the maximum statistical features of the vibration amplitude in time domain at different air injections

Air injection (l/min)	Peak (m/s^2)	RMS (m/s^2)	Peak-to-peak (m/s^2)	Variance (m/s^2)
0.4	520.44	62.65	989.39	3922.40
1	537.20	55.17	992.52	3048.60
1.8	493.38	46.69	930.52	2180.0

Table 6-9 Summary of the minimum statistical features of the vibration amplitude in time domain at different air injections

Air injection (l/min)	Peak (m/s^2)	RMS (m/s^2)	Peak-to-peak (m/s^2)	Variance (m/s^2)
0.4	29.27	6.13	59.75	37.60
1	29.01	6.02	63.31	36.20
1.8	28.22	6.01	59.19	36.0

6.8.8. Frequency Domain Analysis on the Vibration Signal at Different Air Injections

Figure 6-40 depicts the vibration signals in frequency domain at different frequency ranges from 0Hz-1kHz to 1kHz-2kHz under different flow rates, air injection 1 and 1.8(l/min). It can be seen that there is no significant change in the level of amplitude of the vibration signals when the pump works at a capacity lower than 350(l/min). However, a small increase in the level of amplitude of the acoustic signal occurred at flow rate higher than 350(l/min). It is also seen that dominant frequencies includes the rotation frequency and its harmonics, the BPF for all cases being investigation.

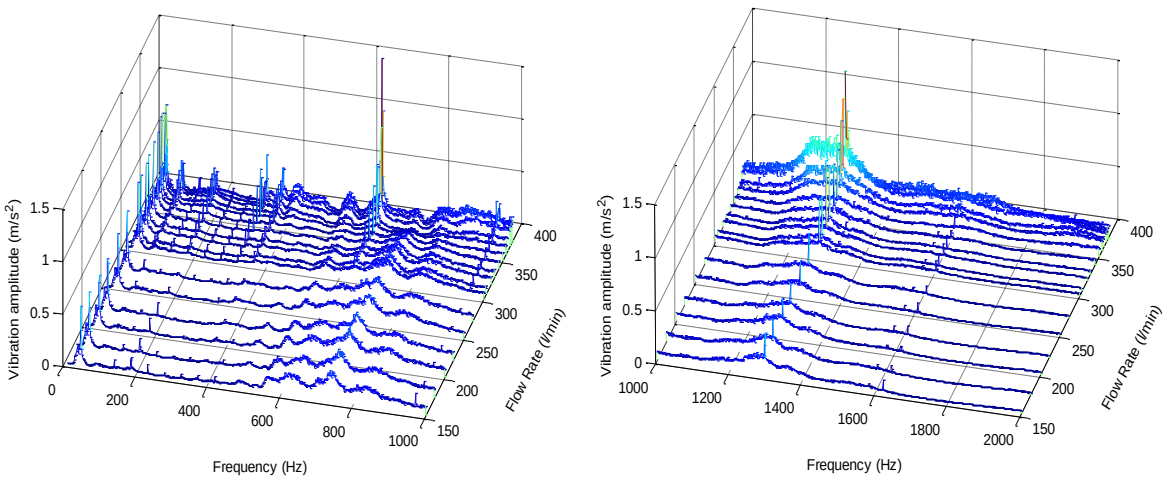

(a) Air injection=1(l/min) (b)

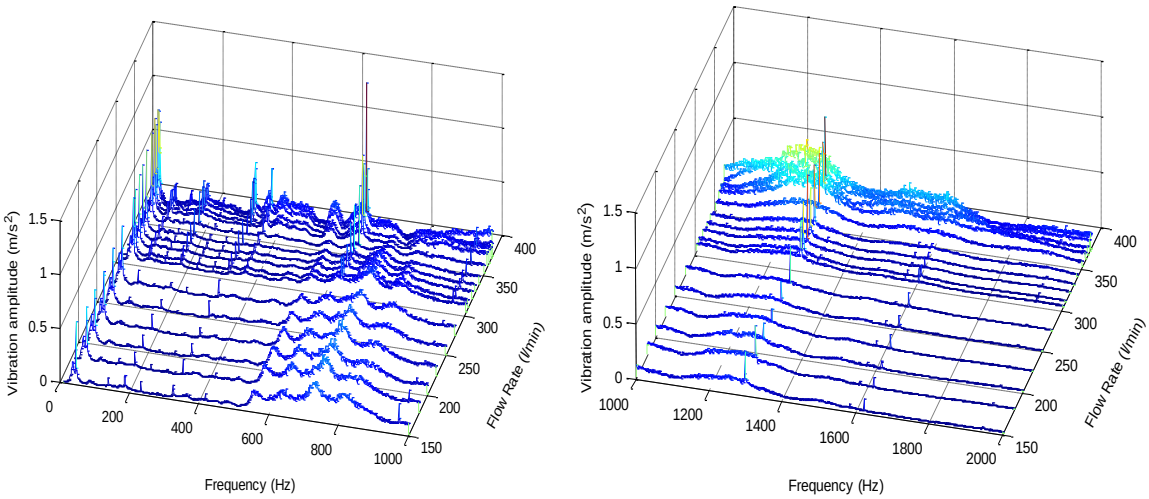

(a) Air injection=1.8(l/min) (b)

Figure 6-40: Vibration signal in frequency domain under various air injections and frequency range from (a) 0Hz-1kHz to (b) 1kHz-2kHz

For comparison purposes between the above cases 0.4, 1, and 1.8(l/min), in frequency domain analysis, all of the results that were obtained from the experimental setup under different air injection rates. The mean and RMS vibration amplitude features follow the same trend as depicted in Figure 6-41 and Figure 6-42 These results indicated that no significant change occurs in the vibration amplitude at flow rate lower than 350(l/min). The rapid increase in the vibration amplitude was at flow rate higher than 350(l/min). This increase in the vibration amplitude due to the increase in the formation of bubbles that causes cavitation. The additional air bubbles leads to decrease in pressure at the eye of impeller, below the water vapour pressure. Furthermore, high amount of air injection within the suction side of the centrifugal pump can be collected back, which forms a pocket around the impeller, particularly at the eye of the impeller which causes more losses in the pump and then possibly leading to air binding.

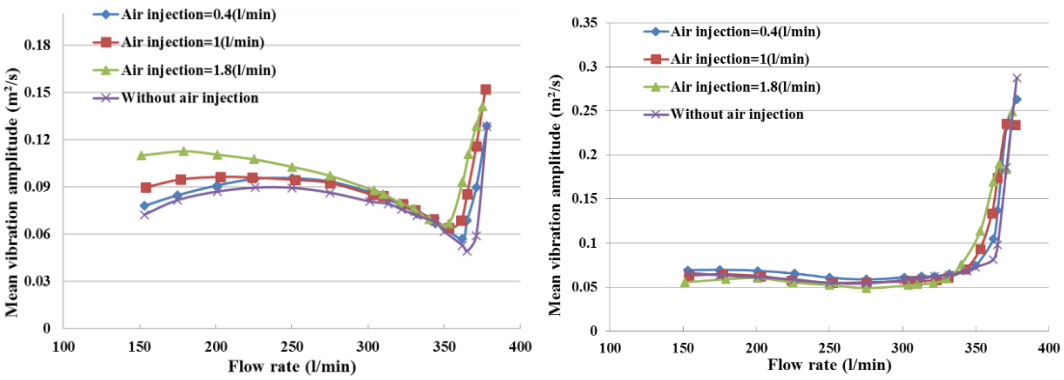

(a) 0Hz-1kHz (b) 1kHz-2kHz

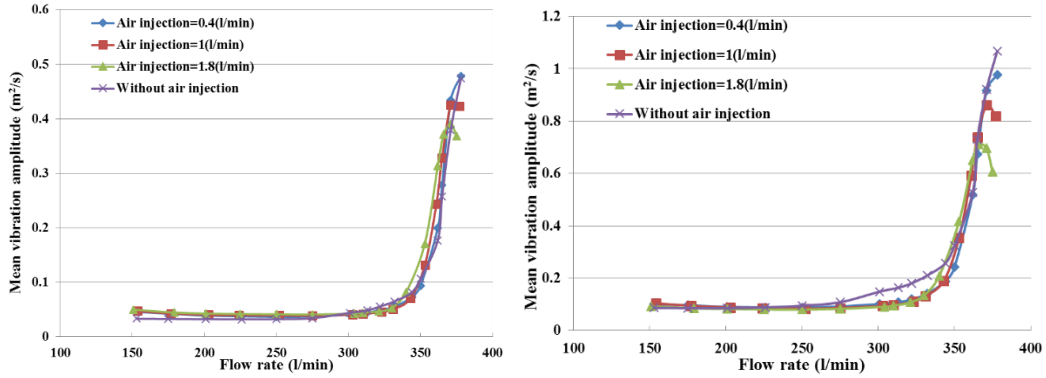

(c) 2kHz-10kHz (d) 10kHz-15kHz

Figure 6-41: Comparison between mean vibration amplitude values in frequency domain for different frequency ranges under different air injections

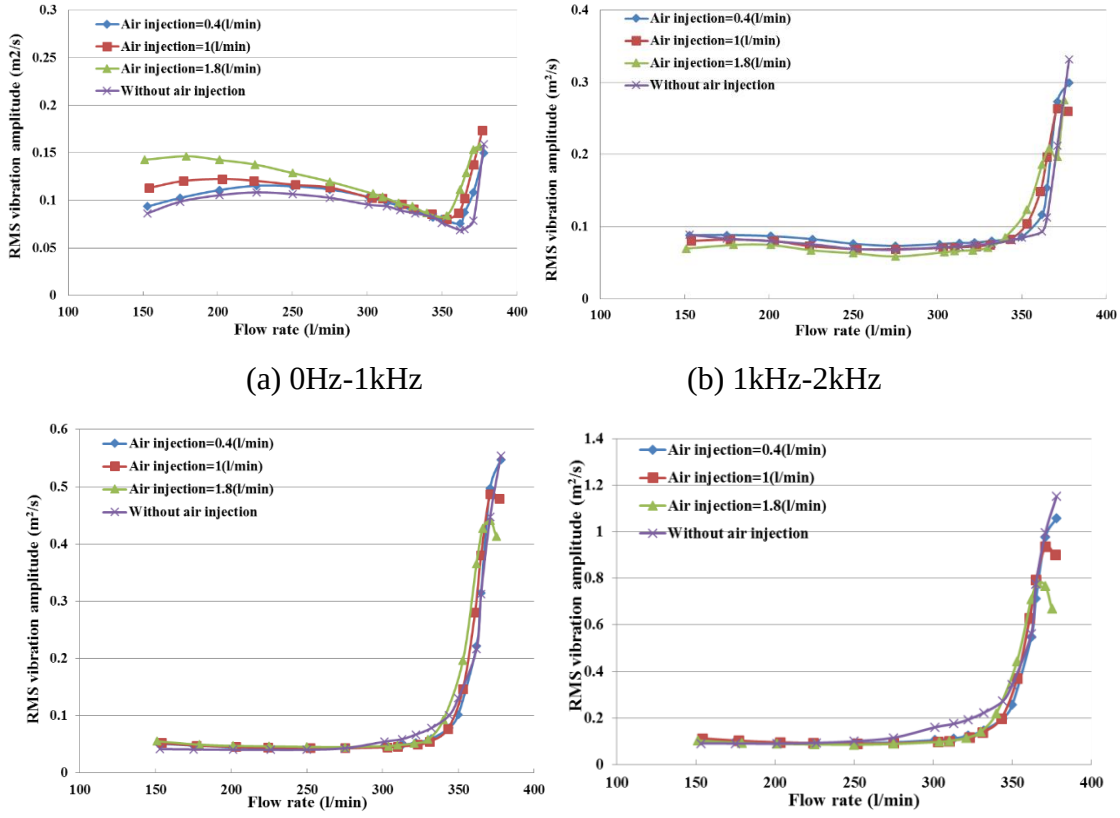

(a) 0Hz-1kHz (b) 1kHz-2kHz

(c) 2kHz-10kHz (d) 10kHz-15kHz

Figure 6-42: Comparison between RMS vibration amplitude values in frequency domain for different and frequency ranges under different air injections

The maximum mean and RMS vibration amplitude values for air injection at 0.4(l/min) were higher than for air injection at 1 and 1.8(l/min) under the different range of frequencies as summarised in Table 6-10 and Table 6-11.

Table 6-10 Summary of the results for the maximum mean vibration amplitude under different air injection and for 0Hz-15kHz

Air injection	Mean value 0Hz-1kHz	Mean value 1kHz-2kHz	Mean value 2kHz-10kHz	Mean value 10kHz-15kHz
(l/min)	(m/s^2)	(m/s^2)	(m/s^2)	(m/s^2)
0.4	0.1287	0.2681	0.4811	0.9766
1	0.1220	0.2417	0.4283	0.8611
1.8	0.1413	0.2492	0.3902	0.7098

Table 6-11 Summary of the results for the maximum RMS vibration amplitude under different air injection and for 0Hz-15kHz

Air injection	Mean value 0Hz-1kHz	Mean value 1kHz-2kHz	Mean value 2kHz-10kHz	Mean value 10kHz-15kHz
(l/min)	(m/s^2)	(m/s^2)	(m/s^2)	(m/s^2)
0.4	0.1497	0.3081	0.5490	1.0585
1	0.1437	0.2673	0.4869	0.9365
1.8	0.1431	0.2660	0.4416	0.7809

6.9. Summary of the Analysis of Different Air Injection within a Centrifugal Pump

Based on the above results in this section, several conclusions can be drawn regarding air injection within a pump and are listed below.

1. The head under both cases (with and without air injection) in the pump follow a continuous downward trend with increasing flow rate.
2. The results showed that there is no significant change in the pump head for both cases (with and without air injection), when the pump works lower than the design flow rate 300(l/min) at low amount of air injection. However, there is a slight difference between the two cases after 300(l/min) flow rate.
3. When the amount of the air injection increases, the head decreases.
4. Analysis on the vibration signals using time wave form showed that there is difference in the level of vibration amplitudes when the pump operates at normal conditions (without cavitation) and under cavitation conditions with air injection.
5. The analysis on the vibration signals in time domain using peak, RMS, peak-to- peak and variance features, with and without air injection, showed that there is a small indication of variance in the vibration level at flow rates below 350(l/min). However, the vibration level witnesses a significant rapid increase when the centrifugal pump operates at flow rate higher than 350(l/min).

6. Analysis on the vibration signals in frequency domain, under different amounts of air injection, revealed different types of frequencies. The first one was the rotational frequency and the second was the BPF and their harmonics.
7. The vibration amplitudes increase with an increase in the flow rate due to the occurrence of the inception and development of cavitation in the pump and also due the effect of air injection within the pump.
8. The use of frequency domain to analyse the vibration signal, is a suitable technique to study the effect of air injection in the pump and also to detect the inception and development of cavitation.
9. Analysing vibration signals in frequency domain using mean and RMS vibration amplitude features showed that the trends for these features have slight changes where flow rate is between 100 and 350(l/min) under both cases (with and without air injection). However, the trends for the above features under both cases rapidly increase after 350(l/min).
10. The trend for the vibration amplitude for both features (mean and RMS) with air injection at a frequency range starting from 2kHz to high-frequency of 15kHz slightly decreases at high flow, but the vibration amplitude without air injection increases with an increase in flow rate.
11. Finally, due to the high interaction between the air injections and the dissolved air caused by the bubbles formation due to cavitation within a pump makes the study of the impact of air injection within a pump more difficult.

The next chapter will analyse and discuss the results that were obtained from the experimental setup through the use of the acoustic technique in order to predict and diagnose the cavitation. With a combination of the vibration and acoustic measurements, dependable techniques are created for monitoring and detecting cavitation within a centrifugal pump. For the case of comparison between both techniques (vibration and acoustic), the structure of the next chapter will be similar to this chapter.

CHAPTER 7

PREDICTION OF CAVITATION WITHIN A CENTRIFUGAL PUMP USING ACOUSTIC ANALYSIS TECHNIQUE

Condition monitoring analysis of the centrifugal pump was a significant research study over recent decades obtaining detailed information regarding the pump performance and the effect of cavitation occurrence within a pump using CFD technique and experimentally using vibration technique in previous chapters. Therefore, in order to achieve other research aims, which lead to increase in the reliability of cavitation detection the use of different techniques, such as acoustic analysis technique, can provide a more robust detection of cavitation. A detailed results analysis, obtained from acoustic signal, was carried out to predict cavitation in the pump under different operating conditions. Also, the acoustic signal was investigated in time domain through the use of the same statistical features as previously mentioned in Chapter six as well as the FFT technique which was used to analyse the acoustic signal in the frequency domain. In addition, this chapter attempted to find a relationship between the cavitation and noise characteristics using acoustic technique for identifying cavitation within a pump. Furthermore, as a basis for developing a comparison and evaluation system amongst different techniques. Also, to find an adequate technique for accurate and reliable detection and diagnosis of different levels of cavitation within a centrifugal pump.

7.1. The used of Acoustic Technique to Diagnose Cavitation in the Centrifugal Pump

Recently, cavitation study has become a focal point of centrifugal pump industry, since it causes many problems in hydraulic machines, especially for turbines and all types of water pumps. It causes the failure, damage and deterioration of the performance and efficiency. Moreover, it increases the noise and vibration level within the system. This study analysed the effectiveness of the acoustic technique using a microphone. The cavitation within the centrifugal pump was predicted initially by analysing experimental acoustic signal in time domain analysis, using time waveform analysis (TWFA) approach along with different statistical features. The second approach was frequency domain, which was used to analyse the spectrum frequency. The effectiveness of the conventional acoustic technique was explained by plotting a three dimensional (waterfall) graph of frequencies against acoustic amplitudes and using different statistical features. The analysis was conducted for various low and high frequency ranges in order to determine a sensitive frequency range to detect cavitation in the pump. The sources of noise in the pump are reviewed in this chapter for different operational conditions. Subsequently, an explanation was provided on how the inception of cavitation influences these sources.

7.2. Sources of Acoustic (Noise) in the Centrifugal Pump

Normally, a certain amount of noise level is expected from different components of the centrifugal pump and pump parts such as an impeller, shaft, seal, bearings and cooling fan. However, the existence of high noise levels might be regarded as an initial indication of possible mechanical malfunctions or vibration issues in the pump. The noise in pumps might occur due to several factors such as the mechanical motion of the pump's parts, fluid movement within the pump and the installed piping system. Basically, the flow field and pressure fluctuations within the pump have periodic characteristics during its operation. In such cases, the compression occurs due to rotating impeller blades close to the volute tongue region. It can be said that impeller rotation is the reason for pressure fluctuation and the primary source of noise (especially if the interaction occurs at the tongue region). In addition, there are several other sources, such as mechanical forces and hydraulic forces that can generate noises within the pump. These hydraulic and mechanical forces could increase the noise level of the pump and eventually damage some parts of the pump leading to a decrease in their performance, such as head and efficiency.

7.2.1. Acoustic (Noise) due to the Mechanical Sources

Vibration is regarded as the first common mechanical source of noise in the pump that mainly occurs due to several reasons. The first reason being pressure fluctuations inside the pump. The second reason being incorrect installations of the pump's parts, such as couplings and seals, which generates mechanical noise and cause bearing rubbing. There are other acoustic sources that participate in generating noise in pumps, for instance, pump shaft and cooling fan [78].

7.2.2. Acoustic (Noise) due to the Hydraulic Sources

The hydraulic forces are regarded the second primary sources of acoustic in the pump. Such factors include direct liquid movement within the centrifugal pump. The fluid and pressure fluctuations interact with rotating impeller blades and the tongue region considered as the main reasons for acoustic noise in the pump. Similar to vibration sources, the hydraulic forces in the pump has several sources such as the hydraulic imbalance, the recirculation in suction and discharge sides, cavitation, flow instabilities, and water hammer [78].

7.2.3. Acoustic (Noise) due to the Cavitation in the Centrifugal Pump

The process of cavitation produces more noise in the pump; such mechanism termed cavitation noise occurs due to the liquid pressure at the inlet eye of impeller. This decreases below the liquid vapour pressure resulting in very small bubbles emerging and collapsing randomly as a consequence of cavitation. Thus, such random bubbles create turbulent acoustic that can be analysed in time and frequency domains. The noise in a centrifugal pump can occur due to internal pressure fluctuations in the tongue region and a number of various mechanisms (e.g. turbulence, flow instabilities, cavitation, high velocities and internal recirculation) [78]. Generally, when the pump works at a condition higher than design flow rate it might produce more turbulence or cavitation as illustrated in the previous chapter. Whereas when the pump operates under low flow rate conditions, the pump may face further internal recirculation. Differences in flow rates induce more pressure variation and eventually lead to the occurrence of high acoustic, which leads to an increase in noise level of the pump [152]. The higher frequencies appear either as a result of interaction between the flowing liquid and the moving components (e.g. impeller blades, impeller with volute and cooling fan) or due to the interaction between the rotating impeller blades with the nearby volute parts.

Cavitation is one of the important factors that cause instability in the pump as shown in previous chapters (five and six). It occurs in the pump due to insufficient or a decrease in the NPSH

when the pump operates under various operation conditions. When cavitation occurs in the pump, it causes various unwanted effects such as reduction in head and efficiency of the pump, damage to the pump part especially impeller through erosion and pitting on the impeller surface. It causes high level of vibration and hence, increases the level of noise. Consequently, the cavitation within the centrifugal pump must be decreased. In order to decrease the effect of cavitation, the inception and development of cavitation should be detected within the pump. To detect and diagnose the inception of cavitation, the emitted acoustic technique could be utilised [84].

7.3. Review of Applications Acoustic Technique

The usage of acoustic condition monitoring has several advantages where the acoustic signals can be easily obtained, evading safety hazards and the necessity for high-temperature acoustic sensors with their related mounting complications [153]. One of the disadvantages that undermine the use of such acoustic condition monitoring is that the surrounding sound from nearby rotating machines tends to contaminate the microphone sound [153]. However, current developments and improvements in acoustic sensors and signal (microphone signals) processing methods have facilitated the extraction of valuable diagnostic information [84].

Using lower frequency range technique (lower than 20kHz) usually has high noise, single related, with different frequencies in the pump such as rotation frequency and blade passing frequency and their harmonics. Using the latter technique in order to detect cavitation in the centrifugal pump is still in development. Another scope of this research study is to promote the use of a microphone with an acoustic range of 0Hz to 15kHz to analyse the acoustic signals for detecting cavitation inception. These signals can be used in order to acquire and provide reliable results for cavitation detection during different operational conditions of the pump. Furthermore, the analyses of acoustic signals are performed using MATLAB code.

In this study, the microphone was used to acquire the acoustic signals for various operational conditions which include different flow rates, pump rotation speeds, different suction valve openings and different amounts of air injection in order to predict the different levels of cavitation. There are several advantages using microphone to predict cavitation. It is a useful sensor mostly due to its simplicity and it is easy to position near or close to any centrifugal pump parts or flow loop piping system. It is not a necessity to select the suitable mounting surface for microphone sensor near the centrifugal pump as compared with vibration sensor (accelerometer). It is therefore easy to set the appropriate space between the pump and the

microphone. Also, it is significant to take into account that the microphone needs space when it is positioned near the pump. For accurate measurement via microphone the surrounding noise should be kept as low as possible [78]. The sample of acoustic signals under the current study was selected at 96kHz with a utilised number of data points up to 2880000. For study purposes, it is vital to know that the microphone frequency response is almost up to 20KHz. Since the acoustic and vibration signals features are almost similar in nature, the acoustic signals were analysed using similar techniques adopted for the vibration signals analysis. This will enable comparison between both signals using common parameters.

This study develops an experimental setup as mentioned that in Chapter four and it consists many parts. The main part is the centrifugal pump, electric motor, and cooling fan. All these parts generate noise through different noise generating mechanisms such as hydrodynamic, mechanical, and electromagnetic respectively. This noise that was generated during the operation of the centrifugal pump is especially first transferred to the pump surroundings and it is transferred to the other flow loop parts such as piping system [78].
The level of the noise signal in time and frequency domains depends on various operation conditions within the centrifugal pump. In order to detect the inception and development of cavitation a detail analysis of the signal will be carried out. In addition, an attempt was made to obtain the correlation between the levels of noise amplitude due to cavitation in time and frequency domains corresponding various operation conditions.

This technique (analyse acoustic signal) can be used in this study in order to increase the reliability of cavitation detection within a centrifugal pump. Use of both techniques (vibration and acoustic) can give a more robust detection cavitation. This chapter will be using similar methodology as mentioned in previous chapter. The methodology for detecting cavitation in a pump consists of different stages. The first one is a collection of acoustic signals from the pump using a microphone, the second stage is the time domain analysis using different statistical features and the final stage is frequency domain analysis. The details of acoustic data analysis in time and frequency domains under different operation conditions and frequency ranges using above methodology are presented and discussed in the next sections.

7.4. Effect of Various Flow Rates to Predict Cavitation within a Pump using Acoustic Technique

The purpose of this analysis is to investigate the effect of various flow rates on cavitation occurrence within a pump. The pump was operated at three stages with different flow rates. The first stage has low flow rate, the second stage represents design flow rate and the last stage has high flow rate. These three stages were considered for a constant rotating speed of N=2755rpm. The complete set of experimental acoustic results can be seen in the next sections.

7.4.1. The Analysis of the Acoustic Signal Based on Time Domain To Detect Cavitation in the pump

In this research study, the inception and development of cavitation in the centrifugal pump were investigated under different experimental measurements with various noise level using acoustic technique. To ensure the accuracy and repeatability of the findings, three readings were taken for each test conditions. The MATLAB code was used to analyse acoustic signals and to identify a set of statistical features for detecting cavitation levels based on acoustic test measurements. These instantaneous acoustic signals were analysed under both time and frequency domains. This analysis enabled prediction cavitation in the pump. Different statistical features were applied for time domain analysis and FFT approach under different frequency ranges were adopted for frequency domain.

In time domain, the amplitude of the above signals varies with respect to time. Based on data analysis from the experimental setup, it was observed that there was a trend to the features induced by acoustic signals with the changes of flow rate and this trend has helped to establish a relationship between induced flow rate and an acoustic signal from the centrifugal pump.

Figure 7-1 depicts the forms of time waves analysis for the acoustic signals based on different flow rates at pump rotation speed of 2755rpm. It can be noticed that when the flow rate is lower than design flow rate of 300(l/min), there is no significant change in the characteristics of acoustic signals. It can be clearly seen there is a significant difference in the characteristics of acoustic signals at a high flow rate higher than 350(l/min) in terms of shapes and amplitudes. There are two possible reasons behind these changes in acoustic signal. The first is due to the high interaction between the impeller and volute. The second is mostly due to the initiation of the cavitation process start in the pump, which is the result in higher NPSHR value than

NPSHA at high flow rate as is mentioned in the previous chapter. By comparing these figures, it can be concluded that acoustic signals are sensitive to detect cavitation within a pump.

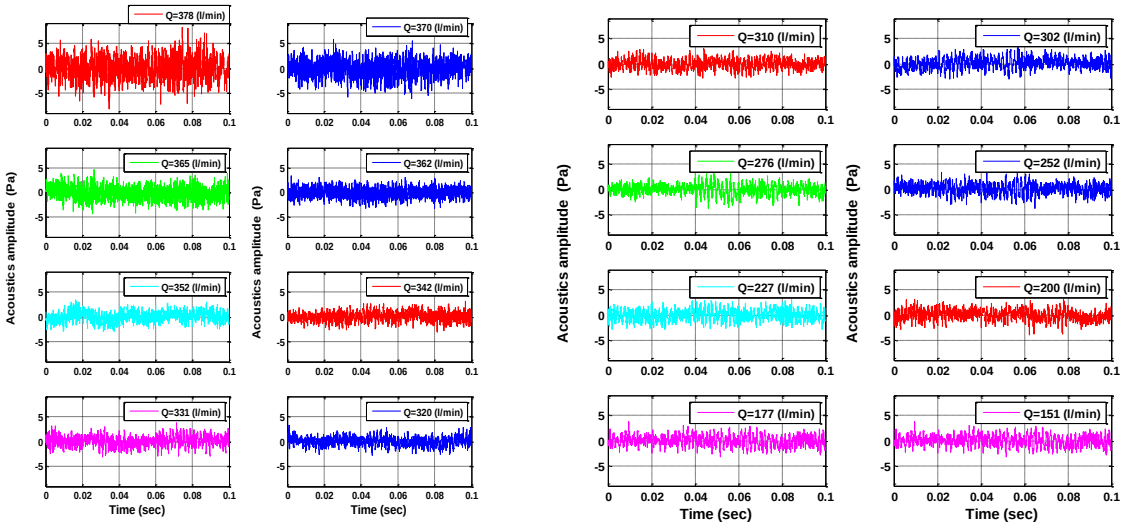

Figure 7-1: Analysis of the acoustic signal in TWFA under various flow rates at N=2755rpm

In order to establish a relationship between the acoustic amplitude and cavitation occurrence within the pump, further more analysis of these acoustic signals is required using effective features, which will be discussed in the next section.

7.4.2. Analysis of the acoustic Signal to Detect Cavitation using Peak, RMS Peak-to-Peak and Variance Features

The various experimental tests were carried out under various pump capacities of flow rates and the following results for microphone signals were obtained. Figure 7-2 (a) depicts these signals that were acquired from an acoustic microphone, at various flow rates, using different statistical features such as peak and RMS values that were calculated using experimental microphone data sets in order to analyse and predict cavitation within the pump. It can be observed that if the pump works lower than design flow rate 300(l/min), then there is further hydraulic noise due to the internal recirculation which occurs at the discharge and suction regions within an impeller. Also, when the pump operates at a higher flow rate than design flow rate 300(l/min), the overall noise increases due to flow turbulence, additional hydraulic noise and cavitation. In addition, from this figure, it can be apparent that when the flow rate is lower than 350(l/min), with a N=2755rpm, there is no significant change in both the trend of peak and RMS features. However, when the flow rate increases from 350(l/min), the amplitude of acoustic signals increase rapidly and hence increase the peak and RMS values as shown in

Figure 7-2 (a). The reason behind the increased level of acoustic amplitude is the occurrence of cavitation. That means, when cavitation happens in the pump, the pressure at the eye of the impeller decreases lower than vapour water pressure. This initiates the formation of small bubbles and subsequent collapse. The collapse of these bubbles consequently changes the level of noise. In other words, when the pump works under high flow rate, the NPSHR will be higher than NPSHA. At this flow rate, a pump will operate under cavitation conditions and this leads to an increase in the level of acoustic signals as was mentioned in the previous chapter. As a result, it can be noticed that increases in the level of acoustic signals provide an initial indication when the pump works under cavitation conditions.

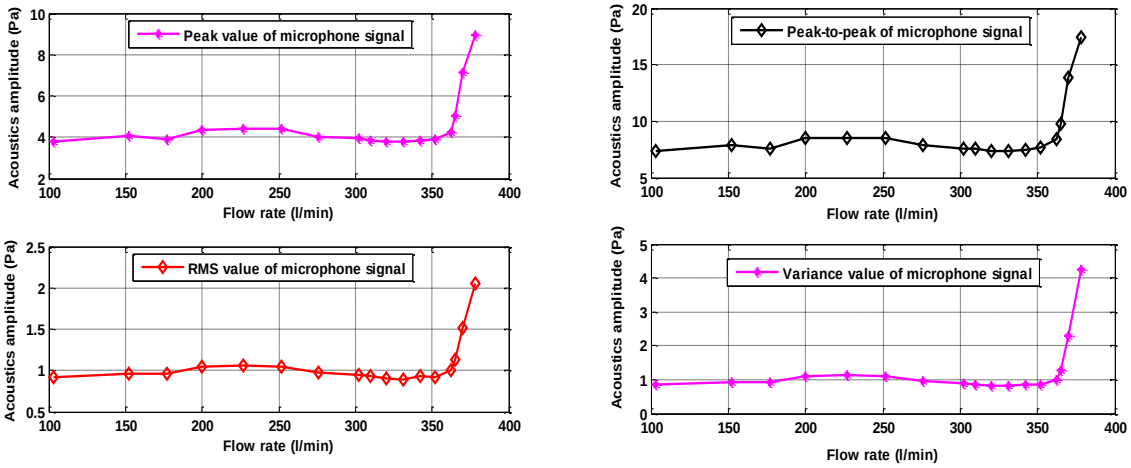

(a) Peak and RMS (b) Peak-to-peak and variance

Figure 7-2: Trends of different statistical features of the acoustic signal in time domain signal at 2755rpm

For further analysis of acoustic microphone signal using different statistical features such as peak-to-peak and variance values, Figure 7-2 (b) depicts the analysis of acoustic signals based on time domain through the use of the above features under different flow rates and a N=2755rpm. It can be observed that the peak-to-peak and variance features have the same trend as compared to peak and RMS features in the previous figures, this means when the flow rate of the pump is increased more than 350(l/min), the acoustic microphone signals are increased. The reason for this is when the flow rate increases, the pump has to operate under cavitation conditions and hence the noise within the pump is increased. As the flow operation conditions within the pump are changing, this leads to an increase in the noise level, the noise level then rapidly increases when the cavitation develops in the pump. The flow rate in the centrifugal pump is a very significant factor because it has more effect on the inception and development of cavitation. When the pump works at high velocity and high flow rate, the cavitation in the

pump starts to develop quicker. It is clear that the cavitation is an important point in the pump, and it should be predicted and diagnosed. Therefore, the characteristics of cavitation noise can be utilised in order to analyse and predict the inception and full development of cavitation in the pump.

As a result, from the above understandings, it can be concluded that the inception and development of cavitation in the pump are highly dependent on the flow rate.

The results revealed that by analysing the acoustic signal obtained by the microphone, using different statistical features could provide a good indication of cavitation. In comparison, between the trends for the same statistical feature such as peak, RMS, peak-to-peak and variance values by using different approaches such as acoustic and vibration signal techniques, it can be observed that both techniques have the same trends. For both cases, there is no significant change on the featured values under low flow rates. However, at higher flow rates (higher than350 (l/min)) the values increase rapidly. The result revealed that the use of vibration signal technique provides a more obvious indication of different levels of cavitation in the pump as compared to acoustic technique signal. The results also showed that the variation in the acoustic level in time domain due to change in the flow rate within a pump agreed with the characteristics of cavitation displayed in Figure 6-4.

7.4.3. The Analysis of the Acoustic Signal Based on Frequency Domain

The recorded acoustic signals were analysed in the frequency domain using FFT technique via MATLAB code. In this present study, the high and lower frequency ranges (lower than 20kHz) were used for detecting cavitation within a centrifugal pump. The important reason of using this technique is to decrease the cost of the microphone. The details of frequency domain under different flow rates and various frequency ranges are presented and discussed in the next sections.

7.4.4. The Analysis of Baseline Frequency at Design Flow Rate

As discussed in the previous chapter, the baseline frequency is important, as it will be utilised as a reference value in order to compare and measure when the pump operates under different operation conditions.

Figure 7-3 depicts the analysis of acoustic signals (baseline spectrum frequency) in frequency domain at a design flow rate equal to 300(l/min) and N=2755rpm. In order to obtain more information regarding the dominant frequencies for this baseline spectrum frequency for this

signal is shown in a frequency range of 0Hz to 1kHz. It can be observed that there are different types of frequencies in this range. As illustrated in Figure 7-3, the dominate frequencies are rotation frequency 45.92Hz and its harmonics 91.84Hz, 137.76Hz, 275,52Hz, and 321.44Hz respectively. The second is blade passing with a frequency of 229.6Hz and also its second harmonic was 459.2Hz. Another frequency that was shown is due to the motor and cooling fan. Furthermore, it can be seen that in this frequency range there are other frequencies with various levels of amplitudes. Because the microphone is very sensitive to any surrounding noise and the electric field around the pump has generated some unwanted noise, these frequencies could be generated due to any sound in the laboratory or due to the electric field flux of the motor. Further noise will appear in the system when the inception of cavitation starts to occur inside the pump. This type of noise is called cavitation noise, which is random in nature.

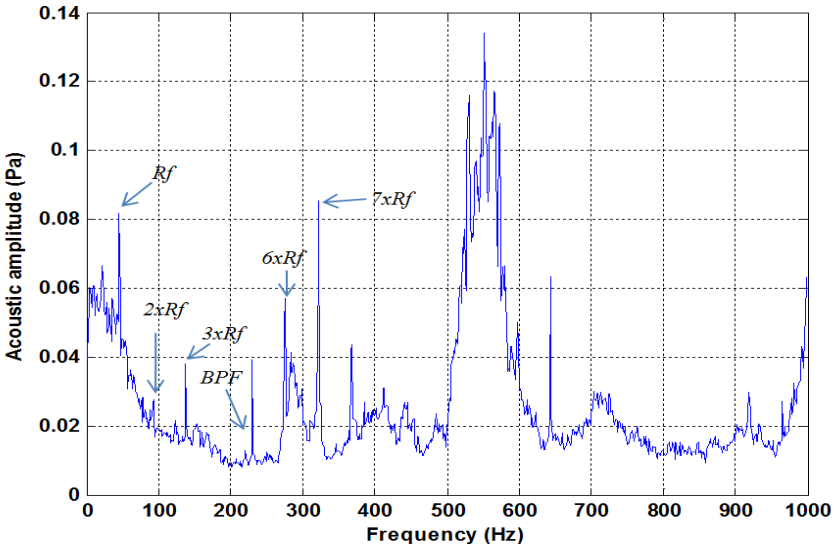

Figure 7-3: Baseline frequency of the acoustic signal range from 0Hz to 1kHz at design flow rate

7.4.5. The Analysis of the Acoustic Signals to Detect Cavitation in Frequency Domain under Various Flow Rates

This current study is aimed to investigate the cavitation within the pump under different operation conditions. For further analysis, in the next section the three-dimensional figure was plotted to illustrate relationship between different parameters. This figure allows for comparing more than one acoustic signal in frequency domain and hence it can be illustrated how the acoustic amplitude in frequency domain changes within the centrifugal pump for various operational conditions.

Figure 7-4 (a) depicts the acoustic signals based on frequency domain, through the use of a low range of frequency 0Hz-1kHz under different flow rates and N=2755rpm. It can be seen that when the pump works at a capacity flow rate less than 350(l/min), there is no significant change in the level of acoustic amplitude signal. However, the important change in the level of acoustic amplitude occurred at the capacity of the pump higher than 350(l/min), the acoustic amplitude is increased when the flow rate is increased. From the above findings, it can be concluded that the reason behind the increased noise level of the centrifugal pump is the high interaction between the impeller and volute and mostly the cavitation inception under high flow rate. The levels of acoustic amplitudes of the frequencies are increased as the flow rate is increased which means it can be used as a good indication for detecting inception and development of cavitation in a pump. It can also be observed that there are various frequencies in the low range of frequency as shown in this figure. The dominate frequencies are rotation frequency 45.9Hz and its harmonics and the second one is BPF which is 229.5Hz for all cases under investigation.

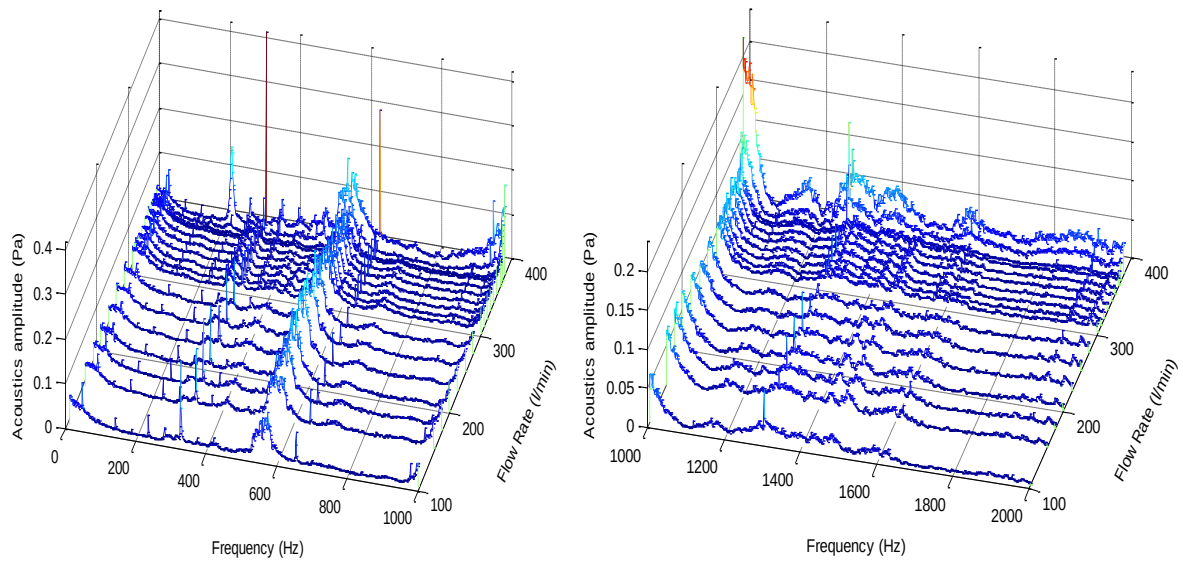

(a) (b)

Figure 7-4: Acoustic signal in frequency domain under various flow rates and frequency range from (a) 0Hz-1kHz to (b) 1kHz-2kHz at 2755rpm

Futheromre, Figure 7-4 (b) depicts the acoustic signals amplitude against frequency with a frequency range of 1kHz to 2kHz under different flow rates and N=2755rpm. It can be seen that at this range of acoustic frequency, the results showed that a small change in acoustic amplitude when the pump works at lower than 350(l/min), but a rapid increase in acoustic amplitude signals was observed at a flow higher than 350(l/min). The reason behind this is because the cavitation has occurred at high flow rate, consequently the NPSHA was lower than

NPSHR in this case. The rotational frequency and BPF is also dominating in this this range as well as observed for the previous range.

To further analyse and detect cavitation within a centrifugal pump, the acoustic signals are plotted in frequency domain at a higher range as shown in Figure 7-5. Two ranges were chosen for this investigation. The first has range of (a) 2kHz to 10kHz and the second one is (b) 10kHz to 15kHz for different flow rates and N=2755rpm. In both cases, (2kHz to 10kHz and 10kHz to 15kHz) when the flow rate is below 350(l/min) no significant change in the amplitude level of acoustic signal was noticed for low band frequencies. However, significant increase is observed at higher than flow rates 350(l/min). At high flow rate, the cavitation creates an increase in the noise level. It can be concluded that the lower noise value indicates the noise level before cavitation inception, whereas the high amplitude noise value indicates the inception cavitation has occurred within the pump, which develops with flow rate increase. This means the cavitation within the pump is a significant factor to increase the level of noise. The increase in the noise level can be observed at the high flow rate, which is due to the development of cavitation within a pump at that time. Due to increase in the flow rate, the velocity of flow increases, which decreases the inlet, pressure in this area. When the cavitation starts to occur, the number of vapour bubbles increases and implosions of bubbles surrounding the surface of the impeller increases the turbulence at the inlet eye of the impeller. Hence, the noise level increases. In addition, it can be clearly seen that the range of frequency 10kHz to 15kHz was more sensitive to predict the cavitation as compared to a range of frequency 2kHz to 10kHz and low range of frequency 0Hz to 2kHz as there are many acoustic amplitudes peaks in frequency range 10kHz to 15kHz as compared to other frequency ranges. As a result, from above findings, it can be concluded that the analysis of acoustic signals in frequency domain using different frequency ranges may provide useful information regarding prediction of cavitation within a pump.

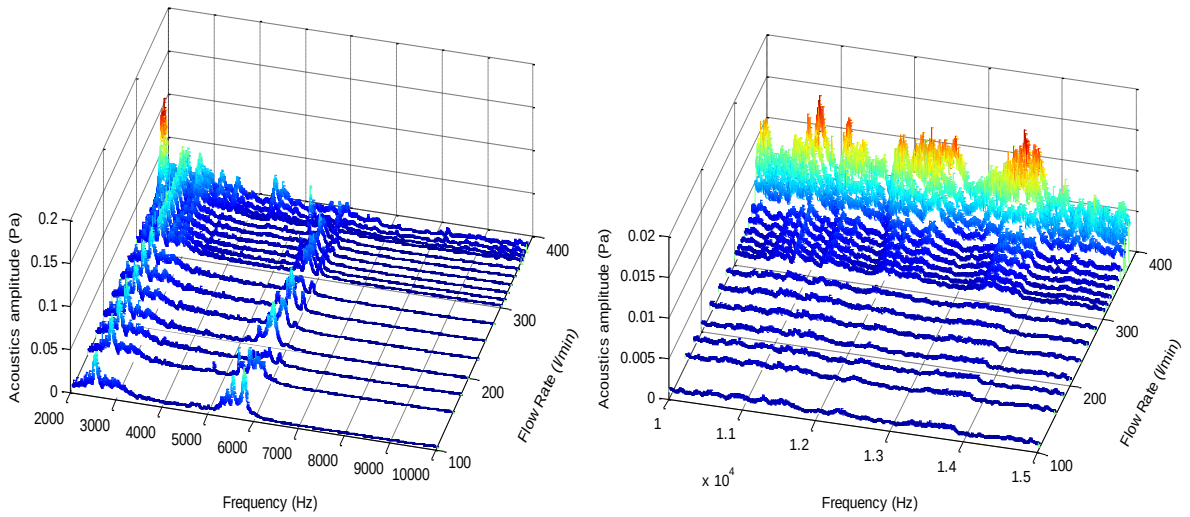

(a) (b)

Figure 7-5: Acoustic signal in frequency domain under various flow rates and frequency range from (a) 2kHz-10kHz to (b) 10kHz-15kHz at 2755rpm

7.4.6. Analysis of the Acoustic Signal in Frequency Domain using Various Statistical Features

As illustrated in the previous section, the use of three-dimension figures for the acoustic amplitude at different frequency ranges can provided more knowledge regarding cavitation process in the pump. This section analysed the acoustic amplitude signals in the frequency domain through the use different statistical features such as mean and RMS values. Different ranges of frequencies were also used in order to obtain more details regarding the acoustic signal.

7.4.7. Analysis of the Acoustic Amplitude in Frequency Domain using Mean Feature

For further investigation, the mean feature of the acoustic signals in frequency domain was analysed under different flow rates with a range of 0Hz to 15kHz, in order to reduce the microphone cost and to find the sensitive range of frequency to detect cavitation.

Figure 7-6 depicts the mean value of the acoustic amplitude signals in the frequency domain under different frequency ranges (0Hz–1kHz), (1kHz–2kHz), (2kHz–10kHz) and (10kHz–15kHz), at various flow rates and N=2755rpm. It can be seen that from mean acoustic amplitude value there is no significant change when the pump operates at a lower flow rate than 300(l/min). However, it can be clearly noticed that the rapid increase in level of acoustic

amplitude occurs at a flow rate higher than 350(l/min) due to cavitation. It occurs at high flow rate that leads NPSHR to be higher than NPSHA. From the above findings, it can be concluded that the use of mean value to analyse the amplitude of acoustic signals in frequency domain can provide a good indication in order to detect cavitation. Increased acoustic amplitude indicates severe cavitation within a pump.

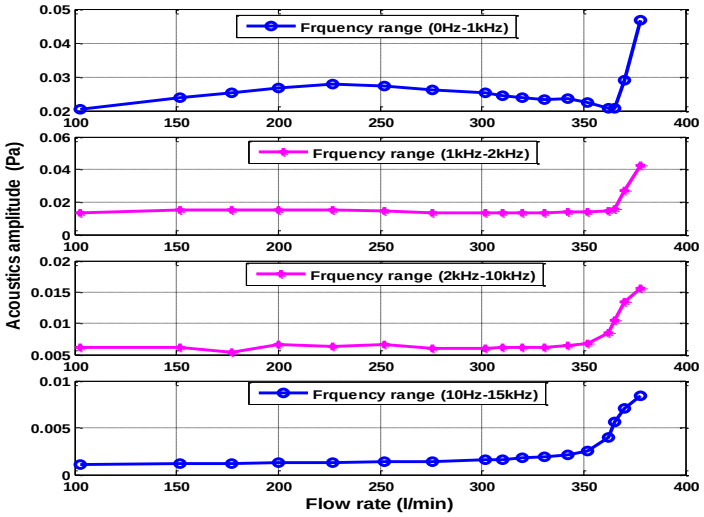

Figure 7-6: Mean acoustic amplitude value of the acoustic frequency range from 0Hz to 10kHz at 2755rpm

7.4.8. Analysis of the Acoustic Amplitude in Frequency Domain using RMS Feature

Figure 7-7 depicts the analysis of acoustic amplitude using RMS feature for different ranges of frequencies which were, (0Hz–1kHz), (1kHz–2kHz), (2kHz–10kHz) and (10kHz–15kHz), under operational conditions including different flow rates and N= 2755rpm. It is clear there is the same trend of the acoustic amplitude as the mean feature. Values of the acoustic amplitude increase rapidly at a high flow rate greater than 350(l/min). During the investigation in this research study, it can be concluded that the analysis of acoustic amplitude for different ranges of frequencies from 0Hz to 15kHz are effective to predict cavitation, especially in the low range of frequency from 1 to 2kHz.

Analysis of acoustic signal in frequency domain using the mean and RMS acoustic amplitude features at various frequency ranges starting from 0Hz to15kHz, shows the same trend when cavitation occurs within the pump. This investigation indicates that a low range frequency can be used to identify the cavitation in the pump. Hence, a low-cost microphone with lower frequency range can be used instead of a microphone which has high-frequency ranges and consequently decreases the cost. The results showed that the variation in the acoustic amplitude

level in frequency domain with respect to changes in the flow rate for different frequency ranges within a pump, agreed with characteristics of cavitation as displayed in Figure 6-4.

In summary, it can be noticed that the trends of results obtained through the use of acoustic technique are similar as compared to vibration technique results. Therefore, it can be concluded that both techniques can be used for condition monitoring of the cavitation in pumps.

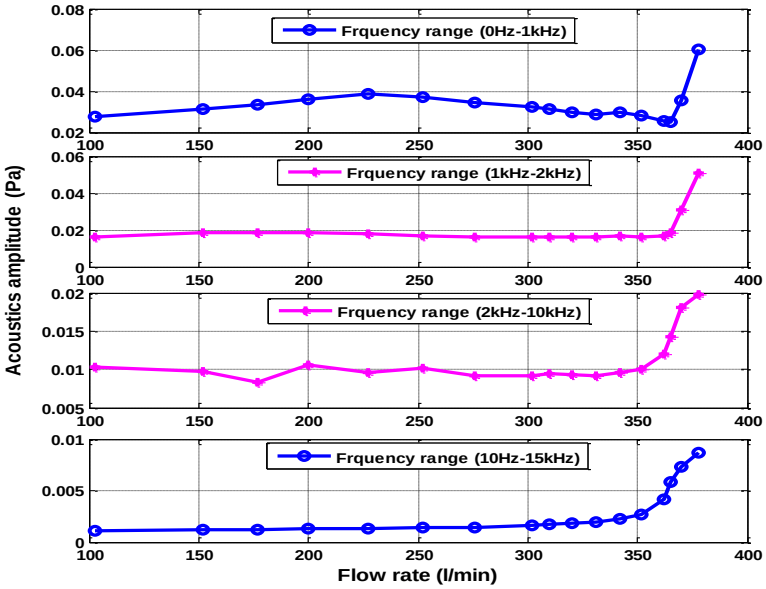

Figure 7-7: RMS acoustic amplitude value of the acoustic frequency range from 0Hz to 15kHz at 2755rpm

7.5. Effect of Various Pump Rotational Speeds to Detect Cavitation within a Pump using Acoustic Technique

As clearly seen in previous chapters, the flow field analysis and cavitation process, as well as instabilities in the flow within a centrifugal pump, were directly changed as a result of the different operating conditions. Therefore, in further investigations, the effects of various pump rotational speeds on detection of the different levels of cavitation in the pump can be studied. To achieve this experimentally, different pump rotational speeds (2610, 2320, and 2030rpm) were chosen for this analysis purpose. The next sections represent the results obtained from the experimental calculation under different rotational speeds.

7.5.1. Analysis of the Acoustic Signal using Various Statistical Features at Different Pump Rotational Speeds

Figure 7-8 depicts the different statistical features namely peak, RMS, peak-to-peak and variance values under various flow rates and different pump rotational speeds of the aforementioned cases for comparison purposes. It can be evident that the maximum peak feature for N=2755rpm is considerably higher than for the other three cases N=2610rpm, N=2320rpm and N=2030rpm by 13.38%, 15.48%, and 35.60%. Also, the maximum RMS value by 11.72%, 29.98%, and 52.53% is considerably higher than for the other cases and the maximum peak-to-peak by 13.02%, 13.45%, and 33.24% with the maximum variance value by 16.66%, 42.19%, and 75.93% respectively. It can also be seen that the minimum peak, RMS, peak-to-peak and variance values for N=2755rpm is considerably also higher than for the other three cases as summarised in Table 7-1 and

Table **7-2** From above findings, it can be concluded that the pump rotational speed is proportionally increased with an increase of the acoustic amplitude. Due to the high interactions between the water and blades of impeller, the interactions between the impeller and volute are also an importance factor contributing to the occurrence of cavitation increasing as the pump rotational speed increases.

Table 7-1 Summary of the maximum statistical features for the acoustic amplitude in time domain at different rotational speeds

Rotational speed (rpm)	Peak (Pa)	RMS (Pa)	peak-to-peak (Pa)	variance (Pa)
2755	0.0466	0.0424	0.0156	0.0084
2610	0.0388	0.0355	0.0155	0.0083
2320	0.0345	0.026	0.0109	0.0062
2030	0.0229	0.0151	0.0064	0.0033

Table 7-2 Summary of the minimum statistical features for the acoustic amplitude in time domain at different rotational speeds

Rotational speed (rpm)	Peak (Pa)	RMS (Pa)	peak-to-peak (Pa)	variance (Pa)
2755	3.7847	0.9163	7.3801	0.8403
2610	3.5571	0.8566	6.9028	0.7343
2320	2.6618	0.6483	5.2194	0.4206
2030	2.1776	0.5264	4.2579	0.2773

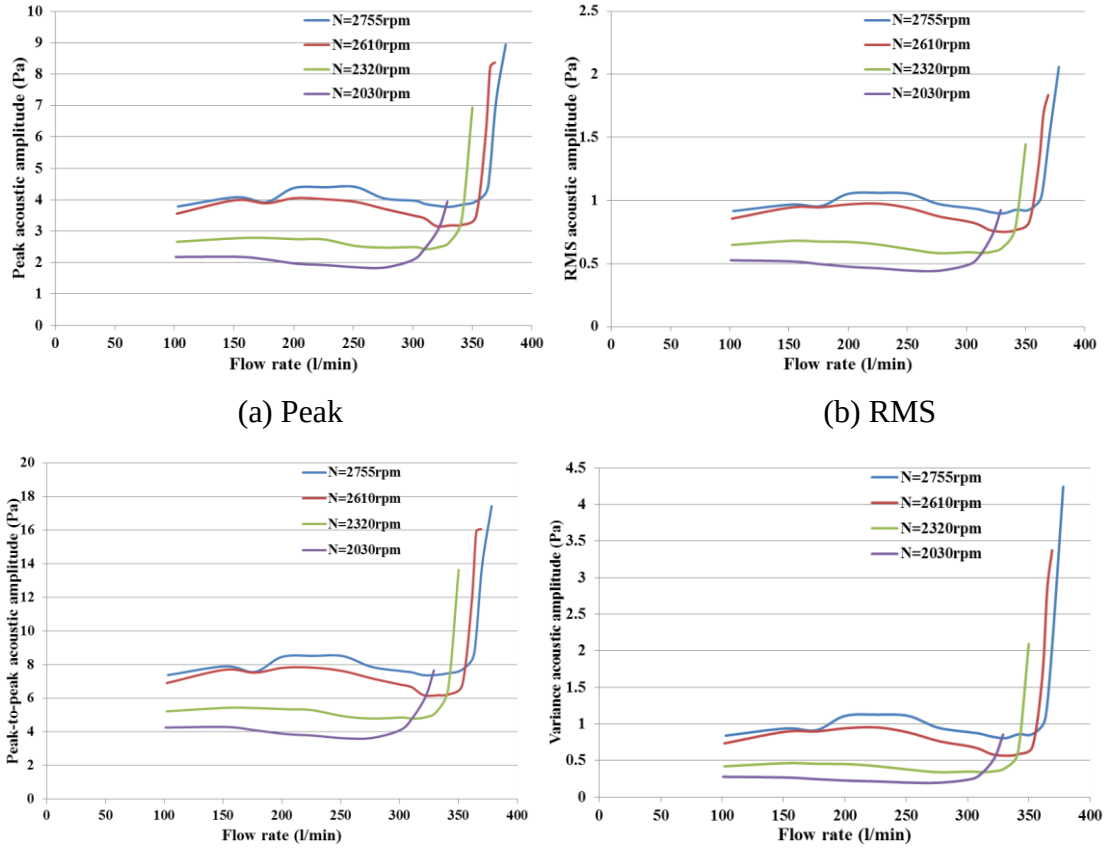

(a) Peak (b) RMS

(c) Peak-to-peak (d) Variance

Figure 7-8: Comparison between different statistical features of the acoustic amplitude in time domain under different rotational speeds

7.5.2. The Analysis of the Acoustic Signal Based on Frequency Domain at Different Pump Rotational Speeds

Figure 7-9 depicts the acoustic signals in frequency domain at different frequency ranges of from 0Hz-1kHz to 1kHz-2kHz under different flow rates and pump rotational speeds are 2610, 2320, and 2030rpm. It can be seen that there is no significant change in the level of amplitude of the acoustic signals when the pump works at a capacity lower than 350(l/min). However, a small increase in the level of amplitude of the acoustic signal occurred at flow rate higher than 350(l/min). It is also seen that there are various frequencies at this low range of frequency as shown in this figure. These dominant frequencies includes the rotation frequency and its harmonics, the BPF and their harmonics and also frequencies that are due to the noise from the environment, especially around the microphone, for all cases being investigation. Furthermore, the acoustic amplitude was increased with rotational speed increased.

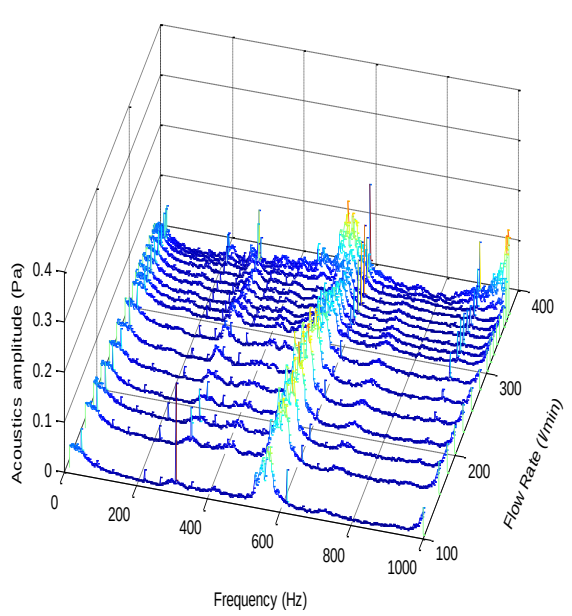

(a)

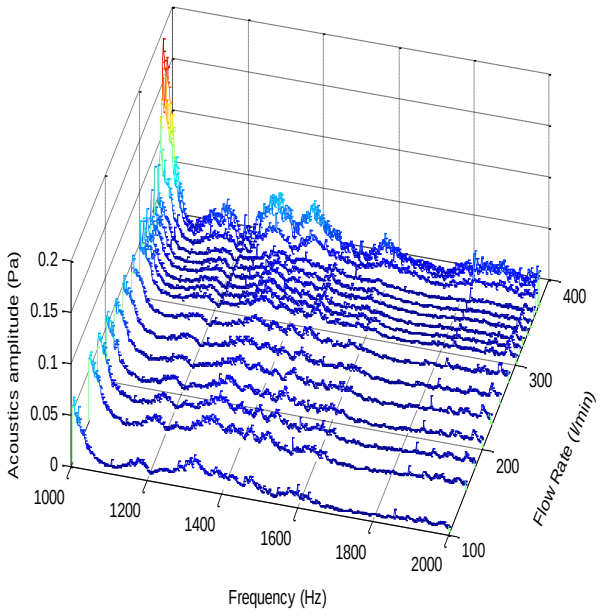

(b)

N=2610rpm

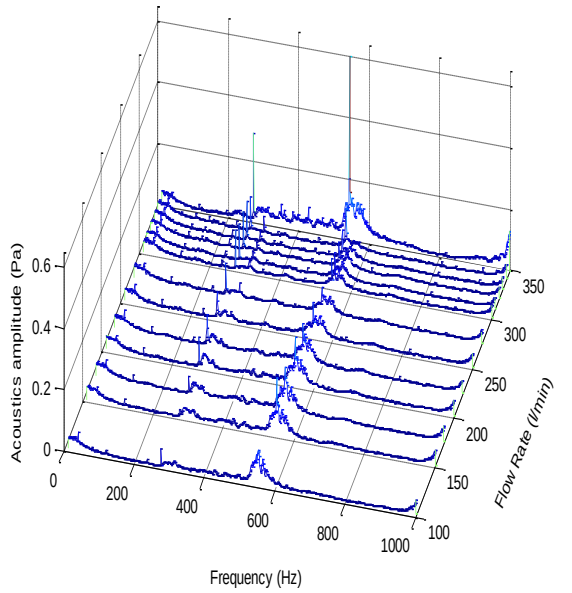

(a)

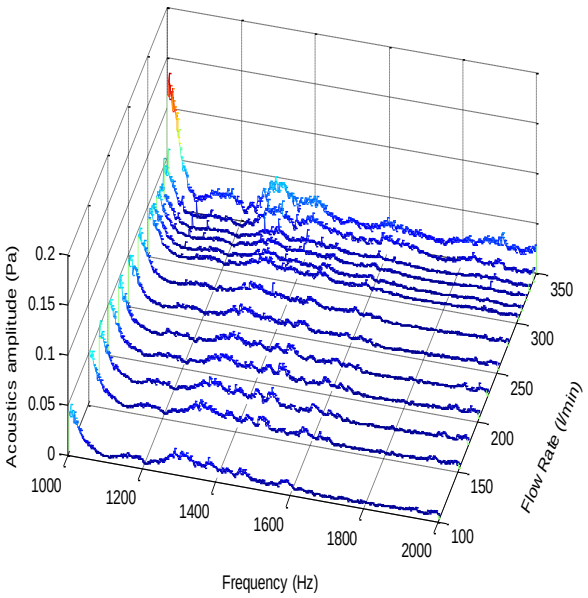

(b)

N=2320rpm

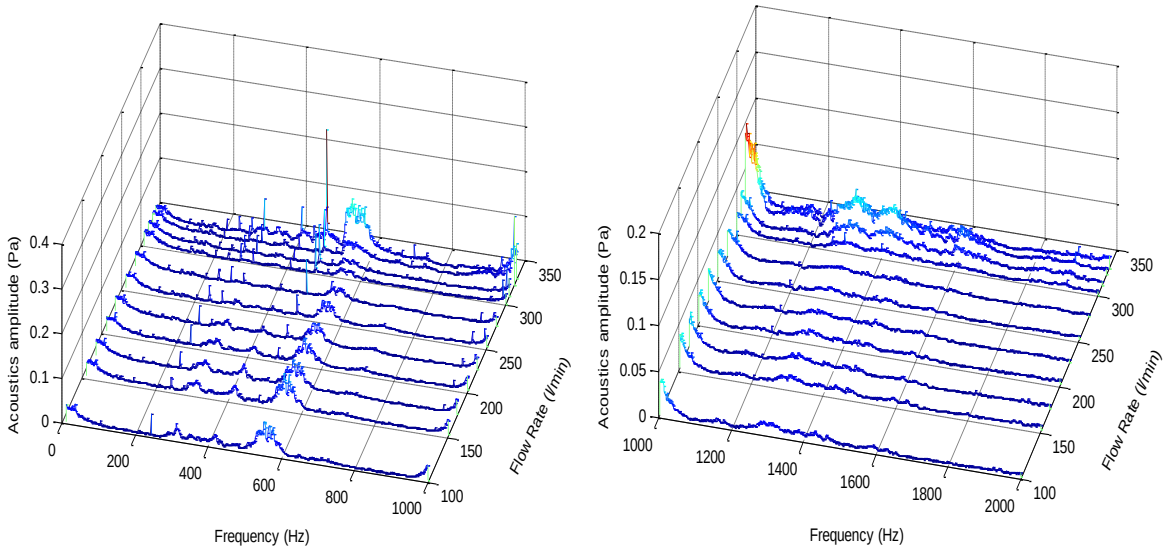

(a) N=2030rpm (b)

Figure 7-9: Acoustic signal in frequency domain under various flow rates and frequency range from (a) 0Hz-1kHz to (b) 1kHz-2kHz

From the above analysis findings, it can be concluded that the reason behind the increase in the acoustic level for the centrifugal pump is due to the inception of cavitation that occurs under high flow rate.

For further investigations, Figure 7-10 depicts the analysis of the acoustic signal in the frequency domain using mean statistical feature values under various flow rates and different pump rotational speeds for the various range of frequencies 0Hz-1kHz, 1kHz-2kHz, 2kHz-10kHz, and 10kHz-15kHz. For comparison purposes of the above cases, it can be seen that the maximum mean value for N=2755rpm is considerably higher than for the other three cases N=2610rpm, N=2320rpm, and N=2030rpm. Also, from above findings, it can be noticed that the pump rotational speed is proportional to the increase of the acoustic amplitude which means when the pump rotational speed is increased this leads to an increase of the acoustic amplitude as summarised in Table 7-3, due to the same reasons as in the previous figure. It is also seen from these figures that the minimum mean acoustic amplitude value increases as the pump rotational speed increases as summarised in Table 7-4.

Table 7-3 Summary of the results comparison for the maximum mean acoustic amplitude features at different rotational speed and frequency ranges

Rotational speed	Mean value 0Hz-1kHz	Mean value 1kHz-2kHz	Mean value 2kHz-10kHz	Mean value 10kHz-15kHz
(rpm)	(Pa)	(Pa)	(Pa)	(Pa)

2755	0.0466	0.0424	0.0156	0.0084
2610	0.0388	0.0355	0.0155	0.0083
2320	0.0345	0.0260	0.0109	0.0062
2030	0.0229	0.0151	0.0064	0.0033

Table 7-4 Summary of the results comparison for the minimum mean acoustic amplitude features of the pump at different rotational speed and frequency ranges

Rotational speed	Mean value 0Hz-1kHz	Mean value 1kHz-2kHz	Mean value 2kHz-10kHz	Mean value 10kHz-15kHz
(rpm)	(Pa)	(Pa)	(Pa)	(Pa)
2755	0.0205	0.0131	0.0061	0.0011
2610	0.019	0.0115	0.0057	0.0012
2320	0.0157	0.0087	0.0042	0.0012
2030	0.0127	0.0062	0.0040	0.0010

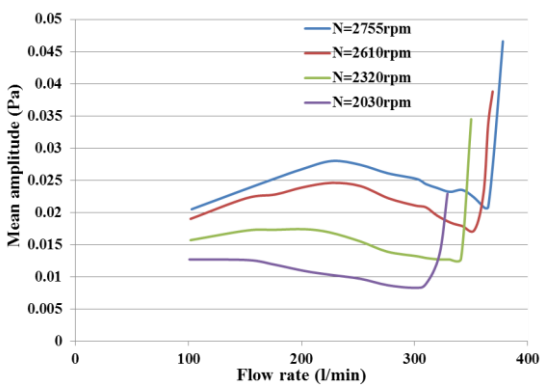

(a) 0Hz-1kHz

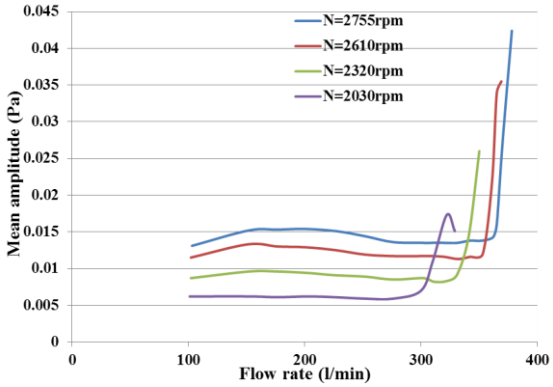

(b) 1kHz-2kHz

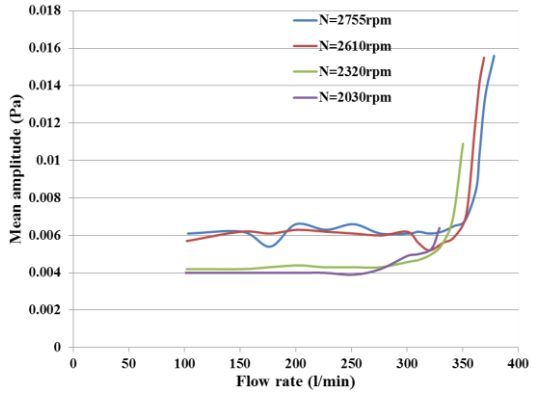

(c) 2kHz-10kHz

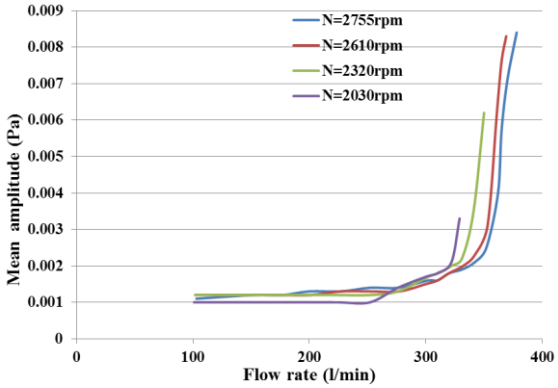

(d) 10kHz-15kHz

Figure 7-10: Comparison between mean acoustic amplitude values in frequency domain for different rotational speeds and frequency ranges

Figure 7-11 depicts the analysis of the acoustic signal in the frequency domain using RMS statistical feature under various flow rates and different pump rotational speeds for the different range of frequencies 0Hz-1kHz, 1kHz-2kHz, 2kHz-10kHz, and 10kHz-15kHz, of the aforementioned cases for comparison purposes. It can be seen that the maximum RMS value for N=2755rpm is considerably higher than for the other three cases N=2610rpm, N=2320rpm,

and N=2030rpm. It is also further noticed that from these figures the maximum and minimum RMS acoustic amplitude value increases as the pump rotational speed increases as summarised in Table 7-5 and Table 7-6.

Table 7-5 Summary of the results comparison for the maximum RMS acoustic amplitude features for the under at different rotational speed and of frequency ranges

Rotational speed	RMS value 0Hz-1kHz	RMS value 1kHz-2kHz	RMS value 2kHz-10kHz	RMS value 10kHz-15kHz
(rpm)	(Pa)	(Pa)	(Pa)	(Pa)
2755	0.0604	0.0510	0.0198	0.0087
2610	0.0499	0.0427	0.0197	0.0085
2320	0.0480	0.0307	0.0132	0.0064
2030	0.0327	0.0220	0.0081	0.0035

Table 7-6 Summary of the results comparison for the minimum RMS acoustic amplitude features for the at different rotational speed and of frequency range

Rotational speed	RMS value 0Hz-1kHz	RMS value 1kHz-2kHz	RMS value 2kHz-10kHz	RMS value 10kHz-15kHz
(rpm)	(Pa)	(Pa)	(Pa)	(Pa)
2755	0.0252	0.0160	0.0084	0.0012
2610	0.0215	0.0134	0.0080	0.0012
2320	0.0164	0.0098	0.0064	0.0012
2030	0.0108	0.0070	0.0054	0.0011

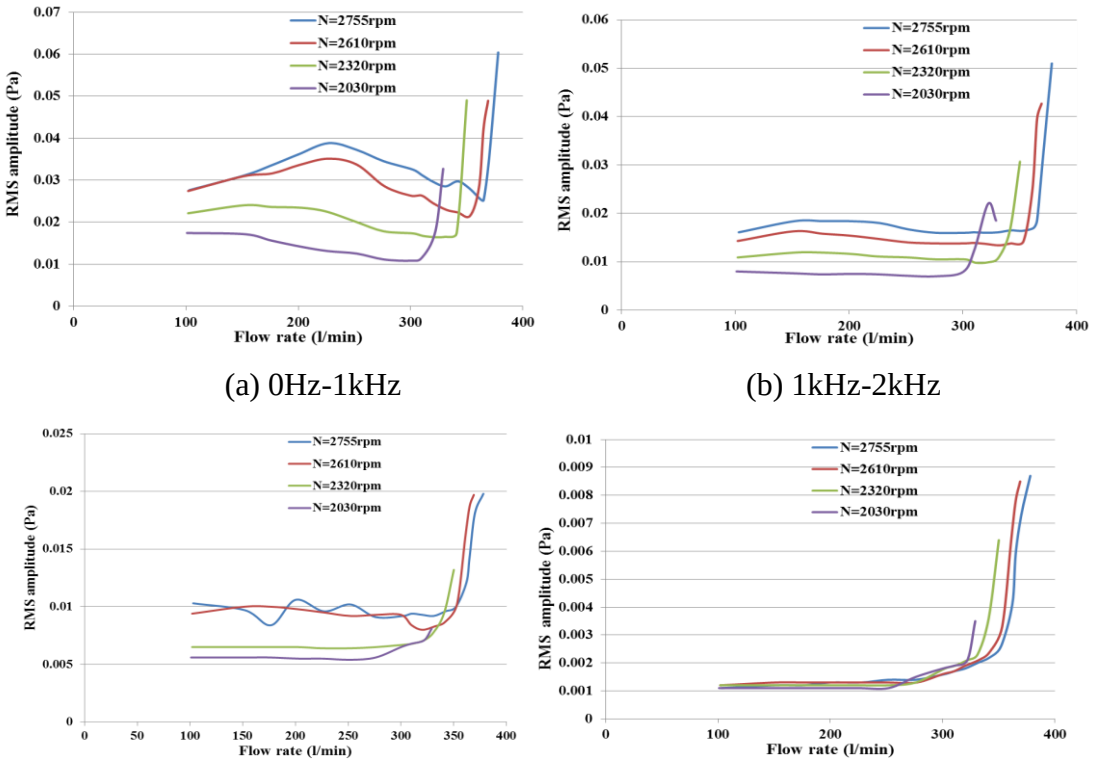

(a) 0Hz-1kHz (b) 1kHz-2kHz

(c) 2kHz-10kHz (d) 10kHz-15kHz

Figure 7-11: Comparison between RMS acoustic amplitude values in frequency domain for different rotational speeds and frequency ranges

7.6. Summary of the Analysis of Different Flow Rates and Pump Rotational Speeds using Acoustic Technique

A detailed analysis into the effect of different flow rates and pump rotational speeds, through the use of acoustic signals, in order to detect cavitation within a centrifugal pump revealed the following results:

1. The acoustic signal analysis in time domain using different statistical features can provide an initial indication to determine when cavitation was occurred in the pump.
2. The level of acoustic amplitude is directly proportional to the pump flow rate, which increases as the flow rate increases.
3. The level of noise signal increases when the pump operates under cavitation condition.
4. The frequency domain was a satisfactory technique to predict the inception and development of cavitation within a pump.
5. There are various frequencies in frequency domain for the acoustic signal, which are the rotation frequency and its harmonics, BPF and other frequencies due to environmental noise around the pump.
6. The analysis on the acoustic signals in frequency domain using different range of frequencies provides good information regarding the prediction of cavitation in the pump.
7. The use of mean and RMS acoustic amplitude values to analyse acoustic frequency under various frequency ranges starting from 0Hz to15kHz provides good indication for detecting cavitation within a pump.
8. The analysis of variation in the level of acoustic amplitude under different flow rate in time domain by using different statistical features and also in frequency domain under different range of frequencies, show a good agreement with the characteristics of cavitation, presented using the NPSH curve in Chapter six.
9. The maximum statistical features in time domain for N=2755rpm are considerably higher than for the other cases.
10. The mean and RMS feature values under N=2755rpm are considerably higher than for the other three cases.
11. The results show that using low-frequency range between 1kHz and 2kHz was sensitive to predict cavitation in the pump. Therefore, it is possible to use a microphone with a low range of frequency, which then leads to decrease in the cost of the sensor when compared to using a microphone with a high range frequency.

12. The results of NPSH in the previous chapter showed that when the value of NPSH is reduced, inception of cavitation starts to occur and develops further within a pump. It can be clearly seen that the level of noise rapidly increases with the increase in the different level of cavitation. It can also be observed that the value of noise level reaches its highest value under full development of cavitation.
13. A series of experimental tests were carried out to collect the acoustic signal from a centrifugal pump. Based on these results, it can be concluded that the acoustic technique is effective to detect the different levels of cavitation.
14. Both techniques (vibration and acoustic) appear to have approximately the same characteristics for detecting the different level of cavitation at various operating conditions.

7.7. Effect of Suction Valve Opening on the Level of Acoustic Signal to Predict Cavitation within a Centrifugal Pump

To analyse the various levels of cavitation under different operation conditions, the effect of the decrease in the inlet pressure of a centrifugal pump can be investigated through controlling the inlet suction valve openings. The acoustic signal can be collected from the experimental setup of the centrifugal pump under different suction valve openings using microphone at various flow rates of 103, 200, 302(l/min), which were selected for this analysis. The flow at the suction and discharge sides of the pump was adjusted through the two valves. The suction valve of the pump is used to control the inlet pressure between the inlet pipe and the inlet impeller in order to simulate cavitation condition through decreasing the pressure at the inlet pipe below the water vapour pressure. The suction valve is first fully open (at 100%) and then changed through throttling of the valve progressively, step by step at 10% intervals until cavitation occurs due to decrease of the inlet pressure in the inlet pipe. The pump rotational speed N=2755rpm is constant. The next sections represent and analyse the acoustic signal that were obtained from the experimental test based on the different suction valve openings.

7.7.1. Analysis on the Acoustic Signals in Time Domain under Different Suction Valve Openings at Flow Rate of 103(l/min)

This section was analysed the acoustic signals in time domain using the same various statistical features such as peak, RMS, peak-to-peak and variance values in order to obtain more details regarding the change in the acoustic amplitude under different suction valve openings and hence, to predict cavitation within a pump based on different operation conditions.

Figure 7-12 depicts the analysis of the acoustic signal for the pump, using the above mentioned features, at different suction valve openings. It can be seen from these figures that there is no significant change in the trend for the acoustic amplitude when the pump operates between suction valve openings of 100% and 40%. However, the trends for the above features rapidly increase when the pump operates between the suction valve openings of 40% to 35%. The main reason is because when the suction valve openings decreases, it leads to decrease in the inlet suction pressure below the water vapour pressure. In that case, cavitation starts to occur within a pump and it rapidly increases when the inlet suction pressure continuously decreases. Due to these conditions, cavitation should be fully developed which then causes quick reduction in the performance of the pump. It can be observed that the above results were agreed with vibration results in previous chapter.

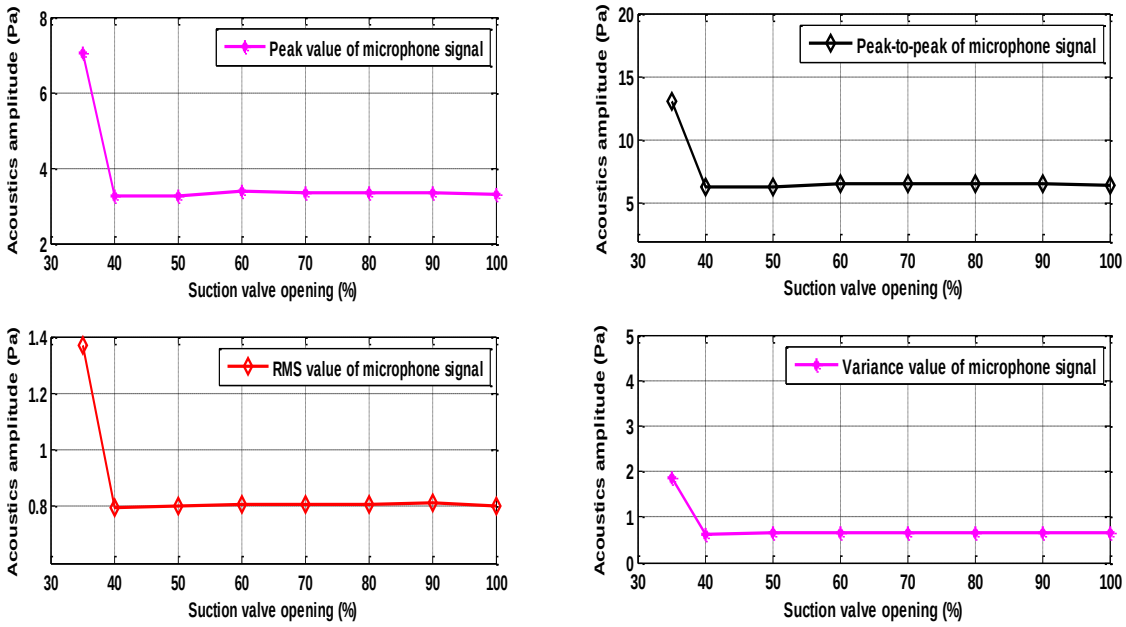

(a) Peak and RMS (b) Peak-to-peak, and variance

Figure 7-12: Trends of different statistical features of the acoustic signal in time domain at different suction valve openings at 103(l/min)

7.7.2. Analysis of the Acoustic Signal in Frequency Domain under Different Suction Valve Openings at Flow Rate of 103(l/min)

Figure 7-13 (a) depicts the acoustic signals in frequency domain under various suction valve openings, corresponding to the occurrence of cavitation within the pump at flow rate of 103(l/min), N=2755rpm and for 0Hz to 1kHz range of frequency. It can be observed that the acoustic peak amplitude was occurred at two dominant distinctive frequencies. The first one is the rotational frequency at 45.9Hz and the second is BPF at 229.58Hz, and their harmonics. It can be seen from this figure that no significant change occurs in the level of acoustic amplitude when the pump operates between suction valve openings of 100% and 40%. However, at this range of frequency, it can be seen that there is a small change in the acoustic amplitude when the pump operates between suction valve openings of 40% and 35%. Therefore, it can be concluded that this range of frequency was effective to predict cavitation within a pump.

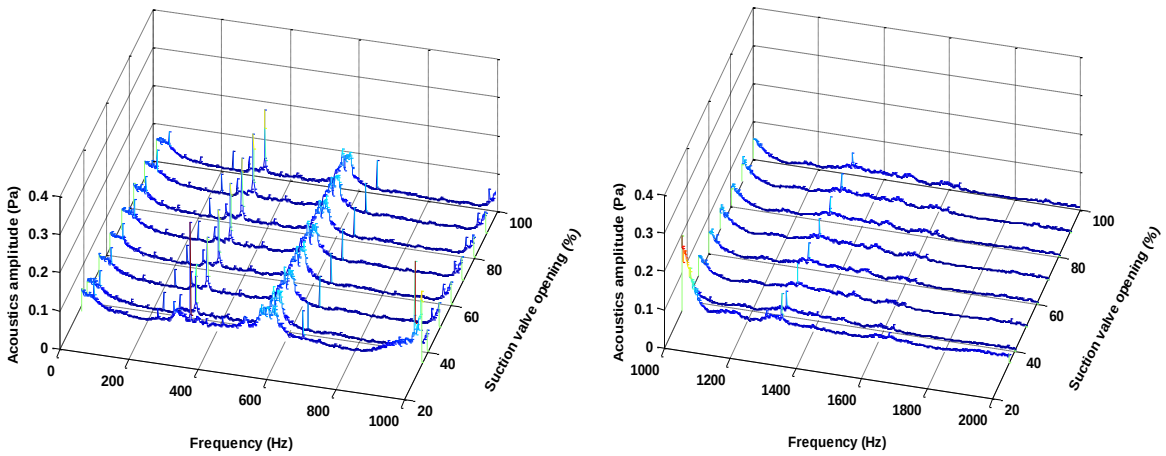

(a) (b)

Figure 7-13: Acoustic signal in frequency domain under various suction valve opening and the frequency range from (a) 0Hz-1kHz to (b) 1kHz-2kHz at 103(l/min)

For more details, Figure 7-13 (b) depicts the analysis on the acoustic signal at range of frequency between 1kHz and 2kHz in order to obtain more information regarding the prediction of cavitation in the pump. The same two dominated frequencies can be observed as in the previous range of frequency. The first one is the rotational frequency while the second is the BPF and their harmonics. It can be observed from this figure that there is no change in the acoustic amplitude between suction valve openings 100% and 40% as changes in the acoustic amplitude occurs when the pump operates between suction valve openings from 40% and 35%. The reason for this is because when cavitation occurs within the pump it generates smaller

bubbles and the collapse of these bubbles inside the pump then create more random noise, hence, the amplitude of acoustic amplitude increases. It can be observed from this that this range of frequency is also effective to predict cavitation as many high peaks occur in the acoustic amplitudes after suction valve opening of 40% as shown in this figure.
It can be noticed that analysis in the level of acoustic amplitude in 1kHz to 2kHz range of frequencies provides suitable indication to predict cavitation.

In order to obtain more information regarding acoustic signal in frequency domain, Figure 7-14 and Figure 7-15 depict the mean and RMS acoustic amplitude features that were calculated from the frequency domain at the different suction valve openings. It can be seen that the mean and RMS acoustic amplitude features for the various range of frequencies have approximately the same trend for the different suction valve openings. Also, there is a small change between the suction valve openings from 100% to 40%, which then increases for the suction valve openings between 40% and 35% due to the operation of the pump at certain flow rate through the fixed discharge valve. After that, the suction valve was progressively closed until the occurrence of cavitation at the suction side of the pump, which leads to the generation of high noise and vibration. The reason for this is due to the high amount of bubbles that were formed making these bubbles clearly visible at the inlet pipe. It can be concluded from these figures that the range of frequency between 0Hz and 2kHz was sensitive for detection of the occurrence of cavitation within a pump under different suction valve openings. Moreover, the above results were agreed with vibration results in previous chapter.

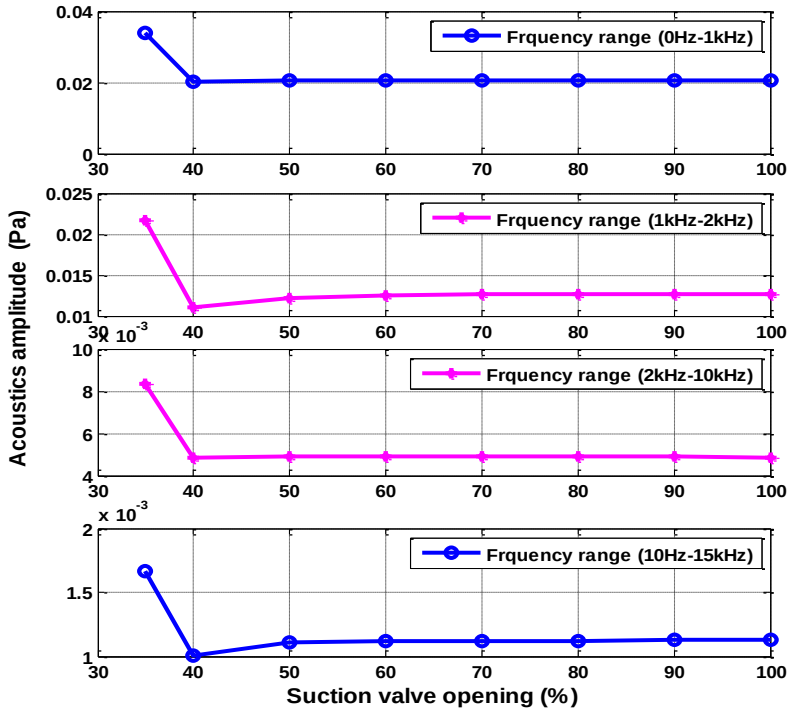

Figure 7-14: Mean acoustic amplitude value of the frequency range from 0Hz to 15kHz at 103(l/min)

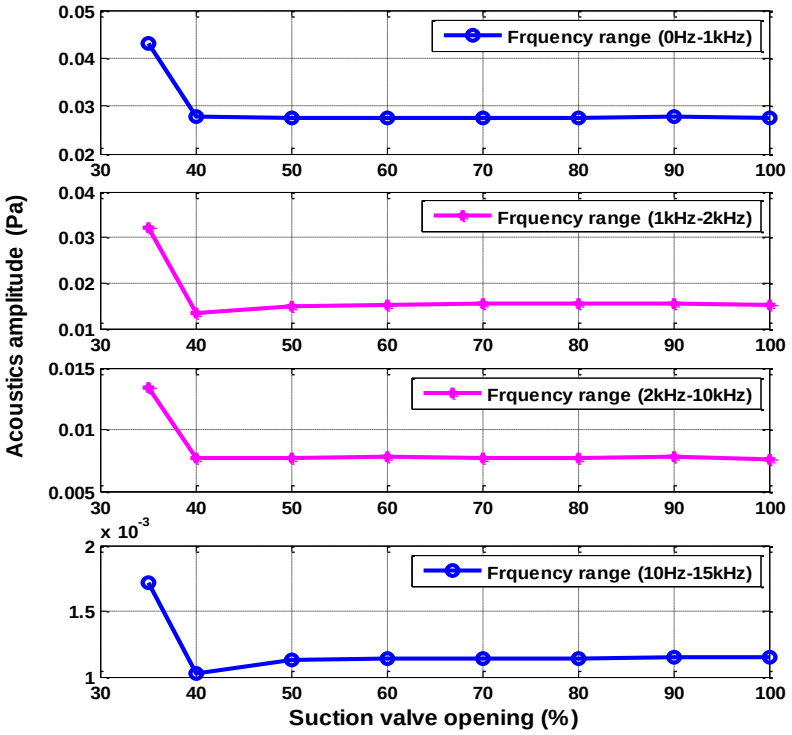

Figure 7-15: RMS acoustic amplitude value of the frequency range from 0Hz to 15kHz at 103(l/min)

7.7.3. Analysis on the Acoustic Signals in Time Domain under Different Suction Valve Openings and Flow Rates

Figure 7-16 depicts the various statistical features which include the peak, RMS, peak-to-peak and variance values under different flow rates and different suction valve openings for comparison purposes for the aforementioned cases. It can be observed that the maximum peak value for Q=302(l/min) is considerably higher than for the other two cases Q=200(l/min), and Q=103(l/min) by 35.59% and 72.03%. Also for the maximum RMS value, it is higher by 32.47%, and 65.81% for the other two cases. For the maximum peak-to-peak, it is higher by 33.88%, and 70.44%, and for the maximum variance value by 54.09%, and 88.34% respectively as shown in Table 7-7. From the above findings, it can be concluded that the suction valve opening is inversely proportional to increase in the acoustic amplitude. This means that when the suction valve opening decreases, it leads to increase in the acoustic amplitude.

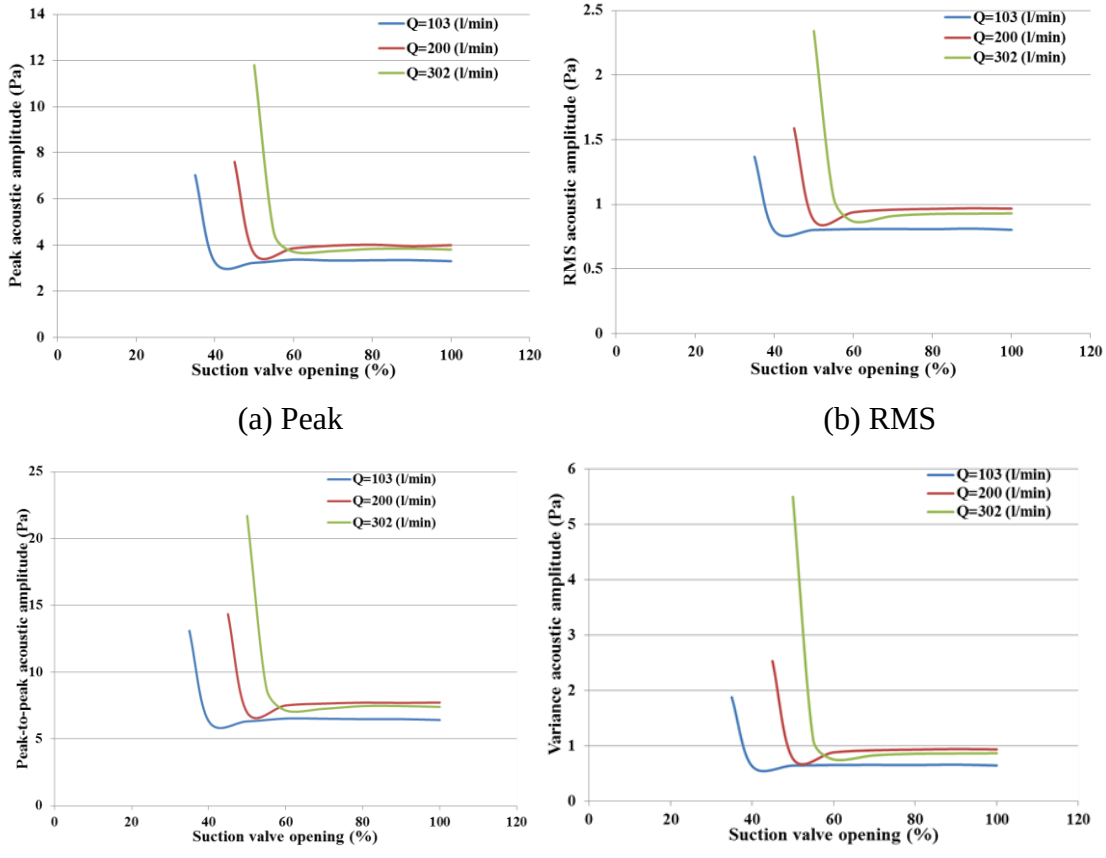

(a) Peak (b) RMS

(c) Peak-to-peak (d) Variance

Figure 7-16: Comparison between different statistical features of the acoustic signal in time domain under different flow rates and suction valve openings

Table 7-7 Summary of the maximum statistical features results for the acoustic amplitude at different flow rates

Flow rate (l/min)	Peak (Pa)	RMS (Pa)	Peak-to-peak (Pa)	Variance (Pa)
103	7.03	1.36	13.09	1.87
200	7.60	1.58	14.34	2.52
302	11.80	2.34	21.69	5.49

It can be concluded that the use of the above statistical features for the acoustic amplitude provides a good indication regarding the cavitation occurrence in the pump. Also, the results showed that the level of acoustic stability of a pump is associated directly with the suction valve opening under different flow rates.

7.7.4. Analysis of the Acoustic Signal in Frequency Domain under Different Suction Valve Openings and Flow Rates

Figure 7-17 depicts the analysis on the acoustic signal at different flow rates of 200 and 302(l/min), N=2755rpm, under different inlet suction valve openings, and for the range of frequency from (0Hz-1kHz) to (1kHz-2kHz). It can be seen that the first peak acoustic amplitude was at frequency 49.5Hz, representing the rotational frequency with the second, third and fourth harmonics at 91.8, 173.75, and 183.66Hz respectively. The second dominant peak acoustic amplitude was at frequency 229.58Hz, representing the BPF. The peak acoustic amplitude considerably increases upon cavitation occurrence in the pump. Furthermore, it is obvious that acoustic amplitude follows the same trend as in the previous case where Q=103(l/min). For Q=200(l/min) no significant change occurred in the level of the acoustic amplitude under suction valve openings between 100 and 50%. However, the change in acoustic amplitude was relatively higher at suction valve openings between 50 and 45%, compared to the suction valve openings between 100 and 50%. Furthermore, for Q=302(l/min) the change in acoustic amplitude was relatively higher at the suction valve openings between 60 and 50% when compared to the suction valve openings between 100 and 60% due to the cavitation condition.

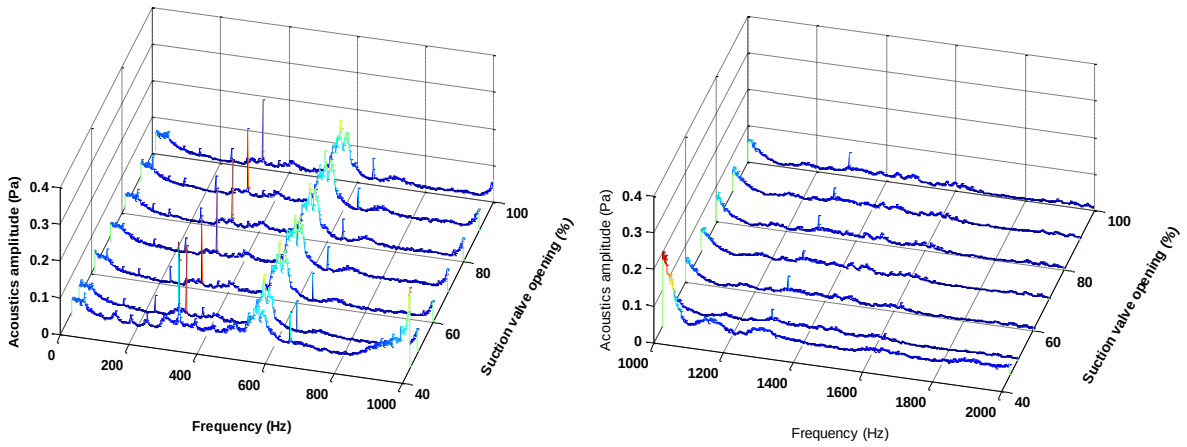

(a) Q=200(l/min) (b)

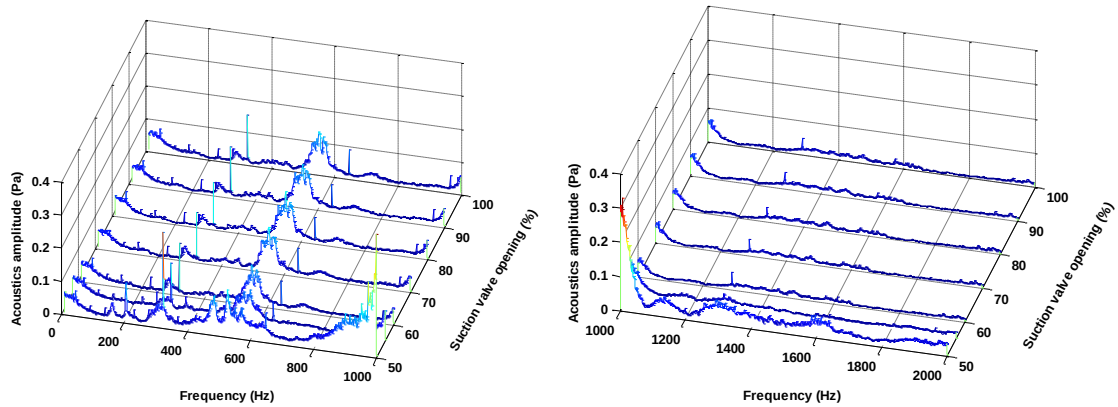

(a) Q=302(l/min) (b)

Figure 7-17: Acoustic signal in frequency domain under various suction valve opening and the frequency range from (a) 0Hz-1kHz to (b) 1kHz-2kHz at 200 and 302(l/min)

For comparison purposes Figure 7-18 and Figure 7-19 depict the mean and RMS acoustic amplitudes in frequency domain for the different range of frequencies including 0Hz-1kHz, 1kHz-2kHz, 2kHz-10kHz, and 10kHz-15kHz, under different suction valve openings and flow rates for the aforementioned cases. The maximum mean acoustic amplitude value at different suction valve openings can be observed at Q=302(l/min) for 0Hz-1kHz range of frequency, is considerably higher than for the other two cases Q=200(l/min), and Q=103(l/min) by 29.42% and 35.66%. In addition, for 1kHz-2kHz range of frequency, it is higher than for the other two cases by 37.35%, and 49.56%. Also for 2kHz-10kHz range of frequency, it is higher by 36.25%, and 47.50%, and for 10kHz-15kHz range of frequency, it is higher by 52.38%, and 59.52% respectively as summarised in Table 7-8. The RMS value has the same mean value trend as it did for when Q=302(l/min), which is also considerably higher than for the other two cases (Q=200(l/min) and Q=103(l/min)) at different suction valve openings as summarised in Table 7-9.

Table 7-8 Summary of the maximum mean acoustic amplitude values at different flow rates and suction valve openings and for frequency range (0Hz-15kHz)

Flow rate	Mean value 0Hz-1kHz	Mean value 1kHz-2kHz	Mean value 2kHz-10kHz	Mean value 10kHz-15kHz
(l/min)	(Pa)	(Pa)	(Pa)	(Pa)
103	0.0341	0.0217	0.0084	0.0017
200	0.0375	0.0270	0.0102	0.0020
302	0.0530	0.0431	0.0160	0.0042

Table 7-9 Summary of the maximum RMS acoustic amplitude values at different flow rates and suction valve openings and frequency range (0Hz-15kHz)

Flow rate	RMS value 0Hz-1kHz	RMS value 1kHz-2kHz	RMS value 2kHz-10kHz	RMS value 10kHz-15kHz
(l/min)	(Pa)	(Pa)	(Pa)	(Pa)
103	0.0432	0.0320	0.0134	0.0017
200	0.0468	0.0382	0.0165	0.0021
302	0.0674	0.0591	0.0240	0.0043

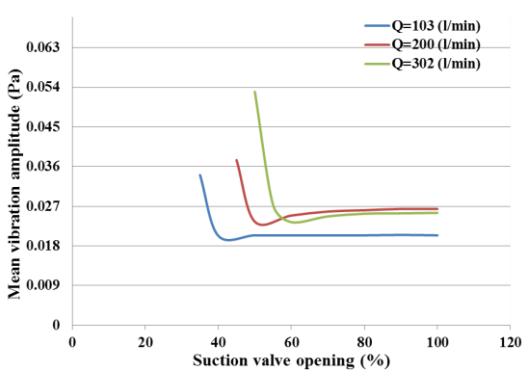

(a) 0Hz-1kHz

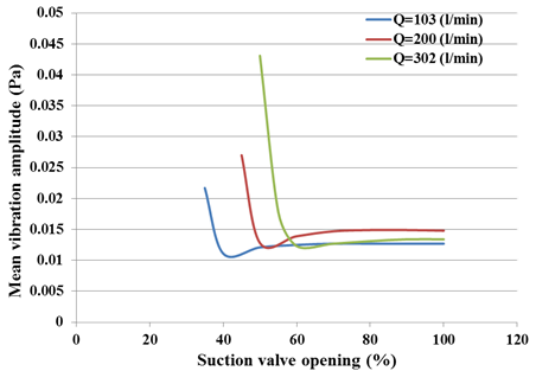

(b) 1kHz-2kHz

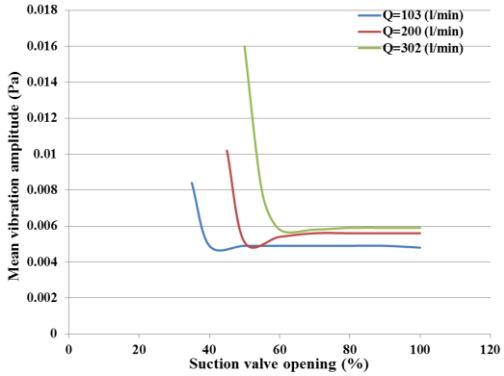

(a) 2kHz-10kHz

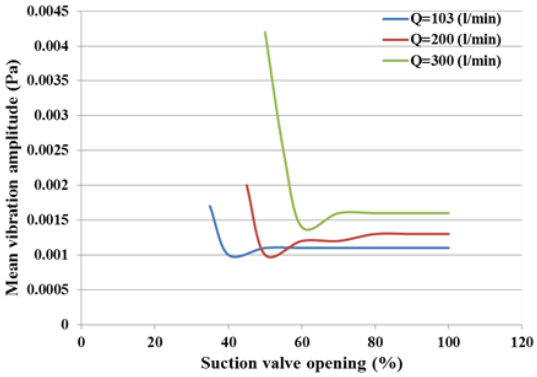

(b) 10kHz-15kHz

Figure 7-18: Comparison between mean acoustic amplitude values in frequency domain for different frequency ranges under different flow rates and suction valve openings

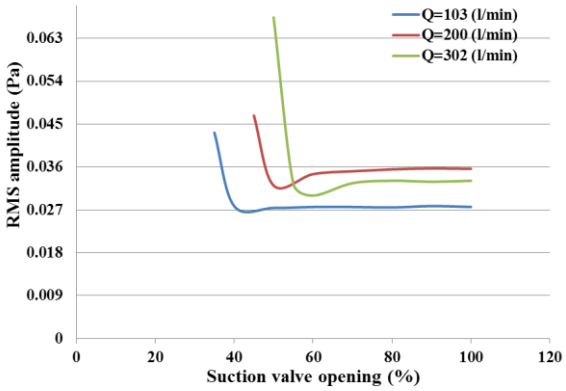

(a) 0Hz-1kHz

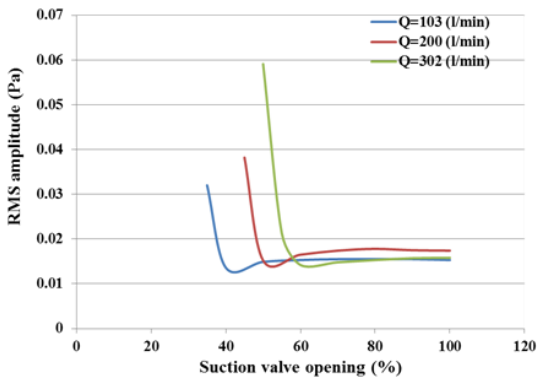

(b) 1kHz-2kHz

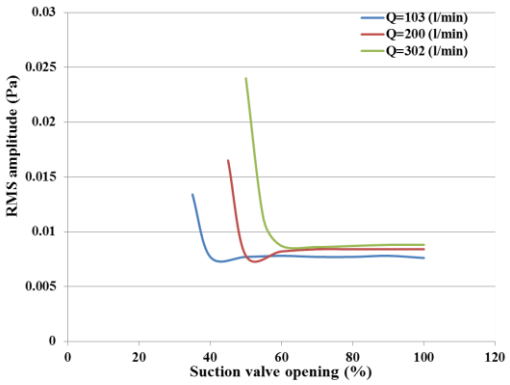

(a) 2kHz-10kHz

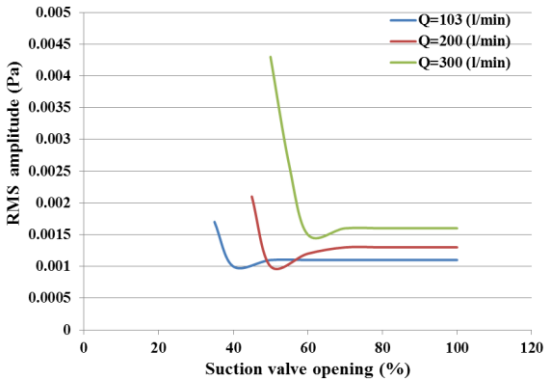

(b) 10kHz-15kHz

Figure 7-19: Comparison between RMS acoustic amplitude values in frequency domain for different frequency ranges under different flow rates and suction valve openings

7.8. Summary of the Analysis of Different Suction Valve Openings

A detailed analysis of the effect of the different suction valve openings on the acoustic signal to predict cavitation in the pump revealed the following results:

1. The acoustic signal analysis in time domain using different statistical features can provide a good indication to determine when cavitation was occurred in the pump under different suction valve openings.
2. Analysis on the acoustic signal using the above mentioned features show different regions. The first region revealed no significant change on the level of acoustic signal. The second region showed that the trends for the above features rapidly increases due to decrease in the suction valve opening and hence, the pump operating under cavitation condition. The third region showed the maximum acoustic level due to when the inlet suction pressure continuously decreases.

3. The maximum amplitude for the peak, RMS, peak-to-peak and variance values in the time domain at different suction valve openings was at Q=302(l/min).
4. Using frequency domain analysis to analyse the acoustic amplitude, was a suitable technique to predict cavitation within a pump at different suction valve openings.
5. The mean and RMS acoustic amplitudes features in frequency domain, at different inlet suction valve openings and various frequency ranges. Different regions were also observed the first region shows that the acoustic amplitudes does not go through any significant change. The second region also shows that acoustic amplitudes increase due to the cavitation occurrence.
6. The mean and RMS for acoustic amplitude in frequency domain increases as the suction valve opening is decreased and the above mentioned statistical features increased with an increase in the flow rate.
7. Based on the above findings, the analysis on the acoustic signal in time domain can provide a primary indicating feature regarding quantifying the detection of the inception and severity different levels of cavitation. A secondary indication can be quantified in the frequency domain analysis for the acoustic signals under different frequency ranges.

7.9. Effect of Different Amounts of Air Injection in the Pump using Acoustic Technique

For this experimental measurement, different rates of air are injected into the suction pipe side of the pump. Also, the pump was tested under various flow rates, corresponding to normal operating conditions (low flow rate) and cavitation conditions (high flow rate). Acoustic signals were collected and analysed in detail in this section in order to study the effect of the different rates of air injections within a centrifugal pump.

7.9.1. Time Domain Analysis on the Acoustic Signal at Air Injection Rate of 0.4(l/min)

Figure 7-20 depicts the acoustic signal of the centrifugal pump in time domain (wave form) obtained at 0.4(l/min) air injection rate, N=2755rpm and under various flow rates. As seen from this figure, there are different levels of the acoustic amplitudes depending on the various flow rates. It can be seen that when the pump operates under low flow rate between 175 and 343(l/min), the levels of acoustic amplitudes was lower than when the pump operates at high flow rate. Hence, the acoustic amplitude signals increase as the flow rate increases. This is mostly due to the start of cavitation occurrence at high flow rate which then develops further when the flow rate is increased, also, due to the effect of air injection within a pump. It can be

observed that when the pump operates under cavitation conditions with air injection as in this case, the trend for the acoustic amplitude was more random with high peaks when compared to normal operation conditions (low flow rate). The reason is due to the occurrence of cavitation and the effect of air injection at the pump. It is also due to the hydraulic losses. By comparing between these figures at the different flow rates, it can be concluded that the acoustic signals are sensitive to predict the effect of cavitation and air injection within a pump.

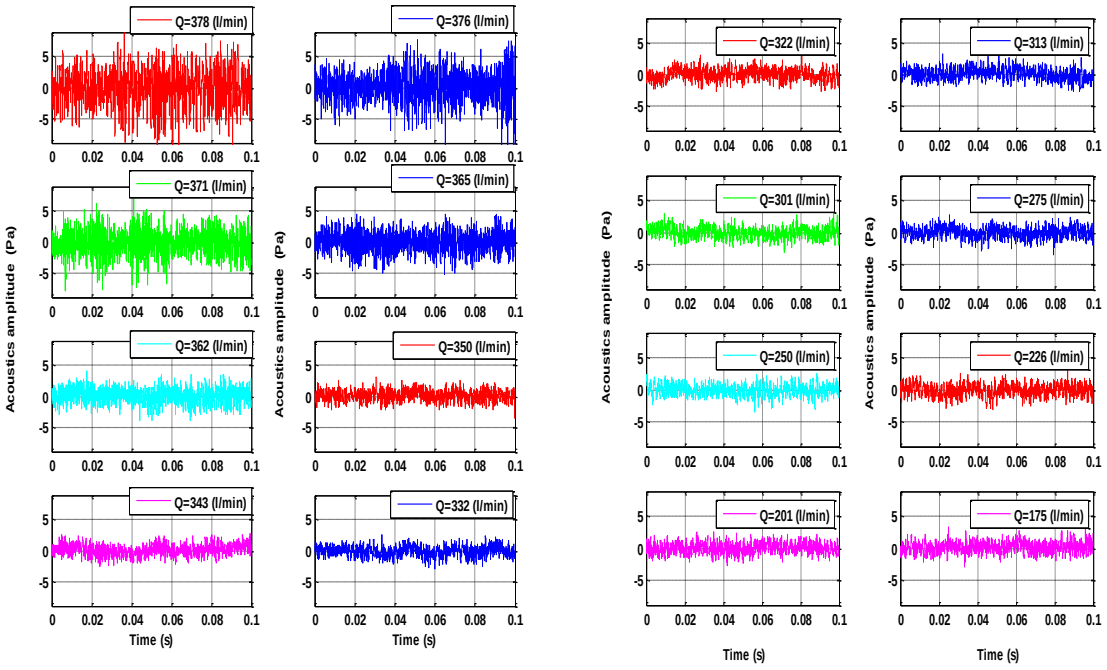

Figure 7-20: Analysis of the acoustic signal in TWFA under various flow rates and air injection 0.4(l/min)

For further investigation regarding the effect of air injection within a centrifugal pump, Figure 7-21 depicts the analysis on the acoustic signal, with and without air injection which were obtained experimentally with operating conditions such as 0.4(l/min) air injection rate, N=2755rpm and at various measurements of flow rates. Statistical features used for this analysis as the same as those in previous sections. It can be seen from this figure that there is a small indication of variance in the analysis of the level of acoustic amplitude at flow rate below 350(l/min) for both cases (with and without air injection). However, the results from experimental measurements revealed the same trends for these statistical features for the acoustic signals at different flow rates, which significantly increase when the pump operates under flow rate higher than 350(l/min) for both cases (with and without air injection). Also, trends for all the features with air injection starts to increase before trends for the features without air injection when the pump operates at flow rate higher than 350(l/min). The reasons

are due to the effect of the air injection within a pump, in addition to the occurrence of cavitation at high flow rate. Furthermore, when the pump operates at flow rate lower than 350(l/min), the trend curves for all the features with air injection were slightly lower than the trends without air injection. This is because of further hydraulic noise losses due to the effect of air injection and the internal recirculation, which occurs at the discharge and suction regions within an impeller.

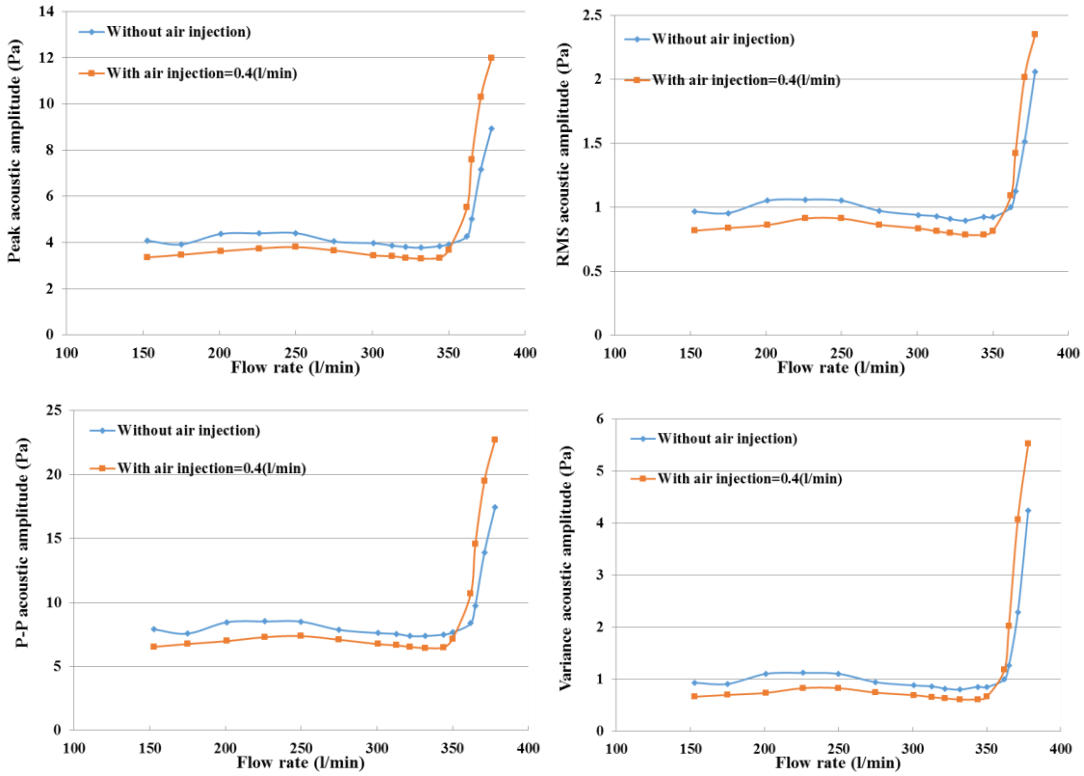

Figure 7-21: Trends for peak, RMS, peak-to-peak and variance features, with and without air injection for the acoustic signal at 2755rpm with air injection rate of 0.4(l/min)

7.9.2. Frequency Domain Analysis on the Acoustic Signal at Air Injection Rate of 0.4(l/min)

Figure 7-22 depicts the frequency domain analysis for the acoustic signal at 0.4(l/min) air injection rate, N=2755rpm, for various measurements of flow rates and for the different range of frequencies which are (a) 0Hz-1kHz and (b) 1kHz-2kHz. It can be seen that different types of frequencies occurred, the first being the rotational frequency of 45.9Hz, which occurred the most, the second, was the BPF occurring at 229.5Hz. It can be seen that the acoustic amplitude increases with increase in the flow rate. This is mostly due to the cavitation occurrence in the pump and the effect of air injection. From the experimental results in frequency domain, it is

observed that there are some peak amplitudes that change with frequencies, which could be due to the environmental noise around the pump as mentioned earlier in the previous sections.

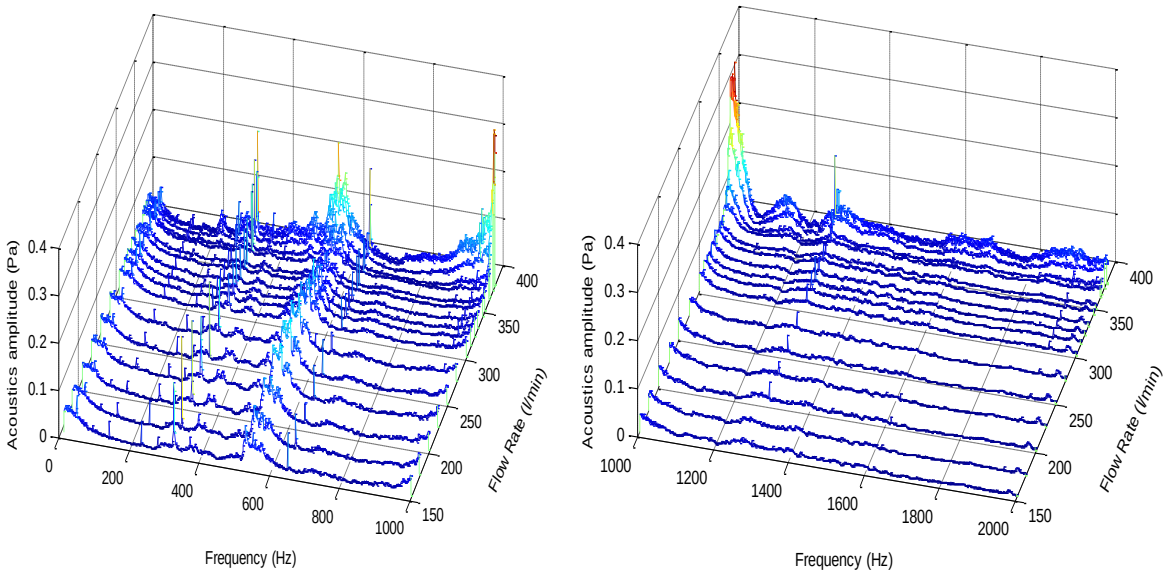

(a) (b)

Figure 7-22: Acoustic signal in frequency domain at various flow rates with frequency range from (a) 0Hz-1kHz to (b) 1kHz-2kHz at 2755rpm and at air injection rate of 0.4(l/min)

Figure 7-23 depicts the analysis of acoustic signal with and without air injection, using mean and RMS acoustic amplitude features. These features were investigated with different range of frequencies including a) 0Hz-1kHz, b) 1kHz-2kHz, c) 2kHz-10kHz, and d) 10kHz-15kHz. The operating conditions for this analysis include different flow rates, air injection rate of 0.4(l/min) and N=2755rpm. It can be seen that these features have the same trend as in the previous sections results which were obtained under different operation conditions. It can be seen that the trends for the mean and RMS acoustic amplitude features, for both cases (with and without air injection), does not change significantly at low flow rate lower than 350(l/min). However, the trends for these features (mean and RMS) rapidly increase after 350(l/min). The experimental results showed that the trends for the above features with air injection, were slightly lower than for the features without air injection at flow rate lower than 350(l/min). The reasons are firstly due to the effect of the rate of air injection which causes more instability in the flow pattern inside the pump. Secondly, the effect of cavitation occurrence within a pump. The trends for these features were approximately the same as the trends that were obtained from vibration results analysis in frequency domain in the previous chapter.

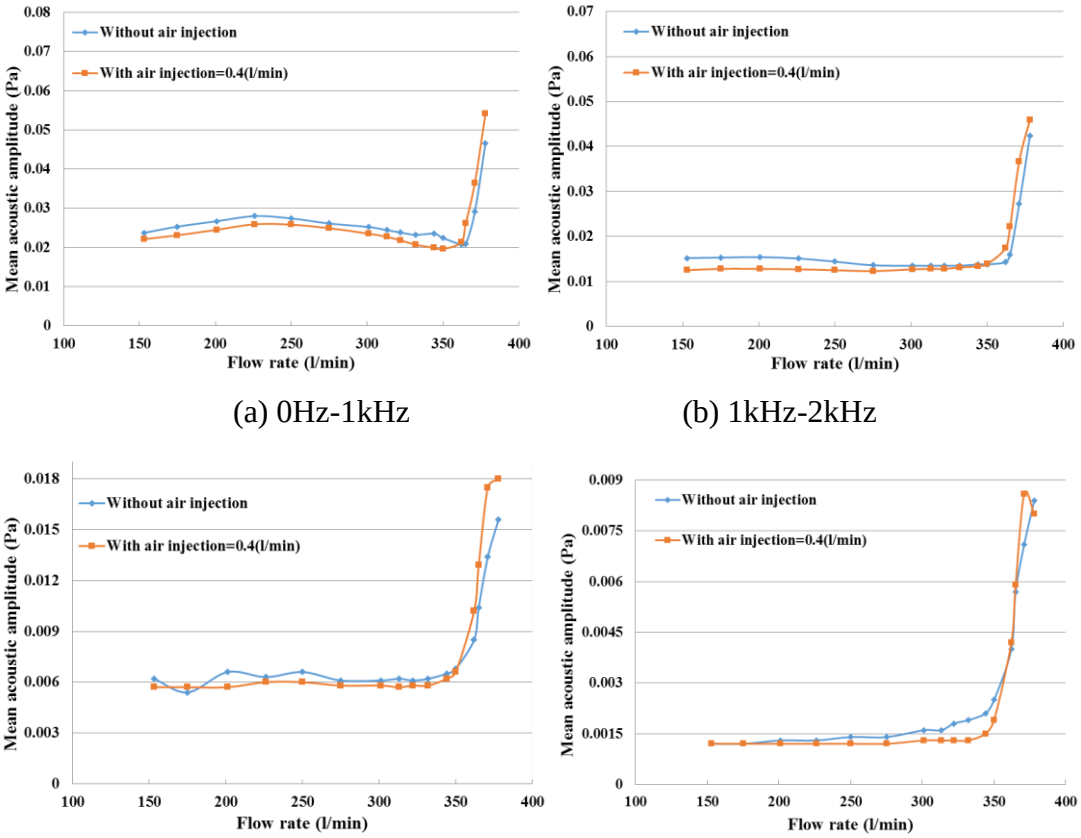

(a) 0Hz-1kHz (b) 1kHz-2kHz

(c) 2kHz-10kHz (d) 10kHz-15kHz

Figure 7-23: Mean vibration amplitude value for frequency range from (0Hz to 15kHz) at 2755rpm with and without air injection at air injection rate of 0.4(l/min)

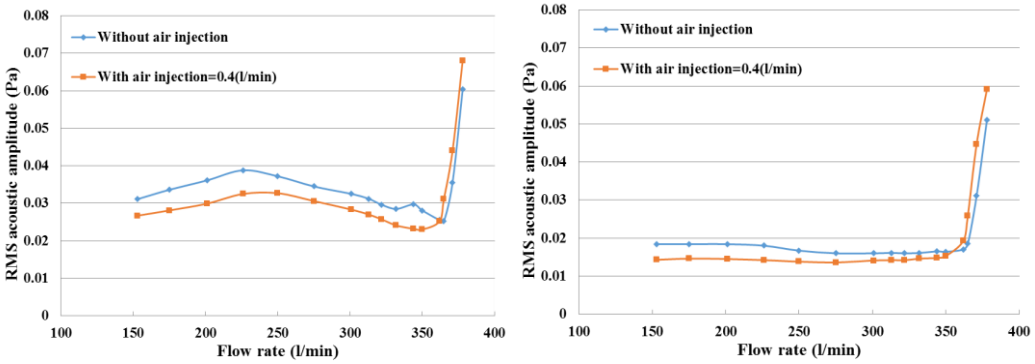

(a) 0Hz-1kHz (b) 1kHz-2kHz

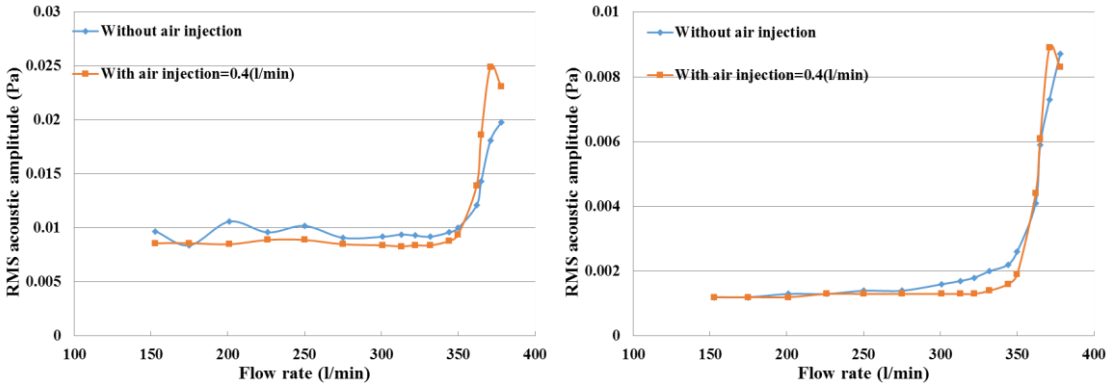

(c) 2kHz-10kHz (d) 10kHz-15kHz

Figure 7-24: RMS vibration amplitude value for frequency range from (0Hz to 15kHz) at 2755rpm with and without air injection

7.9.3. Analysis of the Acoustic Signal Based on Time Domain under Different Amount of Air Injections

For comparison purposes between the different amount of air injections (1 and 1.8(l/min)) under investigation, with and without air injection, based on time domain for the acoustic amplitude, all of these results showed approximately the same trends for the peak, RMS, peak-to-peak and variance values as shown in Figure 7-25. There is no significant change occurrence in the acoustic amplitude for both cases (with and without air injection) under low flow rate, but the rapid increase in the acoustic amplitude for both cases occur at a flow rate higher than 350(l/min). The reason behind this is due to the increase in the formation of bubbles as a result of cavitation, and the additional air injection that leads to decrease in the pressure at the eye of impeller, lower than the water vapour pressure. In this case, this leads to the NPSHA becoming lesser than the NPSHR. At this point, cavitation increases and then develops within a pump as already mentioned in the previous chapter through using the vibration technique. Additionally, injection of high amounts of air within the suction side of the centrifugal pump can form pockets of air bubbles around the impeller, especially at the eye of the impeller causing more hydraulic losses in the pump, probably due to air binding.

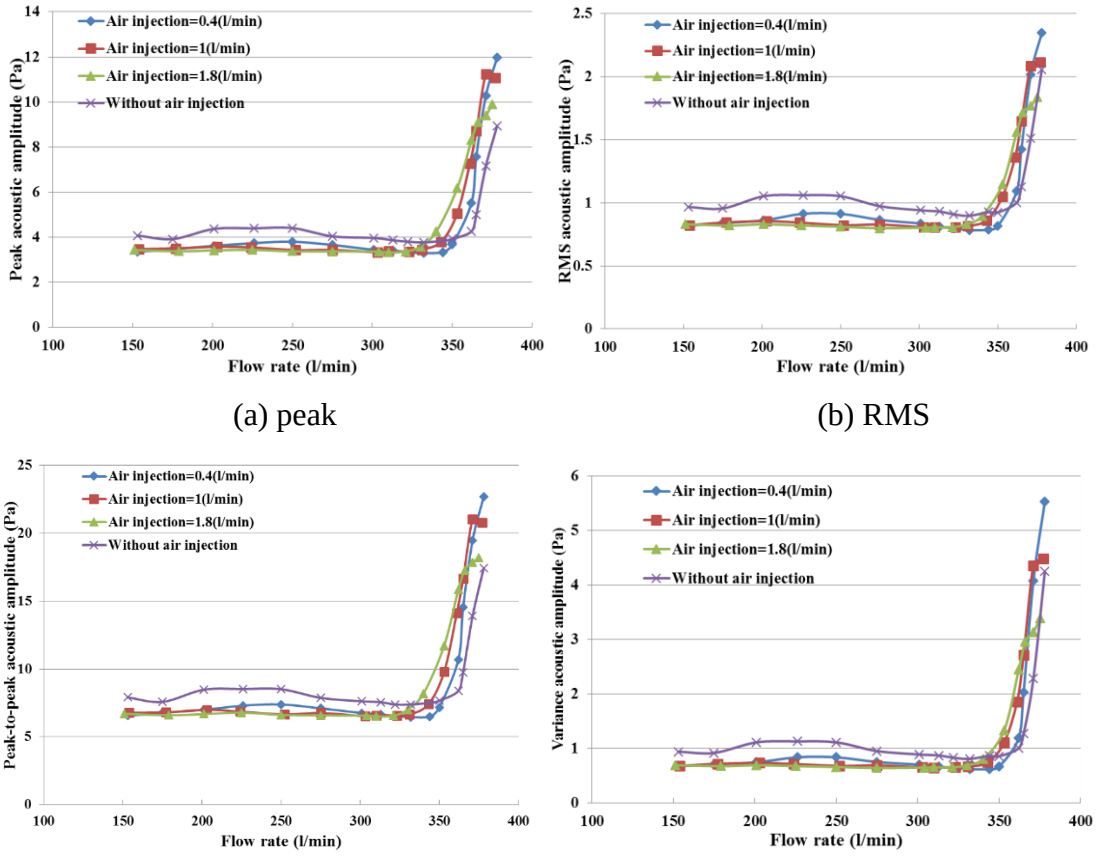

(a) peak (b) RMS

(c) peak-to-peak (d) variance

Figure 7-25: Comparison between different statistical features acoustic signal intime domain with and without air injection under different air injections

Table 7-10 Summary of the maximum statistical features for the acoustic amplitude at different air injections

Air injection (l/min)	Peak (Pa)	RMS (Pa)	Peak-to-peak (Pa)	Variance (Pa)
0.4	11.97	2.34	22.69	5.52
1	11.81	2.19	21.97	4.83
1.8	9.90	1.83	18.18	3.38

7.9.4. Analysis of the Acoustic Signal Based on Frequency Domain under Different Amount of Air Injections

For comparison purposes between the above cases under investigation, with and without air injection, based on frequency domain analysis for the acoustic amplitude, all of these results showed approximately the same trends for the mean and RMS acoustic amplitude values as depicted in Figure 7-26 and Figure 7-27. These results found that there is no significant change occurrence in the acoustic amplitude for both cases (with and without air injection) under low

flow rate, but the rapid increase in the acoustic amplitude for both cases occur at a flow rate higher than 350(l/min). Furthermore, injection of high amounts of air within the suction side of the centrifugal pump can form pockets of air bubbles around the impeller, especially at the eye of the impeller causing air binding.

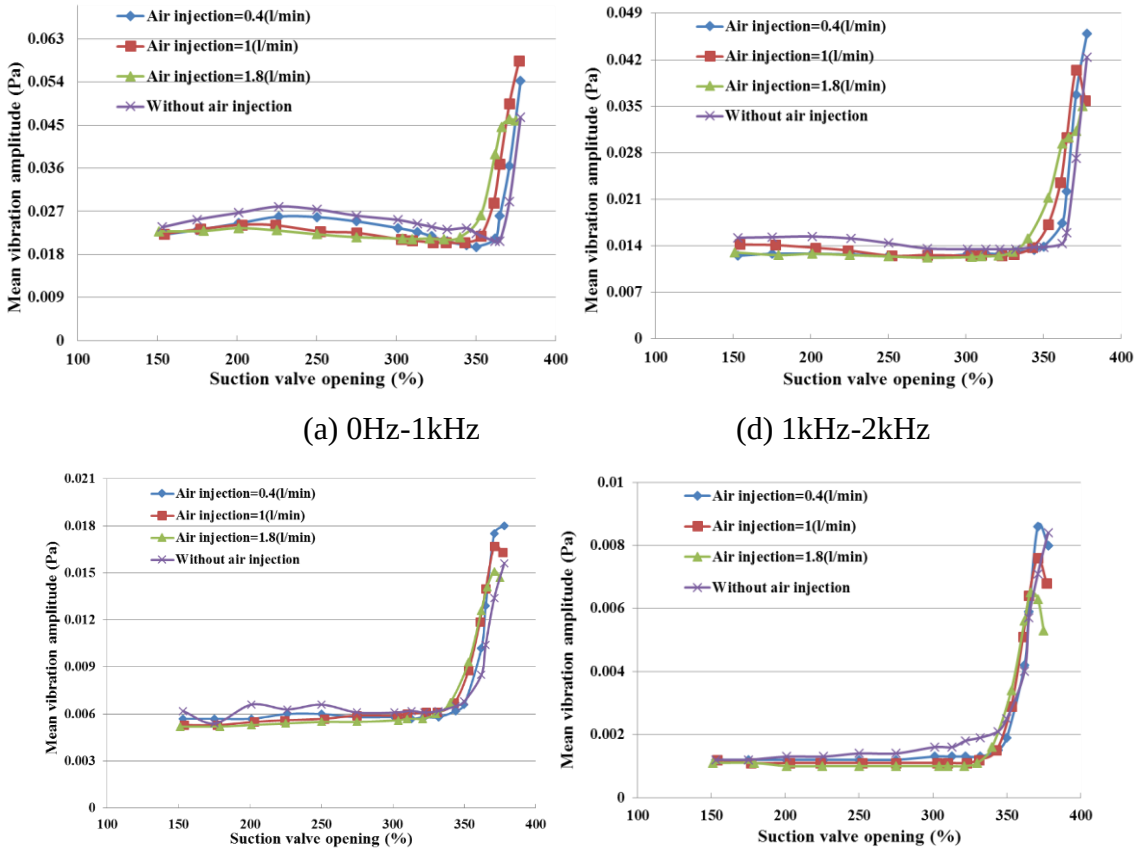

(a) 0Hz-1kHz (d) 1kHz-2kHz

(c) 2kHz-10kHz (d) 10kHz-15kHz

Figure 7-26: Comparison between mean acoustic amplitude values with and without air injection in frequency domain for different frequency ranges and air injections

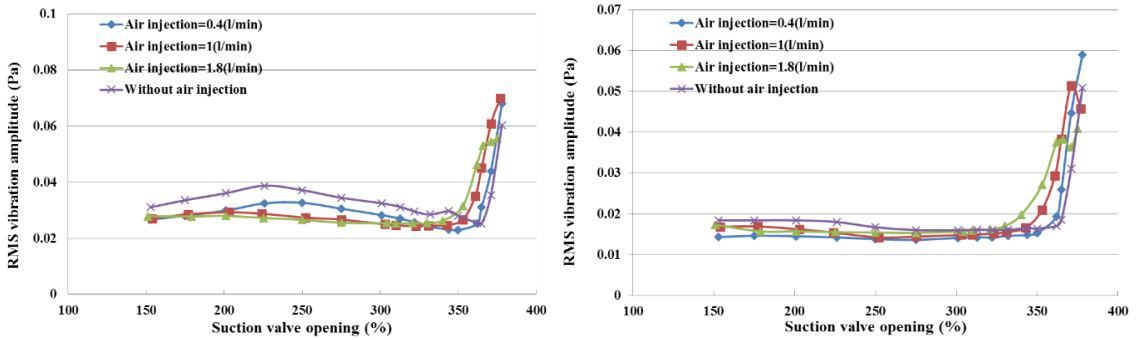

(a) 0Hz-1kHz (d) 1kHz-2kHz

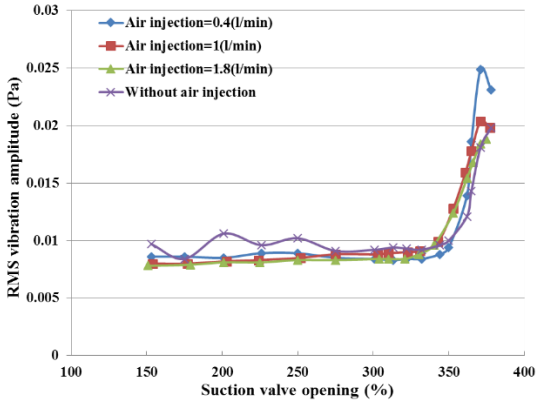

(c) 2kHz-10kHz

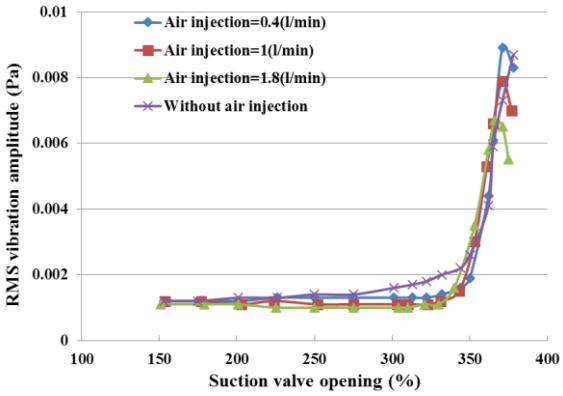

(d) 10kHz-15kHz

Figure 7-27: Comparison between RMS acoustic amplitude values with and without air injection in frequency domain for different frequency ranges and air injections

The mean and RMS acoustic amplitude features for air injection rate of 0.4(l/min) were higher than for air injection rates of 1, and 1.8 (l/min) at different range of frequencies as given in Table 7-11 and Table 7-12.

Table 7-11 Summarises the results of the maximum mean acoustic acoustic under different air injection and of frequency range 0Hz-15kHz

Air injection	Mean value 0Hz-1kHz	Mean value 1kHz-2kHz	Mean value 2kHz-10kHz	Mean value 10kHz-15kHz
(l/min)	(Pa)	(Pa)	(Pa)	(Pa)
0.4	0.0582	0.0460	0.0183	0.0086
1	0.0544	0.0405	0.0168	0.0076
1.8	0.0462	0.0350	0.0151	0.0065

Table 7-12 Summary of the results for the maximum RMS acoustic amplitude at different air injection rate and of frequency range between 0Hz-15kHz

Air injection	Mean value 0Hz-1kHz	Mean value 1kHz-2kHz	Mean value 2kHz-10kHz	Mean value 10kHz-15kHz
(l/min)	(Pa)	(Pa)	(Pa)	(Pa)
0.4	0.0781	0.0591	0.0249	0.0089
1	0.070	0.0523	0.0204	0.0079
1.8	0.0556	0.0409	0.0189	0.0067

7.10. Summary on the Analysis of Different Air Injection Rates within a Centrifugal Pump using Acoustic Technique

Based on above results there can be several conclusions regarding air injection within a pump using acoustic analysis technique:

1. Analysis on the acoustic signals in time domain, using time wave form for the air injection, showed that the levels of the acoustic amplitudes changes depending on the various flow rates.
2. When the pump operates under cavitation conditions with air injection, the trend for the acoustic amplitude became more random with high peaks when compared with normal conditions.
3. Using the acoustic signal was suitable to predict the effect of cavitation and air injection within a pump.
4. The analysis of acoustic signal, with and without air injection in time domain using statistical features show that there is a small indication of variance in the level of acoustic amplitude at flow rate below 350(l/min). However, the same trends for the above features, under different flow rates significantly increase when the pump operates at flow rate higher than 350(l/min).
5. The trends for all the above mentioned features with air injection start to increase before the trends for features without air injection at flow rate higher than 350(l/min).
6. The acoustic amplitude with air injection slightly decreases at high flow. This is due to the high quantity of air injection causing formation of air bubbles at the inlet impeller, particularly at the eye of an impeller and around the impeller causing air binding.
7. The analysis of the acoustic signal with and without air injection in frequency domain using mean and RMS features, under different frequency ranges showed that the trends for these features does not change significantly at flow rate lower than 350(l/min). However, the trends for the above features rapidly increase after 350(l/min).
8. The acoustic amplitude with air injection at frequency range for the above mentioned features start from 2kHz to high-frequency of 15kHz, slightly decreased at high flow.
9. The trends for peak, RMS, peak-to- peak and variance values in time domain and the trends for mean and RMS values in frequency domain for both acoustic and vibration signal, have the same trends. Therefore, it can be concluded from the above finding that any of vibration or acoustic techniques can be used in order to study the cavitation occurrence and effect of air injection within a centrifugal pump.
10. After analysis of both signals (vibration and acoustic) in previous sections, it can be observed that both techniques were effective and capable of detecting cavitation, depending on the noise surrounding the pump. If the level of noise is quite high, the use of vibration technique would be more effective when compared with the acoustic technique.

Detailed experimental measurements and investigations of the vibration and acoustic characteristics for the centrifugal pump were carried out in Chapters 6 and 7 in order to obtain a reliable detection and diagnosis of cavitation within a pump. For further analysis, comparison between the two above techniques can be carried out to obtain the better sensitive technique using cavitation detection index (CDI) which is presented in the next section.

7.11. Cavitation Detection Index (CDI)

Comparison is given below of vibration and acoustic results, to obtain more information and to evaluate sensitivity of techniques for detecting the inception and development of cavitation within a centrifugal pump under different wide ranges of operation conditions. The detection of cavitation index technique was used for the analysis purpose. The simple meaning of this technique is to use normalise features by dividing actual values of statistical features to the maximum values in time domain such as peak, RMS, peak-to-peak and variance, as well as mean and RMS values in frequency domain analysis. More details for normalised results are presented in following section.

7.11.1. Effect of Different Flow Rates

In order to find the sensitive technique for detecting cavitation, within a centrifugal pump, comparison between the vibration and acoustic techniques in both time and frequency domains under different flow rates using detection of cavitation index technique is presented in the next sections.

7.11.1.1. Detection of Cavitation in Time Domain using Different Normalise Features under Different Flow Rates

Figure 7-28 depicts the detection index results of (peak/peak max., RMS/RMS max., peak-to-peak/peak-to-peak max., and variance/variance max.) values for both vibration and acoustic signals under different flow rates start from 100(l/min) to 370(l/min) with a N=2755rpm. It can be seen that all above features, for both vibration and acoustic results, have approximately the same trends. There is no significant change in values of these features when the pump operates under lower than a flow rate of 350(l/min). However, a rapid increase occurs at a flow rate higher than 350(l/min). Also, it can be observed that from these figures all vibration features are more sensitive to detect inception of cavitation as compared to acoustic signal. Trends of these features start to increase after design flow rate of 300(l/min). However, the statistical

features corresponding to acoustic signal start to increase after 350(l/min). The cavitation results of statistical (peak/peak max., RMS/RMS max., and peak-to-peak/peak-to-peak max.) values for the vibration identifies the inception of cavitation is higher than 20% and for acoustic results was higher than 40%. The (variance/variance max.) value for the vibration was higher than 10% and for acoustic approximately higher than 20% respectively. The above values of vibration and acoustic results can be used as a threshold to detect different levels of cavitation. It can also be seen that as the threshold increases, the level of cavitation increases within centrifugal pump. Furthermore, it can be concluded that, the use of above mentioned statistical features to analyse the vibration signal were more sensitive compared to an acoustic signal to detect inception and development of cavitation. In addition, the use of different, normalise statistical features in time domain can prove to be a good indication regarding detection of cavitation within a pump using both techniques.

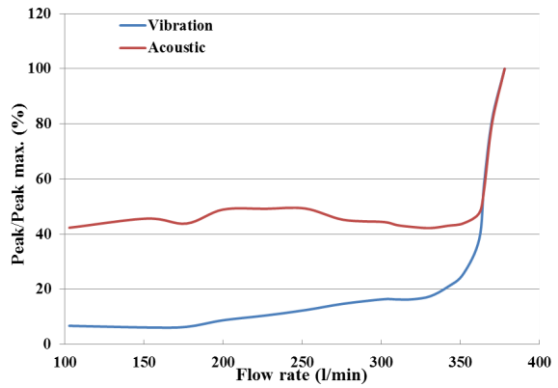

(a) Peak/peak max.

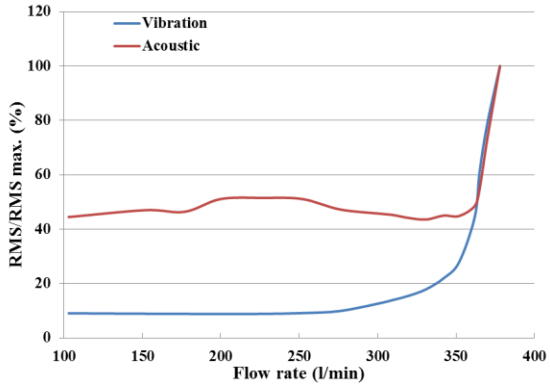

(b) RMS/RMS max.

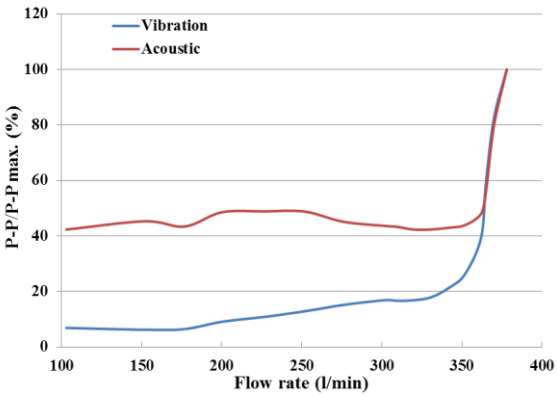

(c) Peak-to-peak/peak-to-peak max.

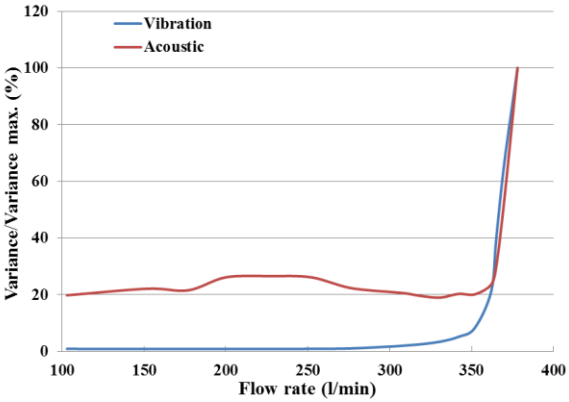

(d) Variance/variance max.

Figure 7-28: Normalised results features in time domain for both vibration and acoustic signals at 2755rpm

7.11.1.2. Detection of Cavitation in Frequency Domain using Different Normalise Features under Different Flow Rates

In the similar manner, Figure 7 29 depicts normalise results of (mean/mean max.) value for the vibration and acoustic signals in frequency domain under different flow rates, starting from 100(l/min) to 370(l/min), N=2755rpm and for various range of frequencies (0Hz-1kHz), (1kHz-2kHz), (2kHz-10kHz), and (10kHz-15kHz). It can be observed that the features mentioned above for both vibration and acoustic results have approximately the same trend. There is no significant change when the pump operates under lower than a flow rate 350(l/min), but the rapid increase was seen at a flow rate higher than 350(l/min). Additionally, it can be seen that from above findings the vibration sensor (accelerometer) provides a suitable indication for detecting inception occurrence of cavitation within a pump under a wide range of flow rates and frequency ranges as compared to acoustic signal using microphone. Due to the acoustic technique, it was not possible to capture the entire changes within pump, particularly small changes that the vibration technique has achieved. It can be observed that the frequency range 10kHz to15kHz was more sensitive for detecting inception of cavitation for both techniques (vibration and acoustic) as there are many vibration and acoustic high amplitudes peaks in this frequency range as compared to other frequency ranges. In both techniques, it was observed from previous sections of this chapter that the frequency ranges of 1-2kHz is effective to detect cavitation. Therefore, sensors with low frequency range can be used to detect inception of cavitation. Additionally, using lower frequency range sensors can decrease the overall cost. The cavitation results of (mean/mean max.) value for the vibration identifies the inception of cavitation detection for frequency range 1kHz-2kHz which was approximately at 20% and for acoustic results was higher than 30%. However, for frequency range 2kHz-10kHz the vibration was lower than 20% and for acoustic around 40% and frequency range 10kHz-15kHz lower than 18% and 20% respectively. The results of (mean/mean max.) values for vibration and acoustic can used as threshold to detect cavitation as well as when this threshold increases shows the level of cavitation increases within the centrifugal pump.

It can be concluded that the analysis of vibration signals using normalisation (mean/mean max.) frequency values was more sensitive to detect inception of cavitation as compared to an acoustic signal. Also, the analysis of vibration and acoustic signal using above normalised feature for high-frequency range was more effective to detect the inception and development

of cavitation. Based on the above results it can be concluded that the use of (mean/mean max.) value for different frequency ranges in frequency domain can be a good indication regarding detecting the inception and development of cavitation within a centrifugal pump.

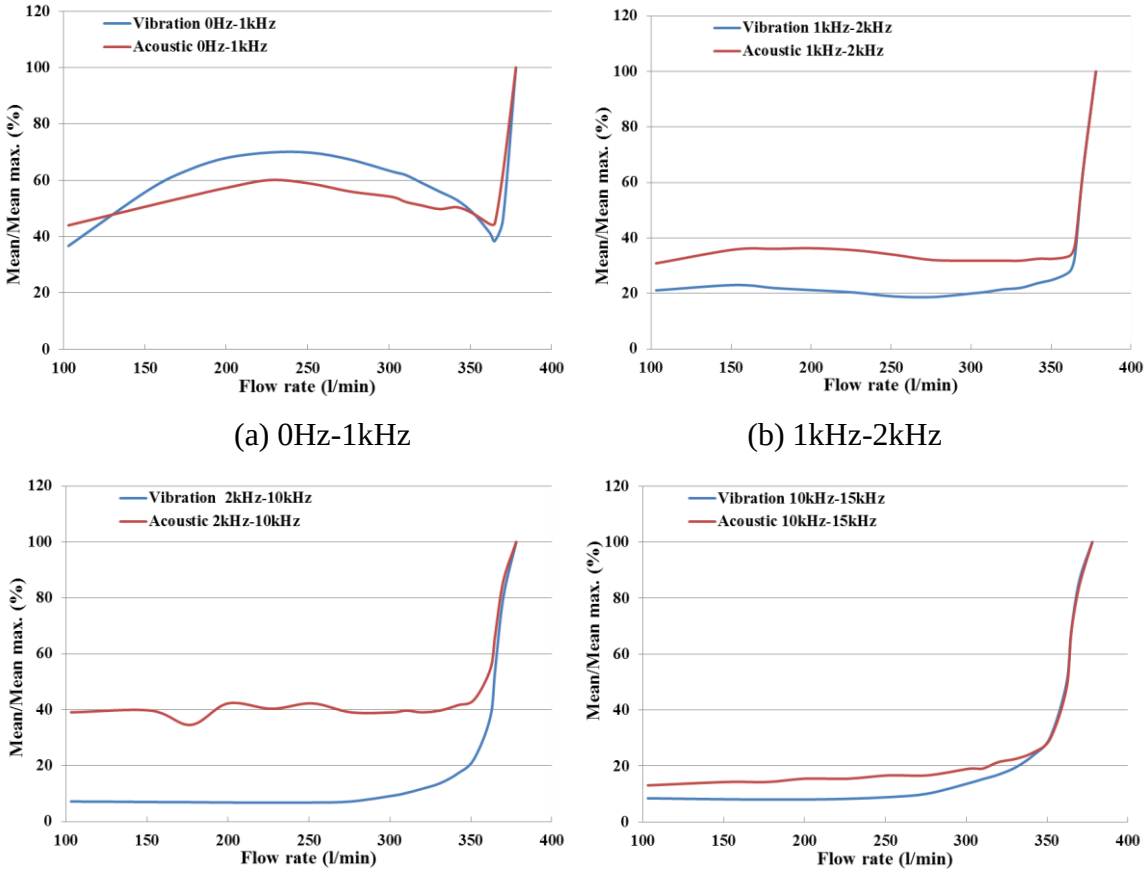

(a) 0Hz-1kHz (b) 1kHz-2kHz

(c) 2kHz-10kHz (d) 10kHz-15kHz

Figure 7-29: Normalised results for (mean/mean max.) value in frequency domain for the vibration and acoustic signals at 2755rpm for the different of frequency range

Figure 7-30 depicts the normalised results of (RMS/RMS max.) value for the vibration and acoustic signals in frequency domain under different flow rates, N=2755rpm and for the different range of frequencies. It can be observed that the (RMS/RMS max.) value for the vibration and acoustic signals have approximately the same trend of (mean/mean max.) value as in previous figures. It can be observed from the vibration and acoustic signals that the normalised (RMS/RMS max.) values under cavitation condition at high flow rate are higher than without cavitation (normal operation conditions) at low flow rate and the severity of cavitation is increased with the increase of flow rate. The cavitation normalised values of (RMS/RMS max.) for vibration and acoustic techniques follow approximately the same trend of cavitation detection index as compared to (mean/mean max.) values in the previous figures.

Based on above results, it can be concluded that the use of (mean/mean max.) and (RMS/RMS max.) values to analyse the vibration and acoustic signals in frequency domain under different flow rates and frequency ranges, can provide useful information regarding detection of cavitation in the pump and hence in order to find the sensitive frequency range for this purpose.

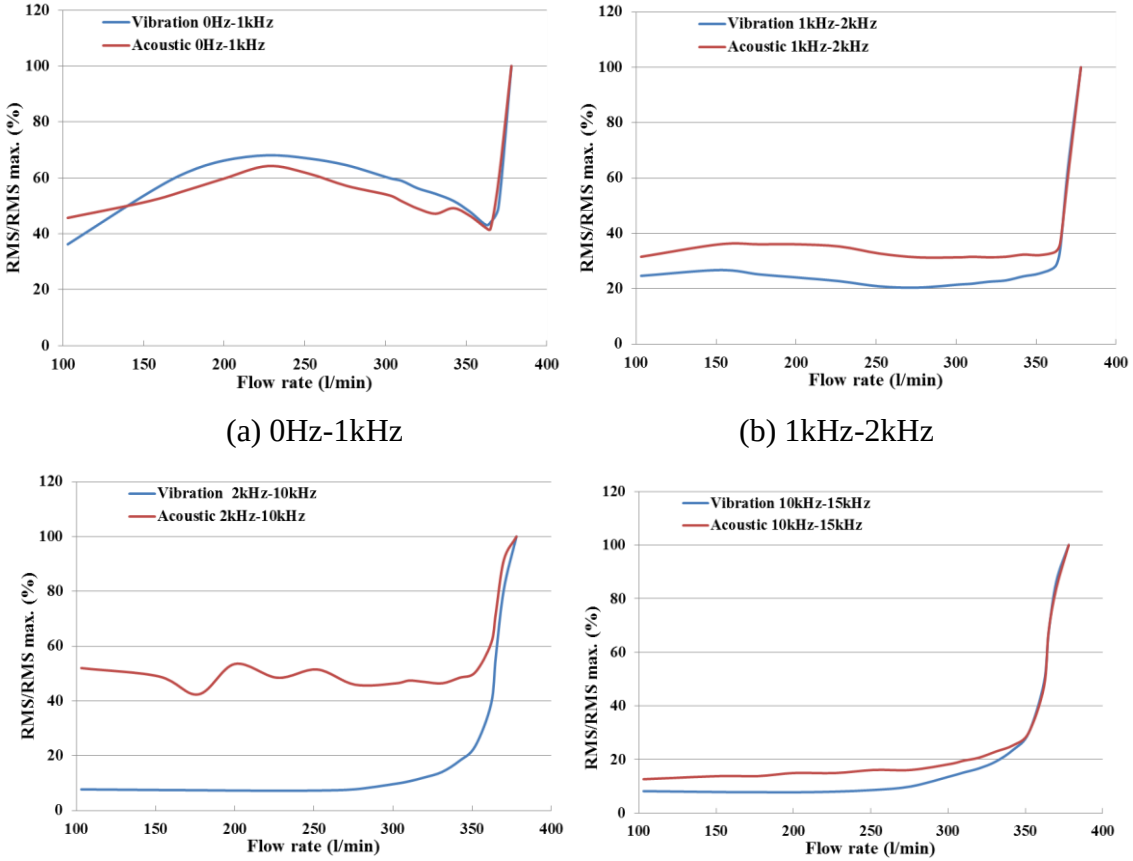

(a) 0Hz-1kHz (b) 1kHz-2kHz

(c) 2kHz-10kHz (d) 10kHz-15kHz

Figure 7-30: Normalise results for (RMS/RMS max) value in frequency domain for the vibration and acoustic signals under different flow rates and frequency range at 2755rpm

7.11.2. Effect of Different Suction Valve Openings

In a similar manner to the previous section, the vibration and acoustic signals can be compared under different suction valve openings as presented in the next sections.

7.11.2.1. Detection of Cavitation in Time Domain using Different Normalise Features under Different Suction Valve Openings

Figure 7-31 depicts the normalised results of (peak/peak max., RMS/RMS max., peak-to-peak/peak-to-peak max., and variance/variance max.) values for both vibration and acoustic signals under different suction valve openings. The pump rotational speed under consideration

is 2755rpm, and the flow rate is 302(l/min). It can be seen that both vibration and acoustic experimental normalised results for (peak/peak max., RMS/RMS max., peak-to-peak/peak-to-peak max., and variance/variance max.) various parameters showed similar trends. It can be observed that the above values have no significant change when the suction valve openings are between 100 and 55% for both vibration and acoustic signals. However, an important change has occurred when the suction valve openings are at about 55% due to the cavitation taking place at the suction pipe as well as at the inlet eye of the impeller due to decrease in the water pressure, which may be lower than water vapour pressure. Also, the vibration technique was found to be more sensitive to detect inception of cavitation as compared to the acoustic technique when carrying out time domain. The cavitation normalised results of (peak/peak max. and peak-to-peak/peak peak-to-peak max.) values for vibration identifies the inception cavitation detection was at higher than 20% and for acoustic results was higher than 30%. The values of (RMS/RMS max.) obtained by vibration technique was around 30% and for acoustic technique 40%. In addition, (variance/variance max.) values was around 10% for vibration and 18% for acoustic technique respectively.

Based on the above results, it can be concluded that both vibration and acoustic are suitable techniques for detecting the level of cavitation in a centrifugal pump, but the vibration technique was found to be more effective as compared to acoustic technique.

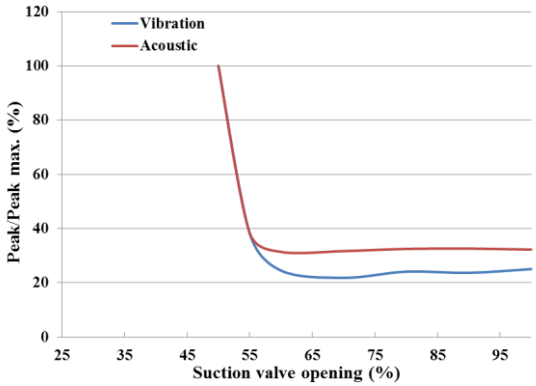

(a) Peak/peak max.

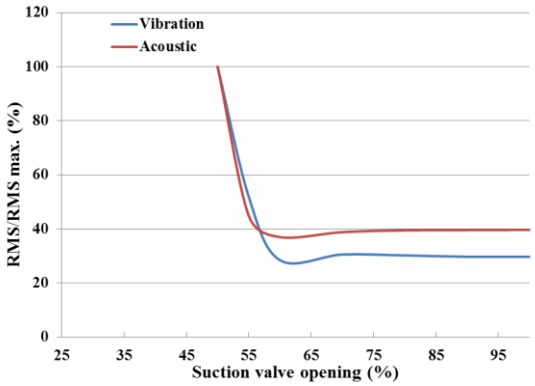

(b) RMS/RMS max.

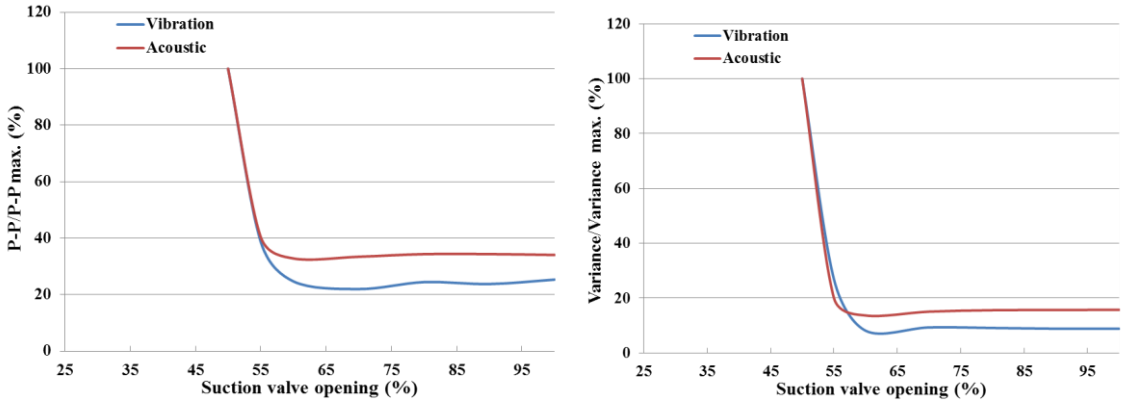

(c) Peak-to-peak/peak-to-peak max. (d) Variance/variance max.

Figure 7-31: Normalised results features in time domain for the vibration and acoustic under different suction valve openings

7.11.2.2. Detection of Cavitation in Frequency Analysis using Different Normalise Features under Different Suction Valve Openings

Figure 7-32 and Figure 7-33 show normalised results of (mean/mean max.) and (RMS/RMS max.) values in the frequency domain for the vibration and acoustic signals at 2755rpm for the different range of frequencies under different suction valve openings and at flow rate of 302(l/min). It can be seen that the vibration and acoustic experimental normalised results (mean/mean max.) and (RMS/RMS max.) have approximately the similar trends. In addition, it can be observed that the features mentioned above have no significant change when the suction valve openings are between 100 and 55% for both vibration and acoustic signals. However, the important change occurs when the suction valve openings are at about 55% opening because of the same reasons that are explained for time domain in the previous section.

In a similar manner to the previous section 7.11.1.2., the frequency range 1kHz-2kHz for both vibration and acoustic results was found to be sensitive to detect cavitation. As well the cavitation normalised results of (mean/mean max.) value for the vibration, it identified the inception of cavitation detection being approximately at 20% and for acoustic results was higher than 30% for this frequency range. However, for frequency range 2kHz-10kHz the vibration was lower than 17% and for acoustic around was higher than 37%. Additionally, frequency range 10kHz-15kHz was lower than 30% and 32% receptively. Furthermore, the cavitation normalised results of (RMS/mean max.) value for the vibration and acoustic under frequency range 1kHz-2kHz are around 20% and 24%, for frequency range 2kHz-10kHz are 18% and 38% and for frequency range 10kHz-15kHz are 30% and 35% respectively.

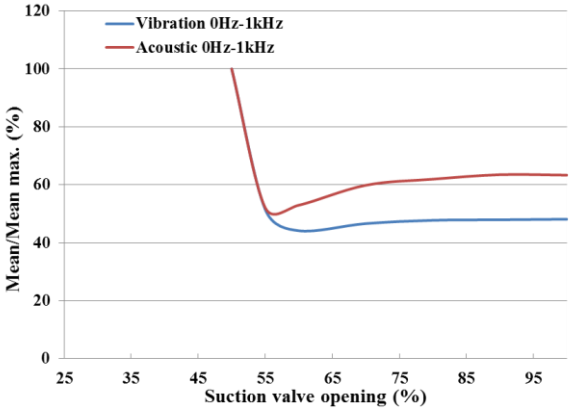

(a) 0Hz-1kHz

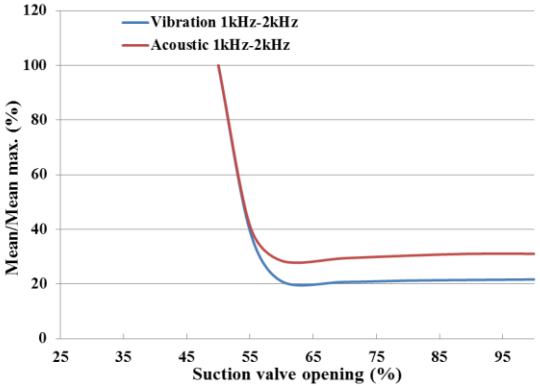

(b) 1kHz-2kHz

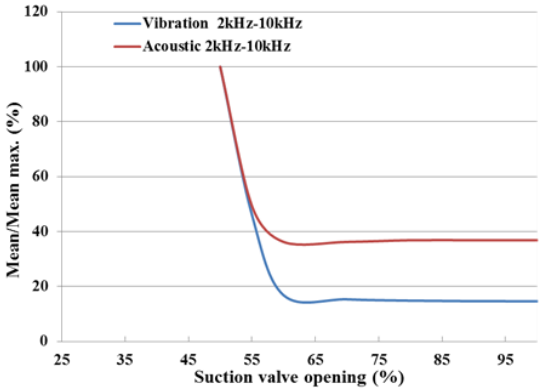

(c) 2kHz-10kHz

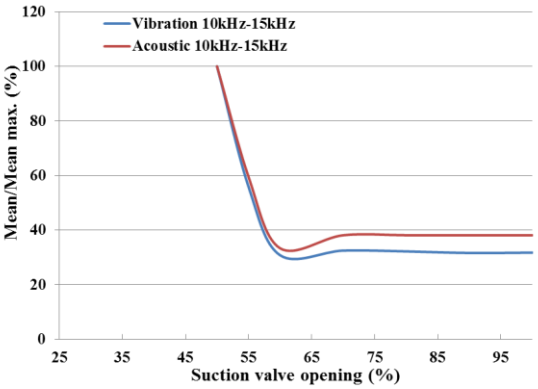

(d) 10kHz-15kHz

Figure 7-32: Normalise results for (mean/mean max.) value in frequency domain for the vibration and acoustic at 2755rpm for different of frequency range and suction valve openings

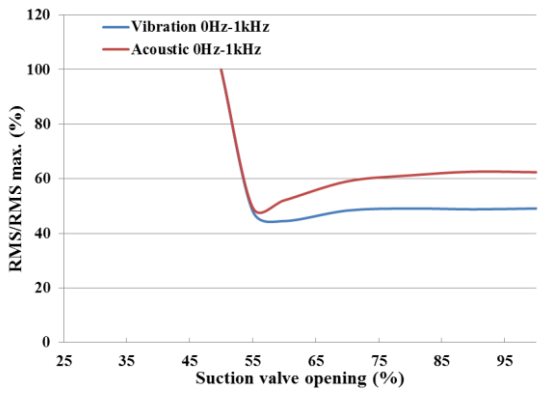

(a) 0Hz-1kHz

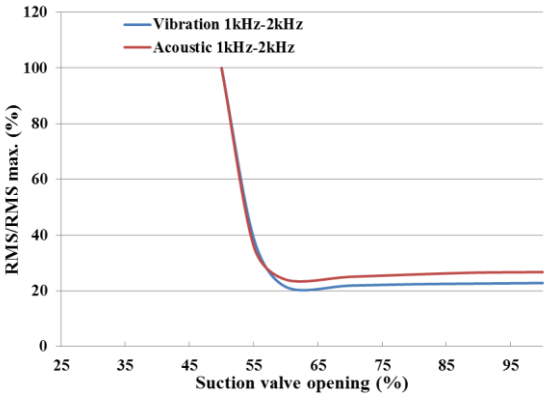

(b) 1kHz-2kHz

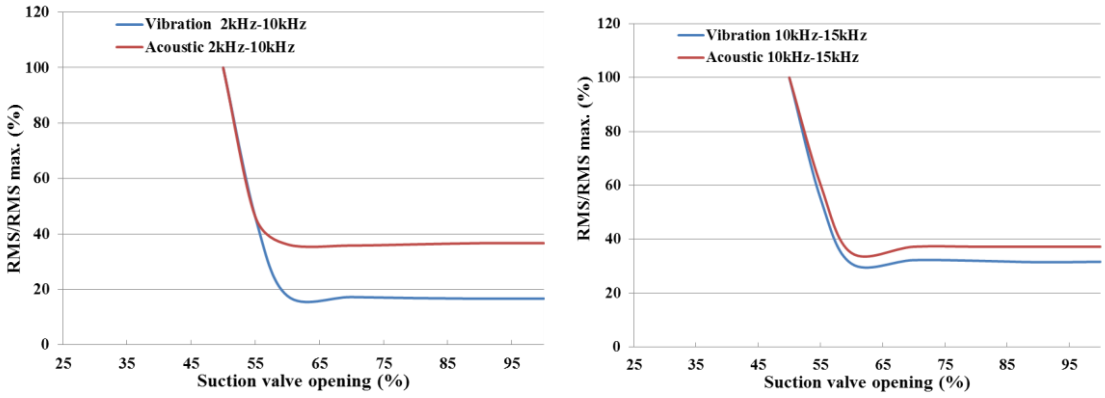

(c) 2kHz-10kHz (d) 10kHz-15kHz

Figure 7-33: Normalise results for (RMS/RMS max.) value in frequency domain for the vibration and acoustic at 2755rpm for different of frequency range and suction valve openings

7.11.3. Effect of Air Injection

In a similar manner, the vibration and acoustic signals can be compared under different amounts of air injection in the next sections using both time and frequency domains analyses.

7.11.3.1. Detection of Cavitation in Time Domain using Different Normalise Features under Air Injection

Figure 7-34 depicts the variation of index cavitation in normalised form for (peak/peak max., RMS/RMS max., peak-to-peak/peak-to-peak max., and variance/variance max.) values for both vibration and acoustic signals under different flow rates. The pump rotational speed of 2755rpm and air injection of 0.4(l/min). It can be seen that all the above features for both vibration and acoustic results have approximately the same trends. There is no significant change when the pump operates at lower flow rates than a flow rate of 350(l/min), but a rapid increase occurs at flow rates higher than the flow rate of 350(l/min) due to the same reasons as mentioned in previous sections. Furthermore, the normalised results of (peak/peak max., RMS/RMS max., and peak-to-peak/ peak-to-peak max.) values for the vibration identifies the inception of cavitation detection is lower than 10% and for acoustic results was higher than 30%. However, the (variance/variance max.) value for the vibration was 5% and for acoustic approximately 15%. Again it can be concluded that based on the above results, the vibration and acoustic techniques are sensitive for detecting cavitation within a centrifugal pump under air injection conditions, but the vibration technique was more sensitive to detect inception of cavitation as compared to acoustic technique.

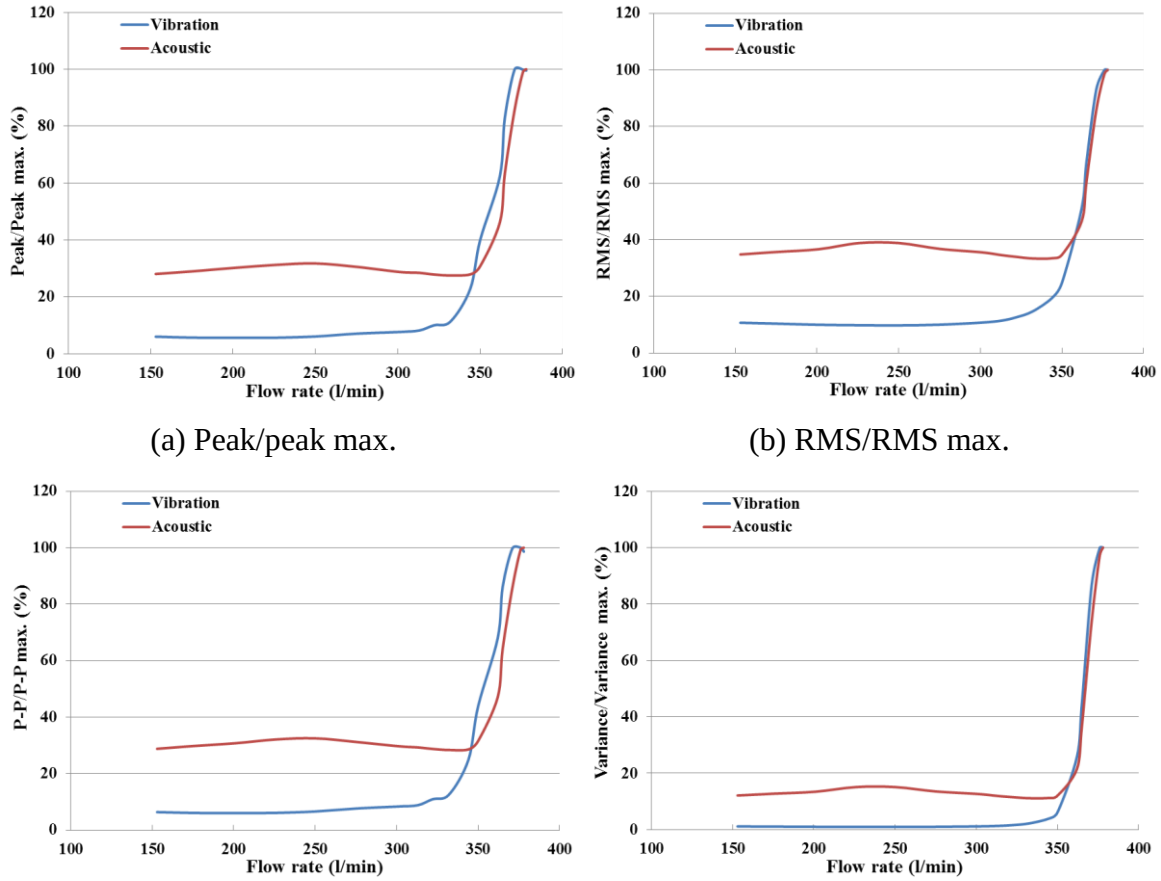

(a) Peak/peak max. (b) RMS/RMS max.

(c) Peak-to-peak/peak-to-peak max. (d) Variance/variance max.

Figure 7-34: Normalise results features in time domain for the vibration and acoustic at air injection 0.4(l/min)

7.11.3.2. Detection of Cavitation in Frequency Domain using Different Normalise Features under Air Injection

Figure 7-35 and Figure 7-36 show normalised results of (mean/mean max.) and (RMS/RMS max.) values in the frequency domain for the vibration and acoustic signals at 2755rpm for the different range of frequencies spectrum with air injection at a rate of 0.4(l/min). It can be seen that the vibration and acoustic experimental normalised results for (mean/mean max.) and (RMS/RMS max.) values have approximate similar trends. It can be seen that at higher flow rates the characteristic values of both vibration and acoustic curves are increased due to the onset of cavitation. In a similar manner in previous sections, the frequency range 1kHz-2kHz for both vibration and acoustic results was sensitive to detect cavitation under air injection. Also, the cavitation normalised results of (mean/mean max.) value for the vibration identified the inception of cavitation detection was approximately at 22% and for acoustic results was higher than 25%. However, for frequency range 2kHz-10kHz the vibration was lower than 10%

and for acoustic around 35%. Additionally, frequency range 10kHz-15kHz was lower than 10% and 15% receptively. Furthermore, the cavitation normalised results of (RMS/RMS max.) value for the vibration and acoustic under frequency range 1kHz-2kHz are around 22% and 25%, for frequency range 2kHz-10kHz are 10% and 36% and for frequency range 10kHz-15kHz are around 10% and 15% respectively. The cavitation normalised results of (RMS/RMS max.) value for the vibration and acoustic techniques under frequency range 1kHz-2kHz are around 22% and 25%. For frequency range 2kHz-10kHz, the values are 10% and 36%, for frequency range 10kHz-15kHz the values obtained are around 10% and 15% respectively.

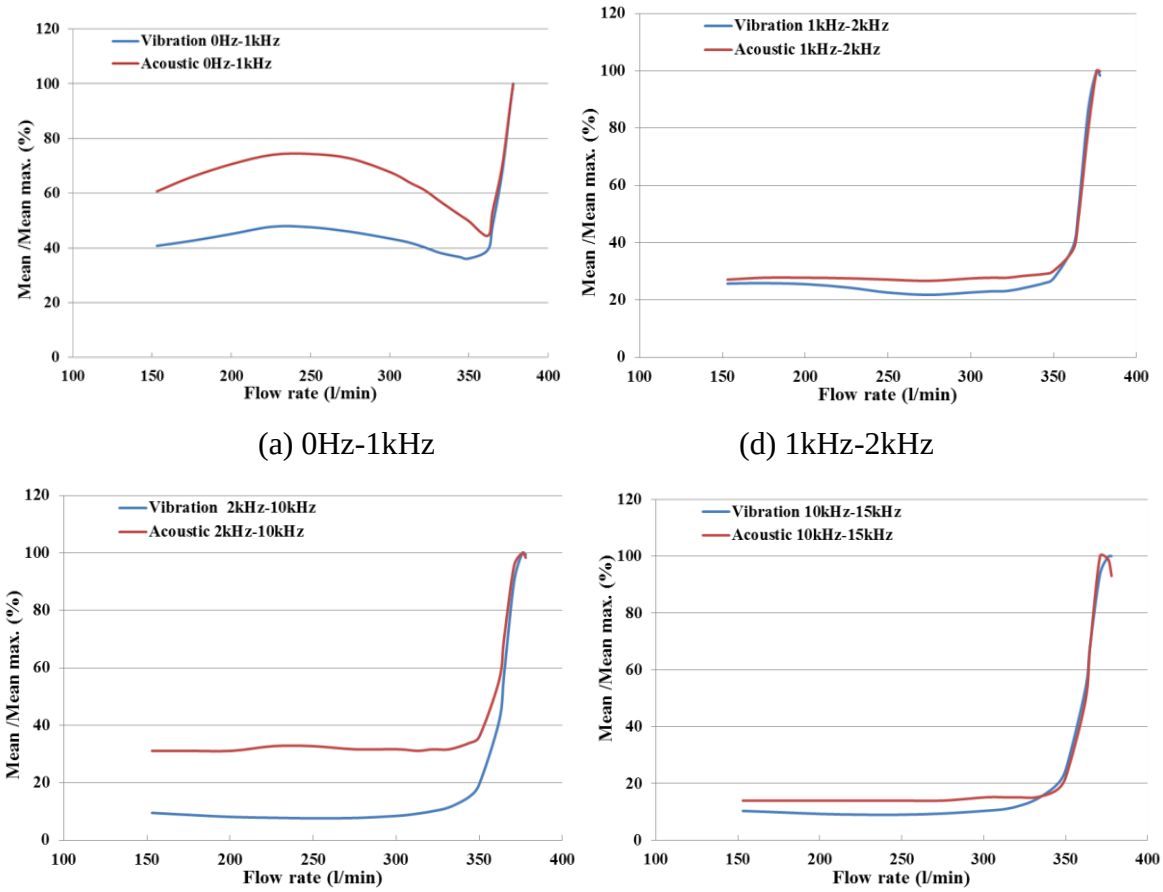

(a) 0Hz-1kHz (d) 1kHz-2kHz

(c) 2kHz-10kHz (d) 10kHz-15kHz

Figure 7-35: Normalise results for (mean/mean max.) value in frequency domain for the vibration and acoustic at 2755rpm for different of frequency range under air injection 0.4(l/min)

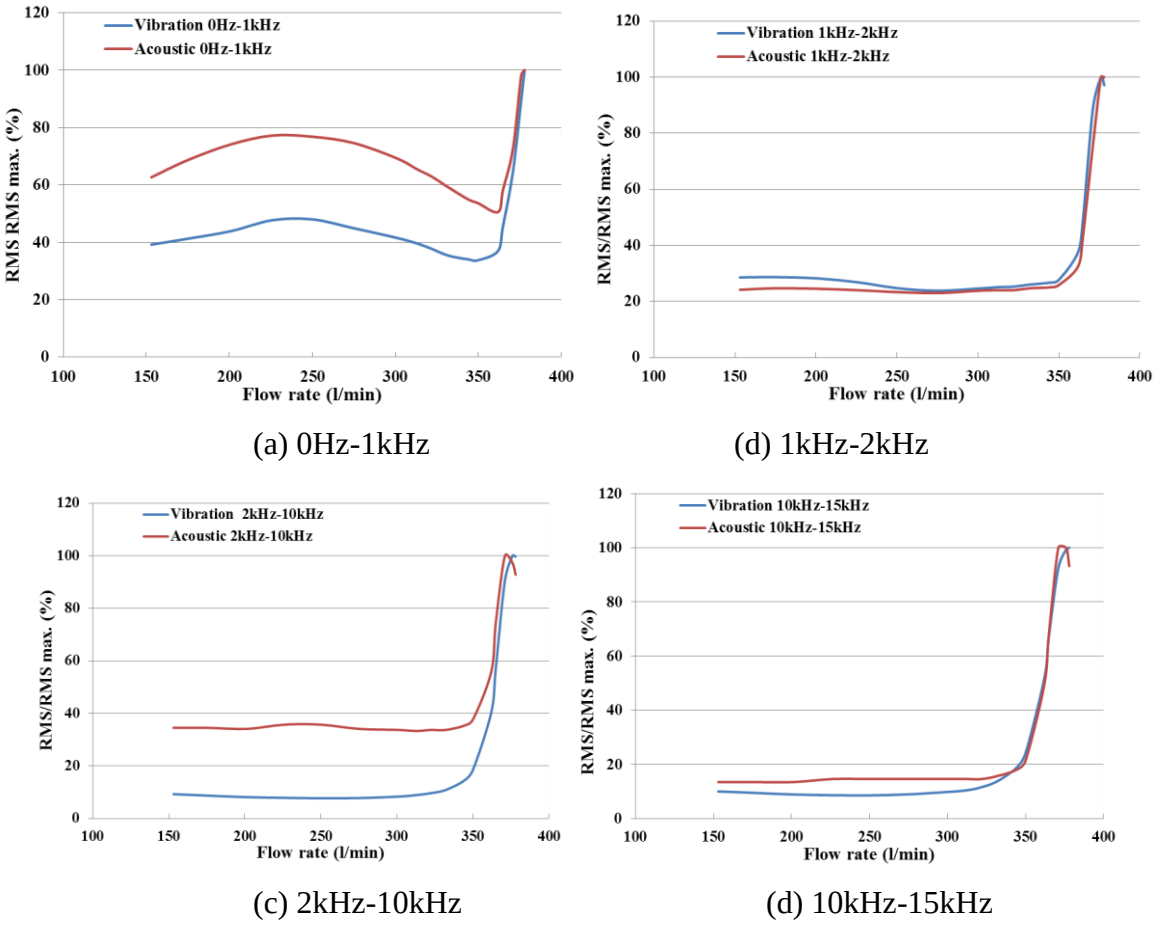

(a) 0Hz-1kHz (d) 1kHz-2kHz

(c) 2kHz-10kHz (d) 10kHz-15kHz

Figure 7-36: Normalise results for (RMS/RMS max.) value in frequency domain for the vibration and acoustic at 2755rpm for different of frequency ranges under air injection 0.4(l/min)

7.12 Summary of the Analysis on the use of Cavitation Detection Index (CDI) Technique to Detect Cavitation under Different Operation Conditions, using Vibration and Acoustic Analyses Techniques

Based on the above results in this section, several following conclusions can be found regarding the use of cavitation detection index (CDI) technique under different operation conditions.

1. The use of detection index normalised features for both vibration and acoustic signals in time domain can be proved as a good indication regarding detecting different levels of cavitation within a centrifugal pump under different operational conditions.
2. The vibration and acoustic techniques are sensitive to detect cavitation but vibration technique was more sensitive as compared to acoustic technique under different operational conditions.

3. The results of normalised features for the vibration amplitude at a flow rate between 100 and 350(l/min) were lower than the results of normalised features for the acoustic amplitude. However, the vibration and acoustic amplitudes were rapidly increased after 350(l/min) due to the development of cavitation within a centrifugal pump.
4. The use of normalised features in time and frequency domains for different frequency ranges can provide a good indication regarding detection of inception and development of cavitation.
5. Based on detection of cavitation results, the vibration method was more sensitive to detect the inception of cavitation within a centrifugal pump as compared to the acoustic method.
6. The frequency range 1kHz-2kHz for both vibration and acoustic results was sensitive to detect cavitation as compared to the frequency range 0Hz-1kHz under different operational conditions. Therefore, sensors with low-frequency range can be used for detecting cavitation which results in a reduction of cost for the sensors as compared to sensors with high-frequency range.
7. After analysing both signals (vibration and acoustic) in previous sections, it can be observed that both techniques were effective and capable of detecting cavitation dependent on noise surrounding the pump. If the level of noise was high, the use of vibration technique is more effective and sensitive as compared to acoustic technique.

7.13 Evaluation of the Cavitation Condition Monitoring Techniques (CMT)

In this research study, the results from the different techniques, including the numerical technique using CFD code, and experimental techniques using vibration and acoustic, under a different range of operational conditions were compared. In order to find the most sensitive technique for the detection of cavitation within the pump as analysed and discussed in detail in the previous chapters. In this section, comparison and evaluation between the various techniques is focused on their ability to detect and diagnose cavitation, based on their cost, installation and ease of application. Furthermore, the major evaluations for the above techniques in this study are summarised as follows:

7.13.1. The CFD Analysis Technique

Currently, turbomachinery such as compressors, turbines and different types of pumps are studied through the use of CFD software to predict their performance. Also, the use of CFD plays a significant part in fluid mechanics due to the development of computer capability and

numerical simulation techniques as CFD is one of the important robust numerical analysis methods. In order to determine the pump performance and diagnose the cavitation phenomenon within the centrifugal pump, different techniques were used in this work to achieve the set aims. The first technique was numerical which is based on CFD code. This technique can provide a more suitable method to visualise and reasonably obtain accurate information regarding the behaviour of fluid flow within a centrifugal pump, under different operating conditions as presented in Chapter five. In order to predict the performance and cavitation of the pump numerically in this study, simulations were carried out through the various operational point of flow rates, pump rotational speeds and different impeller geometrical parameters, in order to cover a wider range of the pump under single-phase and cavitation conditions. Detailed quantitative and quantitative analyses were performed on global and local flow parameters.

This study was assumed that the centrifugal pump is operational in both single-phase and cavitation conditions. Based on transient behaviours and sliding mesh technique, providing a better numerical simulation modelling of the flow within the pump at various operating conditions were carried out and validated against the experimental performance curve. The centrifugal pump model was tested against different impeller geometrical parameters which include the number of blades are (Z=3, 4, and 5), outlet impeller diameters (do=200, 210, and 220mm) and inlet impeller diameters (di=25, 30, and 35mm) under single-phase. Then, it was also modelled under CFD cavitation model in order to clearly visualise the cavitation occurring within the pump, under different impeller geometrical parameters.

In order to obtain more information regarding the detection of cavitation in the pump, useful features for the use of the CFD technique were given. This analysis technique was evaluated based on detection of cavitation, method of detection of cavitation, visualisation of the cavitation, requirements to detect cavitation by CFD code and sensitivity of the CFD code to detect cavitation. Therefore, Table 7-13 summarises the most significant features of the CFD code based on the obtained results given in Chapter five, in order to detect cavitation occurrence within a centrifugal pump under different operation condition. Furthermore, the analysis using CFD methodology can give vital information for further investigations regarding the transient flow pattern in the pump under single-phase and cavitation conditions and can be used on any other types of pumps.

Table 7-13: Summary of the most significant features of the CFD to detect cavitation within a centrifugal pump

No.	Conditions	Remarks
1	Detection of cavitation using CFD code	Using CFD code was important tool to detect cavitation
2	Method of detection of Cavitation	Numerical simulation using CFD code was capable to visualise the cavitation
3	Visualisation of the cavitation	Using vapour volume fraction contour
4	Installation of CFD code	Need licence
5	Cost of CFD licence	Relatively expensive
6	Requirements to detect cavitation by CFD code	It is needed different steps 1.Crerate geometry, 2.Mesh, 3.Solver, 4. Post-processing
7	Time consumption for simulation Using CFD code	Relatively take time due to the time needed for completing a CFD simulation was depended on the complexity of geometry, number of elements (mesh), time step size, number of time steps, maximum iteration for time step, and type of simulation single-phase or cavitation conditions
8	Sensitive of CFD code to detect cavitation	Sensitive
9	Need PC	PC is used to achieve the numerical calculations required for simulating cavitation
10	Cost of the PC	Relatively expensive
11	Detection level of cavitation	It can be detected different levels of cavitation (no cavitation, inception, development, fully development of cavitation) using CFD

7.13.2. The Vibration Analysis Technique

The second main aim of this research study was to construct an experimental setup for the centrifugal pump in order to investigate the pump performance and to predict cavitation under a different wide range of operating conditions using different conditioning monitoring techniques including vibration signal analysis. Detailed different experimental measurements based investigations were carried out to analyse the vibration signal using accelerometer in Chapter six. The results found that cavitation can be predicted within a pump through analysing the vibration signal in time domain for various operation conditions using different statistical features. It can be seen that when cavitation occurrence rapidly increases the level of vibration amplitude increases. Also, the results from experimental measurements showed that the analysis on vibration signal in frequency domain can predict the occurrence of cavitation by using different ranges of frequency from 0Hz to 15kHz, having useful information regarding

the cavitation within a pump. Moreover, it is observed that the range of the frequency from 1Hz to 2kHz is a suitable range to predict cavitation. In this case and from the above findings, accelerometer that has low range of frequency between 1Hz to 2kHz was used due to is effectiveness in predicting cavitation. Furthermore, the use of sensor that has low range of frequency is cheaper than sensor with high range of frequency, leading to decrease in the cost of the sensor and hence, decrease the condition monitoring cost.

This technique was evaluated based on the cost of the sensor, installation of the sensor, ease of application and effect of any vibration within the system. Therefore, Table 7-14 summarises the most significant features of the vibration technique based on the results that were presented in Chapter six in order to detect cavitation occurrence within a centrifugal pump under different experimental operation conditions.

Table 7-14: Summary of the most significant features of the vibration technique to detect cavitation within a centrifugal pump

No.	Conditions	Remarks	
1	Detection of cavitation with a Pump	In time domain analysis (TDA)	In frequency domain analysis (FDA)
		Yes	Yes
2	Effected any vibration within a system	Time domain	Frequency domain
		Yes	Yes
3	Method of detection of cavitation	Online	Offline
		Yes	Yes
4	Installation of accelerometer sensor	Easy to install in the pump	
5	Cost of accelerometer sensor	Relatively expensive	
6	Need signal processing	Needed to analysis the vibration signal in time and frequency domain	
7	Sensitive of sensor to detect Cavitation	Sensitive	
8	Need amplifier for vibration Signal	No	
9	Need DAQ system	Yes	
10	Need PC for analysing raw vibration data	Yes	
11	Cost of PC	Relatively cheap	
12	Installation of MATLAB code	Need licence	
13	Cost of MATLAB licence	Relatively expensive	
14	Frequency range of the sensor	0Hz-15kHz	
15	Sensitive at low frequency range of the sensor to detect cavitation	1kHz-2kHz	
16	Sensitive high frequency range of the sensor to detect cavitation	2kHz-15kHz	
17	Detection level of cavitation	No cavitation, inception, development,	

	at low frequency range	fully development of cavitation
18	Detection level of cavitation at high frequency range	No cavitation, inception, development, fully development of cavitation

7.13.3. The Acoustic Analysis Technique

Detailed different experimental measurement based investigations were carried out to analyse the acoustic signal using microphone in Chapter seven. During these experimental measurements, it was found that the acoustic amplitude in time domain, using different features and also in frequency domain changes in amplitudes when the pump operates at flow rate higher than the design flow rate and hence, cavitation becomes more developed as the flow rate in the pump increases. In the meantime, it can be observed that when the flow rate was higher than 350(l/min), it leads to the pump operating under fully developed of cavitation conditions. For further investigation carried out in this study, both vibration and acoustic signals were analysed using mean and RMS amplitude features based on different range of frequencies. The results revealed that cavitation can be predicted in the pump using low-frequency range between 1Hz and 2kHz and also at high frequency range from 2Hz to 15kHz.

For this current study, the analyses of acoustic signals in time and frequency domains provide approximately the same trend as compared to that of the vibration signal results. The possible reason is because both acoustic and vibration were generated from within the centrifugal pump, through a similar way that was caused by high interaction between the volute and impeller and by the occurrence of cavitation. Furthermore, it can be concluded that using both techniques can be very effective to monitor cavitation in the pump.

In this study, it was observed that the vibration technique was more accurate when compared to the acoustic technique. This is because the acoustic signals were obtained using the microphone as this sensor was very sensitive to any noise around the pump in the lab. However, the acoustic technique can be used for monitoring cavitation condition instead of the vibration technique if the latter technique is not applicable. As mentioned in the previous section, the acoustic technique can be evaluated based on the cost of the sensor, installation of the sensor, ease of application and effect of any noise within a system. Therefore, Table 7-15 summarises the most significant features of the acoustic technique based on the results that were presented in Chapter seven, in order to detect cavitation occurrence within a centrifugal pump under different experimental operation conditions measurements.

Table 7-15: Summary of the most significant features of the acoustic technique to detect cavitation within a centrifugal pump

No.	Conditions	Remarks	
1	Detection of cavitation in the Pump	In time domain Analysis (TDA)	In frequency domain analysis (FDA)
		Yes	Yes
2	Effected any noise within a system	Time domain	Frequency domain
		Yes	Yes
3	Method of detection of cavitation	Online	Offline
		Yes	Yes
4	Installation of microphone sensor	Easy to install near by the pump	
5	Cost of microphone sensor	Relatively expensive	
6	Need signal processing	Needed to analysis the acoustic signal	
7	Sensitive of sensor to detect Cavitation	Sensitive	
8	Need amplifier for acoustic signal	Yes	
9	Need DAQ system	Yes	
10	Need PC for analysing raw acoustic data	Yes	
11	Cost of PC	Relatively cheap	
12	Installation of MATLAB code	Need licence	
13	Cost of MATLAB licence	Relatively expensive	
14	Frequency range of the sensor	0Hz-15kHz	
15	Sensitive at low frequency range of the sensor to detect cavitation	1kHz-2kHz	
16	Sensitive at high frequency range of the sensor to detect cavitation	2kHz-15kHz	
17	Detection level of cavitation at low frequency range	No cavitation, development, fully development of cavitation	
18	Detection level of cavitation at high frequency range	No cavitation, inception, development, fully development of cavitation	

Based on the findings in this thesis, it can be observed that the general behaviour of vibration and acoustic signature was also in agreement with previous studies for different types of pumps [78, 79, 82, 84, 91]. However, detailed investigations of cavitation characteristics use vibration and acoustic analyses techniques under wide ranges of operating conditions and frequency ranges in both time and frequency domains using different statistical features were conducted. In addition, a comparative investigation was carried out between above techniques using cavitation detection index (CDI) in both time and frequency domains. Accordingly, the current work includes comparison and an evaluation of the cavitation condition monitoring using CFD, vibration and acoustic techniques under wide range of operation conditions that were not carried out in most of these studies.

In summary, numerical CFD based methodology, as well as vibration and acoustic technique based on experiments were used in detecting and diagnosing cavitation. CFD, vibration and acoustic techniques were confirmed to be effective techniques in order to analyse the behaviour of cavitation under different operating conditions. When comparison is made among these techniques, they can provide several advantages such as capability to detect the different levels of cavitation. Also, it was observed that the numerical results when using CFD and experimental results when using vibration techniques can detect the inception of cavitation within a pump earlier than the acoustic technique. Furthermore, after computing the numerical and experimental results using the different condition indicators under various operating conditions, cavitation detection within a pump can be achieved using the above mentioned techniques. Furthermore, the numerical and experimental results using CFD, vibration and acoustic detection techniques showed that the inception of cavitation occurs before any drop in the pump performance. Therefore, in order to avoid the effect of cavitation within a pump, it is important to monitor the pump continuously while the pump is in operation.

Extensive numerical and experimental investigations in previous Chapters (5, 6, and 7) were carried out using the different techniques for detecting and diagnosing cavitation within a centrifugal pump. According to the above numerical results, the position, level and characteristics of the visualisation of cavitation flow, whilst observing the flow motion within a centrifugal pump, were detected. Also, the numerical investigation results using both quantitative and qualitative analyses in CFD were used in analysing the results obtained. Qualitative analysis is done by using vapour volume fraction contour for the different operating conditions, whilst quantitative analysis is carried out by using the comparison between the pump head under single-phase and cavitation conditions at different operation conditions. The quantitative and qualitative CFD analyses showed that the inception and different levels (severity) of cavitation in the pump can be accurately captured when compared to both vibration and acoustic technique. Therefore, the order of sensitivity for the above techniques to detect cavitation can be suggested as follows:

1. Numerical simulation using CFD analysis code
2. Experimentation using vibration analysis technique
3. Experimentation using acoustic analysis technique

Based on the above analysis in this research, it can be concluded that using numerical cavitation model in CFD was an effective and reliable tool, as well as assisting and providing good

guidance information for engineers in industry. In order to obtain more information to detect and diagnose the possible areas of cavitation damage that can lead to improvements in the turbomachinery systems in order to avoid real damages. However, the results revealed that the combined use of the above mentioned techniques, numerical and experimental, can increase reliability and provide a more robust detection of cavitation in pumps.

This chapter was presented all analyses and discussions regarding detection of cavitation within a centrifugal pump under different operational conditions using acoustic analysis technique. Moreover, comparison between acoustic technique and vibration technique was carried out, in order to find experimentally, the better sensitive method for detecting the inception and development of cavitation in the pump. Also, the usefulness and evaluation of the above mentioned techniques in finding the most sensitive technique, numerically and experimentally, for predicting and diagnosing cavitation in the pump were carried out. Finally, the next chapter will include conclusions and contributions of knowledge and also suggestions for future work.

CHPTER 8

CONCLUSIONS

This chapter provides detailed conclusions and evaluations of various techniques that were investigated in this research study. These techniques include CFD, vibration, and acoustic based on results that were obtained in previous chapters regarding the pump performance evaluation and detection of cavitation in the centrifugal pump. Also, the main achievements and contributions in this study were summarised in this chapter. Finally, requirements for future work in the area of a centrifugal pump are defined.

8.1. Research Problem Synopsis

In the last decade, centrifugal pumps are broadly used in numerous types of applications such as agriculture, plants of wastewater treatment, gas and oil industry, food industry and power plants [154]. It is becoming one of the most important devices in different industries. Also, cavitation is commonly attributed as being one of the main causes of several unwanted effects. Firstly, deterioration of the pump performance operating at high flow rates and high rotational speeds were revealed in previous chapters. The second significant effect is pitting and erosion of material in parts of the pump. This occurs due to bubbles collapsing near these parts. The third negative effect increases the level of noise and vibration within a pump that happens due to instability in flow which leads to cause more pressure fluctuations [155]. Therefore, based on the above negative impacts it can be clearly seen that the cavitation is an undesirable phenomenon and it should be avoided. In this study, the numerical simulation and experimental techniques were used to analyse the characteristics of cavitation. To achieve this, it is an important point to distinguish the severity level of cavitation within a pump, particularly in industrial environments, and it needs continuous condition monitoring in order to increase the operational life of the pump and decrease the cost of maintenance and attempt to avoid any shutdown in the system. The main aim of this study was the evaluation of various techniques to predict cavitation phenomenon within the centrifugal pump. These techniques include Computational Fluid Dynamics. In this research study, the CFD technique was adopted in order to determine the performance and to predict cavitation within the pump. The investigation was carried out under a wide range of operational conditions and various impeller geometrical parameters. The second and third techniques used to detect cavitation were experimental based on vibration and acoustic. The detailed analysis and results of these techniques can be seen in previous chapters. Also, in this chapter, the advantages of these techniques were summarised based on the results which were obtained from this research study. In the following parts of this chapter, the main aims of this study were summarised along with the main achievements and contributions.

7.2 Research Aims and Main Achievements

The main aims of the present study that were defined based on an extensive literature review in this field are as follows:

Research Aim # 1: CFD based investigation of flow and geometrical parameters on single-phase and cavitation behaviour in the centrifugal pump.

Achievement # 1: In this research detailed Computational Fluid Dynamics based investigations were provided on the flow structure within a centrifugal pump under single-phase and cavitation conditions. A transient numerical simulation was carried out under different operating conditions for the pump. Firstly, the numerical results were validated with experimental results. Also, the numerical statistical analysis results of the pump head under various flow rates were found to agree well with the experimental results. The second aspect corresponds to unsteady flow investigations of the pump, and for this goal, the pump was run at different flow rates under single-phase and cavitation conditions. It allowed extraction head of the pump and the analysis, including the flow structure quantification within the pump based on single-phase and cavitation. Thirdly, the characteristics of pressure fluctuations in the impeller and volute flow domain were analysed in both time and frequency domains in order to obtain a better understanding on the interaction between the impeller and volute effects on the flow field in the pump. Furthermore, three-dimensional centrifugal pump model having various impeller geometrical parameters including the number of blades, inlet and outlet impeller diameters were numerically simulated. The effects of the above geometrical parameters on static pressure, velocity magnitude, vapour volume fraction variations, pressure fluctuations and the pump head of a pump under single-phase and cavitation conditions were investigated. In this study, the effects of different impeller geometrical parameters on the performance of the centrifugal pump were analysed under single-phase and cavitation conditions qualitative and quantitative. The current study was used to determine the pump head and power coefficients for different cases to develop different semi-empirical correlations of the centrifugal pump under various impeller geometric configurations under single-phase and cavitation conditions. This prediction model for the performance of the pump has showed that it is reasonably accurate. Furthermore, this numerical technique has several important advantages that can be summarised as following:

1- Based on the presented results in Chapter five, using the CFD code represents a useful and effective numerical analysis method to determine the pump performance and detect/diagnose different levels of cavitation.
2- CFD analysis technique can provide reasonably accurate results as compared to experimental results.

3- Using CFD modelling can play an important part to visualise the behaviour of the flow field under single-phase and cavitation model.
4- It can be used to reduce the cost of experiments to investigate the effect of various operation conditions and different geometrical parameters as well as their influence on cavitation within a pump.

Research Aim # 2: Experimental investigations on condition monitoring of the centrifugal pump using vibration analysis technique for detecting and diagnosing cavitation phenomenon in a centrifugal pump using time and frequency domains analyses.

Achievement # 2: This study provides detailed condition monitoring results on the centrifugal pump based on vibration analysis technique. As explained in Chapter six, the use of vibration technique to monitor the machines in the last few decades was widely used and hence, it is currently the frequently used applied technique in different industries. This technique has several advantages that can be summarised as follows:

1- This technique usually uses the accelerometer sensor in order to collect vibration data and this sensor is easy to install in the machines, particularly in the different types of pumps.
2- Such type of sensor is widely available under different specifications including different range of frequencies, and it can be work under different temperatures. Also, it is very sensitive to capture any change or fault which occurs in the machine.
3- The analysis of vibration data in the time domain gives useful information regarding any change that occurs in the machine. In this study, different statistical features were used to analyse the vibration signal in time domain and these features can provide a good indicator of changes in the condition within the pump.
4- The analysis of vibration signal in the frequency domain can also give a good indicator, for example, to detect and diagnose cavitation in the centrifugal pump due to the changes in the signal amplitudes under different operating conditions, particularly under cavitation condition as shown in Chapter six in this thesis.

The second aim in this research was to analyse the performance and detect cavitation within a centrifugal pump experimentally using vibration technique under different operating conditions. In order to increase the reliability of detection of cavitation within a pump, the vibration technique can be used as an effective technique for this purpose. The experimental results from the pump setup showed that the vibration signals are highly dependent on different operating conditions within the pump. The results also found that the occurrence of cavitation

in the pump depends on the flow rate and pump rotational speeds and it increases when the flow rate and pump rotational speeds increase. The cavitation causes deterioration in the performance of the pump considerably. Additionally, based on the detailed experimental investigations, the vibration signals in the pump were observed to change at different operating conditions. It was found that vibration signals are sensitive to any change in the pump. The amplitude of vibration signals increases with flow rate increase, hence the analysis of vibration signal in both time and frequency domains provide a good indication to predict cavitation in the pump. Different statistical analysis features showed that the vibration signal can be used as an effective technique in order to diagnose and monitor cavitation.

Research Aim # 3: Experimental investigations on condition monitoring of the centrifugal pump using acoustic analysis technique for detecting and diagnosing cavitation phenomenon in a centrifugal pump using time domain analysis and frequency domain analysis.

Achievement # 3: This study provides a detailed condition monitoring based analysis on the centrifugal pump based on acoustic technique, as explained in Chapter seven. The use of acoustic techniques to monitor the machines was widely practiced in industries due to the important improvements in acoustic sensors and data acquisition systems. This technique has several advantages to predict and diagnose cavitation within a centrifugal pump that can be summarised as following:

1. The acoustic technique can be used to acquire data remotely and can be used to collect and record data from a machine at different environmental operating temperatures and conditions.
2. The acoustic sensor (microphone) is widely available at various specifications comprising different frequency ranges and temperatures. Also, it is sensitive to capture any change or fault that occurs in the machine.
3. The use of microphone to acquire signals is relatively at the same cost as compared to vibration accelerometer.
4. The use of acoustic technique in order to monitor the cavitation within a pump gives the same trend as compared with the vibration technique as shown in Chapter seven in this thesis.

Based on the detailed experimental measurements, the acoustic signals in the centrifugal pump were analysed. In order to increase the reliability and detection of cavitation within a pump, the acoustic techniques can be used as a third technique for this purpose. Due to the combined

use of different techniques (numerically using CFD code and experimentally using vibration as well as acoustic techniques), a more robust detection of cavitation within a pump can take place. The acoustic signals were acquired from the centrifugal pump setup and these signals were analysed in time domain based on the same statistical features that were used to analyse the vibration signals as mentioned in Chapter six. Furthermore, the acoustic signals were analysed in the frequency domain as well using FFT technique in order to find more detailed information regarding the detection of cavitation. The results revealed that when the cavitation takes place in the pump it leads to a rapid increase in the level of the noise and that leads to an increase in the acoustic signal amplitude. The results found that acoustic signals can be used as an effective technique to predict and monitor cavitation in the pump.

8.2. Thesis Conclusions

A comprehensive investigation was carried out to support the existing literature regarding the condition monitoring of the cavitation within a centrifugal pump using different condition monitoring techniques and under the wide range of operating conditions, to provide and enhance the current understanding of the prediction of cavitation process and geometry associated influences on the performance of the pump. The main conclusions from each facet of this current research study are summarised as follows:

Research Objective # 1: To analyse the flow field within the centrifugal pump based on single-phase at different operating conditions using sliding mesh technique (SMT) with transient approach.

From the CFD results, investigations regarding the flow field analysis in the centrifugal pump based on single-phase were carried out in this research, and this objective is divided into two main sections. The first section is including validates numerical results with the experimental results. The second section corresponds to unsteady flow investigation within the centrifugal pump and for this aim; the pump was run at different flow rates under single-phase condition. Additionally, extracting the head of the pump for each 5-degree rotation of impeller as well as analysing the flow structure within the pump based on single-phase condition under various operating conditions using transient simulation approach was also included. From both experiments and CFD results, it can be concluded that there is a good agreement between CFD and the experimental results. Also, CFD results showed that the lower pressure occurs at the inlet of impeller particularly in the eye of the impeller. The higher-pressure regions are

presented within the volute, particularly near or close to the volute tongue region. Also, the head of the centrifugal pump is cyclic with the number of peaks and valleys is equal to the same number of impeller blades. Additionally, it can be found that the head of the pump decreased as the flow rate increased. The pressure fluctuations were analysed in time domain and the numerical results showed that the values of pressure fluctuations around volute were dependent on the angular position of the volute cross-section area as well as flow rates, and the maximum values of pressure fluctuations were noticed at near or close to the tongue region. Also, the values of pressure fluctuations in the impeller were dependent on the distance along the radius of the impeller, which increases with the distance along the radius. Furthermore, the pressure fluctuations in time domain were converted into the frequency domain analysis using FFT technique. The results revealed that there are two dominant frequencies the first one is the rotational frequency and its related harmonics and the second one is blade passing frequency and its related harmonics.

Research Objective # 2: To predict the cavitation phenomenon within the centrifugal pump by using cavitation model in CFD at various operating conditions using sliding mesh technique (SMT) with transient approach.

This study provides a detailed CFD based investigation on the flow detection and diagnostic of cavitation within the centrifugal pump. A three-dimension model for the pump was created to determine the regions of an inlet pipe, outlet pipe, impeller and volute by using CFD. A sliding mesh is applied to consider the flow interaction in an impeller and volute. The assumed physical model was water-liquid and water-vapour during simulation of cavitation flow. The CFD results were analysed corresponding to various flow rates in order to study the effects of wide ranges of flow rates. The results for cavitation were explained through the variation of volume fraction contour. The results showed that the vapour volume fraction was high near the impeller inlet under various flow rates. Hence, the cavitation occurred in the vicinity of low-pressure region. This study concludes that the cavitation inception and development on the impeller can be classified into four levels as the vapour volume fraction at the eye of impeller increases and the deterioration in the head of the pump takes place. The following points emerged from the present investigation:

Level 1: There is no cavitation occurring in this stage when the flow rate range is between 100(l/min) and 250(l/min).

Level 2: The stage of the slow inception of cavitation when the flow rate is between 300(l/min) and 320(l/min).
Level 3: The stage of growth of cavitation, when the range of flow rate is between 320(l/min) and 350(l/min).
Level 4: The stage of development of cavitation, in this final stage when the flow rate is higher than 350(l/min), develops in all passages of the impeller.

It can be observed that the maximum vapour volume fractions were mostly distributed in a special area near the inlet surface blades of an impeller. Subsequently, a progressive increase occurs along each impeller passage. In addition, it can be seen that the vapour volume fractions increased in the radial direction and starts to block the inlet passages of an impeller under high flow rate.

Research Objective # 3: To investigate the effect of the different impeller geometrical parameters including; number of impeller blades, inlet and outlet impeller diameters on the performance of the centrifugal pump under single-phase and cavitation conditions.

To determine the effect of the number of impeller blades on the performance of the centrifugal pump under single-phase and cavitation conditions.

From the CFD results, investigations regarding the effect of the impeller geometrical parameters on the pump performance under single-phase and cavitation conditions were carried out. In order to analyse the effect of the number of impeller blades on the performance of the centrifugal pump, three different number of impeller blades 3, 4, and 5 were selected for the analysis purpose. It can be noticed that the pressure is increased gradually from the inlet to the outlet of the impeller. Under these operating condition, the static pressure at the blade's pressure surface was higher than the suction surface. Further, the lower pressure zone inside the impeller was positioned at the suction surface of the blade inlet and the pressure of suction surface region was found to be increasing with the distance along the radius of the impeller. It can be found that the maximum static pressure is at the outlet of the pump close to the tongue region under both single-phase and cavitation conditions. To further investigate, pressure fluctuations in the time domain in the centrifugal pump, were converted into the frequency domain using FFT technique. Also, it can be observed that the maximum pressure fluctuation amplitude was occurred near the tongue region due to the high effect of the interaction between impeller and volute. Furthermore, it can be found that the amplitudes of pressure fluctuations within the impeller are increased with the distance along impeller radius from the centre. For

comparison purposes between the different number of blades, the number of blade Z=5, the head under single-phase and cavitation conditions are considerably higher than for the other two number of blades namely, 3 and 4. The numerical results showed that as the number of impeller blades increases, the head of the pump and cavitation also increase.

To investigate the effect of the outlet impeller diameter on the performance of the centrifugal pump under single-phase and cavitation conditions.

Detailed CFD based analysis was carried out regarding the influences of the impeller outlet diameter on the performance of the centrifugal pump under single-phase and cavitation conditions. In order to analyse the effect of outlet impeller diameter (do) on the performance of the pump, for analysis purposes, three outlet impeller diameters (do) values of 200mm, 210mm and 220mm were selected. It can be concluded that the impeller outlet diameter considerably influences the performance of the pump. For comparison purposes between different impeller outlet diameters under single-phase and cavitation conditions, it can be found that for do=220mm, the head is considerably higher than for the do=200mm model and slight changes for do=210mm was noticed under both single-phase and cavitation conditions. In addition, it can be seen that the head is considerably higher for do=220mm than do=200mm for both single-phase and cavitation conditions. Furthermore, the numerical results showed that as the outlet impeller diameter increases the cavitation within the pump increases.

To analyse the effect of the inlet impeller diameter on the performance of the centrifugal pump under single-phase and cavitation conditions.

In this research study, the investigations regarding the influence of the inlet impeller diameter on the flow structure within the pump under single-phase and cavitation conditions were carried out. In order to analyse the effect of inlet impeller diameter (di) on the performance of the centrifugal pump, for analysis purposes, three inlet impeller diameters (di) values of 25mm, 30mm and 35mm were selected. For comparison purposes under single-phase and cavitation conditions it can be concluded that for di=25mm, the head is slightly higher than for the other two models under both single-phase and cavitation conditions. Therefore, it can be observed that as (di) increases, the head of the pump slightly decreases as well as the cavitation also slightly increases.

Research Objective # 4: To develop semi-empirical relations for the head and power coefficients in the centrifugal pump under single-phase and cavitation conditions.

Based on the numerical investigations using CFD analysis technique that were conducted in Chapter five and after studying the effects of different pump geometrical parameters, different semi-empirical relations for head and power coefficients of the centrifugal pump were developed in this study using the results of numerical simulations under single-phase and cavitation conditions. The development of above mentioned relations were through the use of multiple regression analysis technique in order to evaluate and study the influences of different geometrical parameters on the performance of a pump.

Research Objective # 5: To detect the cavitation phenomenon in the centrifugal pump based on vibration technique.

In this experimental setup, during the experimental measurements and through the use of signal processing programme to analyse different signals using MATLAB code, cavitation could be monitored from calculating the NPSH of the centrifugal pump under different flow rates. In this study, the results revealed that the reference value of flow rate for occurrence of cavitation was at 350(l/min) under N=2755rpm. The second calculation to predict cavitation in this work was through analysis of the different types of signals. All vibration signals were analysed in time domain using various statistical features in order to predict cavitation in the pump. Then these signals were analysed in frequency domain using FFT technique.

It can be clearly seen under cavitation conditions the trend of vibration amplitude was more random with high peaks as compared with normal conditions. The reason behind that is due to the occurrence of cavitation process within a pump, which generates smaller bubbles, which collapse leading to a change in amplitudes of vibration.

In order to obtain further information regarding the occurrence of cavitation, the vibration signals were analysed in time domain using various types of statistical features such as peak, RMS, peak-to-peak and variance values. It can be noticed that under the low flow rate, the trends of the above features showed no significant change in the level of vibration amplitude. However, the level of vibration amplitude rapidly increases at high flow rate. As a result, using the above features in time domain has the capability to predict cavitation in the pump under high flow rates. For further investigation, the vibration signals in the time domain were converted to the frequency domain using FFT technique to predict and diagnose cavitation using different range of frequencies starting from 0Hz to 15Hz. It can be clearly observed that there is a significant increase in the level of vibration amplitude when the pump is operated under higher than 350(l/min) flow rate. For more details regarding prediction of cavitation, the vibration amplitude signals in the frequency domain were analysed using various statistical

features such as mean and RMS vibration amplitude values. The results also showed that no significant changes occurred in the trends of the above features when a pump operates under low flow rate. However, there is a rapid increase in experimental values corresponding to these features at flow rate higher than 350(l/min) which are due to the occurrence of cavitation. It can be found that the use of FFT technique was an effective technique for detecting cavitation in a pump. Furthermore, the analysis of vibration amplitude in both time and frequency domains were agreed with characteristics of cavitation that was presented using NPSH curve.

Research Objective # 6: To investigate the cavitation within the centrifugal pump based on vibration technique under various pump rotational speeds.

Detailed experimental based examinations were carried out regarding the influences of the different pump rotational speeds on the pump performance and cavitation prediction within a pump using vibration technique. The results revealed that the vibration signal analysis in the time domain can be considered as a first indication of when cavitation has occurred within a pump. Also, the peak and peak-to-peak values were more sensitive to detect cavitation within a pump as compared with RMS and variance features. The frequency domain analysis technique to investigate the vibration amplitude was a satisfactory technique to predict cavitation. In addition, the use of features such as mean and RMS vibration amplitude values to analyse the vibration signal in frequency domain provides more information regarding the prediction of cavitation. It is evident that the trend of head in the pump is continuous downwards trend with increasing flow rate at different rotational speeds. The head under N=2755rpm was considerably higher than for the other cases. Also, cases under different pump rotational speeds (N=2755, N=2610, N=2320, and N=2030rpm) based on time domain analysis were compared. This was carried out by using the statistical features. The vibration signals were also investigated based on frequency domain using the different features such as mean and RMS amplitude values for different range of frequencies. It can clearly be seen that the maximum values corresponding to above features under N=2755rpm were considerably higher than for the other three pump rotational speeds. For further investigation in this study, the vibration signal using mean and RMS amplitudes features for the different range of frequencies revealed that using low-frequency range between 1kHz and 2kHz was sensitive to predict cavitation in the pump. Therefore, it is possible to use an accelerometer with low range of frequency. This leads to a decrease in cost for the sensor as compared to when using a sensor with a high range of frequency.

Research Objective # 7: To detect the cavitation within the pump based on vibration technique under different suction valve openings.

Based on the investigations regarding the effect of different suction valve openings on the pump performance and cavitation prediction within a pump using vibration technique, it can be concluded that the head of the pump decreases when the inlet suction valve openings decreases. This causes cavitation to occur at this point due to reducing the inlet suction pressure under water vapour pressure. The vibration signal analysis in the time domain, using different statistical features can provide a good indication as to when cavitation has occurred under different suction valve openings. The results showed that when the suction valve openings decreased, the above values are increased. Also, the frequency domain analysis technique to investigate the vibration amplitude was a satisfactory technique to predict the inception and development of cavitation within a pump under different suction valve openings. The experimental values of various features such as mean and RMS values in frequency domain have increased as suction valve openings decreased and the above statistical features have increased with the flow rate.

Research Objective # 8: To study the effect of air injection on the performance of the centrifugal pump and detecting cavitation occurrence within a pump based on vibration technique.

Detailed experimental based examinations were carried out regarding the influences of the different amounts of air injections on the pump performance and predict cavitation within a centrifugal pump using vibration technique. It can be concluded that the air injection within a pump has a negative effect due to a decrease in head and caused more unstable flow within a pump due to a higher number of bubbles in addition to bubbles being created by the cavitation process. Also, the experimental results showed that the pump head decreases as the air injection increases in the pump. The use of time domain analysis to analyse the vibration signal can be a suitable technique in order to study the effect of air injection in the pump and detect the inception and development of cavitation. In addition, frequency domain analysis technique also uses the mean and RMS features to analyse the vibration amplitude were a satisfactory technique to study the effect of air injection and predict the inception and development of cavitation within a pump. The experimental results found that an increase in high vibration amplitude in time and frequency domains provides a good indication point to detect cavitation

in a centrifugal pump. The low amount of air injection can cause an increase in the vibration and noise within a pump.

Research Objective # 9: To detect cavitation in the centrifugal pump based on acoustic technique under different flow rates.

Detailed experimental based examinations were carried out regarding the influences of the different flow rates to predict cavitation within a pump using the acoustic analysis technique. It can be concluded that at a flow rate lower than the design flow rate, there is no significant change in the characteristics of acoustic signals. Furthermore, there is a significant difference in the characteristics of acoustic signals at high flow rates that are higher than 350(l/min), in terms of amplitudes of acoustic signals. There are two possible reasons behind this change in acoustic signals. The first is due to the high interaction between the impeller and volute and the second important one is due to the cavitation process occurring in the pump. This is because the NPSHR is higher than NPSHA under high flow rate. The results showed that the level of acoustic amplitude was associated directly with the pump flow rate which increases with flow rate. It can be concluded that acoustic signals are sensitive to predict cavitation within a pump. The results revealed that the effectiveness of using statistical features to analyse acoustic signal such as peak and RMS, peak-to-peak and variance values in the time domain for detection of cavitation in the pump. In order to obtain more information regarding detection of cavitation within a pump, the acoustic signal was converted from time domain analysis to frequency domain using FFT. The results revealed that the analysis of acoustic signals in frequency domain under different frequencies and using mean and RMS acoustic amplitude values provides useful information regarding the prediction of various levels of cavitation within a pump. Furthermore, the analysis of variation in the levels of acoustic amplitude within a pump under different flow rates, in both time and frequency domains were seen to agree with characteristics of cavitation that was presented using NPSH curve in Chapter six.

Research Objective # 10: To investigate the cavitation in the pump based on acoustic technique under various pump rotational speeds.

Based on the investigations regarding the effect of different pump rotational speeds to predict cavitation within a pump using the acoustic technique carried out in this study. It can be concluded that the analysis of the acoustic signal in time domain using different statistical features indicate that the trends of these features are increased when the pump operates under cavitation condition. It can be seen that there are various frequencies in the frequency domain

of acoustic signal. These dominant frequencies are rotation frequency and its harmonics and the second one is BPF. Other frequencies were due to environmental noise around the pump. The experimental results concluded that the for acoustic signals in frequency domain under the different range of frequencies, the mean and RMS acoustic amplitude values increase with the flow rate and pump rotational speed due to the pump operating under cavitation conditions. As a result, the above values provide good information regarding the cavitation prediction in the pump. For comparison purposes between features, in time and frequency domains under different pump rotational speeds (N=2755, N=2610, N=2320, and N=2030rpm), the maximum features values for N=2755rpm are considerably higher than for the other pump rotational speeds. Furthermore, the results showed that using low-frequency range between 1kHz and 2kHz was sensitive to predict cavitation in the pump. Therefore, it possible to use a microphone that has a low range of frequency resulting in a reduction in the sensor cost as compared to when using the microphone with high range of frequency.

Research Objective # 11: To detect the cavitation within the pump based on acoustic technique under various suction valve openings.

Based on the investigations regarding the effect of different suction valve openings to predict cavitation within a pump using the acoustic technique carried out in this study, it can be concluded that when the suction valve openings decrease, it leads to a decrease in the inlet suction pressure below water vapour pressure. This causes cavitation to occur within a pump and it rapidly increases when the inlet suction pressure continuously decreases. The maximum amplitude peak, RMS, peak-to-peak and variance values in the time domain for Q=302(l/min) are higher than for flow rates Q=103(l/min), and Q=200(l/min). The results of different features such as mean and RMS of acoustic amplitude in frequency domain were increased as suction valve openings decreased and the above statistical features were increased with the flow rate.

Research Objective # 12: To analyse the cavitation in the centrifugal pump based on acoustic technique using air injection.

Based on the investigations regarding the effect of the different amounts of air injections to predict cavitation within a centrifugal pump using the acoustic technique as carried out in this study, it can be concluded that the acoustic amplitude signal increased with flow rate increasing due to the cavitation and the effect of air injection within a pump. When the pump operates under cavitation conditions with air injection, the trend of acoustic amplitude was random with high peaks as compared to normal conditions. The maximum peak, RMS, peak-to- peak and

variance values in time domain decrease as air injection increases and the maximum mean and RMS values in frequency domain decrease as air injection increases. Injecting high amounts of air within a suction side of the centrifugal pump results in collection of air bubbles to form a pocket around the impeller, especially at the eye of the impeller, which leads to hydraulic losses in the pump as a result of air binding.

Research Objective # 13: Comparison between vibration and acoustic techniques in order to define the sensitive technique for detecting and diagnosing cavitation in the centrifugal pump.

From the investigations regarding detecting the different level of cavitation within a centrifugal pump, the effects of different operation conditions on cavitation were analysed. From the results presented in Chapters six and seven the cavitation detection index (CDI) technique was used for comparing between vibration and acoustic techniques in order to find the effective technique and sensitive frequency range for detecting occurrence of cavitation. In calculating the cavitation detection index, the actual values for the different statistical features (peak, RMS, peak-to-peak, variance values in time domain and mean, RMS values in frequency domain) were divided with the maximum values for the same above features. It can be concluded that both vibration and acoustic techniques provide good information regarding detecting cavitation in the pump through time domain. However, vibration technique was more sensitive to detect inception of cavitation as compared to acoustic technique. Additionally, the analysis for both techniques in frequency domain showed that both vibration and acoustic techniques are sensitive to detect cavitation at high-frequency range of 10kHz to 15kHz. However, the vibration technique was more sensitive to detect inception of cavitation at low-frequency range of 1kHz to 2kHz as compared to acoustic technique under different operational conditions. Therefore, it can be seen that the use of a sensor with low-frequency range for detecting cavitation can reduce the cost of the sensor. Based on the analysis of vibration and acoustic signal from the pump in time and frequency domains, it can be seen that it is dependent on several operating conditions. It can be observed that these signals are able to identify the pump situation, for example, if the pump operated under normal or abnormal operation conditions. Furthermore, after using both vibration and acoustic techniques in previous chapters, it can be seen that both techniques were effective and capable to detect and diagnose different levels of cavitation depending on noise surrounding the pump; if the level of noise is high, the use of vibration technique is more effective and sensitive as compared to acoustic technique.

8.3. Thesis Contributions

In this present research work the major contributions in the field of cavitation detection within a centrifugal pump are summarised below:

Contribution # 1

The first important contributions of this research study regarding centrifugal pump is a comprehensive investigation on global and local flow field characteristics within a centrifugal pump numerically under single-phase and cavitation conditions. The available literature regarding the pressure, velocity, vapour volume fraction distributions and analysis of pressure fluctuations in time and frequency domains in the pump are severely limited. CFD code was used to carry out extensive investigations on above-mentioned parameters within a centrifugal pump under both single-phase and cavitation conditions as mentioned earlier. The results showed that the CFD could be used as a useful and effective tool to predict and analyse the performance of the pump with reasonable accuracy. In this research, the detailed investigations of cavitation characteristics were carried out in order to provide useful information regarding the inception and development of cavitation within the pump. In this study, both qualitative and quantitative analyses were carried out for various operating conditions and different geometrical configurations of a pump under single-phase and cavitation conditions. These investigations were performed using CFD based tools in order to establish the inter-dependence of various parameters to enable the estimation of the performance characteristics of centrifugal pump. Qualitatively analysis was used for the static pressure and velocity magnitude contours under single-phase conditions and vapour volume fractions contour under cavitation conditions. Whilst quantitative analysis was used for the head and pressure fluctuations in time and frequency domains. The influence of different geometrical parameters such as number of blades and inlet and outlet impeller diameters were investigated. Based on the extensive numerical investigations of these parameters different semi-empirical correlations at different impeller geometrical parameters under single-phase and cavitation conditions for the pump head and power coefficients were developed. The author believes that the use of the above semi-empirical correlations for calculating the head and power coefficients of the pump under single-phase and cavitation conditions is novel as no reports in the literature were seen the use of these semi-empirical correlations for this purpose.

Contribution # 2

Another contribution in this current study was the design and build of a flow loop pumping system of the centrifugal pump. This test rig is capable of studying the characteristic of a pump under different operating conditions (normal or abnormal conditions). The design, construction and capability of this experimental setup were to determine the pump performance then to monitor and detect cavitation phenomenon. This experimental setup can also be used to predict any fault within the pump by using different techniques under various operational conditions such as various flow rates, different pump rotational speeds, different suction valve openings, and using air injection or other operation conditions. Due to this experimental setup including different equipment and quite sensitive sensors such as accelerometer, microphone, different pressure transducers at inlet and outlet of the pump, thermometer, water flow meter, air flow meter, pump rotational speed controller and sensitive data acquisition system were used. Therefore, this test rig can be used to investigate characteristics of the pump in a controlled manner using various techniques simultaneously such as pressure, vibration, and acoustic. All the above-mentioned work was considered as a contribution from this research study to students in the research group at the University of Huddersfield.

Contribution # 3

In this research study, the detailed investigations of cavitation characteristics within a centrifugal pump were carried out using different techniques, such as CFD, vibration and acoustic analysis techniques under wide ranges of operating conditions see Chapters 5, 6, and 7. In order to provide a comprehensive study, useful information and guidance regarding the pump performance and detection/diagnostic, different severity of cavitation (inception, development and full development) within the pump. This research study has provided a good picture and information regarding detection of cavitation numerically and experimentally using the above-mentioned techniques. An extensive study to compare and find an adequate technique for an accurate and reliable monitoring and detection of cavitation amongst the three above-mentioned techniques was carried out. The author believes that the use of the above techniques simultaneously for detection of cavitation in the centrifugal pump under a wide range of operational conditions, numerically and experimentally, as well as to find sensitive and reliable technique for detecting cavitation is an important contribution in this study as no reports in the literature were seen for this purpose. For further and extended study with regard to early detection of cavitation in the pump using both time and frequency domains. This

research study will help future researchers in the same field to define the relative merits of each technique or use another technique (strengths and weaknesses) in order to choose the best technique for monitoring and diagnosing cavitation in the pump.

Contribution # 4

In order to detect the first stages and different levels of cavitation occurrence within a centrifugal pump experimentally under different operation conditions (flow rate, pump rotational speed, suction valve opening, and air injection), in this research, study was carried out for the effectiveness of statistical features, measurements in time and frequency domains. Extensive experimental study to compare between these features based on different techniques (vibration and acoustic) was carried out in Chapters six and seven. This thesis will help researchers for future studies to evaluate and investigate the relative merits of each of these features in time and frequency domain analyses or for use on other features (strengths and weaknesses) for specific applications to monitor the occurrence of cavitation or any faults in the pump.

Contribution # 5

In this research, different experimental techniques such as vibration and acoustic were used to predict cavitation in frequency domain. These techniques includes the use of different range of frequencies, starting from low range of 0Hz-2kHz to high range of between 2kHz to 15kHz in order to determine the most sensitive range of frequency for the detection of cavitation within a centrifugal pump under different operational conditions. The reason behind using this technique is to decrease the computation attempts and reduce the cost of sensors (accelerometer and microphone) that were required. Therefore, this research has found that the range of frequency between 0Hz and 15kHz was more sensitive to detect cavitation in the pump. However, this research also found that the developed tools can be used in the range of frequency from 1Hz to 2kHz to detect cavitation and this range was capable and sensitive enough to predict cavitation process within a centrifugal pump (see Chapters 6 and 7). Based on these findings, it possible to use an accelerometer and microphone with a low range of frequency which leads to a decrease in the cost of sensor as compared to when using sensors with high range of frequency.

This thesis will help researchers for future studies to use the same procedure that was used in this thesis for detecting cavitation under various frequency ranges through the use of different

technique such as acoustic emission (AE) sensor or hydrophone sensor and try to find sensitive frequency range for these techniques to detect cavitation in the pump. These results can be compared with vibration or acoustic techniques results.

Contribution # 6

The main contribution of this experimental work is the use of different techniques such as vibration and acoustic towards conditions based on various conditions monitoring, for detecting cavitation within a centrifugal pump. It was observed in the current experimental study that the use of the above techniques is not only capable of predicting occurrence of cavitation but can also be used for future work to detect the different types of the faults within a pump due to cavitation or any faults. For further and extended study with regard to detecting faults in the pump using both techniques in time and frequency domain analyses. This research study will help future researchers in the same field in the research group at the University of Huddersfield to define the relative merits of each technique or use another technique (strengths and weaknesses) in order to choose the best technique for monitoring and diagnosing faults in the pump.

Contribution # 7

The use of cavitation detection index (CDI) technique that incorporates normalised features for both vibration and acoustic signals in both time and frequency domains proved a good indication regarding detection of different levels of cavitation within a centrifugal pump. Based on these findings, the vibration and acoustic techniques were found to be sensitive to detect cavitation under different operating conditions and different frequency ranges. However, the results showed that the vibration technique was more sensitive to detect different levels of cavitation (no cavitation, inception, development, and fully development of cavitation) as compared to acoustic technique. Furthermore, the use of index with normalised features to analyse vibration signal were more effective technique to detect inception of cavitation as compared to an acoustic signal. The author believes that the use of above index with normalised features for detecting severity of cavitation in the pump in both time and frequency domains is an important contribution in this study as no reports in the literature were carried out.

Contribution # 8

From comparing the findings of the experimental techniques (vibration in Chapter six and acoustic in Chapter seven in both time and frequency domains) and also that of numerical

technique using CFD code in Chapter five, it can be suggested that the sensitivity order of the above techniques to detect cavitation within a centrifugal pump are as follows:

1. Numerical simulation results using CFD code
2. Experimentally using vibration analysis technique
3. Experimentally using acoustic analysis technique

The results revealed that the combined use of these techniques, numerically and experimentally, could increase the reliability and provide a more robust detection of cavitation in the pump. The author believes that the comparison among the three above mentioned techniques to find sensitive technique and suggest order of these techniques to detect cavitation in the centrifugal pump is an important contribution in this research study as no reports in the literature were carried out for this purpose. Furthermore, the numerical and experimental results that were obtained in the current research can provide detailed information and guidelines on prediction of the pump's performance and detection/diagnosis of cavitation within a centrifugal pump under a wide range of operation conditions.

Based on the results in this thesis, the proposed procedure can be used for further and extended work to detect cavitation in different types of pumps. Likewise, the same techniques (CFD, vibration, and acoustic) under wide range of operation conditions and geometrical parameters can be used in the analysing as well. Hence, different relationships or charts could be generated between operational and geometrical parameters through vibrational and acoustical analyses of signals based on experimental data. That can be achieved in both time and frequency domains analyses. Additionally, depending on the CFD results different semi-empirical correlations can be developed using a wide range of operational and geometrical variables with the aid of multiple regression analysis technique.

8.4. Thesis Novelties

The main novelties of the present work are presented below:

1. A wide and comprehensive investigation on global and local flow field characteristics within a centrifugal pump using both qualitative and quantitative analyses were carried out for various operating conditions and different geometrical configurations. Moreover, different semi-empirical equations were developed to estimate the head and power coefficients for the pump under single-phase and cavitation conditions.

2. A very wide range of investigations of cavitation characteristics within a centrifugal pump were carried out experimentally using vibration and acoustic analyses techniques under varied ranges of operating conditions and frequency. Furthermore, the study revealed that cavitation detection index (CDI) technique is a powerful tool, which can be used in both time and frequency domains for detecting the cavitation and comparing the sensitivity of the vibration and acoustic technique in estimating earlier stage of cavitation.
3. A study was conducted to compare usefulness of the different techniques (numerically using CFD and experimentally using vibration and acoustic), which were used simultaneously for detection of cavitation in the pump under a wide range of operational conditions. It was found that the CFD and vibration techniques are effective to detect the inception of cavitation within a pump earlier than the acoustic technique.

8.5. Future Work

For further work which is related to detecting cavitation within a centrifugal pump are described below:

1. This study has used the closed type impeller in the centrifugal pump to obtain more information regarding the cavitation within a pump and to extend the research, it can be used for various kinds of impellers such as open type and semi-open type. Therefore, the same research can be repeated using the above types of impellers and the same techniques applied as those that were used in this thesis, such as CFD, vibration, and acoustic techniques.
2. Repeating the experimental measurements using different ways to simulate the cavitation within a centrifugal pump. Such as decreasing, the water pressure at the suction side through the use of vacuum pump or study the effect of increasing the water temperature using a heater inside the water tank then applied different techniques such as CFD, vibration and acoustic techniques in order to investigate the cavitation in the pump.
3. Light sources and high-speed camera can be used to provide visual observation to predict the inception and development of cavitation in a centrifugal pump. The results can be compared with different techniques such as CFD, vibration and acoustics to find sensitive technique.
4. The strategy of the condition monitoring based on health monitoring and fault prediction is essential for centrifugal pumps. This leads to decrease in maintenance costs and hence avoid any structural damage in the pump. Such condition monitoring system includes detection models that link the severity of faults to the performance of the centrifugal pump. This kind

of research study can be carried out using different techniques such as CFD tools, vibration and acoustic technique

5. The main aim of this study is to predict the inception and development of cavitation occurrence within a centrifugal pump through the use of various techniques. For future research, to use the transparent casing (volute) for the experimental setup of the centrifugal pump in order to obtain more information and a better understanding regarding the occurrence of cavitation and to use the same techniques as stated above or another technique can be attempted.
6. This study has used different techniques to detect cavitation within a centrifugal pump as shown in previous chapters. Therefore, to extend the research, it can be proposed to use the above techniques as well as other techniques to develop the monitoring diagnosis system experimentally using vibration, acoustic, hydrophone and acoustic emission sensors. Also, other techniques such as monitoring motor current and voltage as well as detection of cavitation numerically, using CFD code may be considered equally valid for different types of pumps. Additionally, in order to avoid or prevent a pump from occurrence of cavitation process, the initiating of an alarm to connect with the level of vibration and acoustic amplitudes signals, using the electrical control system can be attempted.
7. The majority of studies in centrifugal pumps concentrates on water as the working fluid, but centrifugal pumps are also used for different applications such as in sewage treatment plants, gas scrubbing and petroleum industries etc. Therefore, for further work, the effect of different working fluid on performance of the pump and detection of cavitation using the same techniques that were used in this research study could be considered.
8. For future research, it can be used various types of inducers in order to decrease or attempt to prevent a centrifugal pump from cavitation through applied different techniques such as CFD, vibration and acoustic.

REFERENCES

1. Staff, P.S. The History of Pumps: Through the Years [cited 6/02/2107]; Available from: http://www.pumpsandsystems.com/topics/pumps/pumps/history-pumps-through-years.
2. 5316-1, B.s., Specification for acceptance tests for centrifugal pump, mixed flow and axial pumps – Part 1: Class C tests. UDC 621.67:620.1. 1976, ISO 2548:1973: UK.
3. RASHAD, A. Ancient Egyptian shaduf. 2015 [cited 06/02/2017]; Available from: http://egy-king.blogspot.co.uk/2015/10/ancient-egyptian-shaduf.html.
4. PUMPS, E. Screw Pump Basics. 2015 [cited 06/02/2017]; Available from: http://empoweringpumps.com/screw-pump-basics/.
5. Nelik, L., Centrifugal & Rotary Pumps: Fundamentals With Applications. 1999: CRC Press.
6. WEE, C.K., Unsteady Flow in Centrifugal Pump at Design and Off-Design Conditions. 2011.
7. Spraker, W., The effects of fluid properties on cavitation in centrifugal pumps. Journal of Engineering for Power, 1965. 87(3): p. 309-318.
8. Girdhar, P. and O. Moniz, Practical Centrifugal Pumps. 2011: Elsevier Science.
9. Al Thobiani, F., The non-intrusive detection of incipient cavitation in centrifugal pumps. 2011, University of Huddersfield.
10. Arnold, K. and M. Stewart, Surface Production Operations, Volume 2:: Design of Gas-Handling Systems and Facilities. Vol. 2. 1999: Gulf Professional Publishing.
11. Design, S. Types of Pumps. 2008 - 2009 [cited 22/07/2017]; Available from: http://pumpseng.blogspot.co.uk/2011/12/types-of-hydraulic-pumps.html.
12. Kamiel, B.P., Vibration-Based Multi-Fault Diagnosis for Centrifugal Pumps. 2015.
13. INC, R.P.S. Basic Configuration and Working of Centrifugal Pumps. 2017; Available from: http://www.rotechpumps.com/basic-configuration-working-centrifugal-pumps-2.
14. Gautam, N., Construction, Working And Advantages Of Centrifugal Pump. 20 Feb 2012
15. Lobanoff, V.S. and R.R. Ross, Centrifugal pumps: design and application. 2013: Elsevier.
16. Liu, G., Effects of geometrical parameters on performance of miniature centrifugal pump. 2014.
17. Time Anderson, N.D., Ladd Folstar, Kerry Lindley, Mike Pollen, and Ken Smith, Introduction to Small Water Systems: A Course for Level 1 Operators. September, 2014.
18. Karassik, I.J., Centrifugal pumps. second edition ed. 1998.

19. Beebe, R.S., Predictive maintenance of pumps using condition monitoring. 2004: Elsevier.
20. Alfayez, L., D. Mba, and G. Dyson, The application of acoustic emission for detecting incipient cavitation and the best efficiency point of a 60kW centrifugal pump: case study. Ndt & E International, 2005. 38(5): p. 354-358.
21. Bachus, L. and A. Custodio, Know and understand centrifugal pumps. 2003: Elsevier.
22. Parrondo, J.L., S. Velarde, and C. Santolaria, Development of a predictive maintenance system for a centrifugal pump. Journal of Quality in Maintenance Engineering, 1998. 4(3): p. 198-211.
23. Brennen, C.E., Hydrodynamics of pumps, 1994. Concepts ETI Inc., Oxford Science Publications: p. 81.
24. Lohrberg, H. and B. Stoffel, Measurement of cavitation erosive aggressiveness by means of structure born noise. http://resolver. caltech. edu/cav: sessionA3. 003, 2001. 8 pages.
25. EQUIPMENTS, F. Understanding Cavitation In Liquids. 2016; Available from: http://www.flowcontrolequip.com/anti-cavitation-trim/.
26. Lee, Y.C., M.D. Ahadlin, and S. Shamsul Anuar, Vibration Analysis Of Cavitation In A Centrifugal Pump. 2007.
27. Zhang, S., et al., Effect of Impeller Inlet Geometry on Cavitation Performance of Centrifugal Pumps Based on Radial Basis Function. International Journal of Rotating Machinery, 2016. Article ID 6048263, 9 pages.
28. Khattab, A. Cavitation in centrifugal pumps. Aug 29, 2014; Available from: http://www.slideshare.net/ahmadkhattab108/pump-cavitation.
29. Okada, T., et al., Relation between impact load and the damage produced by cavitation bubble collapse. Wear, 1995. 184(2): p. 231-239.
30. Jensen, J. and K. Dayton, Detecting cavitation in centrifugal pumps. ORBIT, Second quarter, 2000. 5 pages.
31. www.pumpfundamentals.com. PUMP AND PUMP SYSTEM GLOSSARY. Available from: http://www.pumpfundamentals.com/pump_glossary.htm#top.
32. Smith, P. and T. Kraenzler, Reducing effects of corrosion and erosion. World Pumps, 2017. p. 38-41.
33. Tian, X., Enhanced information extraction from noisy vibration data for machinery fault detection and diagnosis. 2017, Huddersfield: UK.
34. Devi, S., et al., A comparative study between vibration and acoustic signals in HTC cooling pump and chilling pump. International Journal of Engineering and Technology, 2010. 2(3): p. 273.

35. Schroeder, M., et al., Springer handbook of acoustics. 2007.
36. Liu, F., Condition Monitoring and Prognosis for Subsea Multiphase Pump. 2015.
37. Higgs, P.A., et al. A survey on condition monitoring systems in industry. in ASME 7th Biennial Conference on Engineering Systems Design and Analysis. 2004. American Society of Mechanical Engineers (pp. 19-22).
38. Raymond, S.B., Predicitive Maintenance of Pumps Using Condition Monitoring. 2004.
39. Systems, X.A.W. Pump cavitation and how to avoid it
    Best practices in pump system design. August 2015; Available from: http://buildings.xylemappliedwater.com/files/2015/09/Cavitation-White-Paper_FINAL-2.pdf.
40. Kim, J., et al. Design optimization of a centrifugal pump impeller and volute using computational fluid dynamics. in IOP Conference Series: Earth and Environmental Science. 2012 (Vol. 15, No. 3, p. 032025). IOP Publishing.
41. Sidhesware, R. and O. Hebbal, Validation Of Hydraulic Design Of A Metallic Volute Centrifugal Pump. International Journal of Engineering Research & Technology (IJERT) ISSN, 2013: p. 2278-0181.
42. Rajendran, S. and D.K. Purushothaman, Analysis of a centrifugal pump impeller using ANSYS-CFX. International Journal of Engineering Research and Technology, 2012. 1(3) Vol. 1 Issue 3, 6 pages.
43. Patel, M. and A. Doshi, Effect of Impeller Blade Exit Angle on the Performance of Centrifugal Pump. Int J. Emerging Technology and Advanced Engineering, 2013. 3(1): p. 91-99.
44. Shah, S., S. Jain, and V. Lakhera, CFD based flow analysis of centrifugal pump. Proceedings ofInternational Conferenceon Fluid Mechanics and Fluid Power. Chennai, India, paper# TM08, 2010.
45. Kagami, R.L., E. LuizZaparoli, and C.R. de Andrad. Cfd Analysis of An Automotive Centrifugal Pump. in 14th Brazilian Congress of Thermal Sciences and Engineering, October18-22. 2012, 4 pages.
46. Houlin, L., et al., Improvement of SIMPLE Algorithm in Centrifugal Pump for CFD. Appl. Math, 2013. 7(5): p. 1845-1856.
47. Yang, S., F. Kong, and B. Chen, Research on pump volute design method using CFD. International Journal of Rotating Machinery, 2011 Volume 2011, Article ID 137860, 7 pages.

48. Chakraborty, S., et al., Performance prediction of Centrifugal Pumps with variations of blade number. Journal of Scientific & Industrial Research, 2013. 72: p. 373-378.
49. Gupta, M., S. Kumar, and A. Kumar, Numerical study of pressure and velocity distribution analysis of centrifugal pump. International Journal of Thermal Technologies, 2011. 1(1): p. 117-121.
50. Chakraborty, S. and K. Pandey, Numerical Studies on Effects of Blade Number Variationson Performance of Centrifugal Pumps at 4000 RPM. International Journal of Engineering and Technology, 2011. 3(4): p. 410.
51. Shi, W., et al., Numerical prediction and performance experiment in a deep-well centrifugal pump with different impeller outlet width. Chinese Journal of Mechanical Engineering, 2013. 26(1): p. 46-52.
52. Liu, H., X. Wu, and M. Tan, Numerical investigation of the inner flow in a centrifugal pump at the shut-off condition. Journal of Theoretical and Applied Mechanics, 2013. 51, pp. 649-660.
53. Yulin, W., L. Shuhong, and S. Jie, Numerical Simulation on the Steady and Unsteady Internal Flows of a Centrifugal Pump. 18 pages. 2010: INTECH Open Access Publisher.
54. Barrio, R., J. Parrondo, and E. Blanco, Numerical analysis of the unsteady flow in the near-tongue region in a volute-type centrifugal pump for different operating points. Computers & Fluids, 2010. 39(5): p. 859-870.
55. Meakhail, T.A., M. Salem, and I. Shafie, Steady and unsteady flow inside a centrifugal pump for two different impellers. International Journal of Energy and Power Engineering, 2014. 3(2): p. 65-76.
56. Zhang, F., et al., Investigation of transient flow in a centrifugal charging pump during charging operating process. Advances in Mechanical Engineering, 2014. 6: p. 860257.
57. Cui, B., et al., Unsteady flow characteristic of low-specific-speed centrifugal pump under different flow-rate conditions. Journal of Thermal Science, 2015. 24(1): p. 17-23.
58. Dai, C., F.-y. Kong, and L. Dong, Pressure fluctuation and its influencing factors in circulating water pump. Journal of Central South University, 2013. 20: p. 149-155.
59. W.M. Koné, D.S., 2,3B. Dro, K. Yao, and K. Kamanzi). detection of Cavitation in Centrifugal Pumps. 2011.
60. Abbas, M.K., Cavitation In Centrifugal Pumps. Diyala Journal of Engineering Sciences, ISSN, 1999. 8716: p. 22-23.

61. Kim, M.J., H.B. Jin, and W.J. Chung. A Study on Prediction of Cavitation for Centrifugal Pump. in Proceedings of World Academy of Science, Engineering and Technology. 2012 pp.612-617. World Academy of Science, Engineering and Technology (WASET).
62. Li, W., et al., Numerical Prediction and Performance Experiment in an Engine Cooling Water Pump with Different Blade Outlet Widths. Mathematical Problems in Engineering, Volume 2017, Article ID 8945712, 11 pages.
63. Niazi, E., M. Mahjoob, and A. Bangian. Experimental and numerical study of cavitation in centrifugal pumps. in ASME 2010 10th Biennial Conference on Engineering Systems Design and Analysis. American Society of Mechanical Engineers (pp. 395-400).
64. Li, X., et al., Numerical simulation of leading edge cavitation within the whole flow passage of a centrifugal pump. Science China Technological Sciences, 2013. 56(9): p. 2156-2162.
65. Misiewicz, A. and J. Skrzypacz, Cavitation behaviours of low specyfic speed pump impellers designed according to the „tight inlet" rule. Open Engineering, 2011. 1(2): p. 195-201.
66. A., H.A.M.K.N., Experimental and Numerical Study on Cavitation Effects in Centrifugal Pumps. Volume 20 February 2014: p. 73-86.
67. Kesba, O.K., M.K. Mihoubi, and M. Bourkia, Study of the effect of cavitation upon the wheels of different types of materials for pump. Mechanics & Industry, 2013. 14(4): p. 299-304.
68. Lei, T., et al., Numerical simulation of unsteady cavitation flow in a centrifugal pump at off-design conditions. Proceedings of the Institution of Mechanical Engineers, Part C: Journal of Mechanical Engineering Science, 2014, Vol. 228(11) p. 1994–2006.
69. Fukaya, M., Y. Tamura, and Y. Matsumoto. Prediction of Impeller Speed Dependence of Cavitation Intensity in Centrifugal Pump Using Cavitating Flow Simulation with Bubble Flow Model. in Proceedings of the 7th International Symposium on Cavitation, CAV. 2009, 7 pages.
70. Al-Hashmi, S.A., Statistical Analysis of Acoustic Signal for Cavitation Detection. International Journal of Emerging Technology and Advanced Engineering, 2013, p. 55-66.
71. Steinmann, A., H. Wurm, and A. Otto, Numerical and experimental investigations of the unsteady cavitating flow in a vortex pump. Journal of Hydrodynamics, Ser. B, 2010. 22(5): p. 324-329.

72. Shukla, S.N. and J. Kshirsagar. Numerical Prediction of Cavitation in Model Pump. in ASME 2008 International Mechanical Engineering Congress and Exposition. 2008 pp. 91-98. American Society of Mechanical Engineers.
73. Zhu, R., et al., Features of Transient Flow during Collapse of Nuclear Power Pump Cavitation. Applied Mathematics & Information Sciences, 2014. 8(3): p. 1185.
74. Liu, H.-l., et al., Influence of the empirical coefficients of cavitation model on predicting cavitating flow in the centrifugal pump. International Journal of Naval Architecture and Ocean Engineering, 2014. 6(1): p. 119-131.
75. Homa, D. and W. Wróblewski. Modelling of flow with cavitation in centrifugal pump. in Journal of Physics: Conference Series. 2014 (Vol. 530, No. 1, p. 012032). IOP Publishing.
76. Zhang, N., et al., Investigation on vibration characteristics in a centrifugal pump with special slope volute. Advances in Mechanical Engineering, 2015. 7(2): p. 936218.
77. Stopa, M.M., B.J. Cardoso Filho, and C.B. Martinez. Detection of incipient cavitation phenomenon in a centrifugal pump. in 2012 (pp. 1-6) IEEE Industry Applications Society Annual Meeting.
78. Chudina, M., Noise as an Indicator of Cavitation in a Centrifugal Pump. Acoustical Physics, 2003. 49(4): p. 463-474.
79. Černetič, J., J. Prezelj, and M. Čudina, Use of noise and vibration signal for detection and monitoring of cavitation in kinetic pumps. The Journal of the Acoustical Society of America, 2008. 123(5): p. 3316-3316.
80. Albraik, A., et al. Diagnosis of centrifugal pump faults using vibration methods. in Journal of Physics: Conference Series. 2012 (Vol. 364, No. 1, p. 012139). IOP Publishing.
81. Suhane, A., Experimental Study on Centrifugal Pump to Determine the Effect of Radial Clearance on Pressure Pulsations, Vibrations and Noise. Int. J. Eng. Res. Appl, 2012. 2(4): p. 1823-1829.
82. Farokhzad, S., N. Bakhtyari, and H. Ahmadi, Vibration Signals Analysis and Condition Monitoring of Centrifugal Pump. Technical Journal of Engineering and Applied Sciences, 2013: p. 1081.
83. Luo, Y., Sun, H., Yuan, S. Q., & Yuan, J. P. (2015). Research on statistical characteristics of vibration in centrifugal pump. Technical Journal of the Faculty of Engineering, 38(1), p. 49-61.
84. Čdina, M., Detection of cavitation phenomenon in a centrifugal pump using audible sound. Mechanical Systems and Signal Processing, 2003. 17(6): p. 1335-1347.

85. Sakthivel, N., V. Sugumaran, and S. Babudevasenapati, Vibration based fault diagnosis of monoblock centrifugal pump using decision tree. Expert Systems with Applications, 2010. 37(6): p. 4040-4049.
86. Tan, C.Z. and M.S. Leong, An experimental study of cavitation detection in a centrifugal pump using envelope analysis. Journal of System Design and Dynamics, 2008. 2(1): p. 274-285.
87. McCormick, A. and A. Nandi, Classification of the rotating machine condition using artificial neural networks. Proceedings of the Institution of Mechanical Engineers, Part C: Journal of Mechanical Engineering Science, 1997. 211(6): p. 439-450.
88. Al Thobiani, F., F. Gu, and A. Ball, The monitoring of cavitation in centrifugal pumps based on the analysis of vibro-acoustic measurements. CM 2010 and MFPT 11 pages.
89. Čudina, M. and J. Prezelj, Detection of cavitation in operation of kinetic pumps. Use of discrete frequency tone in audible spectra. Applied Acoustics, 2009. 70(4): p. 540-546.
90. Nasiri, M., M. Mahjoob, and H. Vahid-Alizadeh. Vibration signature analysis for detecting cavitation in centrifugal pumps using neural networks. in Mechatronics (ICM), 2011 IEEE International Conference pp. 632-635.
91. Zargar, O.A., Detecting Cavitation in a Vertical Sea water Centrifugal Lift Pump Related to Iran Oil Industry Cooling Water Circulation System. World Academy of Science, Engineering and Technology, International Journal of Mechanical, Aerospace, Industrial, Mechatronic and Manufacturing Engineering, 2014. 8(1): p. 124-129.
92. Hosain, M.L. and R.B. Fdhila, Literature Review of Accelerated CFD Simulation Methods towards Online Application. Energy Procedia, 2015. 75: p. 3307-3314.
93. Kevin W. Linfield, a.R.G.M. Pros and Cons of CFD and Physical Flow Modeling. August, 2008; Available from: http://www.airflowsciences.com/sites/default/files/docs/Pros-and-Cons-of-CFD-and-Physical-Flow-Modeling.pdf.
94. Experience), C.M.S.C.E.C.M.A.W.V. 4 Advantages and Disadvantages of CFD. 12Jun / 2013; Available from: https://cfdmodelingservices.wordpress.com/2013/06/12/4-advantages-and-disadvantages-of-cfd/.
95. La Roche-Carrier, N., G. Dituba Ngoma, and W. Ghie, Numerical Investigation of a First Stage of a Multistage Centrifugal Pump: Impeller, Diffuser with Return Vanes, and Casing. ISRN Mechanical Engineering, 2013. Article ID 578072, 15 pages.
96. Jaiswal, N., CFD Analysis of Centrifugal Pump: A Review. Int. Journal of Engineering Research and Applications, 2014. 4(5): p. 175-178.

97. Online, C. Near-wall treatment for k-omega models. 3 November 2011; Available from: https://www.cfd-online.com/Wiki/Near-wall_treatment_for_k-omega_models.
98. Limbach, P., et al., Numerical and experimental investigation of the cavitating flow in a low specific speed centrifugal pump and assessment of the influence of surface roughness on head prediction. 2016. 9 pages.
99. Müller, T., P. Limbach, and R. Skoda, Influence of Geometry Simplifications and Numerical Parameters in 3D URANS Liquid-Gas Flow Simulations of a Radial Pump with an Eulerian Mono-Dispersed Two-Phase Model. 2016. 9 pages.
100. Hua, T., L. Yi, and Z. Yu-Liang, Numerical analysis of a prototype centrifugal pump delivering solid-liquid two-phase flow. Journal of Applied Sciences, 2013. 13(17): p. 3416.
101. Cui, B., et al., Research on performance of centrifugal pump with different-type open impeller. Journal of Thermal Science, 2013. 22(6): p. 586-591.
102. Cui, B., et al., Influence of blade outlet angle on performance of low-specific-speed centrifugal pump. Journal of Thermal Science, 2013. 22(2): p. 117-122.
103. Park, K., Optimal design of a micro vertical axis wind turbine for sustainable urban environment. 2013, University of Huddersfield: p. 45.
104. Asim, T., Computational Fluid Dynamics based Diagnostics and Optimal Design of Hydraulic Capsule Pipelines. 2013, University of Huddersfield: p. 55.
105. Pavesi, G., Impeller volute and diffuser interaction. 2006, DTIC Document.
106. ANSYS, I. ANSYS Fluent Theory Guide Release 15.0. November 2013; Available from: https://uiuc-cse.github.io/me498cm fa15/lessons/fluent/refs/ANSYS%20Fluent%20Theory%20Guide.pdf.
107. Liu, H.-l., et al., Application of modified κ-ω model to predicting cavitating flow in centrifugal pump. Water Science and Engineering, 2013. 6(3): p. 331-339.
108. Fluent, A., 12.0 Theory Guide. Ansys Inc, 2009. 5.
109. Li, Z. and T. Terwisga. On the capability of multiphase RANS codes to predict cavitation erosion. in Second International Symposium on Marine Propulsors. 2011. 8 pages.
110. Riglin, J.D., Cavitation Study of a Microhydro Turbine. 2012.
111. Center, F.U.S. Solver Settings Solver Settings Introductory FLUENT Training. December 2006;Availablefrom:http://www.engr.uconn.edu/~barbertj/CFD%20Training/Fluent/4%20Solver%20Settings.pdf.

112. Yong, W., et al. Prediction research on cavitation performance for centrifugal pumps. in Intelligent Computing and Intelligent Systems, ICIS 2009. IEEE International Conference (Vol. 1, pp. 137-140).
113. Liu, J., et al. Critical cavitation coefficient analysis of a space low specific centrifugal pump with micro gravity. in IOP Conference Series: Materials Science and Engineering. 2016 (Vol. 129, No. 1, p. 012049). IOP Publishing.
114. Li, H., et al. Advanced computational modeling of steady and unsteady cavitating flows. in ASME 2008 International Mechanical Engineering Congress and Exposition (pp. 413-423). American Society of Mechanical Engineers.
115. Tang, X.-l., et al., Numerical investigations on cavitating flows with thermodynamic effects in a diffuser-type centrifugal pump. Journal of Mechanical Science and Technology, 2013. 27(6): p. 1655-1664.
116. Xu, Y., et al. Influence of blade angle distribution along leading edge on cavitation performance of a centrifugal pump. in IOP Conference Series: Materials Science and Engineering. 2015 (Vol. 72, No. 3, p. 032019). IOP Publishing.
117. Ning, C., et al. Numerical calculation for cavitation flow of inducer. in IOP Conference Series: Materials Science and Engineering. 2015 (Vol. 72, No. 3, p. 032025). IOP Publishing.
118. Qiu, N., et al. Research on cavitation characteristic of inducer. in IOP Conference Series: Materials Science and Engineering. 2013 (Vol. 52, No. 6, p. 062010). IOP Publishing.
119. Guo, X., et al., Analysis of Cavitation Performance of Inducers. 2012: INTECH Open Access Publisher 16 pages.
120. F32/200AH, P.P. Standardised “EN 733” centrifugal pumps. Available from: http://www.pedrollo.co.uk/pump-shop/acatalog/F_2014.pdf.
121. h, J.D.S.m.i.t., Vibration Measurement and Analysis. 1989: Butterworths.
122. (GST), G.S.T. The CA-YD-1182 is a general purpose integrated electronics (IEPE) accelerometer. 2015; Available from: www.globalsensortech.com/icpe-accelerometer-ca-yd-1182.
123. (GST), G.S.T. Free field microphone CHZ-223. 2015; Available from: http://www.globalsensortech.com/free-field-microphone-chz-223.
124. (GST), G.S.T. Microphone pre-amplifier YG-201. 2015; Available from: http://www.globalsensortech.com/microphone-pre-amplifier-yg-201.
125. Ltd, I.S.S. IMP Industrial Pressure Transmitter. 2016 [cited; Available from: http://www.impress-sensors.co.uk/products/sensor-products/pressure

measurement/industrial-pressure-transducers-transmitters/standard-range-pressure-transmitter/imp-industrial-pressure-transmitter.html.

126. FLOMEC. TM Series Electronic Water Meters Owner's Manual. 2015; Available from: http://gpi.net/downloads/920786-03.pdf.
127. FLOWMC. 1 ½ in. PVC water meter with NPT fittings and local electronic LCD computer that reads Gallons, Litres and Cubic Feet. Use with water and mild chemicals. [cited 2017; Available from: http://catalog.gpi.net/item/economy-electronic-digital-meters/tm-series-water-meter/tm150-n-water-meter.
128. INC, O.E. Mass Flow meters With or Without Integral Display FMA1700 and FMA1800 2017; Available from: http://www.omega.com/pptst/FMA1700_1800.html.
129. PROTO-PIC. Rapid 10A 0-30V Triple Output Digital DC Regulated PSU. 2017; Available from:https://www.proto-pic.co.uk/rapid-10a-0-30v-triple-output-digital-dc-regulated-psu.html.
130. Smith, S.W., The scientist and engineer's guide to digital signal processing. 1997.
131. Connection Technology Center, I., R. Boulevard, and N.Y. Victor. Beginning Vibration Analysis.2015[cited25/03/2017];Availablefrom:http://www.ctconline.com/pdf/pubTechPapers/01-Beginning%20Vibration%20Analysis.pdf.
132. HANDBOOK), B.O.C.N., Measurement Uncertainty Analysis Principles and Methods 2010.
133. Li, G., et al. Numerical analysis of transient flow in centrifugal pump at off-design conditions. in Fluid Machinery and Fluid Engineering, ISFMFE-6th International Symposium on p. 19. 2014. IET.
134. Shi, F. and H. Tsukamoto, Numerical study of pressure fluctuations caused by impeller-diffuser interaction in a diffuser pump stage. Journal of Fluids Engineering, 2001. 123(3): p. 466-474.
135. Tao, Y., et al., Influence of blade thickness on transient flow characteristics of centrifugal slurry pump with semi-open impeller. Chinese Journal of Mechanical Engineering, 2016. 29(6): p. 1209-1217.
136. Pei, J., W.-j. Wang, and S.-q. Yuan, Statistical analysis of pressure fluctuations during unsteady flow for low-specific-speed centrifugal pumps. Journal of Central South University, 2014. 21: p. 1017-1024.
137. Hedi, M., K. Hatem, and Z. Ridha, Numerical analysis of the flow through in centrifugal pumps. 6 pages. International Journal of thermal Technology, 2012. 2(4).

138. Stickland, M.T.a.S., T.J. and Blanco-Marigorta, E. and Fernandez-Francos, J. and Gonzalez-Perez, J. and Santolaria-Morros, C. Numerical flow simulation in a centrifugal pump with impeller-volute interaction. 2000; 8 pages Available from: http://strathprints.strath.ac.uk/7436/.
139. Messina, J., Pump Handbook. Vol. 3. 1986, New York: McGraw-Hill.
140. Huang, S. and Y.-l. WU, Analysis of Flow Field Asymmetry and Force on a Centrifugal Pump by 3-D Numerical Simulation [J]. Fluid Machinery, 2006. 2: p. 008.
141. Hanimann, L., et al. Cavitation modeling for steady-state CFD simulations. in IOP Conference Series: Earth and Environmental Science. 2016 (Vol. 49, No. 9, p. 092005). IOP Publishing.
142. Li, P., Y. Huang, and J. Li. Cavitation simulation and NPSH prediction of a double suction centrifugal pump. in IOP Conference Series: Earth and Environmental Science. 2012 (Vol. 15, No. 6, p. 062025). IOP Publishing.
143. Ding, H., F. Visser, and Y. Jiang. A practical approach to speed up NPSHR prediction of centrifugal pumps using CFD cavitation model. Fluids Engineering Division Summer Meeting collocated with the ASME Heat Transfer Summer Conference and the ASME 2012 10th International Conference on Nanochannels, Microchannels, and Minichannels. American Society of Mechanical Engineers pp. 505-514; 10 pages.
144. Cimbala, J.M., Fluid Mechanics: Fundamentals and Applications. Vol. 1. 2006: Tata McGraw-Hill Education.
145. Moisés Solis, F.B., Sofiane Khelladi, and Ricardo Noguera. Numerical study on pressure fluctuation in centrifugal pump influence of radial gap and splitter blades. 2011; Available from: https://www.hindawi.com/journals/isrn/2011/479594/. Article ID 479594, 14 pages.
146. Dai, C., F.-y. Kong, and L. Dong, Pressure fluctuation and its influencing factors in circulating water pump. Journal of Central South University, 2013. 20(1): p. 149-155.
147. Zhang, W., Z. Yu, and B. Zhu, Influence of Tip Clearance on Pressure Fluctuation in Low Specific Speed Mixed-Flow Pump Passage. Energies, 2017. 10(2): p. 148.
148. Tuzson, J., Centrifugal pump design. 2000: John Wiley & Sons.
149. Schmitz, S., Reducing pump noise in cooling tower applications. World pumps, 2004. 2004(456): p. 24-29.
150. Hernandez-Solis, A., Diagnosis of Centrifugal Pumps. 2006: Skolan för elektro-och systemteknik, Kungliga Tekniska högskolan.

151. Goyal, D. and B. Pabla, The vibration monitoring methods and signal processing techniques for structural health monitoring: A review. Archives of Computational Methods in Engineering, 2016. 23(4): p. 585-594.
152. Guelich, J. and U. Bolleter, Pressure pulsations in centrifugal pumps. Journal of Vibration and Acoustics, 1992. 114(2): p. 272-279.
153. Ramroop, G., et al. Airborne Acoustic Condition Monitoring of a Gearbox System. in 2001 5th Annual Maintenance and Reliability Conference (MARCON 2001). 11 pages.
154. Jones, G.M., et al., Pumping station design. 2006: Gulf Professional Publishing.
155. Grist, E., Cavitation and the centrifugal pump: a guide for pump users. 1998: CRC press.

APPENDIX A

- y+ calculation for different centrifugal parts under different flow rates

Table A.1 Summarises the calculation of y+ for volute

No.	Flow rate	Density	Kinematic viscosity	Shear stress	u*	y	y+
	(l/min)	(kg/m^3)	$m^2/s *10^{-6}$	Pa		(m)	(-)
1	100	998.2	1.004	106.28	0.326	0.00009	29.24
2	150	998.2	1.004	155.40	0.394	0.000077	30.26
3	200	998.2	1.004	196.17	0.443	0.00007	30.90
4	250	998.2	1.004	226.07	0.475	0.000063	29.86
5	300	998.2	1.004	245.97	0.496	0.00006	29.66
6	320	998.2	1.004	255.50	0.505	0.000062	31.24

Table A.2 Summarises the calculation of y+ for inlet pipe

No.	Flow rate	Density	Kinematic viscosity	Shear stress	u*	y	y+
	(l/min)	(kg/m^3)	$m^2/s *10^{-6}$	Pa		(m)	(-)
1	100	998.2	1.004	2.84	0.053	0.0006	31.87
2	150	998.2	1.004	5.05	0.071	0.00043	30.46
3	200	998.2	1.004	8	0.089	0.00038	33.88
4	250	998.2	1.004	11.76	0.108	0.00027	29.18
5	300	998.2	1.004	16.01	0.126	0.00025	31.52
6	320	998.2	1.004	17.80	0.133	0.00023	30.59

Table A.3 Summarises the calculation of y+ for outlet pipe

No.	Flow rate	Density	Kinematic viscosity	Shear stress	u*	y	y+
	(l/min)	(kg/m^3)	$m^2/s *10^{-6}$	Pa		(m)	(-)
1	100	998.2	1.004	8.52	0.092	0.00032	29.44
2	150	998.2	1.004	22.8	0.151	0.00022	33.11
3	200	998.2	1.004	36.28	0.190	0.00017	32.28
4	250	998.2	1.004	51.37	0.226	0.00013	29.37
5	300	998.2	1.004	70.85	0.266	0.00012	31.84
6	320	998.2	1.004	77.40	0.278	0.00011	30.50

- **y+ sensitivity**

Table A.4 Summarises the calculation of y+ sensitivity for impeller

No.	Flow rate	Density	Kinematic Viscosity	Shear stress	u*	y	y+
	(l/min)	(kg/m^3)	$m^2/s *10^{-6}$	Pa		(m)	(-)
1	300	998.2	1.004	339.90	0.583	0.000035	20.34
2	300	998.2	1.004	342.96	0.586	0.000052	30.35
3	300	998.2	1.004	344.99	0.587	0.00007	40.98

Table A.5 Summarises the calculation of y+ sensitivity for volute

No.	Flow rate	Density	Kinematic Viscosity	Shear stress	u*	y	y+
	(l/min)	(kg/m^3)	$m^2/s *10^{-6}$	Pa		(m)	(-)
1	300	998.2	1.004	236.59	0.486	0.000041	19.88
2	300	998.2	1.004	245.97	0.496	0.00006	29.66
3	300	998.2	1.004	252.67	0.503	0.000085	42.59

Table A.6 Summarises the calculation of y+ sensitivity for inlet pipe

No.	Flow rate	Density	Kinematic Viscosity	Shear stress	u*	y	y+
	(l/min)	(kg/m^3)	$m^2/s *10^{-6}$	Pa		(m)	(-)
1	300	998.2	1.004	15.90	0.126	0.00016	20.11
2	300	998.2	1.004	16.01	0.126	0.00025	31.52
3	300	998.2	1.004	15.61	0.126	0.00033	41.48

Table A.7 Summarises the calculation of y+ sensitivity for outlet pipe

No.	Flow rate	Density	Kinematic Viscosity	Shear stress	u*	y	y+
	(l/min)	(kg/m^3)	$m^2/s *10^{-6}$	Pa		(m)	(-)
1	300	998.2	1.004	66.77	0.258	0.000075	19.32
2	300	998.2	1.004	70.85	0.266	0.00012	31.84
3	300	998.2	1.004	74.66	0.273	0.00016	43.58

APPENDIX B

Table B-1 Details of piping system components

Item	No	Description	Cost	Photo
Clear PVCu Pipe	2	PVCu Clear Pipe 16 BAR 2.5m Length 32mm	£ 42.902	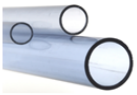
Clear PVCu Pipe	1	PVCu Clear Pipe 16 BAR 1.25m Length 50mm	£ 34.068	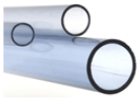
Short Radius Bend 90°	2	PVCu Bend 90 Swept Plain 2"	£ 32.448	
Elbow 90°	2	PVCu Elbow 90 Plain 1 1/4"	£ 4.44	
Tee 90°	1	PVCu Tee 90 Plain 2 1/2"	£ 9.384	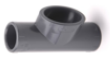
Reducing Bush	1	PVCu Reducing Bush Plain 2 1/2" x 2"	£ 2.988	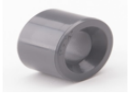
Reducing Bush	2	PVCu Reducing Bush Plain 1 1/2" x 1 1/4"	£ 2.424	

Ball Valves	1	Brass Ball Valve NPT F/F 1 1/4"	£ 29.676	
Ball Valves	1	Brass Ball Valve NPT F/F 2"	£ 66.852	
Adaptor Plain F / BSP M	2	PVCu Adaptor Female Plain x Threaded Male 1 1/4"	£ 4.824	
Adaptor Plain F / BSP M	2	PVCu Adaptor Female Plain x Threaded Male 2"	£ 8.4	
Socket	4	PVCu Socket Plain 1 1/4"	£ 5.328	
Socket	5	PVCu Socket Plain 2"	£ 11.1	
Union	1	PVCu Union Plain x Threaded 1 1/4"	£ 9.775	
Union	1	PVCu Union Plain x Threaded 2"	£ 12.855	

Flow Meter Plain Inch	1	Digital Flow Meter 38 to 380 LPM Plain 1 1/2"	£ 322.392	
PVCU Solvent Cement	1	Solvent Cement for PVCu 500ml Tin	£17.436	
Cleaning Fluid	1	Cleaning Fluid For PVCu And ABS 500ml Tin	£12.384	
PTFE Tape	1	PTFE Tape 12m Roll Pack of 10	£6.516	
Thread	1	Studding 1M	£1.36	
Galv Back Plate	3	THREADED BACK PLATE GALV	£2.12	
RUBBER LINED CLIPS	3	110 mm EPDM RUBBER LINED CLIPS	£ 17.4	
sheet steel metal	1	dimensions (70cm*60cm*1cm)	£ 90.5	

Operating flow loop for the centrifugal pump

To operate the centrifugal pump, follow the below next stages:

1. Fill the main water tank
2. Make sure that the main switch is off and choose pump the 4kW has a red plug
3. Check flow loop system, check all valves and pressure taps in the flow loop
4. Plug the pump socket into the power supply provided by lifting the red lid up and carefully plug it as shown in the figure B-1 (a) below.
5. Turn on the below switch of the socket as shown in the figure B-1 (b)
6. Switch on the main wall power supply on as it is shown in B-1 (c) below

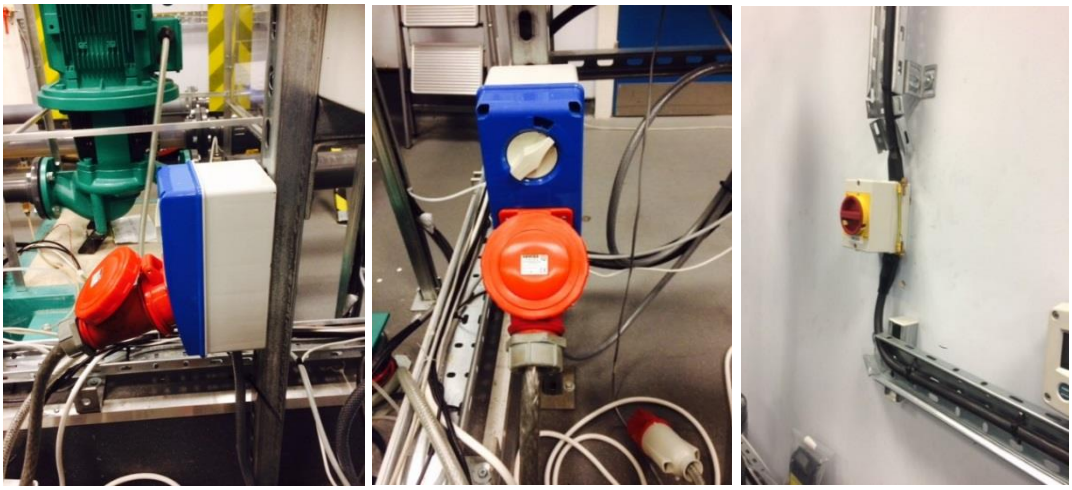

(a) (b) (c)

Figure B-1 shows (a) Plugging the pump into the socket, (b) Plugging the pump into the socket and switch it on, (c) The main wall power supply switch

7. Go to the main control panel and switch the power supply on
8. Wait for the control panel to warm up before doing the next step.
9. Wait to show the massage in the Parker control panel as shown in the figure below
10. Double check the flow loop and everything is set for experiment
11. Select motor current from the Parker control panel through the use of key M then press the key after
12. Change the motor current to 8.9A by using key M by through using the Up/Down keys

(a) (b) (c)

Figure B-2 shows (a) Motor drive Parker control panel, (b) Select parameters from the motor control panel, (c) Change the motor current

13. Then press (Escape) Key E

14. In order to select the number of steps Using the touch screen as shown below
15. Click key Next
16. Go to operator screen then click set-up as shown in the figure below
17. Select the number of steps required

(a) (b) (c)

Figure B-2 shows (a) The main control panel touch screen, (b) The main control panel touch screen, (c) Number of steps required

18. Insert the time laps and the speed percentage in the recipe screen

Figure B-10 Time laps and speed percentage

19. Go to operator screen and select the auto and flow then change the set point for example, to 800 this mean the rotational speed of the pump is 50%

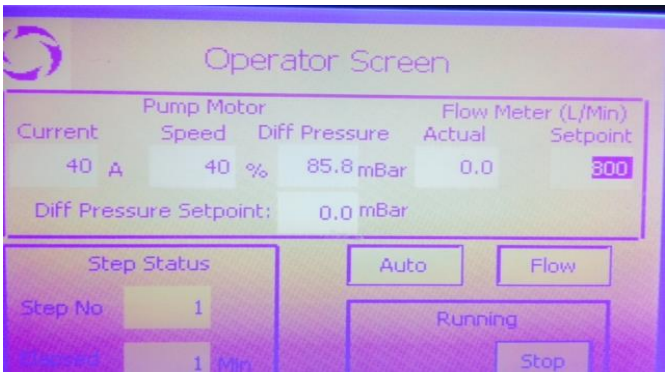

Figure B-11 The main control panel touch screen

20. Select Start from the main touch screen to start up the pump
21. It can be changed the rotational speed of the pump by change the set point for example 800 = 50%, 1200=75%, and 1440=90%

22. To stop the running of the pump, press stop key in the main touch screen operator in the control panel then switch off the main control panel, switch off pump socket and finally switch off the main power supply.
23. After finishing experiment, switch off all the main power supplies and unplug the socket
24. Shut all the valves in the loop and clean up any water spillage around the floor in the bund area
25. Empty the water tank

Centrifugal Pump Type F32/200AH Pedrollo

Figure B.12 Centrifugal pump type F32/200AH Pedrollo

Curves and Performance Data at Pump Rotational Speed N=2900rpm

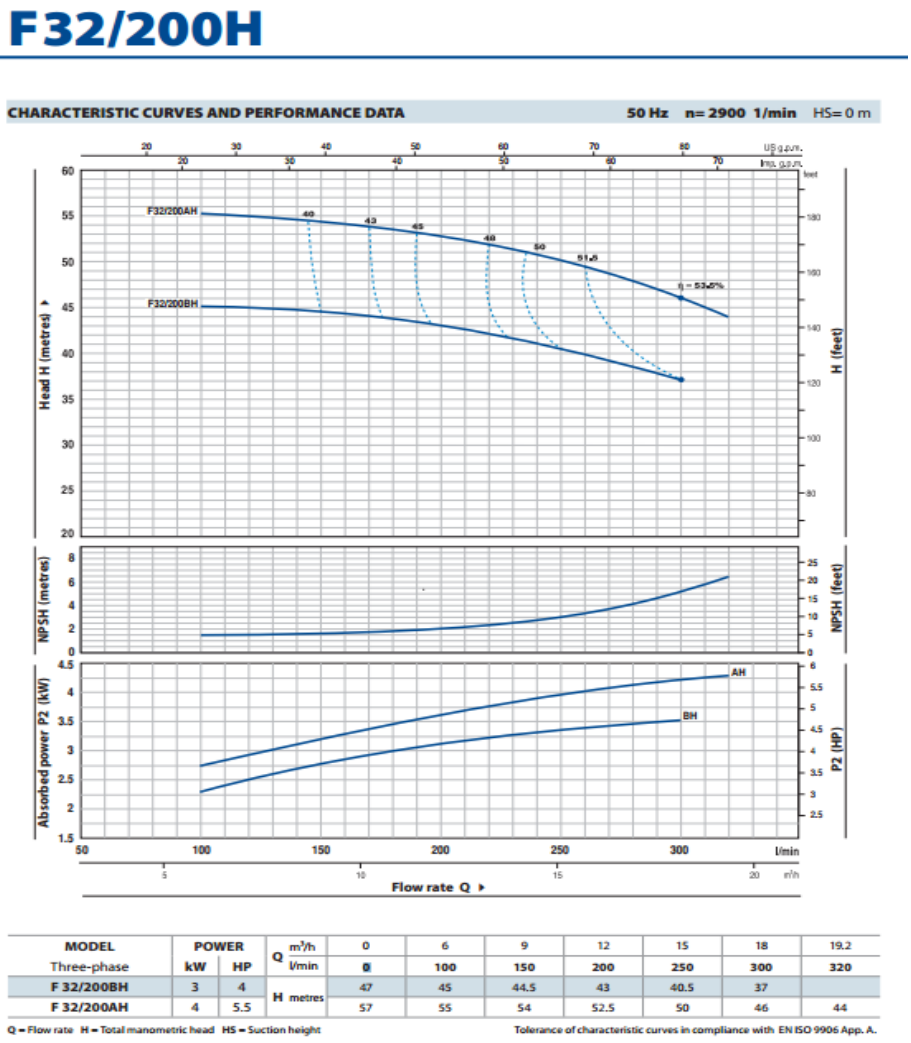

MODEL	POWER		Q m³/h	0	6	9	12	15	18	19.2
Three-phase	kW	HP	Q l/min	0	100	150	200	250	300	320
F 32/200BH	3	4	H metres	47	45	44.5	43	40.5	37	
F 32/200AH	4	5.5		57	55	54	52.5	50	46	44

Figure B.13 Centrifugal pump preformance curves data from pedrollo company at rotational speed N=2900rpm, and inlet and outlet diameters 50mm, 32mm

Centrifugal Pump Components

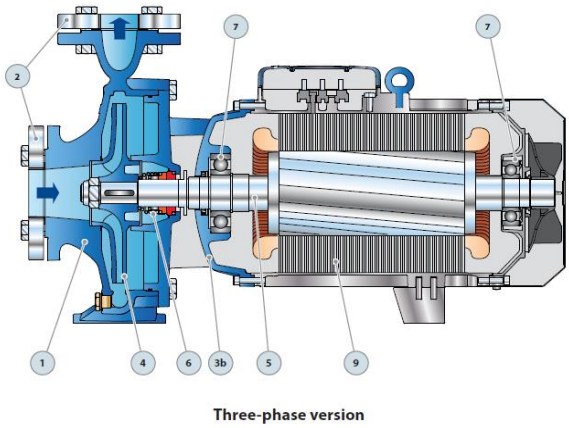

Figure B.14 Centrifugal pump components

Centrifugal Pump Components (Constraction Characteristics)

F

POS.	COMPONENT	CONSTRUCTION CHARACTERISTICS
1	PUMP BODY	Cast iron, complete with flanged suction and delivery ports
2	COUNTERFLANGES	Steel, complete with ISO 228/1 thread
3a	BODY BACKPLATE	Cast iron
3b	MOTOR BRACKET	Cast iron
4	IMPELLER	Brass for F32/160, F32/200, F40/160, F40/200, F50/125, F50/160 Cast iron for F40/250, F50/200, F50/250, F65/125, F65/160, F65/200, F65/250, F80/160, F80/200, F80/250, F100/160, F100/200, F100/250
5	MOTOR SHAFT	Stainless steel EN 10088-3 - 1.4104

6 MECHANICAL SEAL

Pump Model		Seal Model	Shaft Diameter	Materials: Stationary ring	Rotational ring	Elastomer
F32/160 F50/125	F40/160	FN-20	Ø 20 mm	Graphite	Ceramic	NBR
F32/200 F50/160	F40/200 F65/125	FN-24	Ø 24 mm	Graphite	Ceramic	NBR
F50/200 F65/200 F100/160	F65/160 F80/160	FN-32 NU	Ø 32 mm	Graphite	Ceramic	NBR
F40/250	F50/250	FN-38	Ø 38 mm	Graphite	Ceramic	NBR
F65/250 F80/250B	F80/200 F100/200	FN-40	Ø 40 mm	Graphite	Ceramic	NBR
F80/250A	F100/250	FH-45 NU	Ø 45 mm	Graphite	Ceramic	NBR

7 BEARINGS

Pump	Model
Fm32/160C F32/160C F32/160B F40/160C F50/125C	6206 ZZ - C3 / 6204 ZZ
Fm32/160B F32/160A Fm40/160C F40/160B Fm50/125C F50/125B	6206 ZZ - C3 / 6205 ZZ
F40/160A F50/125A	6306 ZZ - C3 / 6206 ZZ - C3

Pump	Model
F32/200 F40/200 F50/160 F65/125	6307 ZZ - C3 / 6206 ZZ - C3
F40/250 F50/200 F50/250 F65/160 F65/200 F80/160 F100/160	6310 ZZ - C3 / 6308 ZZ - C3
F65/250 F80/200 F80/250B F100/200	6312 ZZ - C3 / 6212 ZZ - C3
F80/250A F100/250	6314 ZZ - C3 / 6314 ZZ - C3

8 CAPACITOR

Pump Single-phase	Capacitance (230 V or 240 V)
Fm32/160C	45 µF 450 VL
Fm32/160B	70 µF 450 VL
Fm40/160C	70 µF 450 VL
Fm50/125C	70 µF 450 VL

9 ELECTRIC MOTOR

Fm: single-phase 230 V - 50 Hz with thermal overload protector built-in to the winding (up to 1.5 kW)
F: three-phase 230/400 V - 50 Hz up to 4 kW
400/690 V - 50 Hz from 5.5 to 75 kW
= Pumps fitted with the three-phase motor option offer IE2 (IEC 60034-30) class high performance
– Insulation: F class
– Protection: IP 55

Figure B.15 Centrifugal pump components and specification

Centrifugal Pump Dimensions and Specifications

F

DIMENSIONS AND WEIGHT

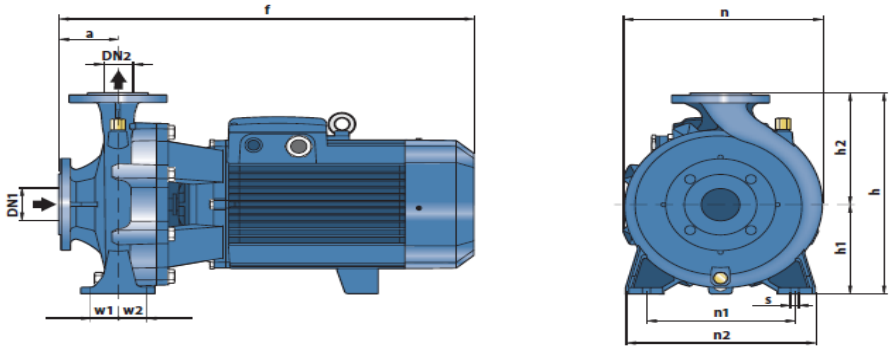

MODEL		PORTS		DIMENSIONS mm										kg *	
Single-phase	Three-phase	DN1	DN2	a	f	h	h1	h2	n	n1	n2	w1	w2	s	1~	3~
Fm 32/160C	F 32/160C	50	32	80	412	292	132	160	242	190	240	35	35		39.2	37.0
Fm 32/160B	F 32/160B														42.6	38.5
–	F 32/160A				431										–	42.6
–	F 32/200C				469	340	160	180	270						–	52.0
–	F 32/200B				515										–	57.0
–	F 32/200A														–	61.0
–	F 32/200BH				469										–	47.9
–	F 32/200AH														–	51.1

Figure B.16 Centrifugal pump dimensions

Centrifugal Pump Absorption (Model and Voltage)

F

ABSORPTION

MODEL	VOLTAGE (three-phase)		
Three-phase	230÷240 V	400÷415 V	690÷720 V
F 32/200BH	12.6 A	7.3 A	4.2 A
F 32/200AH	15.4 A	8.9 A	5.1 A

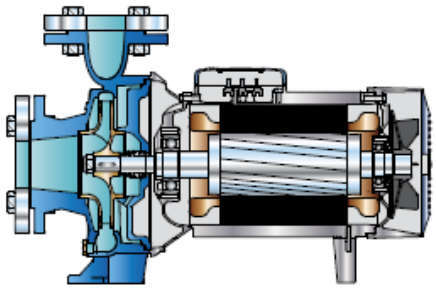

Three-phase version

Figure B.17 Centrifugal pump specifications

APPENDIX C

Table C.1 Head coefficient of the centrifugal pump under various impeller geometrical parameters at single-phase

H CFD	CH CFD	H equation	CH equation	Z	do	di	H	CH
(m)	(-)	(m)	(-)	(-)	(m)	(m)	(%)	(%)
31.80	0.093	32.37	0.095	3	0.2	0.025	-1.78	1.75
33.02	0.097	34.26	0.101	4	0.2	0.025	-3.76	3.63
33.60	0.099	35.80	0.105	5	0.2	0.025	-6.54	6.14
34.94	0.093	34.09	0.091	3	0.21	0.025	2.42	-2.48
38.19	0.102	36.08	0.096	4	0.21	0.025	5.53	-5.85
39.34	0.105	37.70	0.100	5	0.21	0.025	4.15	-4.33
34.73	0.084	35.81	0.087	3	0.22	0.025	-3.11	3.02
37.99	0.092	37.90	0.092	4	0.22	0.025	0.24	-0.24
39.13	0.095	39.61	0.096	5	0.22	0.025	-1.21	1.19
31.51	0.092	32.02	0.094	3	0.2	0.03	-1.61	1.59
32.77	0.096	33.89	0.099	4	0.2	0.03	-3.41	3.30
33.73	0.099	35.42	0.104	5	0.2	0.03	-4.98	4.74
34.82	0.093	33.72	0.090	3	0.21	0.03	3.16	-3.26
37.89	0.101	35.69	0.095	4	0.21	0.03	5.80	-6.16
38.83	0.103	37.29	0.099	5	0.21	0.03	3.94	-4.10
34.66	0.084	35.43	0.086	3	0.22	0.03	-2.21	2.16
37.64	0.091	37.49	0.091	4	0.22	0.03	0.38	-0.38
38.75	0.094	39.18	0.095	5	0.22	0.03	-1.11	1.09
31.02	0.091	31.73	0.093	3	0.2	0.035	-2.28	2.23
32.63	0.096	33.58	0.099	4	0.2	0.035	-2.92	2.84
33.79	0.099	35.09	0.103	5	0.2	0.035	-3.85	3.71
34.57	0.092	33.41	0.089	3	0.21	0.035	3.35	-3.47
37.52	0.100	35.36	0.094	4	0.21	0.035	5.74	-6.08
38.60	0.103	36.95	0.098	5	0.21	0.035	4.25	-4.44
34.31	0.083	35.10	0.085	3	0.22	0.035	-2.30	2.25
37.57	0.091	37.15	0.090	4	0.22	0.035	1.10	-1.11
38.59	0.094	38.82	0.094	5	0.22	0.035	-0.61	0.60

Table C.2 Power coefficient of the centrifugal pump under various impeller geometrical parameters at single-phase

P CFD	CP CFD	P equation	CP equation	Z	do	di	P	CP
(kw)	(-)	(kw)	(-)	(-)	(m)	(m)	(%)	(%)
2.521	0.0003	2.669	0.00034	3	0.2	0.025	-5.88	-5.68
2.383	0.00031	2.819	0.00036	4	0.2	0.025	-18.27	-18.05
2.774	0.00036	2.940	0.00038	5	0.2	0.025	-6.01	-5.81
2.77	0.00028	2.677	0.00027	3	0.21	0.025	3.48	3.66
2.398	0.00024	2.827	0.00028	4	0.21	0.025	-17.87	-17.65
3.095	0.00031	2.949	0.00030	5	0.21	0.025	4.72	4.89

2.873	0.00023	2.684	0.00021	3	0.22	0.025	6.56	6.74
3.074	0.00024	2.834	0.00022	4	0.22	0.025	7.78	7.95
3.162	0.00025	2.957	0.00023	5	0.22	0.025	6.50	6.67
2.519	0.00032	2.641	0.00034	3	0.2	0.03	-4.87	-4.67
2.364	0.00030	2.789	0.00036	4	0.2	0.03	-17.96	-17.74
2.789	0.00036	2.910	0.00037	5	0.2	0.03	-4.31	-4.11
2.773	0.00028	2.649	0.00027	3	0.21	0.03	4.49	4.67
2.974	0.000303	2.797	0.00028	4	0.21	0.03	5.93	6.11
3.085	0.00031	2.918	0.00029	5	0.21	0.03	5.41	5.59
2.875	0.00023	2.656	0.00021	3	0.22	0.03	7.60	7.77
3.068	0.00024	2.805	0.00022	4	0.22	0.03	8.57	8.74
3.157	0.00025#	2.926	0.00023	5	0.22	0.03	7.33	7.51
2.518	0.00032	2.618	0.00034	3	0.2	0.035	-3.95	-3.75
2.398	0.00031	2.765	0.00036	4	0.2	0.035	-15.2	-15.07
2.814	0.00036	2.884	0.00037	5	0.2	0.035	-2.48	-2.29
2.785	0.00028	2.625	0.00026	3	0.21	0.035	5.74	5.91
2.977	0.00030	2.772	0.00028	4	0.21	0.035	6.86	7.04
3.091	0.00031	2.89	0.00029	5	0.21	0.035	6.42	6.60
2.879	0.00023	2.632	0.00021	3	0.22	0.035	8.57	8.74
3.075	0.00024	2.780	0.00022	4	0.22	0.035	9.60	9.77
3.161	0.00025	2.900	0.00023	5	0.22	0.035	8.25	8.42

Table C.3 Head coefficient of the centrifugal pump under various impeller geometrical parameters at cavitation condition

H CFD	CH CFD	H equation	CH equation	Z	do	di	H	CH
(m)	(-)	(m)	(-)	(-)	(m)	(m)	(%)	(%)
31.53	0.092	31.86	0.093	3	0.2	0.025	-1.04	1.03
30.81	0.090	33.41	0.098	4	0.2	0.025	-8.45	7.79
32.73	0.096	34.67	0.102	5	0.2	0.025	-5.91	5.58
34.25	0.091	33.59	0.089	3	0.21	0.025	1.94	-1.98
36.86	0.098	35.22	0.094	4	0.21	0.025	4.44	-4.65
37.65	0.101	36.54	0.097	5	0.21	0.025	2.94	-3.02
34.53	0.084	35.32	0.086	3	0.22	0.025	-2.28	2.22
37.47	0.091	37.03	0.090	4	0.22	0.025	1.14	-1.16
38.37	0.093	38.43	0.093	5	0.22	0.025	-0.13	0.13
31.13	0.091	31.40	0.092	3	0.2	0.03	-0.89	0.88
30.67	0.090	32.93	0.097	4	0.2	0.03	-7.39	6.88
32.77	0.096	34.17	0.101	5	0.2	0.03	-4.28	4.10
34.10	0.091	33.10	0.088	3	0.21	0.03	2.91	-2.99
36.62	0.097	34.71	0.092	4	0.21	0.03	5.20	-5.49
37.30	0.099	36.02	0.096	5	0.21	0.03	3.43	-3.55
34.30	0.083	34.81	0.084	3	0.22	0.03	-1.46	1.44
37.29	0.090	36.50	0.088	4	0.22	0.03	2.12	-2.16
38.25	0.093	37.87	0.092	5	0.22	0.03	0.99	-1.01
30.73	0.091	31.02	0.091	3	0.2	0.035	-0.93	0.92
30.49	0.089	32.53	0.095	4	0.2	0.035	-6.67	6.26
32.57	0.095	33.75	0.099	5	0.2	0.035	-3.62	3.49

33.76	0.090	32.70	0.087	3	0.21	0.035	3.13	-3.23
36.15	0.096	34.29	0.091	4	0.21	0.035	5.13	-5.41
37.20	0.099	35.58	0.095	5	0.21	0.035	4.34	-4.54
33.96	0.082	34.38	0.083	3	0.22	0.035	-1.23	1.22
36.99	0.090	36.06	0.087	4	0.22	0.035	2.53	-2.59
38.20	0.093	37.41	0.091	5	0.22	0.035	2.07	-2.11

Table C.4 Power coefficient of the centrifugal pump under various impeller geometrical parameters at cavitation condition

P CFD	CP CFD	P equation	CP equation	Z	do	di	P	CP
(kW)	(-)	(kW)	(-)	(-)	(m)	(m)	(%)	(%)
2.258	0.000294	2.637	0.000343	3	0.2	0.025	-16.78	-16.56
2.319	0.000302	2.799	0.000364	4	0.2	0.025	-17.73	-17.50
2.724	0.000355	2.932	0.000382	5	0.2	0.025	-7.65	-7.45
2.744	0.000280	2.649	0.000270	3	0.21	0.025	3.45	3.63
2.915	0.000297	2.812	0.000287	4	0.21	0.025	3.52	3.70
3.025	0.000309	2.946	0.000300	5	0.21	0.025	2.64	2.82
2.838	0.000229	2.660	0.000215	3	0.22	0.025	6.25	6.43
3.033	0.000245	2.824	0.000228	4	0.22	0.025	6.86	7.04
3.068	0.000248	2.958	0.000239	5	0.22	0.025	3.56	3.74
2.469	0.000321	2.593	0.000337	3	0.2	0.03	-4.99	-4.79
2.377	0.000309	2.752	0.000358	4	0.2	0.03	-15.80	-15.59
2.733	0.000356	2.883	0.000375	5	0.2	0.03	-5.49	-5.29
2.742	0.000280	2.604	0.000266	3	0.21	0.03	5.02	5.19
2.913	0.000297	2.765	0.000282	4	0.21	0.03	5.08	5.25
3.028	0.000309	2.896	0.000295	5	0.21	0.03	4.34	4.52
2.834	0.000229	2.616	0.000211	3	0.22	0.03	7.68	7.85
3.033	0.000245	2.777	0.000224	4	0.22	0.03	8.43	8.60
3.086	0.000249	2.909	0.000235	5	0.22	0.03	5.75	5.93
2.454	0.000319	2.556	0.000333	3	0.2	0.035	-4.13	-3.94
2.391	0.000311	2.713	0.000353	4	0.2	0.035	-13.47	-13.26
2.758	0.000359	2.842	0.00037	5	0.2	0.035	-3.03	-2.84
2.741	0.000279	2.567	0.000262	3	0.21	0.035	6.33	6.51
2.914	0.000297	2.726	0.000278	4	0.21	0.035	6.44	6.62
3.035	0.000309	2.855	0.000291	5	0.21	0.035	5.92	6.09
2.839	0.000229	2.579	0.000208	3	0.22	0.035	9.15	9.32
3.048	0.000246	2.737	0.000221	4	0.22	0.035	10.17	10.34
3.151	0.000255	2.867	0.000232	5	0.22	0.035	8.99	9.16

Table C.5 Statistical analysis results of the pump head under various impeller geometrical parameters at single-phase

Inlet impeller diameter	Outlet impeller diameter	No. of impeller blades	Head avge.	Head min.	Head max.	Head (max.-min.)
(mm)	(mm)	(-)	(m)	(m)	(m)	(m)
		3	31.80	28.69	34.30	5.609
	200	4	33.02	31.19	34.61	3.412

25		5	33.60	32.25	34.83	2.577
	210	3	34.94	31.46	37.75	6.289
		4	38.19	35.89	40.19	4.297
		5	39.34	38.01	40.54	2.542
	220	3	34.73	30.07	37.93	7.859
		4	37.99	34.65	40.46	5.811
		5	39.13	36.97	40.74	3.778
30	200	3	31.51	28.36	34.01	5.638
		4	32.77	30.96	34.38	3.425
		5	33.73	32.32	35.05	2.728
	210	3	34.82	31.33	37.64	6.307
		4	37.89	35.58	39.87	4.284
		5	38.83	37.49	39.98	2.485
	220	3	34.66	30.06	37.79	7.724
		4	37.64	34.20	39.98	5.785
		5	38.75	36.50	40.50	4.005
35	200	3	31.02	27.89	33.47	5.587
		4	32.63	30.79	34.26	3.470
		5	33.79	32.48	34.95	2.467
	210	3	34.57	31.14	37.33	6.186
		4	37.52	35.24	39.49	4.248
		5	38.60	37.26	39.78	2.522
	220	3	34.31	29.72	37.44	7.721
		4	37.57	34.19	39.94	5.758
		5	38.59	36.41	40.21	3.798

Table C.6 Statistical analysis results of the pump head under various impeller geometrical parameters at cavitation conditions

Inlet impeller diameter	Outlet impeller diameter	No. of impeller blades	Head avge.	Head min.	Head max.	Head (max.-min.)
(mm)	(mm)	(-)	(m)	(m)	(m)	(m)
25	200	3	31.53	28.28	33.91	5.626
		4	30.81	28.53	32.77	4.244
		5	32.73	31.40	34.08	2.680
	210	3	34.25	30.60	37.08	6.480
		4	36.86	34.21	39.13	4.919
		5	37.65	36.48	38.82	2.338
	220	3	34.53	29.74	37.44	7.705
		4	37.47	34.91	39.48	4.575
		5	38.37	36.55	39.73	3.174
30	200	3	31.13	28.03	33.38	5.357
		4	30.67	28.39	32.62	4.235
		5	32.77	31.52	34.07	2.552
	210	3	34.10	30.13	37.01	6.863
		4	36.62	33.66	38.57	4.908
		5	37.30	35.98	38.33	2.344
		3	34.30	30.90	37.12	6.215

	220	4	37.29	34.40	39.31	4.916
		5	38.25	36.37	39.49	3.111
35	200	3	30.73	28.25	33.01	4.751
		4	30.49	28.58	32.11	3.524
		5	32.57	31.29	33.77	2.477
	210	3	33.76	30.23	36.18	5.943
		4	36.15	33.68	38.04	4.359
		5	37.20	35.96	38.34	2.378
	220	3	33.96	30.38	36.69	6.309
		4	36.99	34.52	38.918	4.392
		5	38.20	36.39	39.71	3.315

APPENDIX D

The accelerometer qualification certification

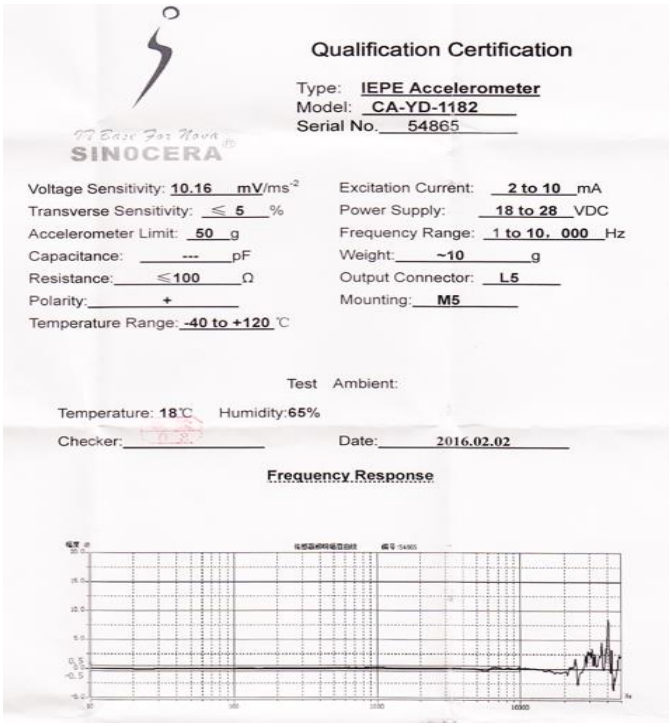

Qualification Certification

Type: IEPE Accelerometer
Model: CA-YD-1182
Serial No. 54865

SINOCERA

Voltage Sensitivity:	10.16 mV/ms^{-2}	Excitation Current:	2 to 10 mA
Transverse Sensitivity:	≤ 5 %	Power Supply:	18 to 28 VDC
Accelerometer Limit:	50 g	Frequency Range:	1 to 10，000 Hz
Capacitance:	--- pF	Weight:	~10 g
Resistance:	≤100 Ω	Output Connector:	L5
Polarity:	+	Mounting:	M5
Temperature Range:	-40 to +120 ℃		

Test Ambient:
Temperature: 18℃ Humidity:65%
Checker: Date: 2016.02.02

Frequency Response

Calibration chart for the microphone sensor

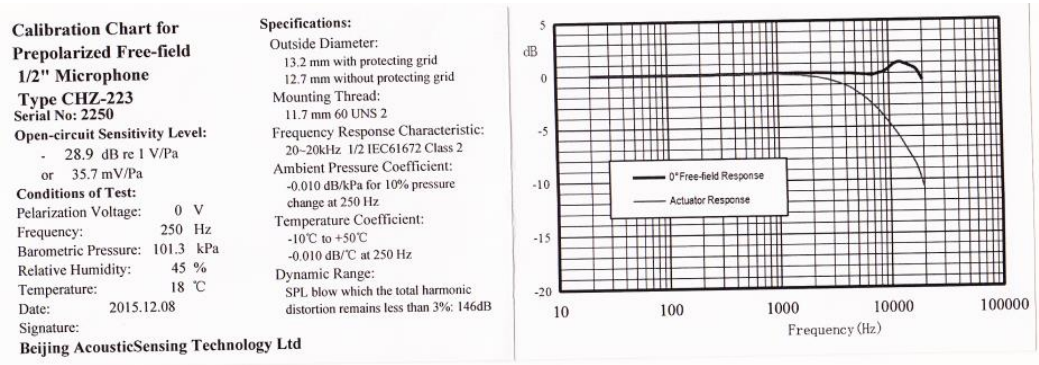

Calibration Chart for Prepolarized Free-field 1/2" Microphone Type CHZ-223
Serial No: 2250
Open-circuit Sensitivity Level:
- 28.9 dB re 1 V/Pa
or 35.7 mV/Pa

Conditions of Test:
Pelarization Voltage: 0 V
Frequency: 250 Hz
Barometric Pressure: 101.3 kPa
Relative Humidity: 45 %
Temperature: 18 ℃
Date: 2015.12.08
Signature:
Beijing AcousticSensing Technology Ltd

Specifications:
Outside Diameter:
13.2 mm with protecting grid
12.7 mm without protecting grid
Mounting Thread:
11.7 mm 60 UNS 2
Frequency Response Characteristic:
20~20kHz 1/2 IEC61672 Class 2
Ambient Pressure Coefficient:
-0.010 dB/kPa for 10% pressure change at 250 Hz
Temperature Coefficient:
-10℃ to +50℃
-0.010 dB/℃ at 250 Hz
Dynamic Range:
SPL blow which the total harmonic distortion remains less than 3%: 146dB

Specification of ICP microphone preamplifier

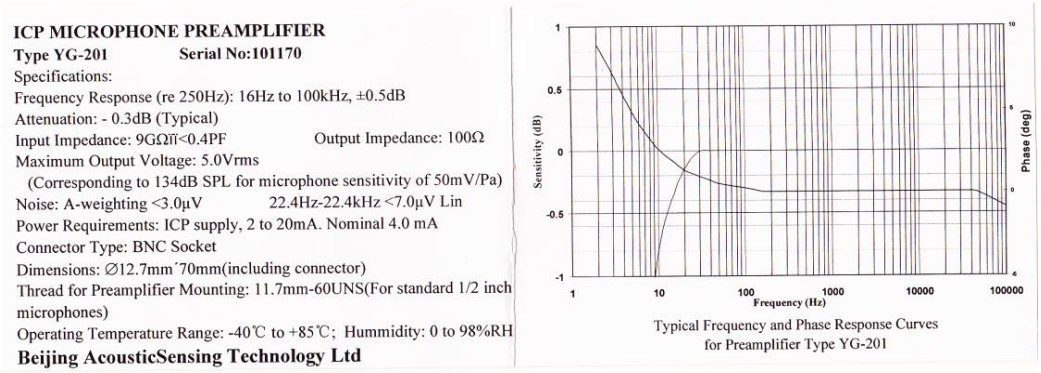

ICP MICROPHONE PREAMPLIFIER
Type YG-201 Serial No:101170
Specifications:
Frequency Response (re 250Hz): 16Hz to 100kHz, ±0.5dB
Attenuation: - 0.3dB (Typical)
Input Impedance: 9GΩ∏<0.4PF Output Impedance: 100Ω
Maximum Output Voltage: 5.0Vrms
(Corresponding to 134dB SPL for microphone sensitivity of 50mV/Pa)
Noise: A-weighting <3.0μV 22.4Hz-22.4kHz <7.0μV Lin
Power Requirements: ICP supply, 2 to 20mA. Nominal 4.0 mA
Connector Type: BNC Socket
Dimensions: ∅12.7mm*70mm(including connector)
Thread for Preamplifier Mounting: 11.7mm-60UNS(For standard 1/2 inch microphones)
Operating Temperature Range: -40℃ to +85℃; Hummidity: 0 to 98%RH
Beijing AcousticSensing Technology Ltd

Typical Frequency and Phase Response Curves for Preamplifier Type YG-201

Calibration certificate for the pressure transducer (range 0-10bar)

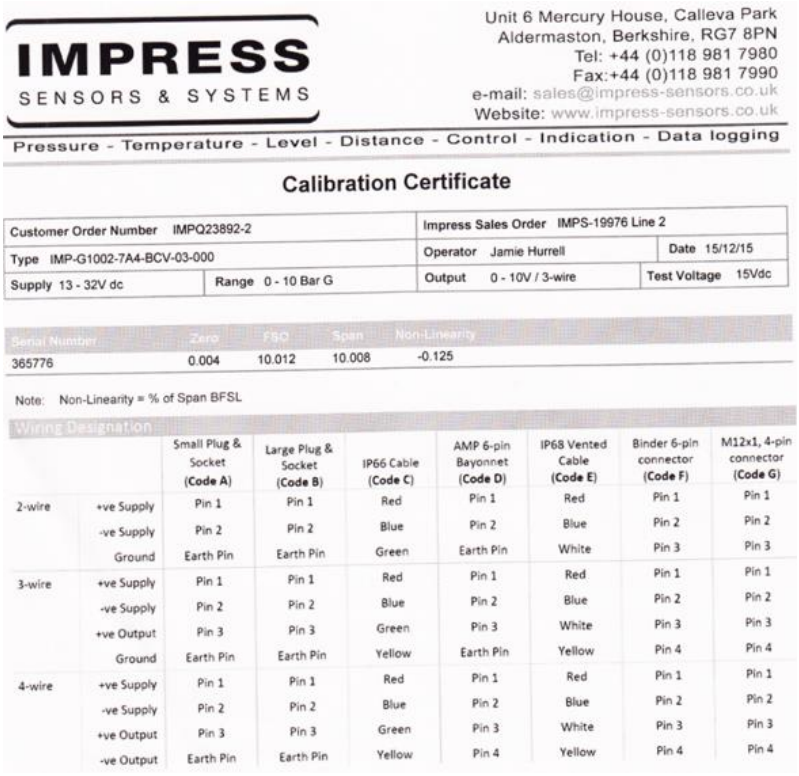

IMPRESS
SENSORS & SYSTEMS

Unit 6 Mercury House, Calleva Park
Aldermaston, Berkshire, RG7 8PN
Tel: +44 (0)118 981 7980
Fax:+44 (0)118 981 7990
e-mail: sales@impress-sensors.co.uk
Website: www.impress-sensors.co.uk

Pressure - Temperature - Level - Distance - Control - Indication - Data logging

Calibration Certificate

Customer Order Number IMPQ23892-2		Impress Sales Order IMPS-19976 Line 2	
Type IMP-G1002-7A4-BCV-03-000		Operator Jamie Hurrell	Date 15/12/15
Supply 13 - 32V dc	Range 0 - 10 Bar G	Output 0 - 10V / 3-wire	Test Voltage 15Vdc

Serial Number	Zero	FSO	Span	Non-Linearity
365776	0.004	10.012	10.008	-0.125

Note: Non-Linearity = % of Span BFSL

Wiring Designation

		Small Plug & Socket (Code A)	Large Plug & Socket (Code B)	IP66 Cable (Code C)	AMP 6-pin Bayonnet (Code D)	IP68 Vented Cable (Code E)	Binder 6-pin connector (Code F)	M12x1, 4-pin connector (Code G)
2-wire	+ve Supply	Pin 1	Pin 1	Red	Pin 1	Red	Pin 1	Pin 1
	-ve Supply	Pin 2	Pin 2	Blue	Pin 2	Blue	Pin 2	Pin 2
	Ground	Earth Pin	Earth Pin	Green	Earth Pin	White	Pin 3	Pin 3
3-wire	+ve Supply	Pin 1	Pin 1	Red	Pin 1	Red	Pin 1	Pin 1
	-ve Supply	Pin 2	Pin 2	Blue	Pin 2	Blue	Pin 2	Pin 2
	+ve Output	Pin 3	Pin 3	Green	Pin 3	White	Pin 3	Pin 3
	Ground	Earth Pin	Earth Pin	Yellow	Earth Pin	Yellow	Pin 4	Pin 4
4-wire	+ve Supply	Pin 1	Pin 1	Red	Pin 1	Red	Pin 1	Pin 1
	-ve Supply	Pin 2	Pin 2	Blue	Pin 2	Blue	Pin 2	Pin 2
	+ve Output	Pin 3	Pin 3	Green	Pin 3	White	Pin 3	Pin 3
	-ve Output	Earth Pin	Earth Pin	Yellow	Pin 4	Yellow	Pin 4	Pin 4

Calibration certificate for the pressure transducer (range 0-5bar)

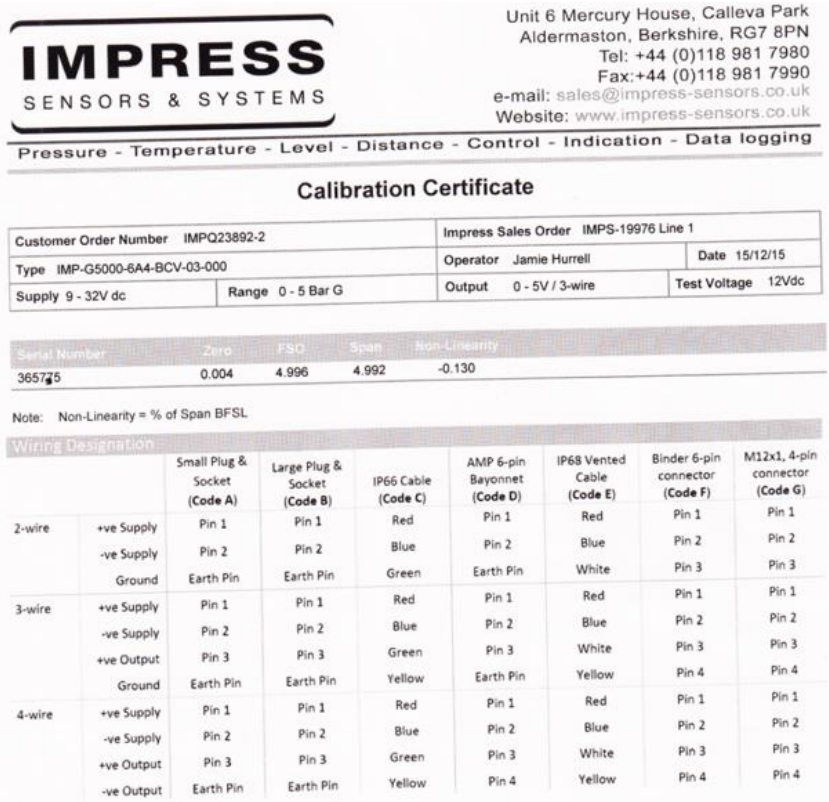

IMPRESS
SENSORS & SYSTEMS

Unit 6 Mercury House, Calleva Park
Aldermaston, Berkshire, RG7 8PN
Tel: +44 (0)118 981 7980
Fax:+44 (0)118 981 7990
e-mail: sales@impress-sensors.co.uk
Website: www.impress-sensors.co.uk

Pressure - Temperature - Level - Distance - Control - Indication - Data logging

Calibration Certificate

Customer Order Number IMPQ23892-2		Impress Sales Order IMPS-19976 Line 1	
Type IMP-G5000-6A4-BCV-03-000		Operator Jamie Hurrell	Date 15/12/15
Supply 9 - 32V dc	Range 0 - 5 Bar G	Output 0 - 5V / 3-wire	Test Voltage 12Vdc

Serial Number	Zero	FSO	Span	Non-Linearity
365775	0.004	4.996	4.992	-0.130

Note: Non-Linearity = % of Span BFSL

Wiring Designation

		Small Plug & Socket (Code A)	Large Plug & Socket (Code B)	IP66 Cable (Code C)	AMP 6-pin Bayonnet (Code D)	IP68 Vented Cable (Code E)	Binder 6-pin connector (Code F)	M12x1, 4-pin connector (Code G)
2-wire	+ve Supply	Pin 1	Pin 1	Red	Pin 1	Red	Pin 1	Pin 1
	-ve Supply	Pin 2	Pin 2	Blue	Pin 2	Blue	Pin 2	Pin 2
	Ground	Earth Pin	Earth Pin	Green	Earth Pin	White	Pin 3	Pin 3
3-wire	+ve Supply	Pin 1	Pin 1	Red	Pin 1	Red	Pin 1	Pin 1
	-ve Supply	Pin 2	Pin 2	Blue	Pin 2	Blue	Pin 2	Pin 2
	+ve Output	Pin 3	Pin 3	Green	Pin 3	White	Pin 3	Pin 3
	Ground	Earth Pin	Earth Pin	Yellow	Earth Pin	Yellow	Pin 4	Pin 4
4-wire	+ve Supply	Pin 1	Pin 1	Red	Pin 1	Red	Pin 1	Pin 1
	-ve Supply	Pin 2	Pin 2	Blue	Pin 2	Blue	Pin 2	Pin 2
	+ve Output	Pin 3	Pin 3	Green	Pin 3	White	Pin 3	Pin 3
	-ve Output	Earth Pin	Earth Pin	Yellow	Pin 4	Yellow	Pin 4	Pin 4

LIST OF PUBLICATIONS

1. Al-Obaidi, A., Pradhan, S., Asim, T., Mishra, R., & Zala, K. (2014). Numerical studies of the velocity distribution within the volute of a centrifugal pump.

2. Mohamed, F., Park, K. S., Pradhan, S., Mishra, R., Zala, K., Asim, T., & Al-Obaidi, A. (2014). The effect of blade angles of the vertical axis wind turbine on the output performance.